NASA-CR-176103

DOE/CS/54209-27(Vol.2)
(DE85017587)

NASA-CR-176103
19850024981

Energy
CONSERVATION

EVALUATION OF SEMICONDUCTOR DEVICES FOR ELECTRIC AND HYBRID VEHICLES (EHV) AC-DRIVE APPLICATIONS

Final Report

By
F. C. Lee
D. Y. Chen
M. Jovanovic
D. C. Hopkins

March 25, 1985

LIBRARY COPY
NOV 1 4 1985
LANGLEY RESEARCH CENTER
LIBRARY, NASA
HAMPTON, VIRGINIA

Work Performed Under Contract No. AI01-78CS54209

Virginia Polytechnic Institute and State University
Blacksburg, Virginia

Technical Information Center
Office of Scientific and Technical Information
United States Department of Energy

NF01762

BEST

AVAILABLE

COPY

DISCLAIMER

This report was prepared as an account of work sponsored by an agency of the United States Government. Neither the United States Government nor any agency thereof, nor any of their employees, makes any warranty, express or implied, or assumes any legal liability or responsibility for the accuracy, completeness, or usefulness of any information, apparatus, product, or process disclosed, or represents that its use would not infringe privately owned rights. Reference herein to any specific commercial product, process, or service by trade name, trademark, manufacturer, or otherwise does not necessarily constitute or imply its endorsement, recommendation, or favoring by the United States Government or any agency thereof. The views and opinions of authors expressed herein do not necessarily state or reflect those of the United States Government or any agency thereof.

This report has been reproduced directly from the best available copy.

Available from the National Technical Information Service, U. S. Department of Commerce, Springfield, Virginia 22161

Price: Printed Copy A18
Microfiche A01

Codes are used for pricing all publications. The code is determined by the number of pages in the publication. Information pertaining to the pricing codes can be found in the current issues of the following publications, which are generally available in most libraries: *Energy Research Abstracts (ERA)*, *Government Reports Announcements* and Index *(GRA* and I), *Scientific and Technical Abstract Reports (STAR)*, and publication NTIS-PR-360 available from NTIS at the above address.

DOE/CS/54209-27(Vol.2)
(JPL-9950-1038(Vol.2))
(DE85017587)
Distribution Category UC-96

EVALUATION OF SEMICONDUCTOR DEVICES FOR ELECTRIC AND HYBRID VEHICLE (EHV) AC-DRIVE APPLICATIONS

Final Report

Volume II

March 25, 1985

Prepared for

JET Propulsion Laboratory
California Institute of Technology
Pasadena, CA. 91109

Contract No. 956684

RE-1521170

by

F.C. Lee, D.Y. Chen, M. Jovanovic and D. C. Hopkins

Electrical Engineering Department
Virginia Polytechnic Institute
and State University
Blacksburg, Va. 24061

N85-33294#

This Page Intentionally Left Blank

TABLE OF CONTENTS

Volume II

APPENDIX A

TEST DATA OF SWITCHING TIMES CHARACTERIZATION OF BIPOLAR TRANSISTORS

A.1 Test Data for Westinghouse KD324510

Fig. A.1.1

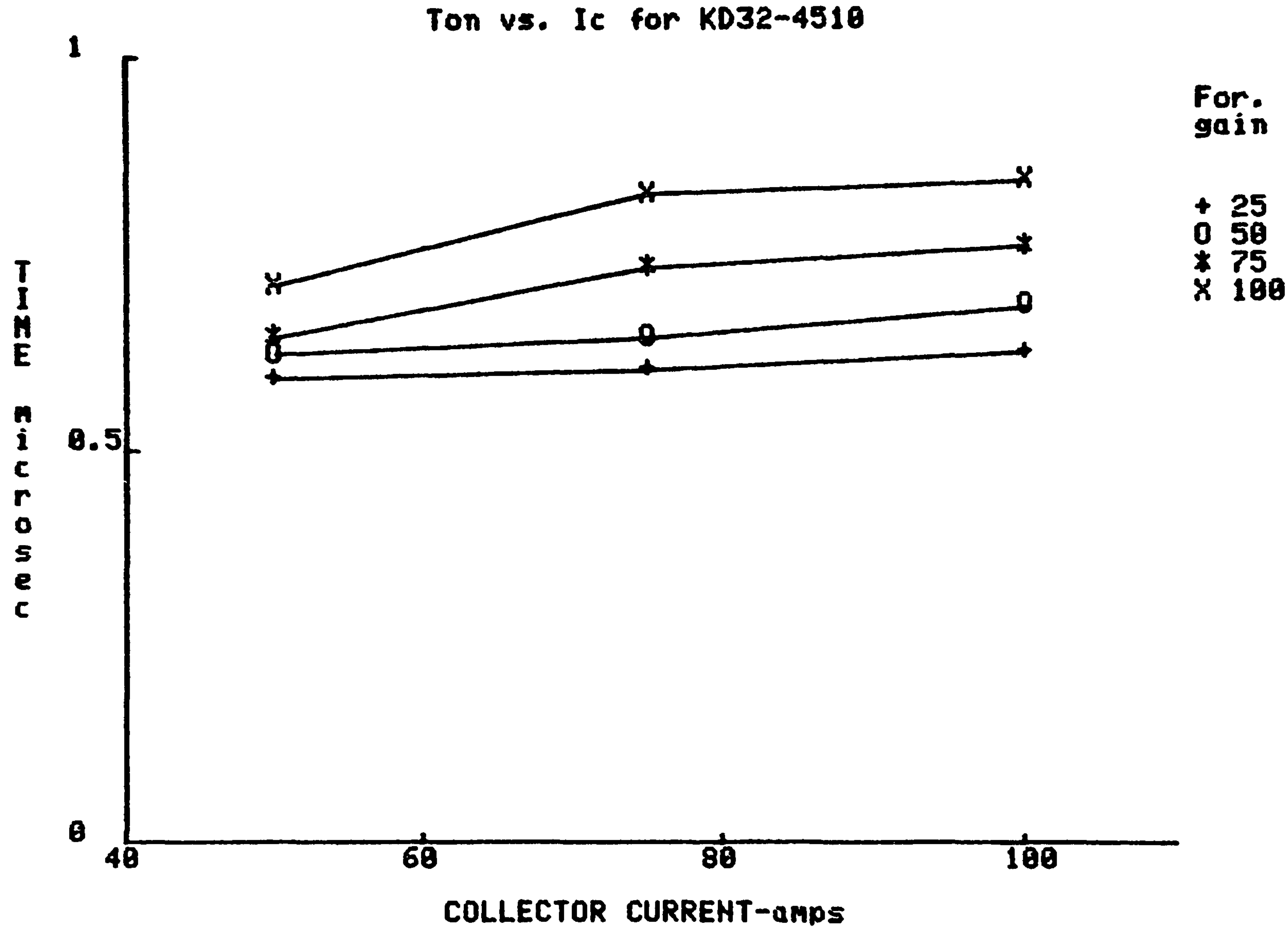
Ton vs. Ic for KD32-4510
1
0.5
0
TIME microsec
40
60
80
100
COLLECTOR CURRENT-amps
For. gain
+ 25
O 50
* 75
X 100

Fig. A.1.2

Ts vs. Ic for KD32-4510 @ Gf=50

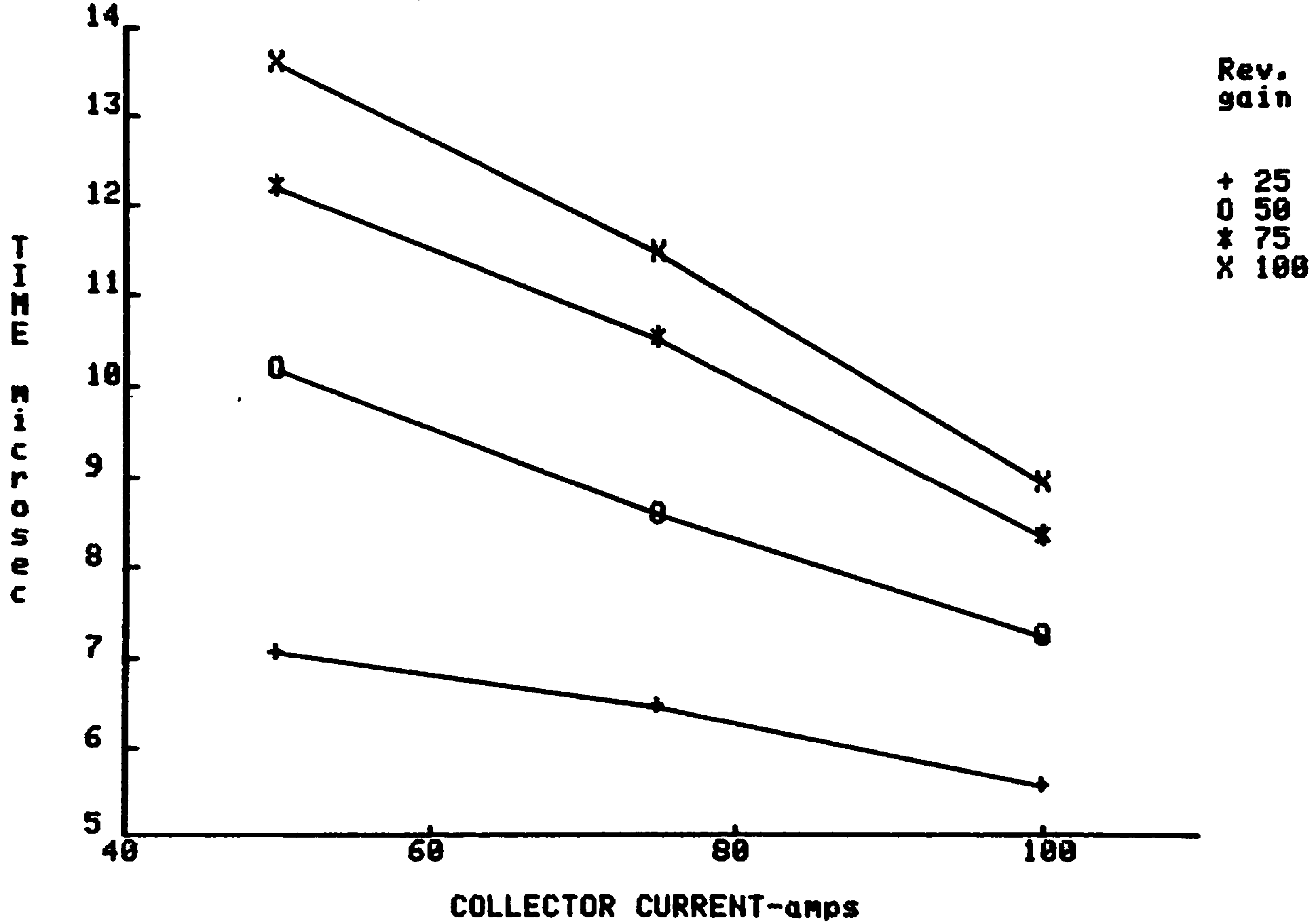

Fig. A.1.3

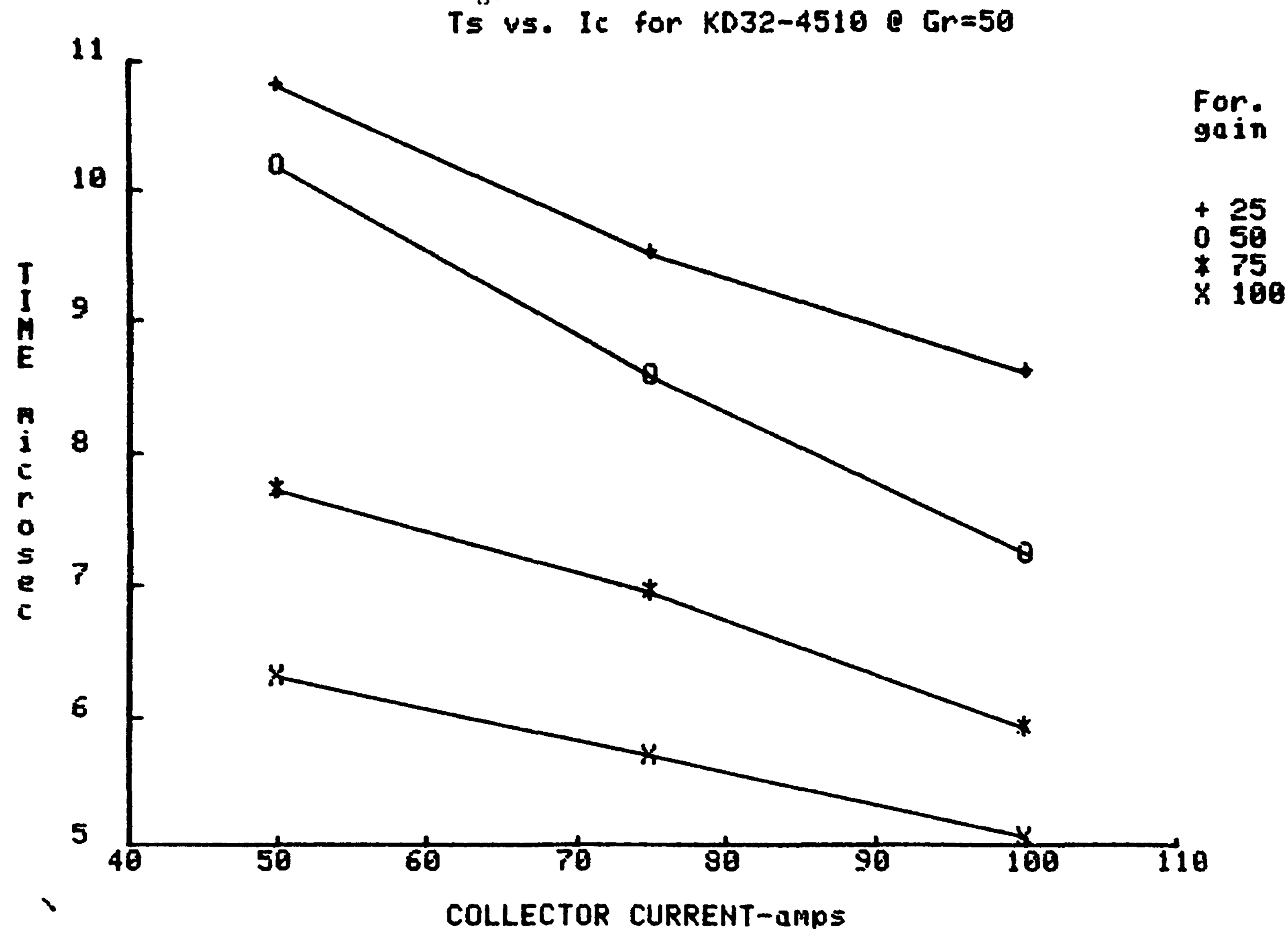

Ts vs. Ic for KD32-4510 @ Gr=50
TIME microsec
COLLECTOR CURRENT-amps
11
10
9
8
7
6
5
40
50
60
70
80
90
100
110
For. gain
+ 25
O 50
* 75
X 100

Fig. A.1.4

Tf vs. Ic for KD32-4510 @ Gf=50

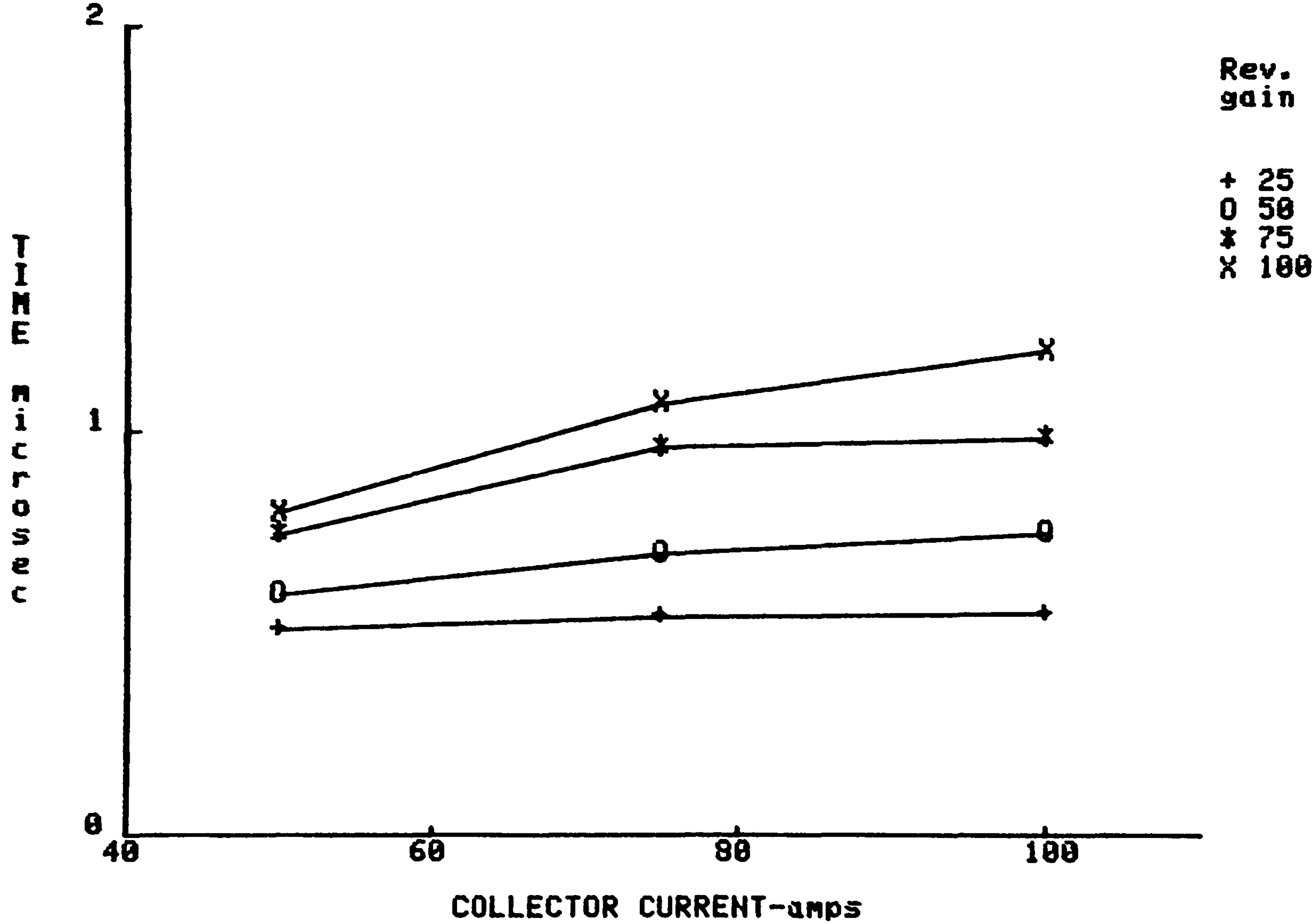

Fig. A.1.5

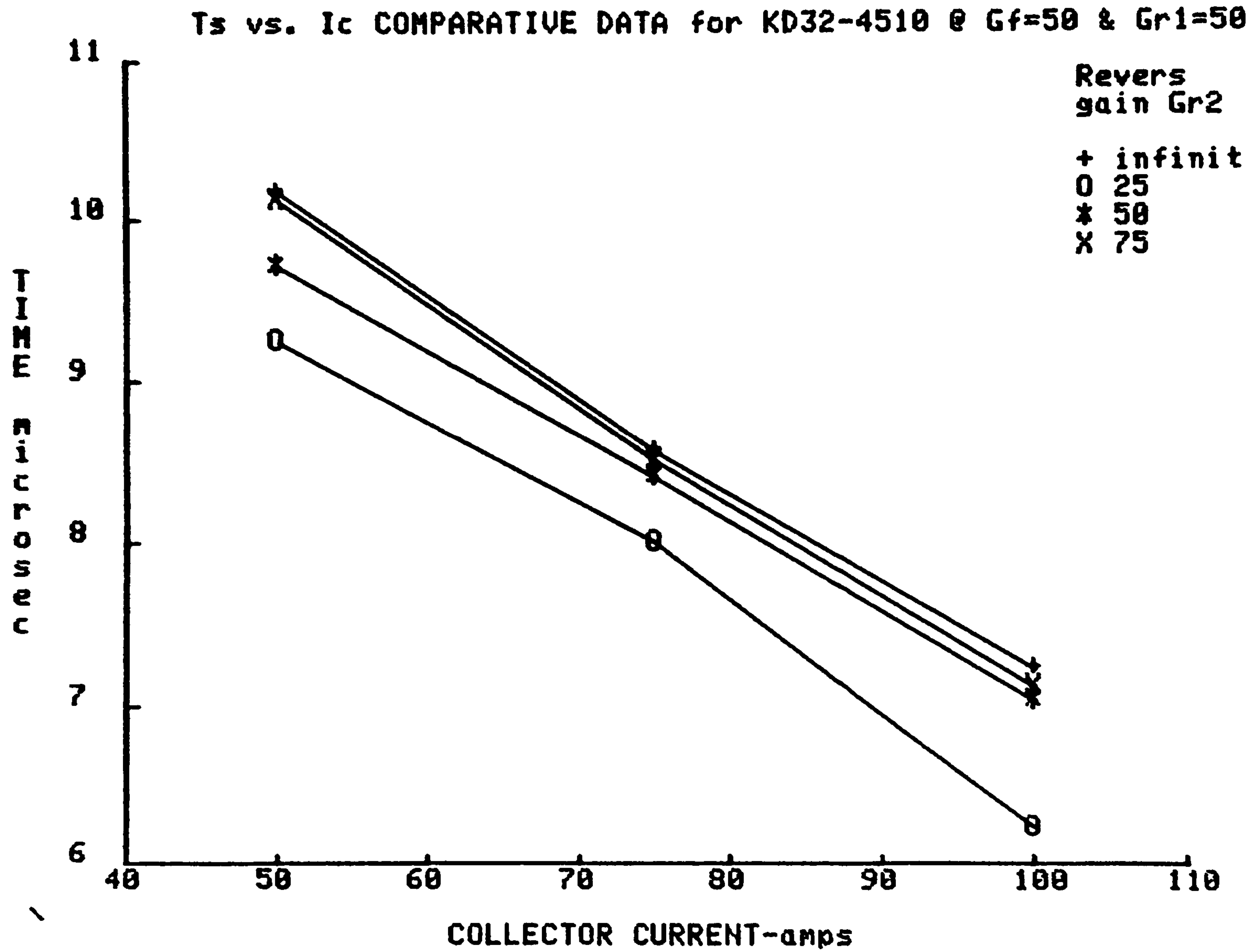

Ts vs. Ic COMPARATIVE DATA for KD32-4510 @ Gf=50 & Gr1=50
Revers gain Gr2
+ infinit
O 25
* 50
X 75
TIME microsec
11
10
9
8
7
6
40
50
60
70
80
90
100
110
COLLECTOR CURRENT-amps

Fig. A.1.6

Tf vs. Ic COMPARATIVE DATA for KD32-4510 @ Gf=50 & Gr1=50

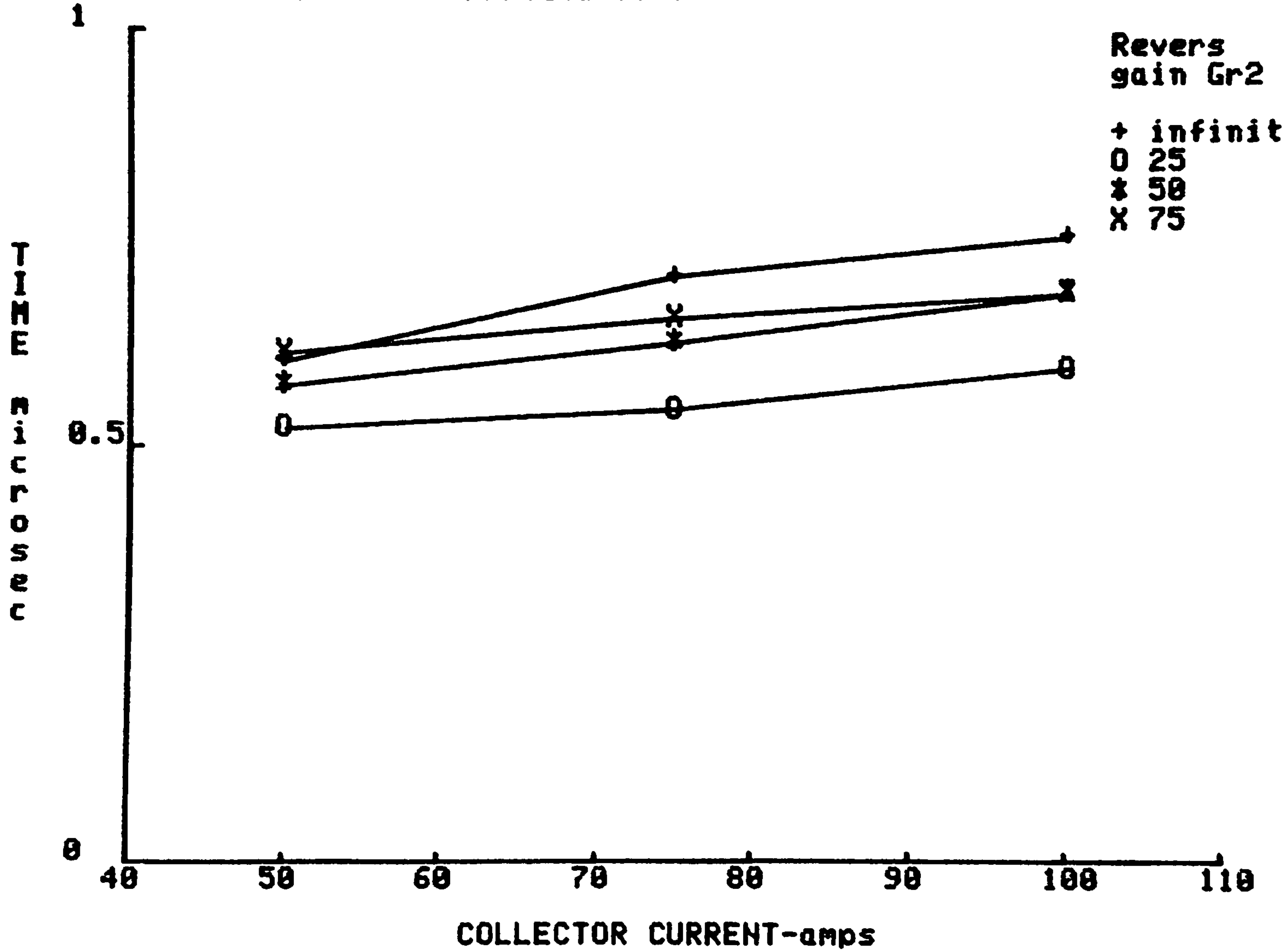

Fig. A.1.7

Qon vs Ic for KD324510 @ Vce=200V

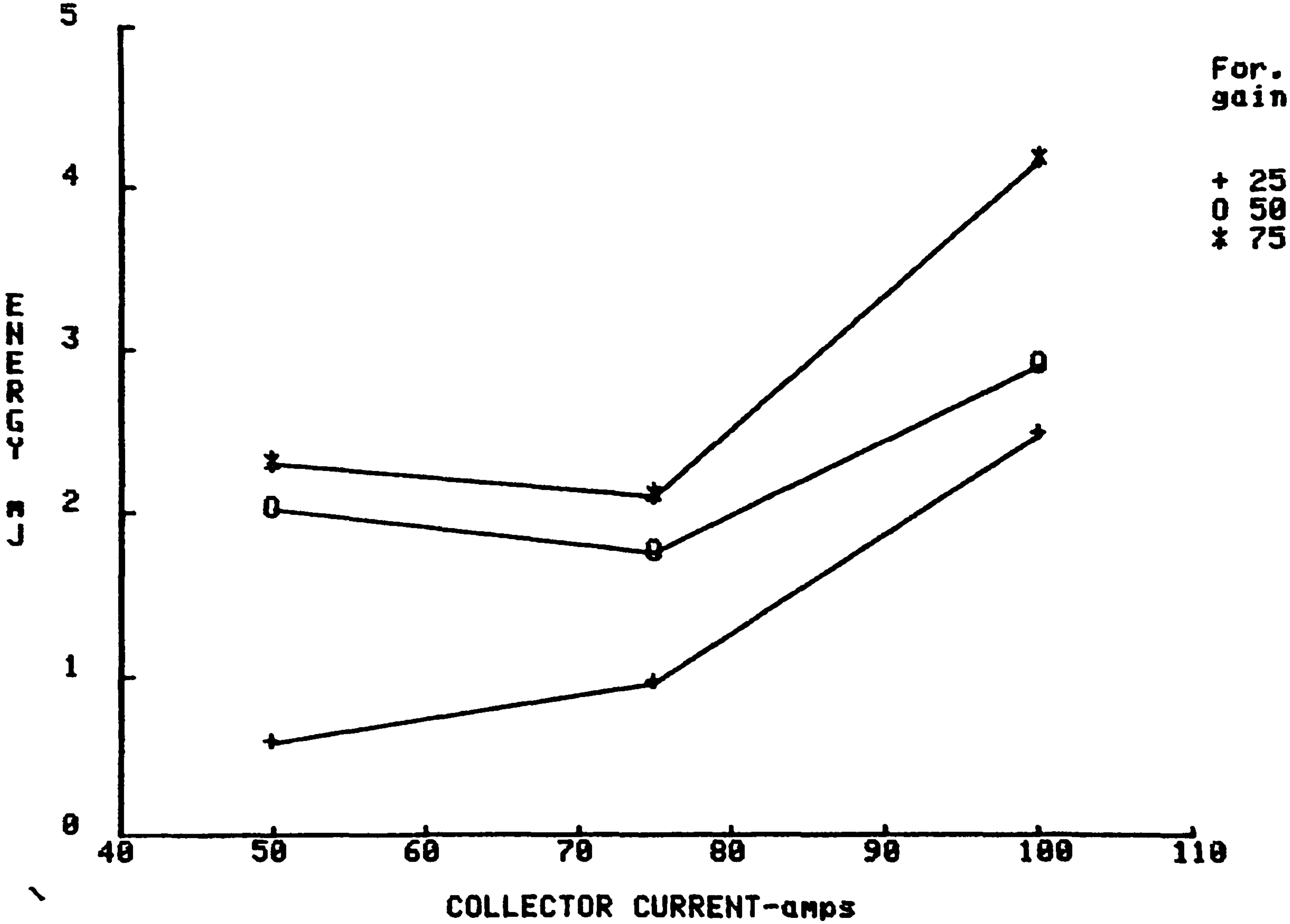

Fig. A.1.8

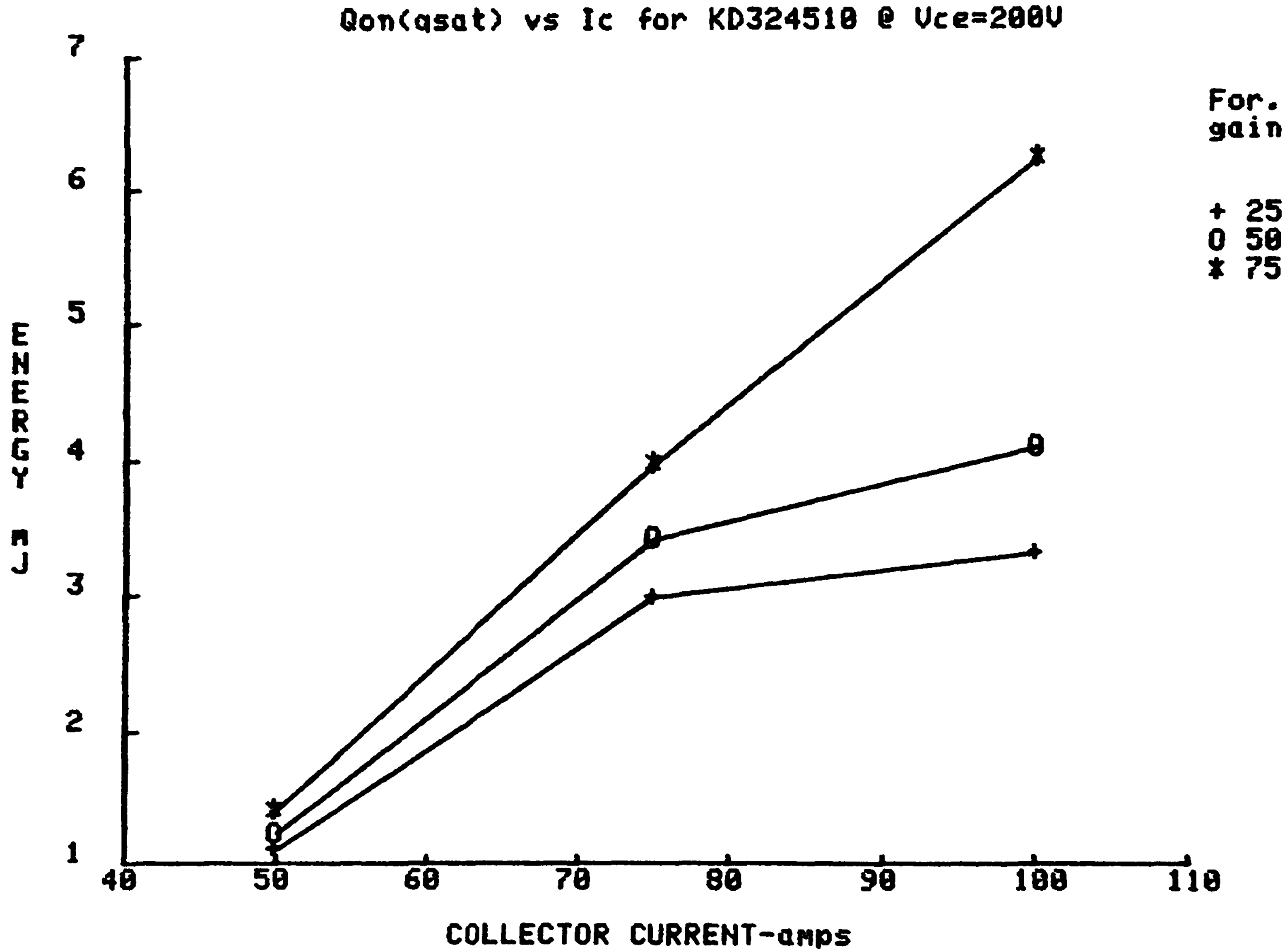
Qon(qsat) vs Ic for KD324510 @ Vce=200V
ENERGY mJ
1
2
3
4
5
6
7
40
50
60
70
80
90
100
110
COLLECTOR CURRENT-amps
For. gain
+ 25
O 50
* 75

Fig. A.1.9

Qon(tot) vs Ic for KD324510 @ Vce=200V

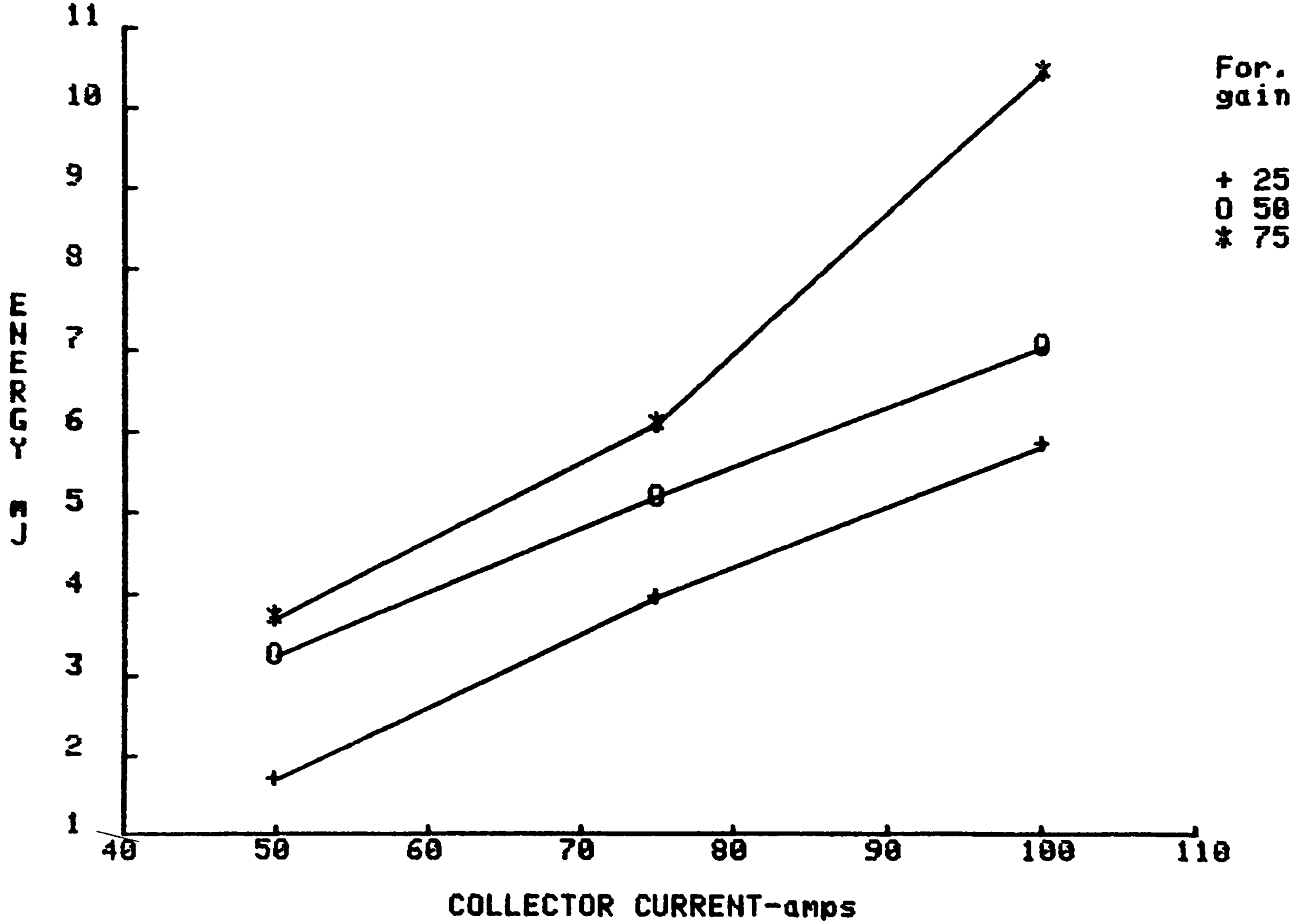

Fig. A.1.10

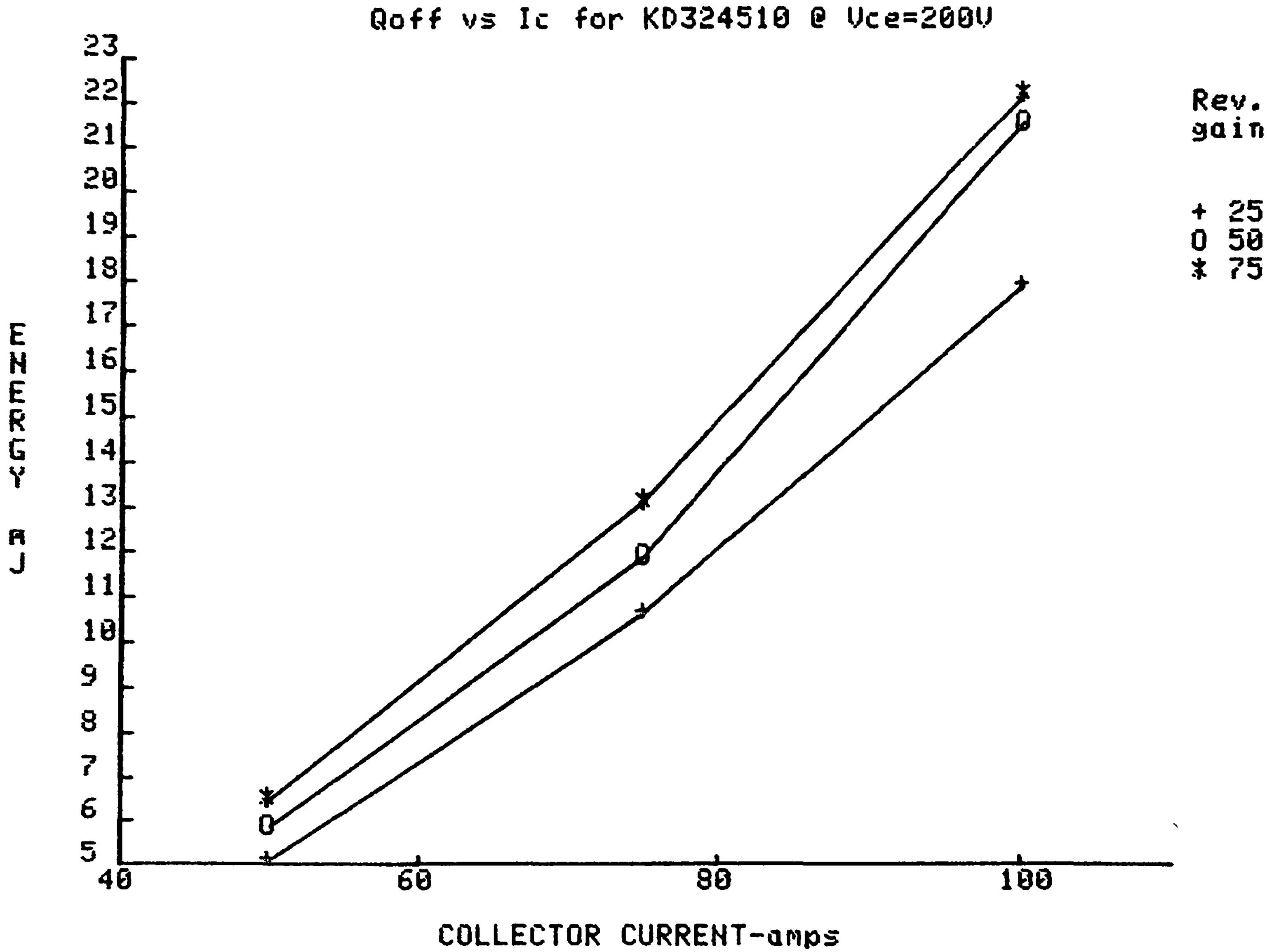

Qoff vs Ic for KD324510 @ Vce=200V
ENERGY mJ
23
22
21
20
19
18
17
16
15
14
13
12
11
10
9
8
7
6
5
40
60
80
100
COLLECTOR CURRENT-amps
Rev. gain
+ 25
O 50
* 75

Fig. A.1.11

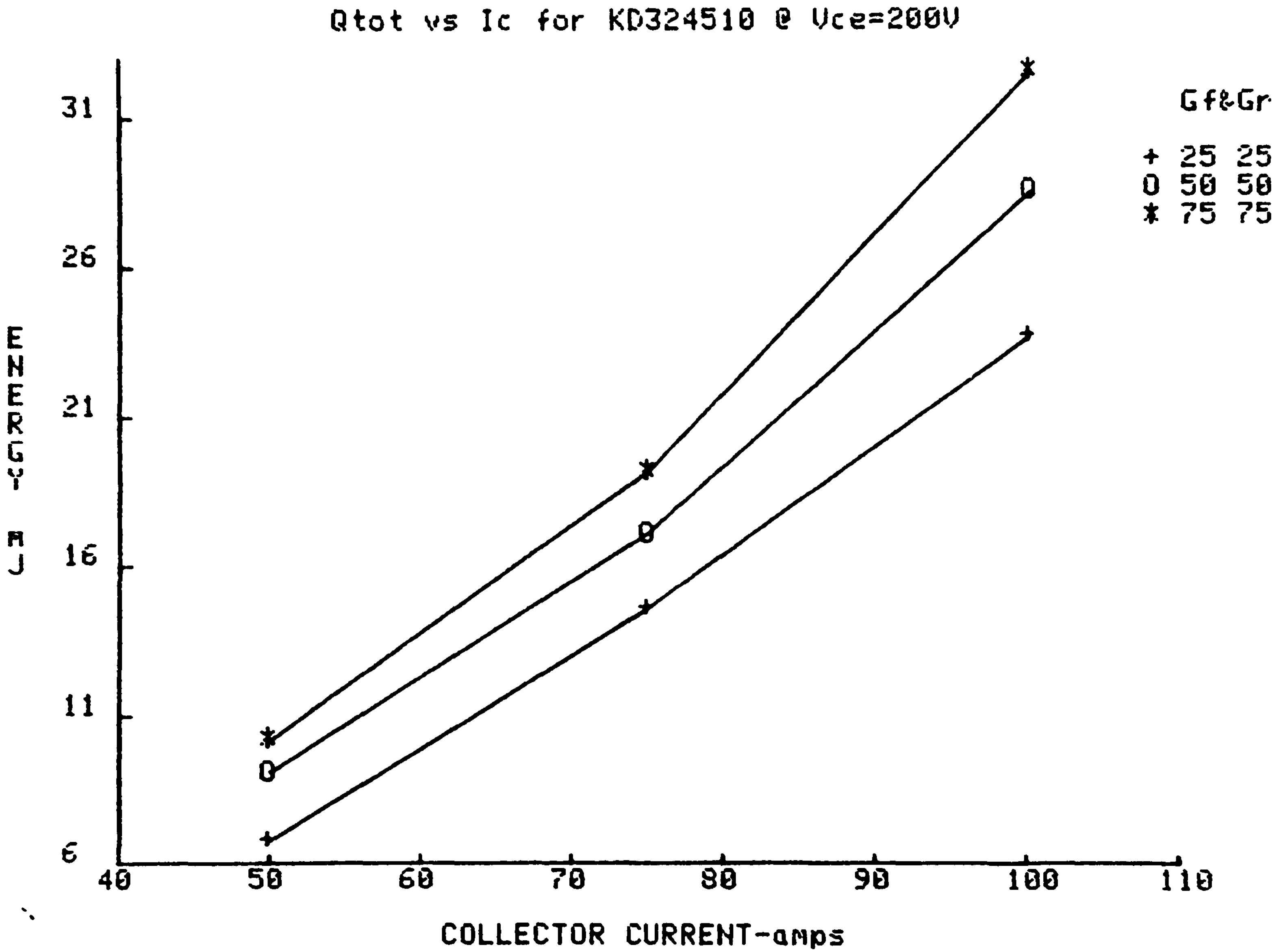
Qtot vs Ic for KD324510 @ Vce=200V
Gf&Gr
+ 25 25
O 50 50
* 75 75
ENERGY mJ
31
26
21
16
11
6
40
50
60
70
80
90
100
110
COLLECTOR CURRENT-amps

Fig. A.1.12

Switching Loadline Characteristics: Vce vs. Ic
for Turn-on of Power Trans. with Inductive Load

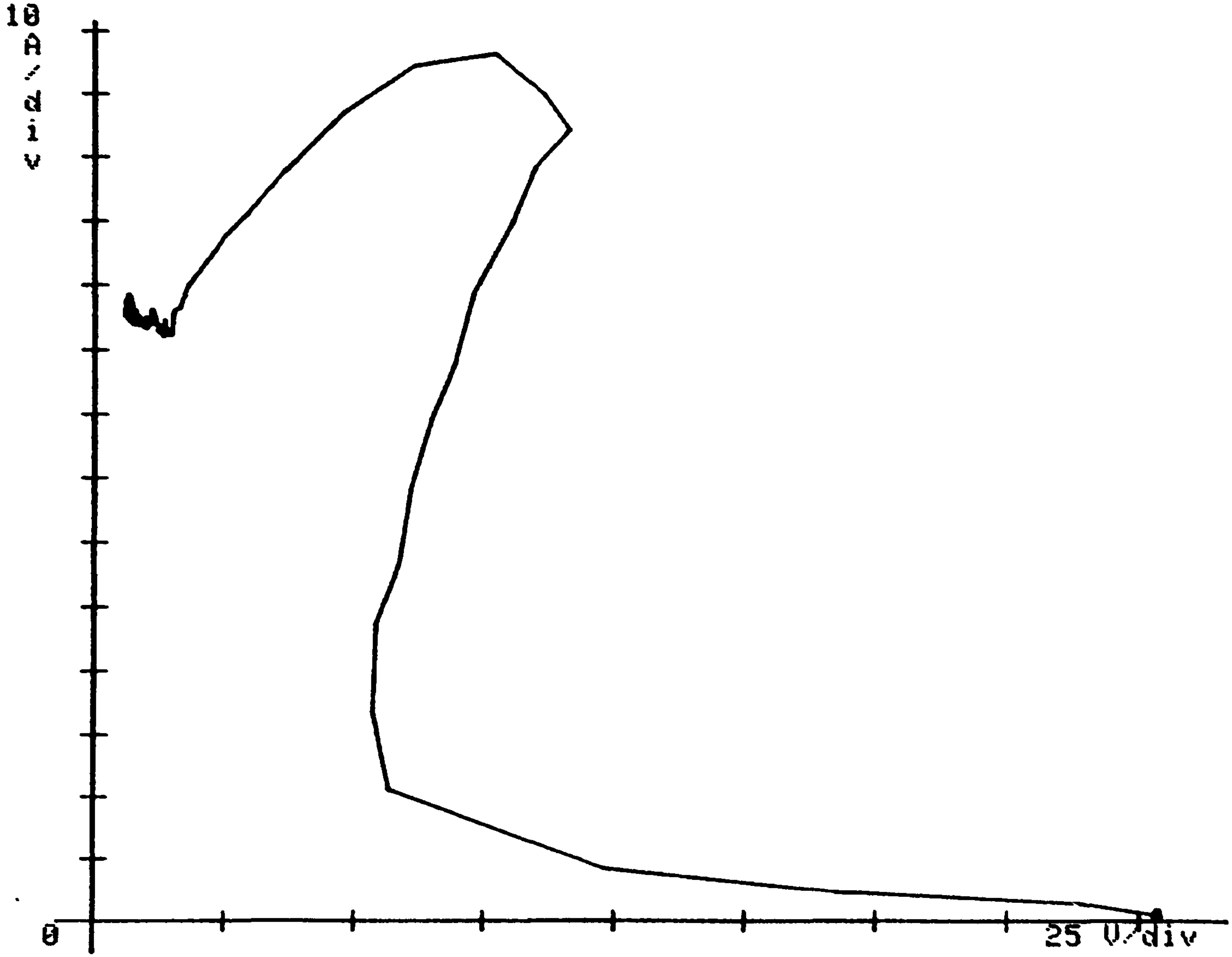

Fig. A.1.13

Switching Loadline Characteristics: Vce vs. Ic
for Turn-off of Power Trans. with Inductive Load

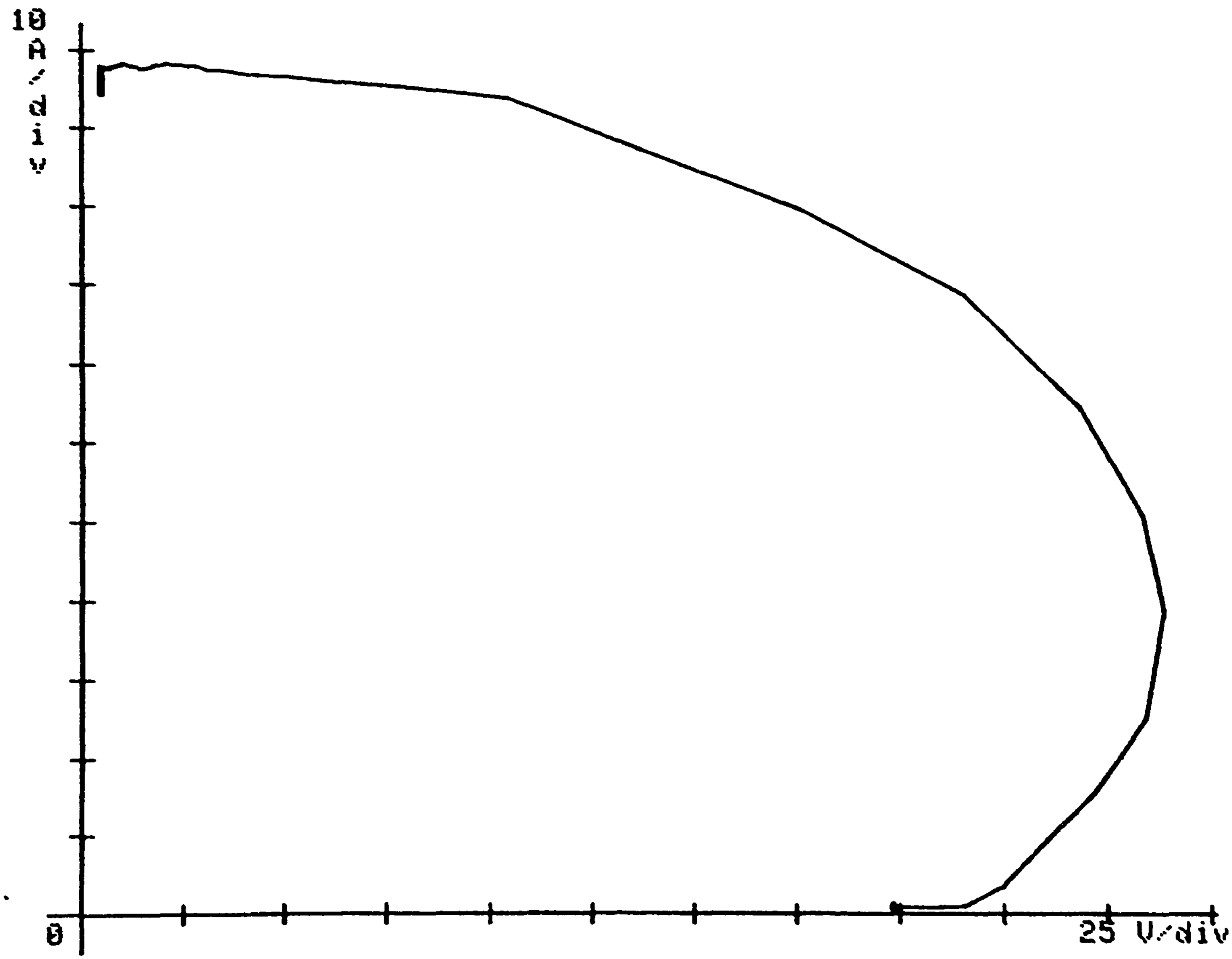

Fig. A.1.14

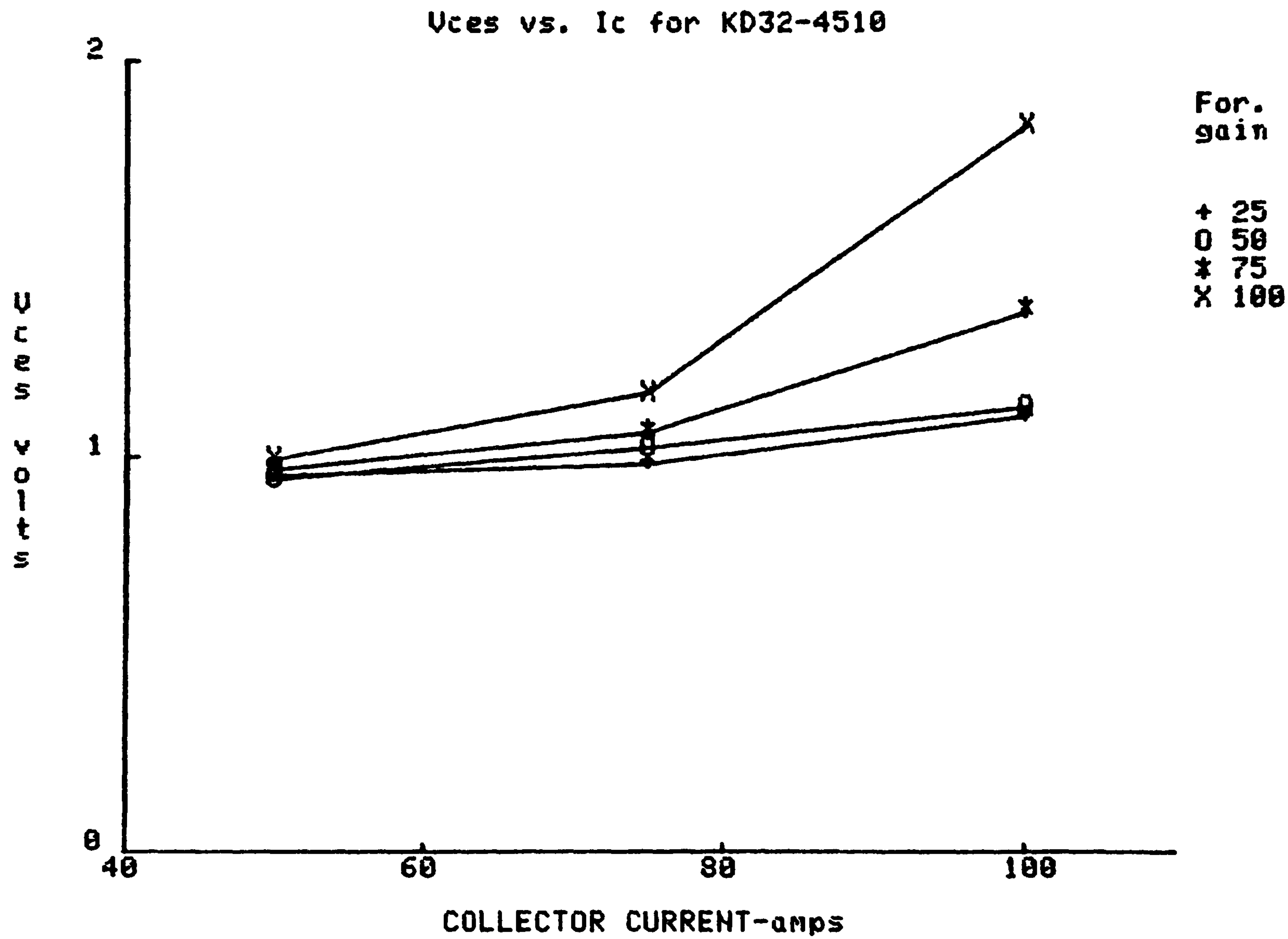
Vces vs. Ic for KD32-4510
2
1
0
Vces volts
40
60
80
100
COLLECTOR CURRENT-amps
For. gain
+ 25
O 50
* 75
X 100

Fig. A.1.15

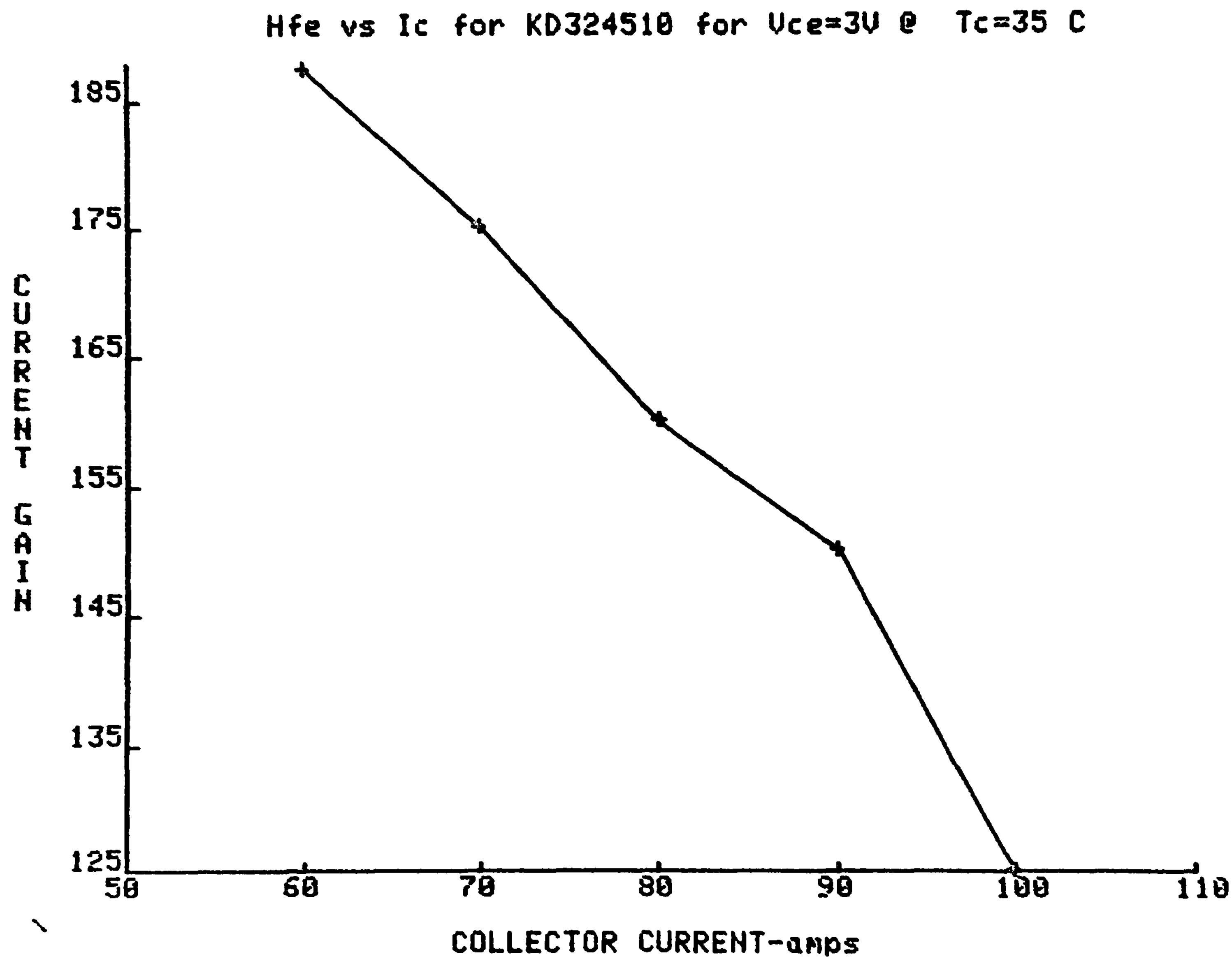
Hfe vs Ic for KD324510 for Vce=3V @ Tc=35 C
CURRENT GAIN
185
175
165
155
145
135
125
50
60
70
80
90
100
110
COLLECTOR CURRENT-amps

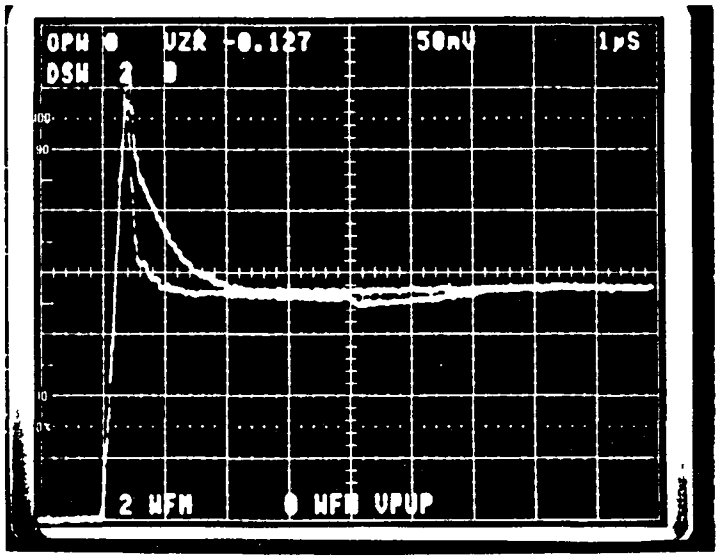

Fig. A.1.16 Diode recovery and dv/dt test for KD324510
Upper trace: Base open
Lower trace: Base reverse biased
(Scale: horizontal 1 μs/div; vertical 20 A/div)

A.2 Test Data for Westinghouse DA11503008

Fig. A.2.1

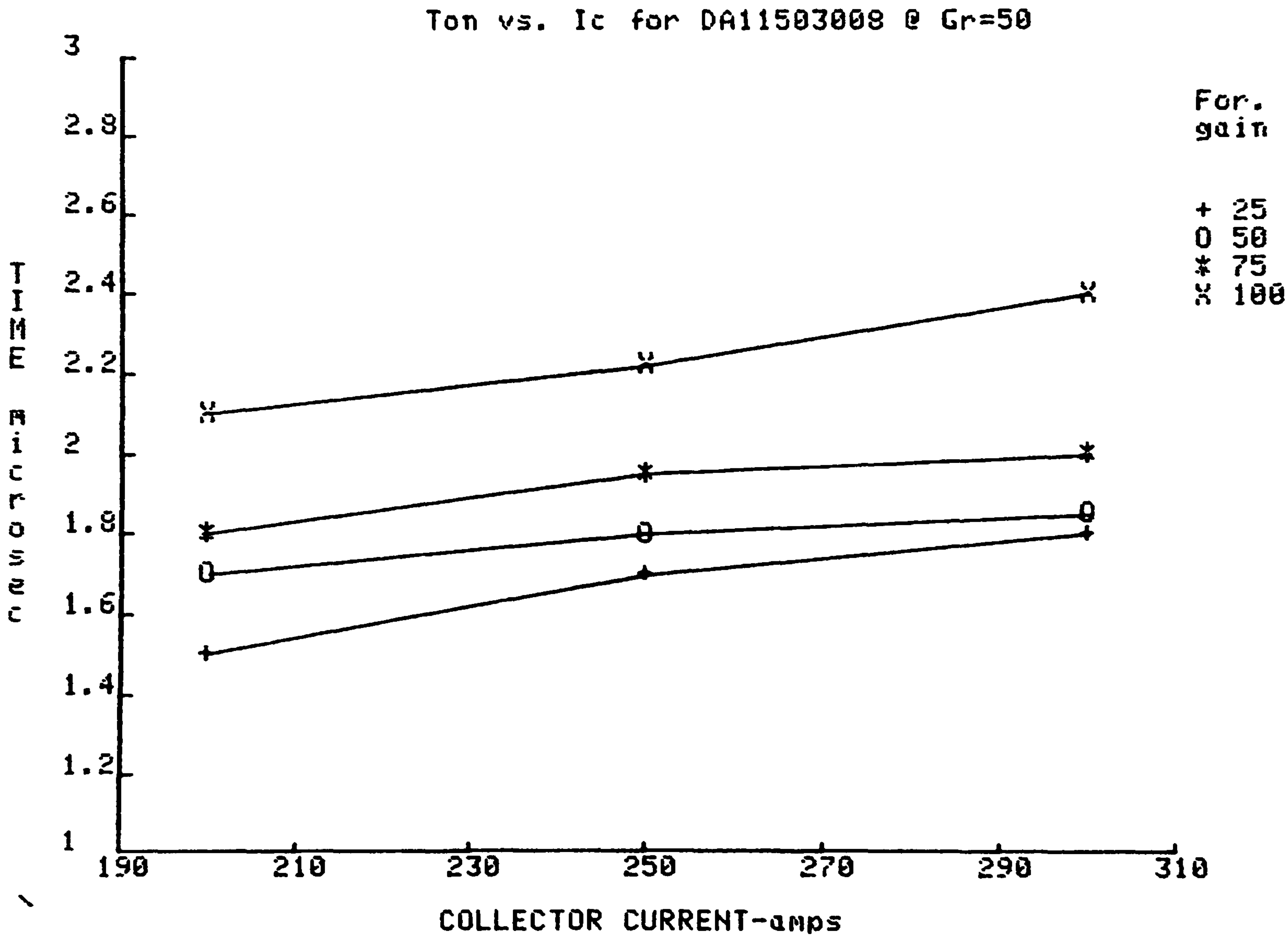
Ton vs. Ic for DA11503008 @ Gr=50
TIME microsec
COLLECTOR CURRENT-amps
For. gain
+ 25
O 50
* 75
X 100
3
2.8
2.6
2.4
2.2
2
1.8
1.6
1.4
1.2
1
190
210
230
250
270
290
310

Fig. A.2.2

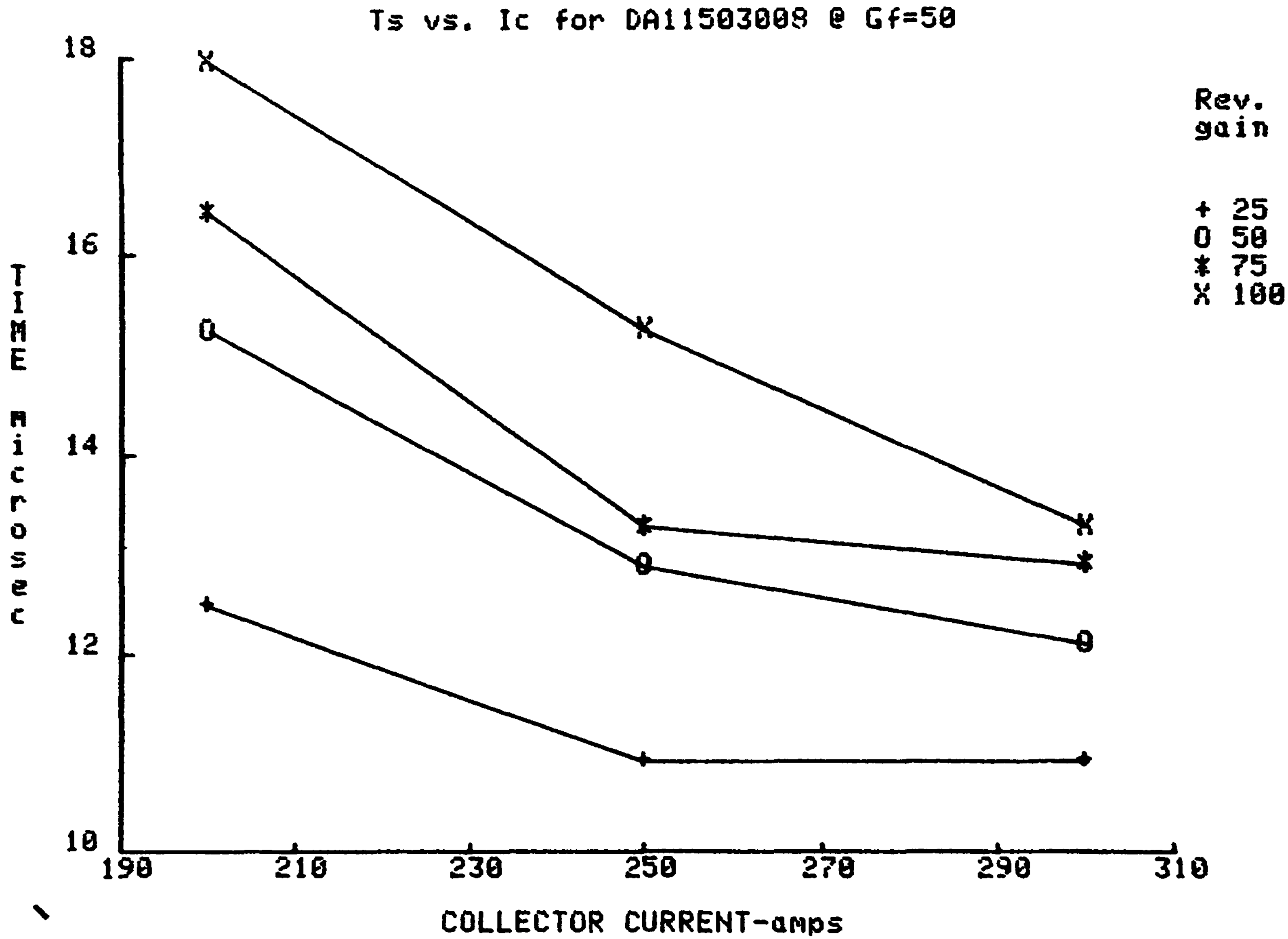
Ts vs. Ic for DA11503008 @ Gf=50
TIME microsec
COLLECTOR CURRENT-amps
18
16
14
12
10
190
210
230
250
270
290
310
Rev. gain
+ 25
O 50
* 75
X 100

Fig. A.2.3

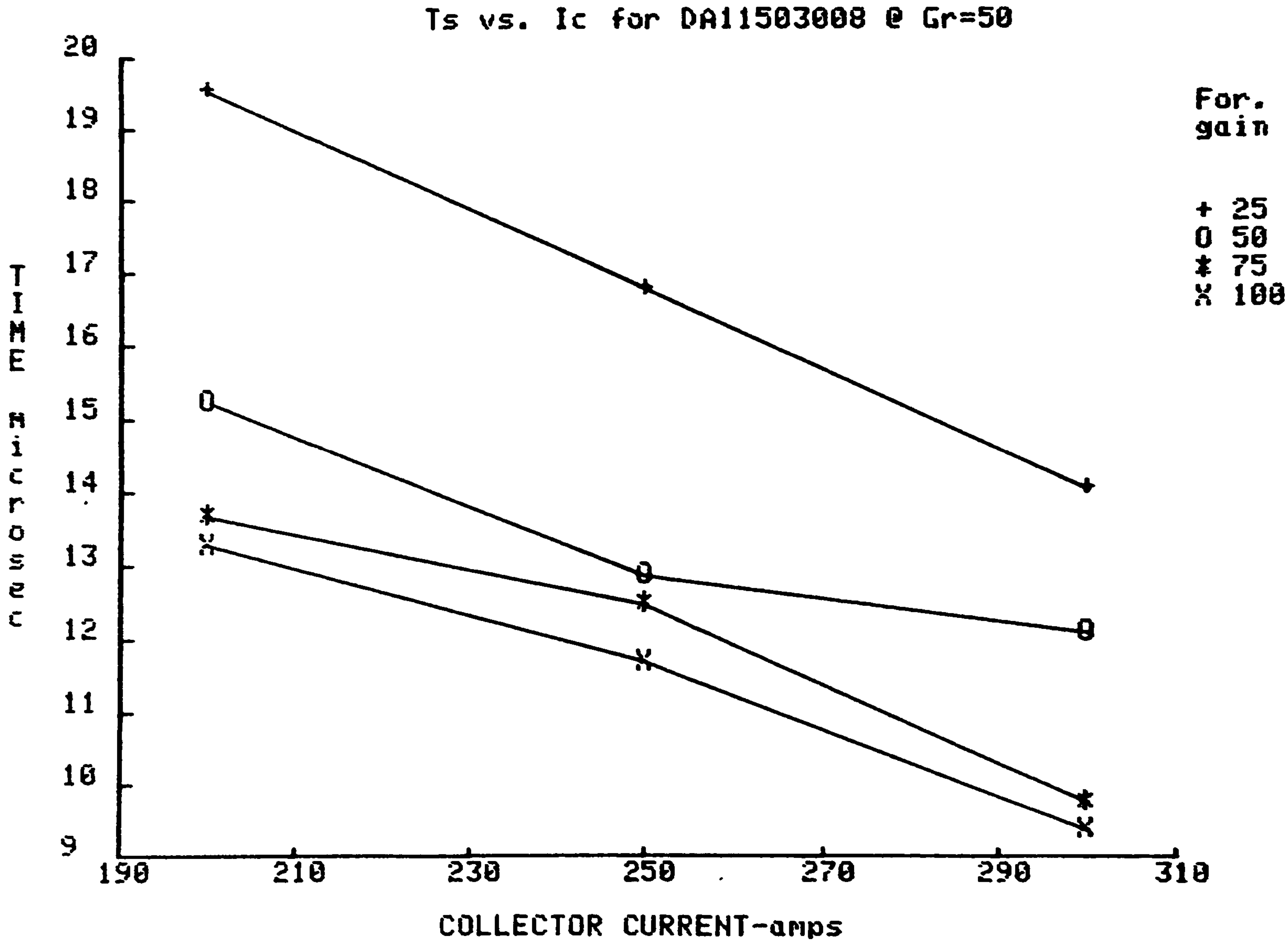
Ts vs. Ic for DA11503008 @ Gr=50
20
19
18
17
16
15
14
13
12
11
10
9
TIME microsec
190
210
230
250
270
290
310
COLLECTOR CURRENT-amps
For. gain
+ 25
O 50
* 75
X 100

A.22

Fig. A.2.4

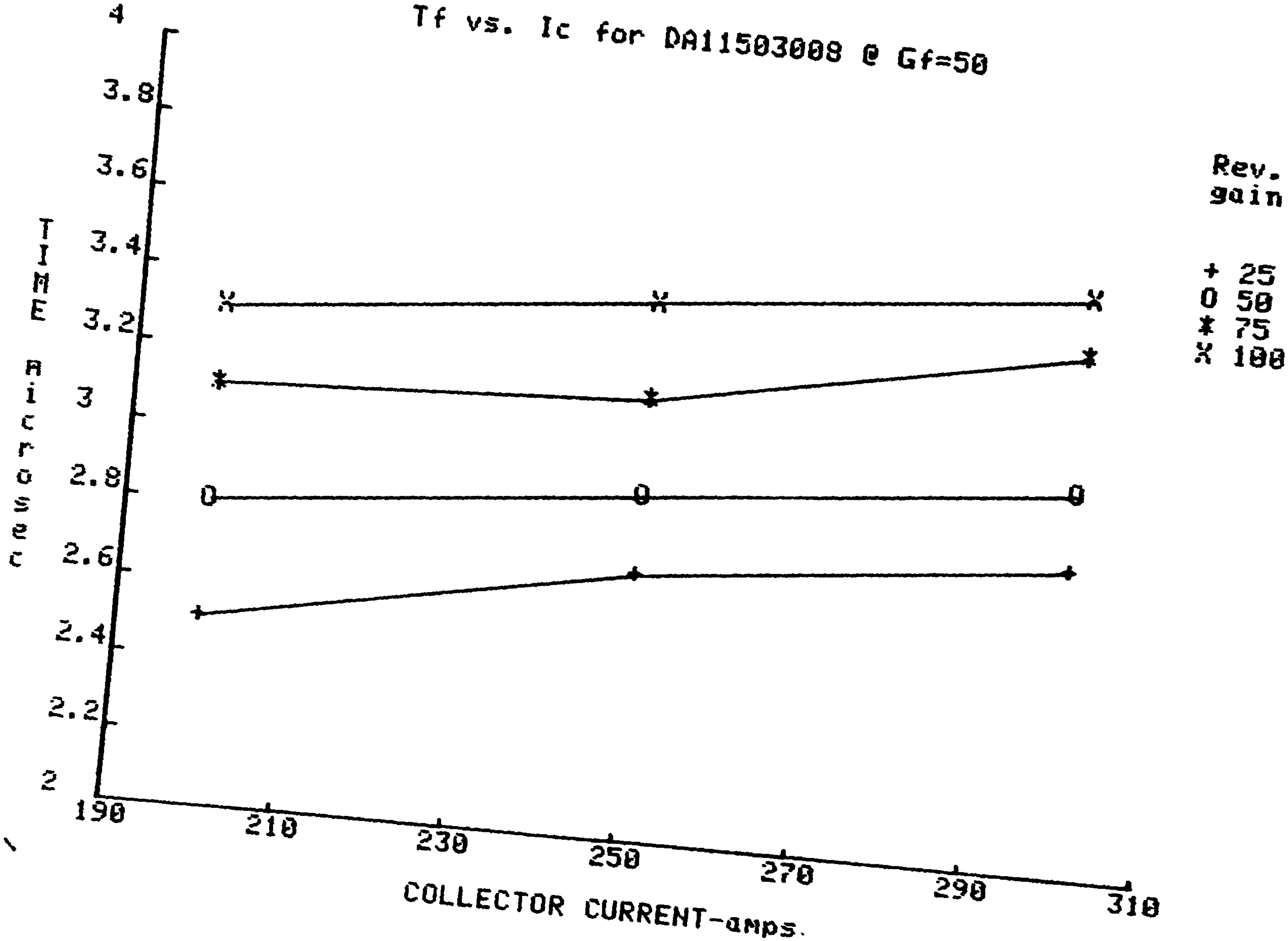

Tf vs. Ic for DA11503008 @ Gf=50
TIME microsec
4
3.8
3.6
3.4
3.2
3
2.8
2.6
2.4
2.2
2
190
210
230
250
270
290
310
COLLECTOR CURRENT-amps.
Rev. gain
+ 25
0 50
* 75
X 100

Fig. A.2.5

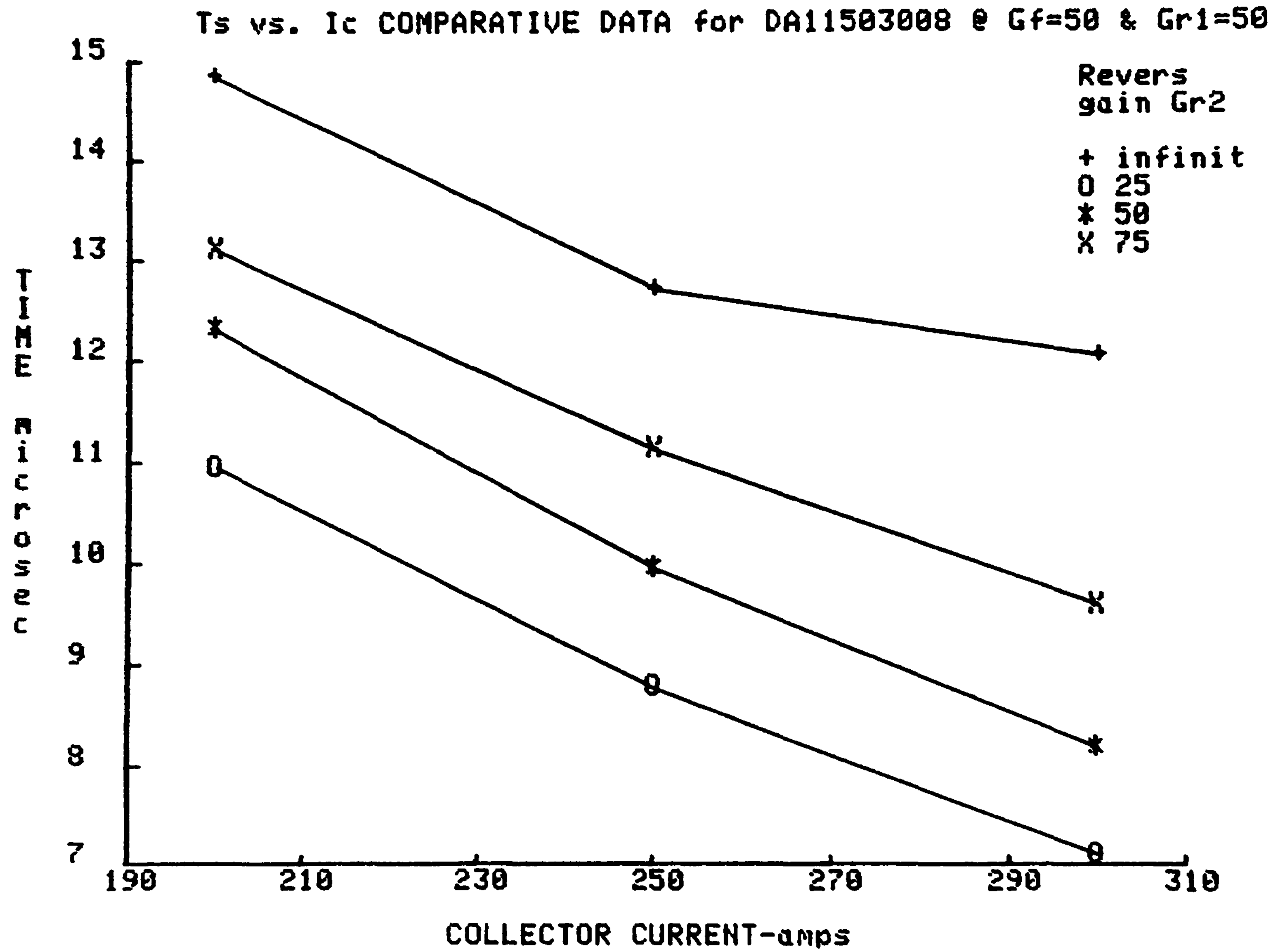
Ts vs. Ic COMPARATIVE DATA for DA11503008 @ Gf=50 & Gr1=50
TIME microsec
COLLECTOR CURRENT-amps
Revers gain Gr2
+ infinit
O 25
* 50
X 75
15
14
13
12
11
10
9
8
7
190
210
230
250
270
290
310

Fig. A.2.6

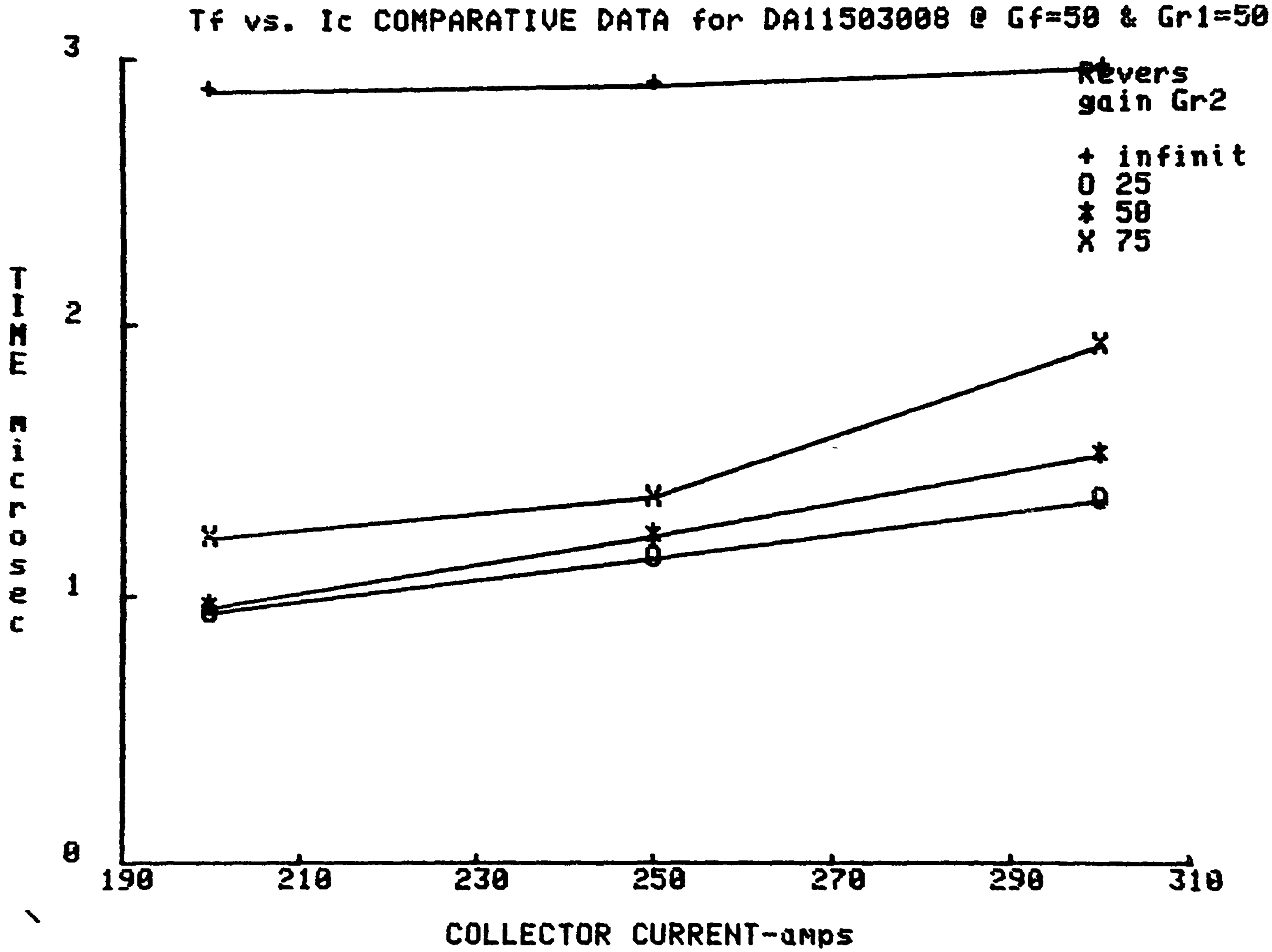

Tf vs. Ic COMPARATIVE DATA for DA11503008 @ Gf=50 & Gr1=50
Revers gain Gr2
+ infinit
O 25
* 50
X 75
TIME microsec
3
2
1
0
190
210
230
250
270
290
310
COLLECTOR CURRENT-amps

Fig. A.2.7

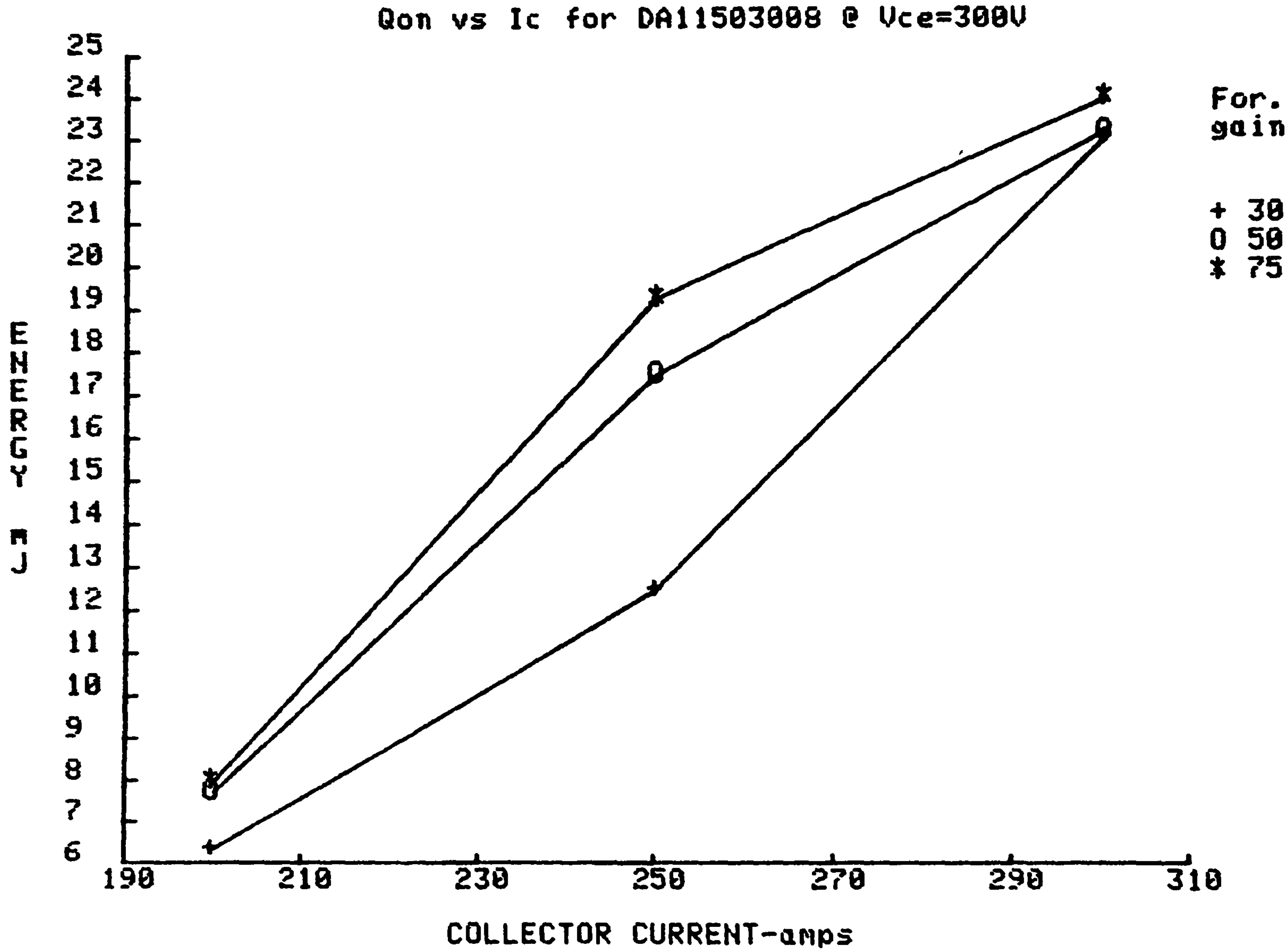

Qon vs Ic for DA11503008 @ Vce=300V
ENERGY mJ
25
24
23
22
21
20
19
18
17
16
15
14
13
12
11
10
9
8
7
6
190
210
230
250
270
290
310
COLLECTOR CURRENT-amps
For. gain
+ 30
O 50
* 75

Fig. A.2.8

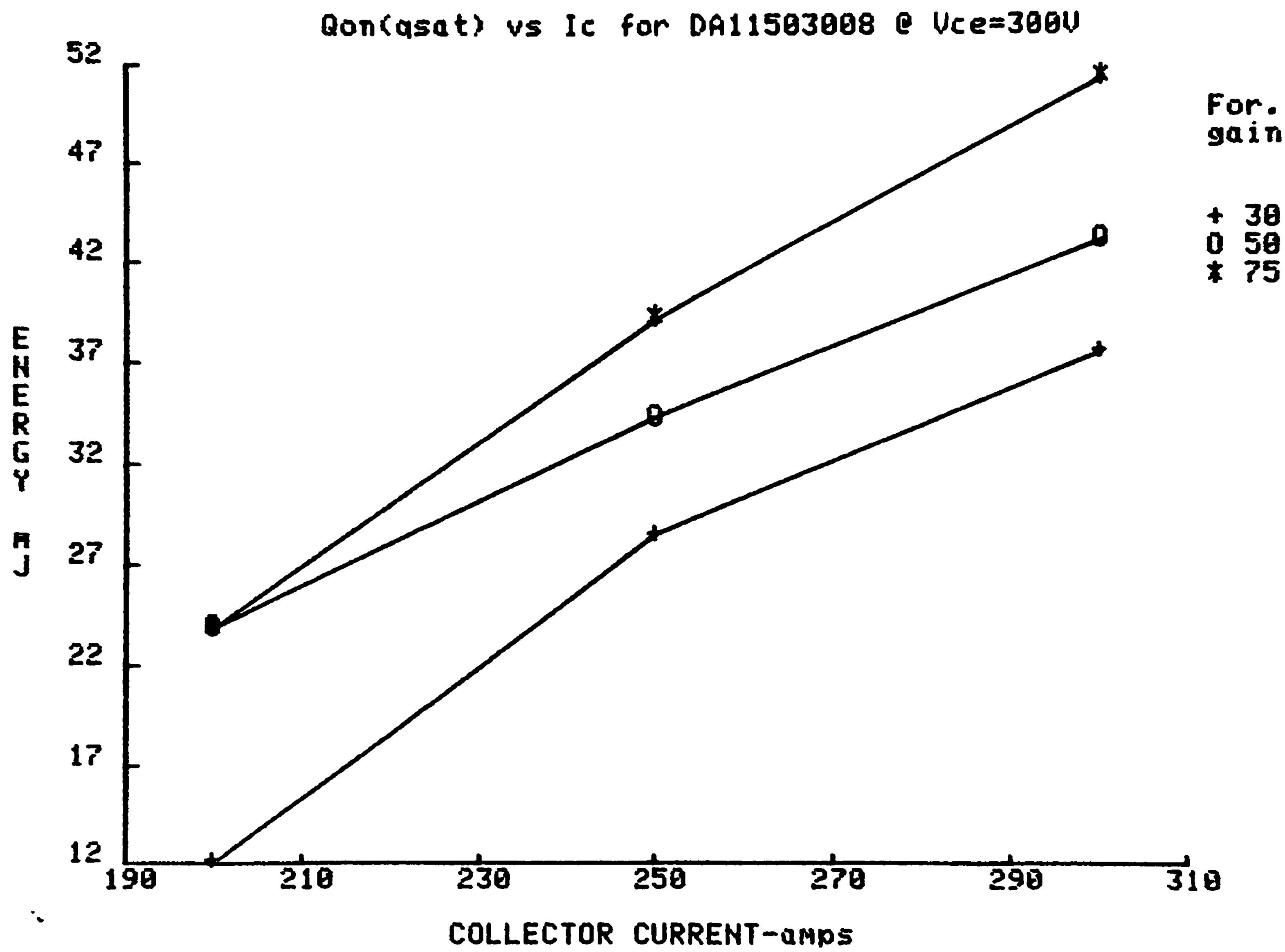

Qon(qsat) vs Ic for DA11503008 @ Vce=300V
52
47
42
37
32
27
22
17
12
ENERGY mJ
190
210
230
250
270
290
310
COLLECTOR CURRENT-amps
For. gain
+ 30
0 50
* 75

A.27

Fig. A.2.9

Qon(tot) vs Ic for DA11503008 @ Vce=300V

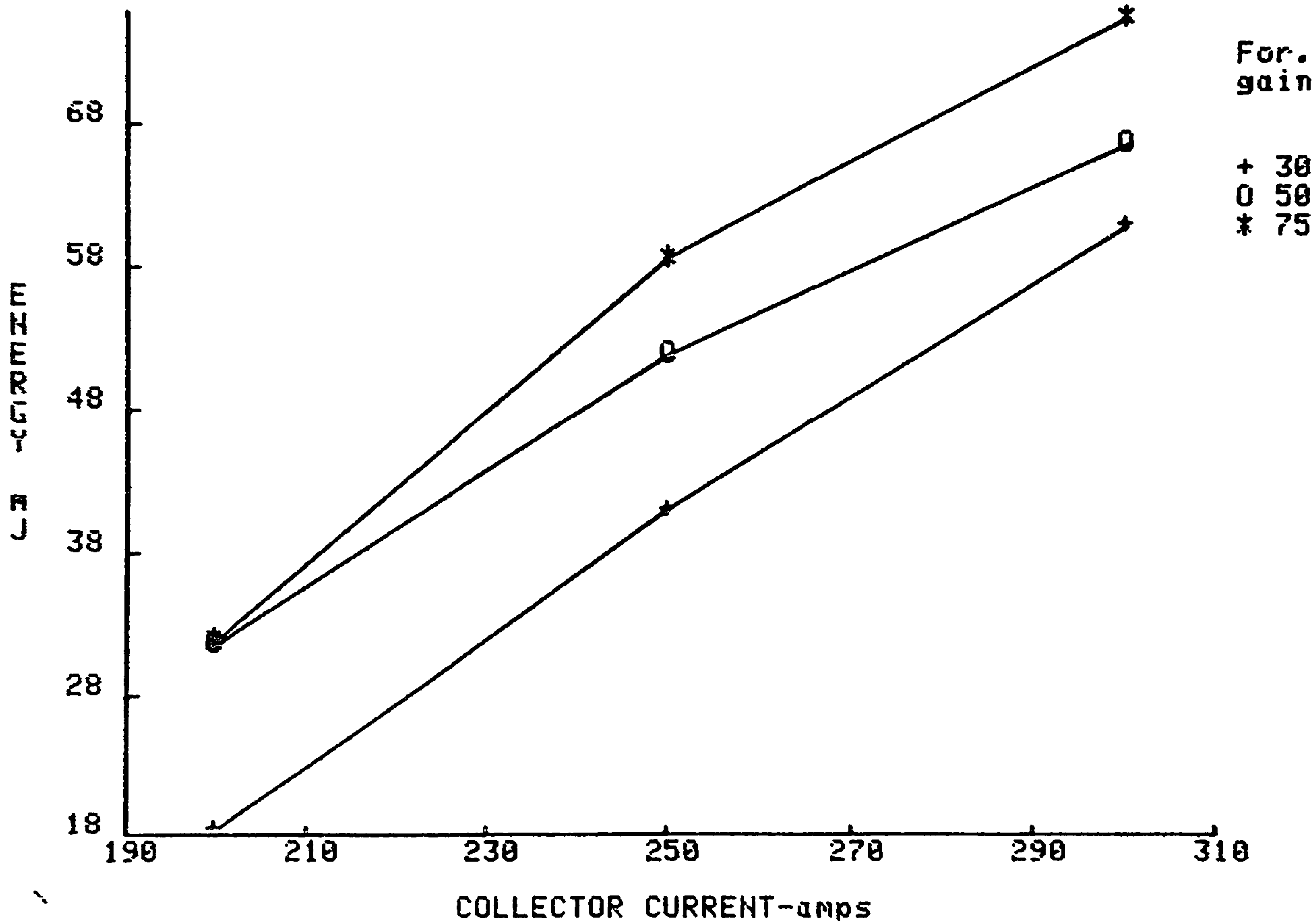

Fig. A.2.10

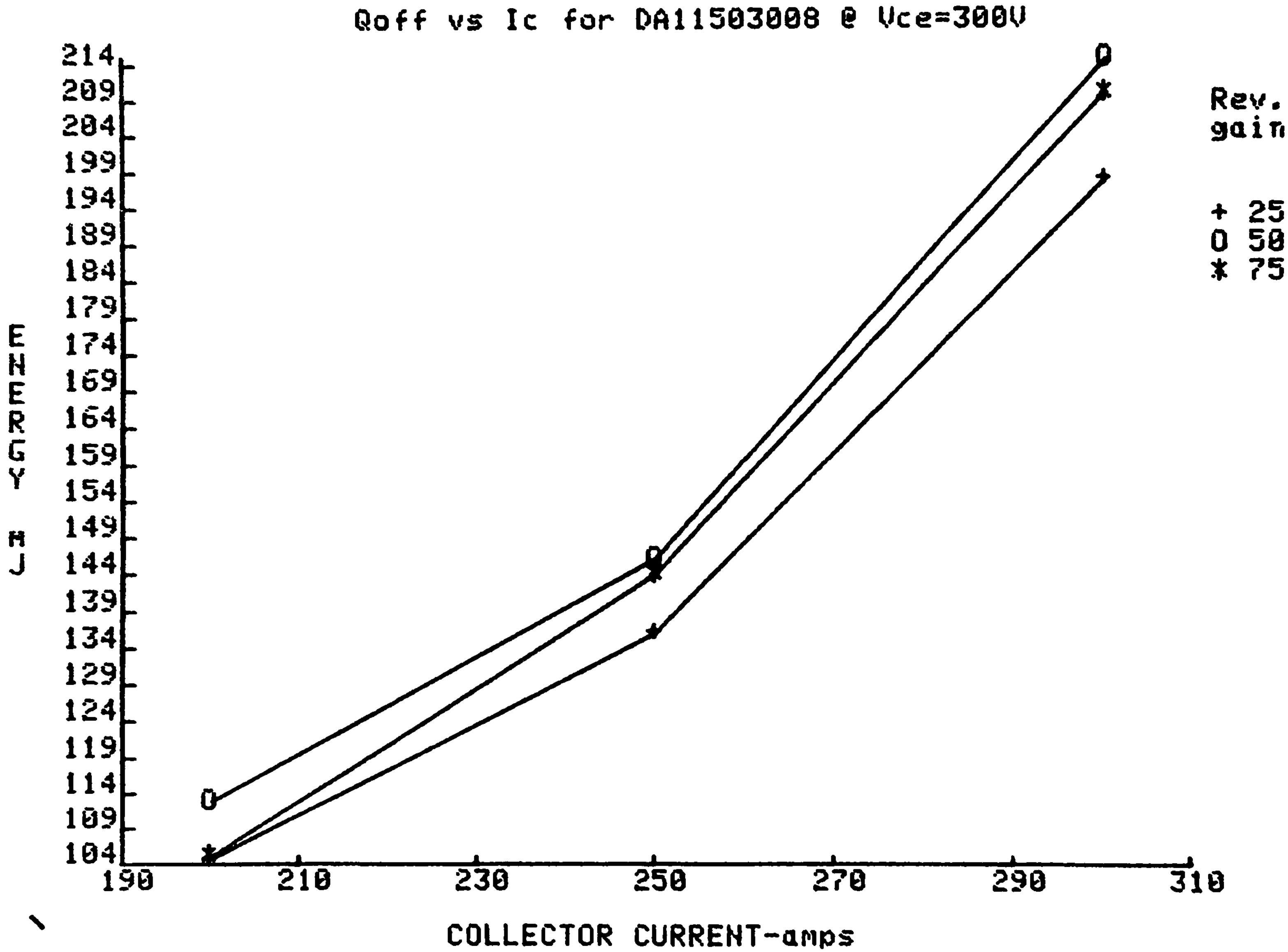
Qoff vs Ic for DA11503008 @ Vce=300V
214
209
204
199
194
189
184
179
174
169
164
159
154
149
144
139
134
129
124
119
114
109
104
ENERGY mJ
190
210
230
250
270
290
310
COLLECTOR CURRENT-amps
Rev. gain
+ 25
O 50
* 75

Fig. A.2.11

Qtot vs Ic for DA1150300B @ Vce=300V

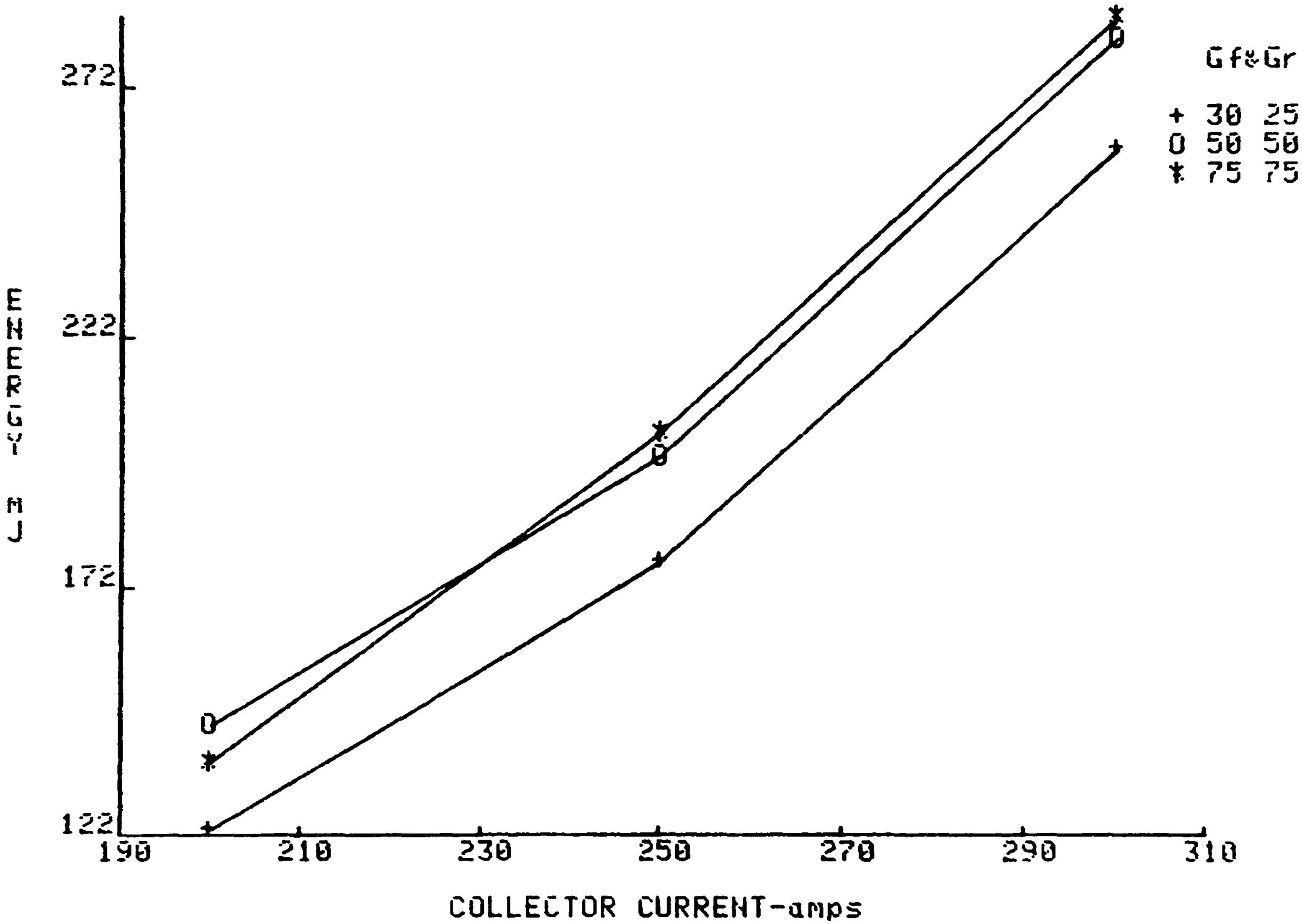

Fig. A.2.12

Switching Loadline Characteristics: Vce vs. Ic
for Turn-on of Power Transistor with Inductive Load

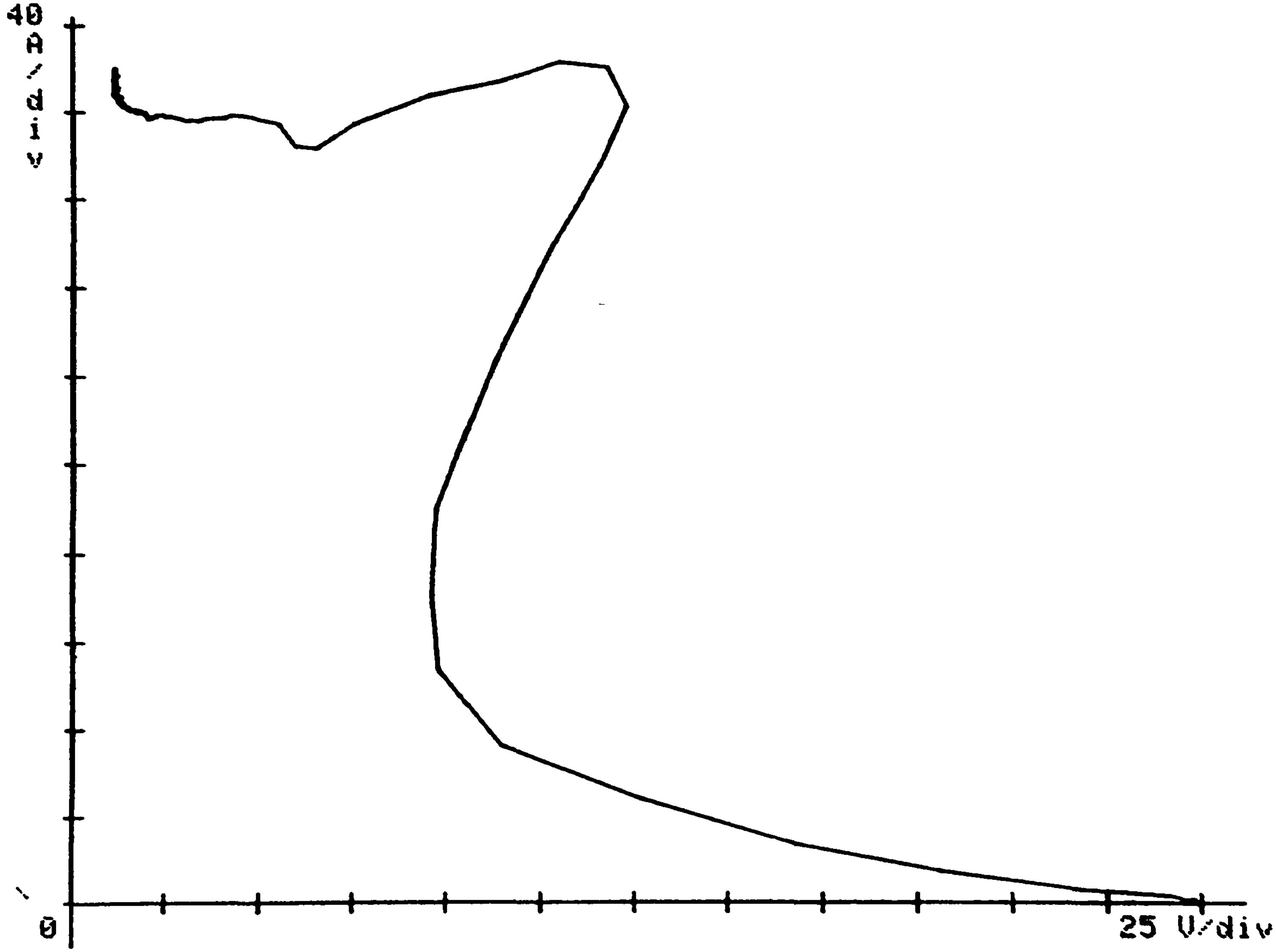

Fig. A.2.13

Switching Loadline Characteristics: Vce vs. Ic
for Turn-off of Power Trans. with Inductive Load

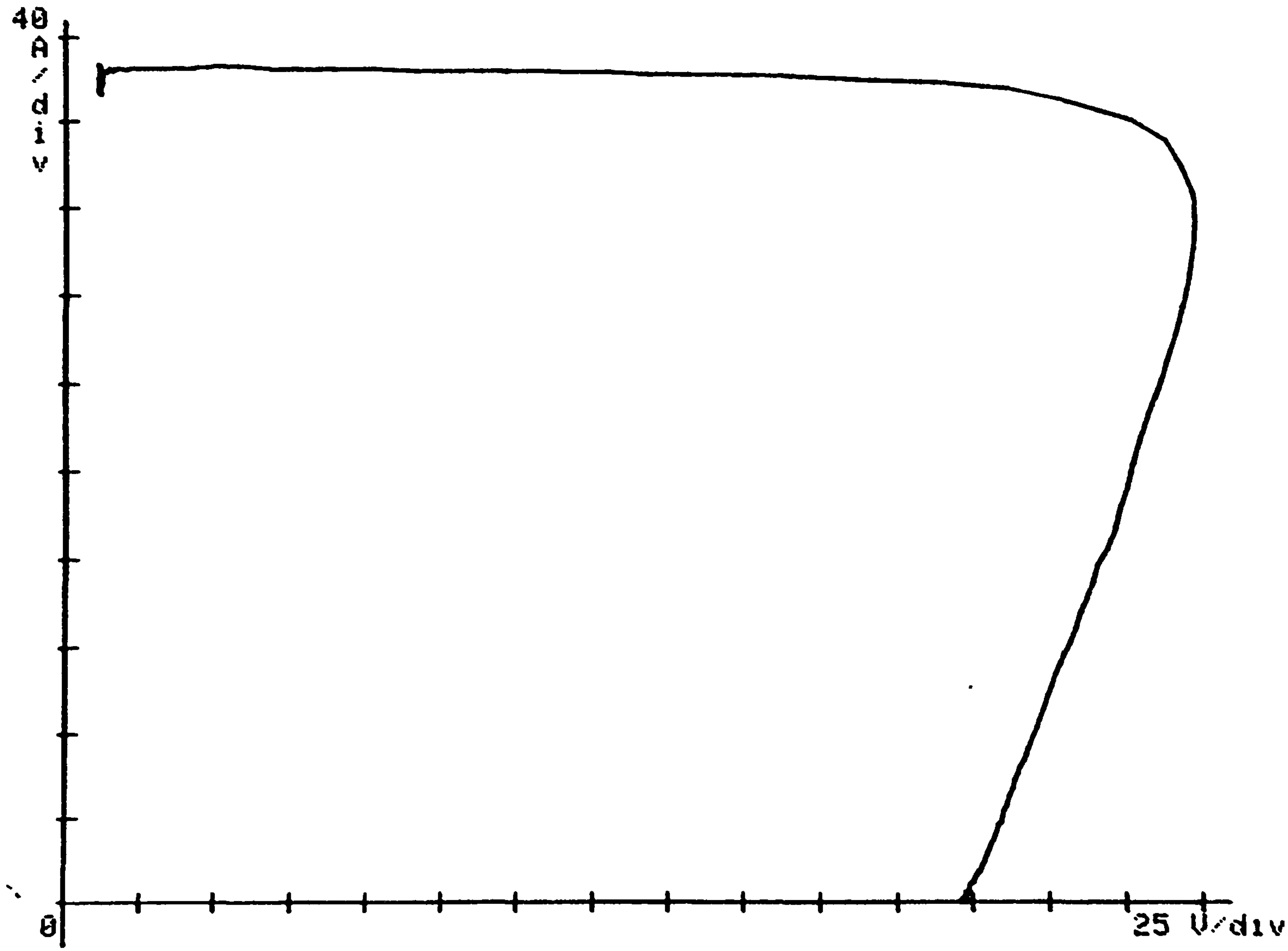

Fig. A.2.14

Vces vs. Ic for DA11503008

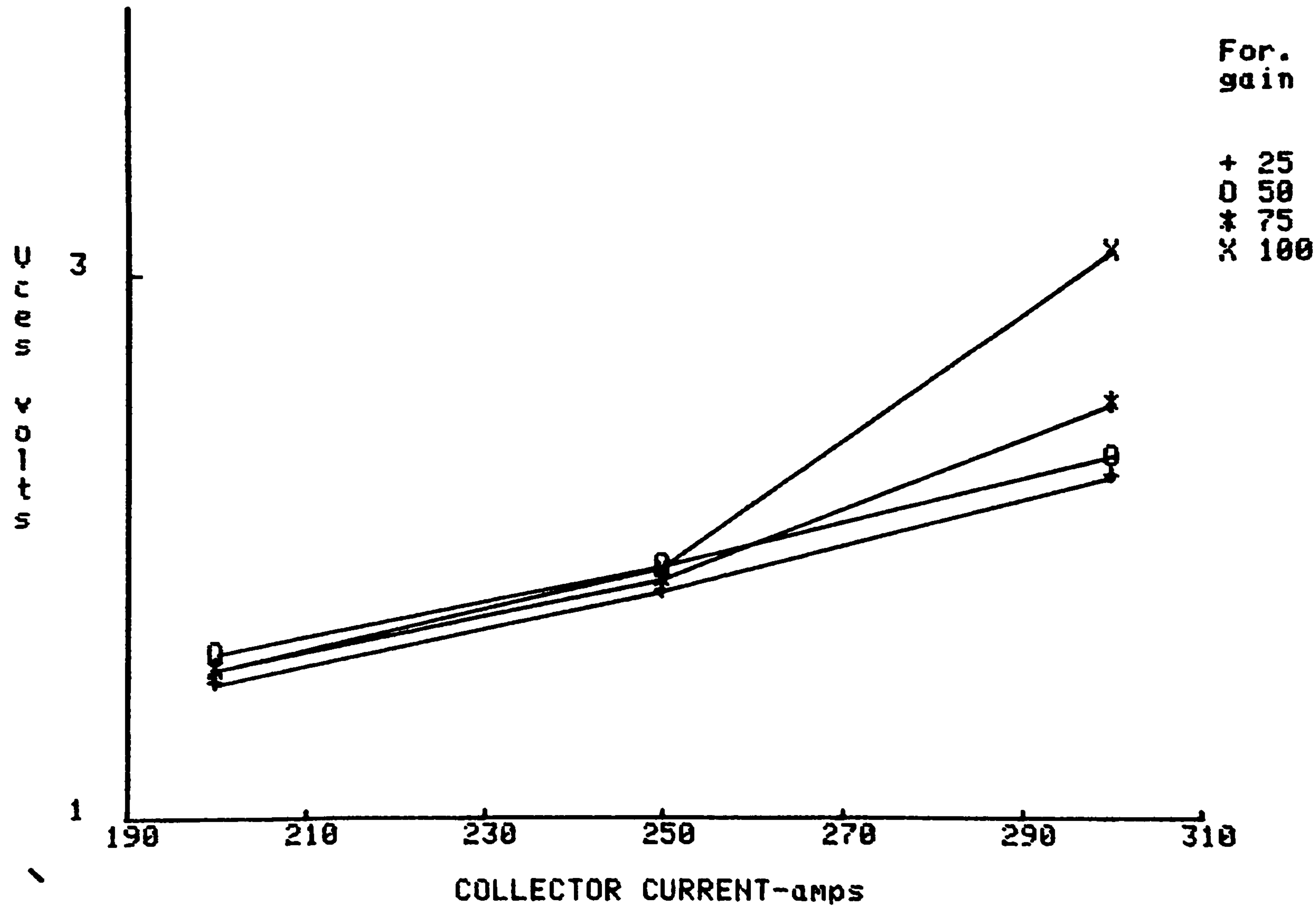

Fig. A.2.15

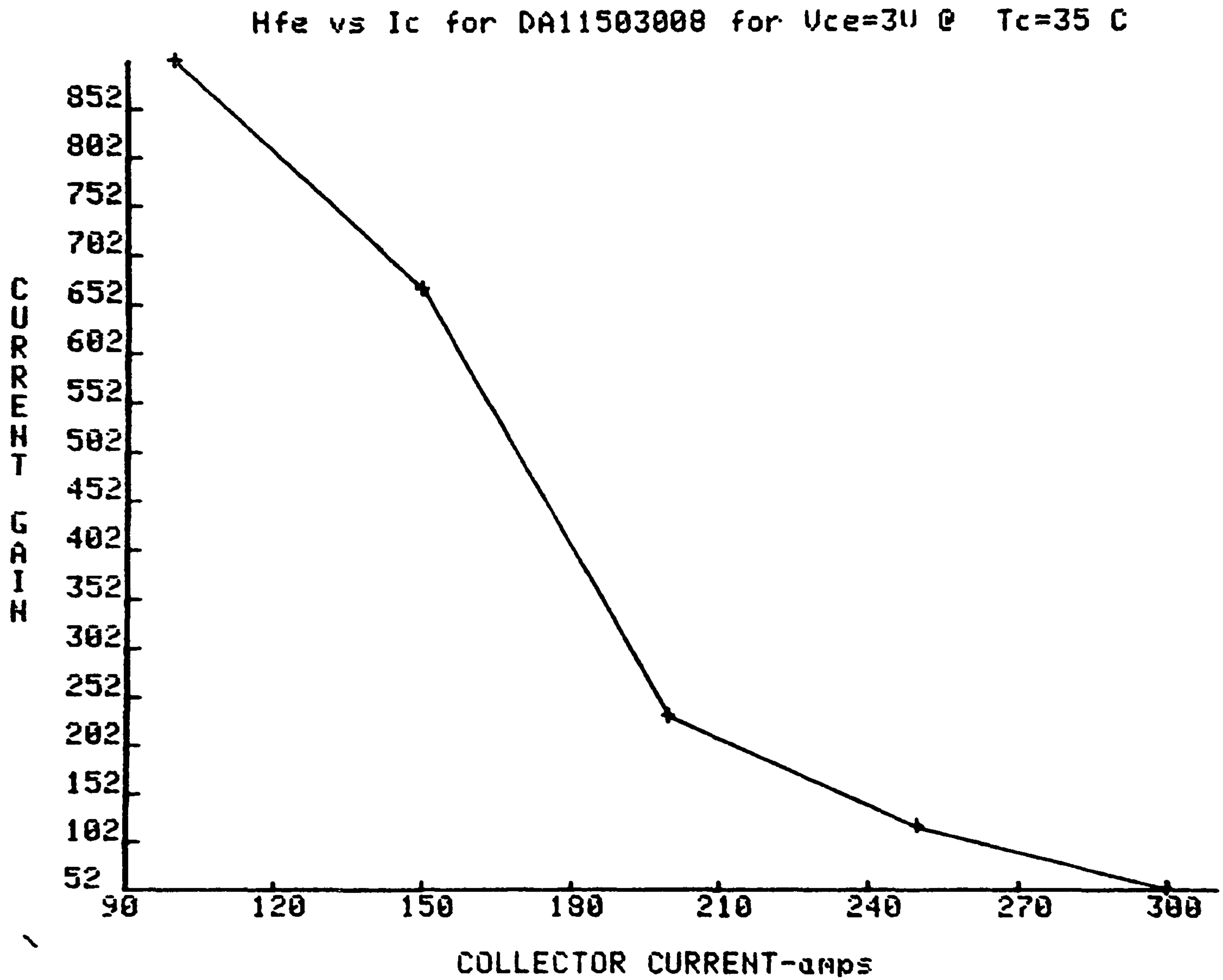
Hfe vs Ic for DA11503008 for Vce=3V @ Tc=35 C
CURRENT GAIN
852
802
752
702
652
602
552
502
452
402
352
302
252
202
152
102
52
90
120
150
180
210
240
270
300
COLLECTOR CURRENT-amps

A.3 Test Data for Fuji ETN81-055

Fig. A.3.1

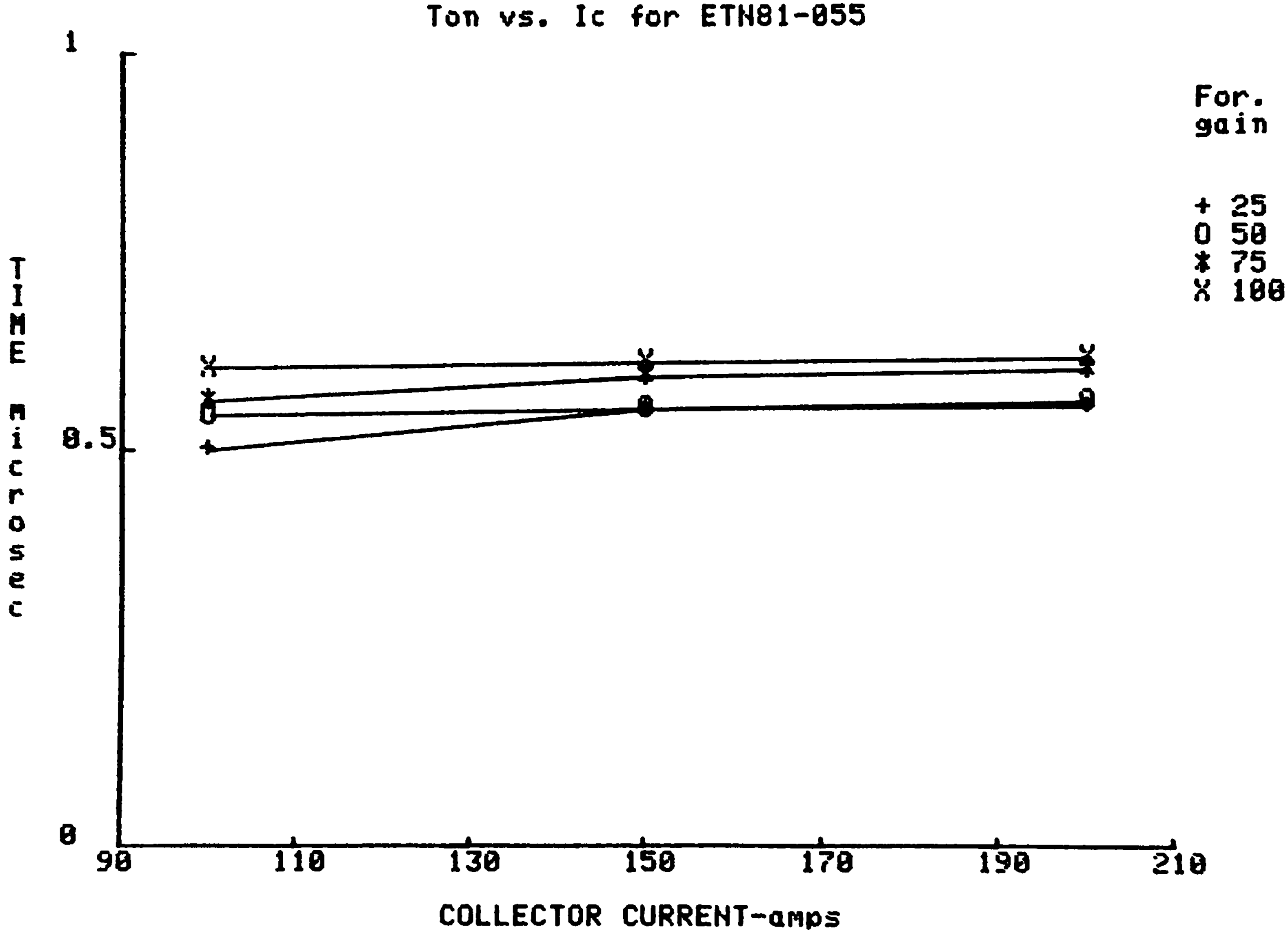
Ton vs. Ic for ETN81-055
1
0.5
0
TIME microsec
90
110
130
150
170
190
210
COLLECTOR CURRENT-amps
For. gain
+ 25
O 50
* 75
X 100

Fig. A.3.2

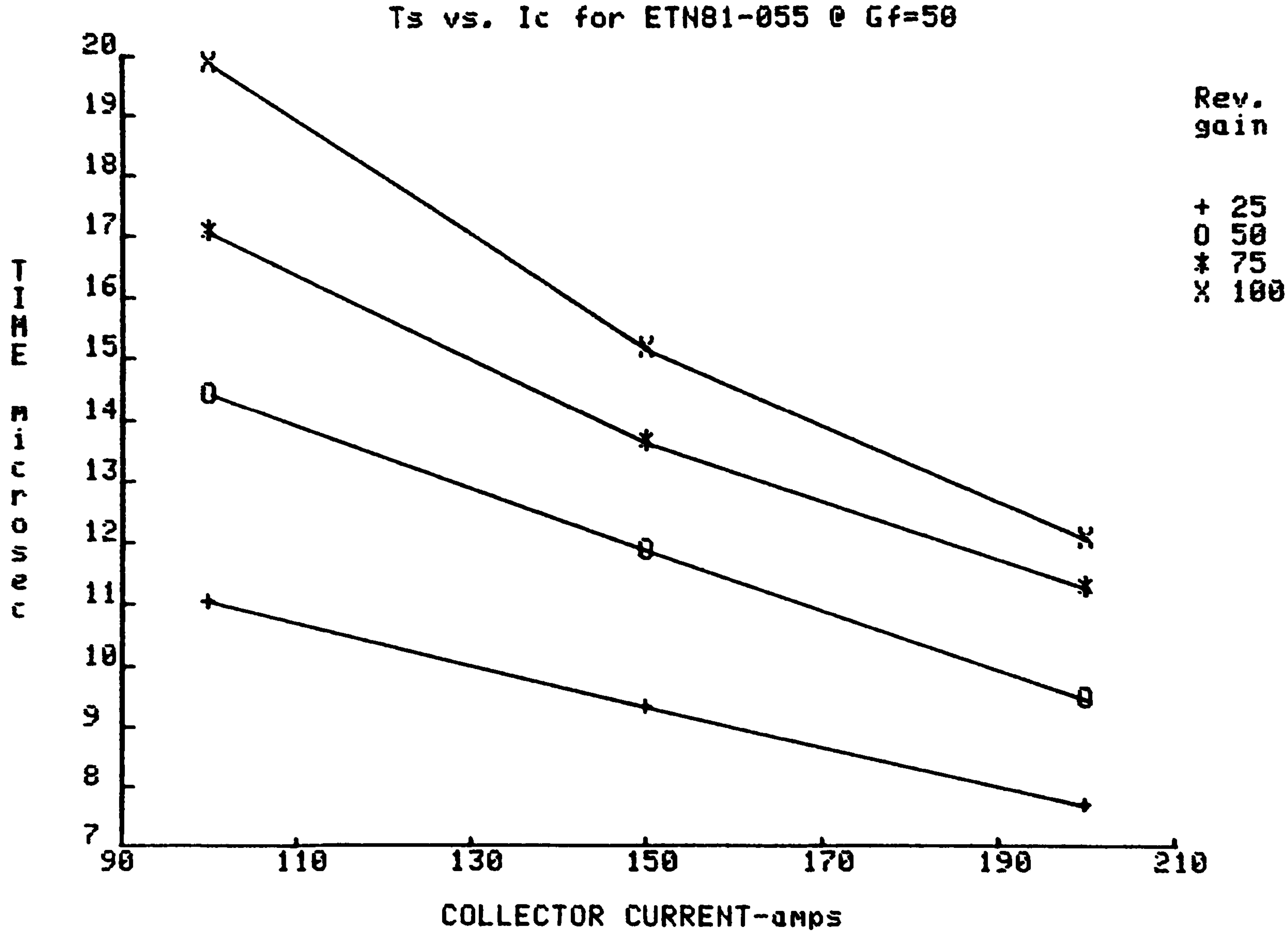
Ts vs. Ic for ETN81-055 @ Gf=50
TIME microsec
20
19
18
17
16
15
14
13
12
11
10
9
8
7
90
110
130
150
170
190
210
COLLECTOR CURRENT-amps
Rev.
gain
+ 25
O 50
* 75
X 100

Fig. A.3.3

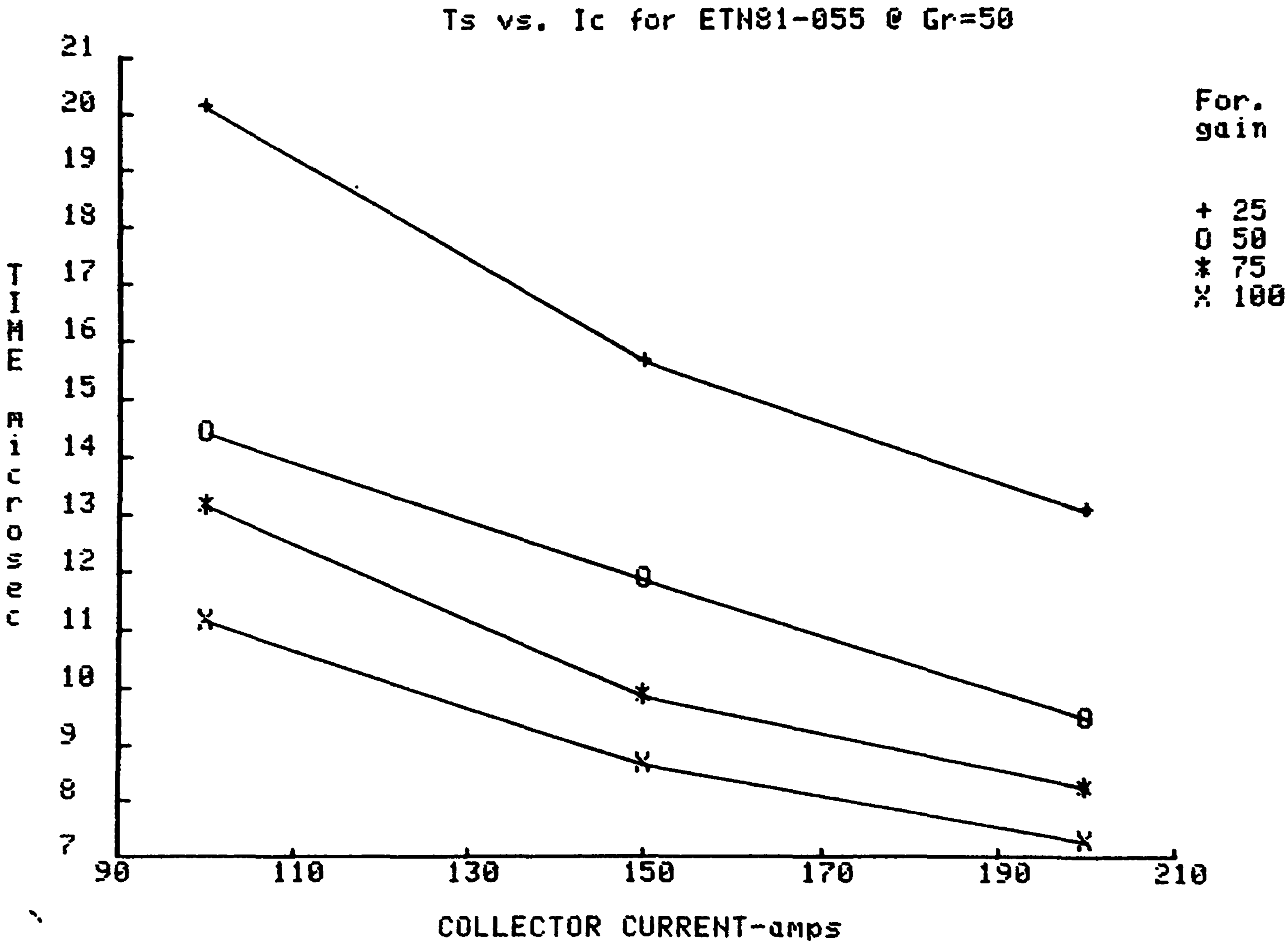

Ts vs. Ic for ETN81-055 @ Gr=50
TIME microsec
COLLECTOR CURRENT-amps
For. gain
+ 25
O 50
* 75
X 100
21
20
19
18
17
16
15
14
13
12
11
10
9
8
7
90
110
130
150
170
190
210

0

Fig. A.3.4

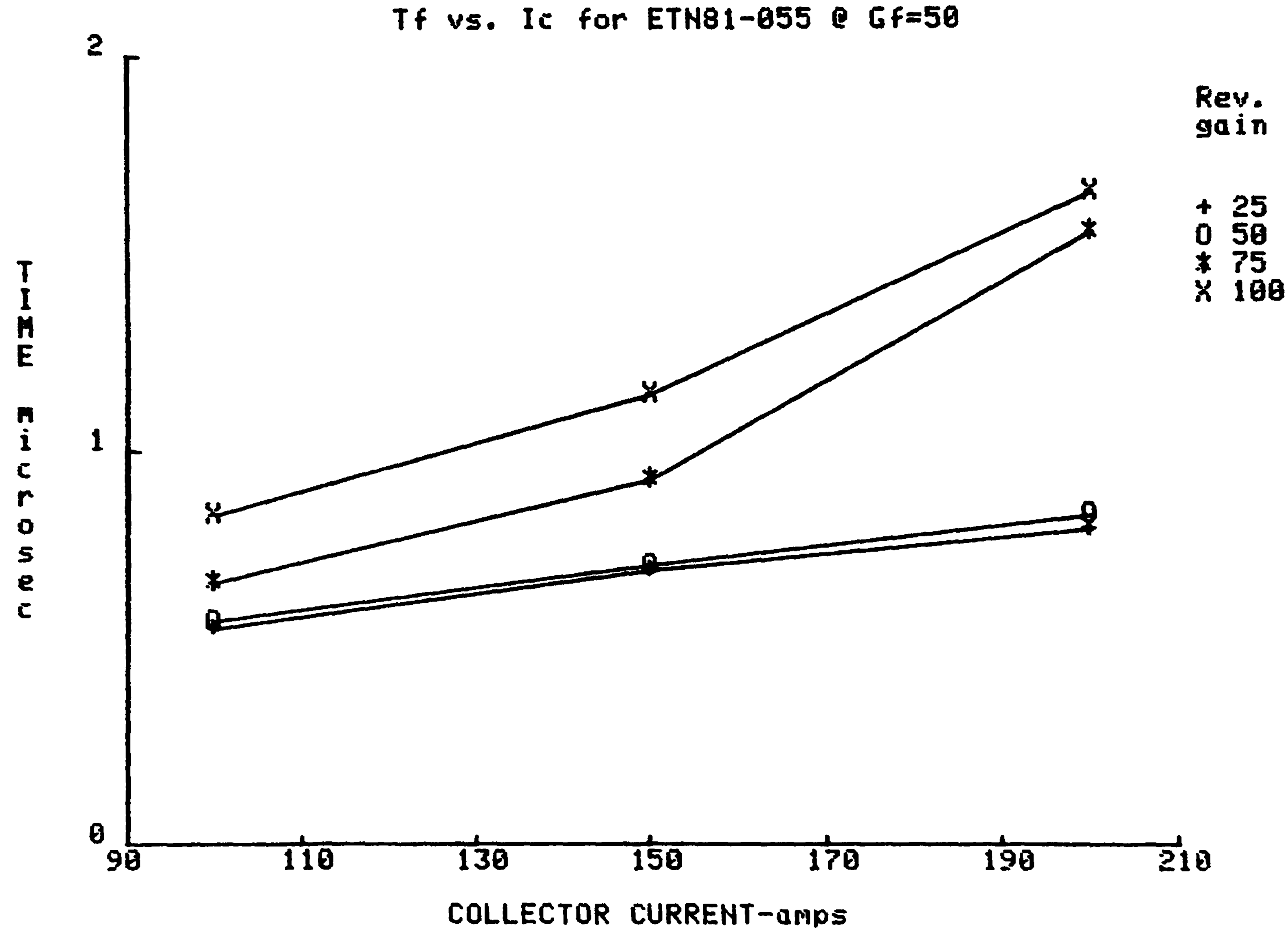

Tf vs. Ic for ETN81-055 @ Gf=50
TIME microsec
2
1
0
90
110
130
150
170
190
210
COLLECTOR CURRENT-amps
Rev. gain
+ 25
O 50
* 75
X 100

Fig. A.3.5

Ts vs. Ic COMPARATIVE DATA for ETN81-055 @ Gf=50 & Gr1=50

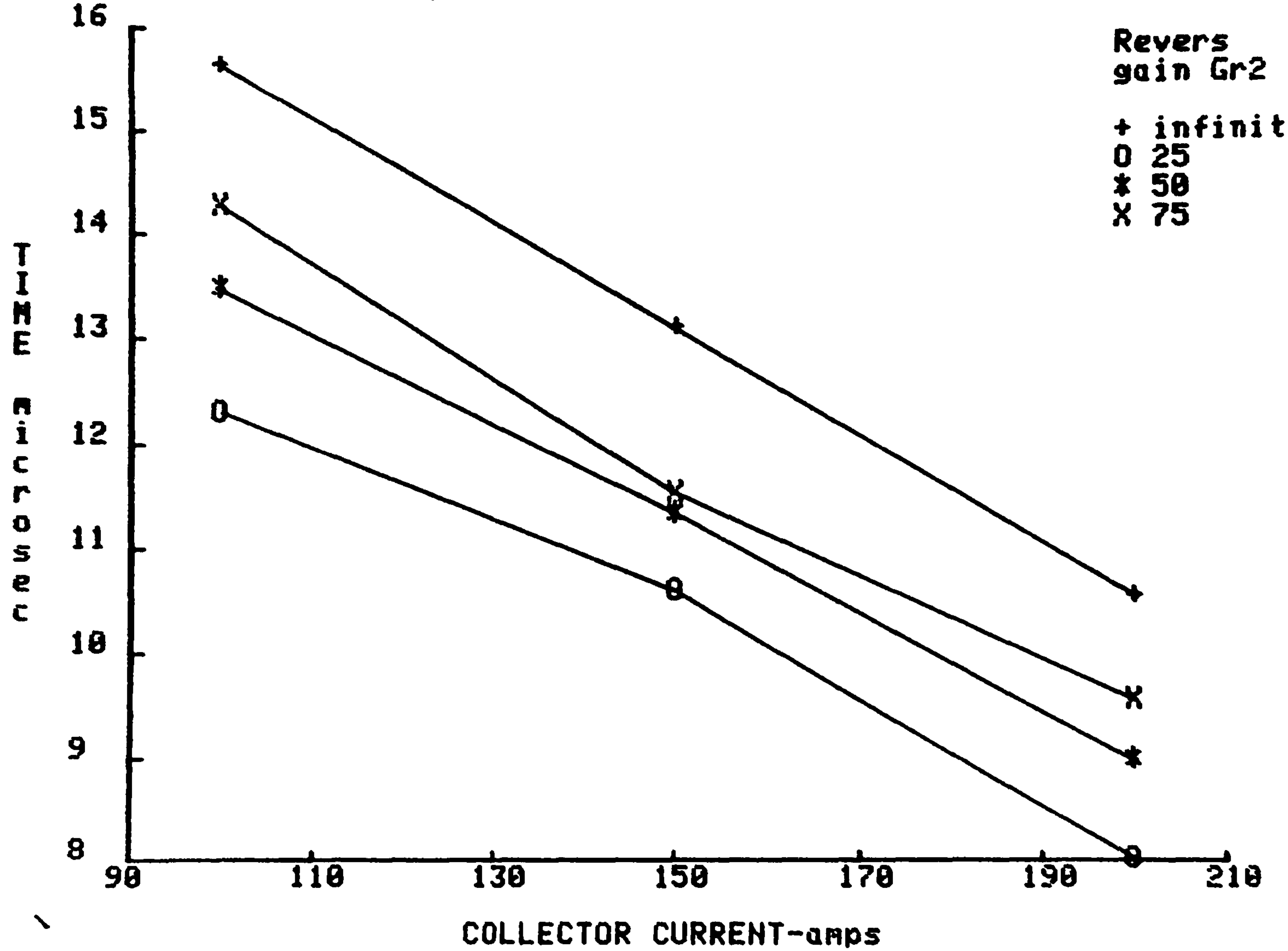

Fig. A.3.6

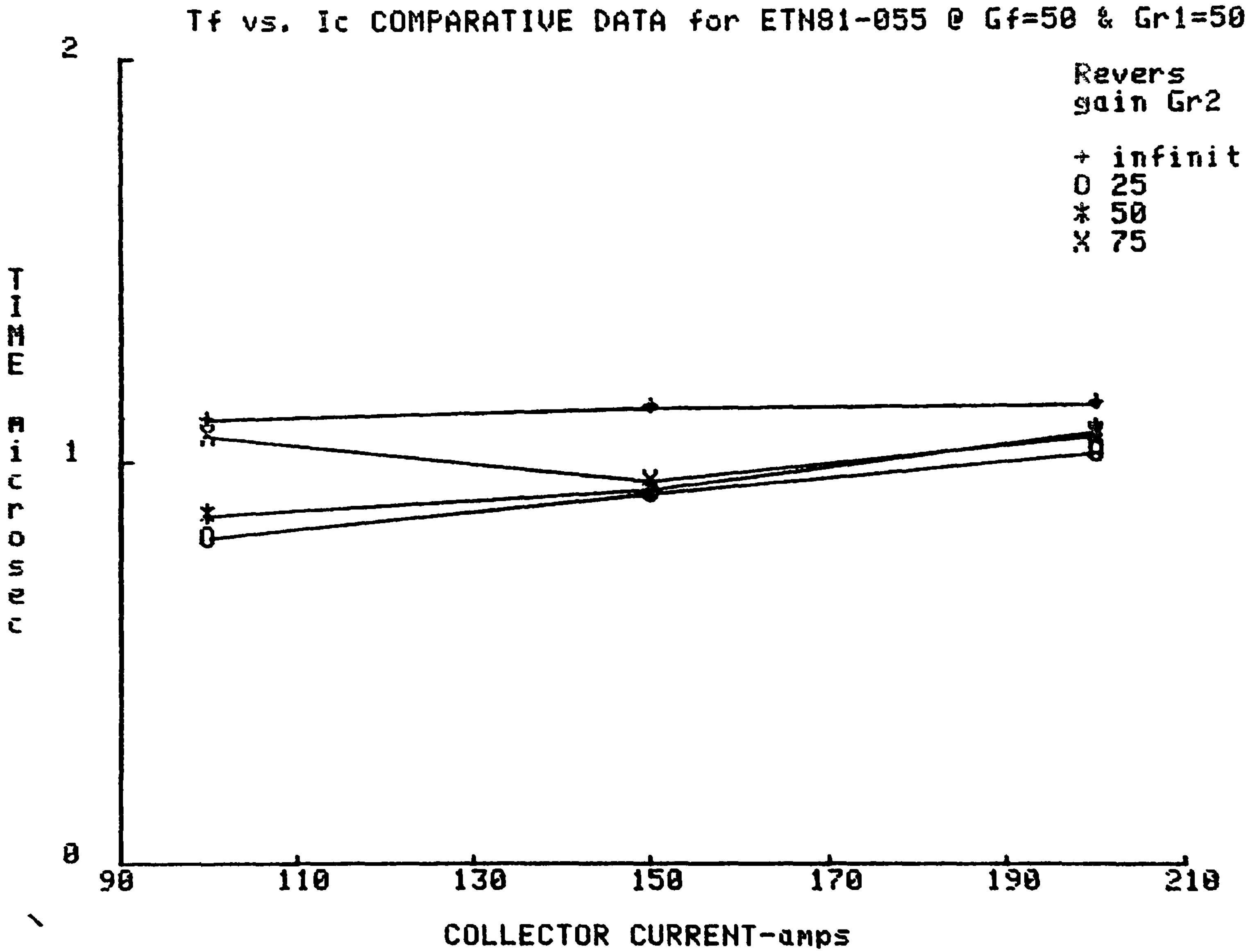

Tf vs. Ic COMPARATIVE DATA for ETN81-055 @ Gf=50 & Gr1=50
Revers
gain Gr2
+ infinit
O 25
* 50
X 75
TIME microsec
2
1
0
90
110
130
150
170
190
210
COLLECTOR CURRENT-amps

A.41

Fig. A.3.7

Qon vs Ic for ETN81-055 @ Vce=300V

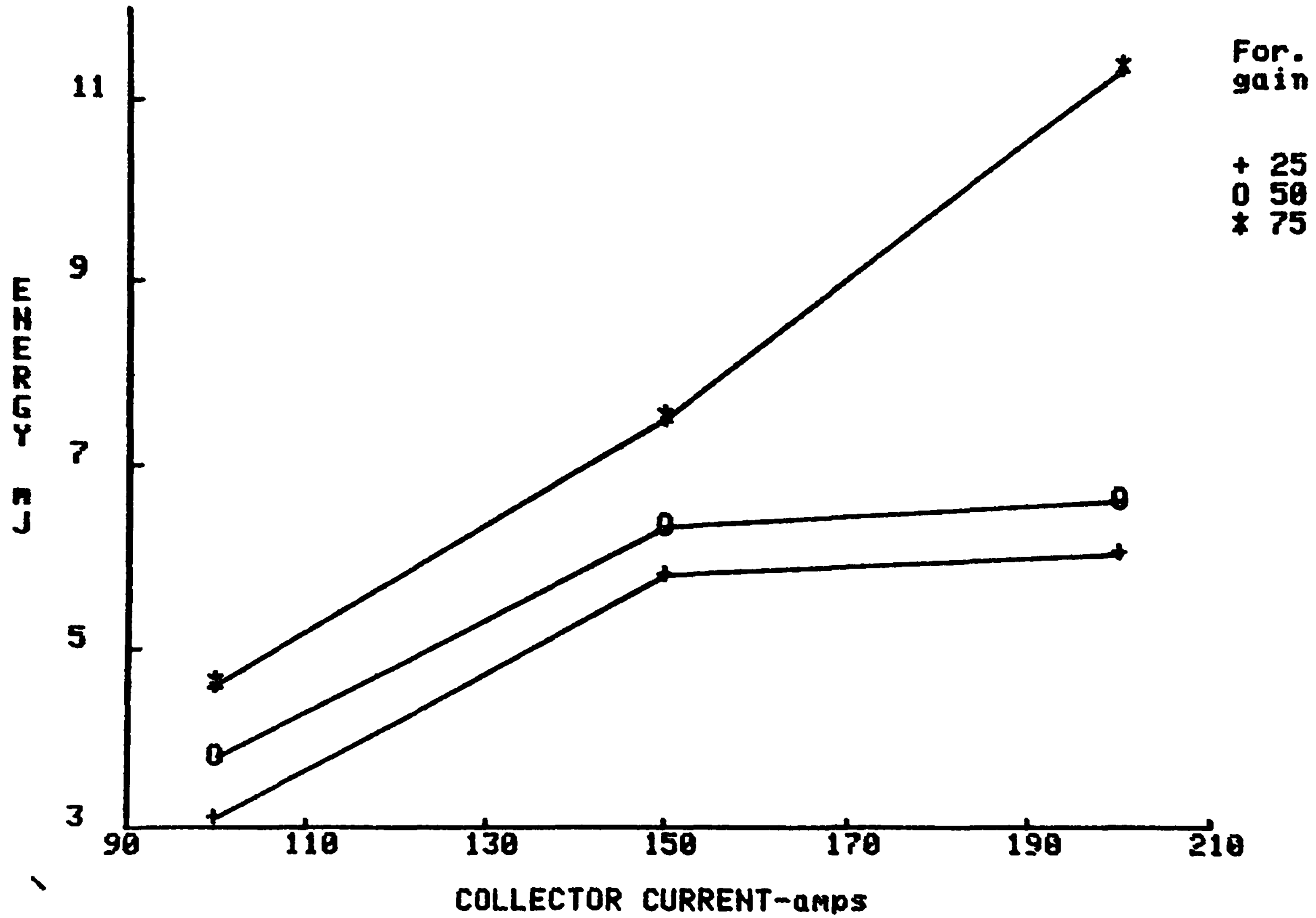

Fig. A.3.8

Qon(qsat) vs Ic for ETN81-055 @ Vce=300V

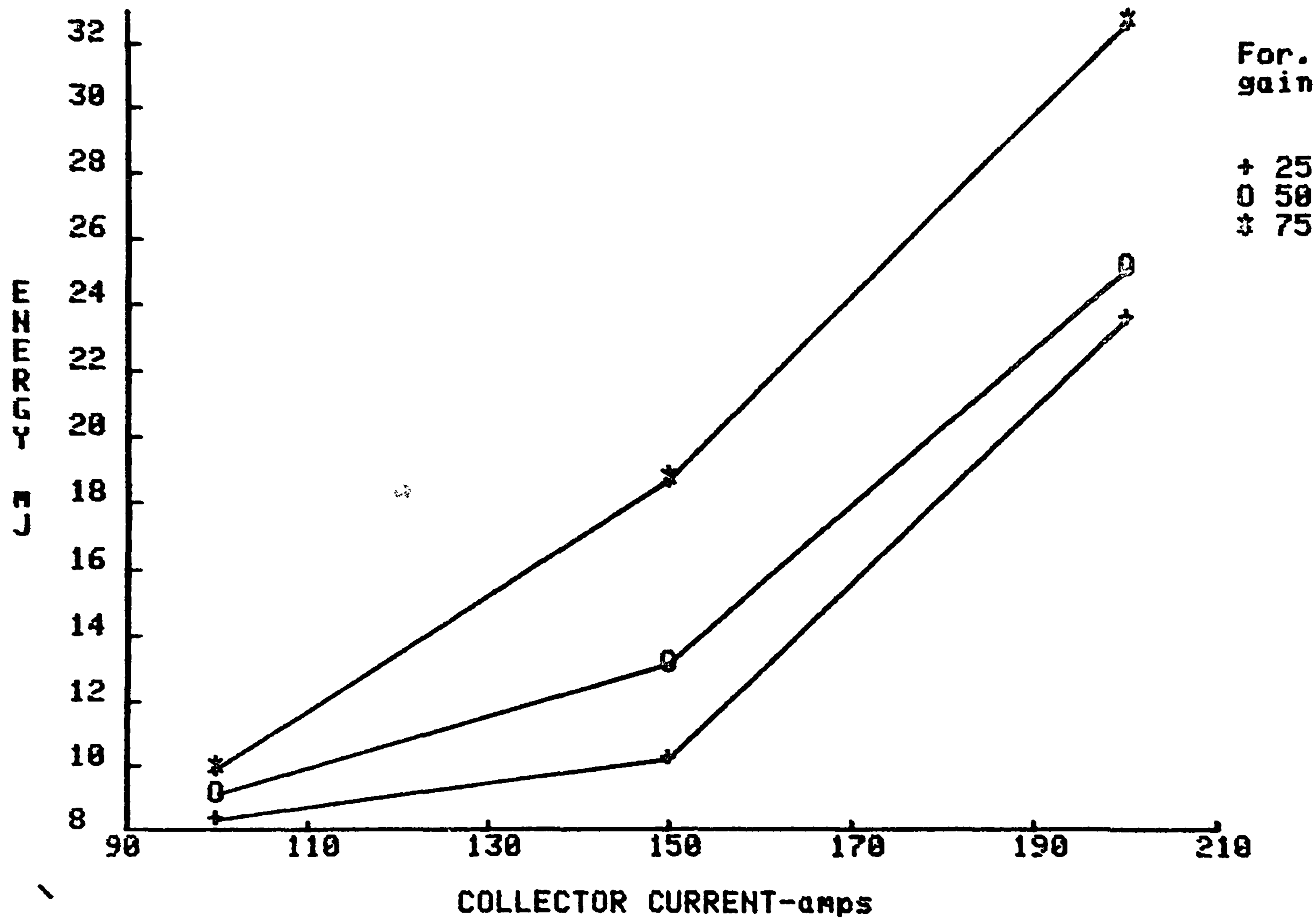

Fig. A.3.9

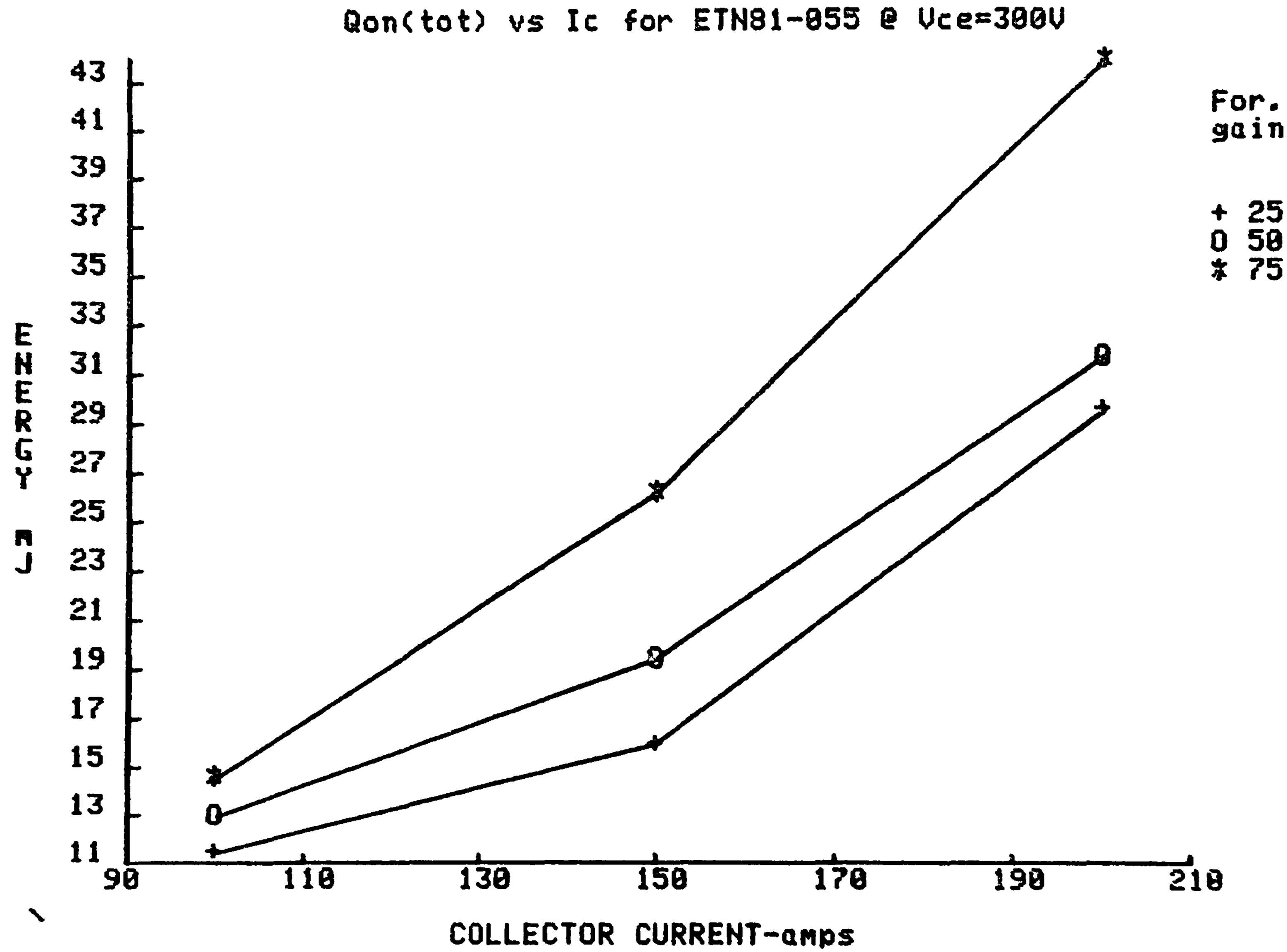
Qon(tot) vs Ic for ETN81-055 @ Vce=300V
ENERGY mJ
43
41
39
37
35
33
31
29
27
25
23
21
19
17
15
13
11
90
110
130
150
170
190
210
COLLECTOR CURRENT-amps
For. gain
+ 25
O 50
* 75

Fig. A.3.10

Qoff vs Ic for ETN81-055 @ Vce=300V

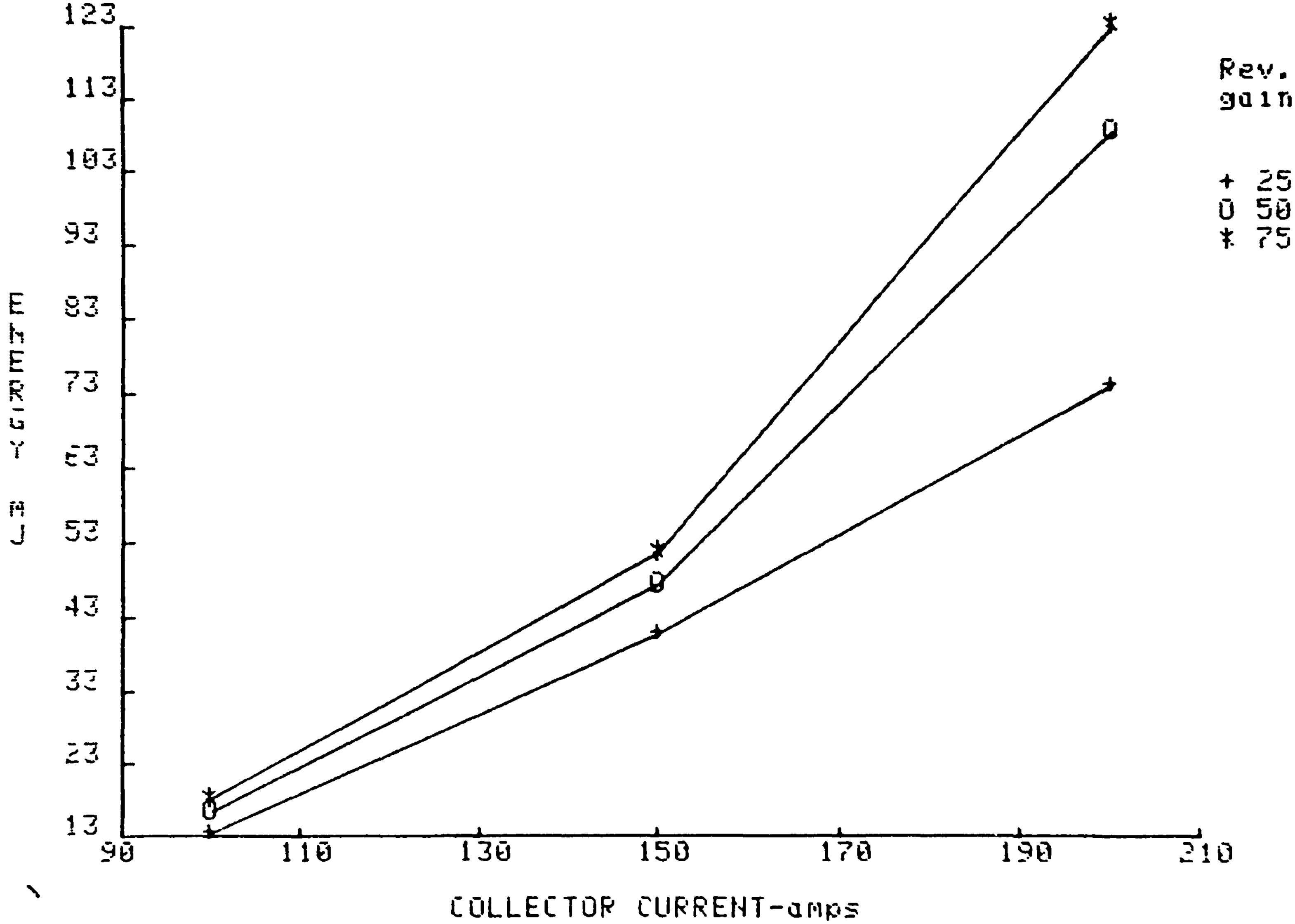

Fig. A.3.11

Qtot vs Ic for ETN81-055 @ Vce=300V

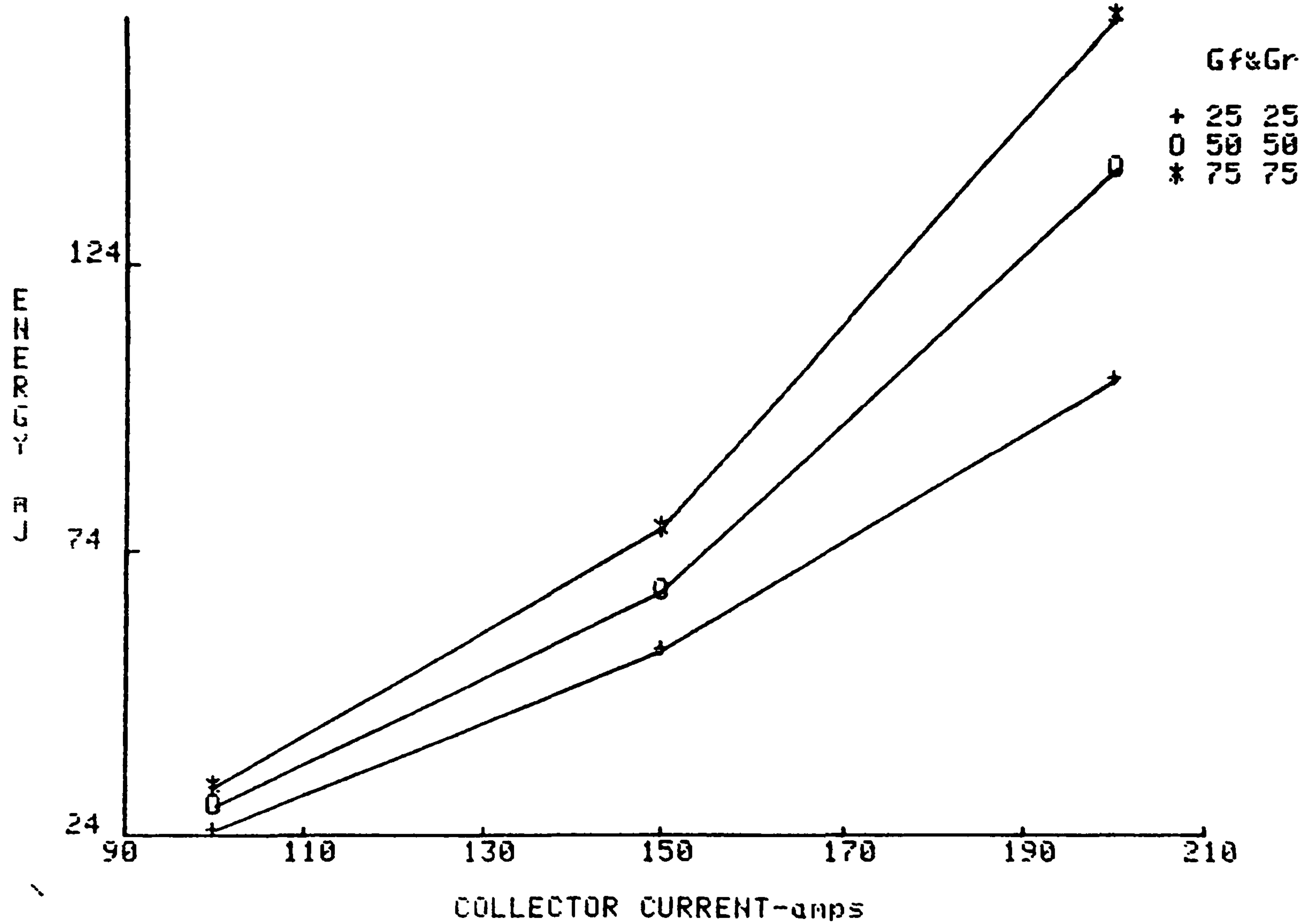

Fig. A.3.12

Switching Loadline Characteristics: Vce vs. Ic
for Turn-on of Power Transistor with Inductive Load

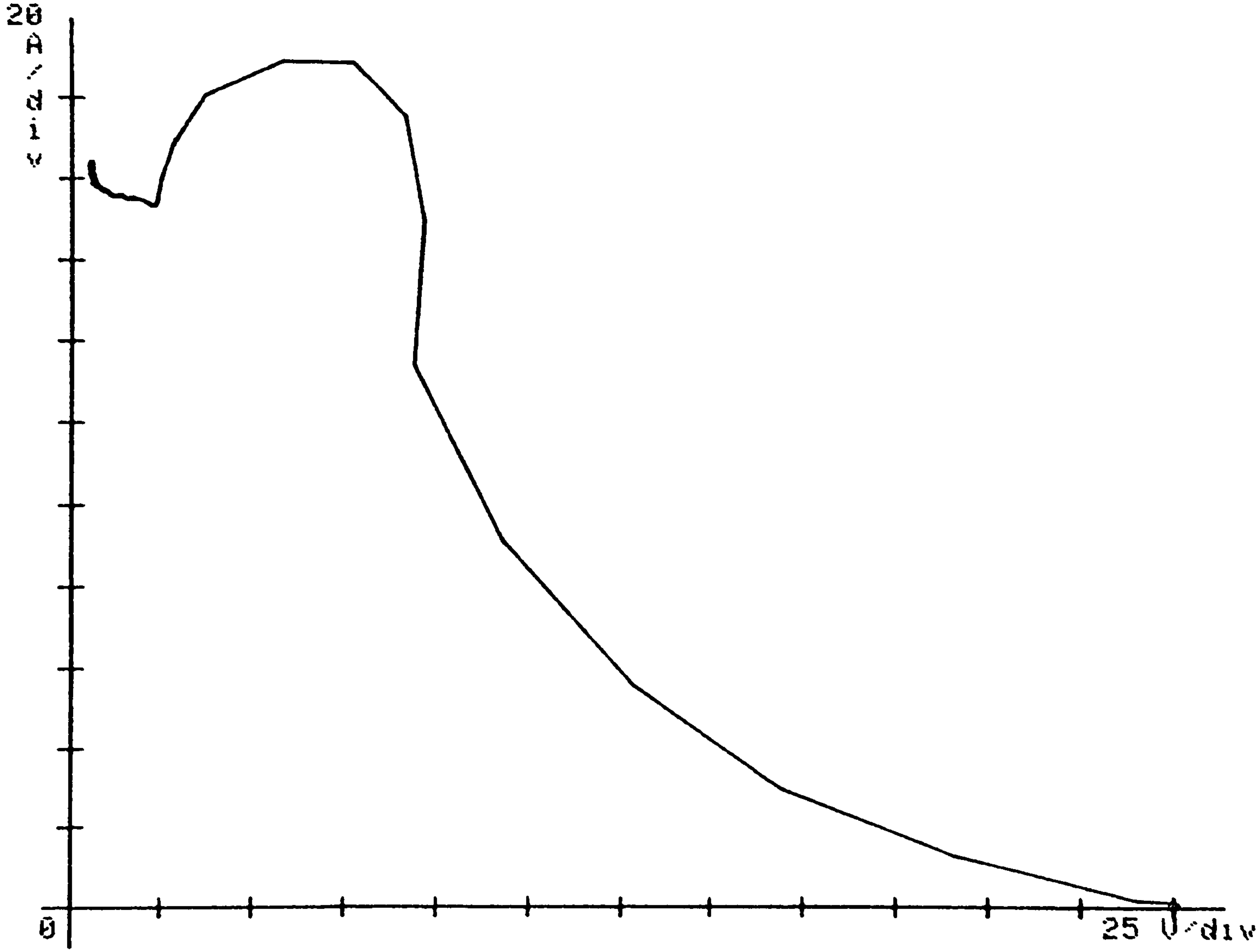

Fig. A.3.13

Switching Loadline Characteristics: Vce vs. Ic
for Trun-off of Power Trans. with Inductive Load

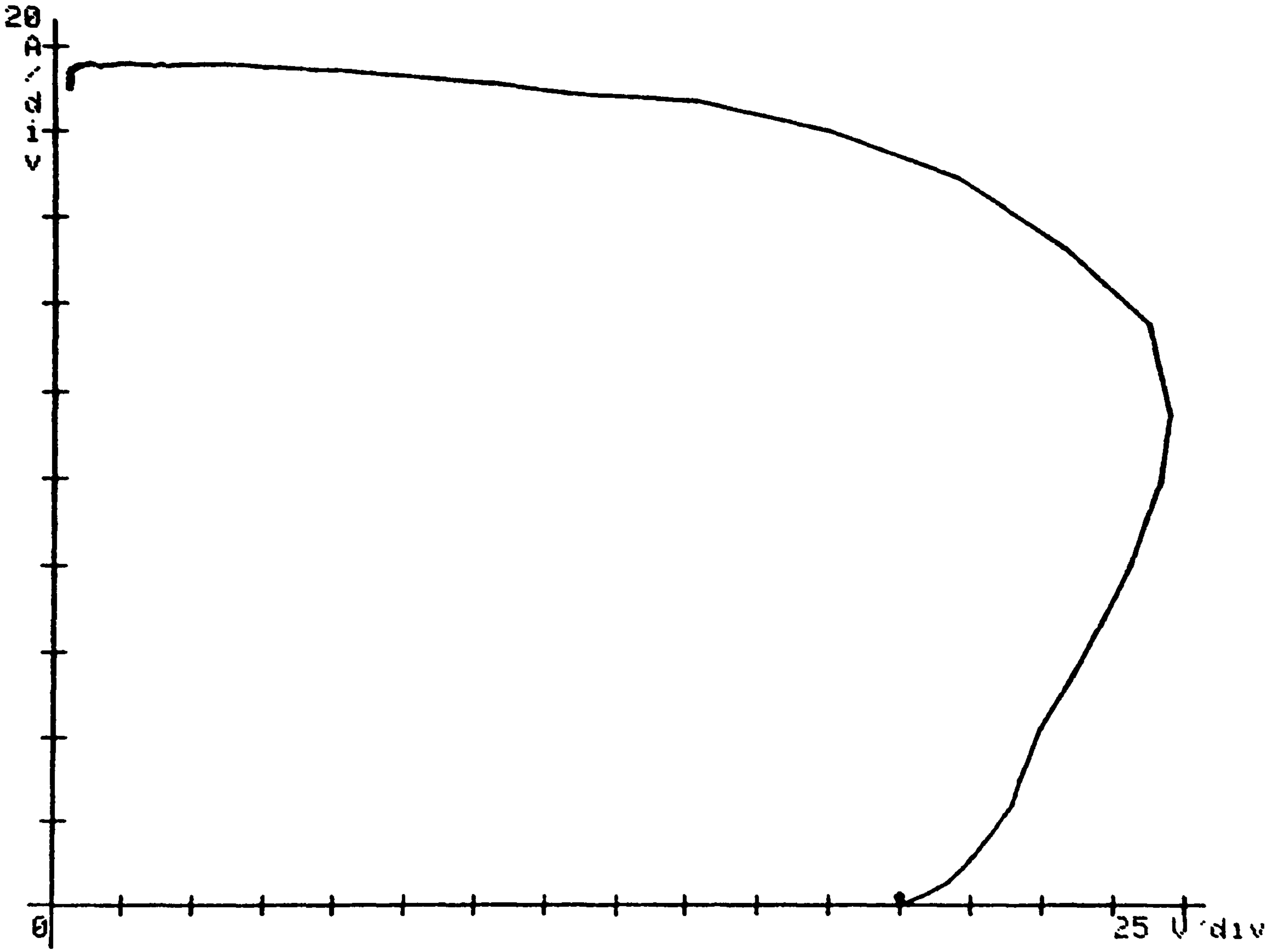

Fig. A.3.14

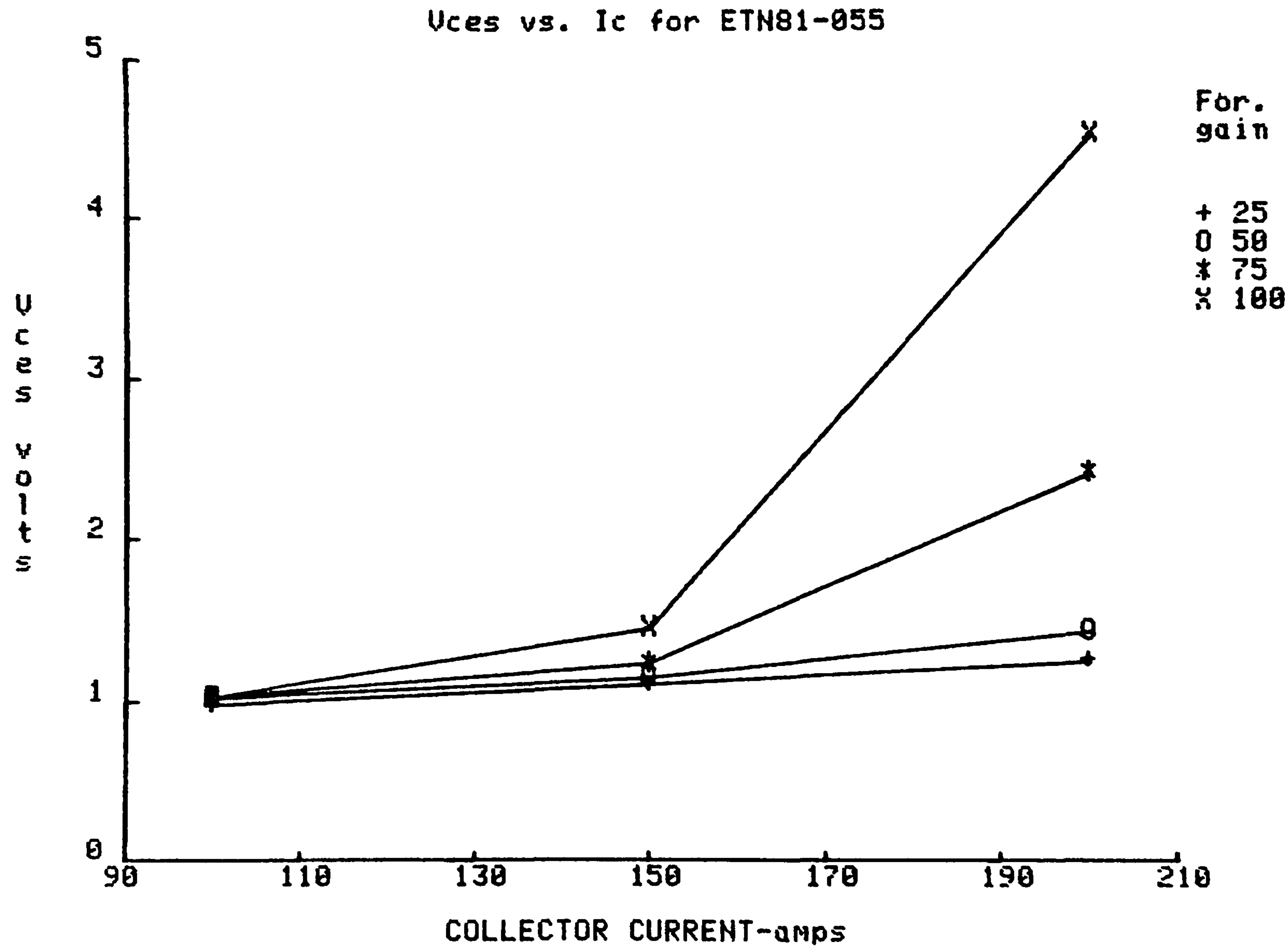
Vces vs. Ic for ETN81-055
Vces volts
COLLECTOR CURRENT-amps
0
1
2
3
4
5
90
110
130
150
170
190
210
For. gain
+ 25
O 50
* 75
X 100

Fig. A.3.15

Hfe vs Ic for ETN81-055 for Vce=3V @ Tc=35 C

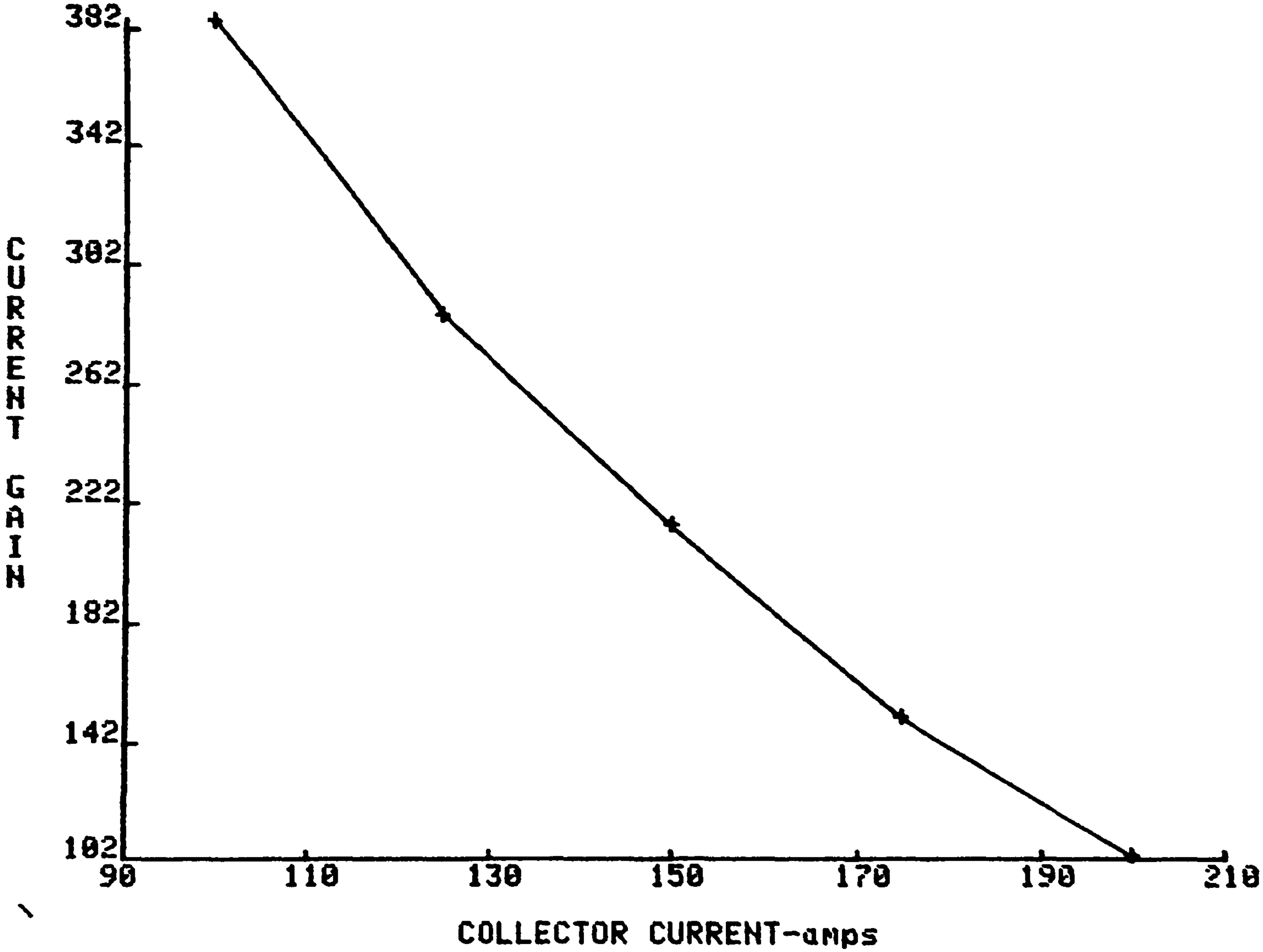

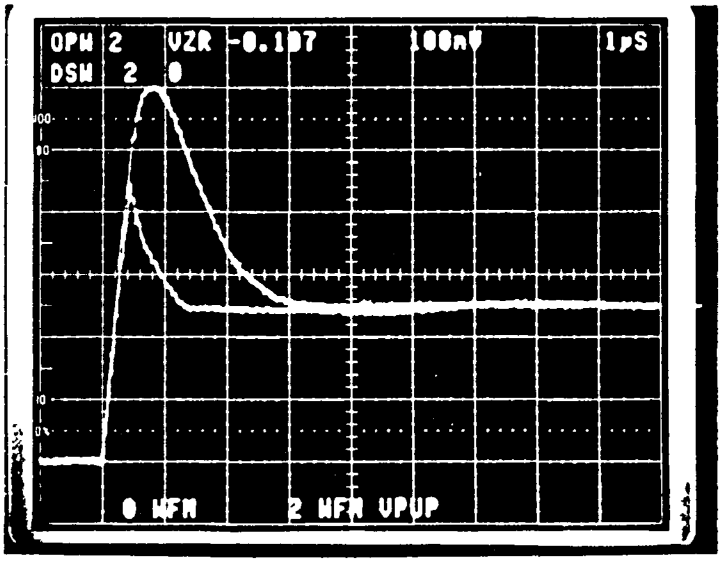

Fig. A.3.16 Diode recovery and dv/dt test for ETN81-055
Upper trace: Base open
Lower trace: Base reverse biased
(Scale: horizontal 1 µs/div; vertical 40 A/div)

A.4 Test Data for Fuji EVM31-050

Figure A.41 missing

Fig. A.4.2

Ts vs. Ic for EVM31-050 @ Gf=50

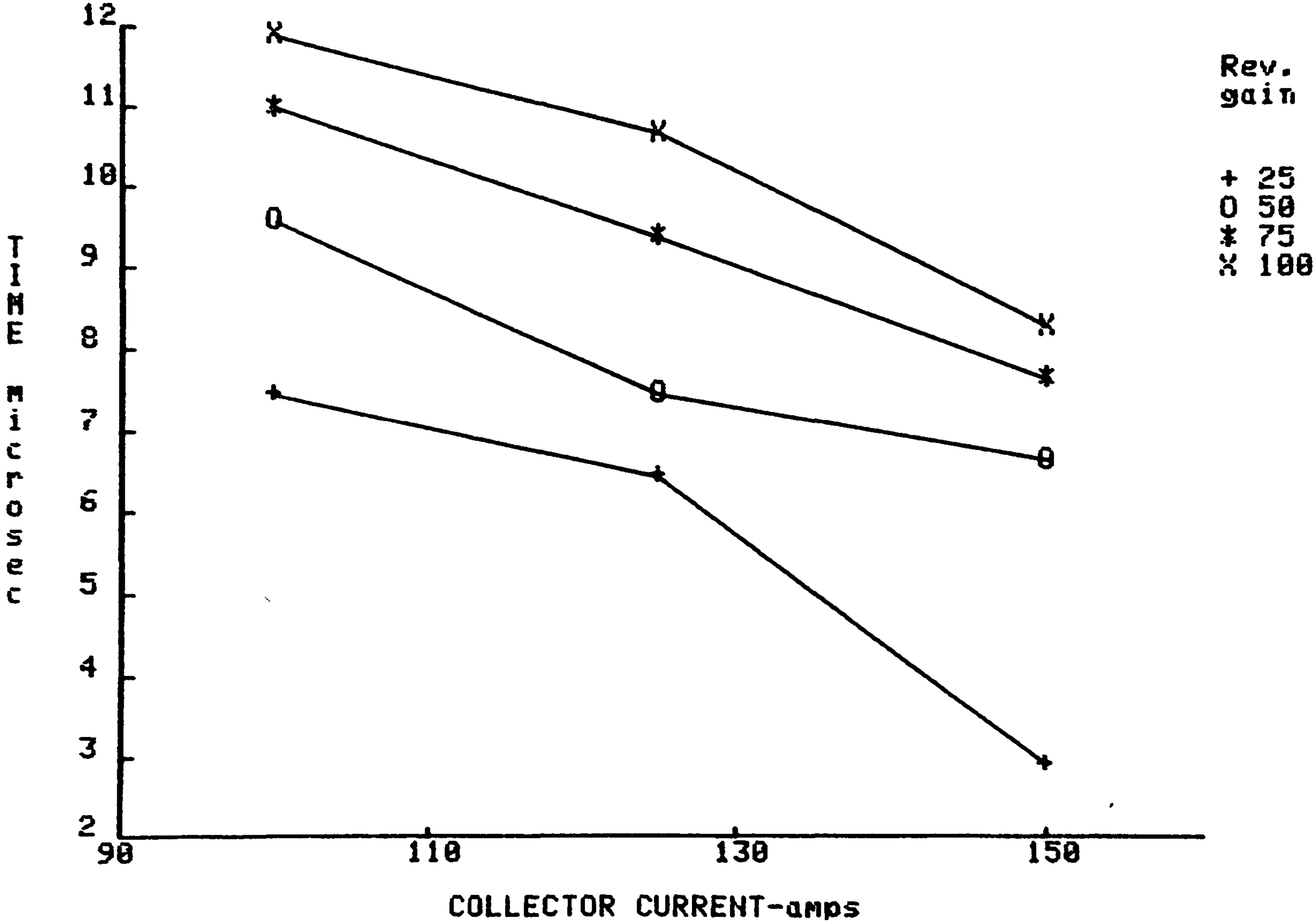

Fig. A.4.3

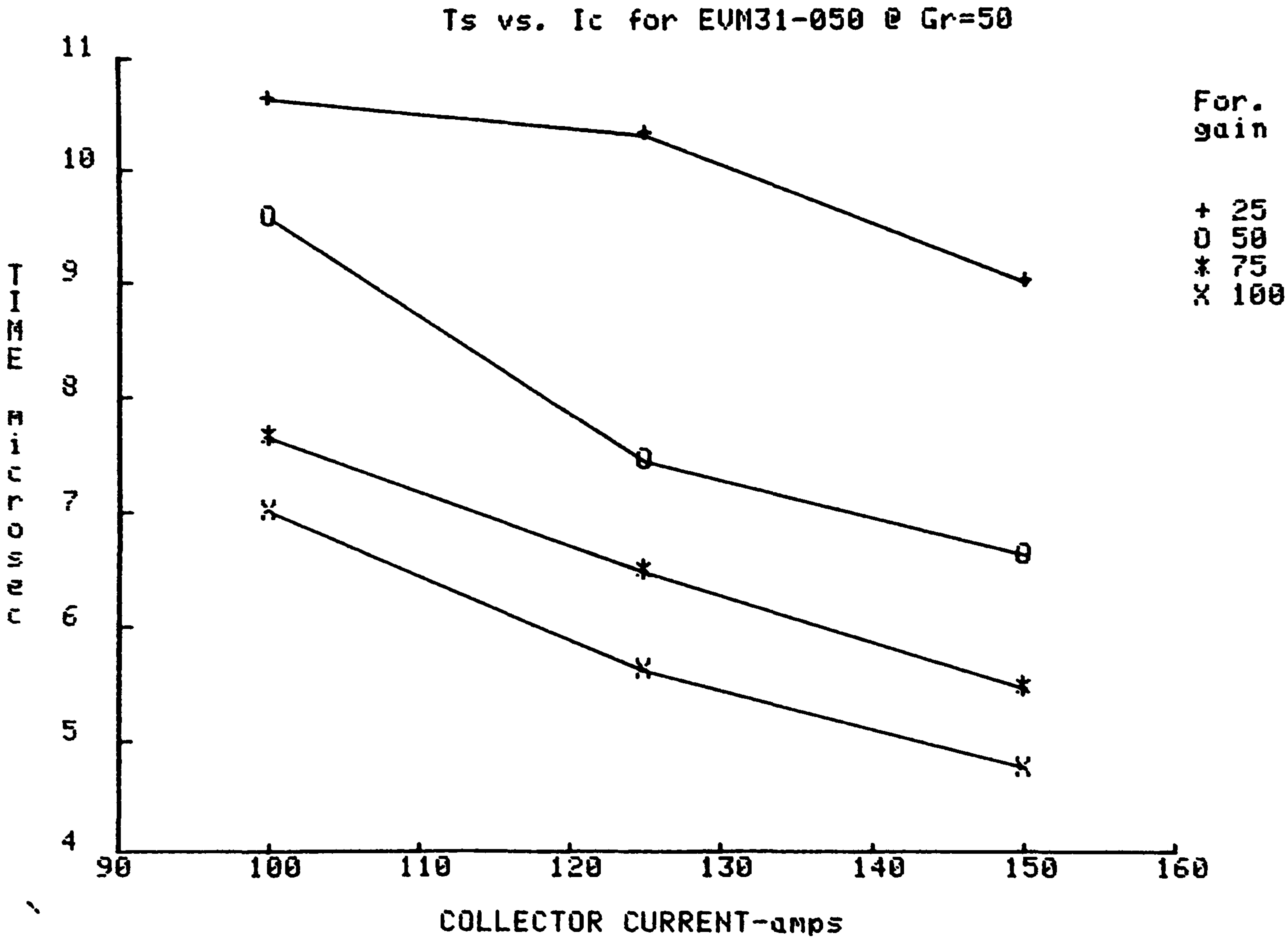

Ts vs. Ic for EVM31-050 @ Gr=50
TIME microsec
11
10
9
8
7
6
5
4
90
100
110
120
130
140
150
160
COLLECTOR CURRENT-amps
For. gain
+ 25
O 50
* 75
X 100

Fig. A.4.4

Tf vs. Ic for EVM31-050 @ Gf=50

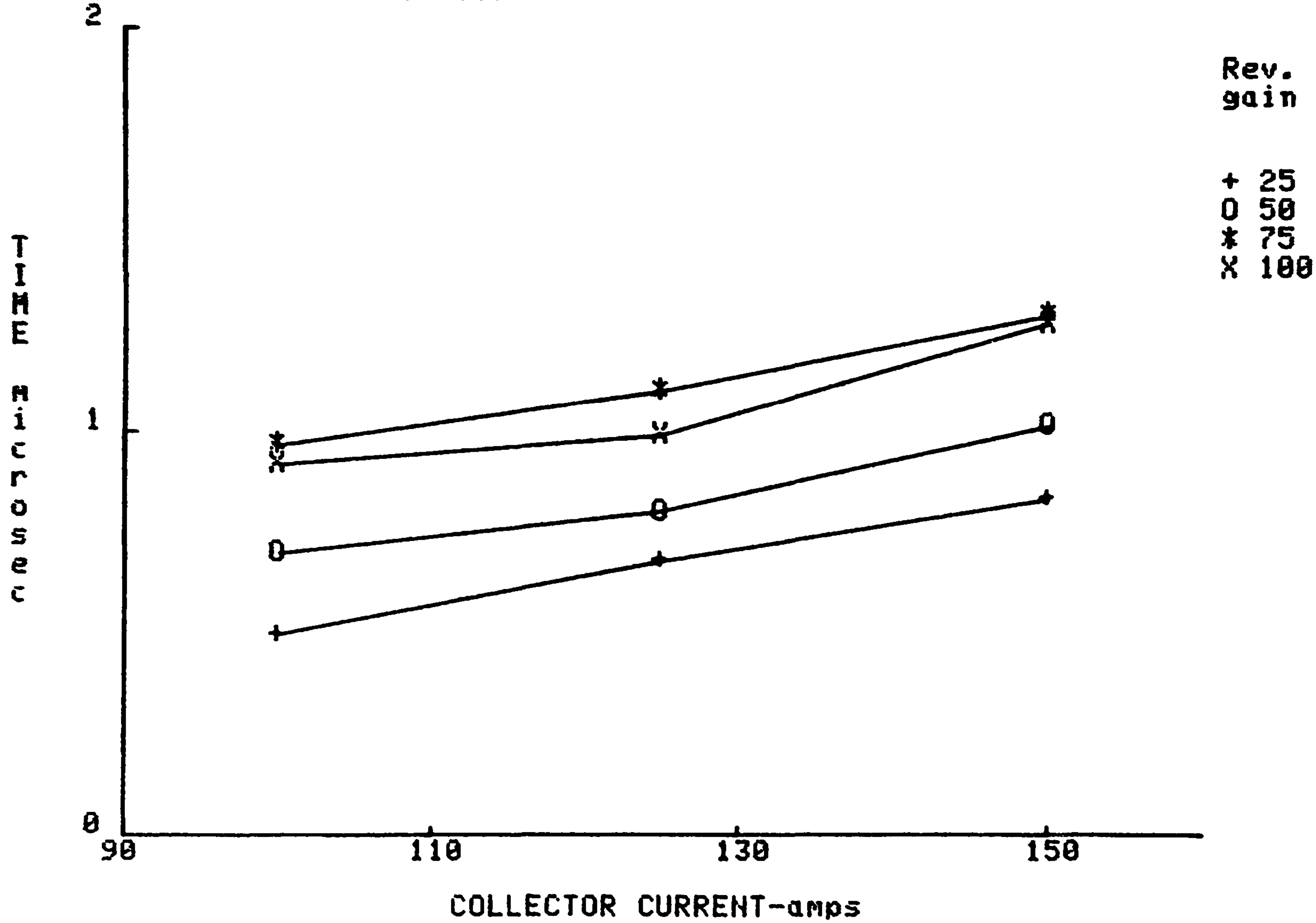

Fig. A.4.7

Qon vs Ic for EVM31-050 @ Vce=300V

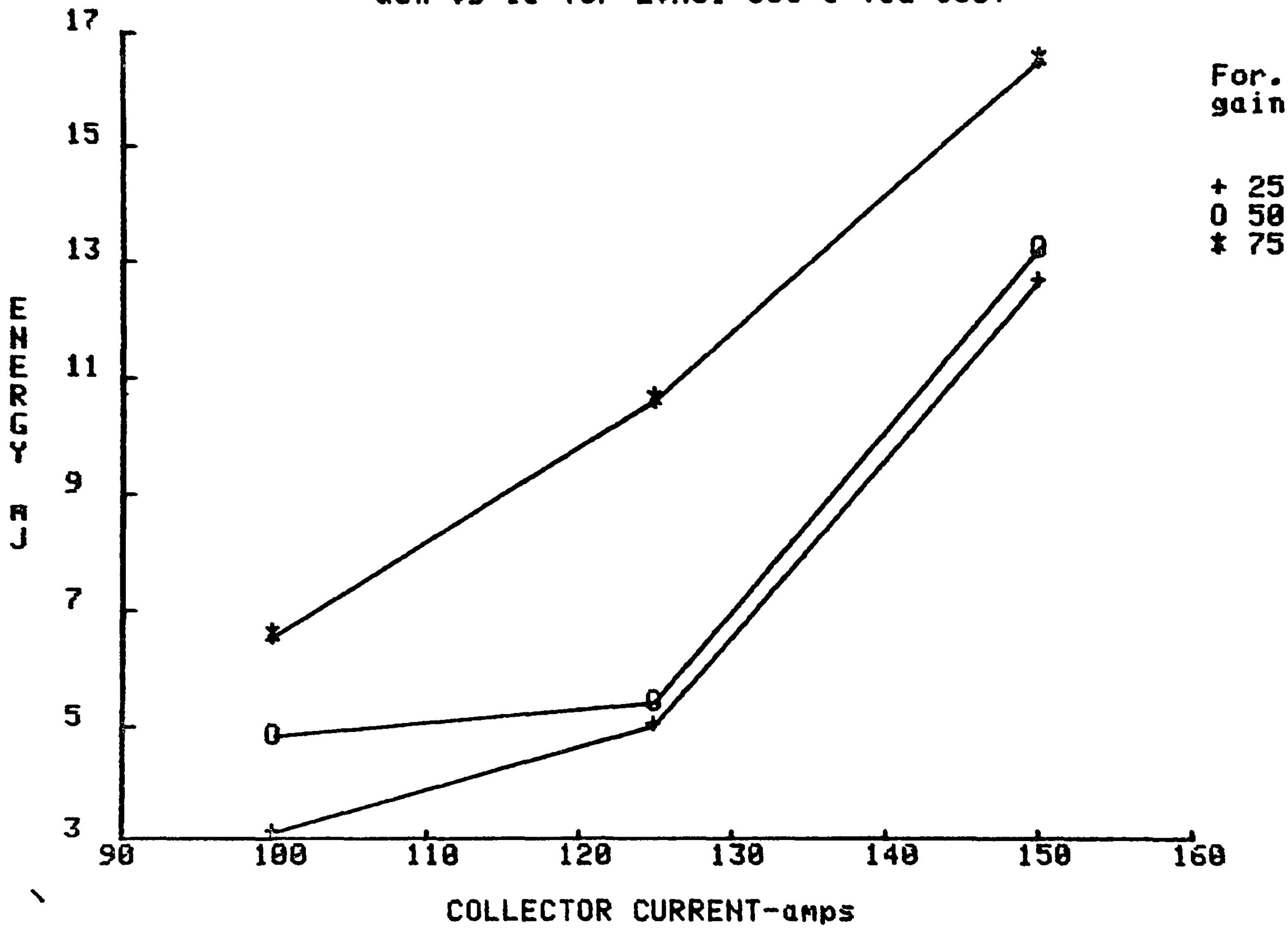

Fig. A.4.8

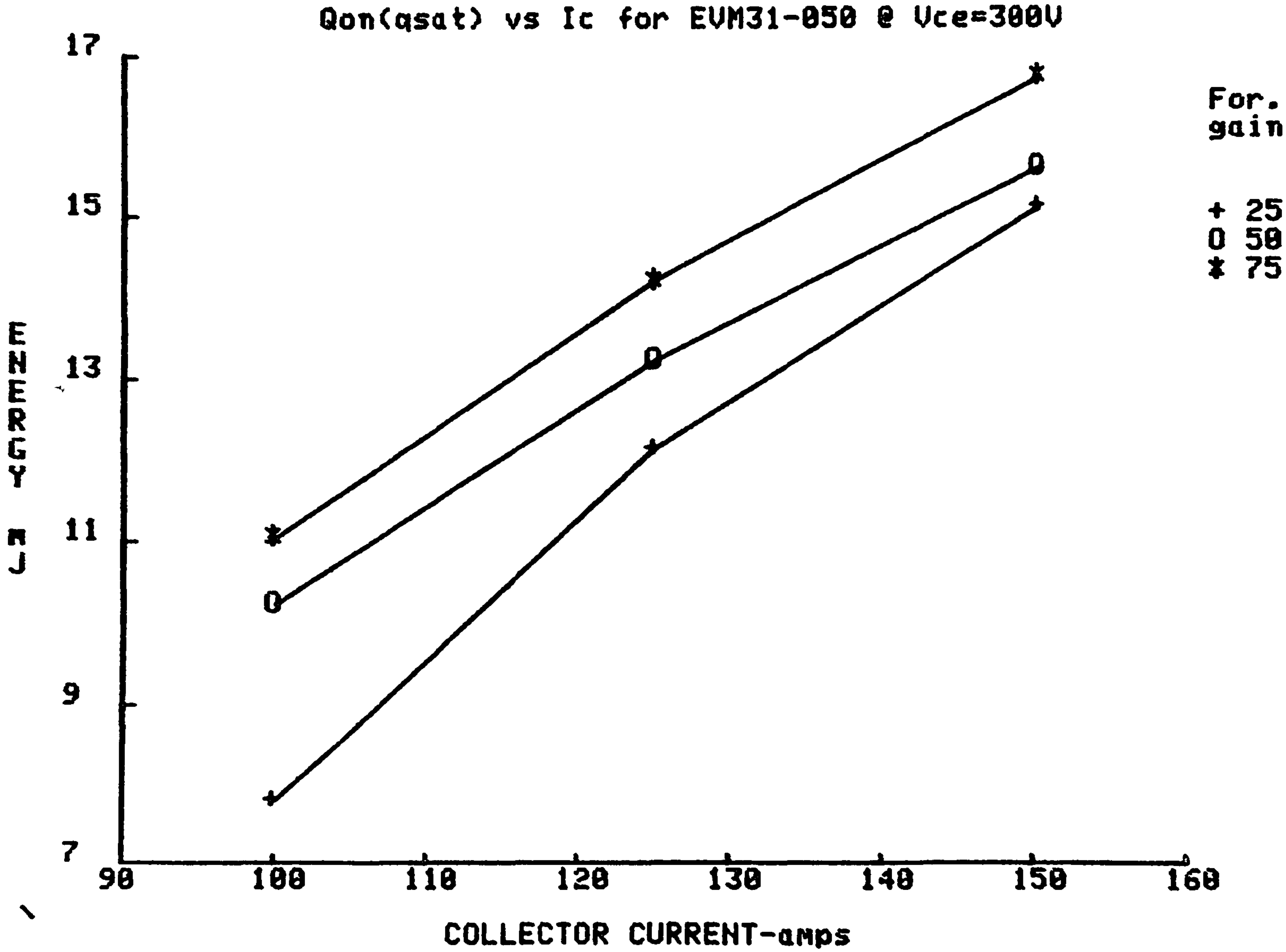
Qon(qsat) vs Ic for EVM31-050 @ Vce=300V
17
15
13
11
9
7
ENERGY mJ
For. gain
+ 25
0 50
* 75
90
100
110
120
130
140
150
160
COLLECTOR CURRENT-amps

Fig. A.4.9

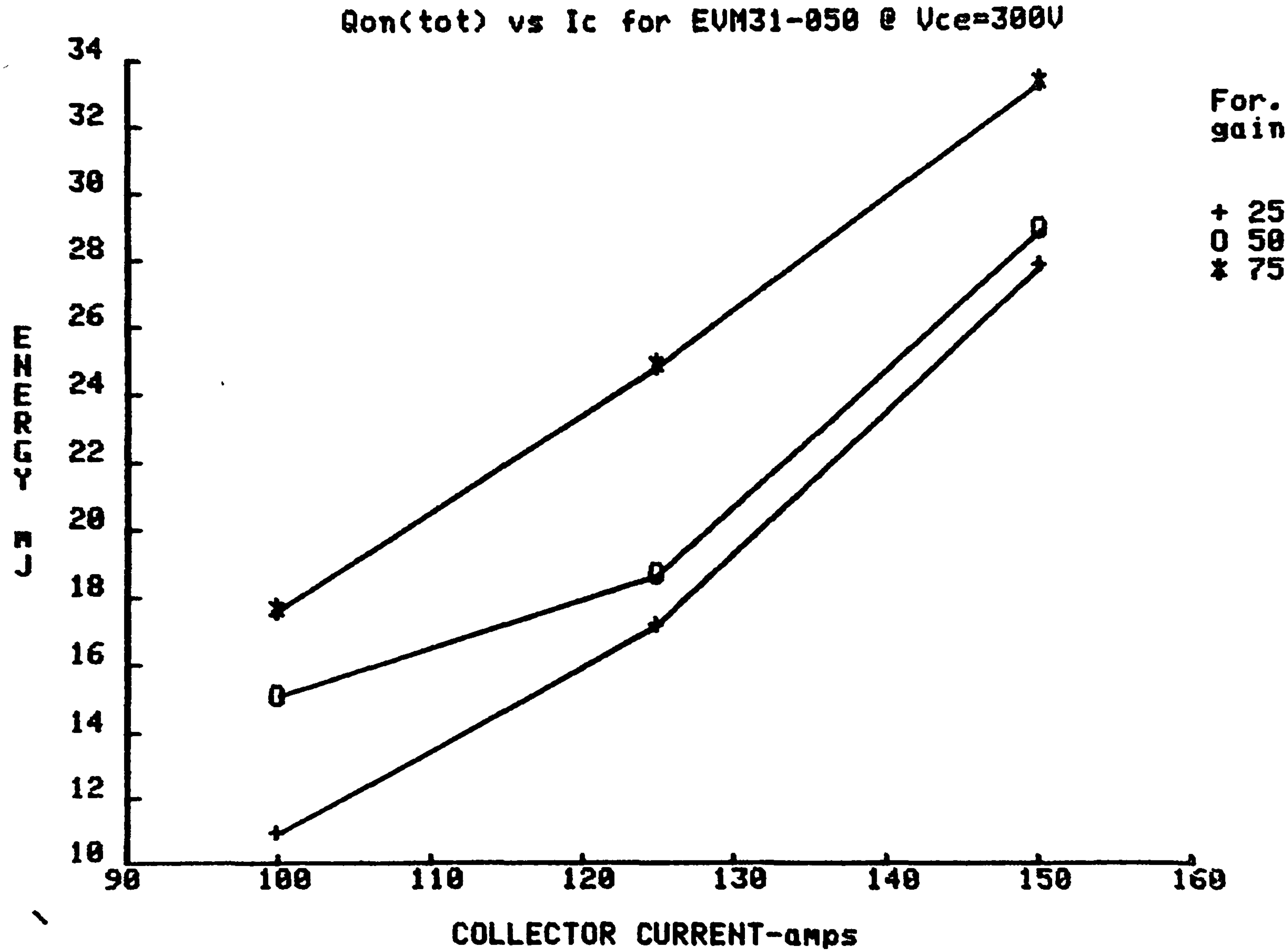
Qon(tot) vs Ic for EVM31-050 @ Vce=300V
ENERGY mJ
34
32
30
28
26
24
22
20
18
16
14
12
10
90
100
110
120
130
140
150
160
COLLECTOR CURRENT-amps
For. gain
+ 25
0 50
* 75

Fig. A.4.10

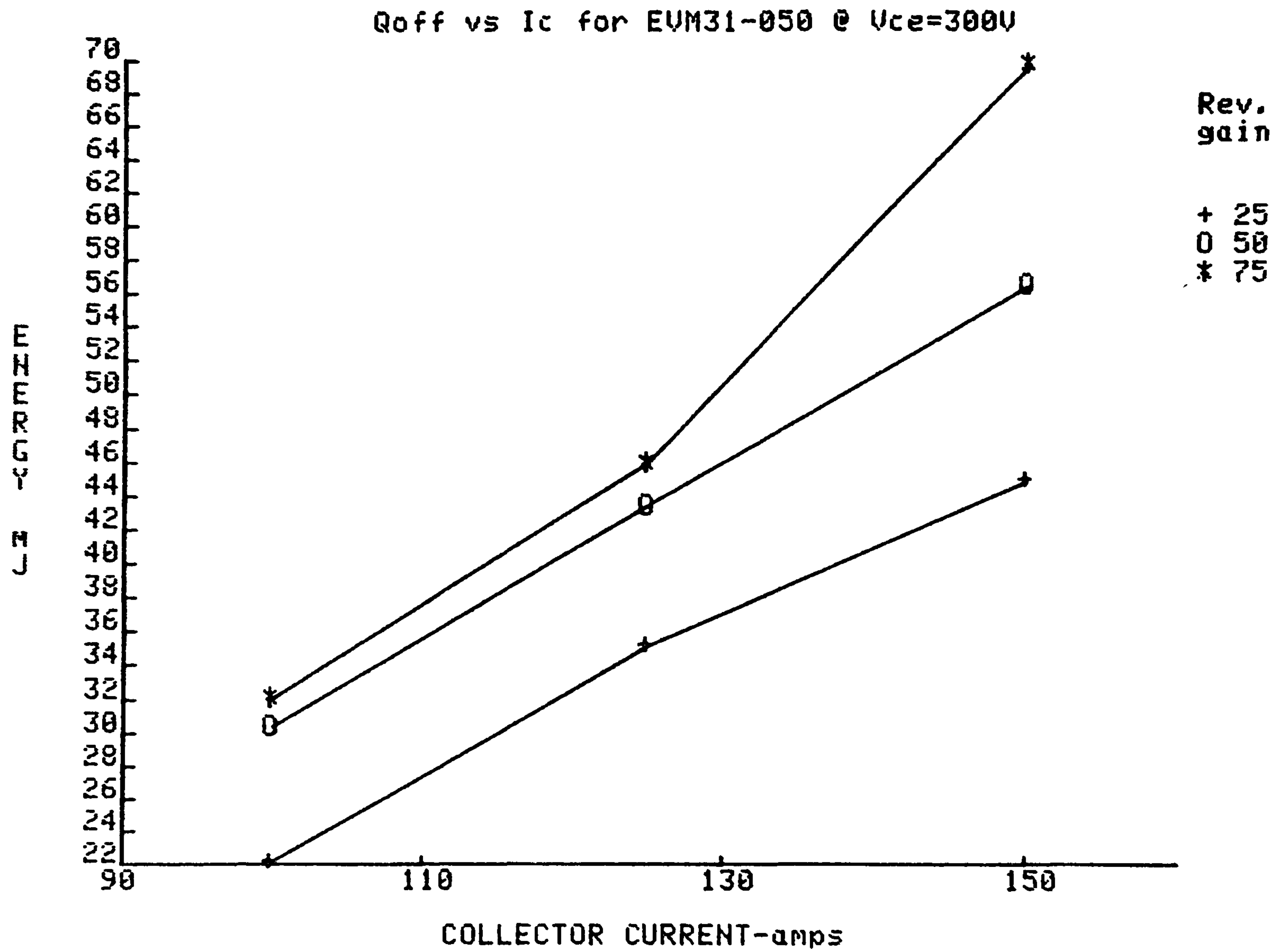
Qoff vs Ic for EVM31-050 @ Vce=300V
70
68
66
64
62
60
58
56
54
52
50
48
46
44
42
40
38
36
34
32
30
28
26
24
22
ENERGY mJ
90
110
130
150
COLLECTOR CURRENT-amps
Rev. gain
+ 25
0 50
* 75

Fig. A.4.11

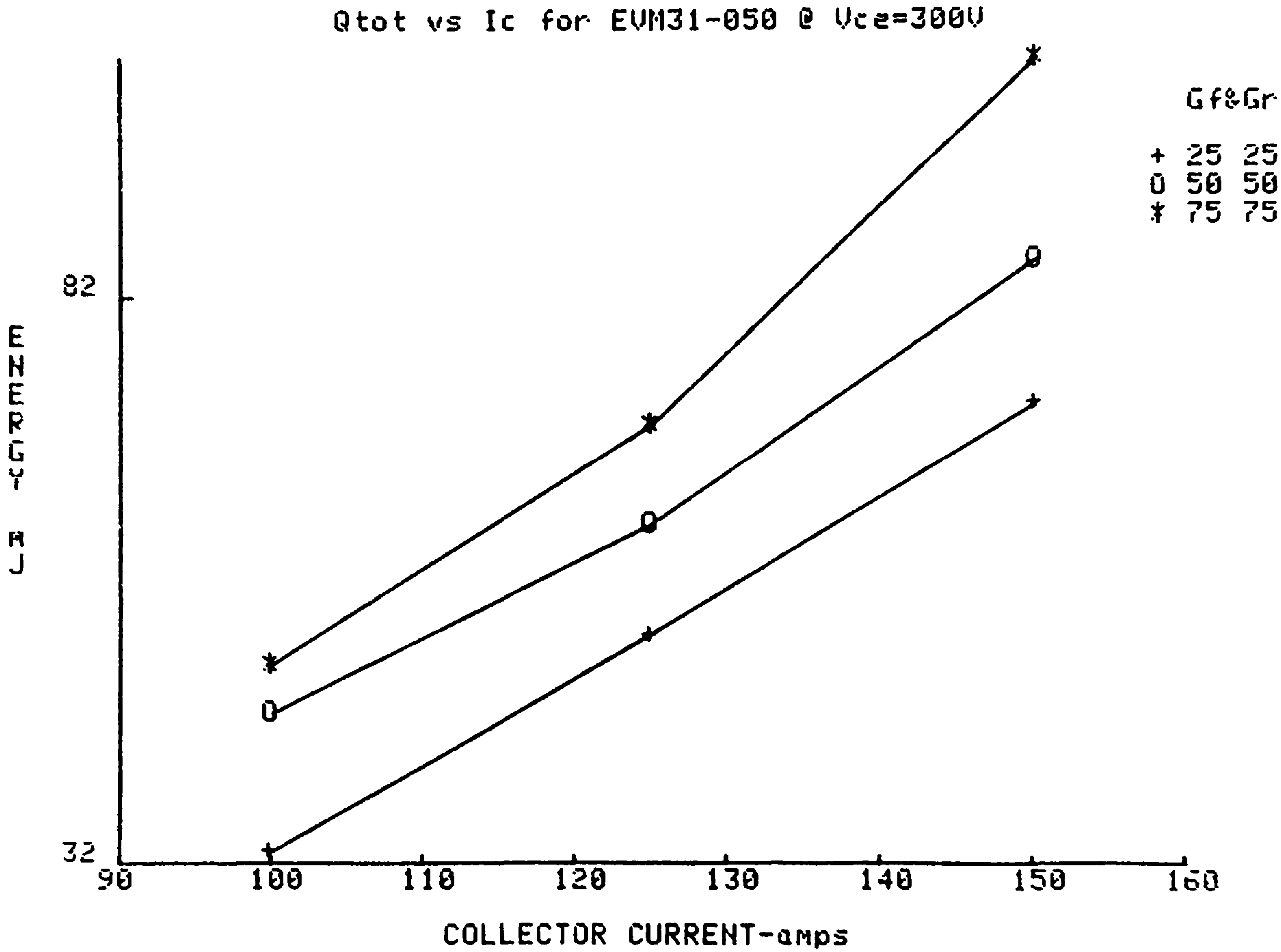

Qtot vs Ic for EVM31-050 @ Vce=300V
ENERGY- mJ
82
32
90
100
110
120
130
140
150
160
COLLECTOR CURRENT-amps
Gf&Gr
+ 25 25
0 50 50
* 75 75

Fig. A.4.12

Switching Loadline Characteristics: Vce vs. Ic
for Turn-on of Power Transistor with Inductive Load

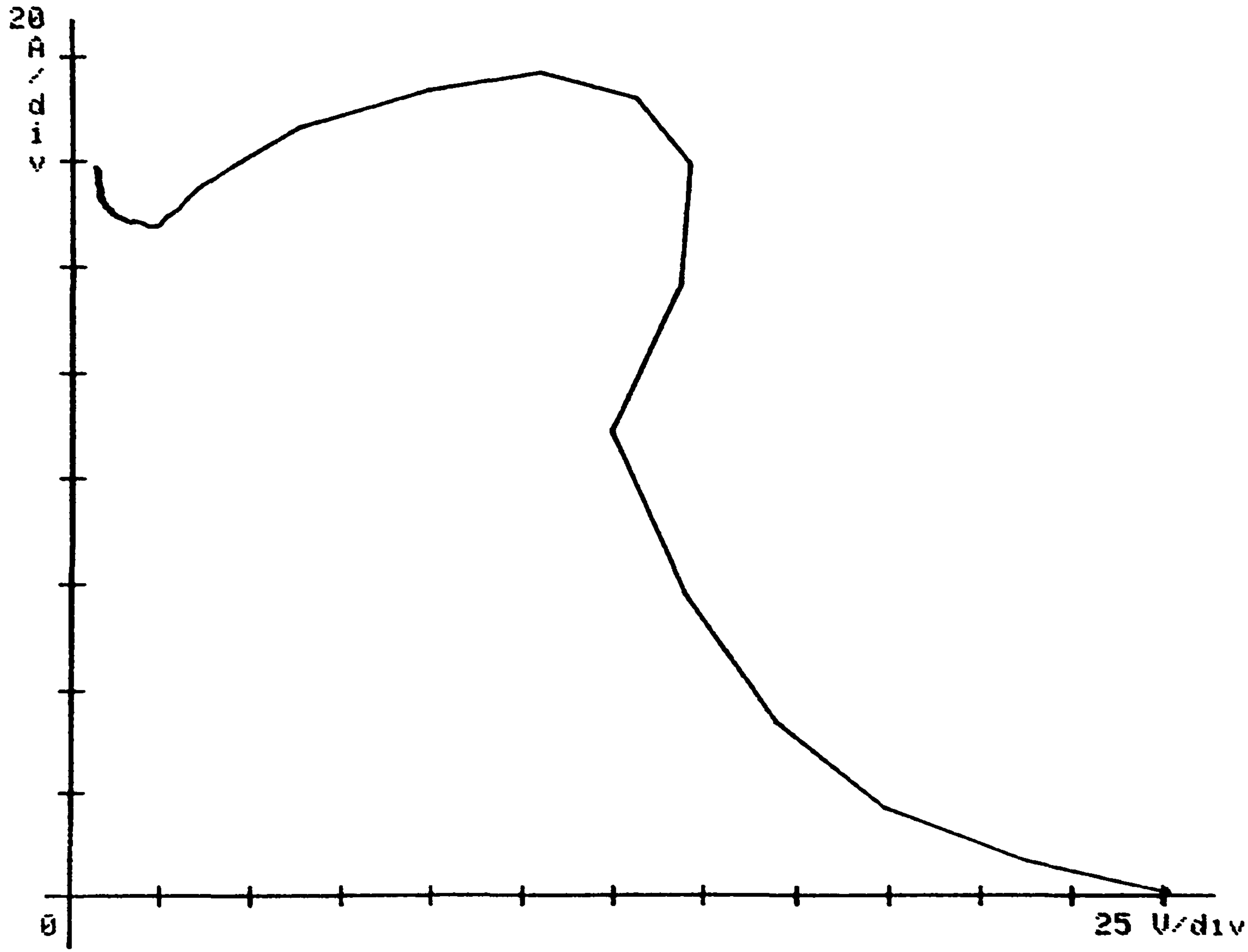

Fig. A.4.13

Switching Loadline Characteristics: Vce vs. Ic
for Turn-off of Power Trans. with Inductive Load

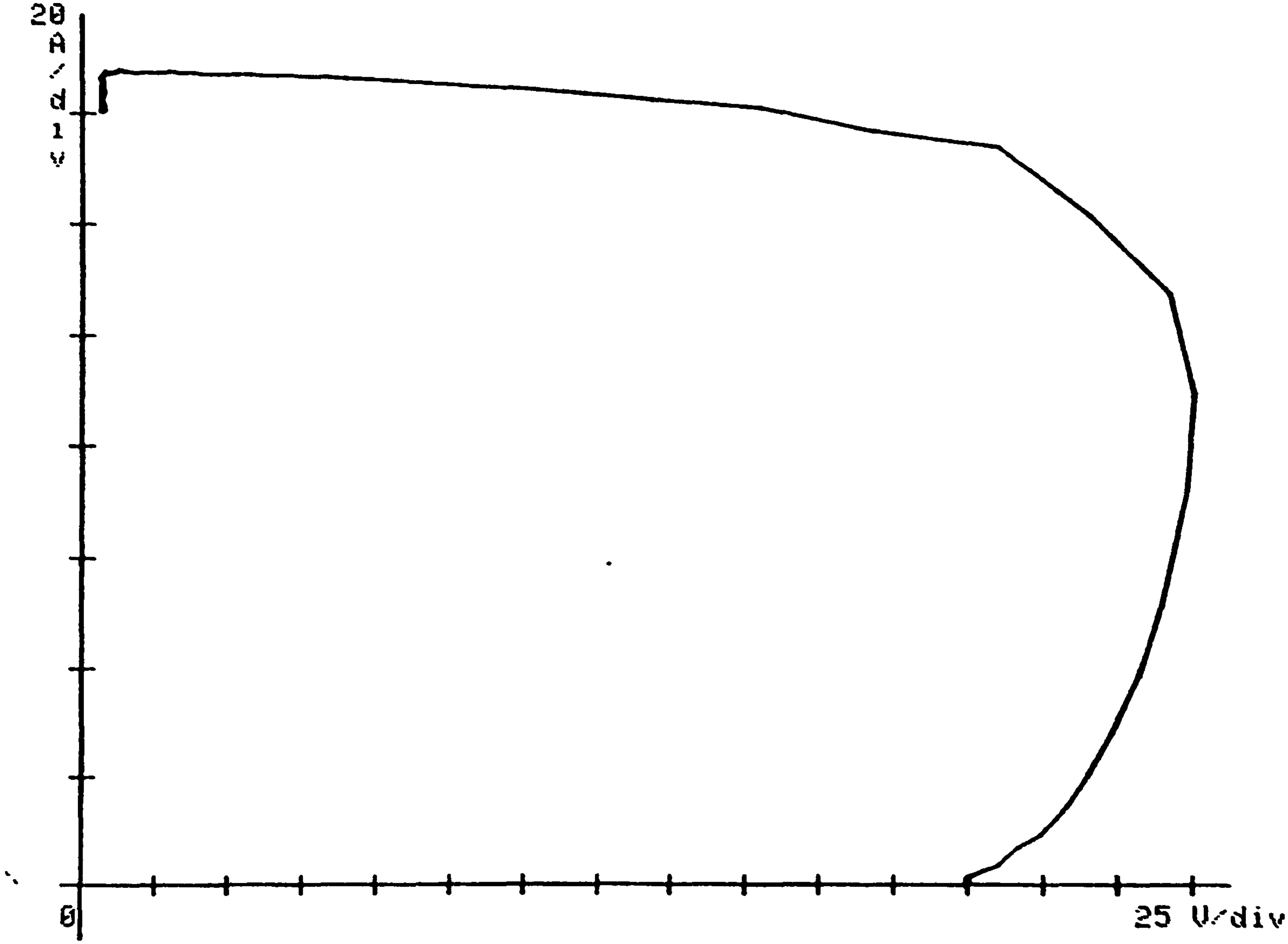

Fig. A.4.14

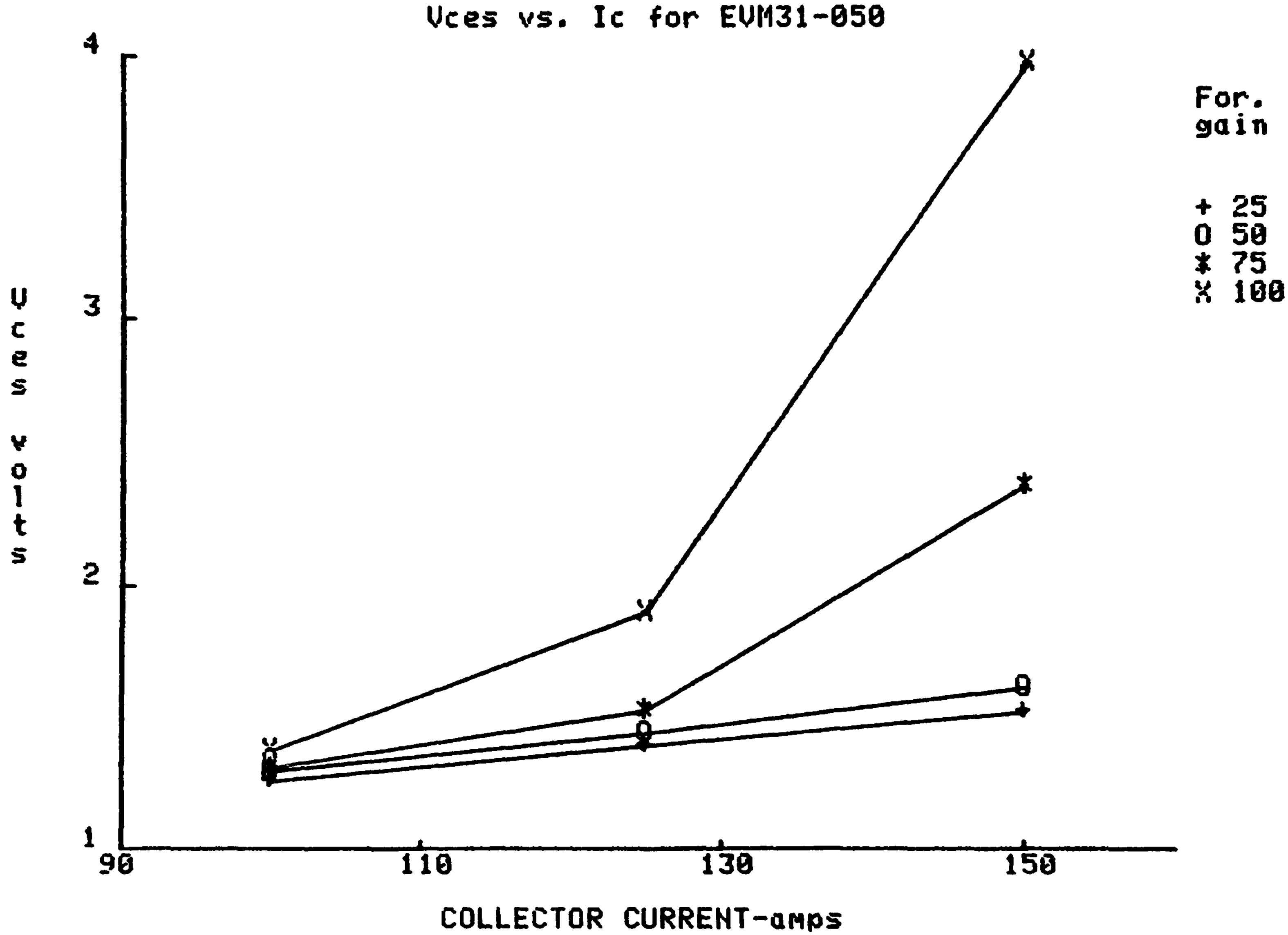
Vces vs. Ic for EVM31-050
Vces volts
4
3
2
1
90
110
130
150
COLLECTOR CURRENT-amps
For. gain
+ 25
O 50
* 75
X 100

Fig. A.4.15

Hfe vs Ic for EVM31-050 for Vce=3V @ Tc=35 C

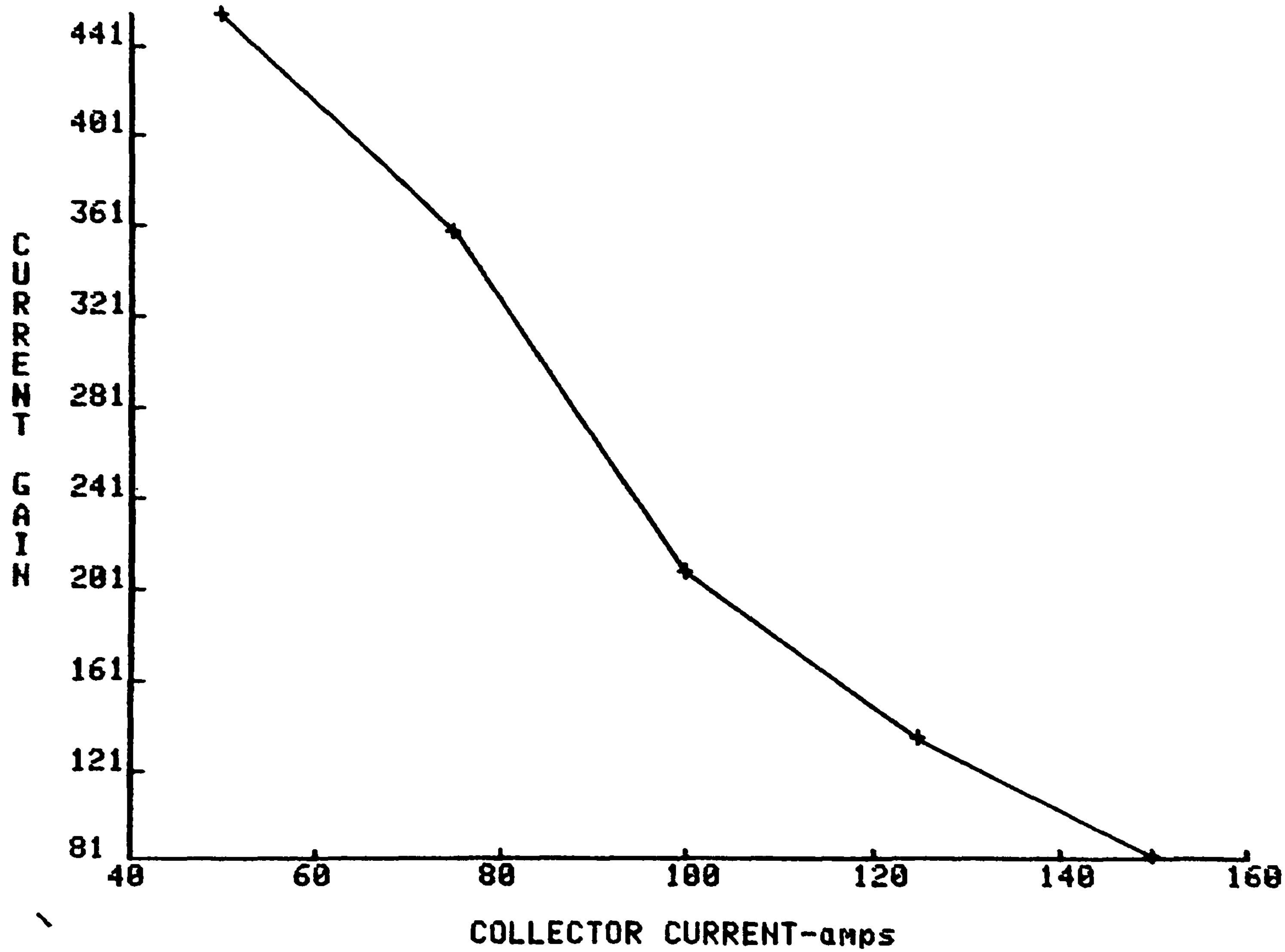

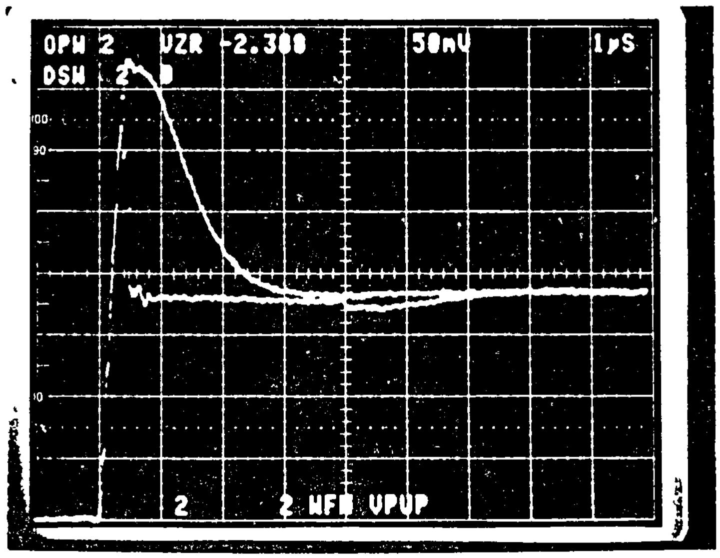

Fig. A.4.16 Diode recovery and dv/dt test for EVM31-050
Upper trace: Base open
Lower trace: Base reverse biased
(Scale: horizontal 1 µs/div; vertical 20 A/div)

A.5 Test Data for Mitsubishi QM150DY-H

Fig. A.5.1

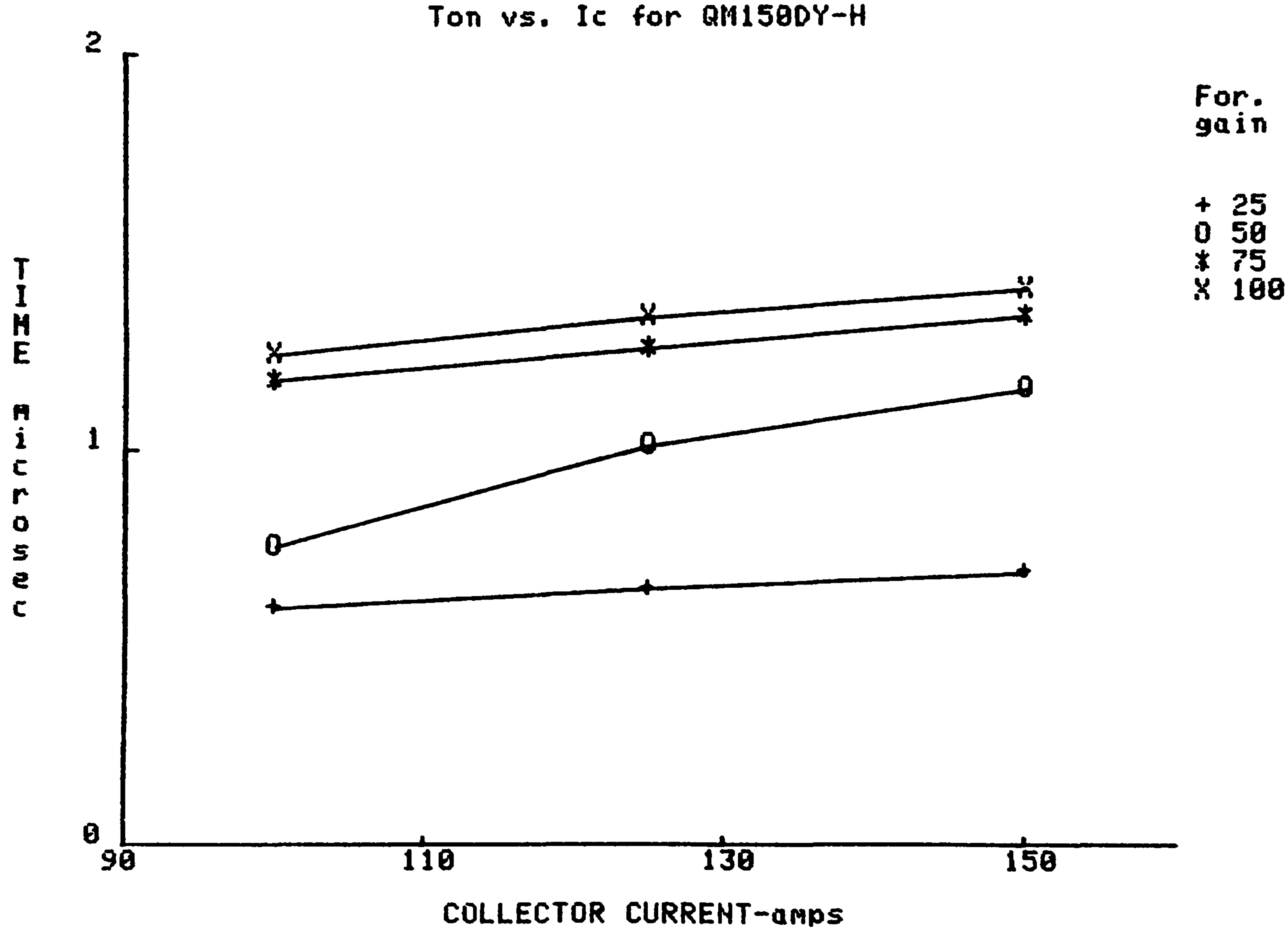
Ton vs. Ic for QM150DY-H
TIME microsec
2
1
0
90
110
130
150
COLLECTOR CURRENT-amps
For. gain
+ 25
O 50
* 75
X 100

Fig. A.5.2

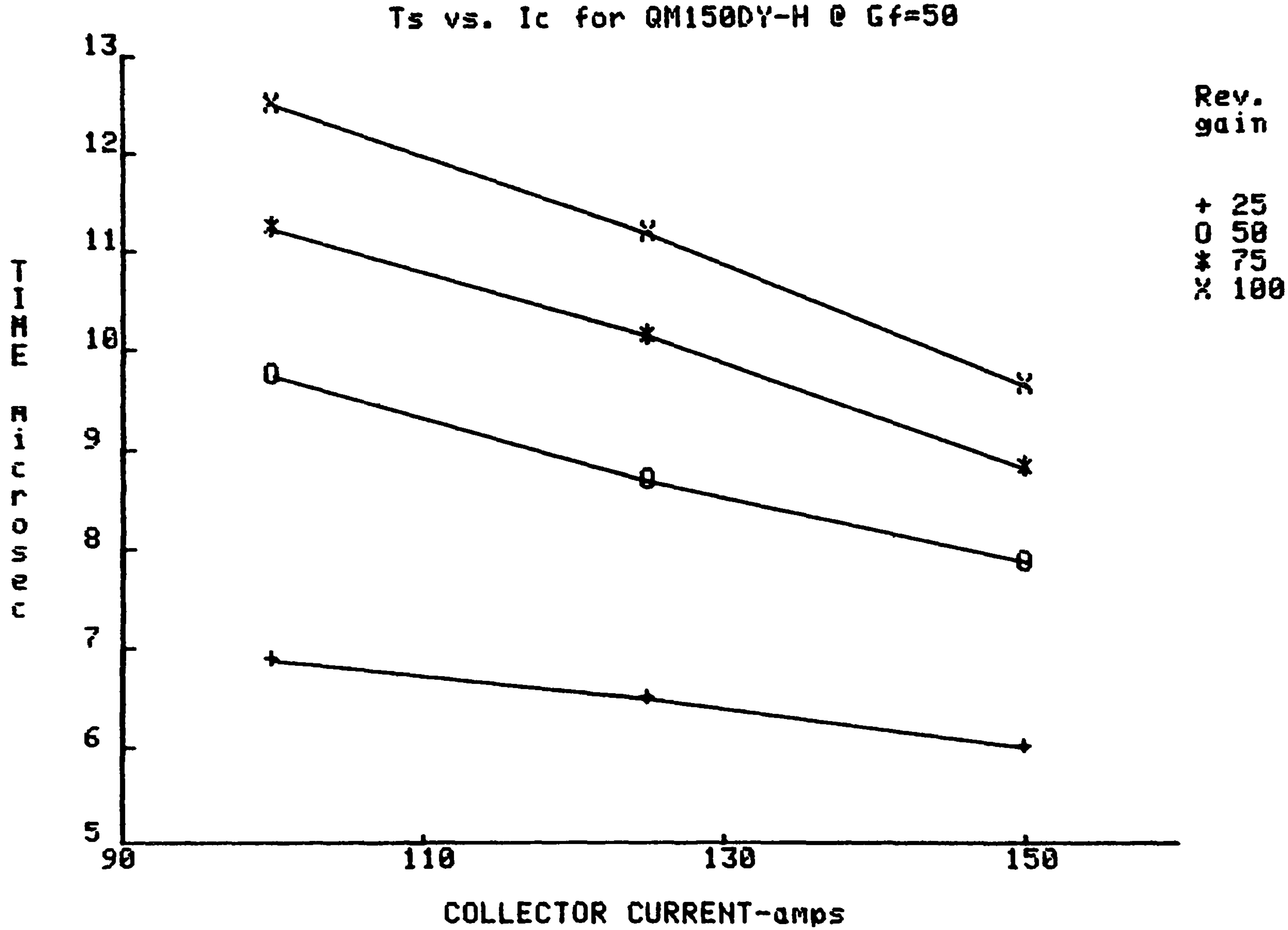

Ts vs. Ic for QM150DY-H @ Gf=50
TIME microsec
13
12
11
10
9
8
7
6
5
90
110
130
150
COLLECTOR CURRENT-amps
Rev. gain
+ 25
O 50
* 75
X 100

Fig. A.5.3

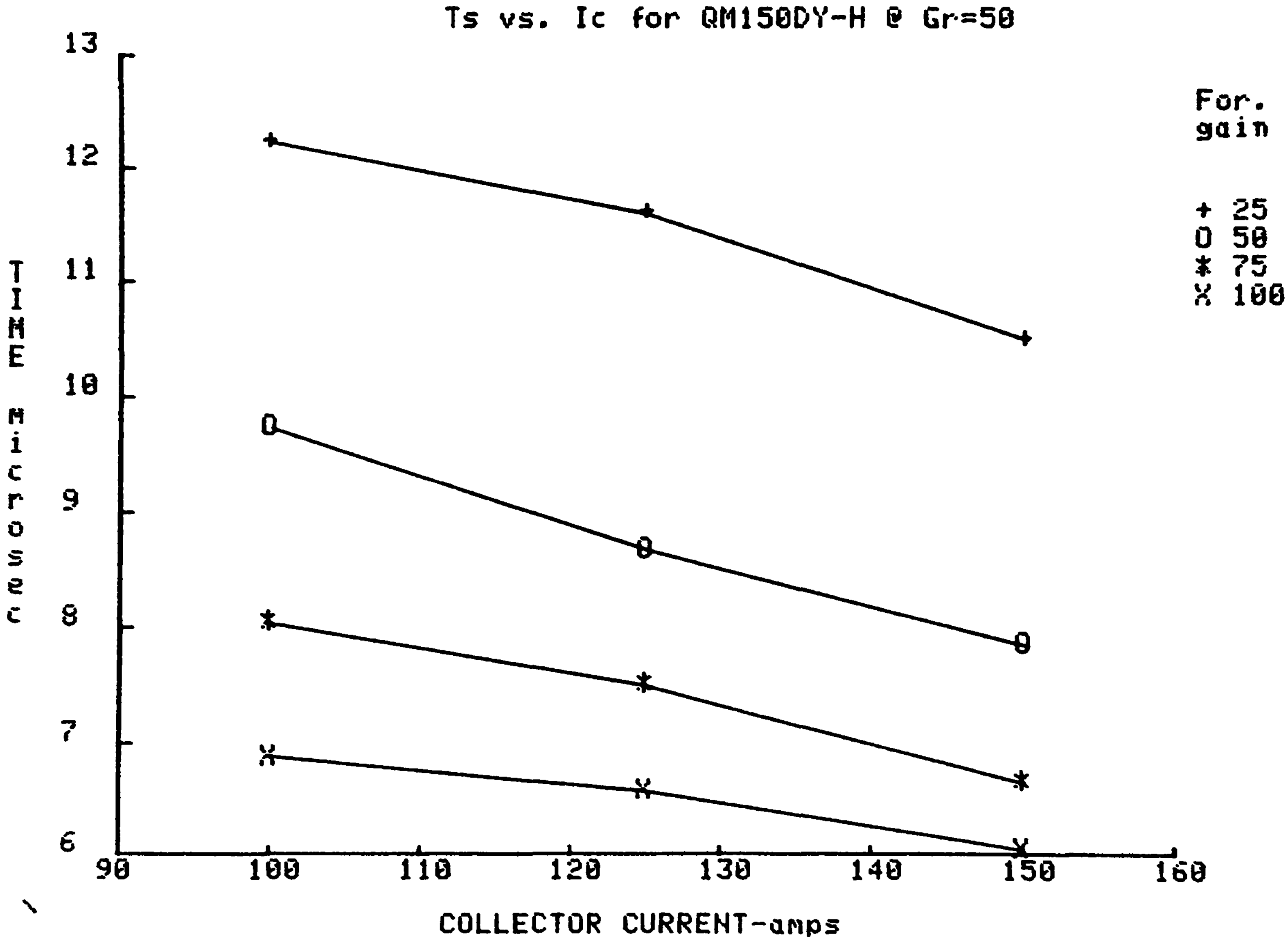
Ts vs. Ic for QM150DY-H @ Gr=50
TIME microsec
13
12
11
10
9
8
7
6
90
100
110
120
130
140
150
160
COLLECTOR CURRENT-amps
For. gain
+ 25
O 50
* 75
X 100

Fig. A.5.4

Tf vs. Ic for QM150DY-H @ Gf=50

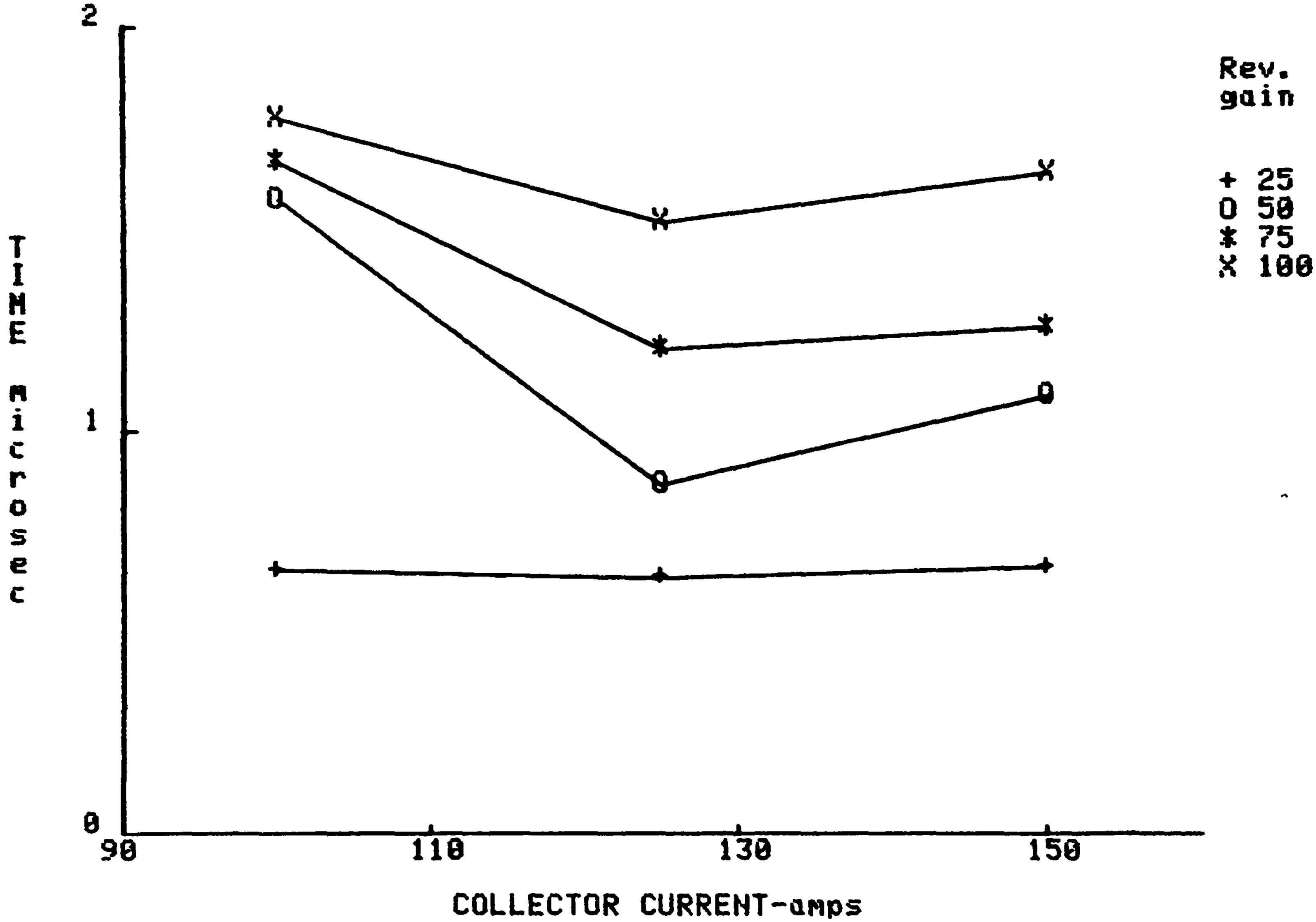

Fig. A.5.5

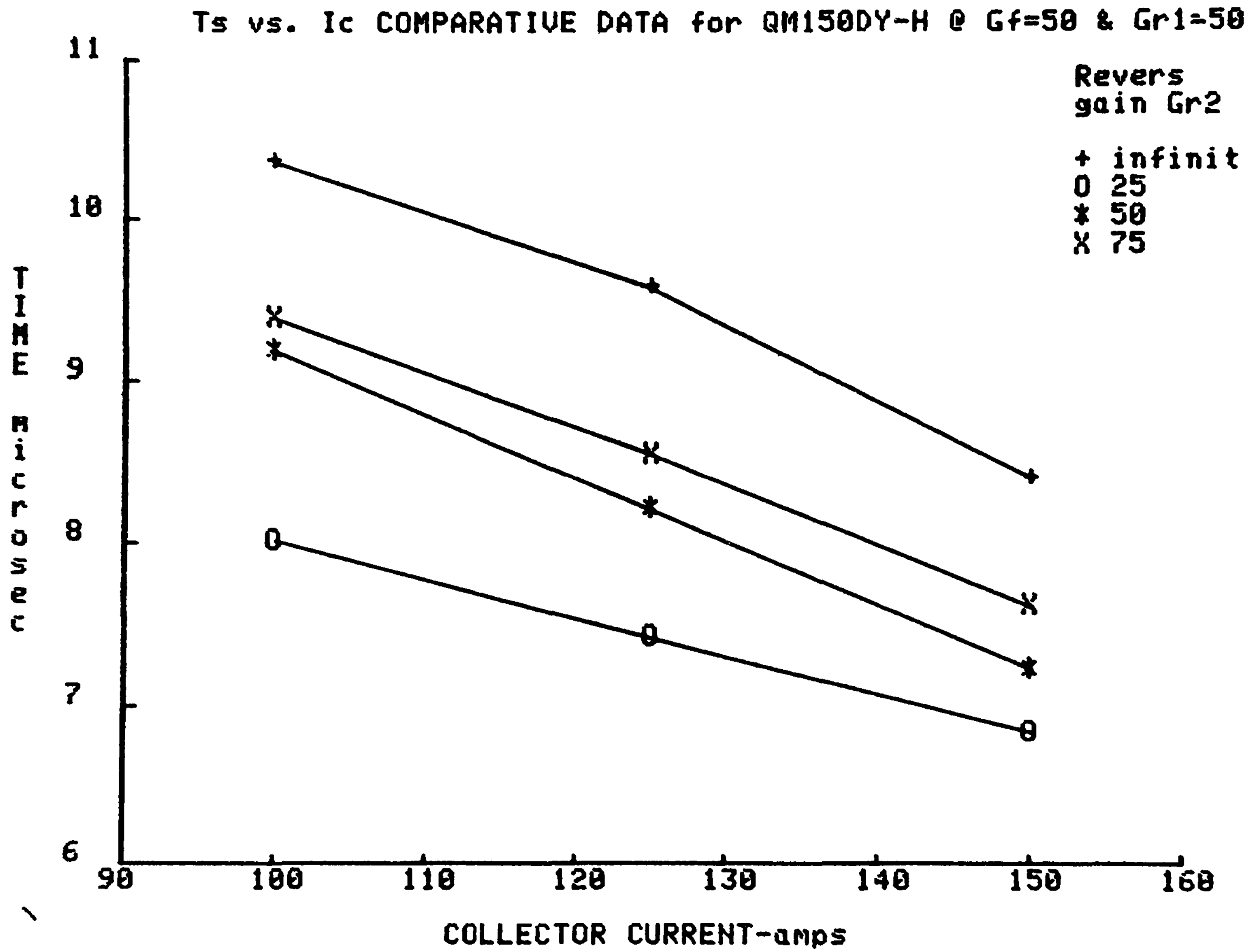

Ts vs. Ic COMPARATIVE DATA for QM150DY-H @ Gf=50 & Gr1=50
Revers gain Gr2
+ infinit
O 25
* 50
X 75
TIME microsec
11
10
9
8
7
6
90
100
110
120
130
140
150
160
COLLECTOR CURRENT-amps

Fig. A.5.6

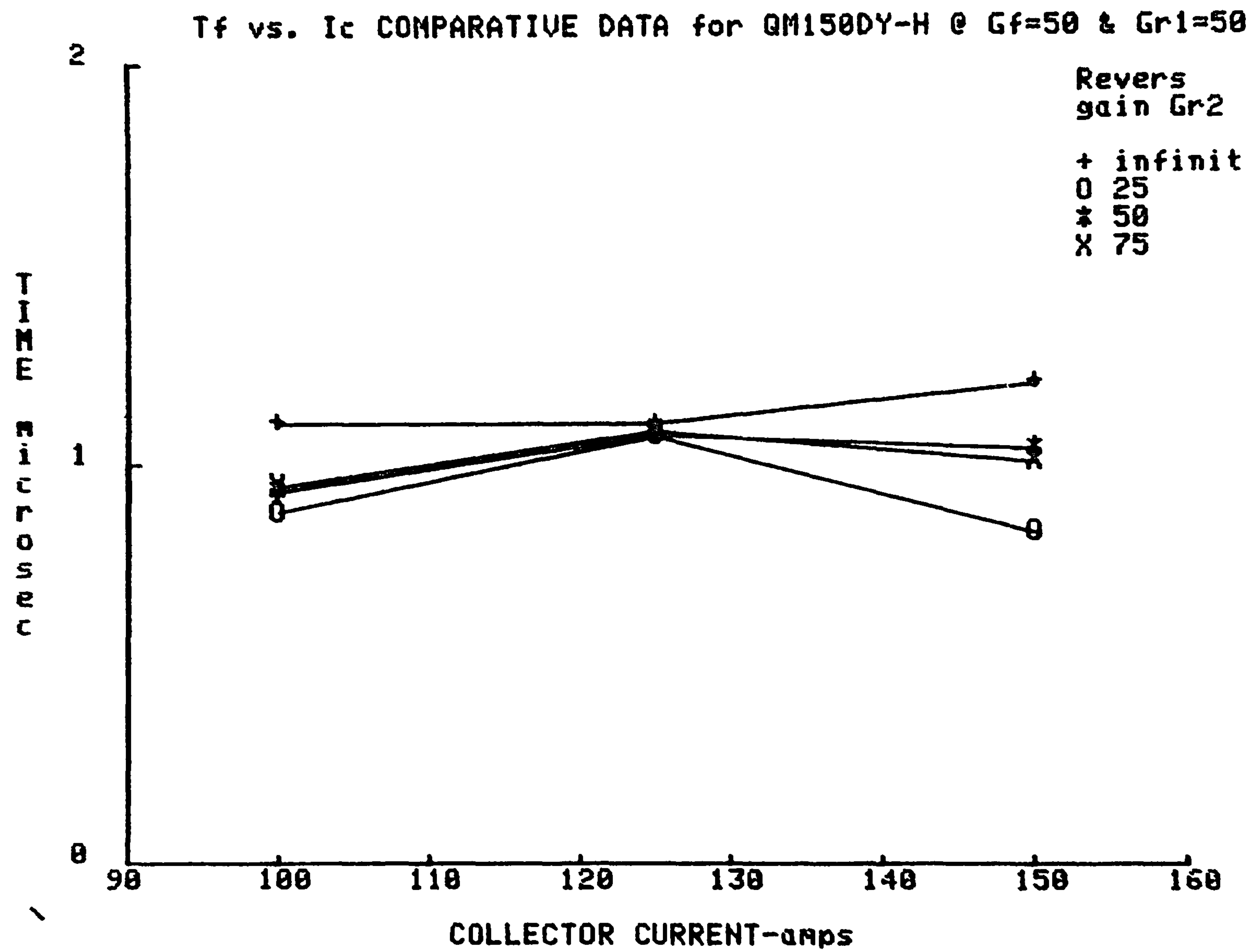

Tf vs. Ic COMPARATIVE DATA for QM150DY-H @ Gf=50 & Gr1=50
Revers
gain Gr2
+ infinit
0 25
* 50
X 75
TIME microsec
2
1
0
90
100
110
120
130
140
150
160
COLLECTOR CURRENT-amps

Fig. A.5.7

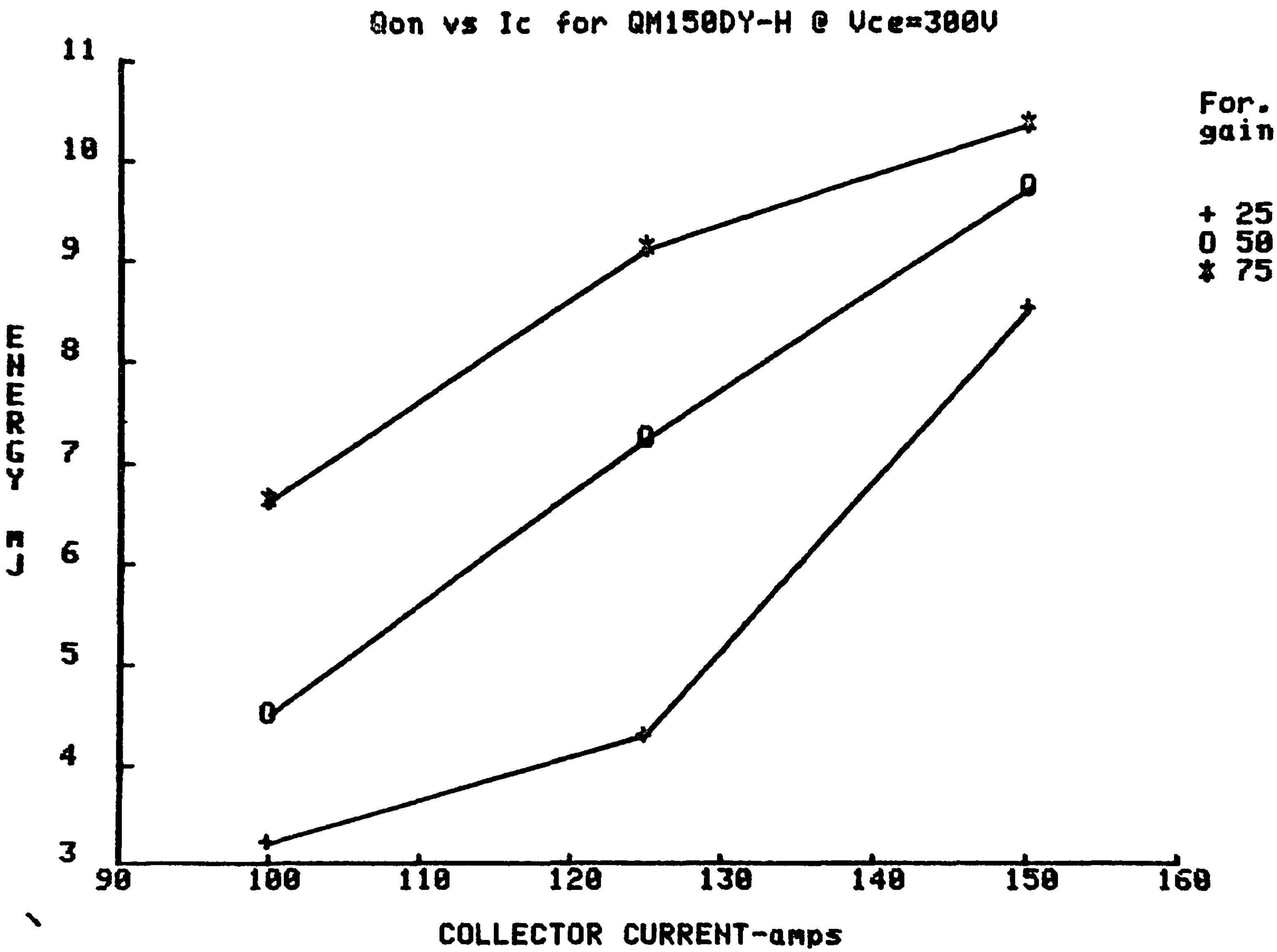
Qon vs Ic for QM150DY-H @ Vce=300V
ENERGY mJ
11
10
9
8
7
6
5
4
3
90
100
110
120
130
140
150
160
COLLECTOR CURRENT-amps
For. gain
+ 25
0 50
* 75

Fig A.5.8

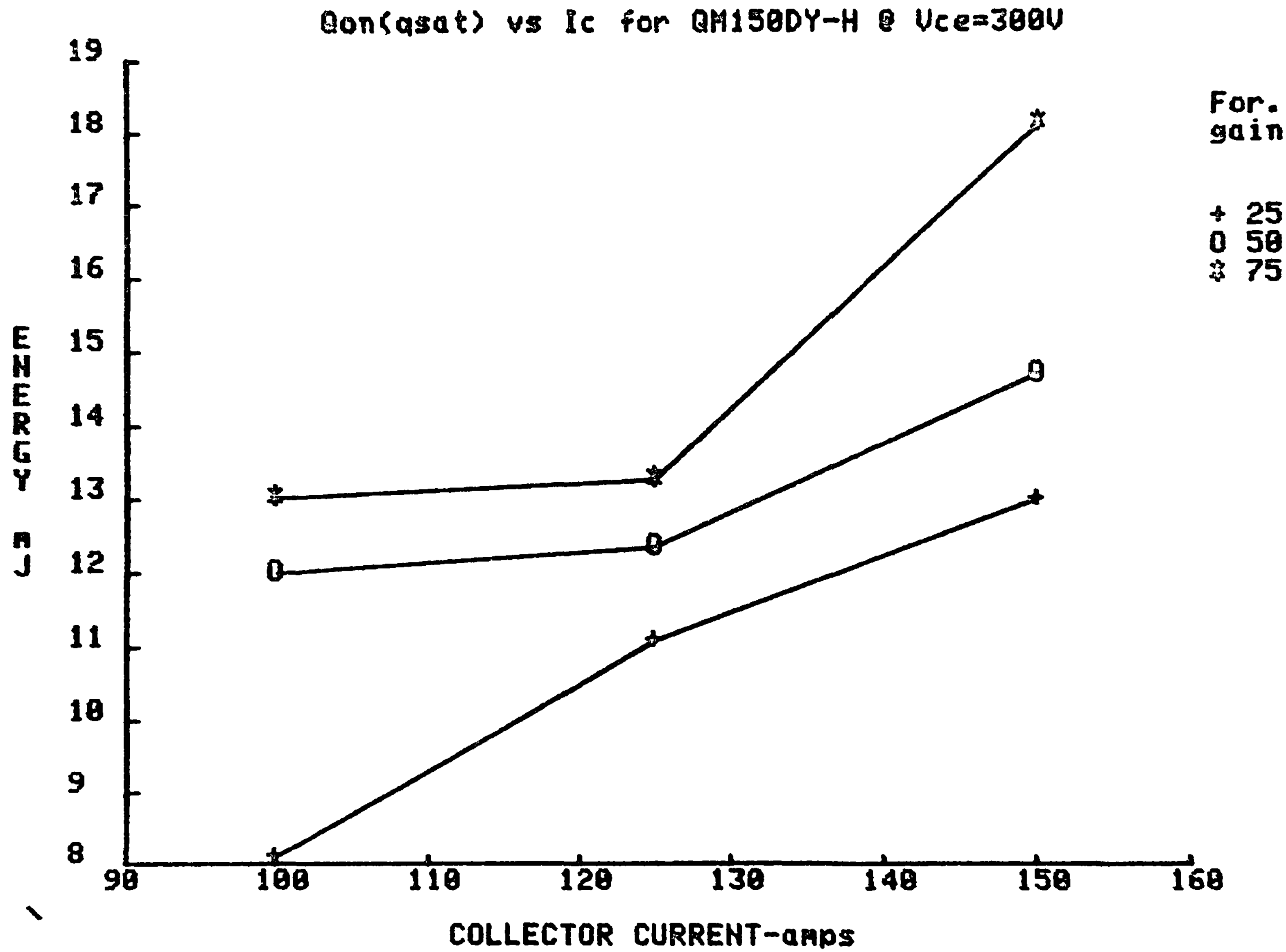

Qon(qsat) vs Ic for QM150DY-H @ Vce=300V
ENERGY mJ
19
18
17
16
15
14
13
12
11
10
9
8
90
100
110
120
130
140
150
160
COLLECTOR CURRENT-amps
For. gain
+ 25
0 50
☆ 75

Fig A.5.9

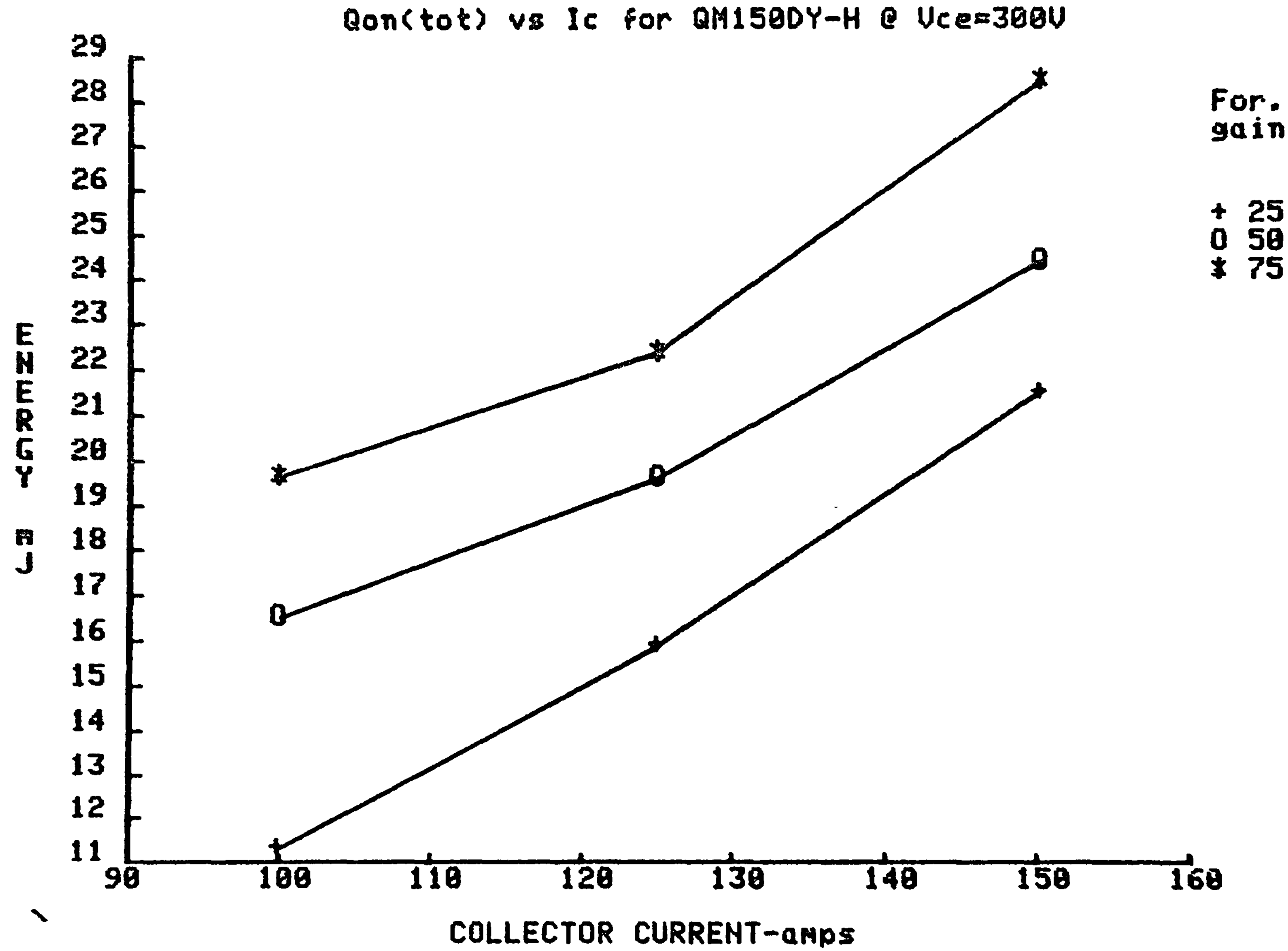

Qon(tot) vs Ic for QM150DY-H @ Vce=300V
ENERGY mJ
COLLECTOR CURRENT-amps
For. gain
+ 25
0 50
* 75
29
28
27
26
25
24
23
22
21
20
19
18
17
16
15
14
13
12
11
90
100
110
120
130
140
150
160

Fig. A.5.10

Qoff vs Ic for QM150DY-H @ Vce=300V

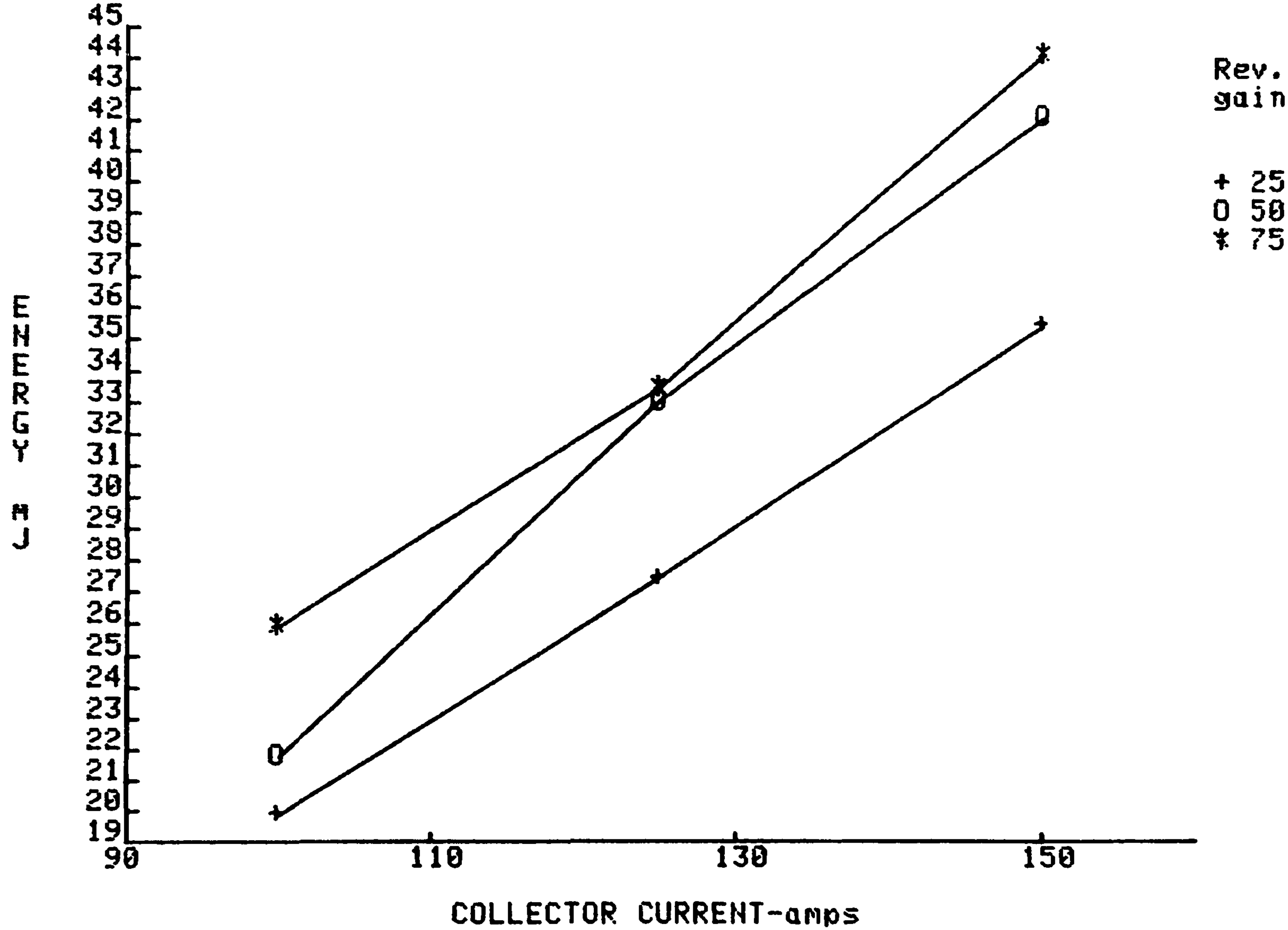

Fig. A.5.11

Qtot vs Ic for QM150DY-H @ Vce=300V

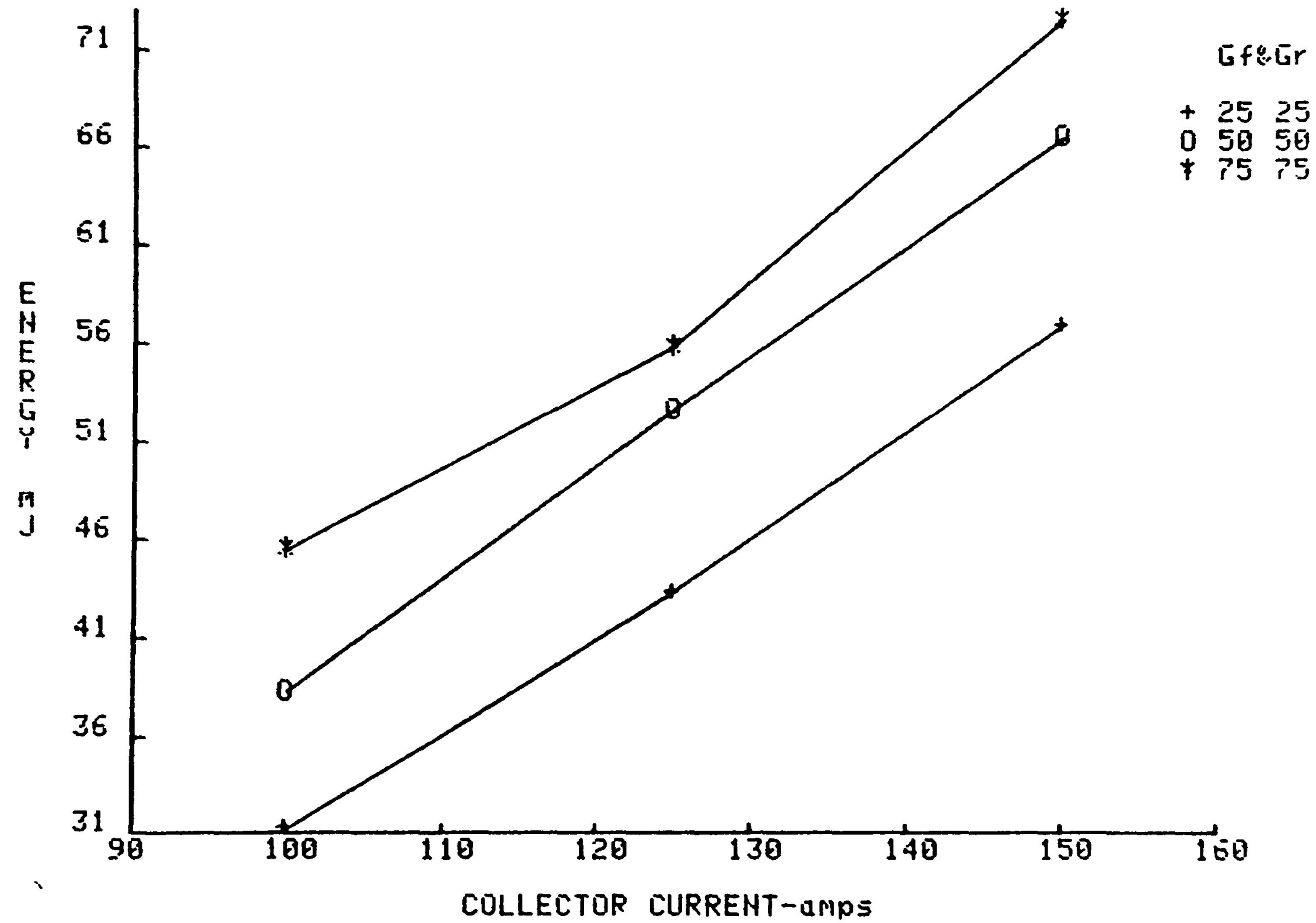

Fig. A.5.12

Switching Loadline Characteristics: Vce vs. Ic
for Turn-on of Power Transistor with Inductive Load

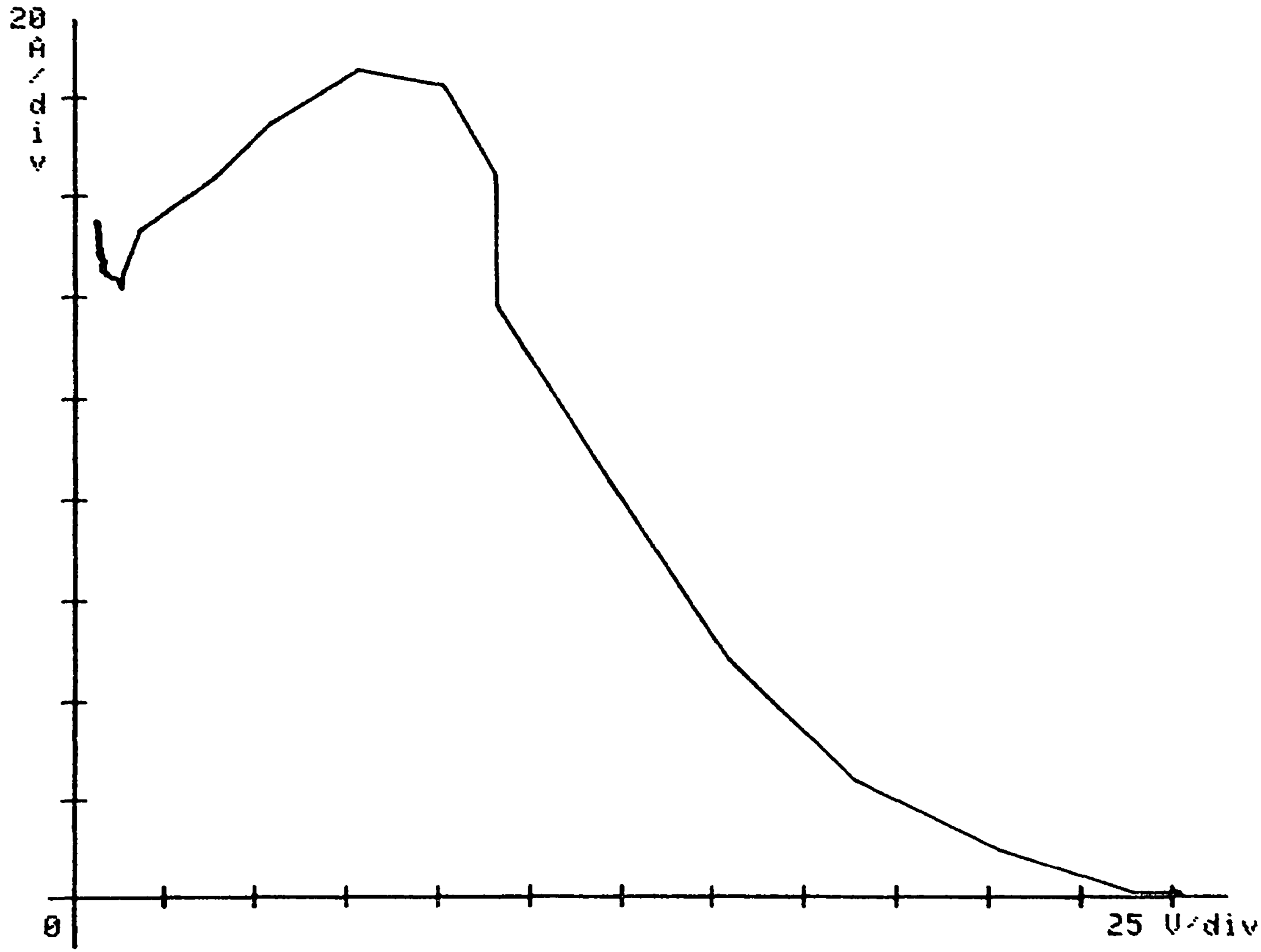

Fig. A.5.13

Switching Loadline Characteristics: Vce vs. Ic
for Turn-off of Power Trans. with Inductive Load

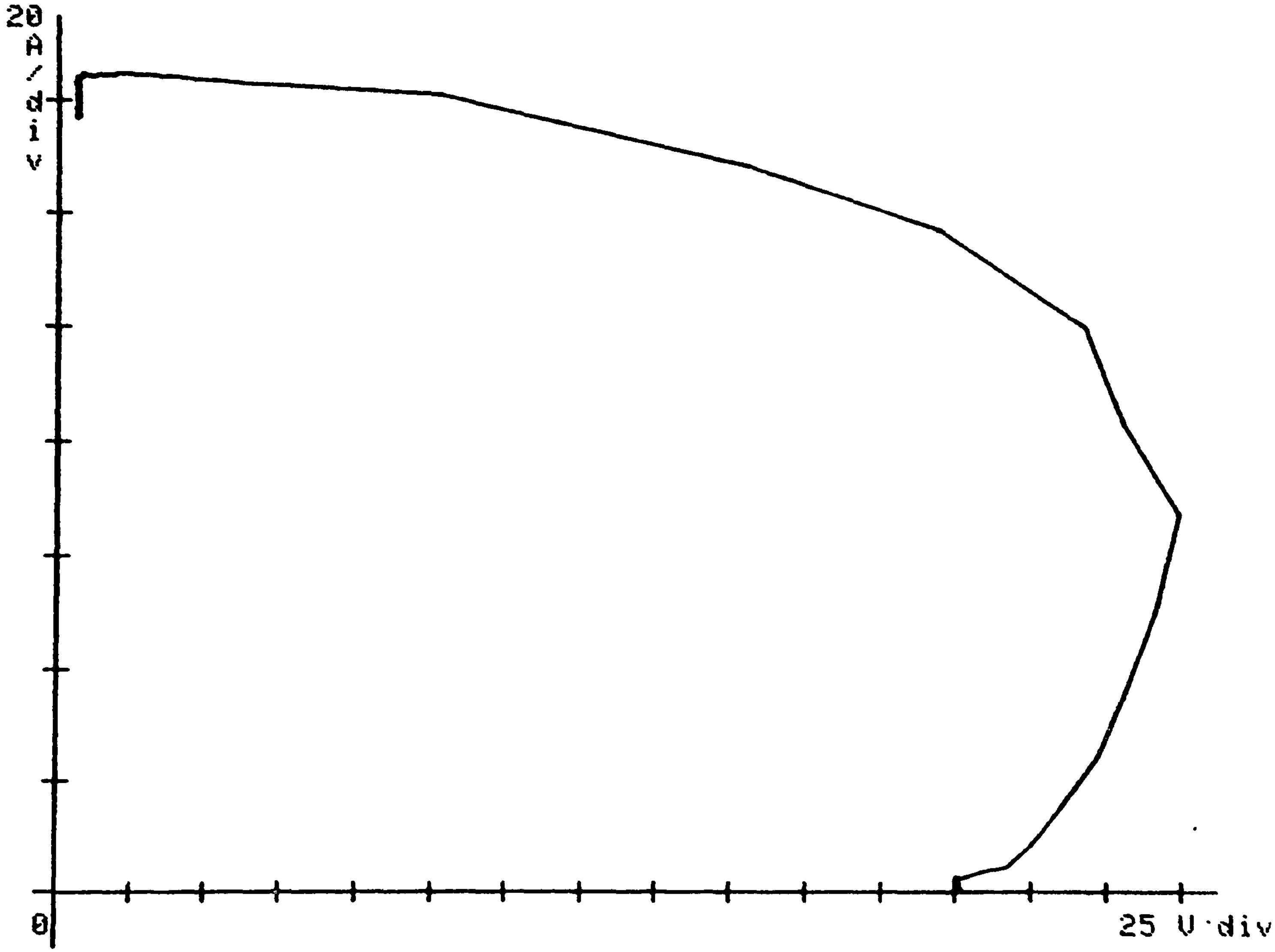

Fig. A.5.14

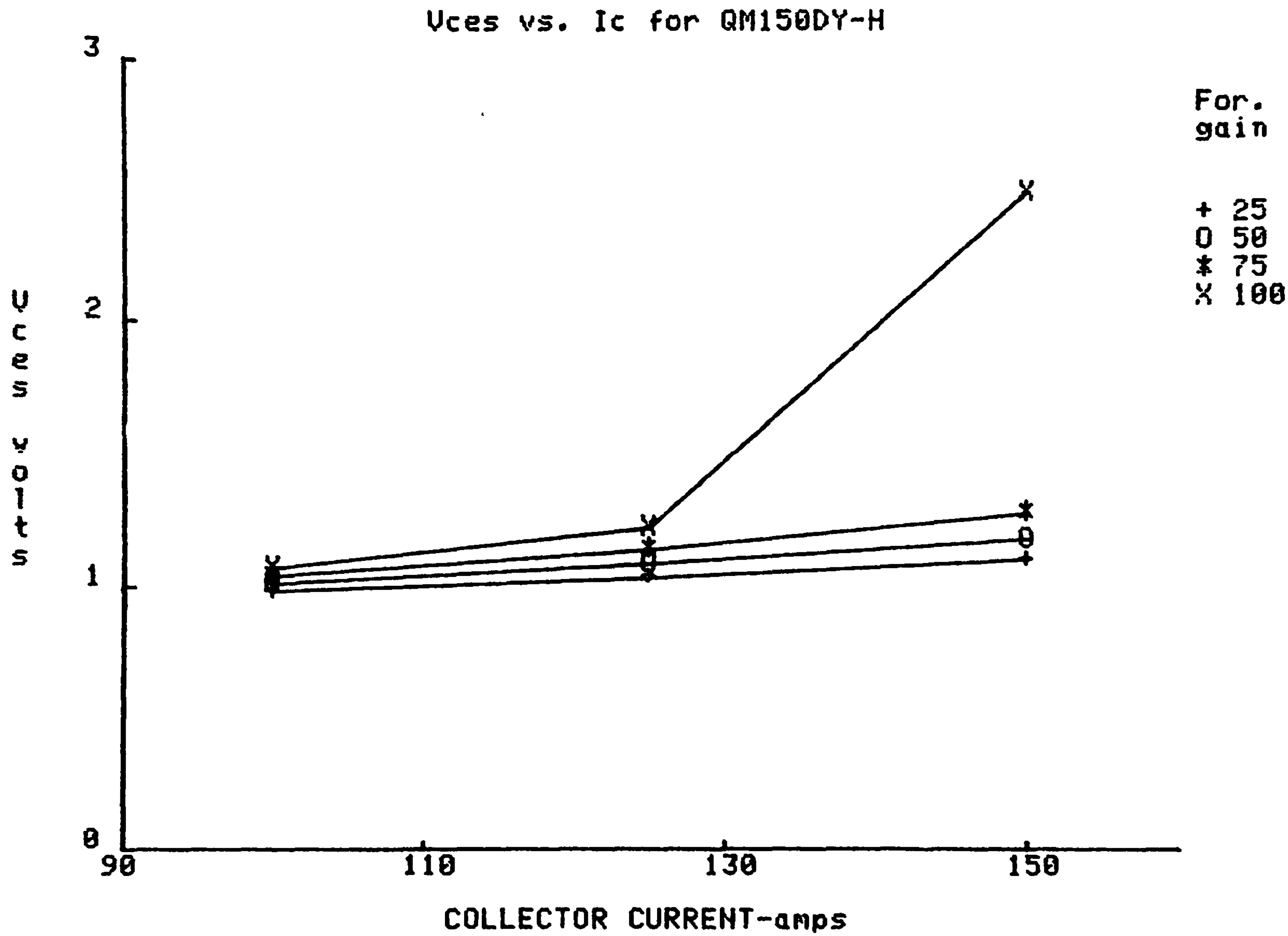

Vces vs. Ic for QM150DY-H
Vces volts
COLLECTOR CURRENT-amps
0
1
2
3
90
110
130
150
For. gain
+ 25
O 50
* 75
X 100

A.81

Fig. A.5.15

Hfe vs Ic for QM150DY-H for Vce=3V @ Tc=35 C

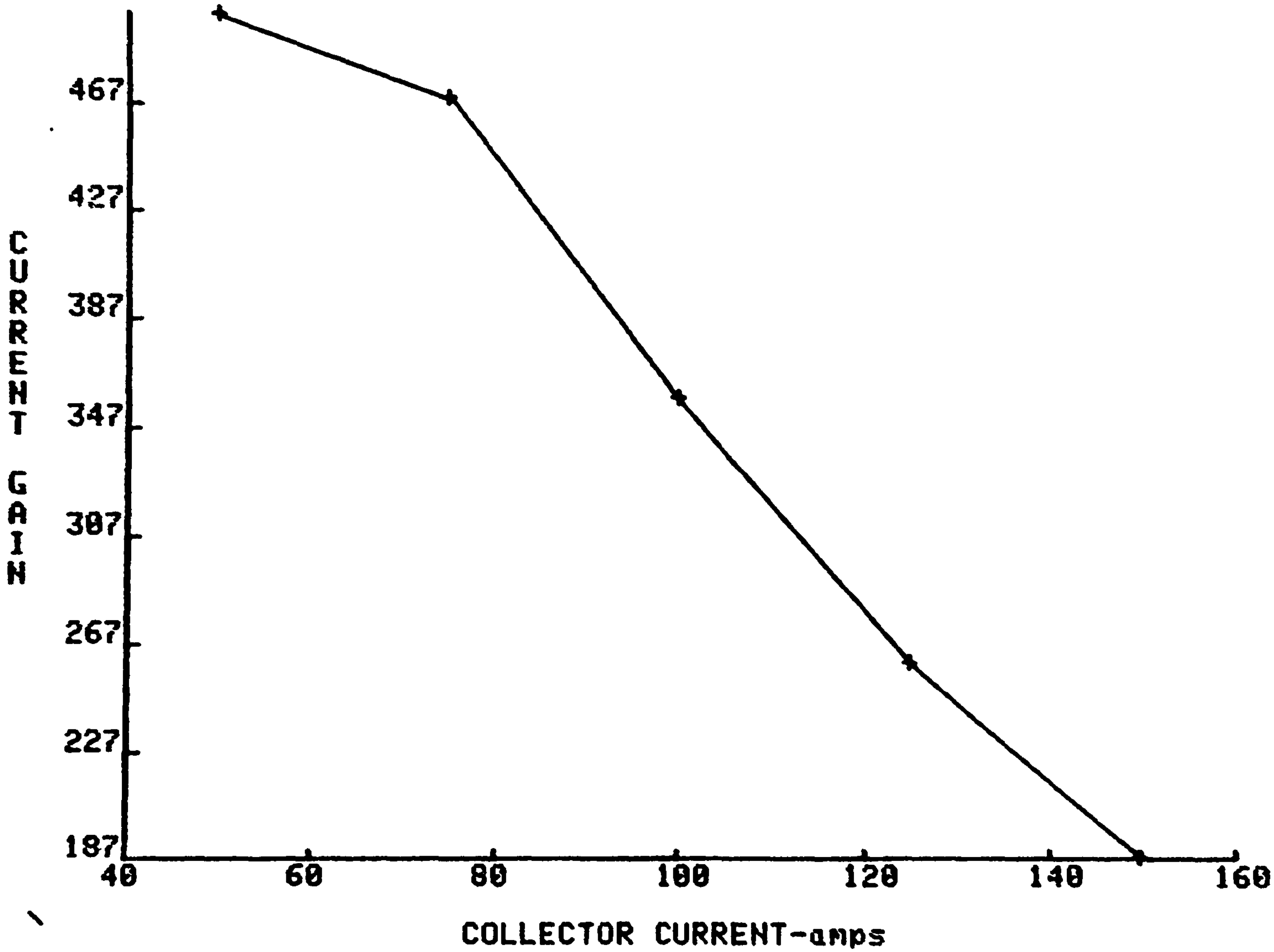

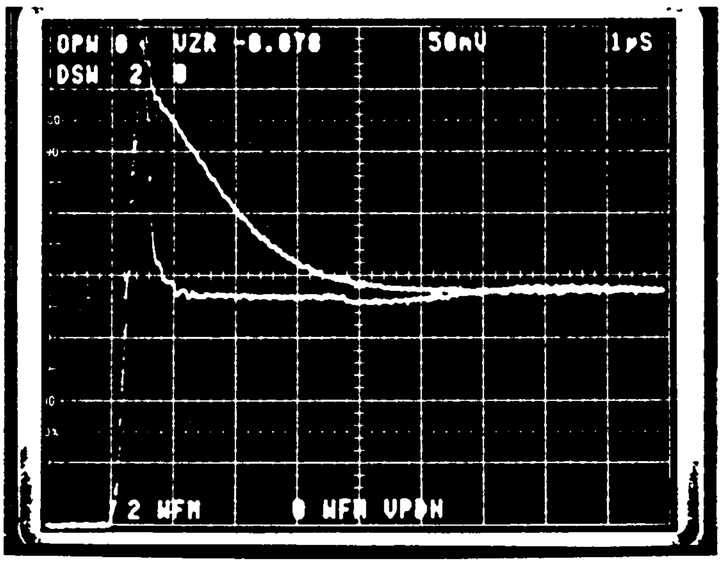

Fig. A.5.16 Diode recovery and dv/dt test for QM150DY-H

Upper trace: Base open

Lower trace: Base reverse biased

(Scale: horizontal 1 μs/div; vertical 20 A/div)

A.6 Test Data for Mitsubishi QM300HA-H

Fig. A.6.1

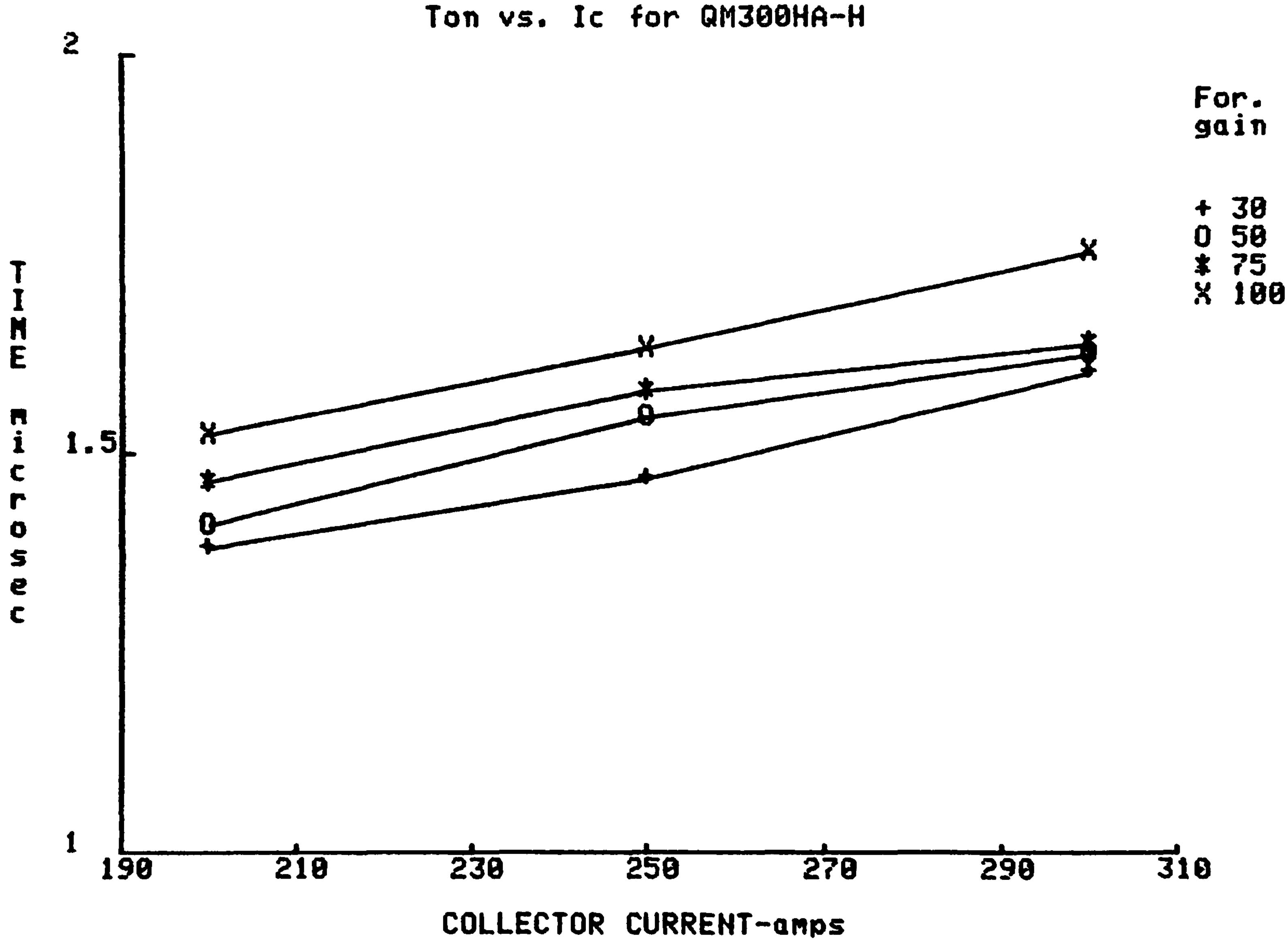
Ton vs. Ic for QM300HA-H
2
1.5
1
TIME microsec
190
210
230
250
270
290
310
COLLECTOR CURRENT-amps
For. gain
+ 30
O 50
* 75
X 100

Fig. A.6.2

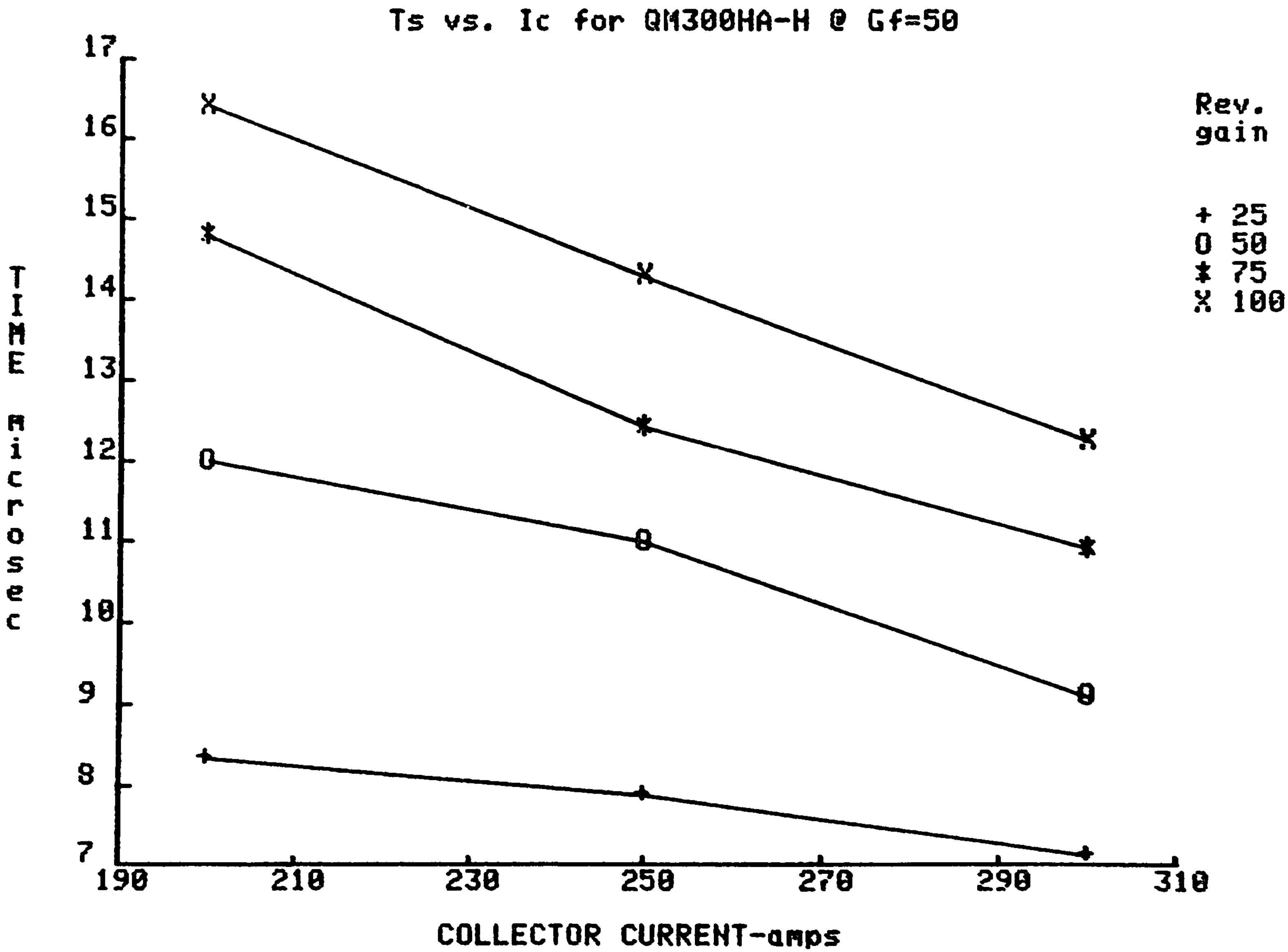
Ts vs. Ic for QM300HA-H @ Gf=50
TIME microsec
17
16
15
14
13
12
11
10
9
8
7
190
210
230
250
270
290
310
COLLECTOR CURRENT-amps
Rev. gain
+ 25
0 50
* 75
X 100

Fig. A.6.3

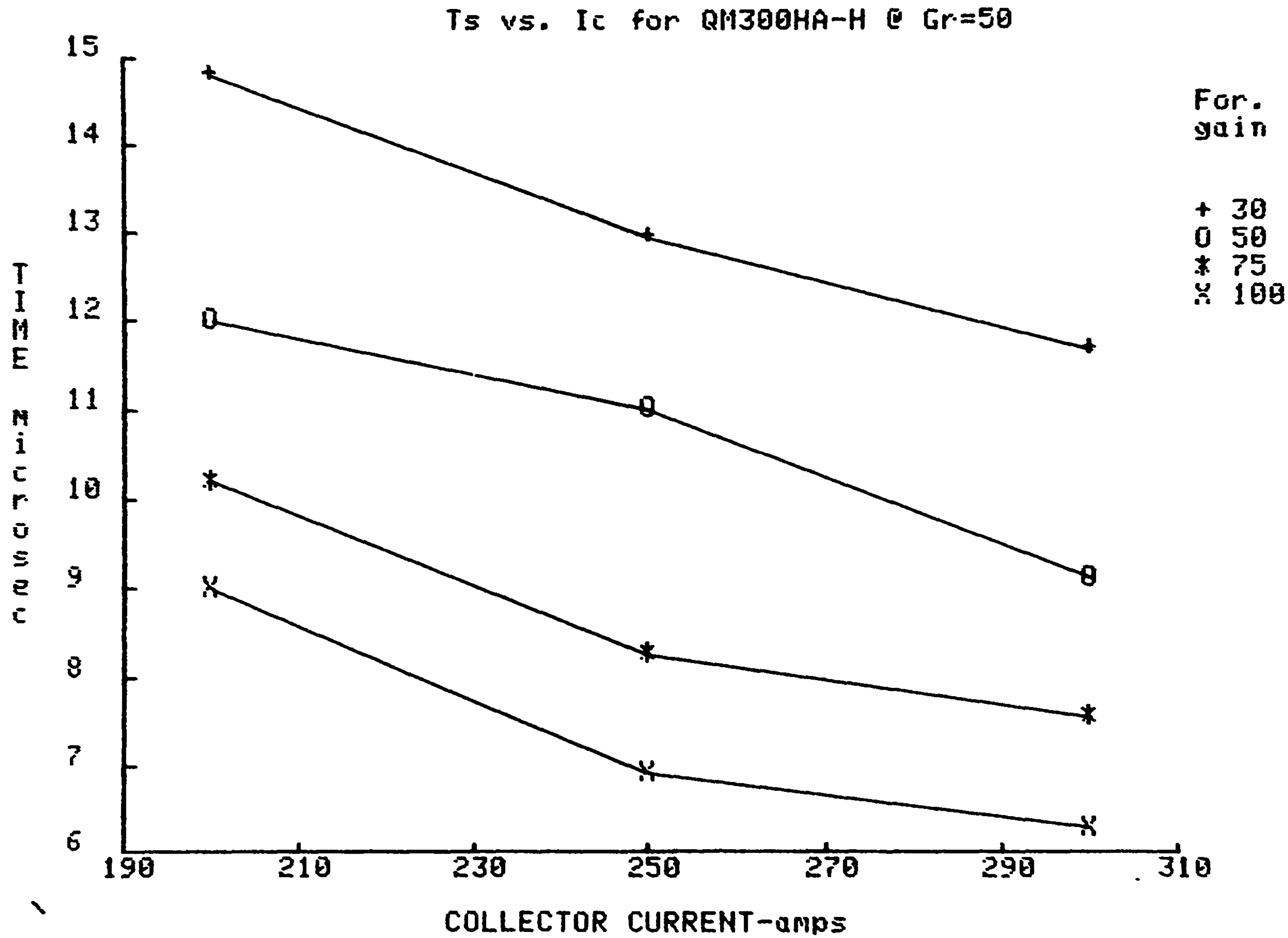
Ts vs. Ic for QM300HA-H @ Gr=50
TIME Microsec
15
14
13
12
11
10
9
8
7
6
190
210
230
250
270
290
310
COLLECTOR CURRENT-amps
For.
gain
+ 30
O 50
* 75
X 100

Fig. A.6.4

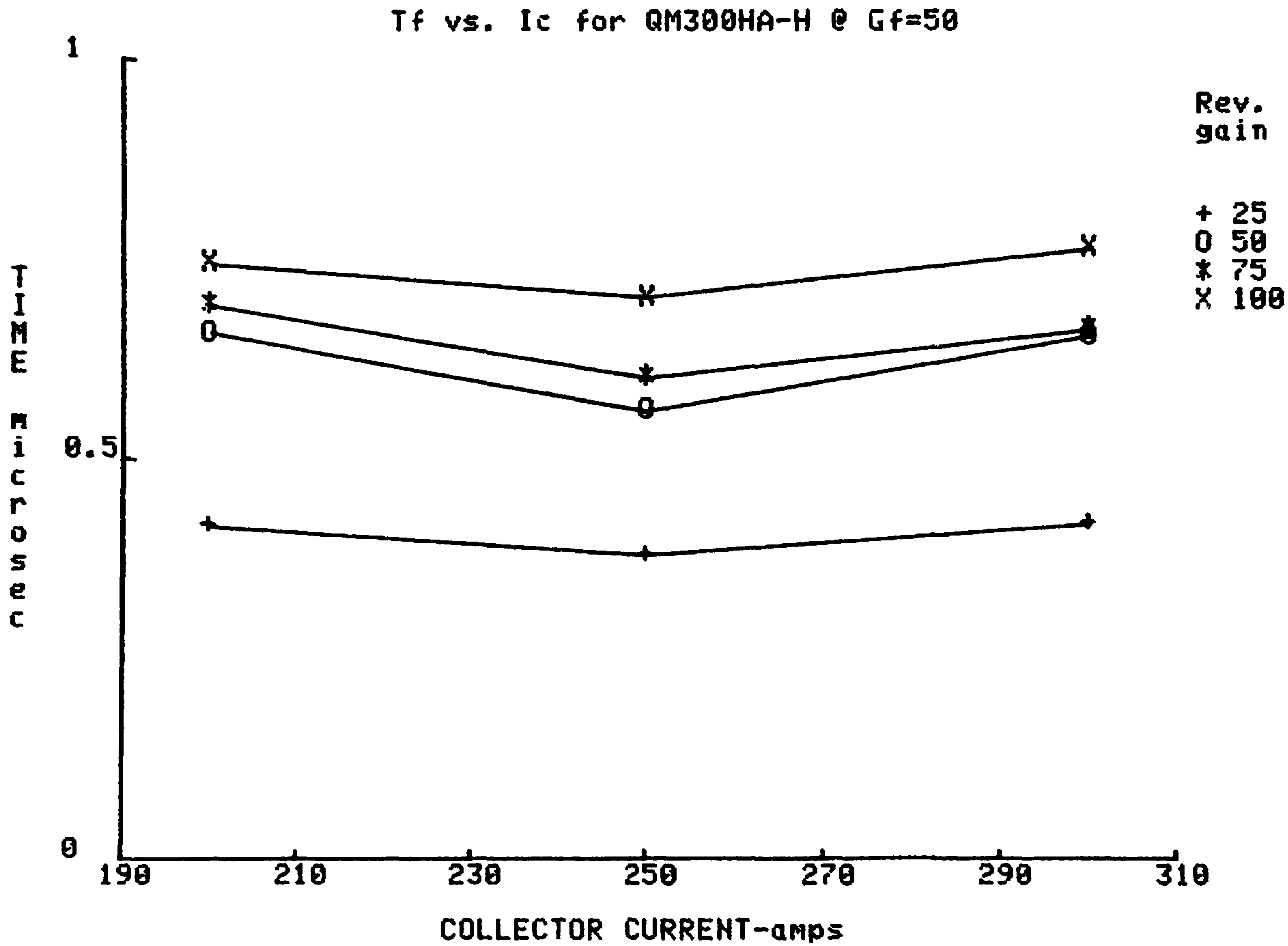
Tf vs. Ic for QM300HA-H @ Gf=50
1
0.5
0
TIME microsec
190
210
230
250
270
290
310
COLLECTOR CURRENT-amps
Rev. gain
+ 25
O 50
* 75
X 100

Fig. A.6.7

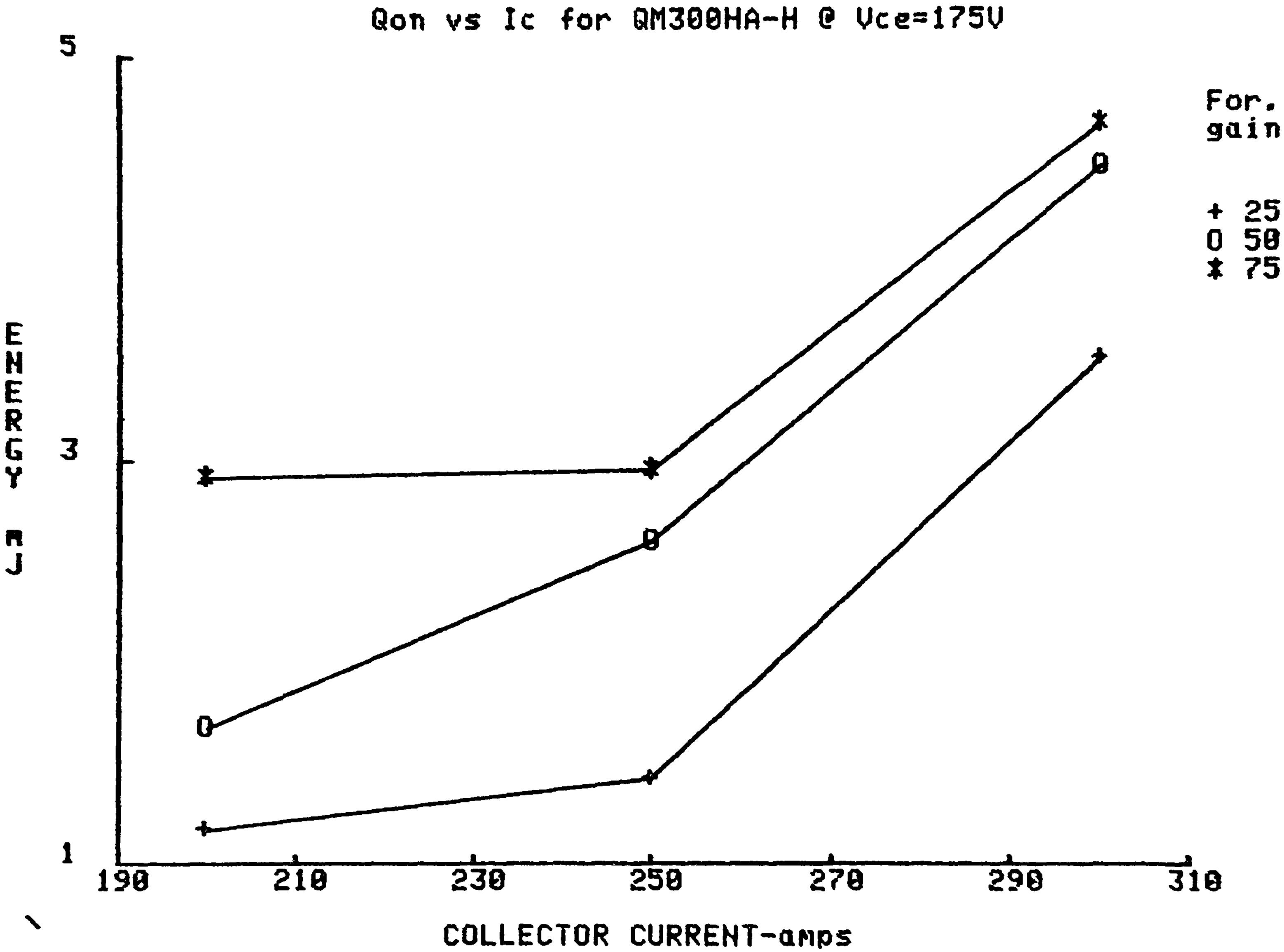

Qon vs Ic for QM300HA-H @ Vce=175V
ENERGY mJ
5
3
1
190
210
230
250
270
290
310
COLLECTOR CURRENT-amps
For. gain
+ 25
0 50
* 75

Fig. A.6.8

Qon(qsat) vs Ic for QM300HA-H @ Vce=175V

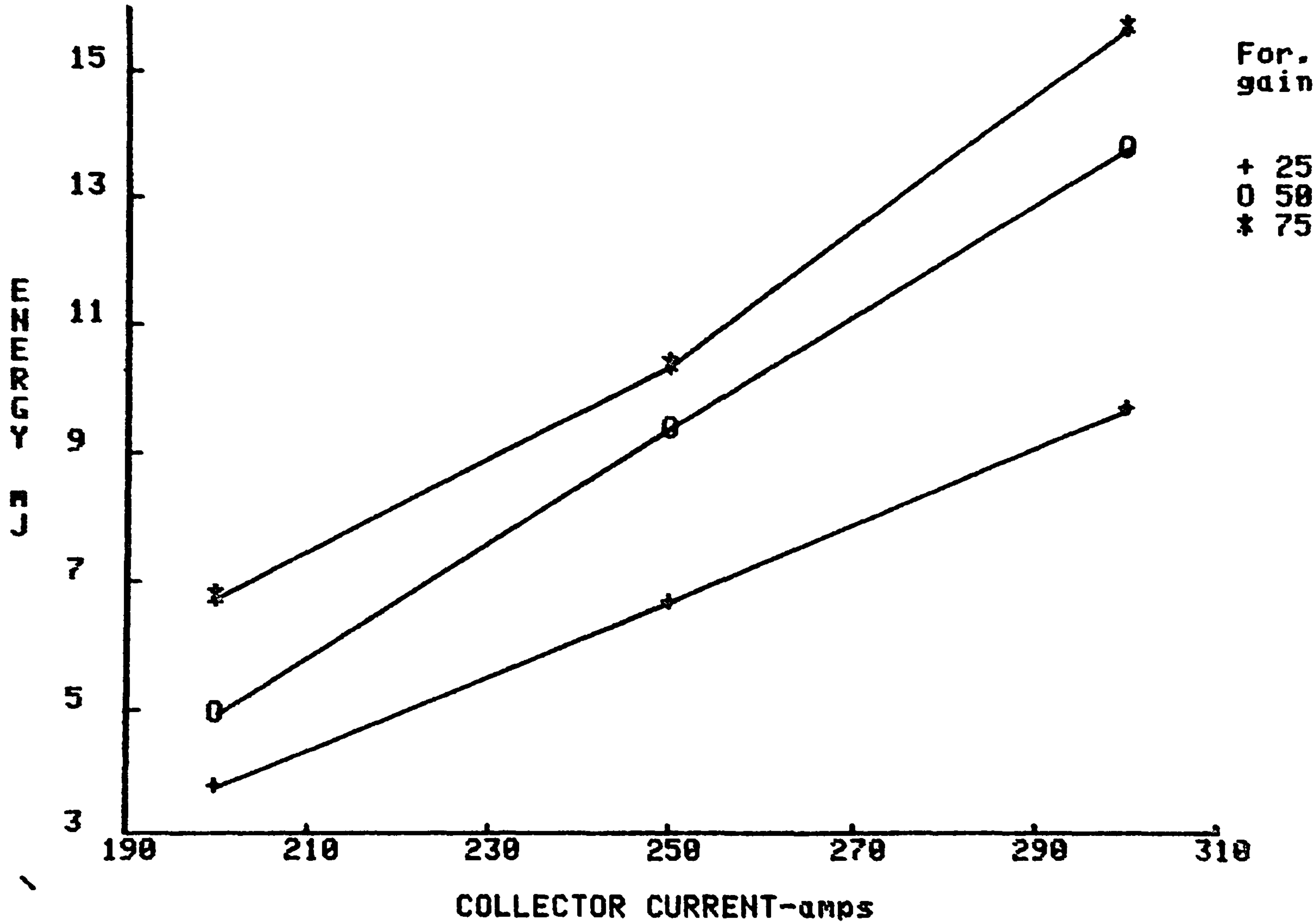

Fig. A.6.9

Qon(tot) vs Ic for QM300HA-H @ Vce=175V

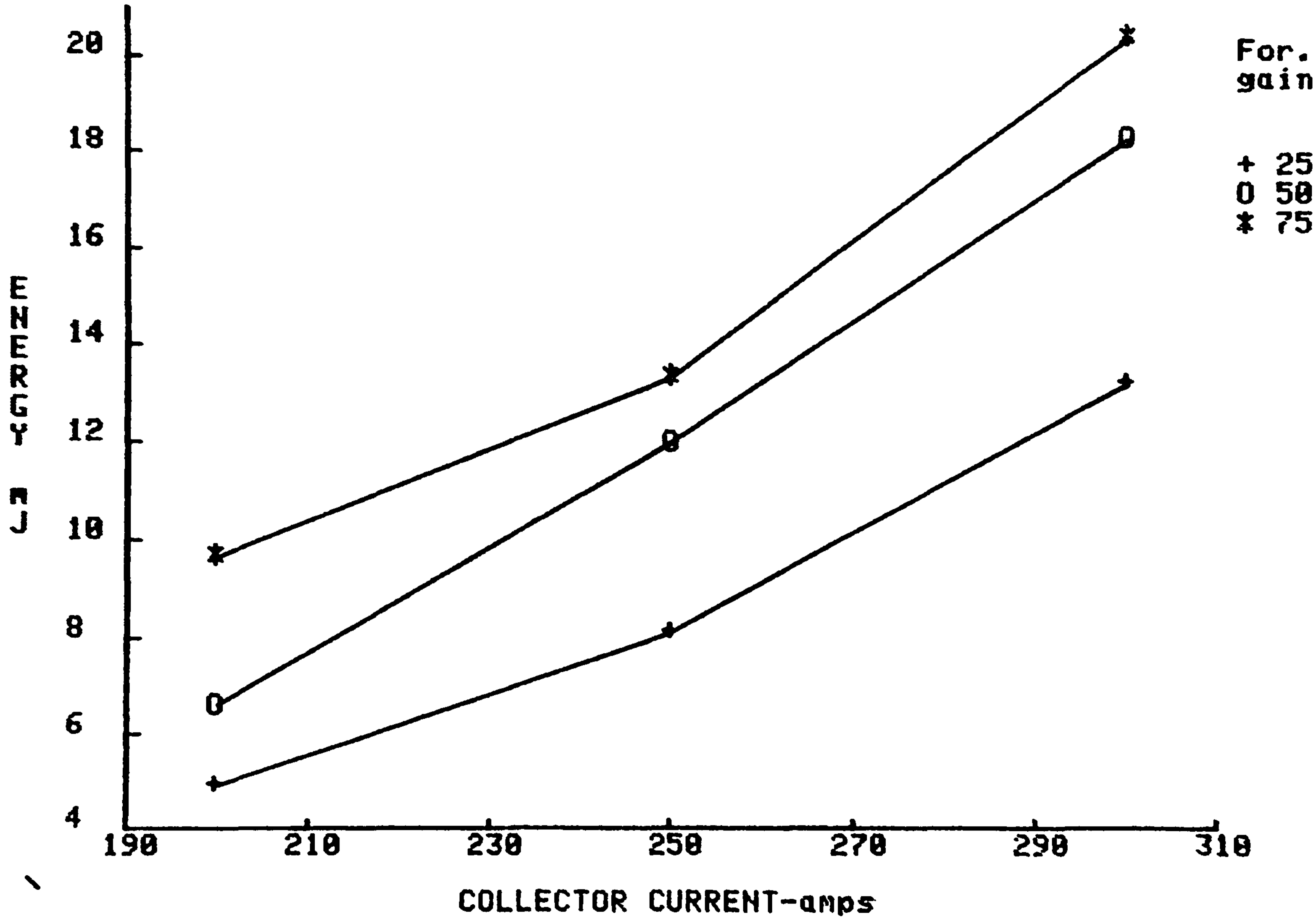

Fig. A.6.10

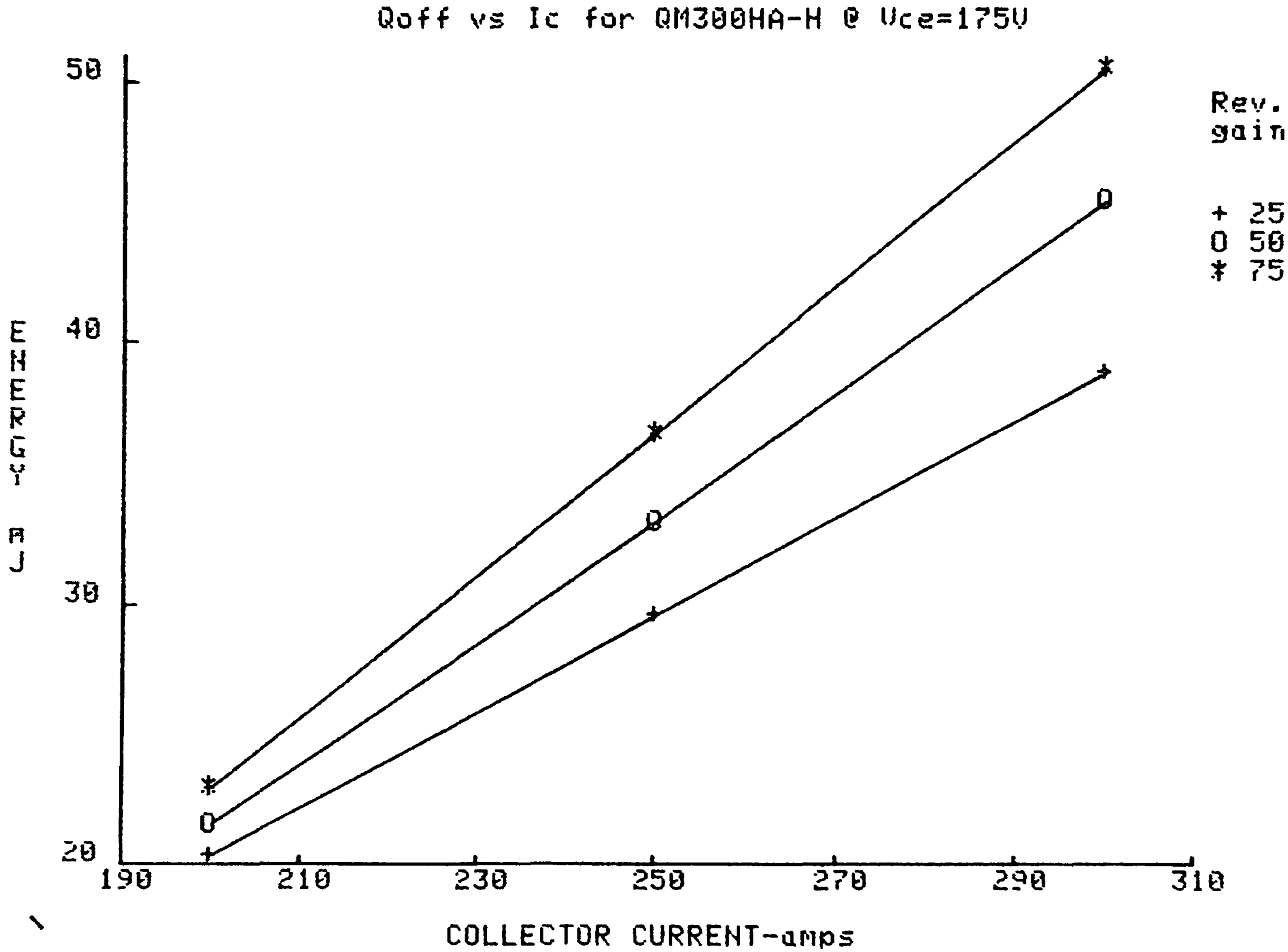
Qoff vs Ic for QM300HA-H @ Vce=175V
ENERGY mJ
50
40
30
20
190
210
230
250
270
290
310
COLLECTOR CURRENT-amps
Rev. gain
+ 25
O 50
* 75

Fig. A.6.11

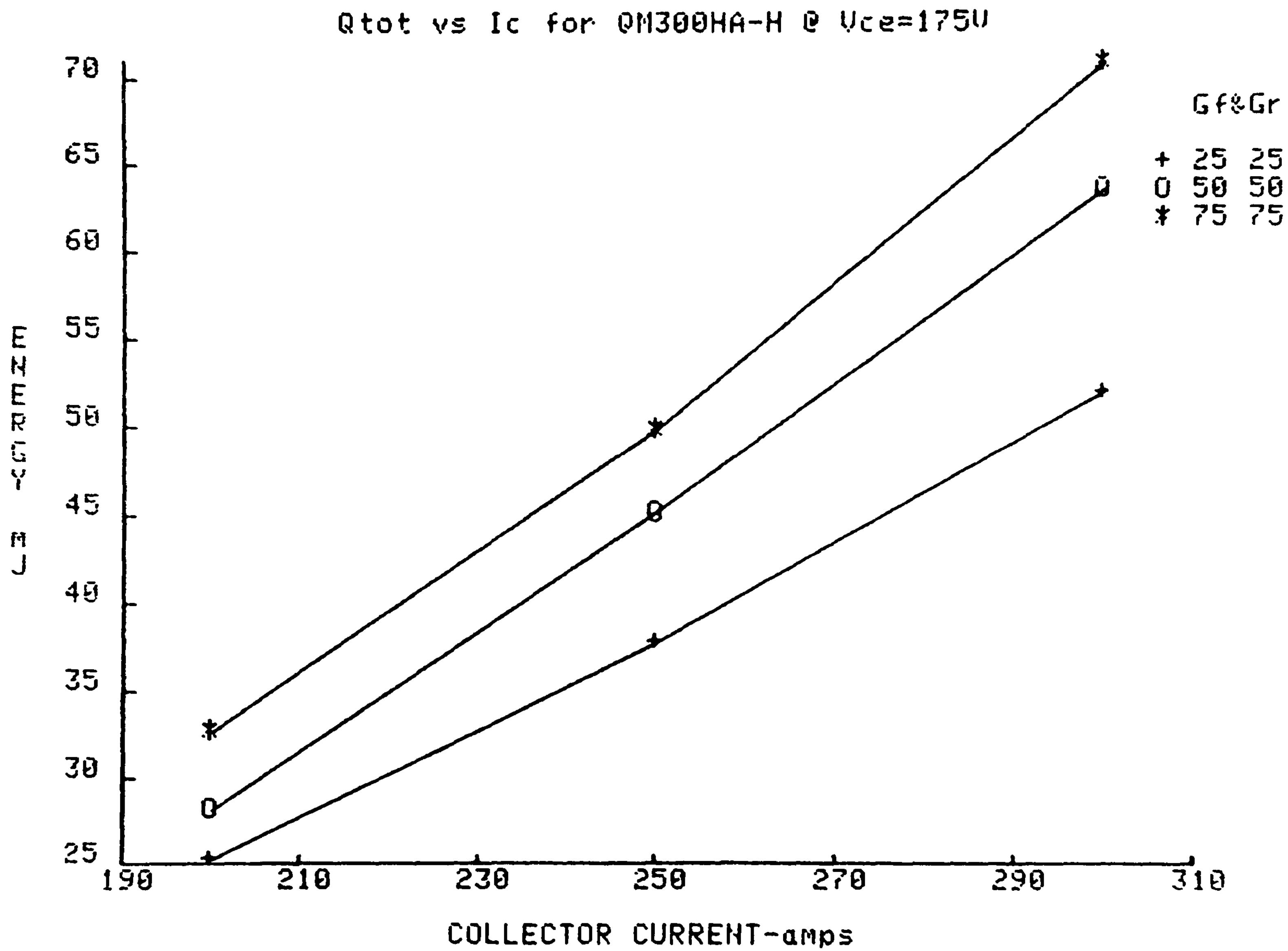
Qtot vs Ic for QM300HA-H @ Vce=175V
ENERGY mJ
70
65
60
55
50
45
40
35
30
25
190
210
230
250
270
290
310
COLLECTOR CURRENT-amps
Gf&Gr
+ 25 25
O 50 50
* 75 75

Fig. A.6.12

Switching Loadline Characteristics: Vce vs. Ic
for Turn-on of Power Trans. with Inductive Load

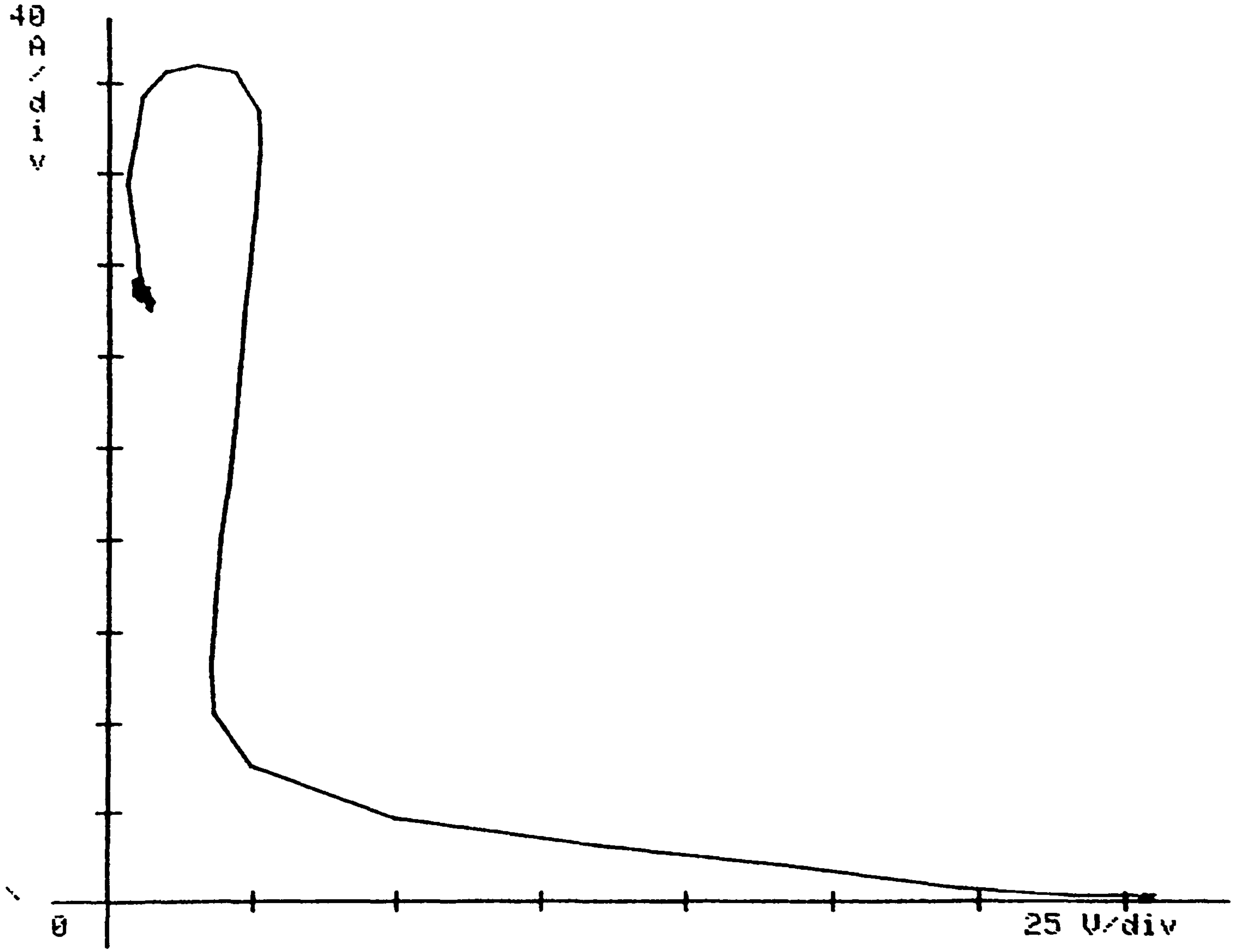

Fig. A.6.13

Switching Loadline Characteristics: Uce vs. Ic
for Turn-off of Power Trans. with Inductive Load

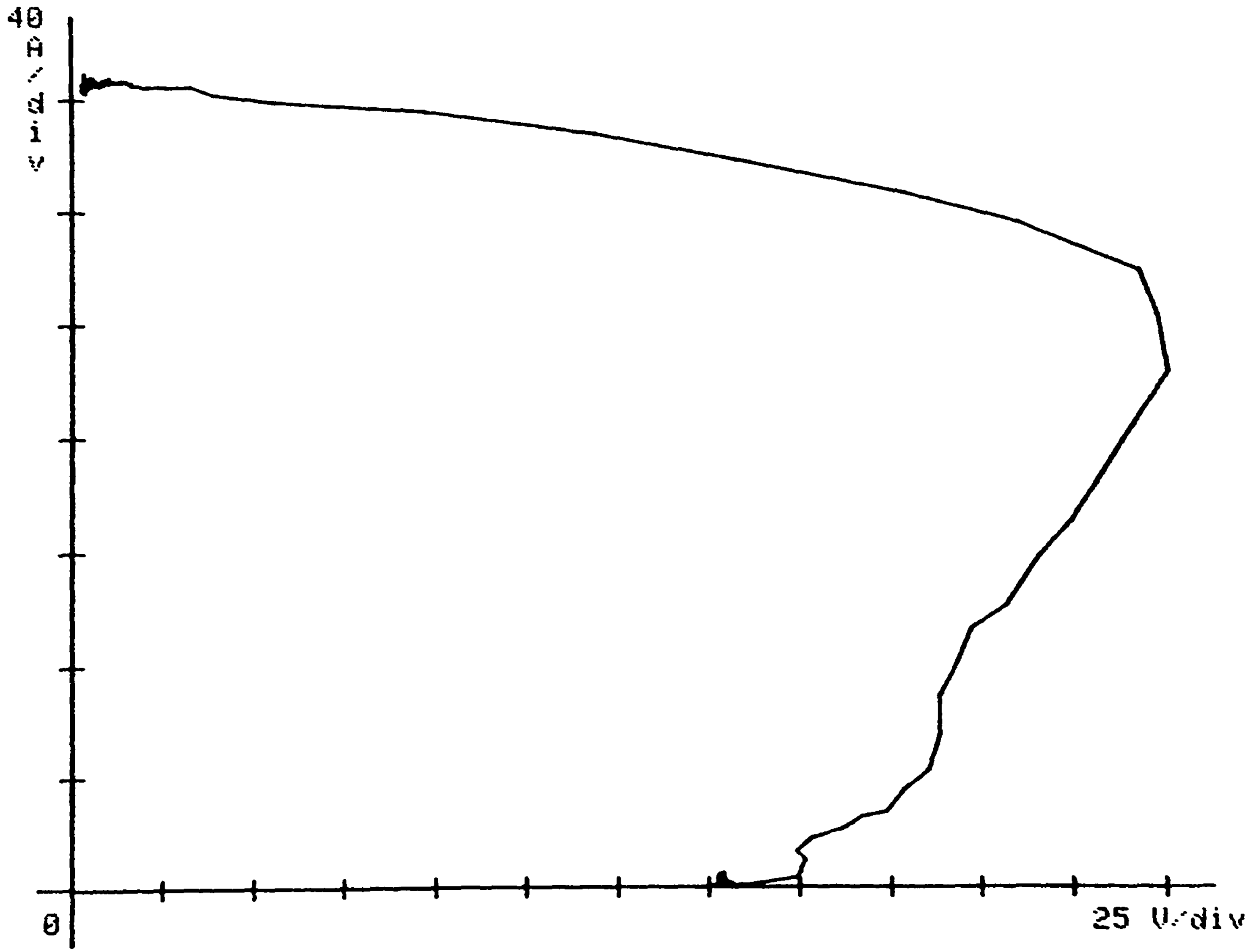

Fig. A.6.14

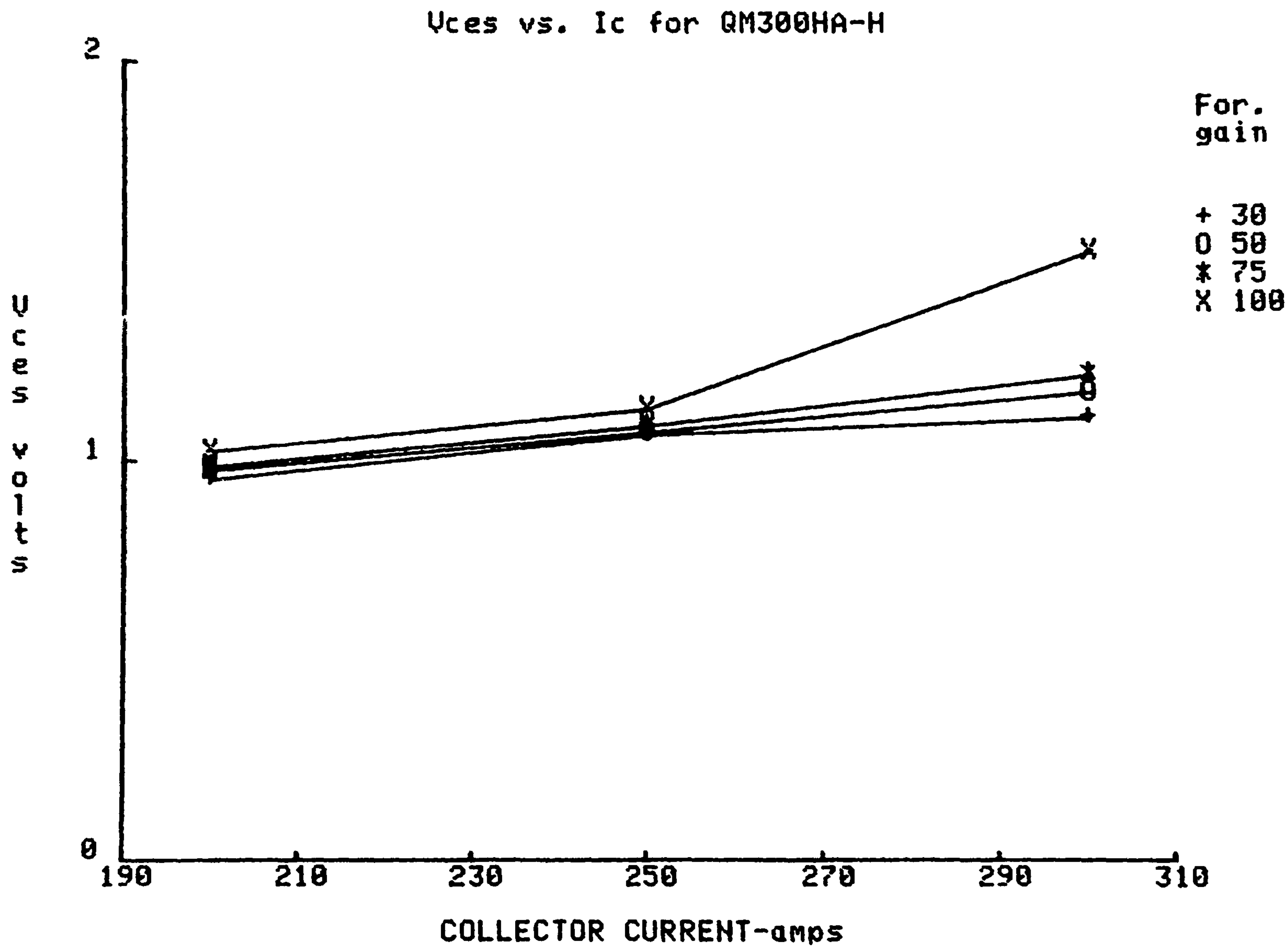
Vces vs. Ic for QM300HA-H
2
1
0
V c e s v o l t s
190
210
230
250
270
290
310
COLLECTOR CURRENT-amps
For. gain
+ 30
O 50
* 75
X 100

Fig. A.6.15

Hfe vs Ic for QM300HA-H for Vce=3V @ Tc=35 C

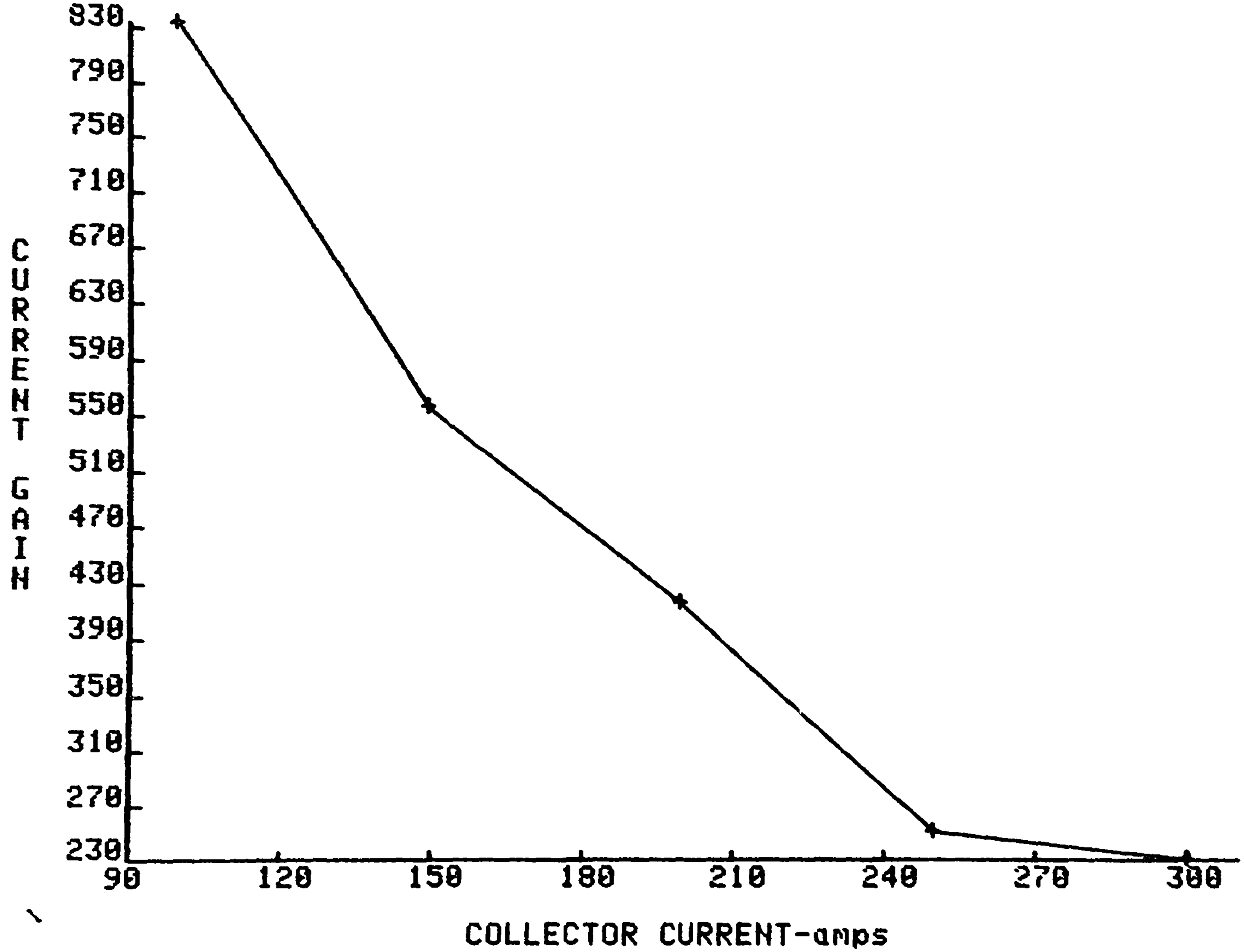

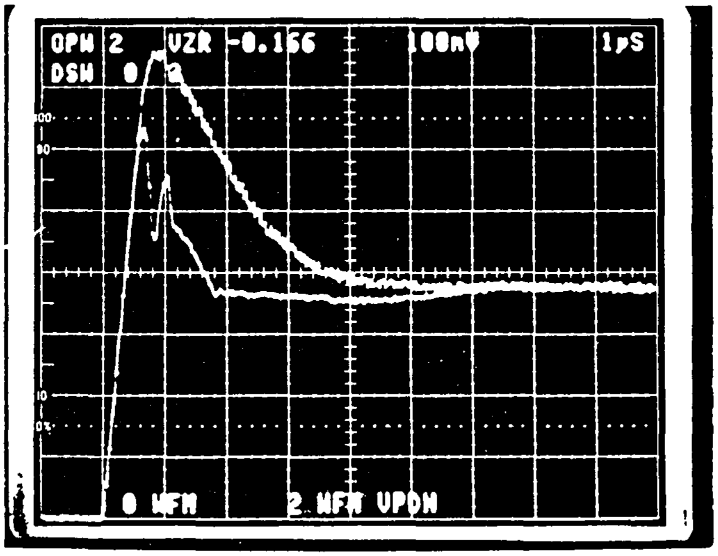

Fig. A.6.16 Diode recovery and dv/dt test for QM300HA-H
Upepr trace: Base open
Lower trace: Base reverse biased
(Scale: horizontal 1 µs/div; vertical 40 A/div)

A.7 Test Data for Mitsubishi QM300HA-2H

Fig. A.7.1

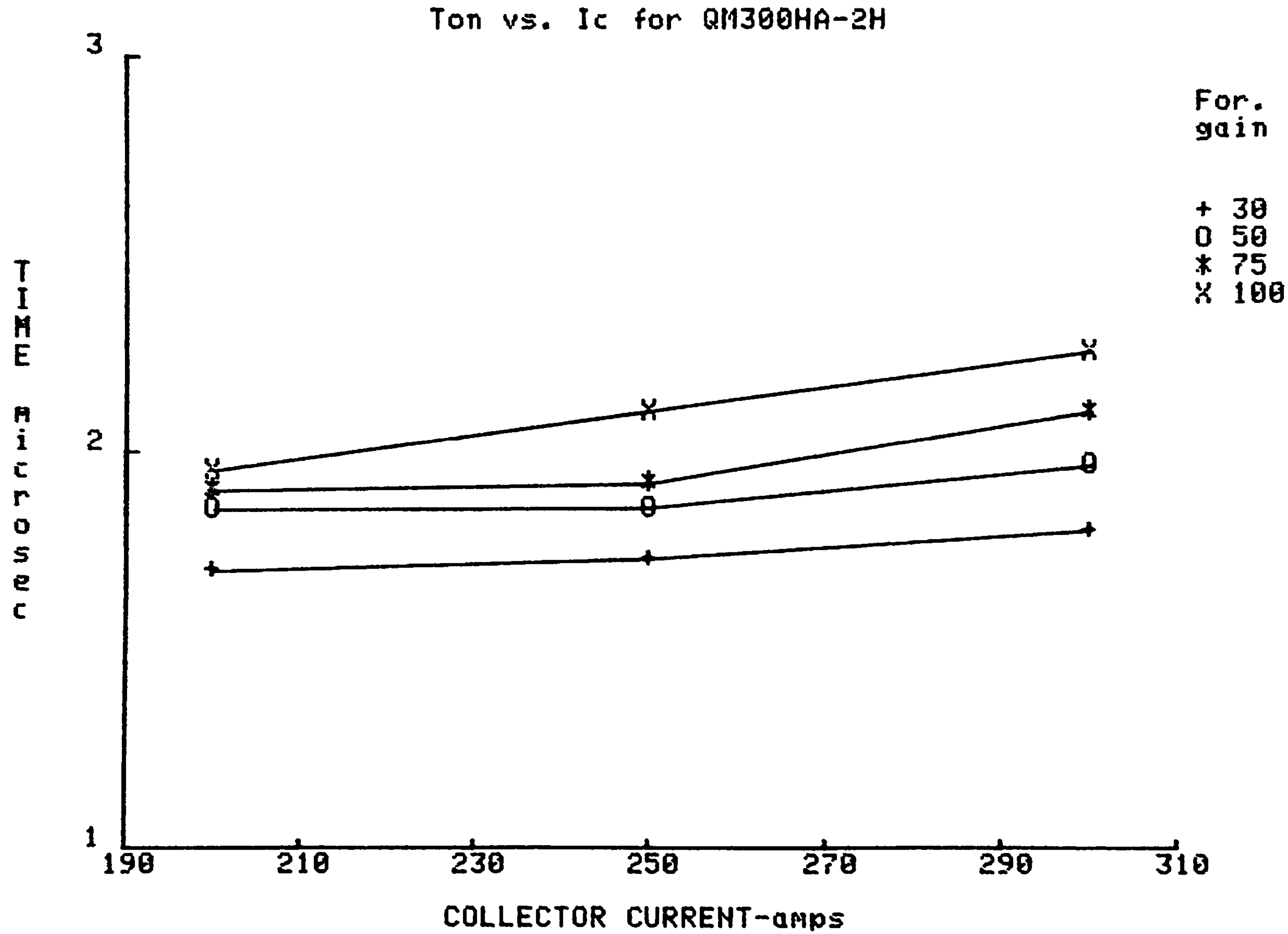

Ton vs. Ic for QM300HA-2H
TIME microsec
3
2
1
190
210
230
250
270
290
310
COLLECTOR CURRENT-amps
For. gain
+ 30
O 50
* 75
X 100

Fig. A.7.2

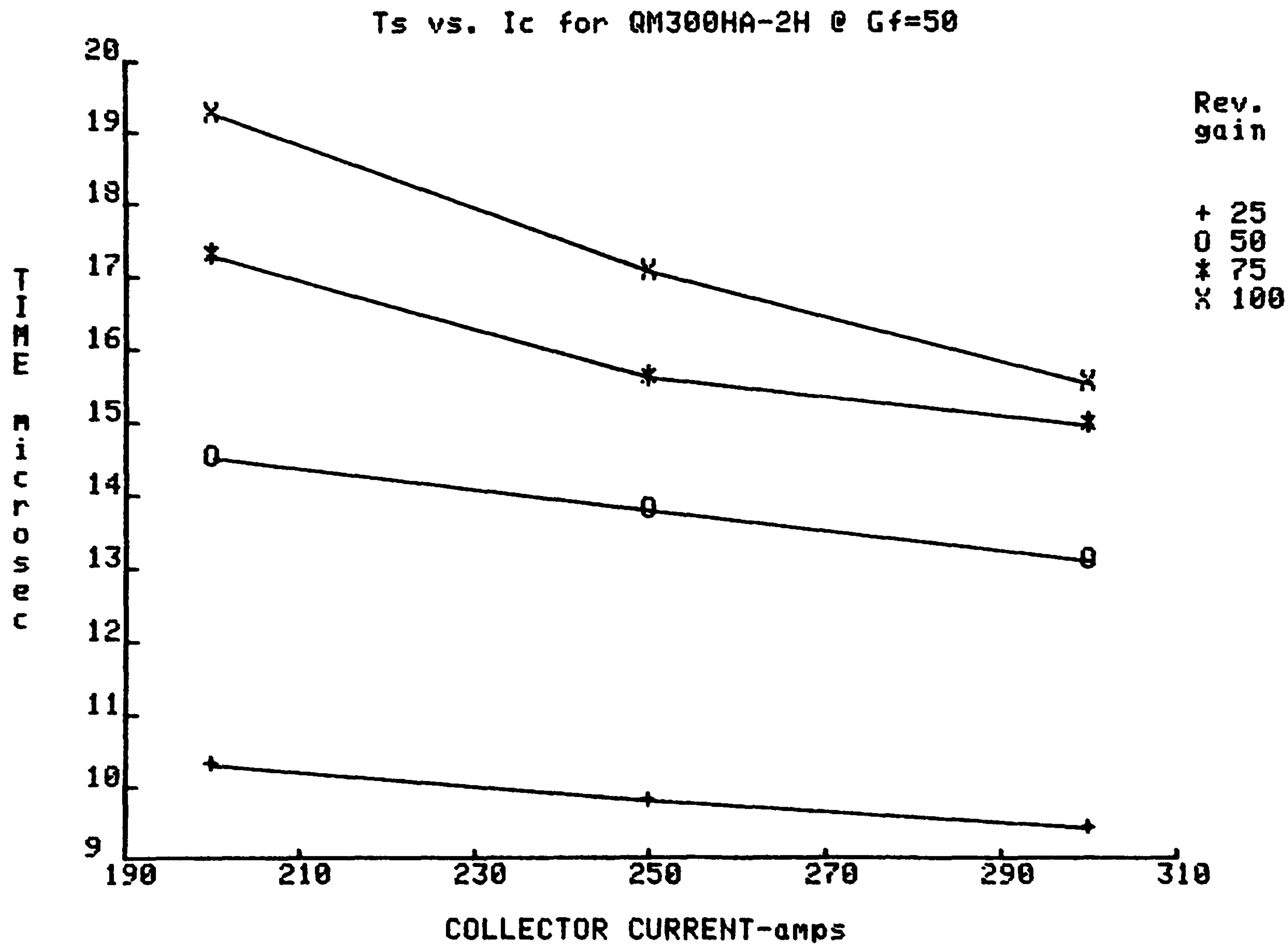

Ts vs. Ic for QM300HA-2H @ Gf=50
TIME microsec
20
19
18
17
16
15
14
13
12
11
10
9
190
210
230
250
270
290
310
COLLECTOR CURRENT-amps
Rev. gain
+ 25
O 50
* 75
X 100

Fig. A.7.3

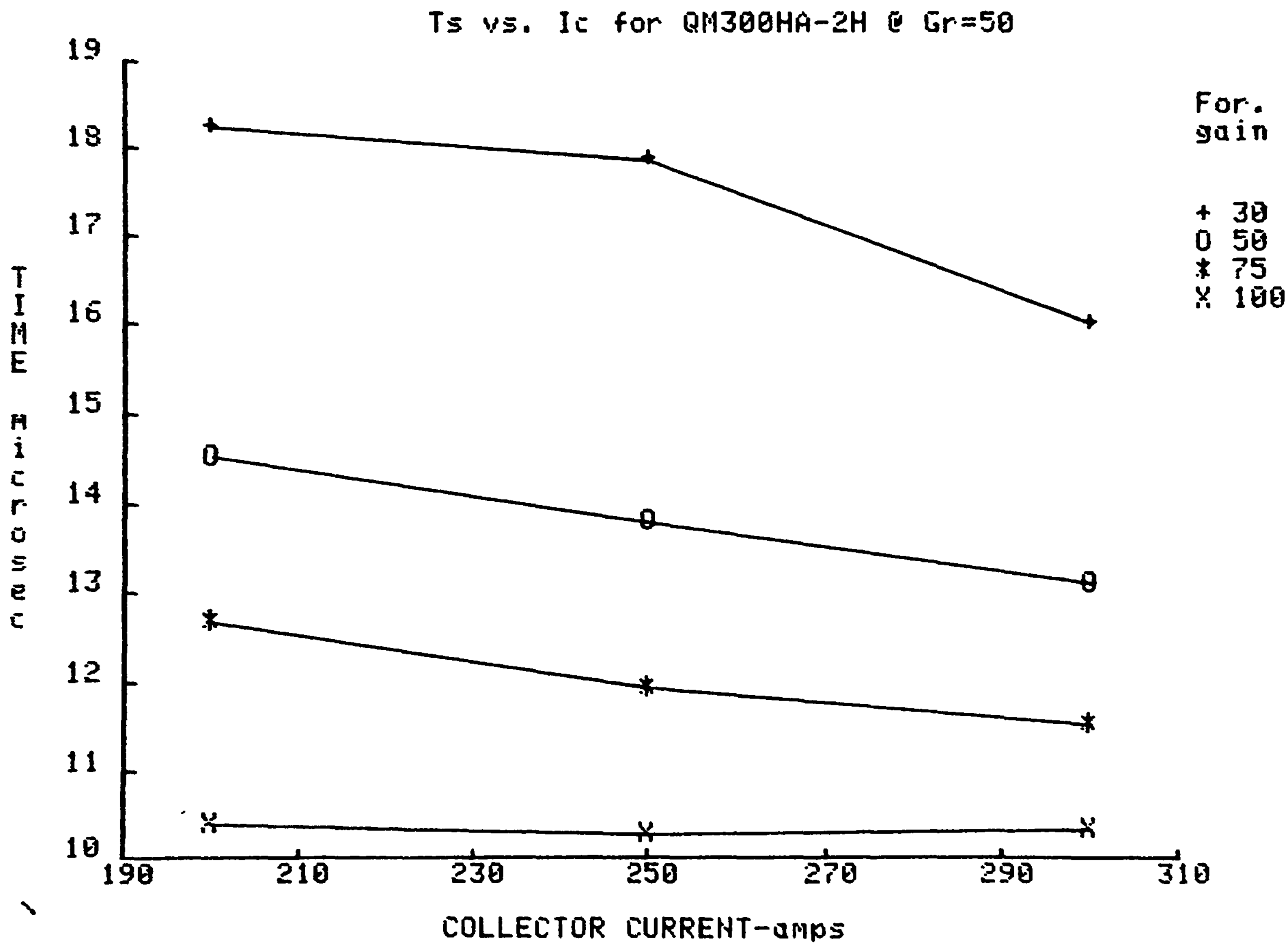
Ts vs. Ic for QM300HA-2H @ Gr=50
TIME microsec
COLLECTOR CURRENT-amps
For. gain
+ 30
O 50
* 75
X 100
19
18
17
16
15
14
13
12
11
10
190
210
230
250
270
290
310

A.102

Fig. A.7.4

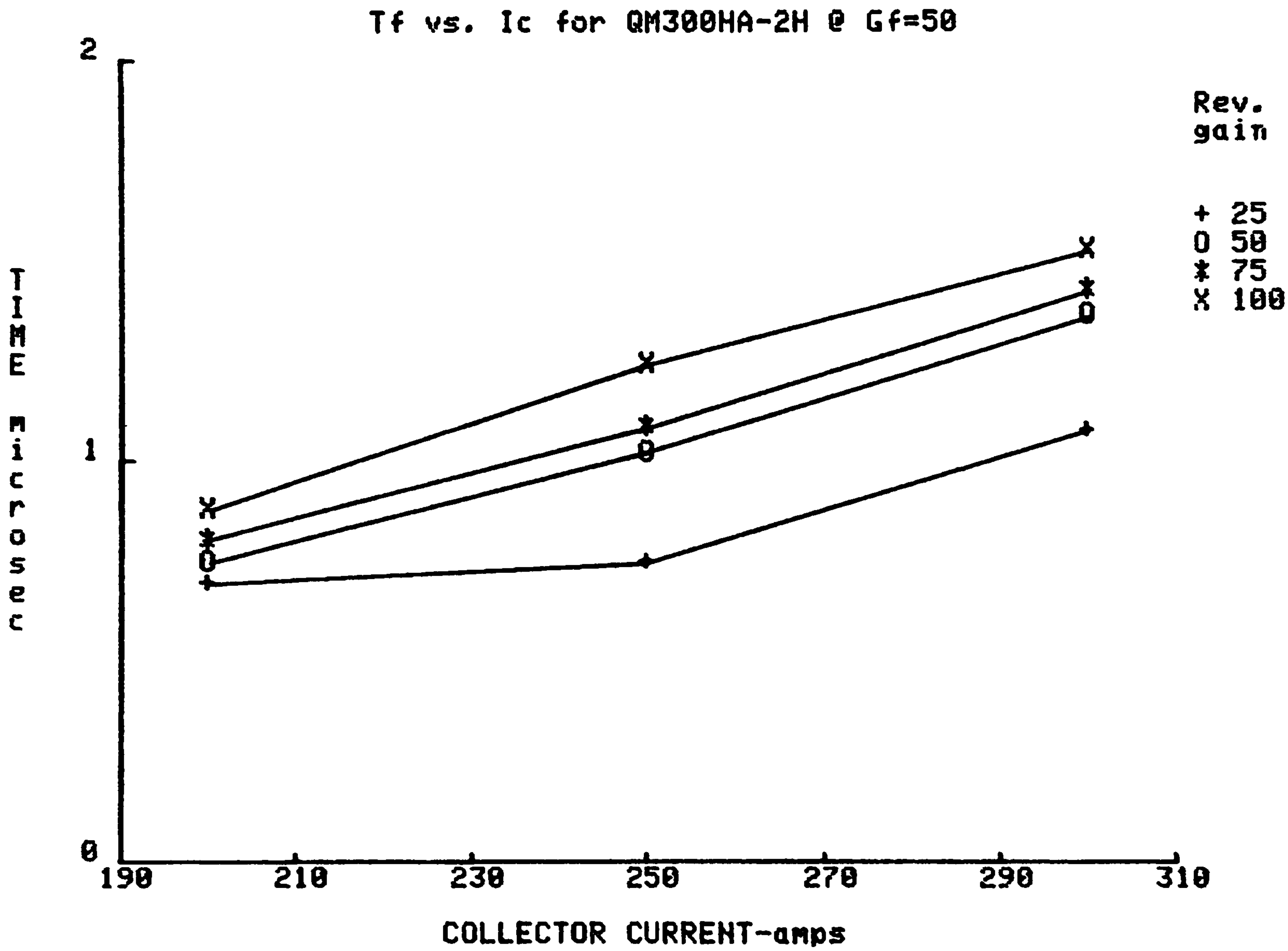

Tf vs. Ic for QM300HA-2H @ Gf=50
TIME microsec
2
1
0
190
210
230
250
270
290
310
COLLECTOR CURRENT-amps
Rev. gain
+ 25
O 50
* 75
X 100

Fig. A.7.5

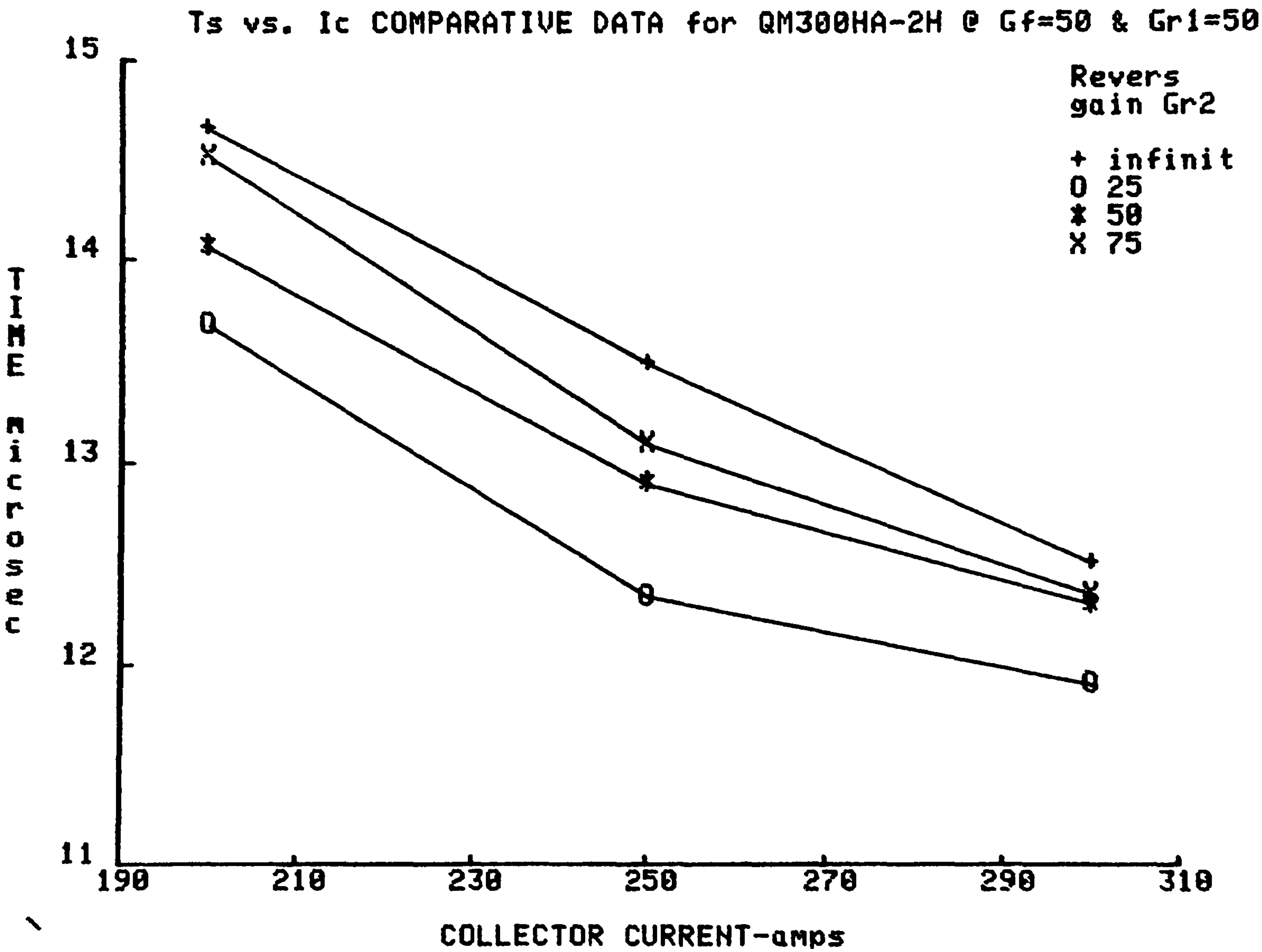

Ts vs. Ic COMPARATIVE DATA for QM300HA-2H @ Gf=50 & Gr1=50
Revers gain Gr2
+ infinit
O 25
* 50
X 75
TIME microsec
15
14
13
12
11
190
210
230
250
270
290
310
COLLECTOR CURRENT-amps

Fig. A.7.6

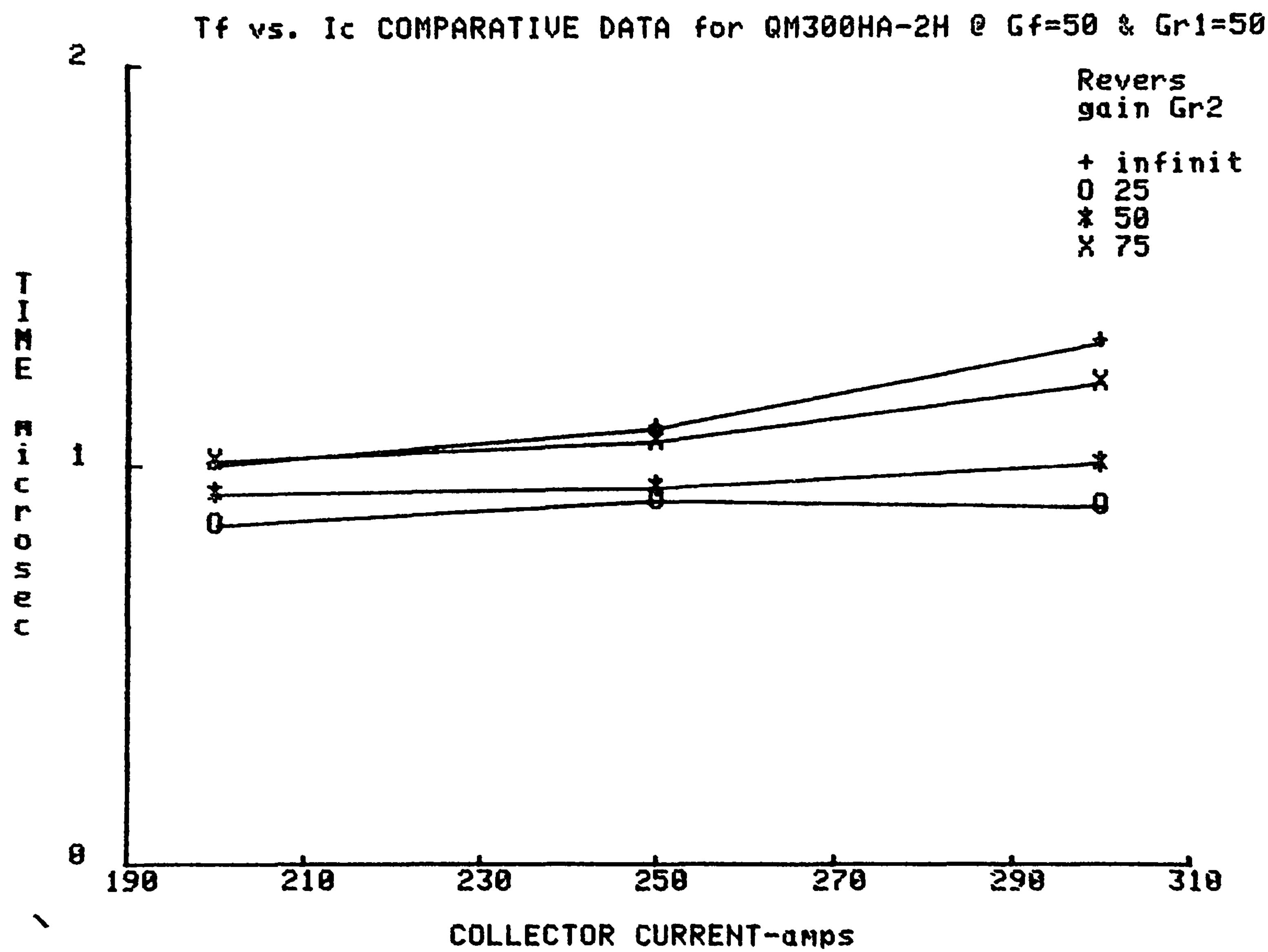
Tf vs. Ic COMPARATIVE DATA for QM300HA-2H @ Gf=50 & Gr1=50
Revers gain Gr2
+ infinit
O 25
* 50
X 75
TIME microsec
2
1
0
190
210
230
250
270
290
310
COLLECTOR CURRENT-amps

Fig. A.7.7

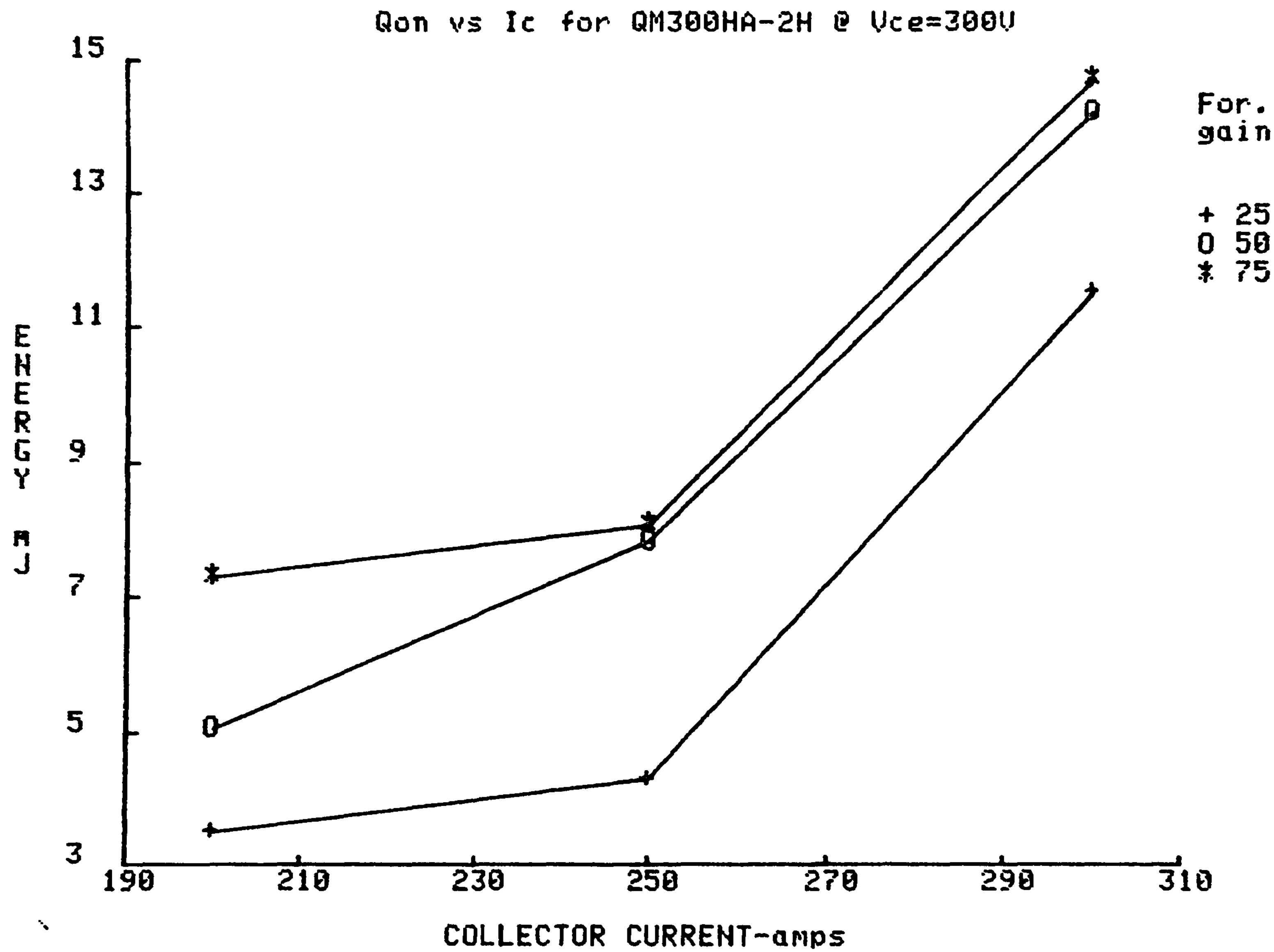
Qon vs Ic for QM300HA-2H @ Vce=300V
15
13
11
9
7
5
3
ENERGY mJ
190
210
230
250
270
290
310
COLLECTOR CURRENT-amps
For. gain
+ 25
O 50
* 75

Fig. A.7.8

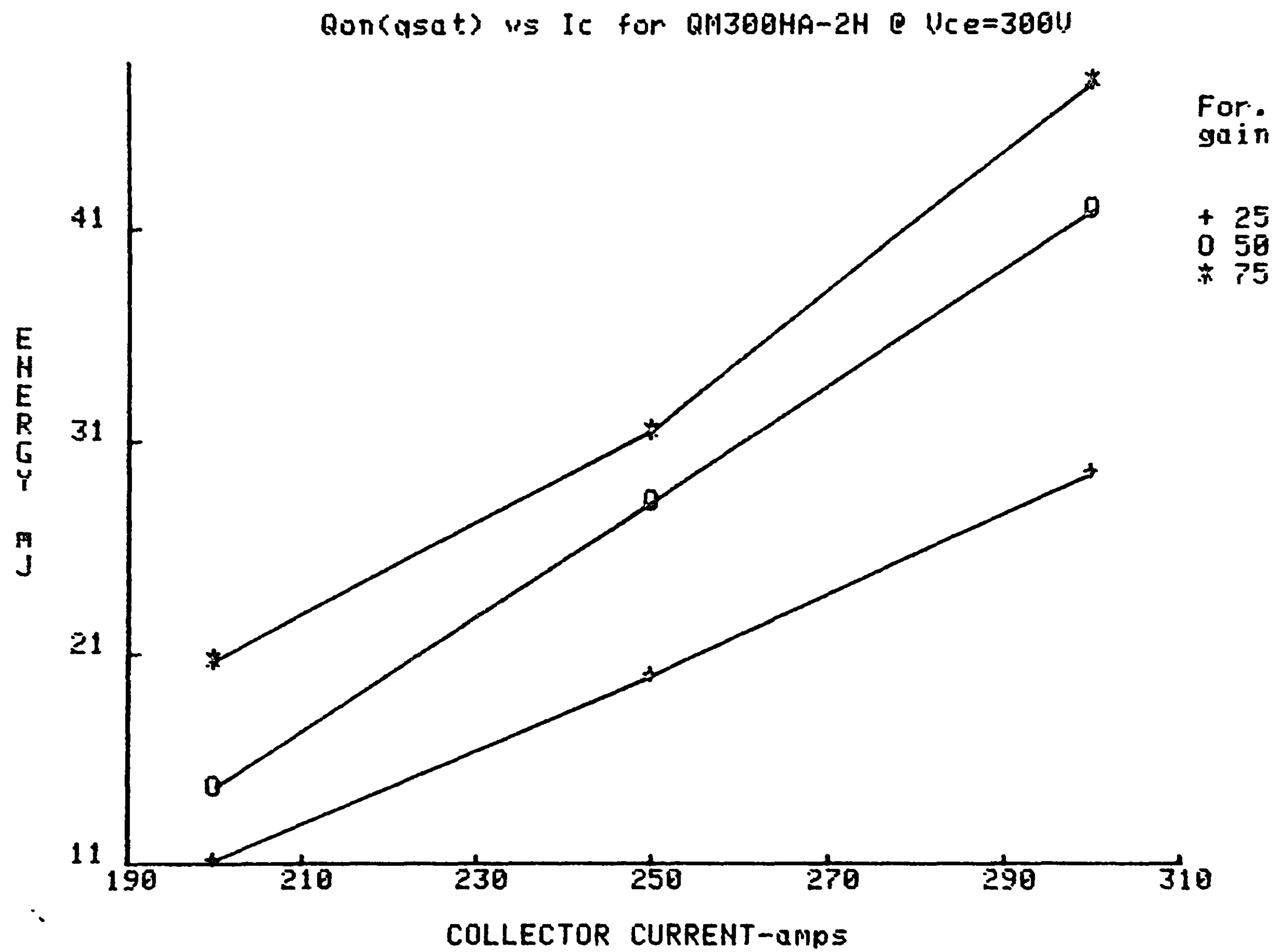

Qon(qsat) vs Ic for QM300HA-2H @ Vce=300V
ENERGY mJ
41
31
21
11
190
210
230
250
270
290
310
COLLECTOR CURRENT-amps
For. gain
+ 25
O 50
* 75

Fig. A.7.9

Qon(tot) vs Ic for QM300HA-2H @ Vce=300V

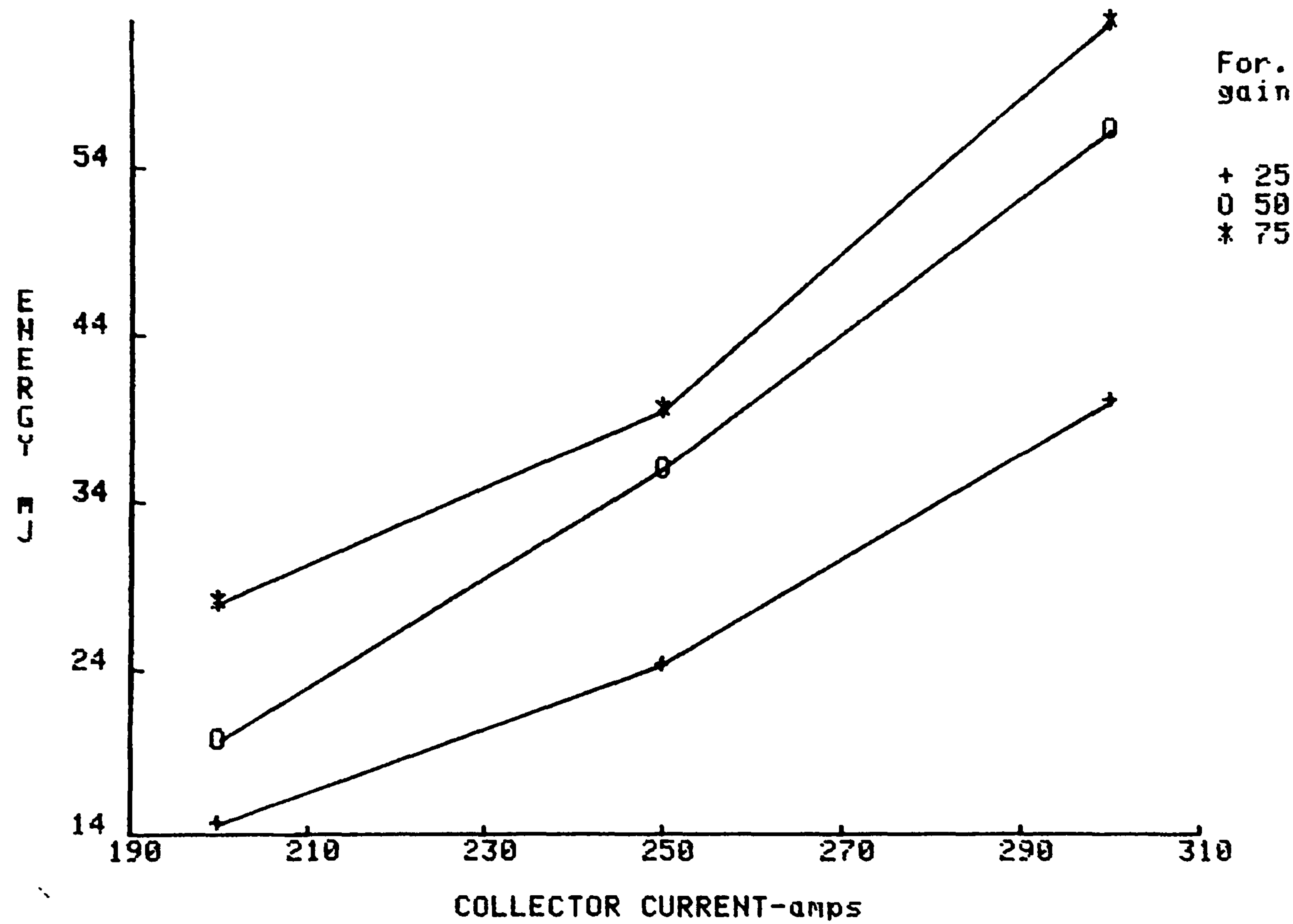

Fig. A.7.10

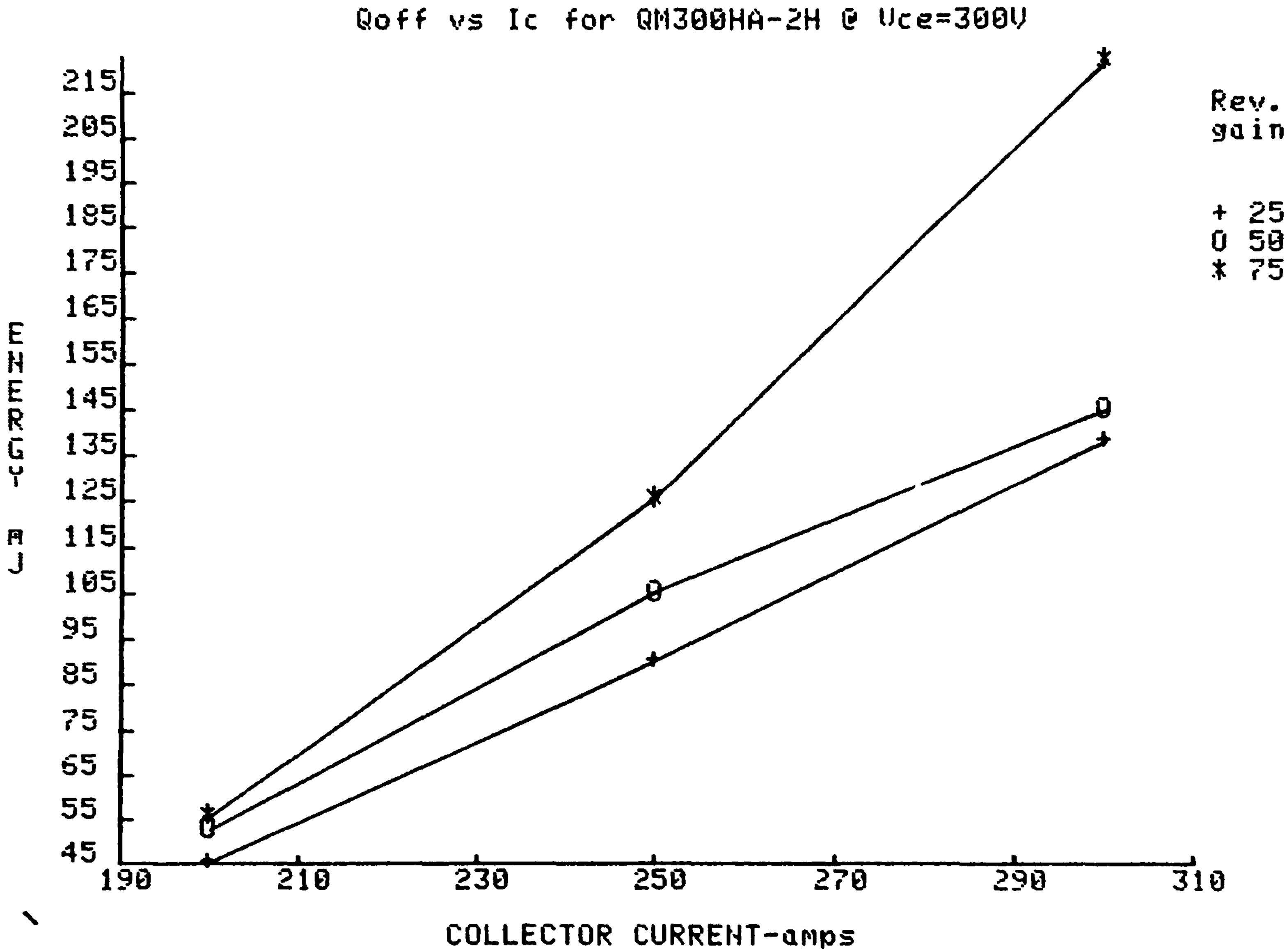
Qoff vs Ic for QM300HA-2H @ Vce=300V
ENERGY mJ
215
205
195
185
175
165
155
145
135
125
115
105
95
85
75
65
55
45
190
210
230
250
270
290
310
COLLECTOR CURRENT-amps
Rev. gain
+ 25
0 50
* 75

Fig. A.7.11

Qtot vs Ic for QM300HA-2H @ Vce=300V

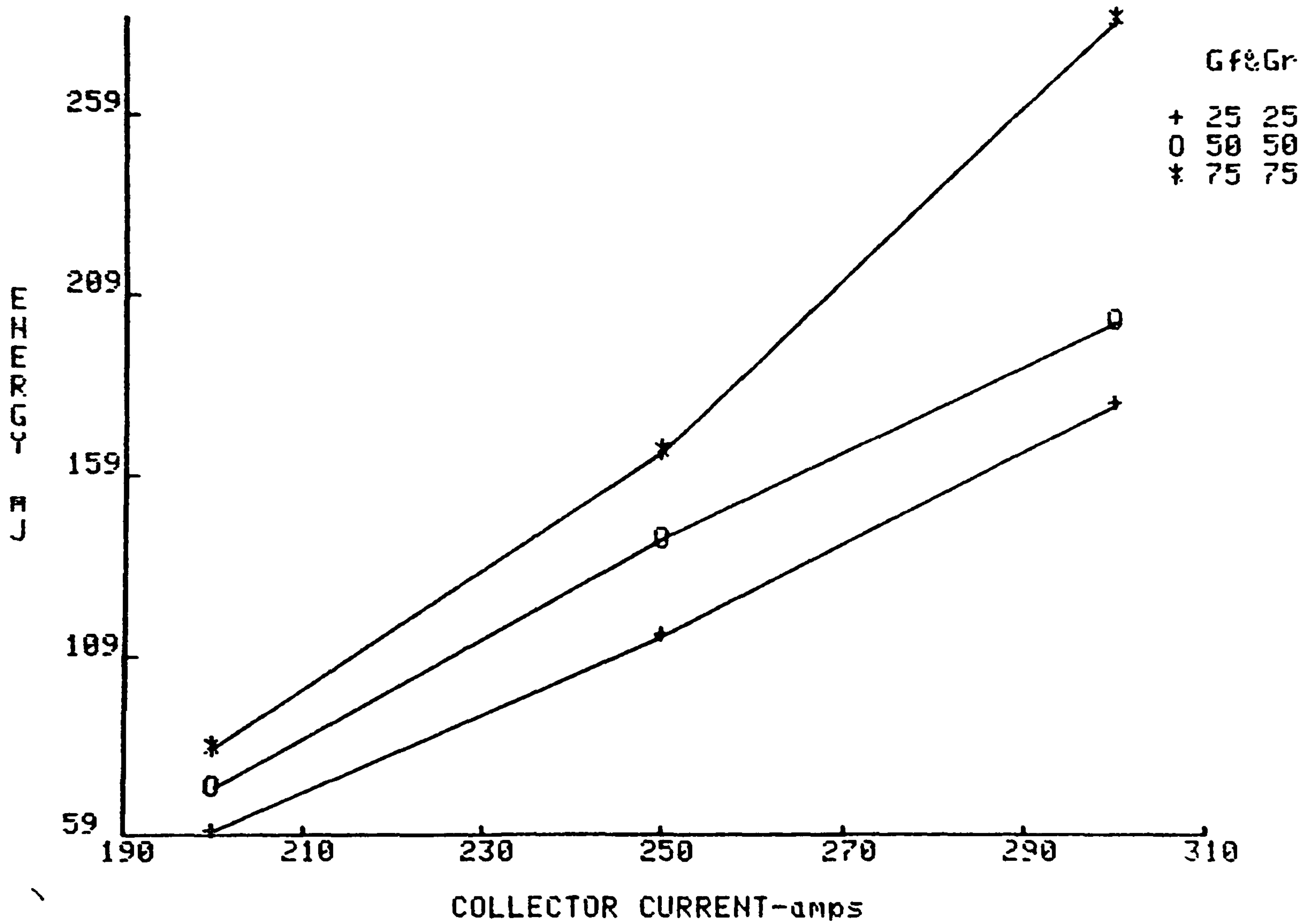

Fig. A.7.12

Switching Loadline Characteristics: Uce vs. Ic
for Turn-on of Power Transistor with Inductive Load

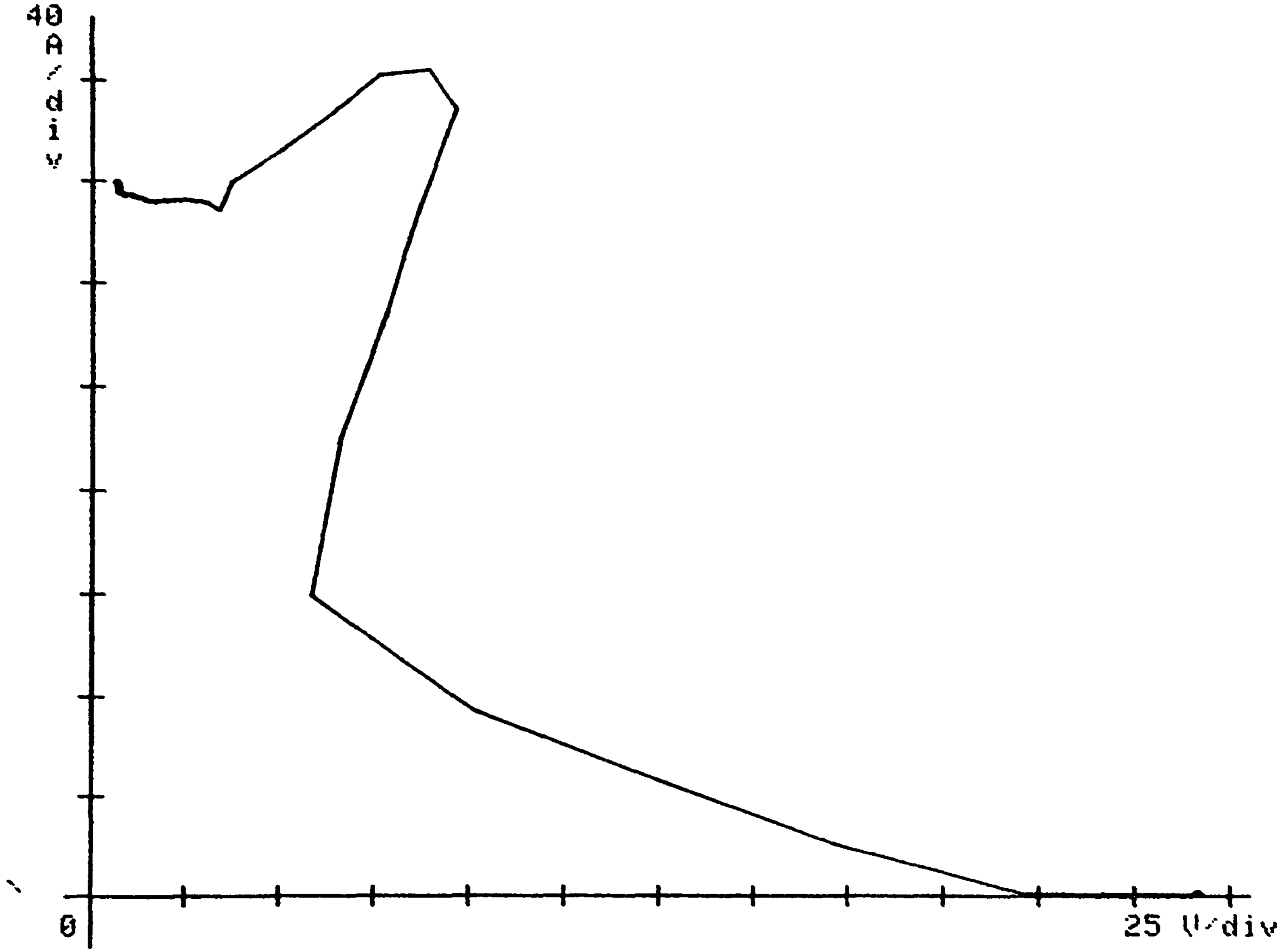

Fig. A.7.13

Switching Loadline Characteristics: Vce vs. Ic
for Turn-off of Power Trans. with Inductive Load

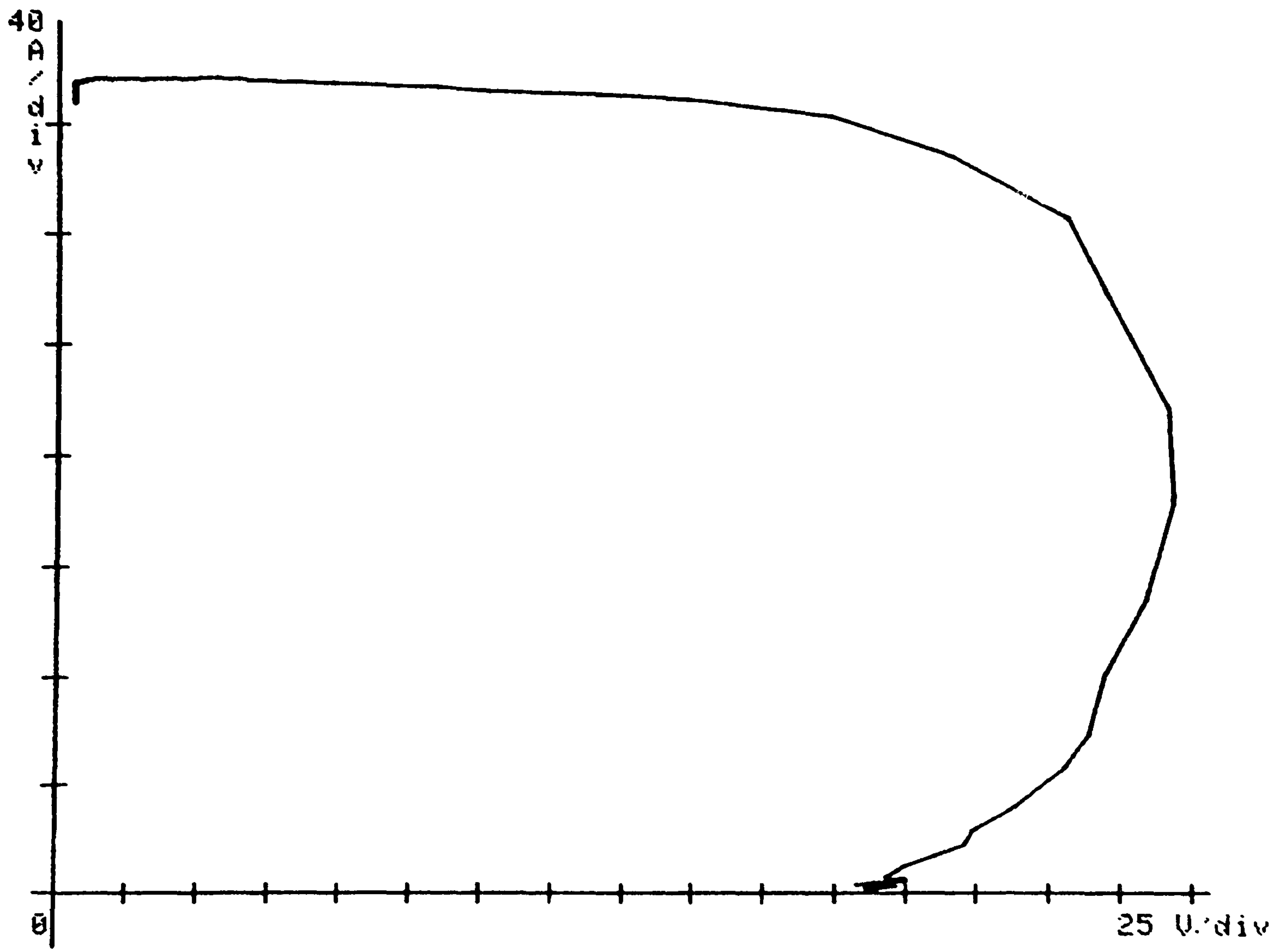

Fig. A.7.14

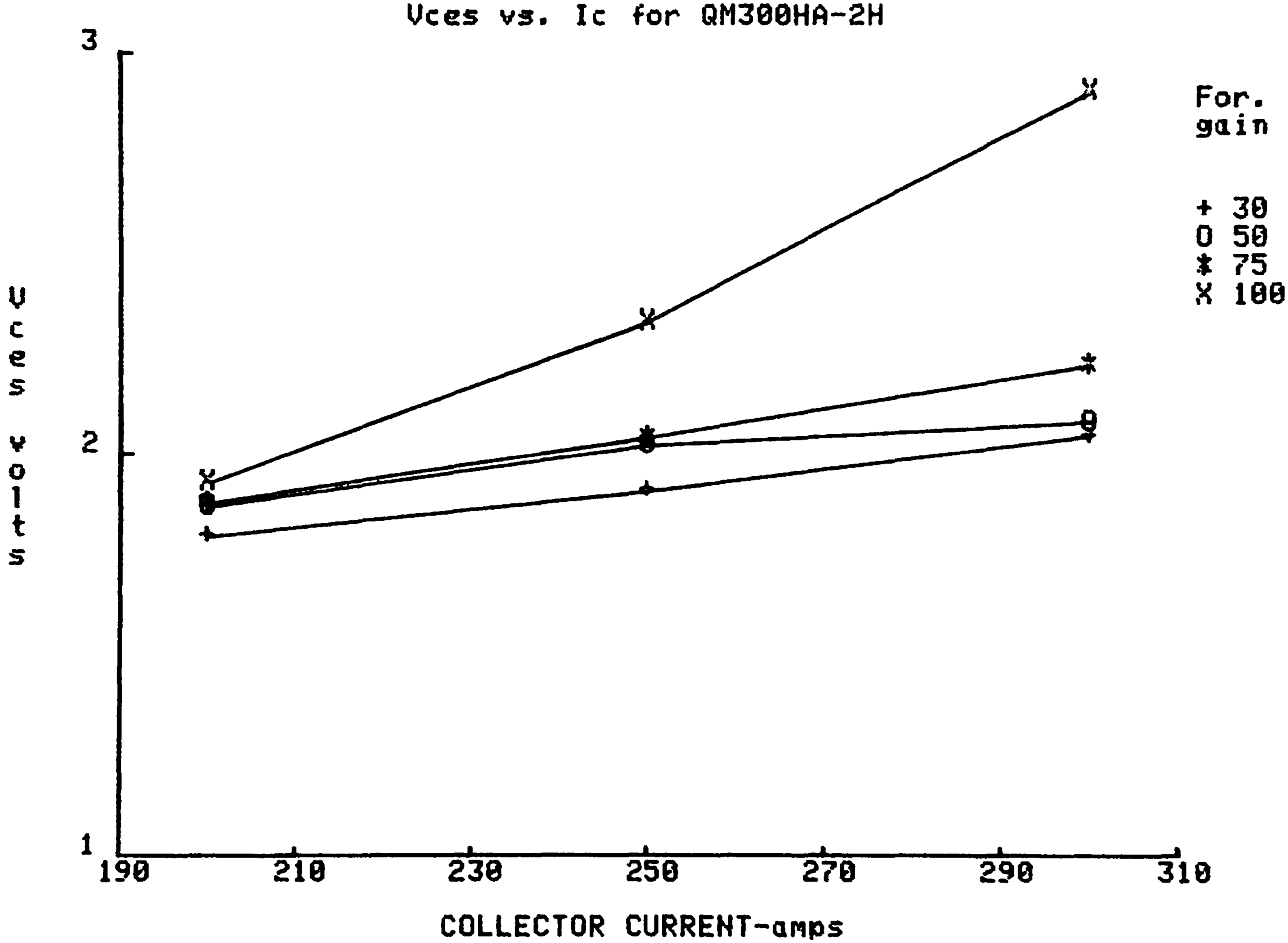

Vces vs. Ic for QM300HA-2H
Vces volts
3
2
1
190
210
230
250
270
290
310
COLLECTOR CURRENT-amps
For. gain
+ 30
O 50
* 75
X 100

Fig. A.7.15

Hfe vs Ic for QM300HA-2H for Vce=3V @ Tc=35 C

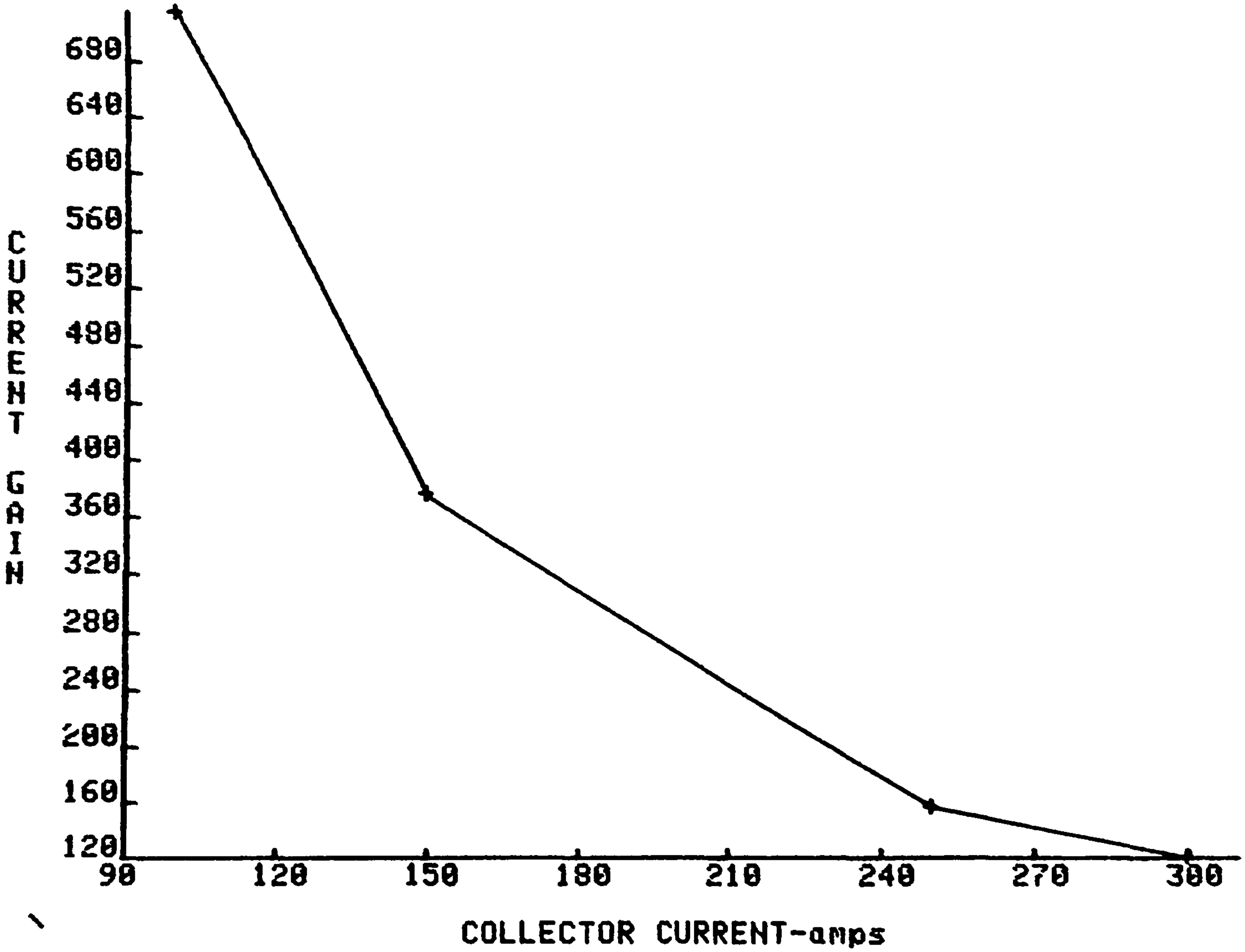

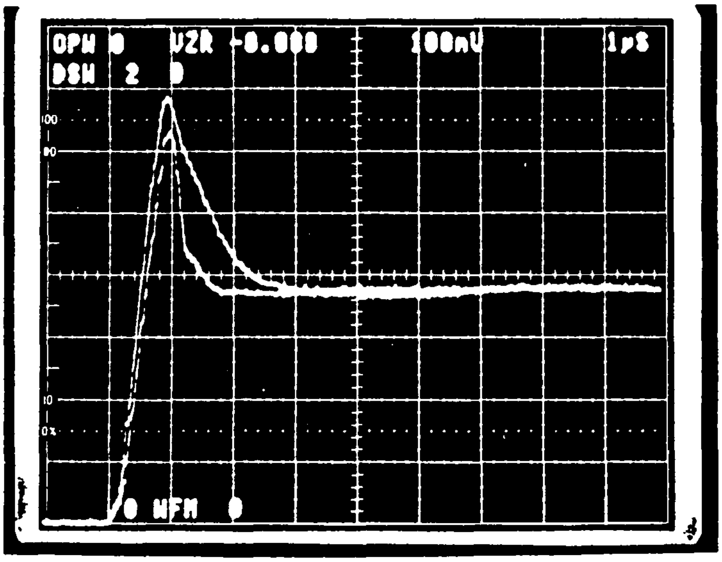

Fig. A.7.16 Diode recovery and dv/dt test for QM300HA-2H
Upper trace: Base open
Lower trace: Base reverse biased
(Scale: horizontal 1 μs/div; vertical 40 A/div)

A.8 Test Data for Toshiba ST200M

Fig. A.8.1

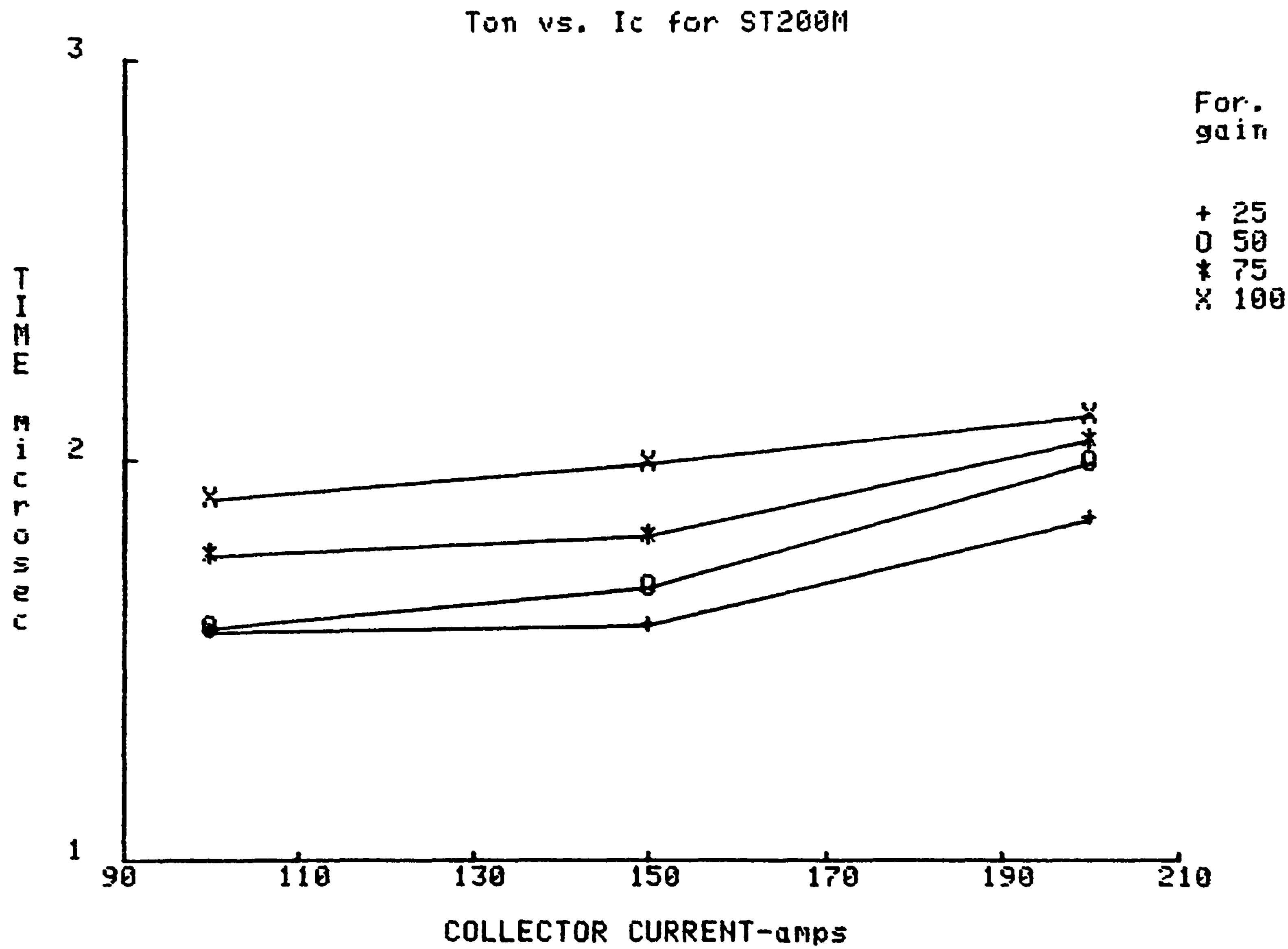

Ton vs. Ic for ST200M
3
2
1
TIME microsec
90
110
130
150
170
190
210
COLLECTOR CURRENT-amps
For. gain
+ 25
O 50
* 75
X 100

Fig. A.8.2

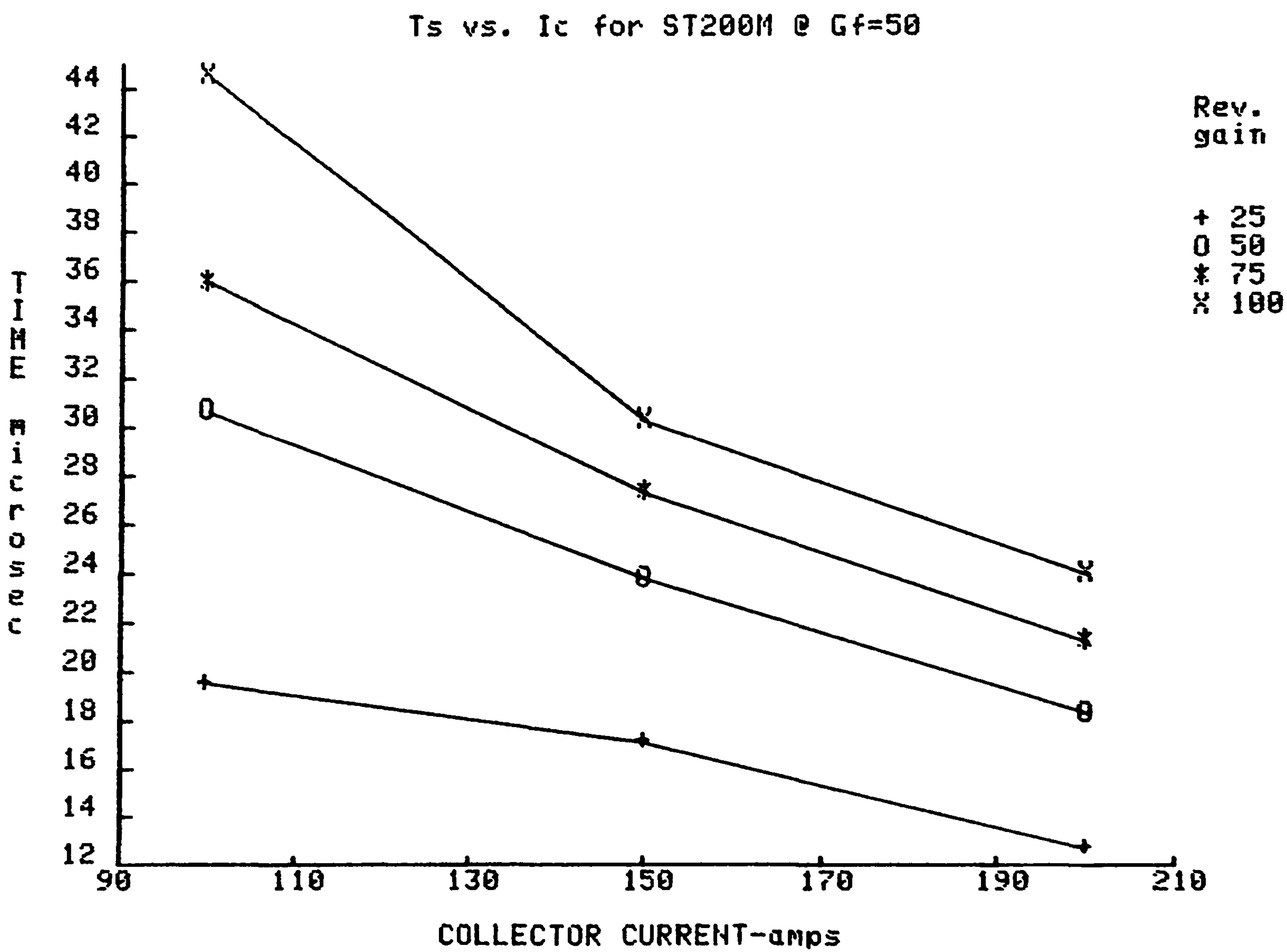

Ts vs. Ic for ST200M @ Gf=50
TIME microsec
44
42
40
38
36
34
32
30
28
26
24
22
20
18
16
14
12
90
110
130
150
170
190
210
COLLECTOR CURRENT-amps
Rev. gain
+ 25
O 50
* 75
X 100

Fig. A.8.3

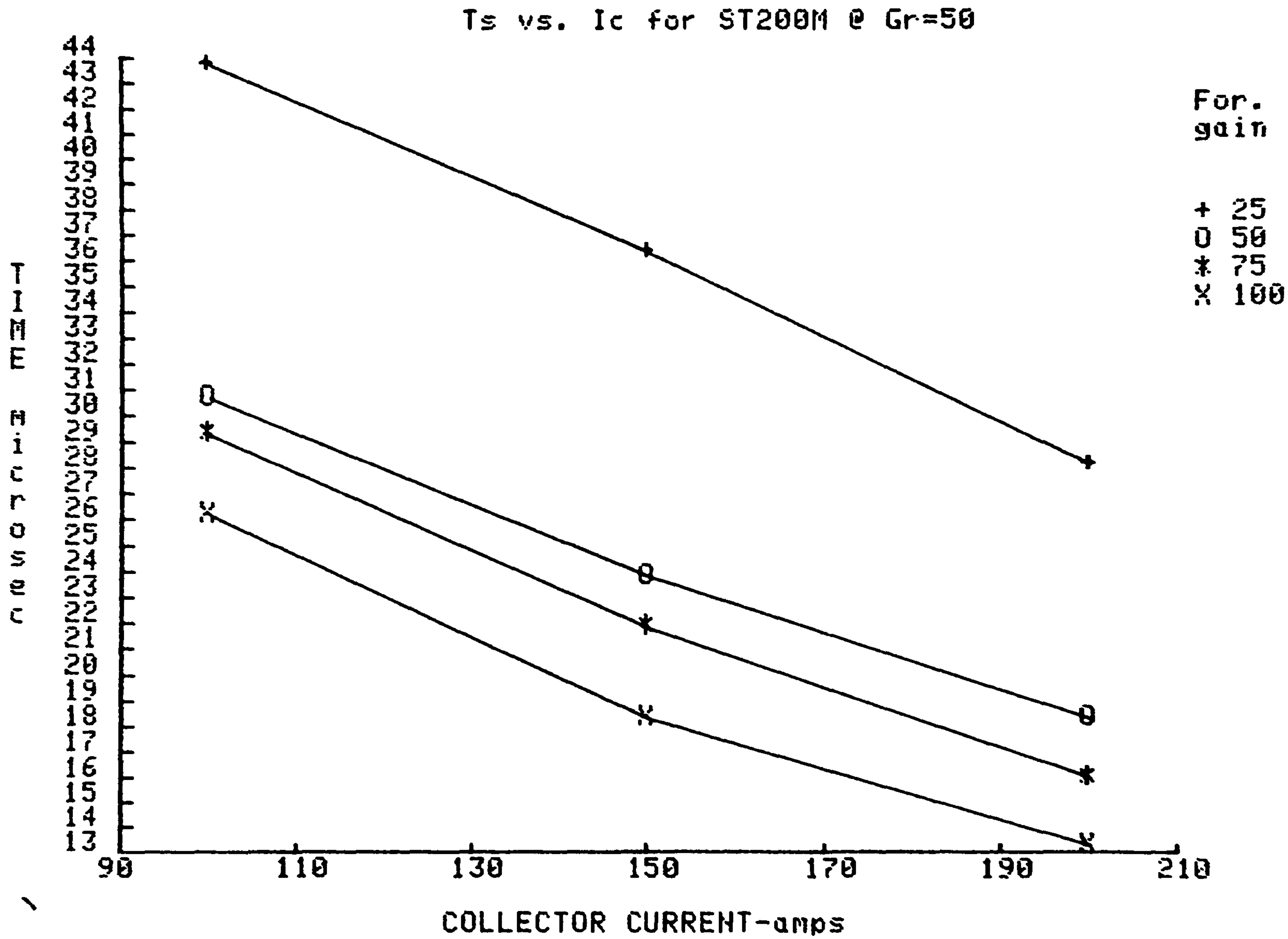

Ts vs. Ic for ST200M @ Gr=50
TIME microsec
COLLECTOR CURRENT-amps
For. gain
+ 25
O 50
* 75
X 100

Fig. A.8.4

Tf vs. Ic for ST200M @ Gf=50

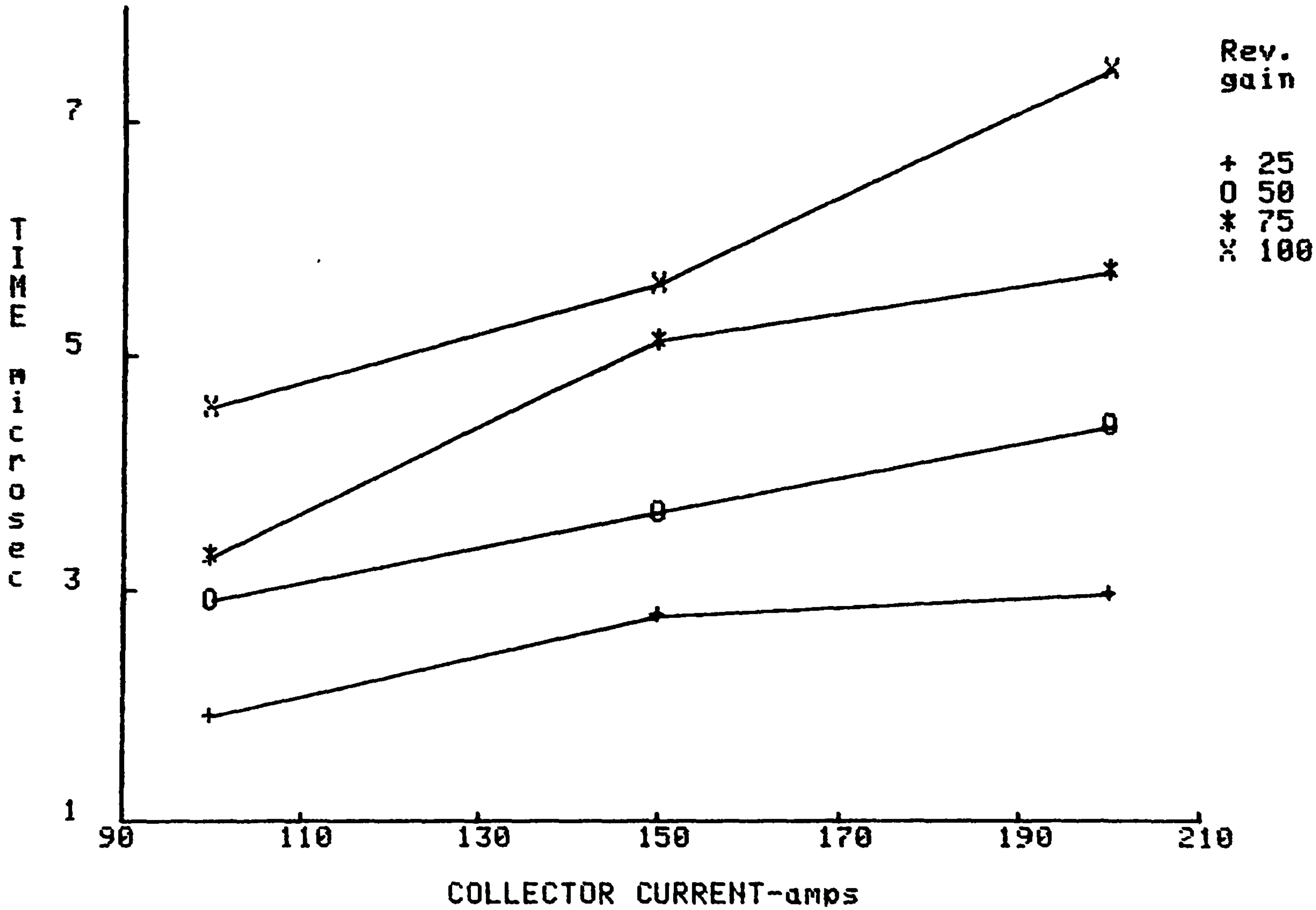

Fig. A.3.5

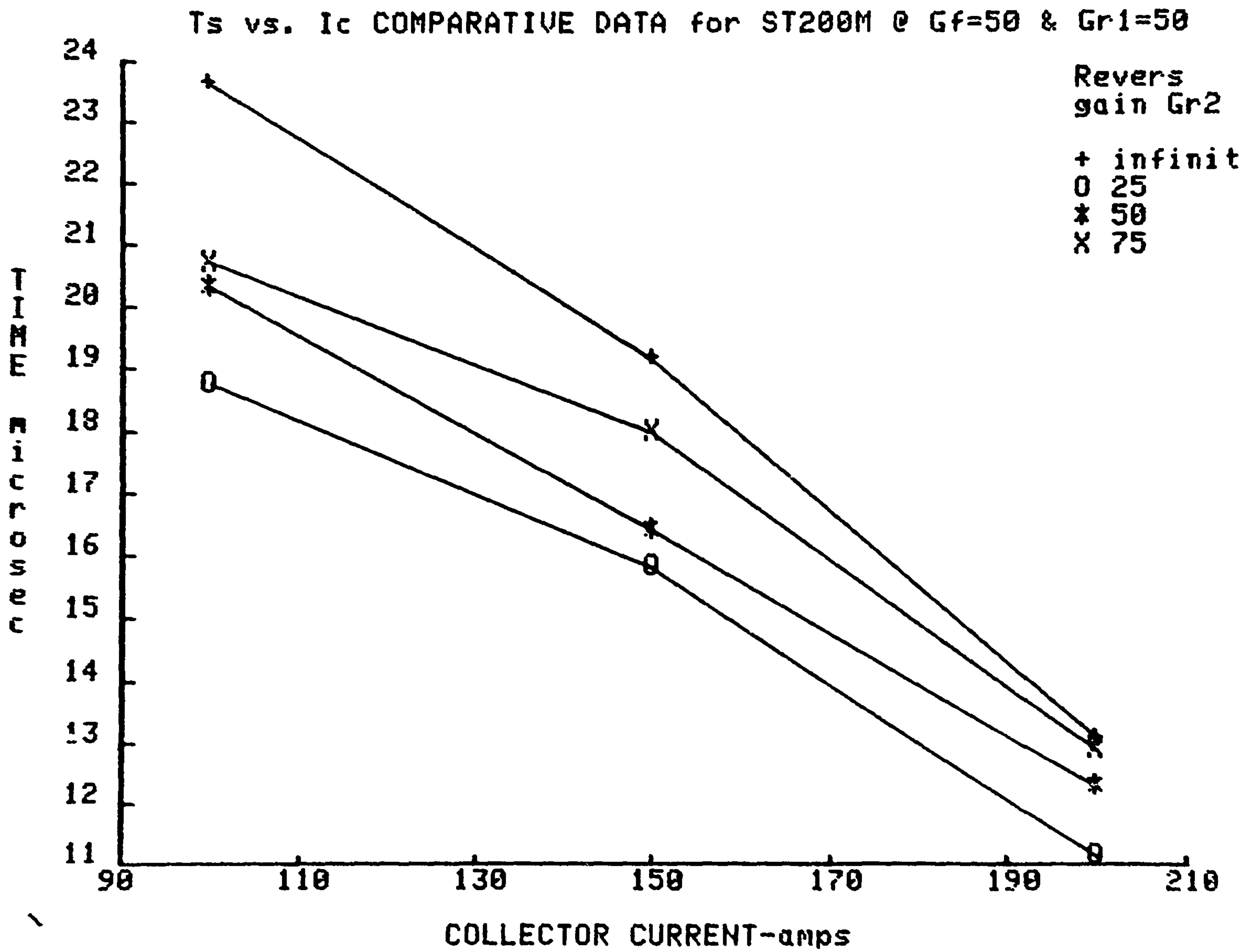

Ts vs. Ic COMPARATIVE DATA for ST200M @ Gf=50 & Gr1=50
TIME microsec
24
23
22
21
20
19
18
17
16
15
14
13
12
11
90
110
130
150
170
190
210
COLLECTOR CURRENT-amps
Revers
gain Gr2
+ infinit
O 25
* 50
X 75

Fig. A.8.6

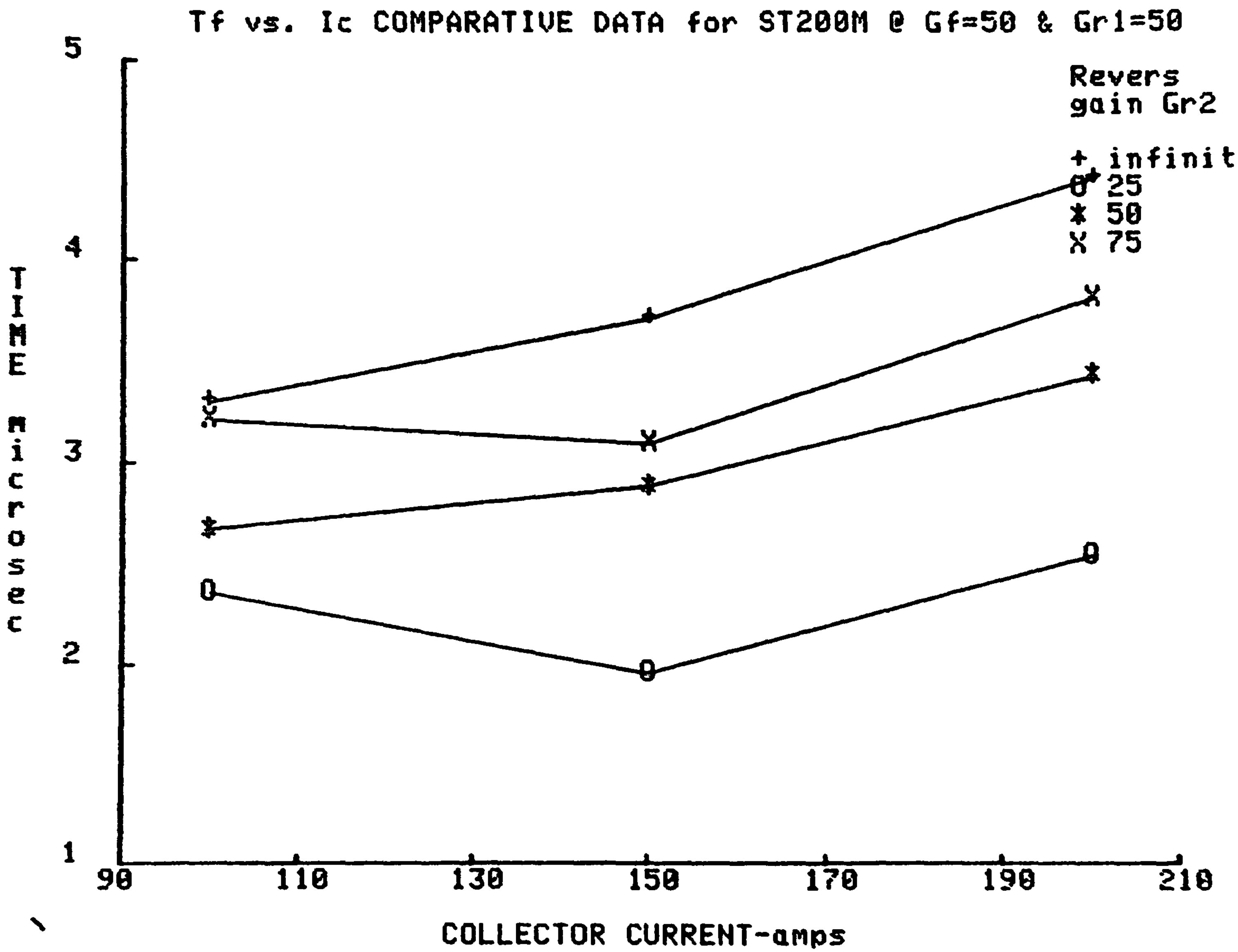
Tf vs. Ic COMPARATIVE DATA for ST200M @ Gf=50 & Gr1=50
Revers gain Gr2
+ infinit
0 25
* 50
X 75
TIME microsec
5
4
3
2
1
90
110
130
150
170
190
210
COLLECTOR CURRENT-amps

A.122

Fig. A.8.7

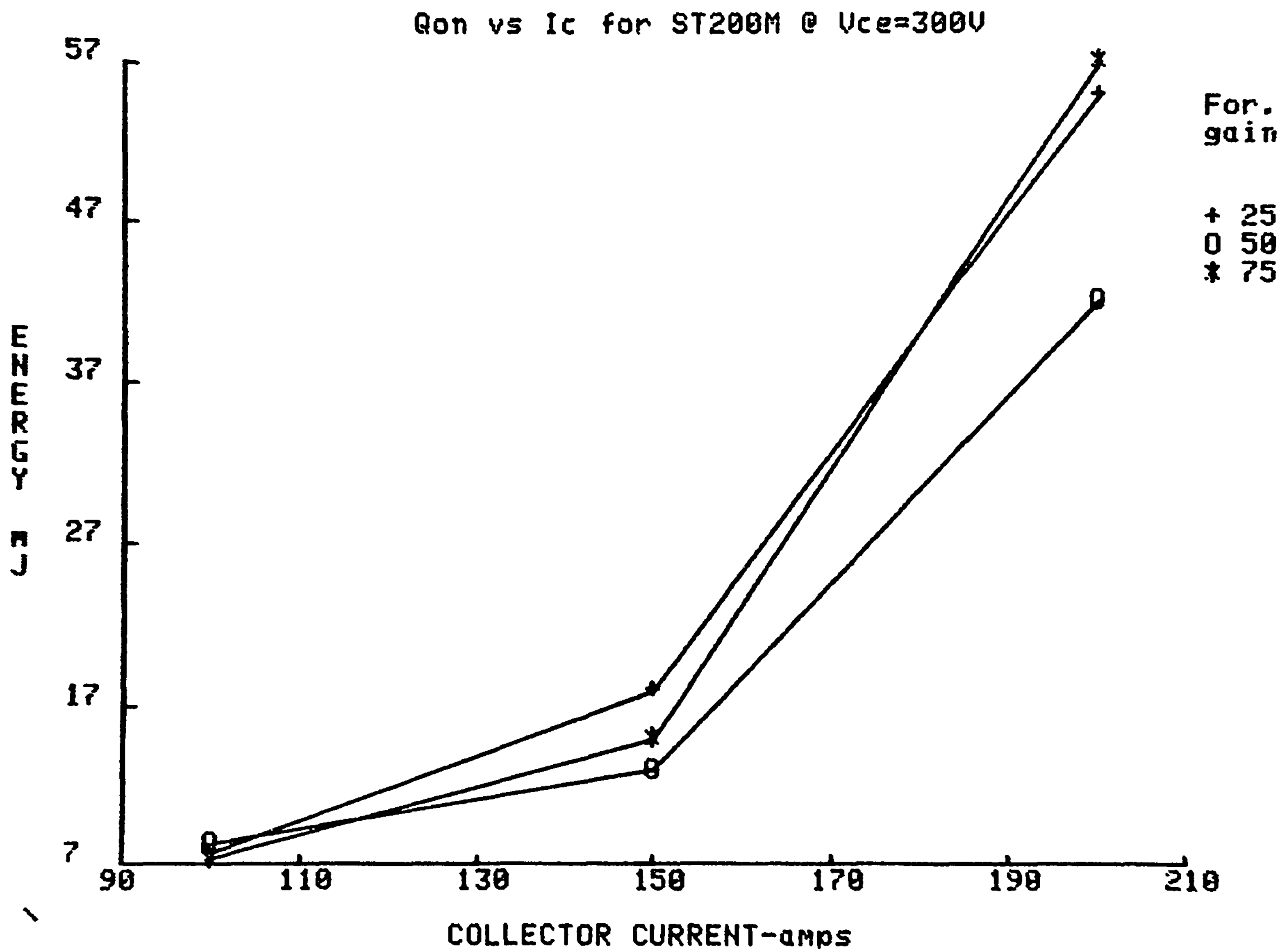
Qon vs Ic for ST200M @ Vce=300V
57
47
37
27
17
7
ENERGY mJ
90
110
130
150
170
190
210
COLLECTOR CURRENT-amps
For. gain
+ 25
O 50
* 75

Fig. A.8.8

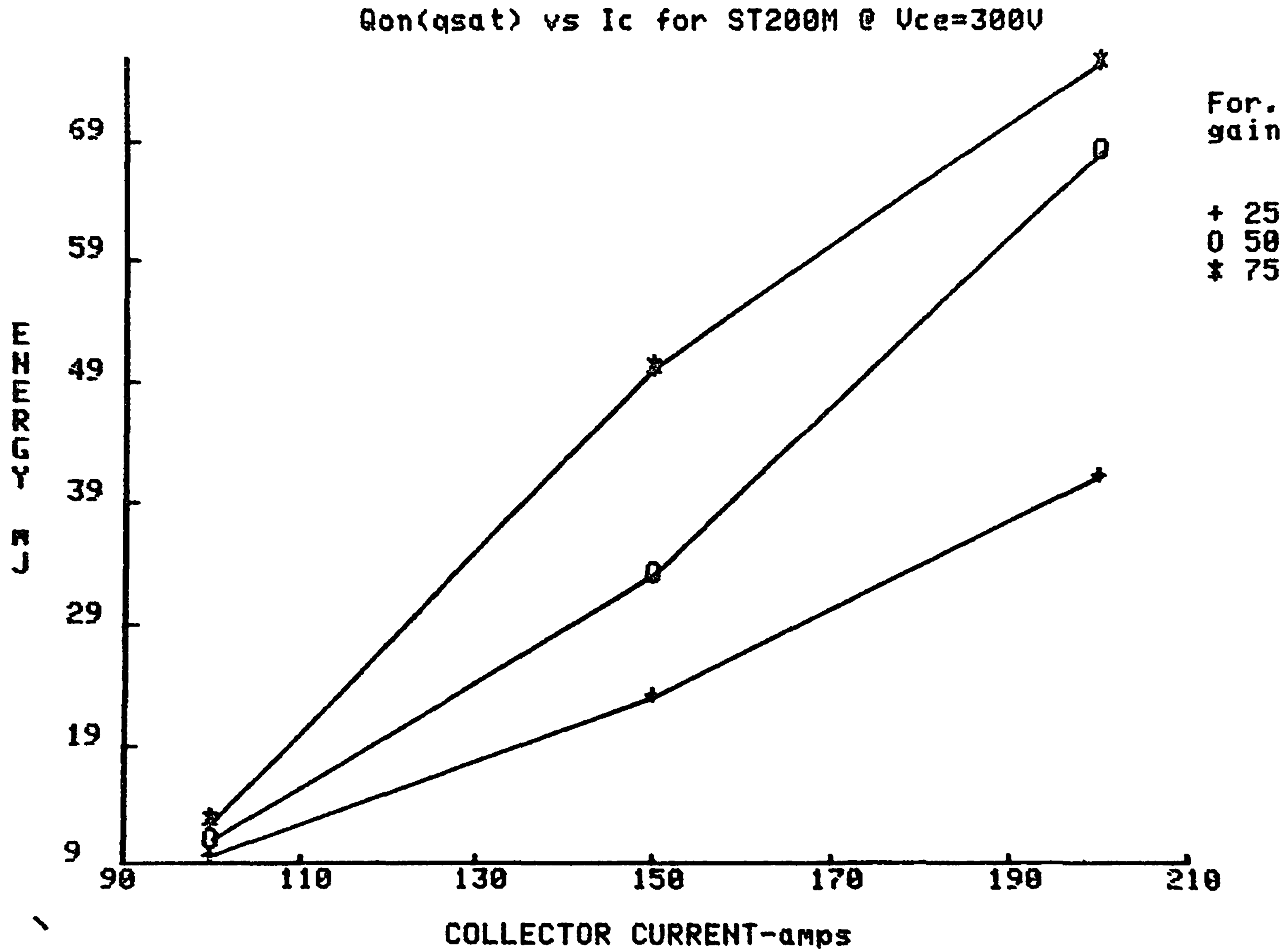
Qon(qsat) vs Ic for ST200M @ Vce=300V
ENERGY mJ
69
59
49
39
29
19
9
90
110
130
150
170
190
210
COLLECTOR CURRENT-amps
For. gain
+ 25
O 50
* 75

A.124

Fig. A.8.9

Qon(tot) vs Ic for ST200M @ Vce=300V

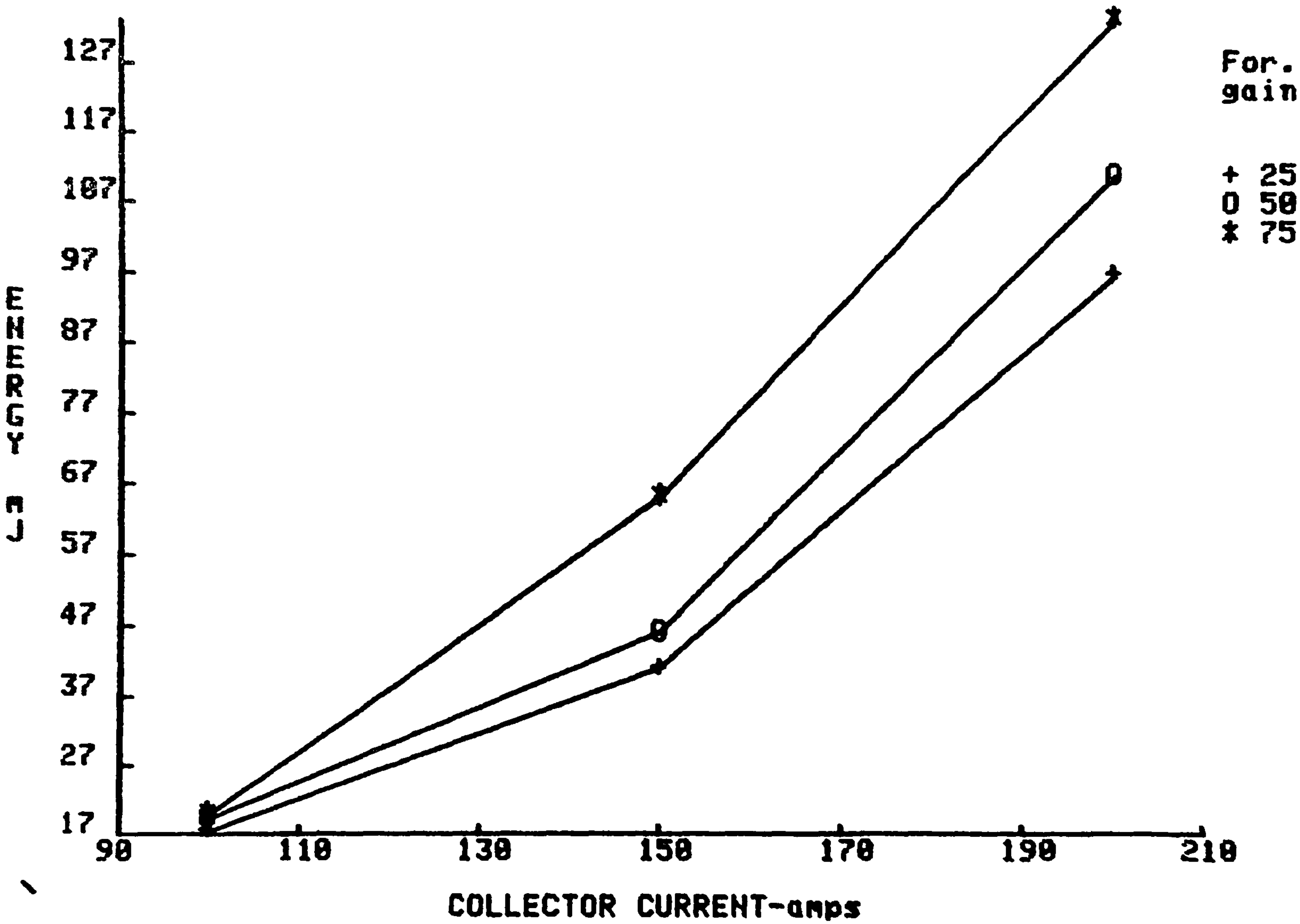

Fig. A.8.10

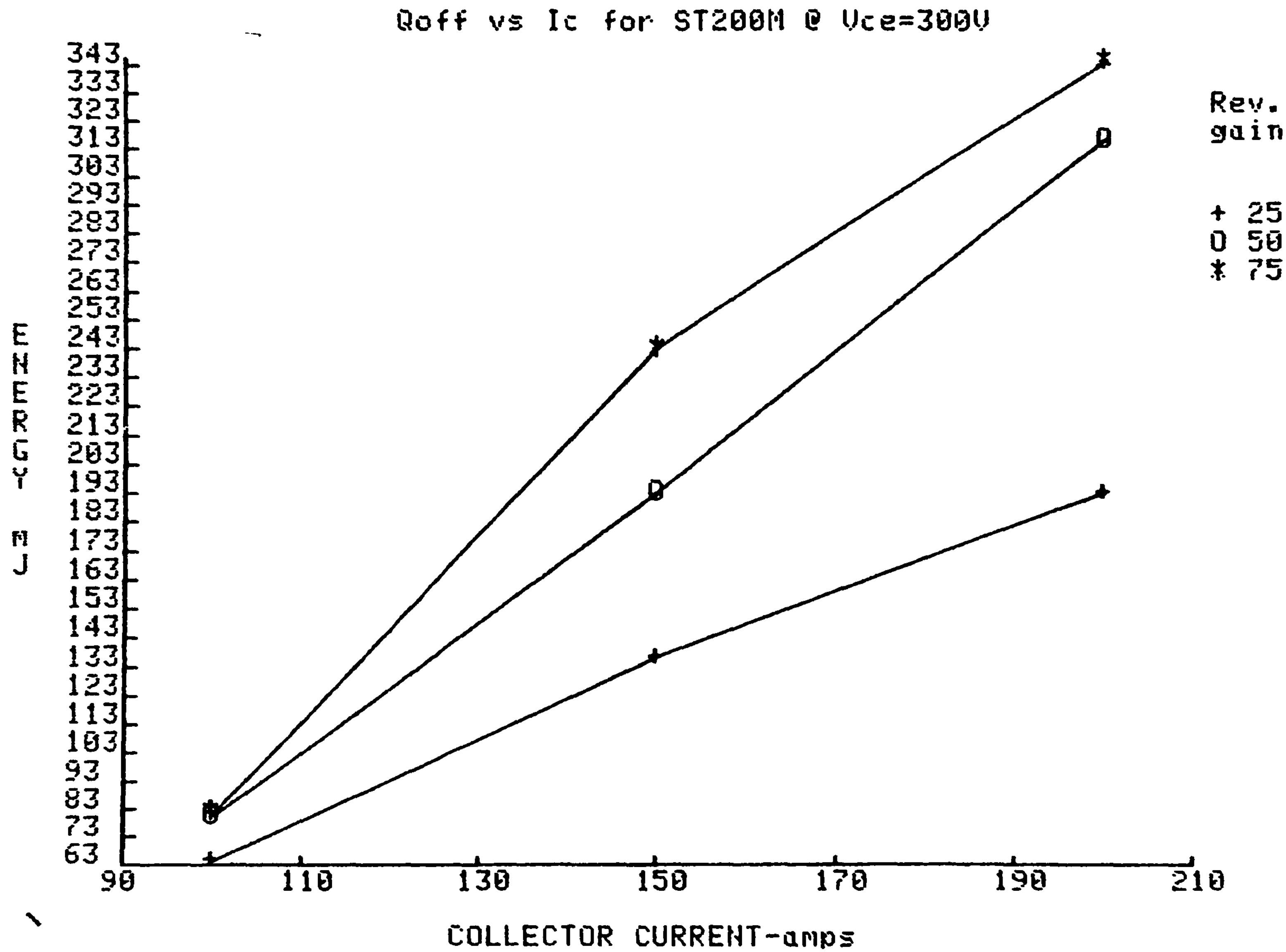
Qoff vs Ic for ST200M @ Vce=300V
ENERGY mJ
343
333
323
313
303
293
283
273
263
253
243
233
223
213
203
193
183
173
163
153
143
133
123
113
103
93
83
73
63
90
110
130
150
170
190
210
COLLECTOR CURRENT-amps
Rev. gain
+ 25
O 50
* 75

Fig. A.8.11

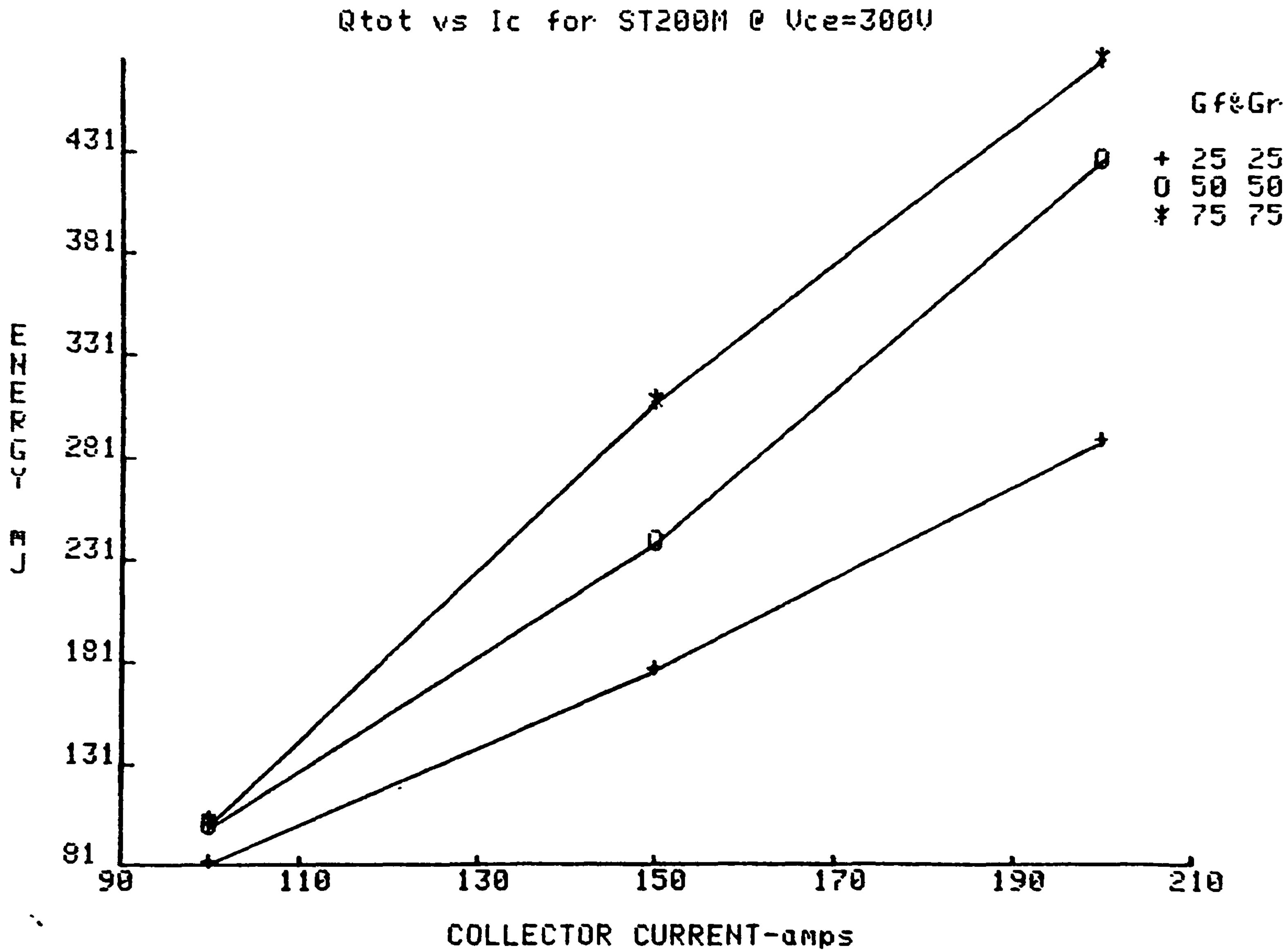
Qtot vs Ic for ST200M @ Vce=300V
ENERGY-mJ
431
381
331
281
231
181
131
81
90
110
130
150
170
190
210
COLLECTOR CURRENT-amps
Gf&Gr
+ 25 25
0 50 50
* 75 75

Fig. A.8.12

Switching Loadline Characteristics: Vce vs. Ic
for Turn-on of Power Transistor with Inductive Load

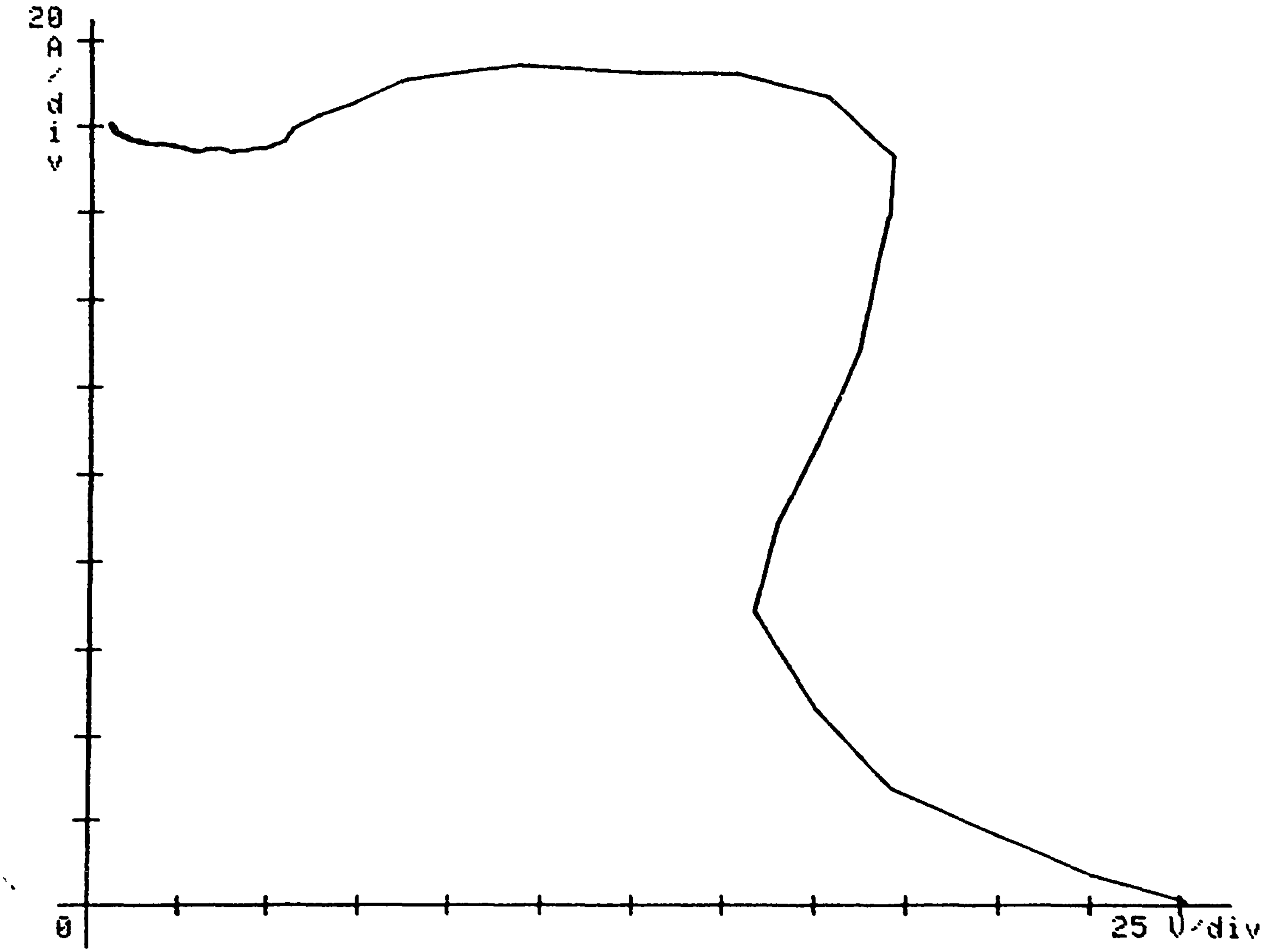

Fig. A.8.13

Switching Loadline Characteristics: Uce vs. Ic
for Turn-off of Power Trans. with Inductive Load

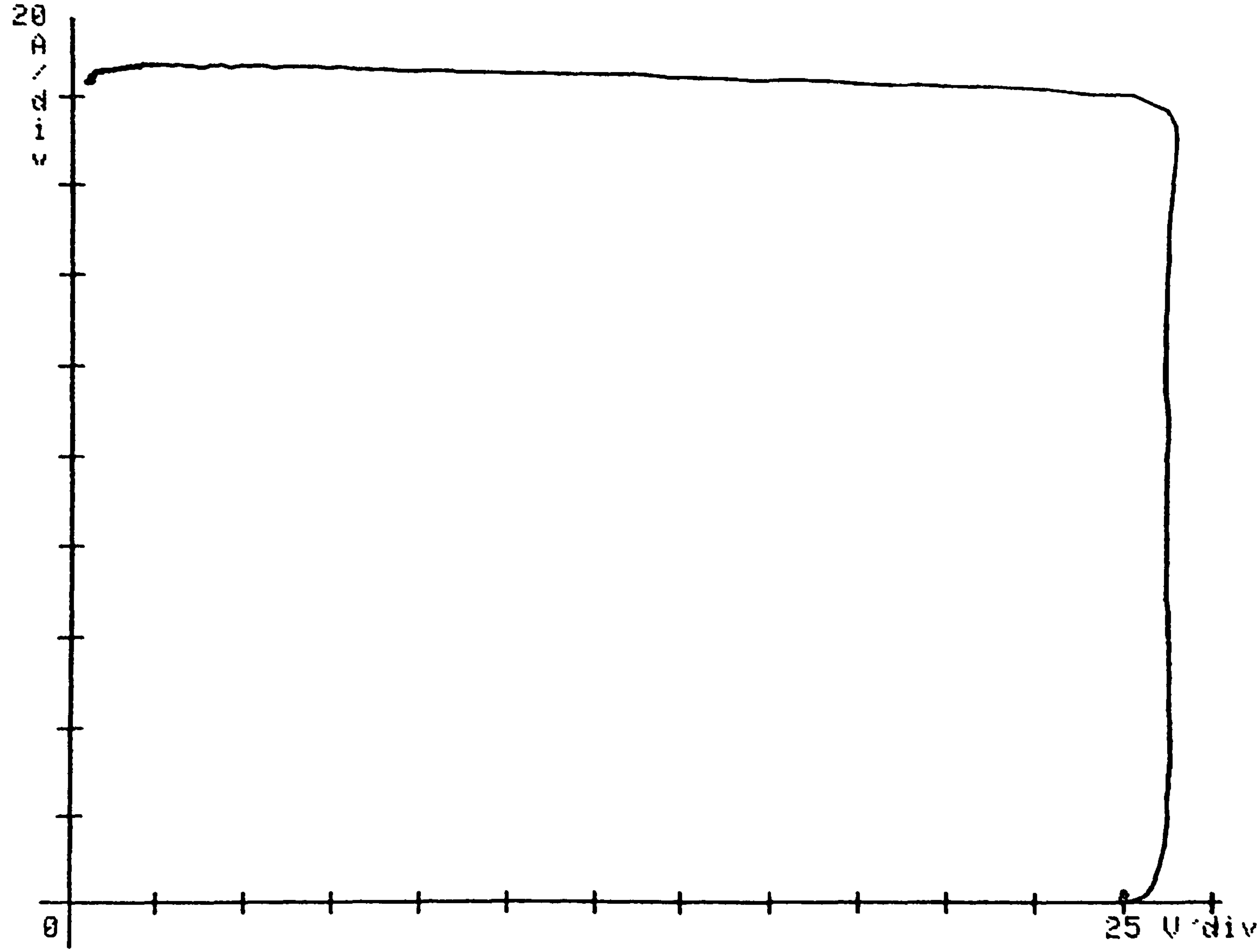

Fig. A.8.14

Vces vs. Ic for ST200M

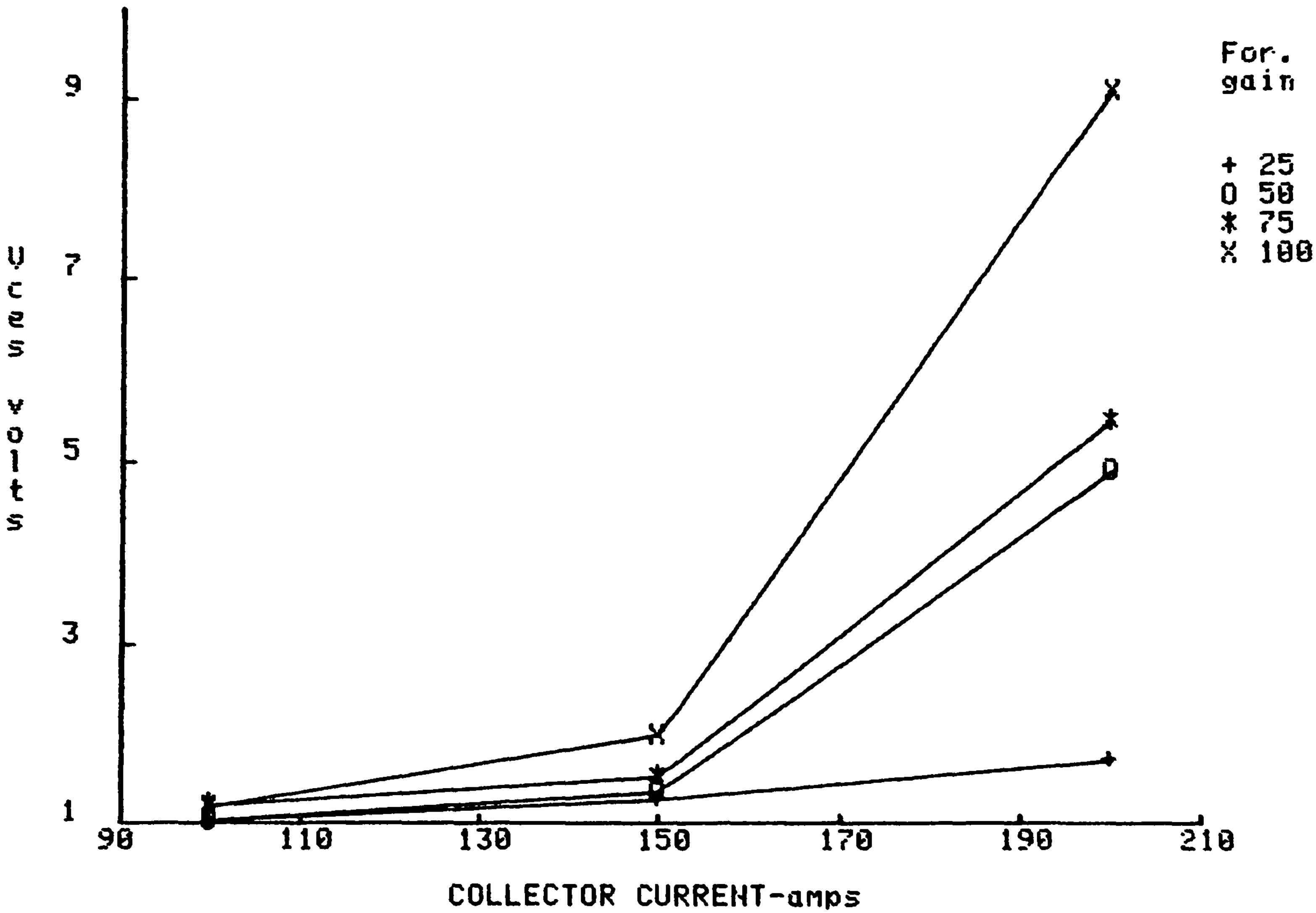

Fig. A.8.15

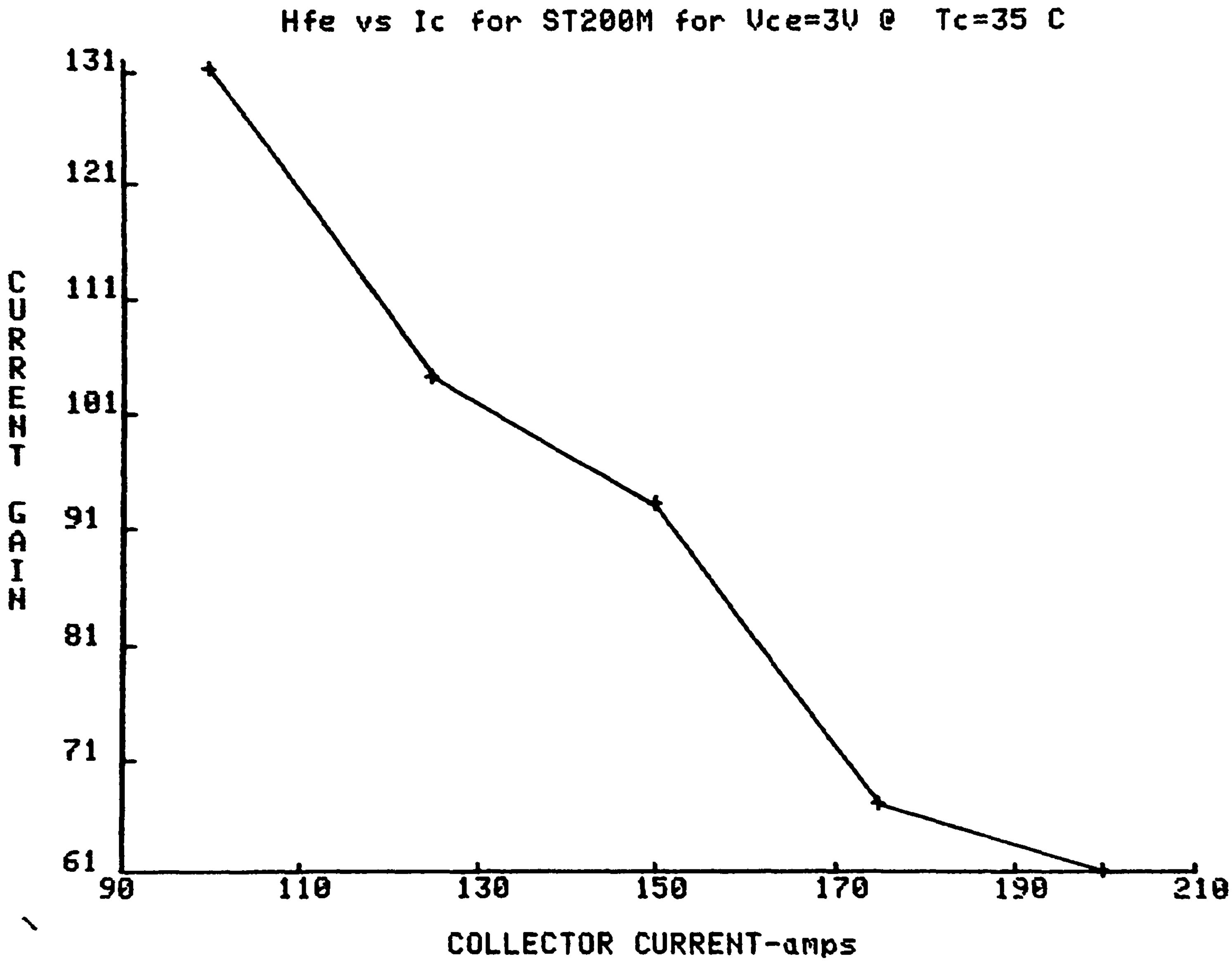
Hfe vs Ic for ST200M for Vce=3V @ Tc=35 C
CURRENT GAIN
131
121
111
101
91
81
71
61
90
110
130
150
170
190
210
COLLECTOR CURRENT-amps

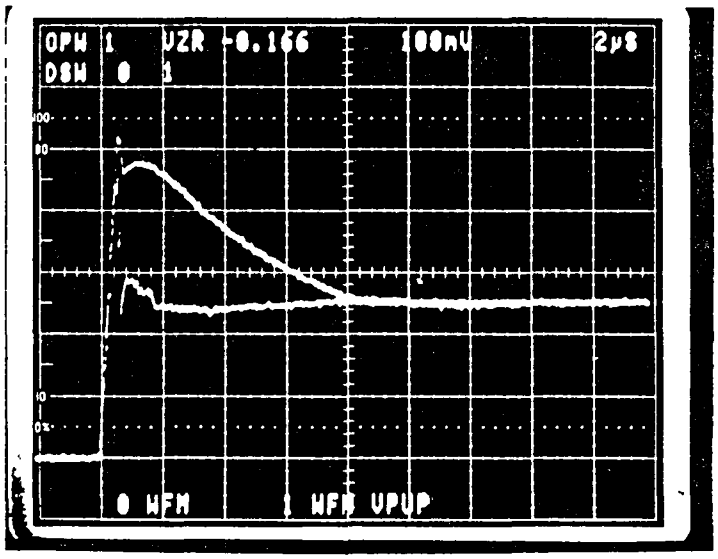

Fig. A.8.16 Diode recovery and dv/dt test for ST200M

Upper trace: Base open

Lower trace: Base reverse biased

(Scale: horizontal 1 μs/div; vertical 40 A/div)

A.9 Test Data for Toshiba ST300M21

Fig. A.9.1

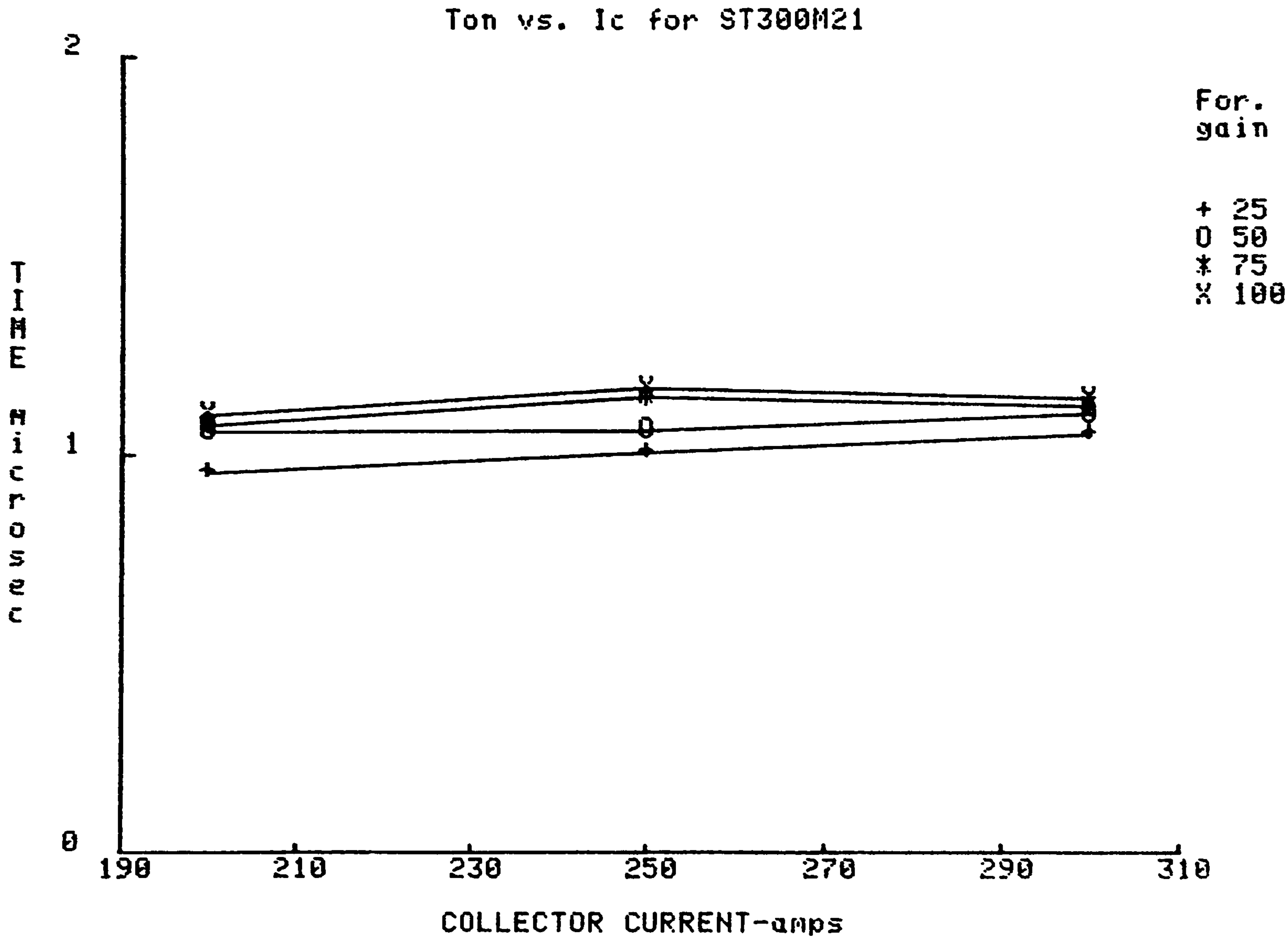

Ton vs. Ic for ST300M21
2
1
0
TIME Microsec
190
210
230
250
270
290
310
COLLECTOR CURRENT-amps
For. gain
+ 25
O 50
* 75
X 100

Fig. A.9.2

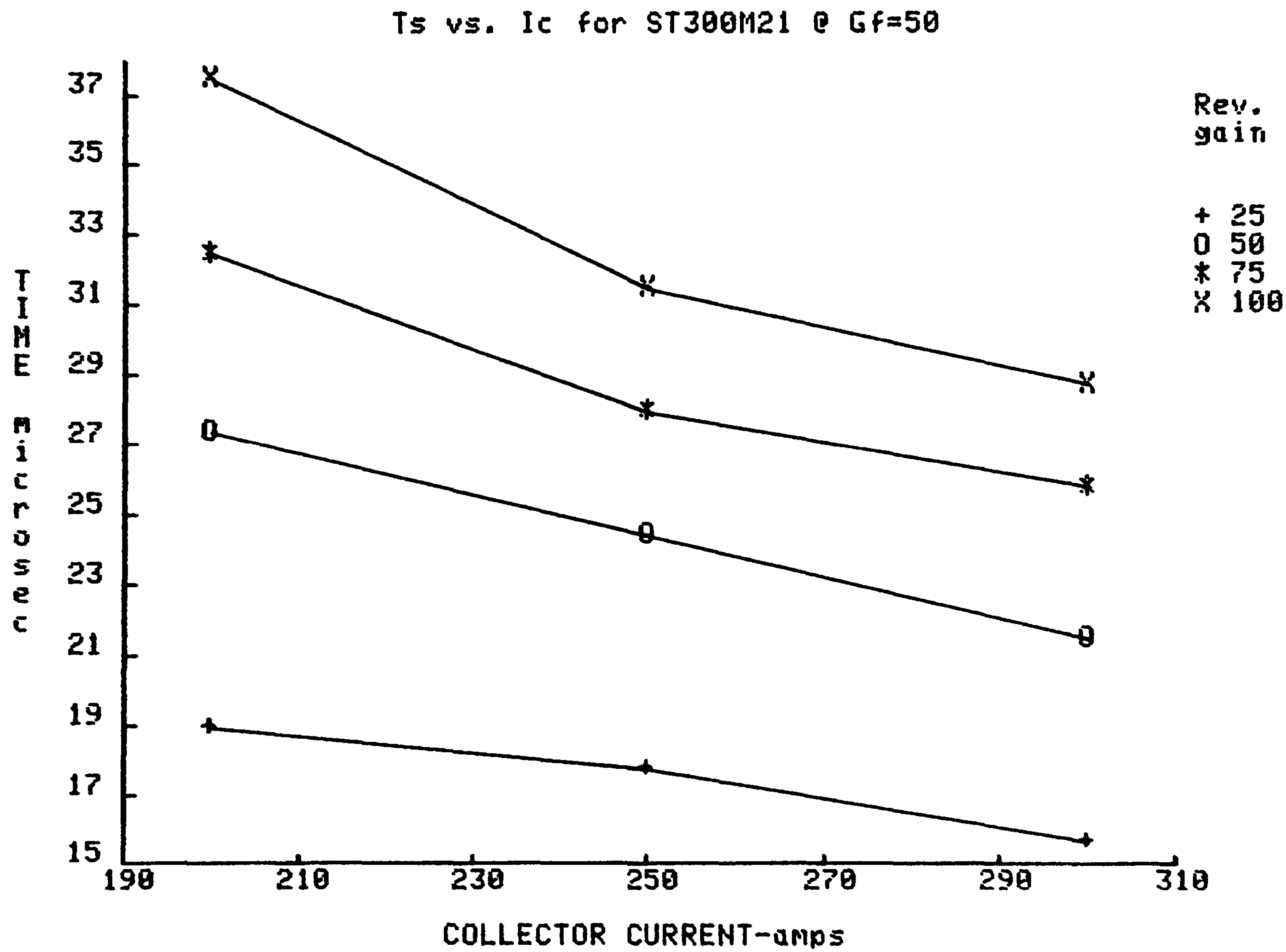
Ts vs. Ic for ST300M21 @ Gf=50
TIME microsec
37
35
33
31
29
27
25
23
21
19
17
15
190
210
230
250
270
290
310
COLLECTOR CURRENT-amps
Rev. gain
+ 25
O 50
* 75
X 100

Fig. A.9.3

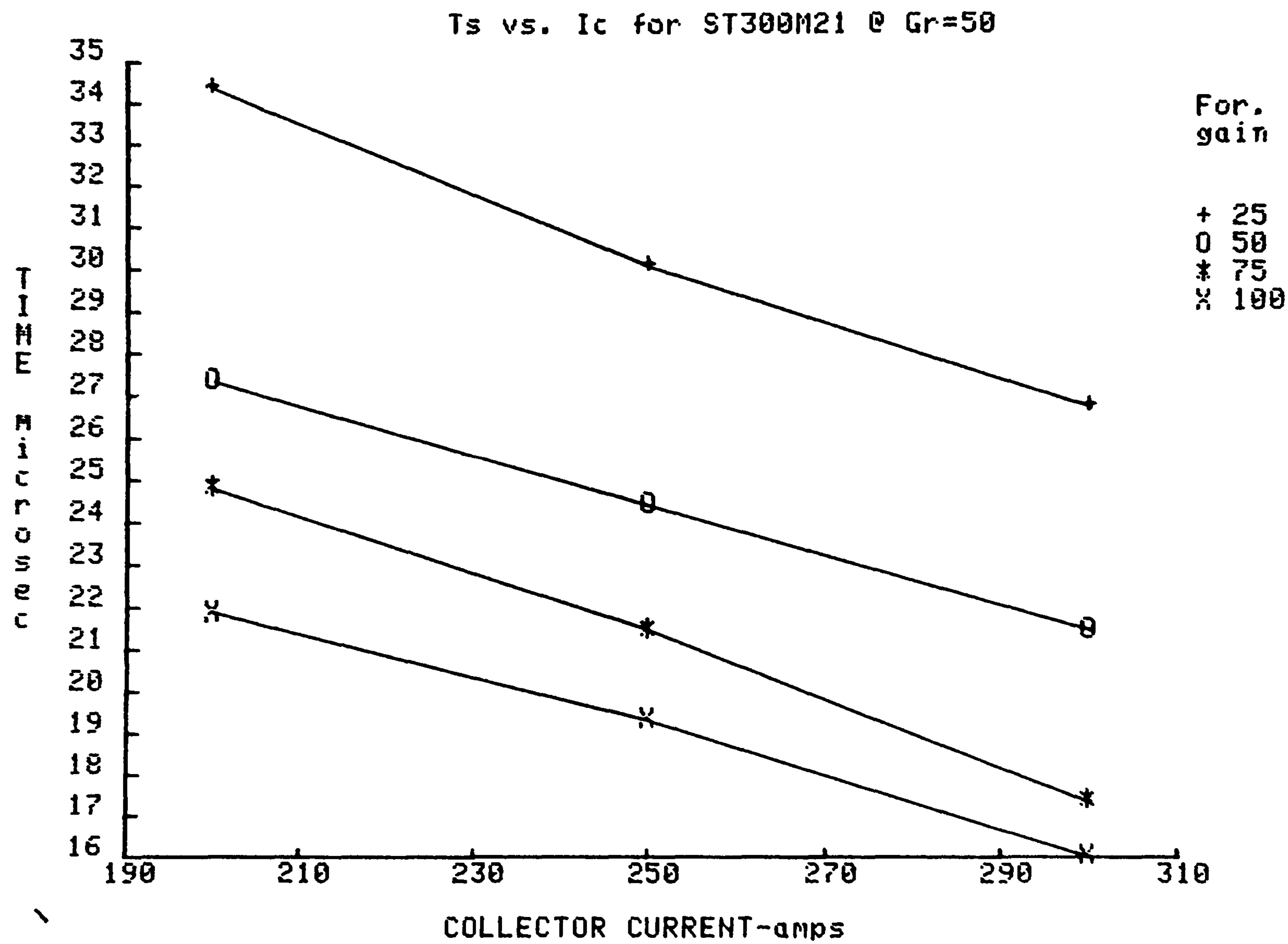
Ts vs. Ic for ST300M21 @ Gr=50
TIME Microsec
35
34
33
32
31
30
29
28
27
26
25
24
23
22
21
20
19
18
17
16
190
210
230
250
270
290
310
COLLECTOR CURRENT-amps
For. gain
+ 25
O 50
* 75
X 100

Fig. A.9.4

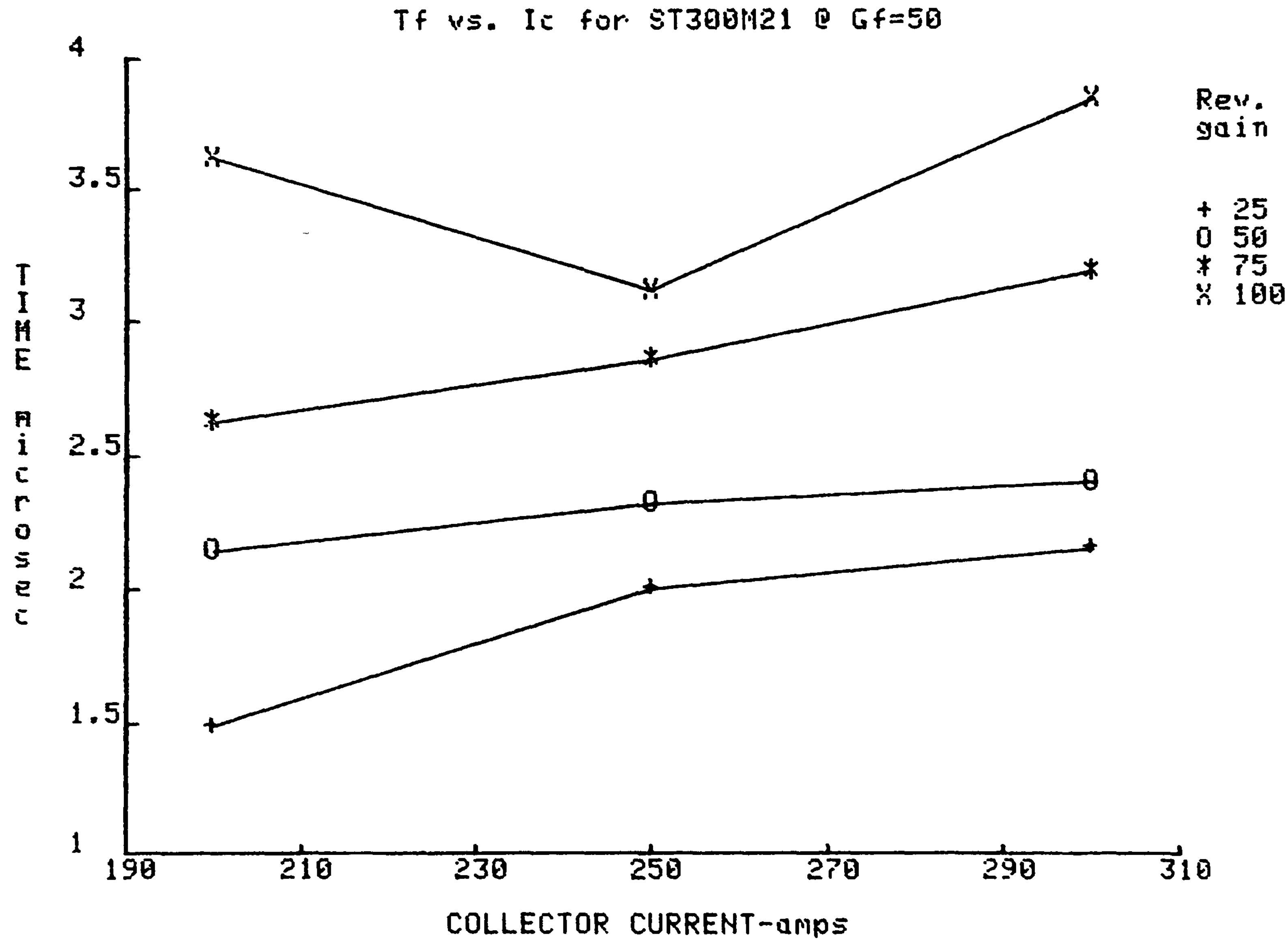
Tf vs. Ic for ST300M21 @ Gf=50
TIME microsec
4
3.5
3
2.5
2
1.5
1
190
210
230
250
270
290
310
COLLECTOR CURRENT-amps
Rev. gain
+ 25
O 50
* 75
X 100

Fig. A.9.7

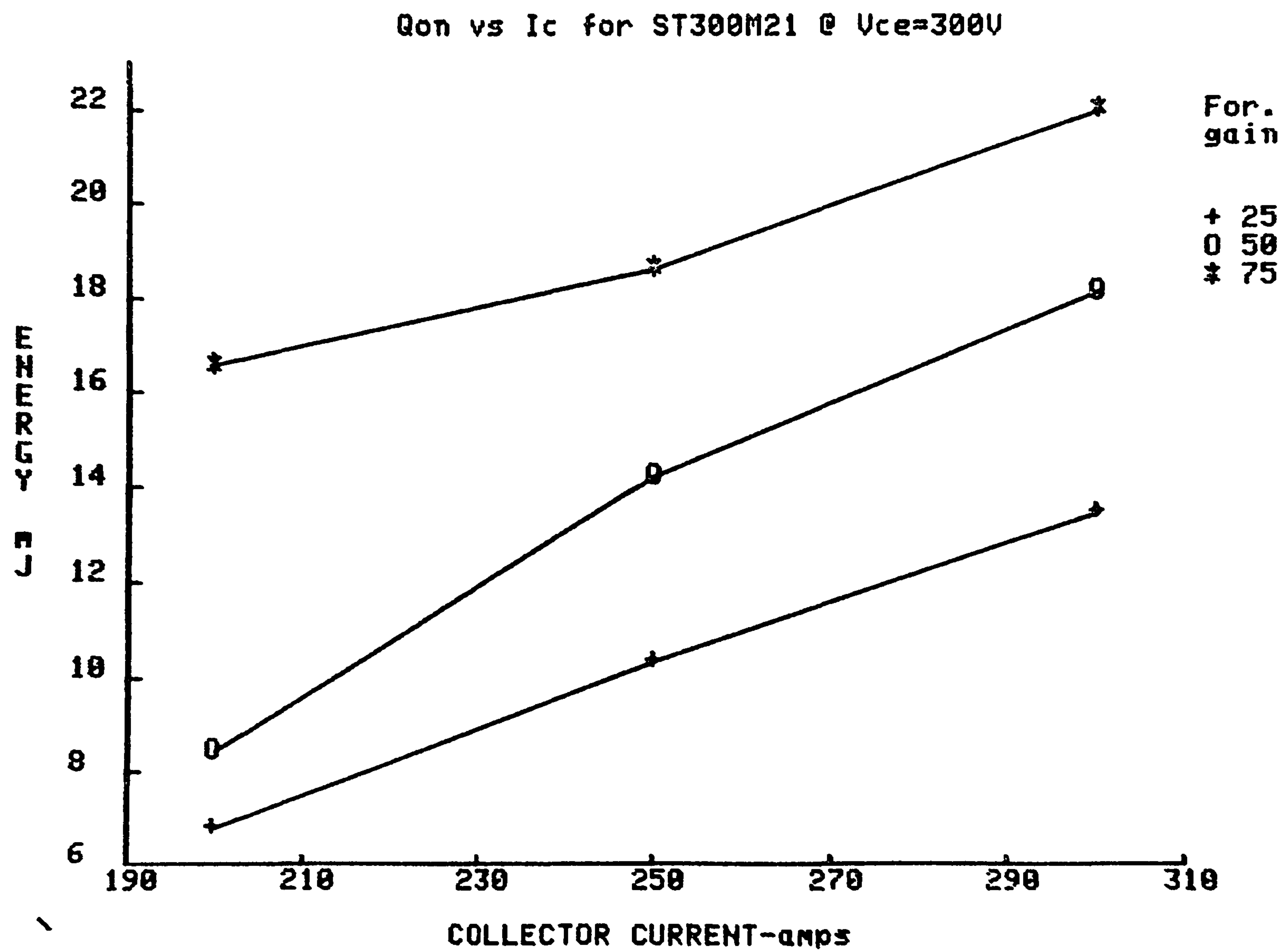

Qon vs Ic for ST300M21 @ Vce=300V
ENERGY mJ
22
20
18
16
14
12
10
8
6
190
210
230
250
270
290
310
COLLECTOR CURRENT-amps
For. gain
+ 25
0 50
* 75

Fig. A.9.8

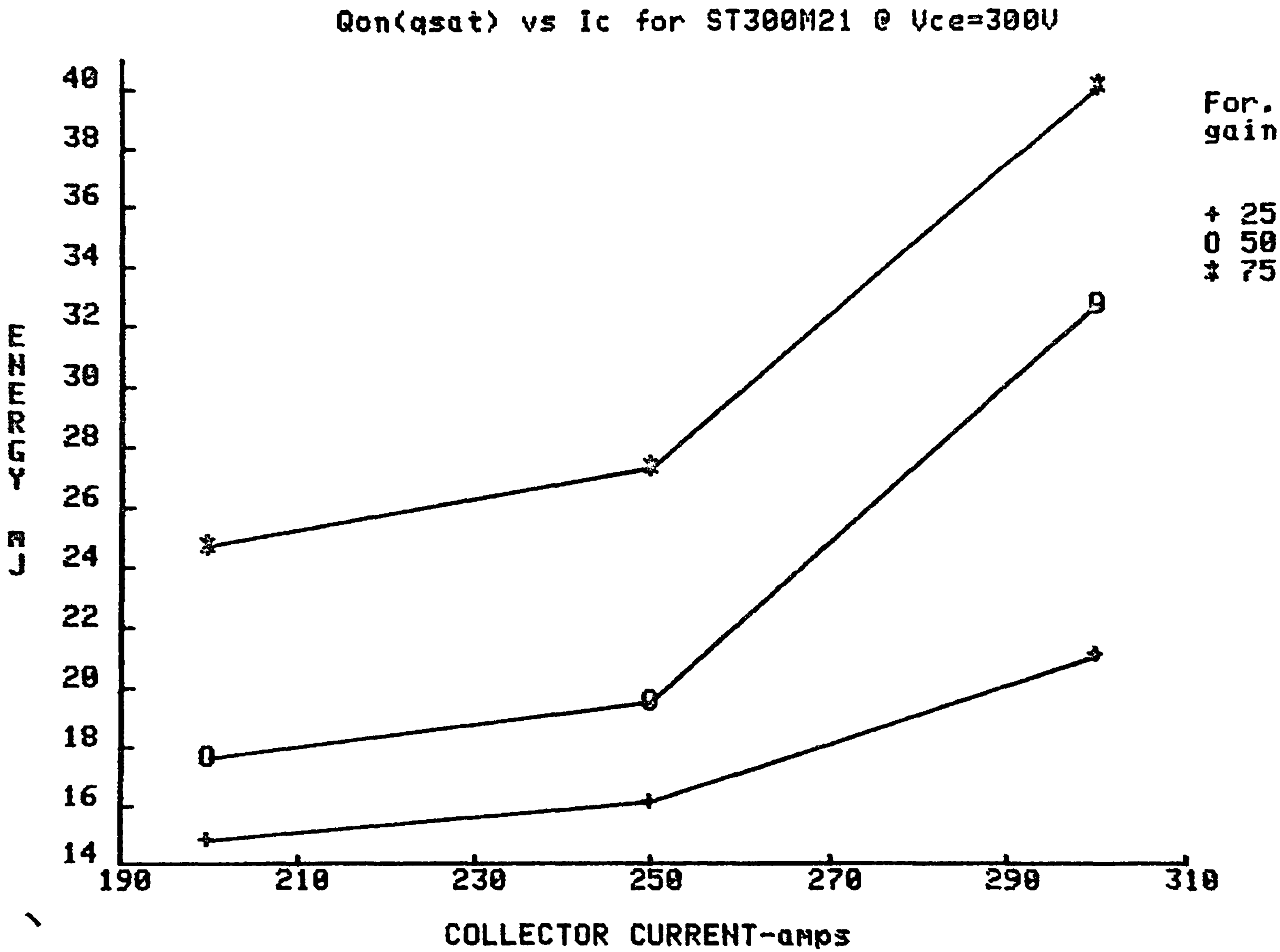
Qon(qsat) vs Ic for ST300M21 @ Vce=300V
ENERGY mJ
40
38
36
34
32
30
28
26
24
22
20
18
16
14
190
210
230
250
270
290
310
COLLECTOR CURRENT-amps
For. gain
+ 25
O 50
* 75

Fig. A.9.9

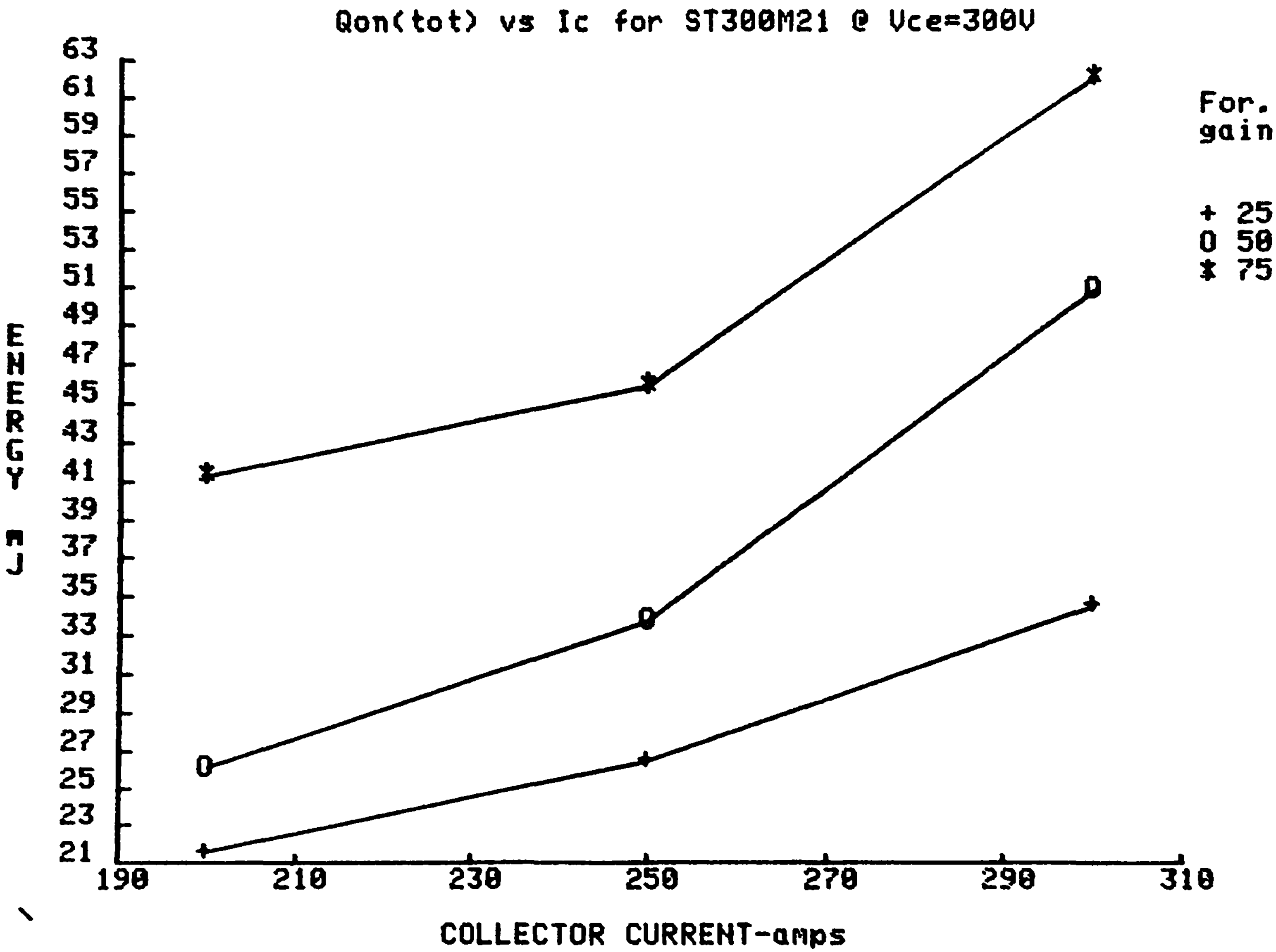
Qon(tot) vs Ic for ST300M21 @ Vce=300V
ENERGY mJ
COLLECTOR CURRENT-amps
For. gain
+ 25
O 50
* 75
63
61
59
57
55
53
51
49
47
45
43
41
39
37
35
33
31
29
27
25
23
21
190
210
230
250
270
290
310

Fig. A.9.10

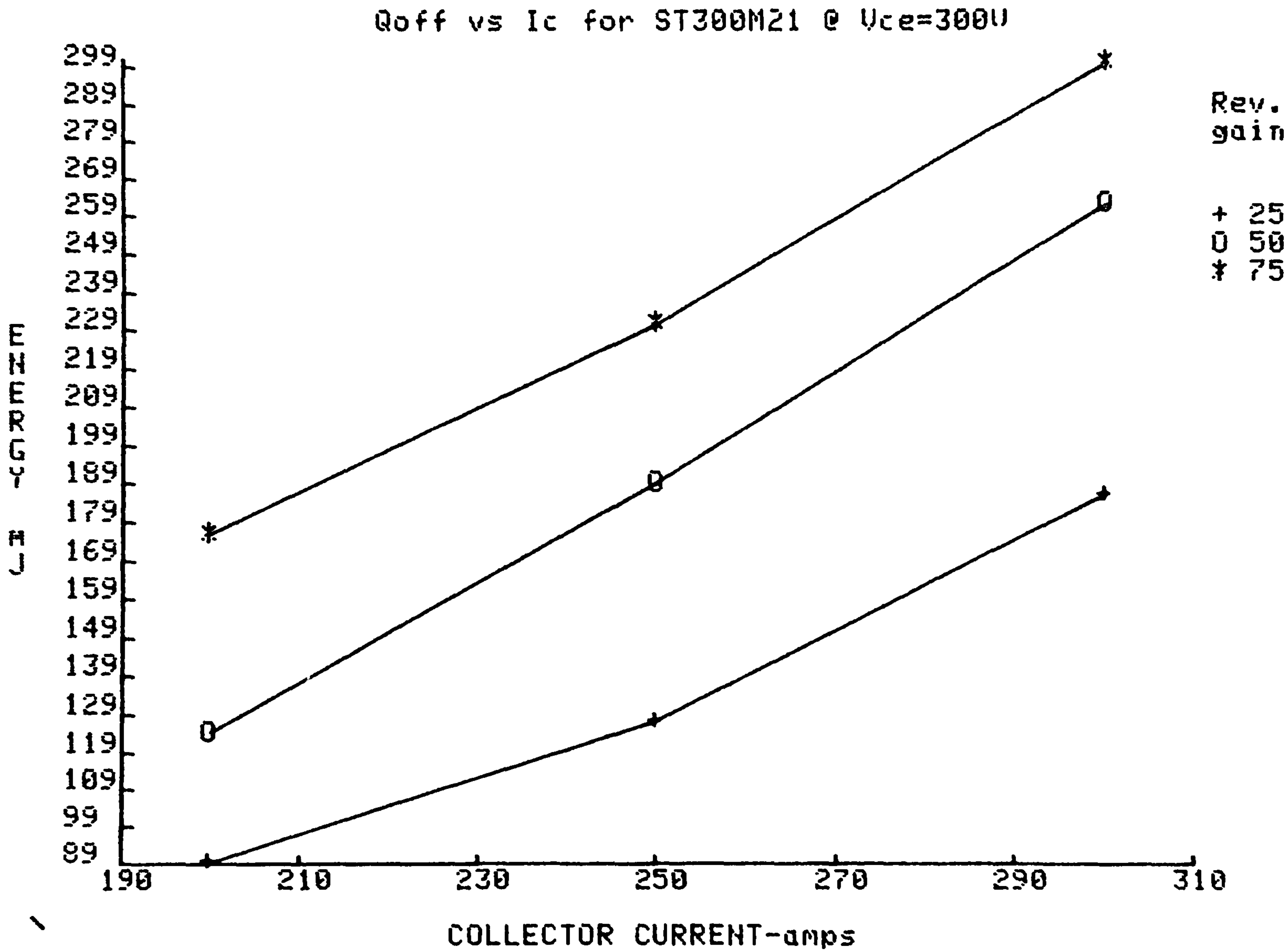
Qoff vs Ic for ST300M21 @ Vce=300V
299
289
279
269
259
249
239
229
219
209
199
189
179
169
159
149
139
129
119
109
99
89
ENERGY mJ
190
210
230
250
270
290
310
COLLECTOR CURRENT-amps
Rev. gain
+ 25
O 50
* 75

Fig. A.9.11

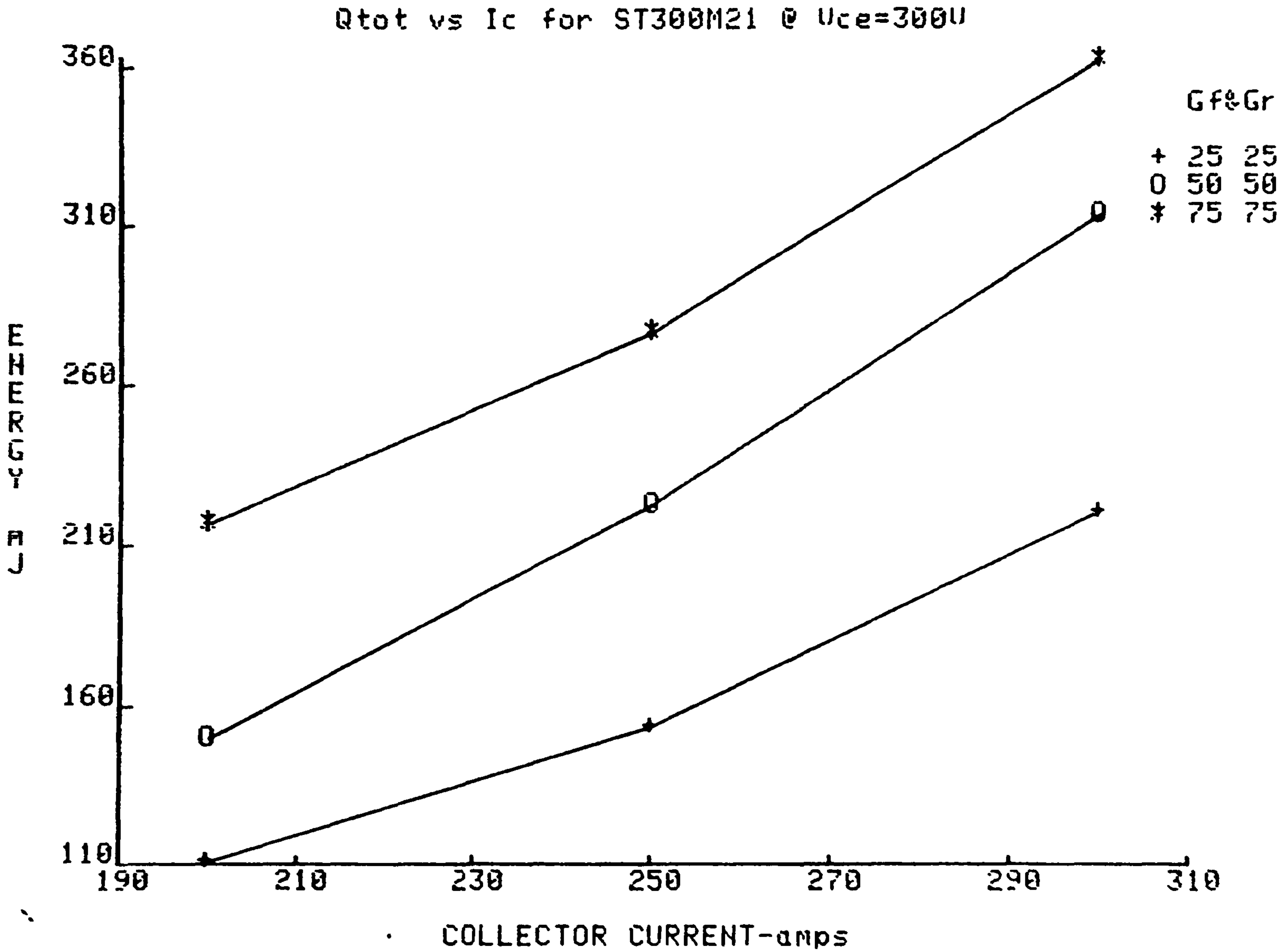
Qtot vs Ic for ST300M21 @ Vce=300V
360
310
260
210
160
110
ENERGY mJ
190
210
230
250
270
290
310
COLLECTOR CURRENT-amps
Gf&Gr
+ 25 25
O 50 50
* 75 75

Fig. A.9.12

Switching Loadline Characteristics: Uce vs. Ic
for Turn-on of Power Transistor with Inductive Load

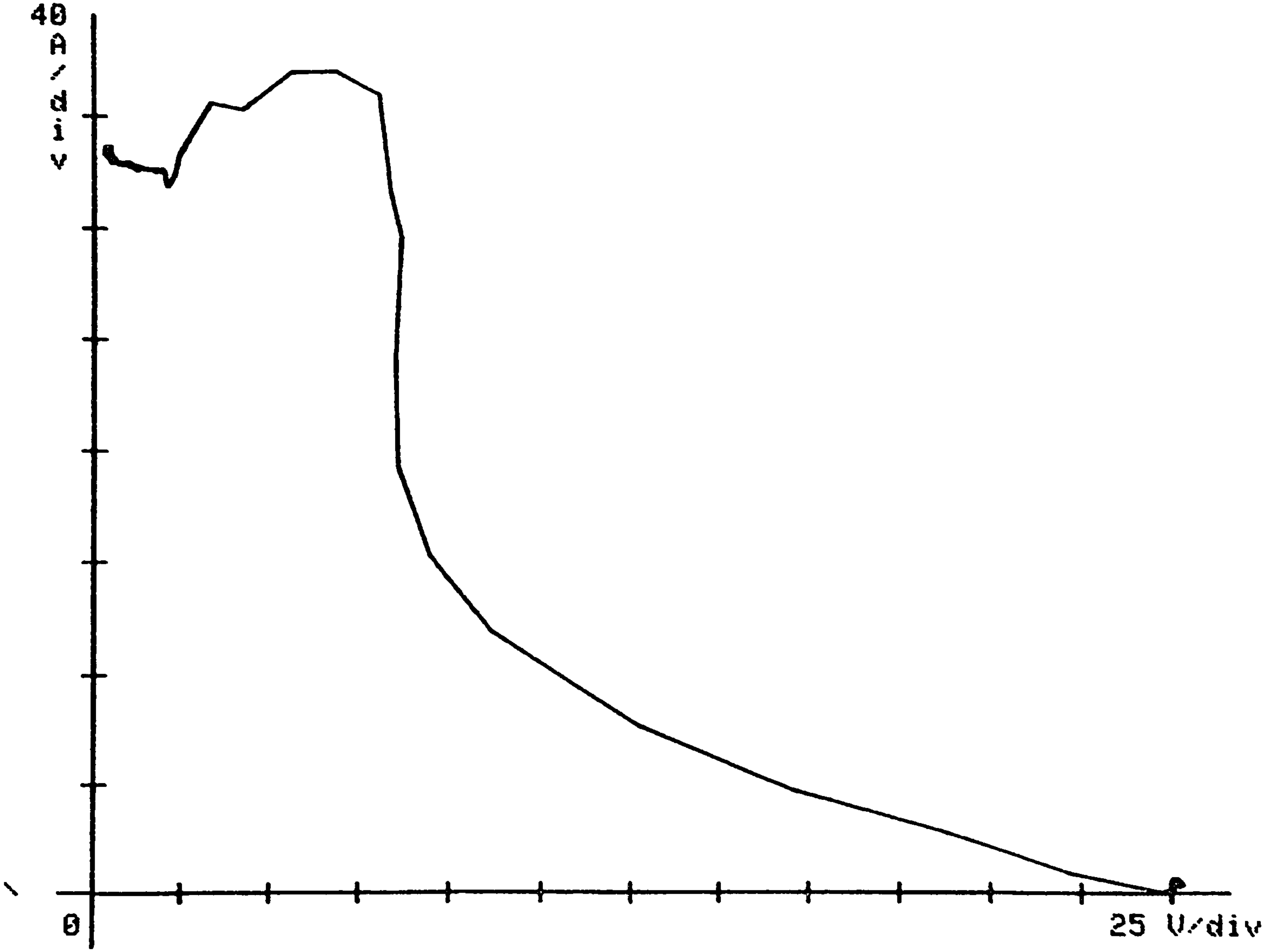

Fig. A.9.13

Switching Loadline Characteristics: Vce vs. Ic
for Turn-off of Power Trans. with Inductive Load

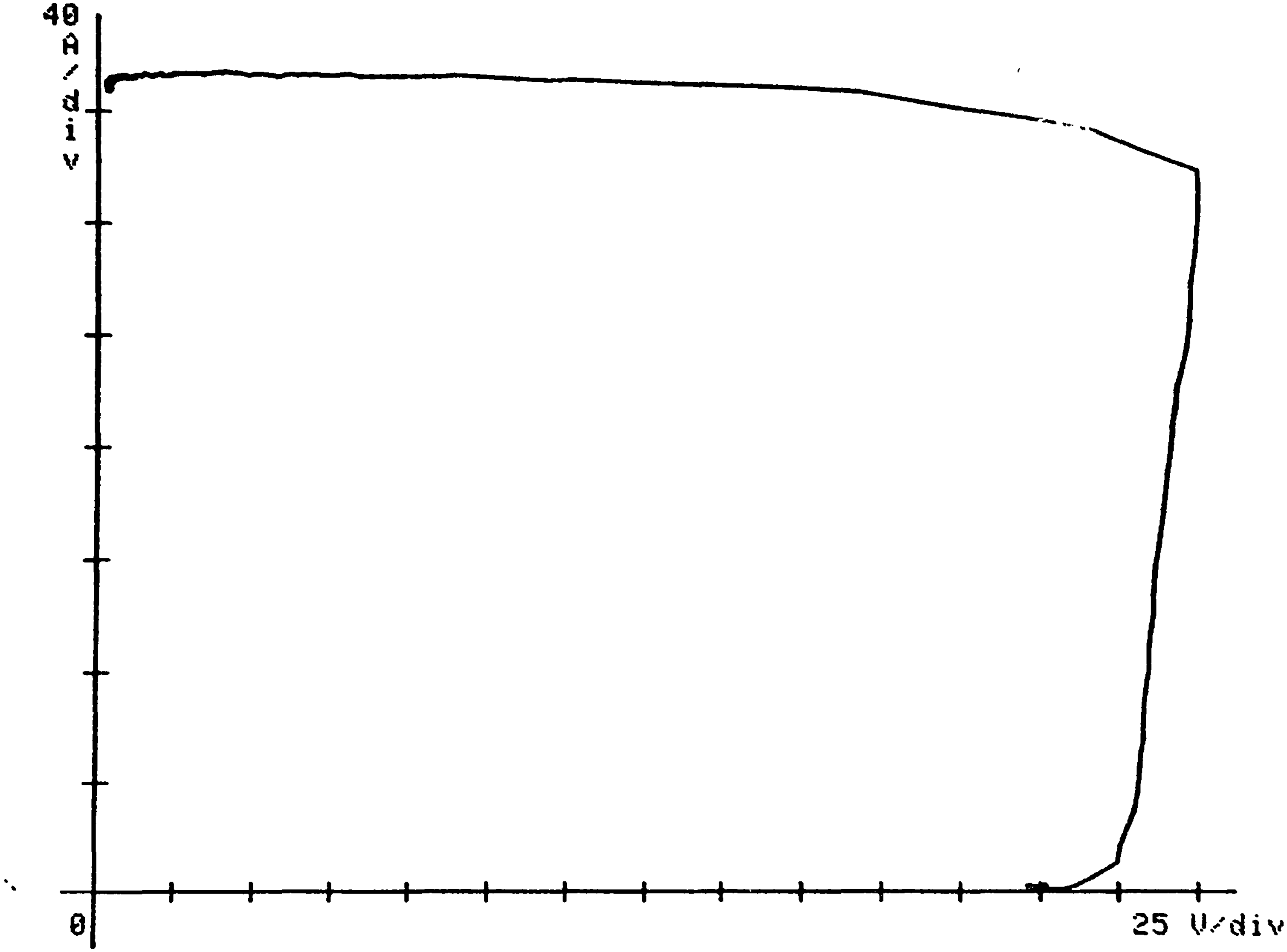

Fig. A.9.14

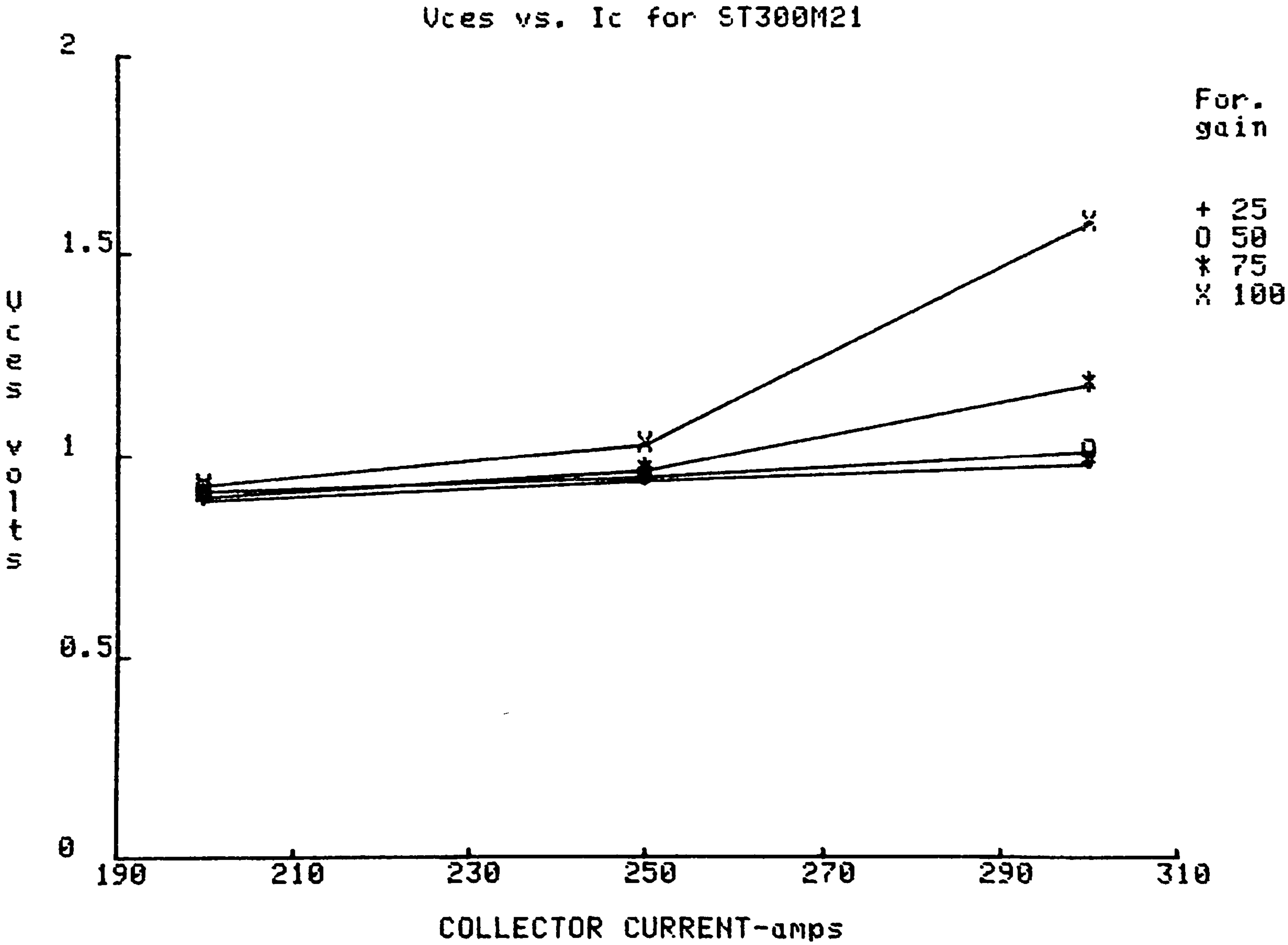

Vces vs. Ic for ST300M21
2
1.5
1
0.5
0
Vces volts
190
210
230
250
270
290
310
COLLECTOR CURRENT-amps
For.
gain
+ 25
O 50
* 75
X 100

Fig. A.9.15

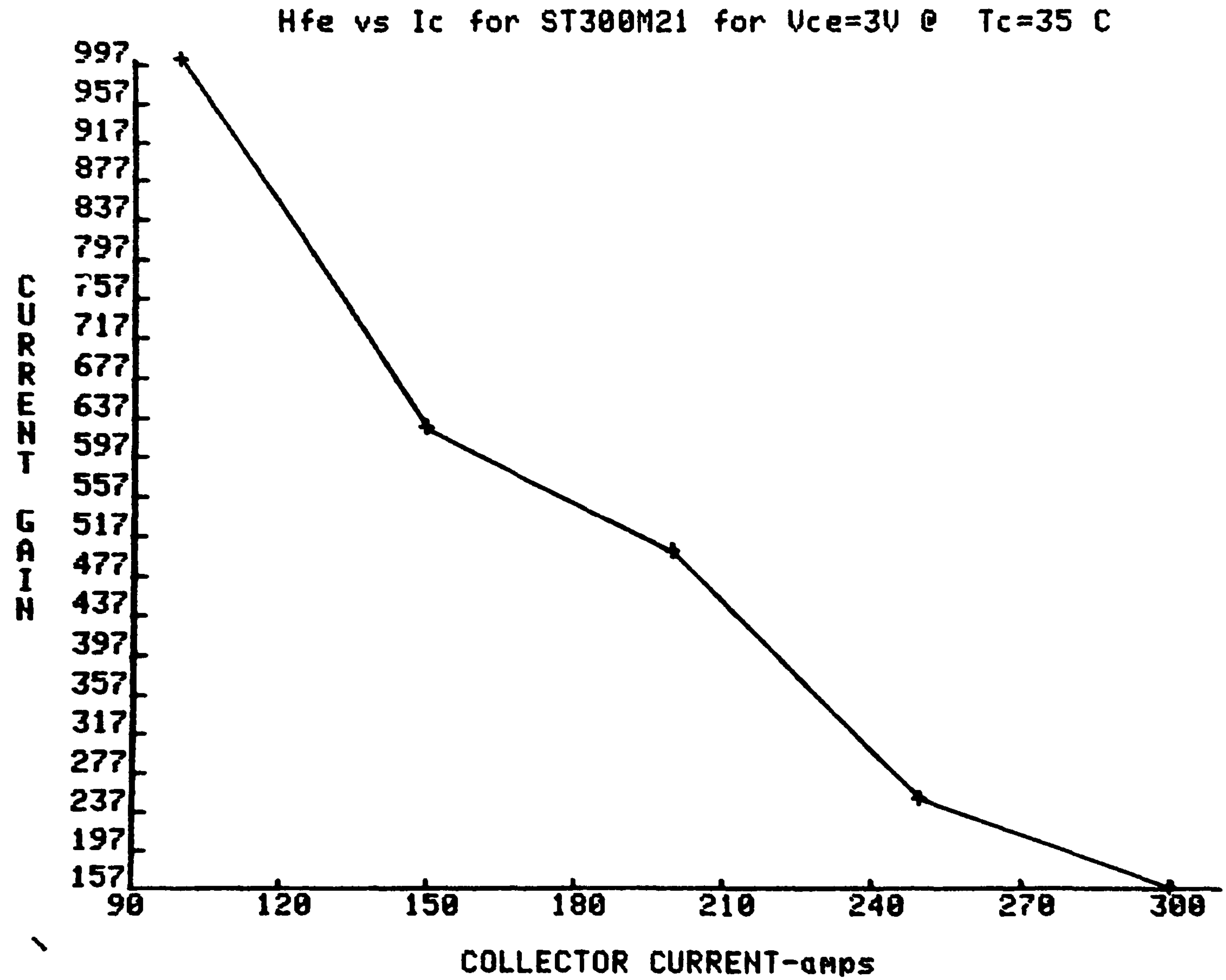

Hfe vs Ic for ST300M21 for Vce=3V @ Tc=35 C
CURRENT GAIN
997
957
917
877
837
797
757
717
677
637
597
557
517
477
437
397
357
317
277
237
197
157
90
120
150
180
210
240
270
300
COLLECTOR CURRENT-amps

A.10 Test Data for Toshiba ST400G

Fig. A.10.1

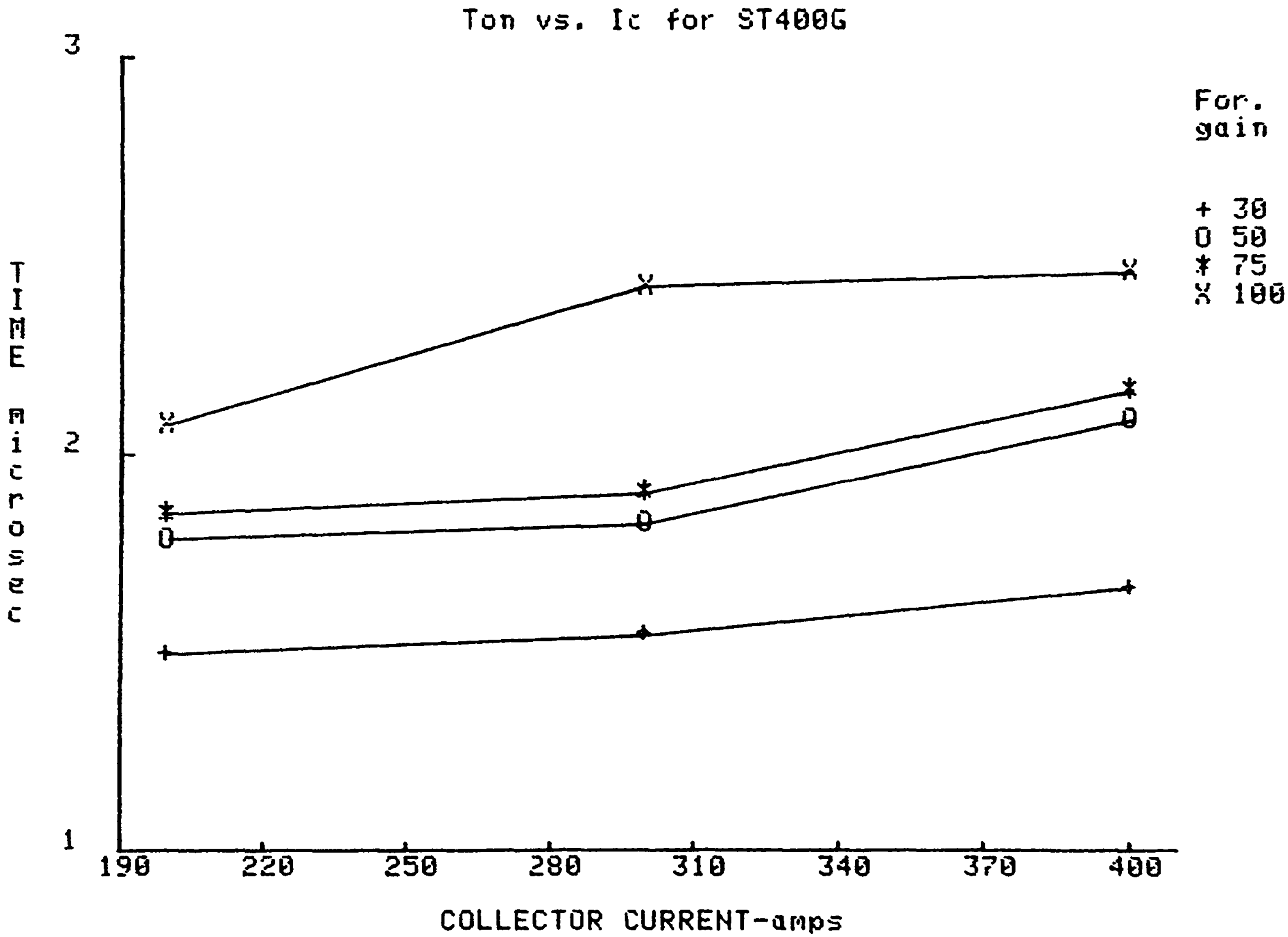
Ton vs. Ic for ST400G
3
2
1
TIME microsec
For. gain
+ 30
O 50
* 75
X 100
190
220
250
280
310
340
370
400
COLLECTOR CURRENT-amps

Fig. A.10.2

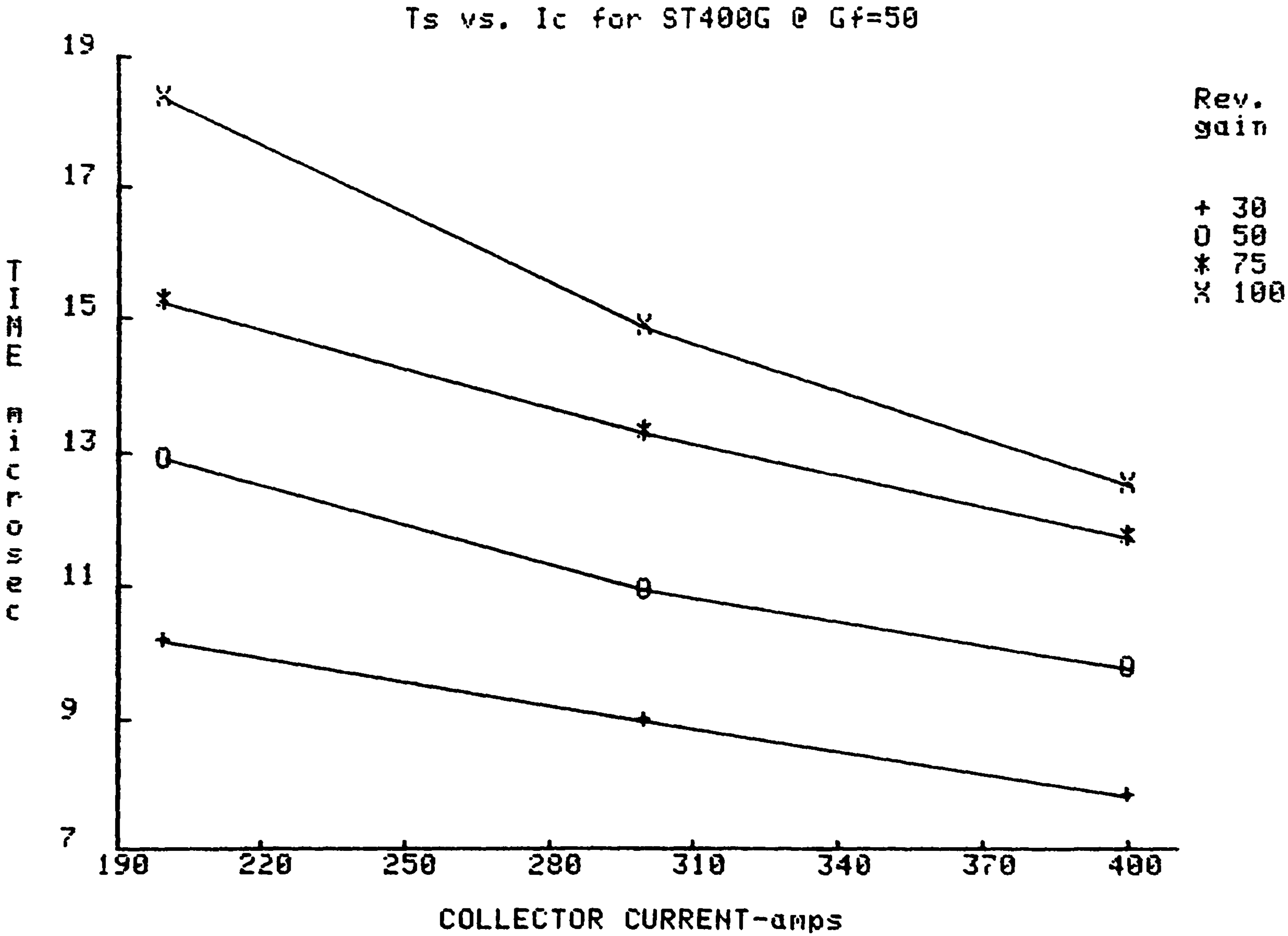

Ts vs. Ic for ST400G @ Gf=50
TIME microsec
19
17
15
13
11
9
7
190
220
250
280
310
340
370
400
COLLECTOR CURRENT-amps
Rev. gain
+ 30
O 50
* 75
X 100

Fig. A.10.3

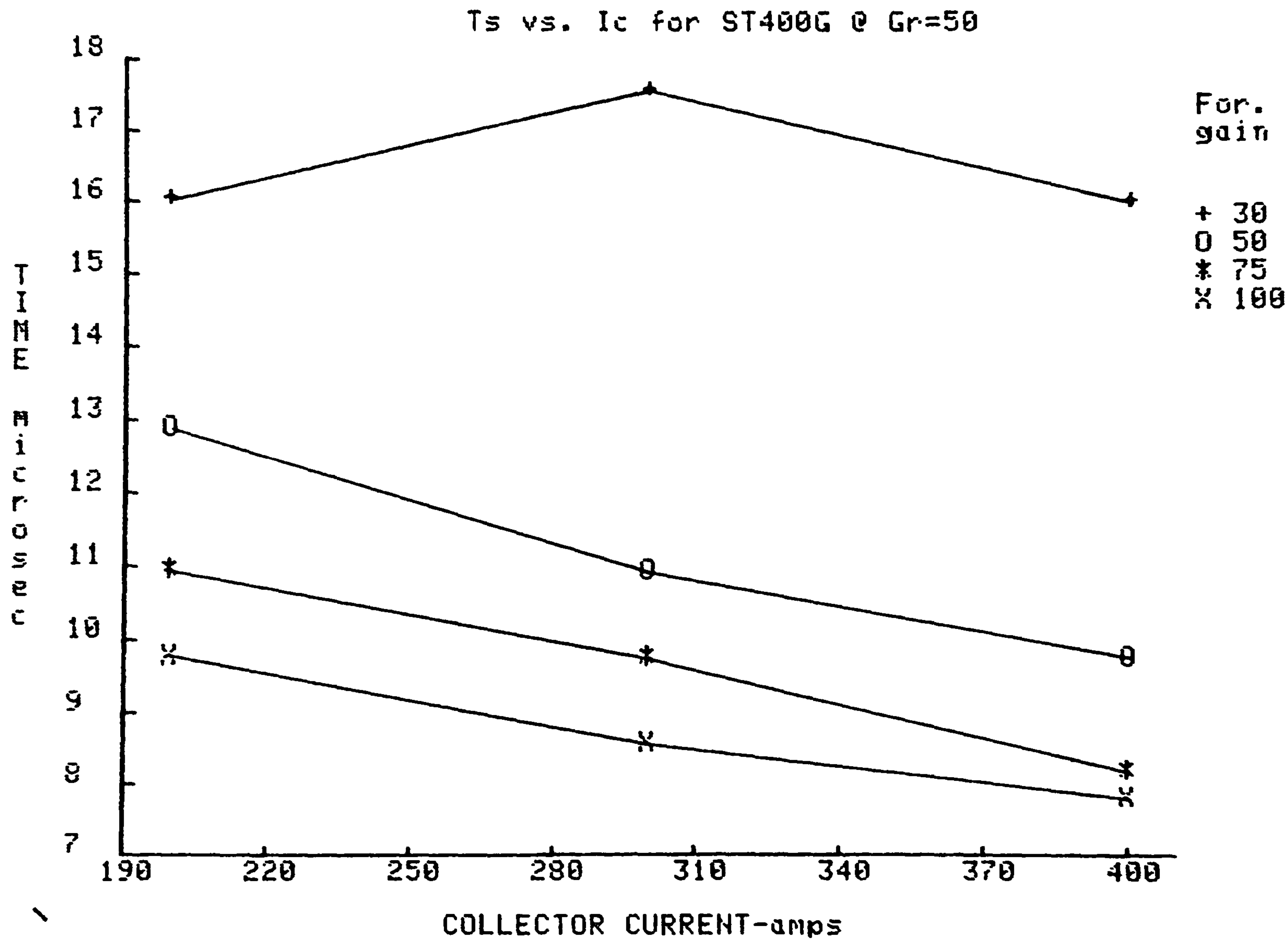

Ts vs. Ic for ST400G @ Gr=50
TIME microsec
18
17
16
15
14
13
12
11
10
9
8
7
190
220
250
280
310
340
370
400
COLLECTOR CURRENT-amps
For. gain
+ 30
O 50
* 75
X 100

Fig. A.10.4

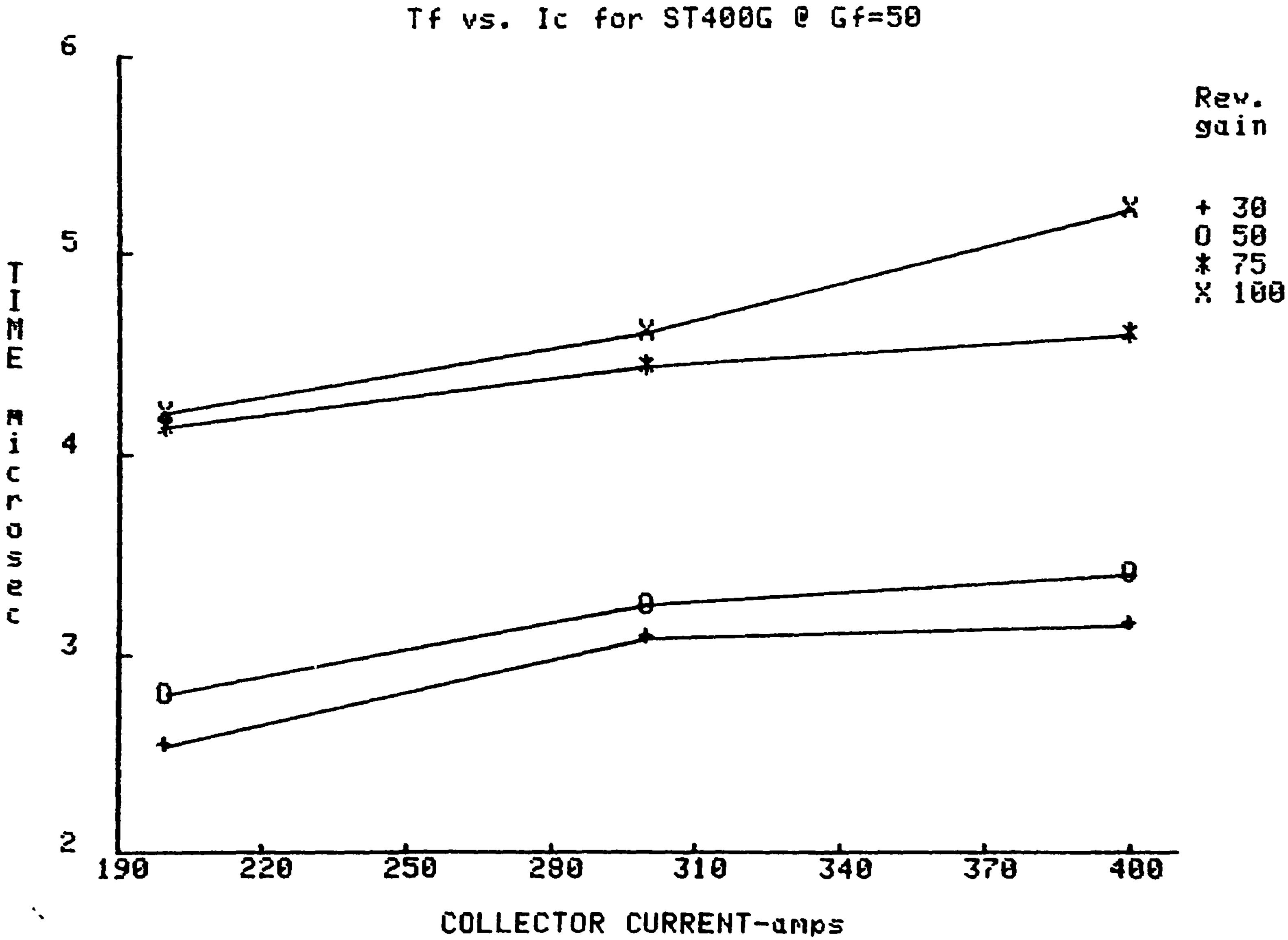

Tf vs. Ic for ST400G @ Gf=50
TIME microsec
COLLECTOR CURRENT-amps
6
5
4
3
2
190
220
250
280
310
340
370
400
Rev. gain
+ 30
O 50
* 75
X 100

Fig. A.10.5

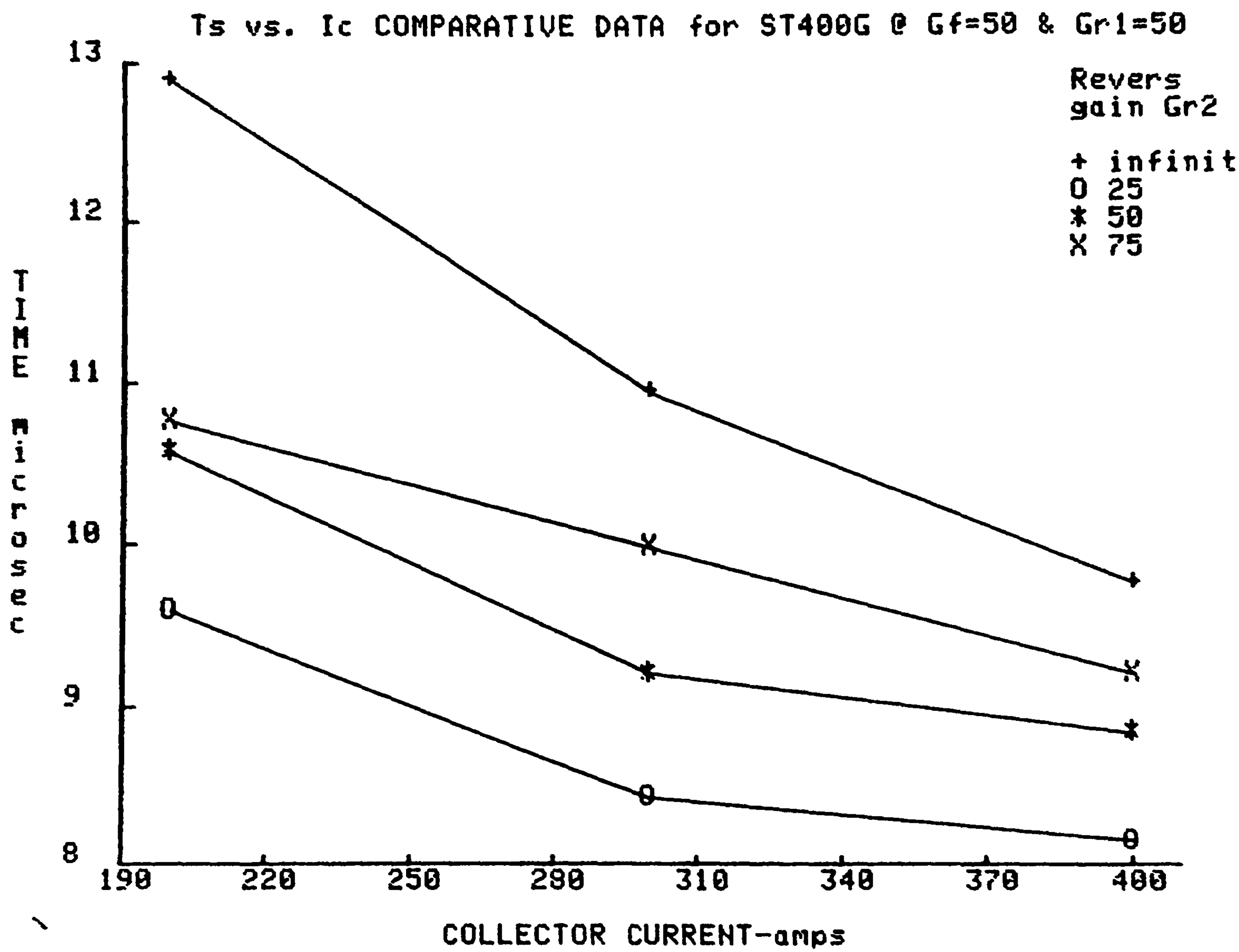

Ts vs. Ic COMPARATIVE DATA for ST400G @ Gf=50 & Gr1=50
TIME microsec
13
12
11
10
9
8
190
220
250
280
310
340
370
400
COLLECTOR CURRENT-amps
Revers gain Gr2
+ infinit
O 25
* 50
X 75

Fig. A.10.6

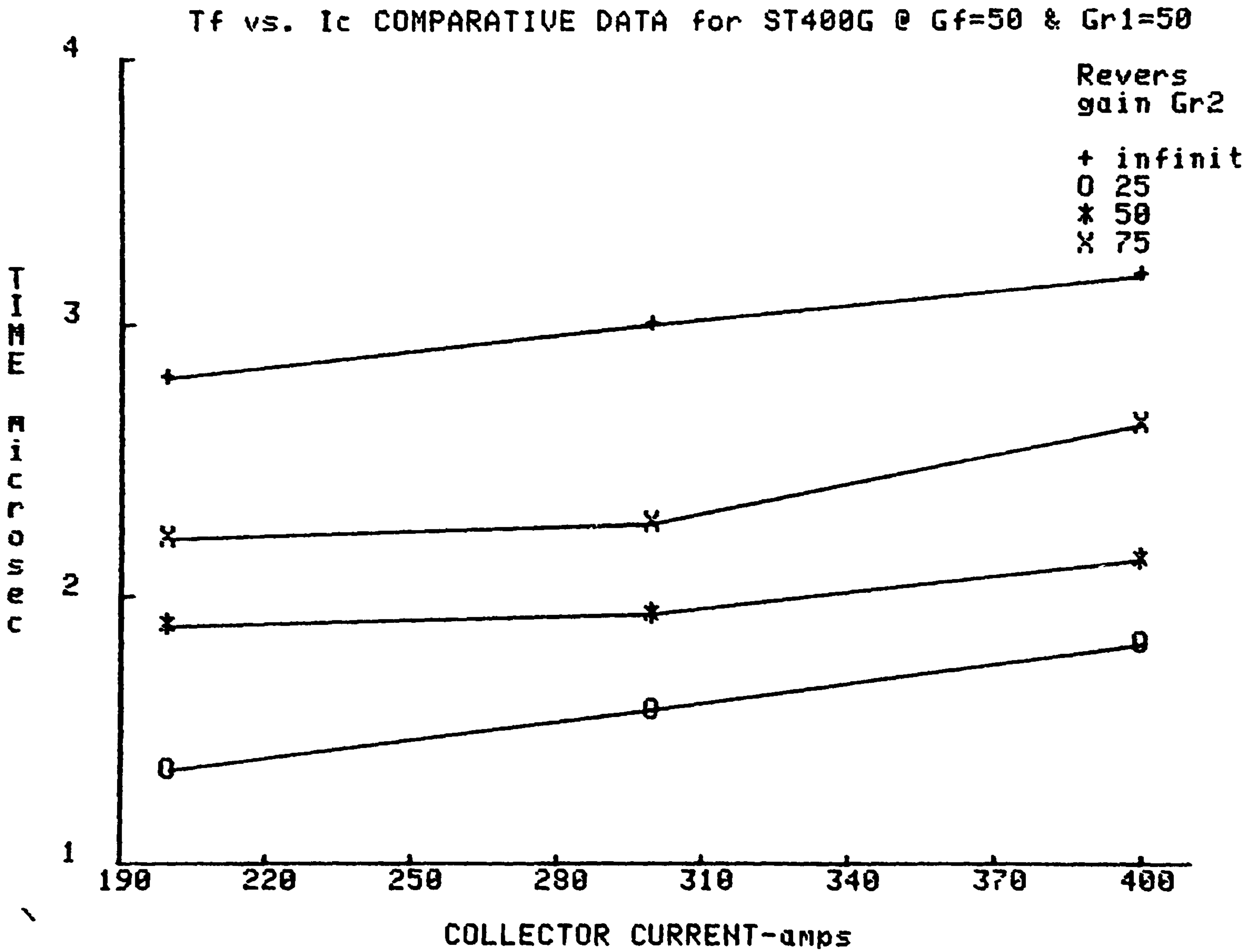
Tf vs. Ic COMPARATIVE DATA for ST400G @ Gf=50 & Gr1=50
Revers gain Gr2
+ infinit
O 25
* 50
X 75
TIME microsec
4
3
2
1
190
220
250
280
310
340
370
400
COLLECTOR CURRENT-amps

Fig. A.10.7

Qon vs Ic for ST400G @ Vce=300V

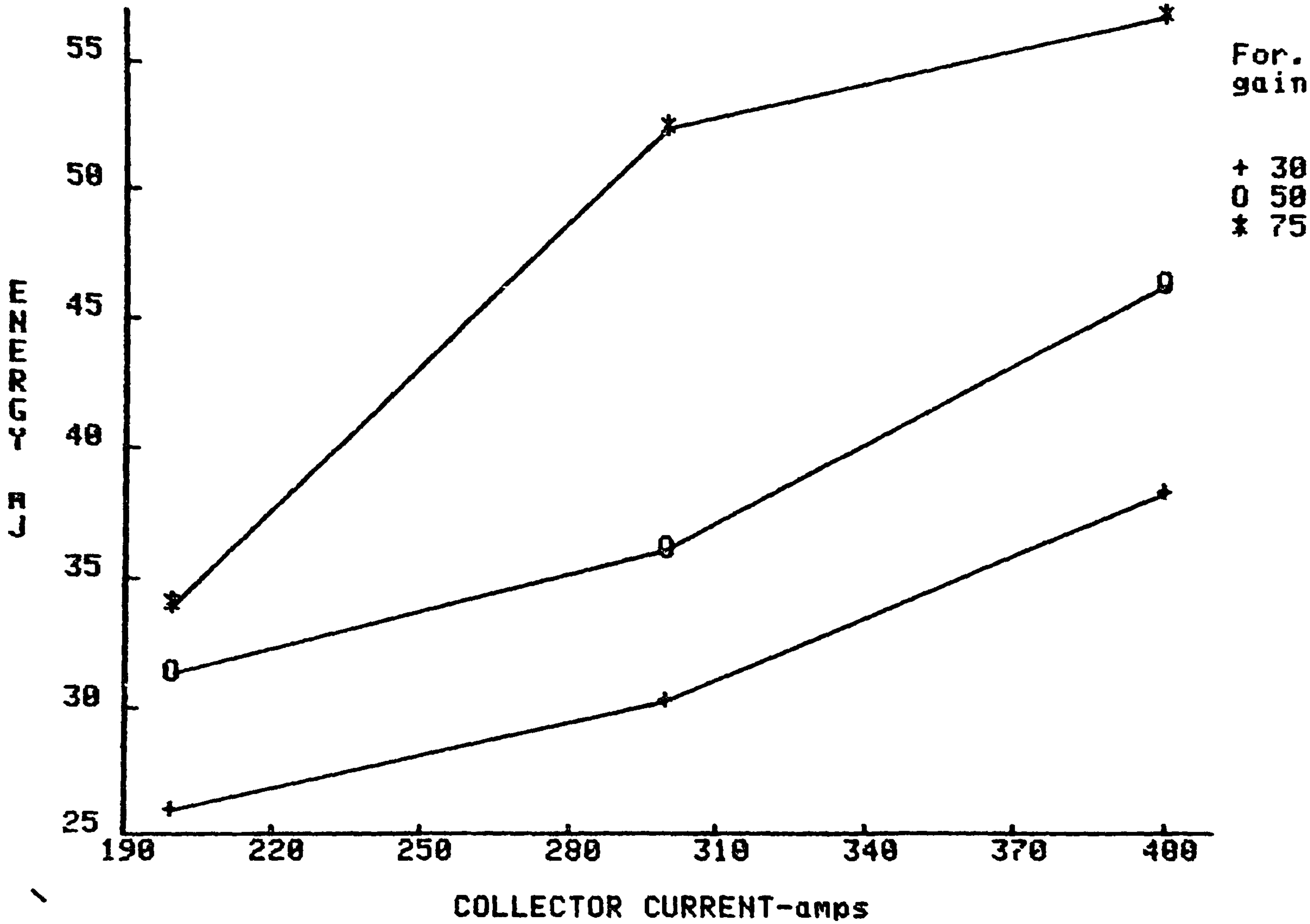

Fig. A.10.8

Qon(qsat) vs Ic for ST400G @ Vce=300V

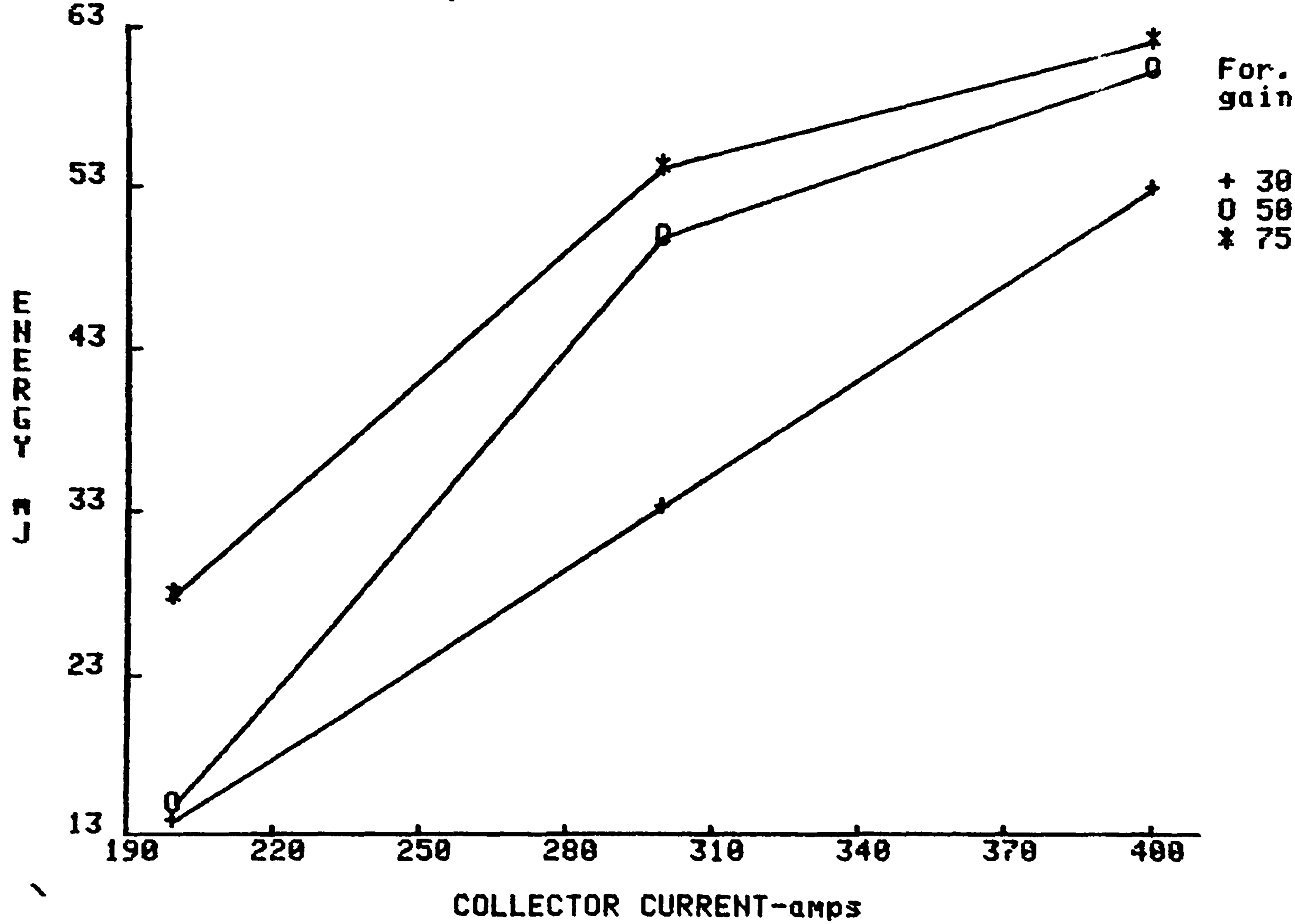

Fig. A.10.9

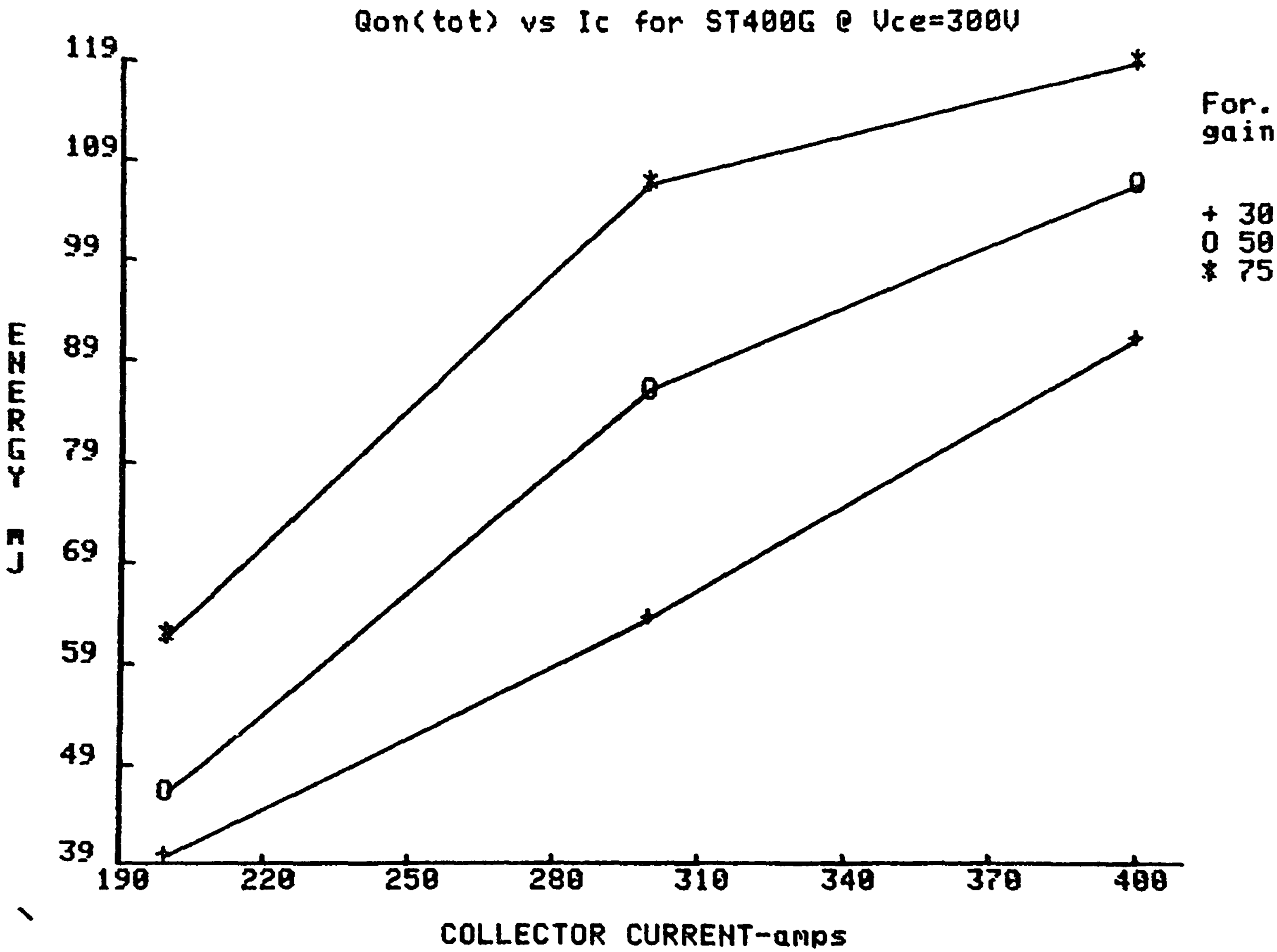
Qon(tot) vs Ic for ST400G @ Vce=300V
119
109
99
89
79
69
59
49
39
ENERGY mJ
190
220
250
280
310
340
370
400
COLLECTOR CURRENT-amps
For.
gain
+ 30
0 50
* 75

Fig. A.10.10

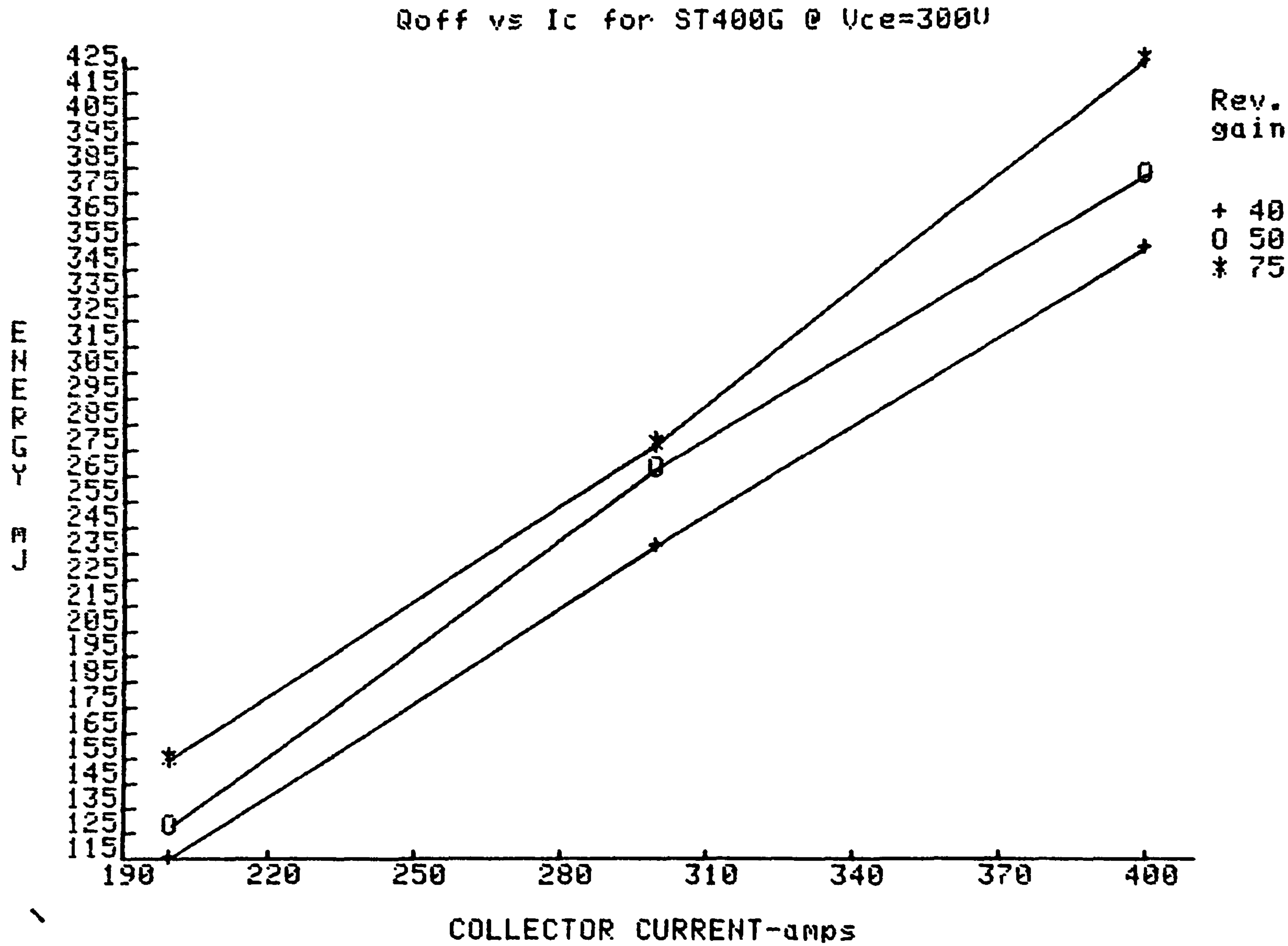
Qoff vs Ic for ST400G @ Vce=300V
ENERGY mJ
425
415
405
395
385
375
365
355
345
335
325
315
305
295
285
275
265
255
245
235
225
215
205
195
185
175
165
155
145
135
125
115
190
220
250
280
310
340
370
400
COLLECTOR CURRENT-amps
Rev. gain
+ 40
O 50
* 75

Fig. A.10.11

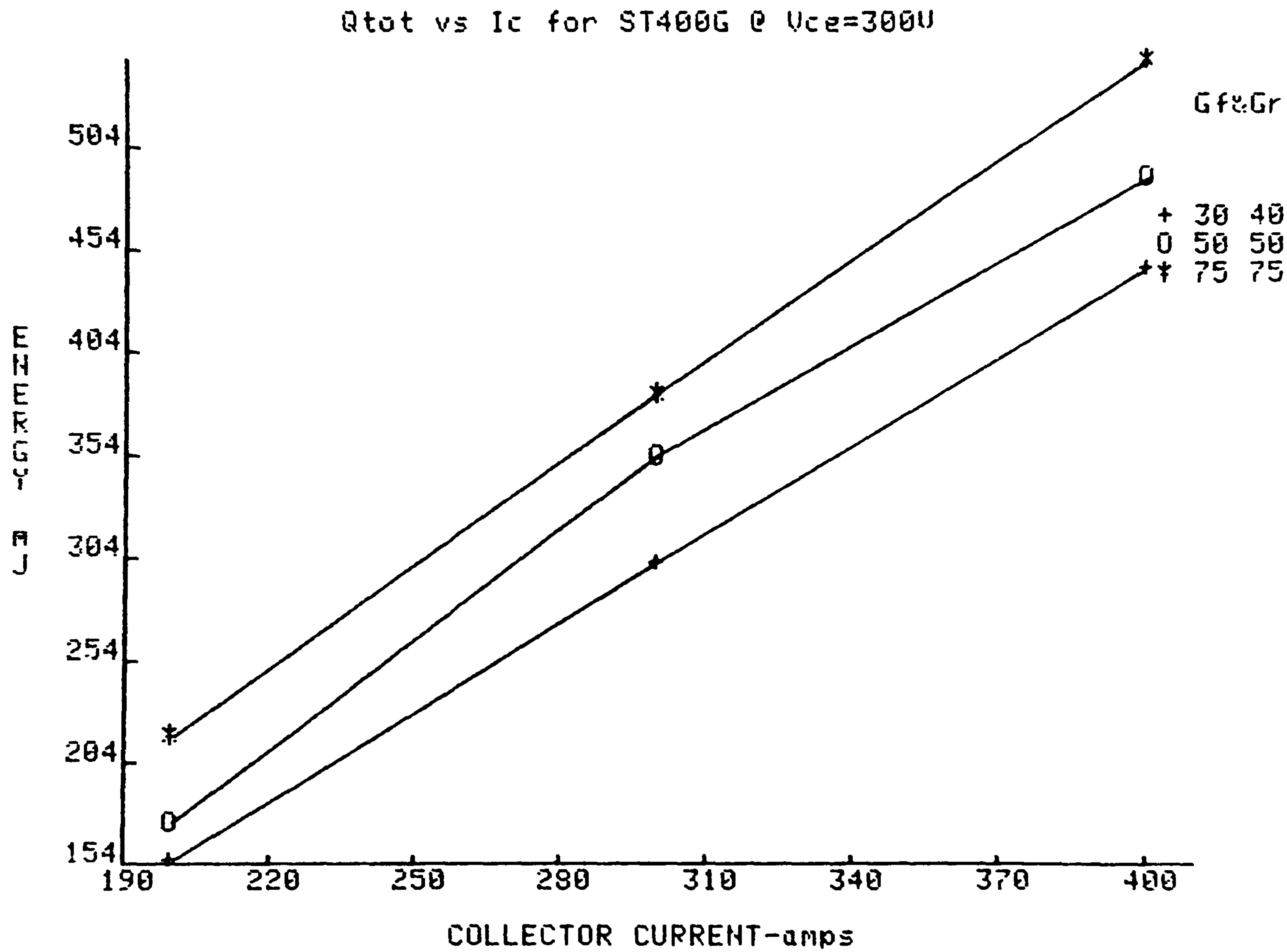
Qtot vs Ic for ST400G @ Vce=300V
Gf&Gr
+ 30 40
0 50 50
* 75 75
ENERGY mJ
504
454
404
354
304
254
204
154
190
220
250
280
310
340
370
400
COLLECTOR CURRENT-amps

Fig. A.10.12

Switching Loadline Characteristics: Vce vs. Ic
for Turn-on of Power Trans. with Inductive Load

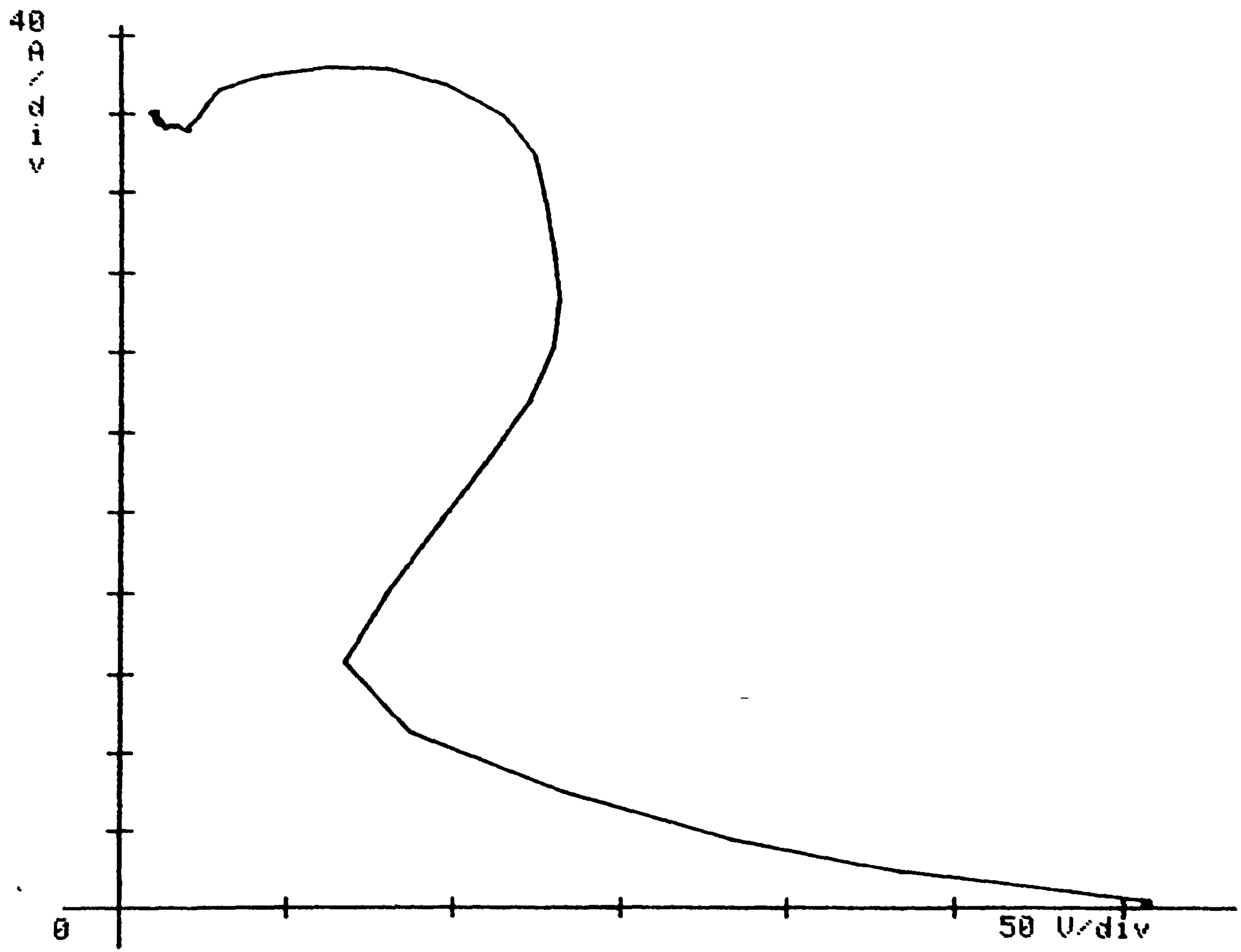

Fig. A.10.13

Switching Loadline Characteristics: Vce vs. Ic
for Turn-off of Power Trans. with Inductive Load

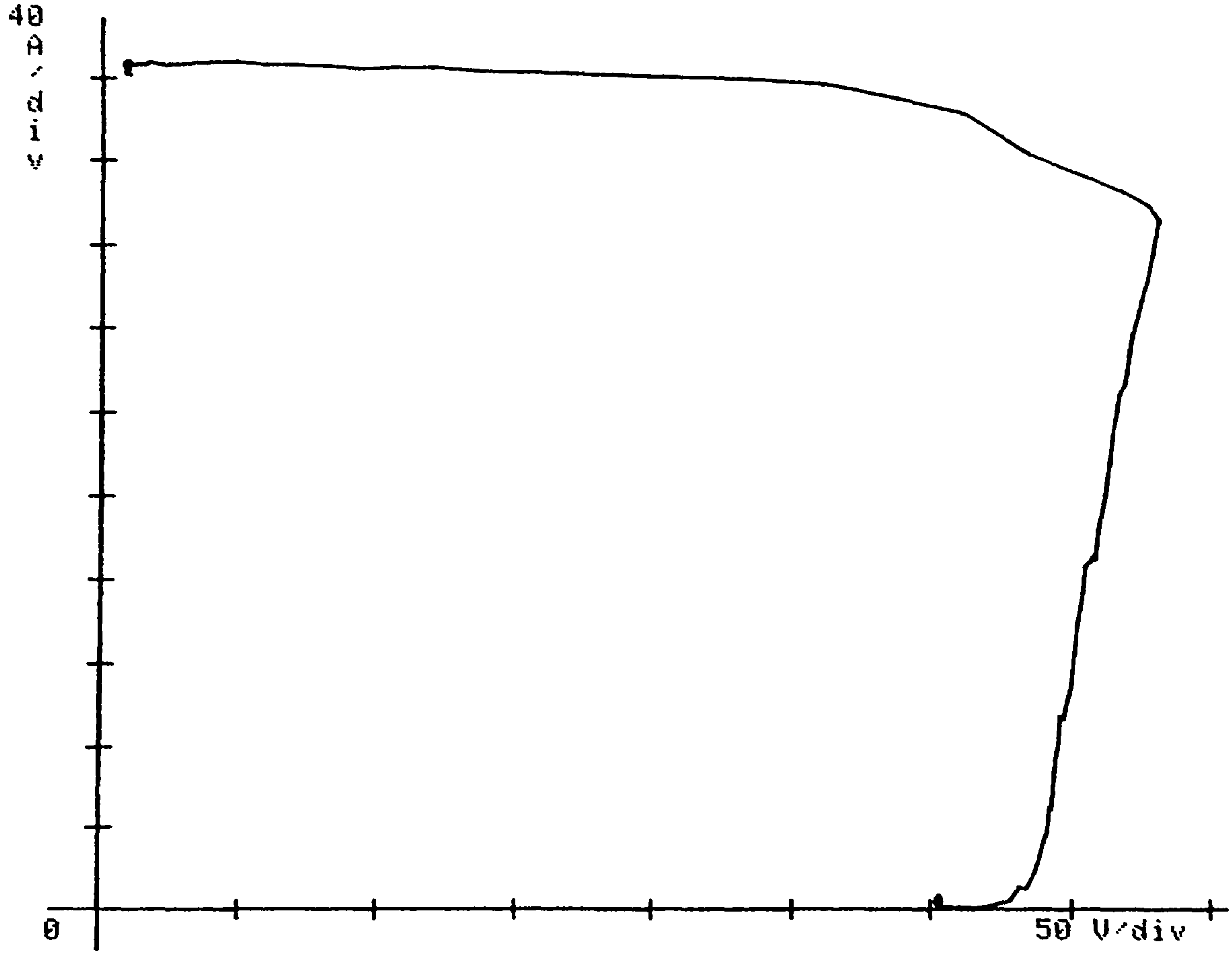

Fig. A.10.14

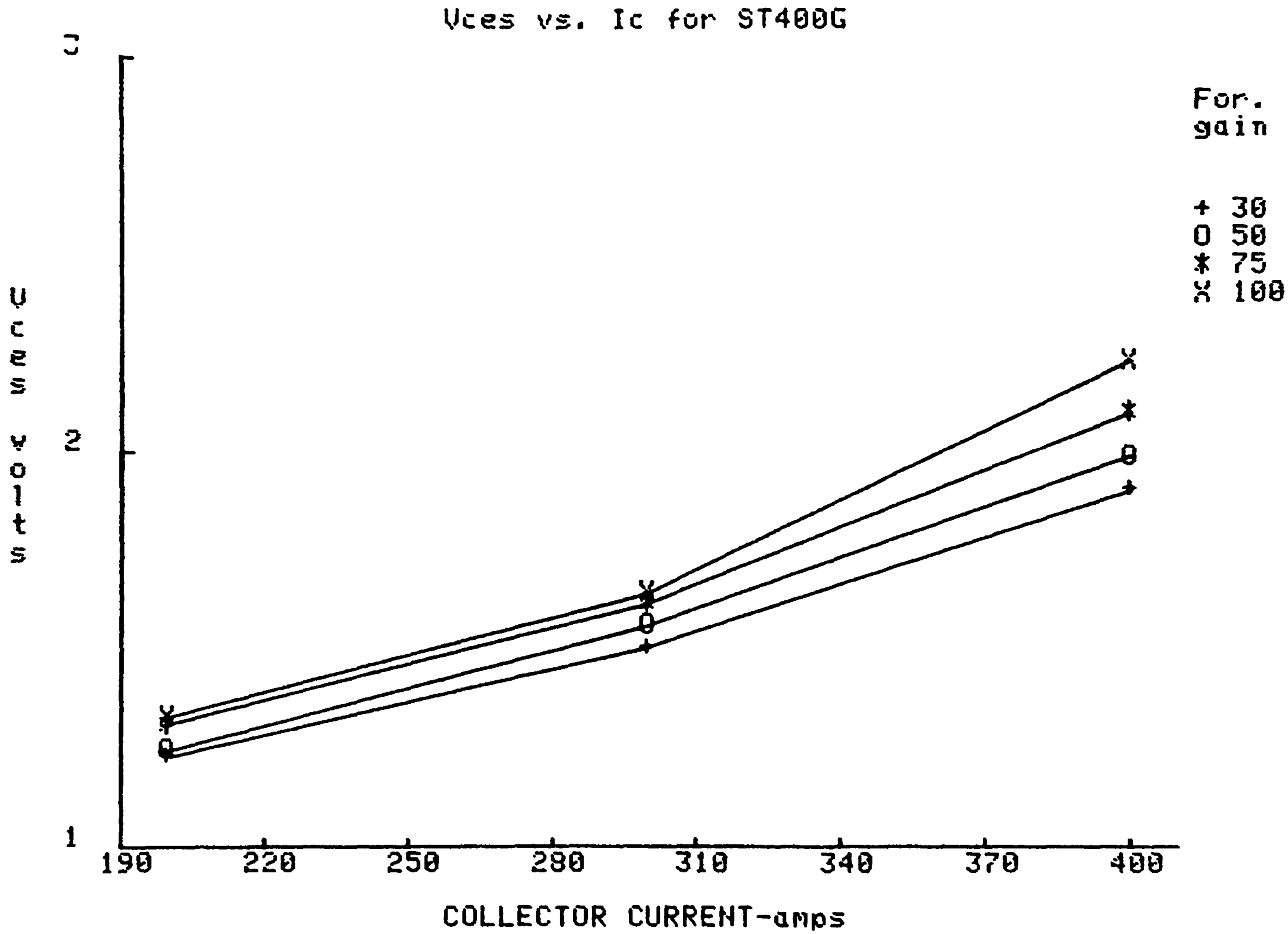
Vces vs. Ic for ST400G
3
2
1
Vces volts
190
220
250
280
310
340
370
400
COLLECTOR CURRENT-amps
For.
gain
+ 30
O 50
* 75
X 100

Fig. A.10.15

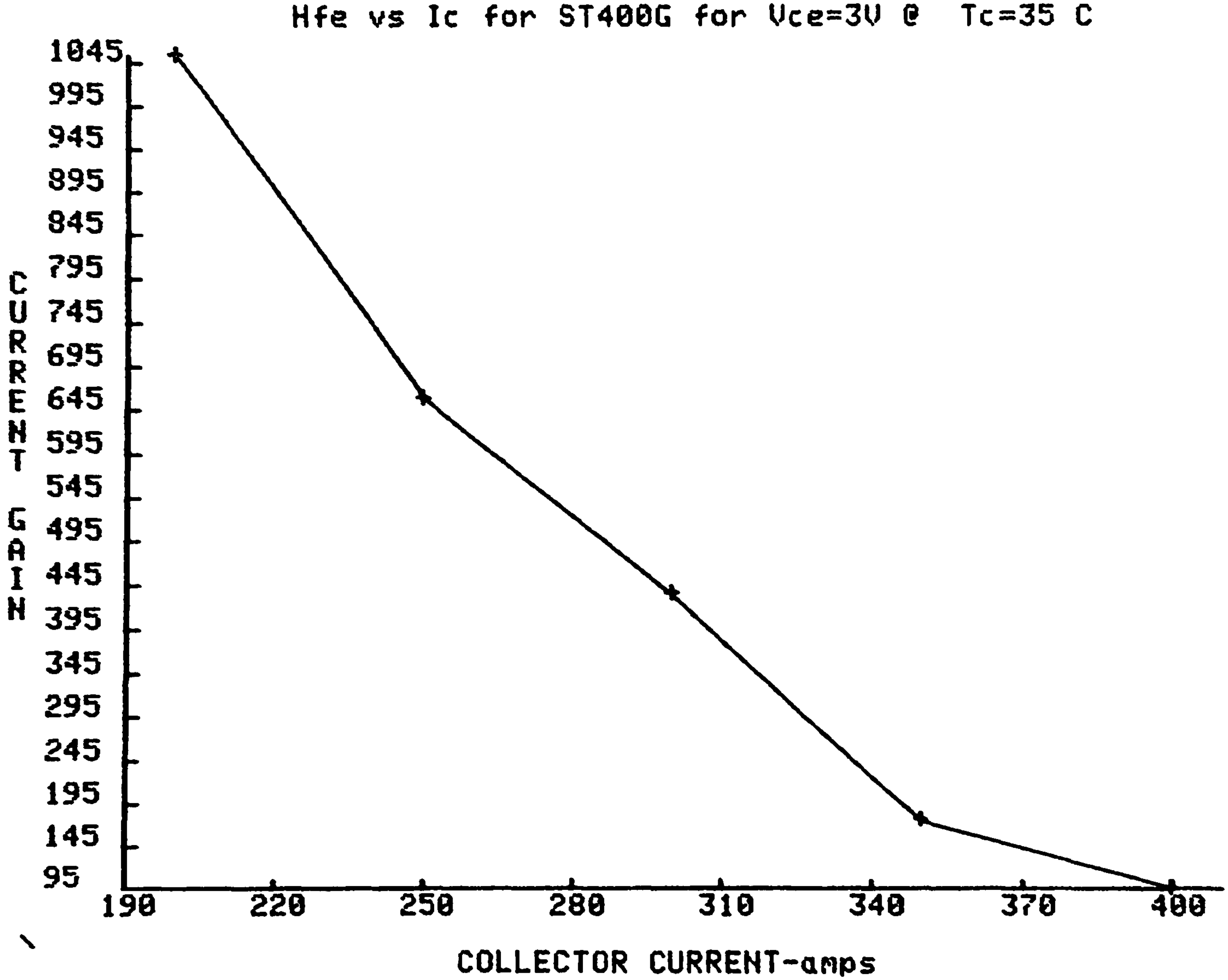
Hfe vs Ic for ST400G for Vce=3V @ Tc=35 C
CURRENT GAIN
1045
995
945
895
845
795
745
695
645
595
545
495
445
395
345
295
245
195
145
95
190
220
250
280
310
340
370
400
COLLECTOR CURRENT-amps

A.11 Test Data for Toshiba ST400G21

A.164

Fig.A.11.1

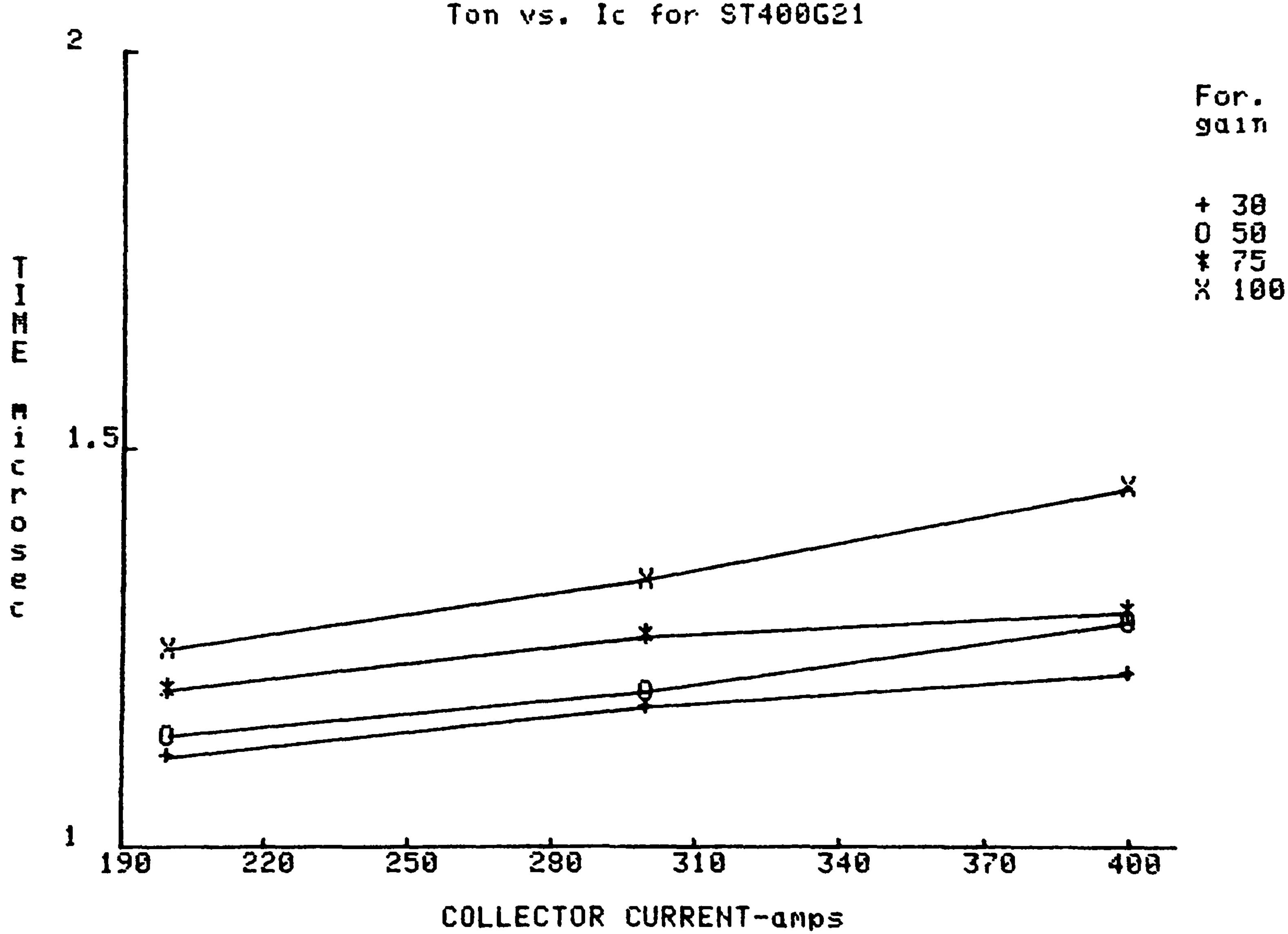

Fig. A.11.2

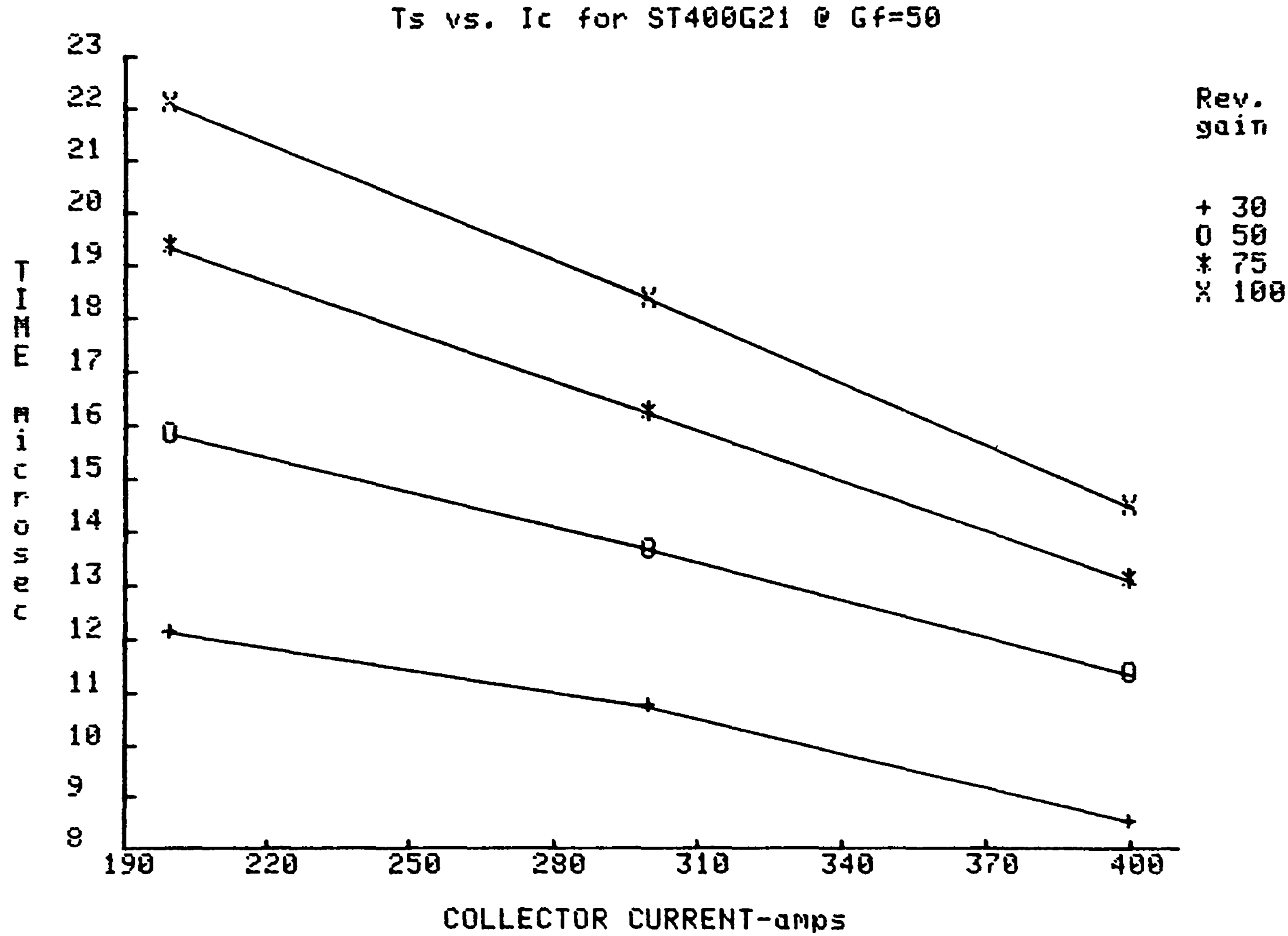
Ts vs. Ic for ST400G21 @ Gf=50
TIME microsec
COLLECTOR CURRENT-amps
Rev. gain
+ 30
0 50
* 75
X 100
23
22
21
20
19
18
17
16
15
14
13
12
11
10
9
8
190
220
250
280
310
340
370
400

Fig. A.11.3

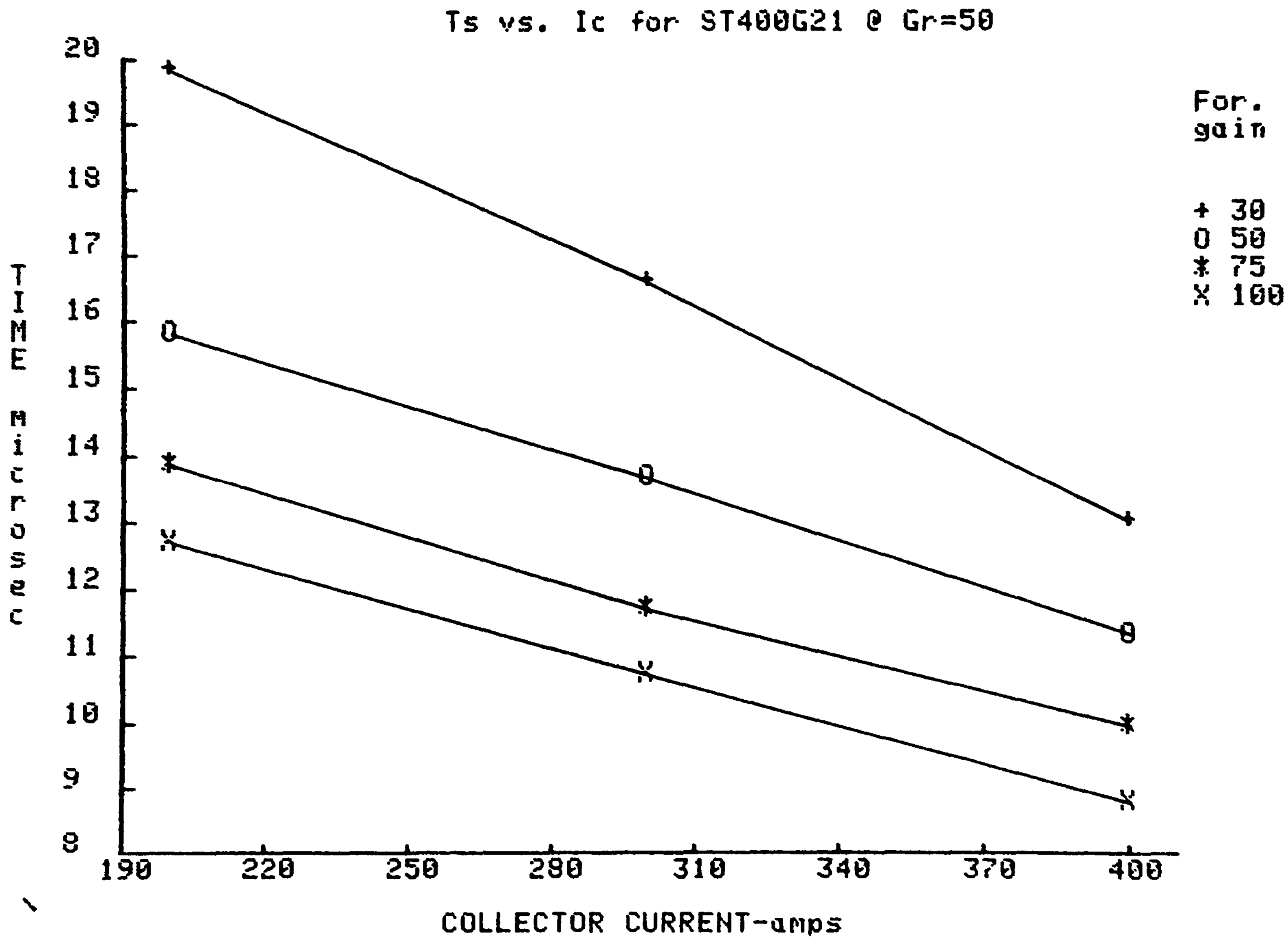

A.166

Fig. A.11.4

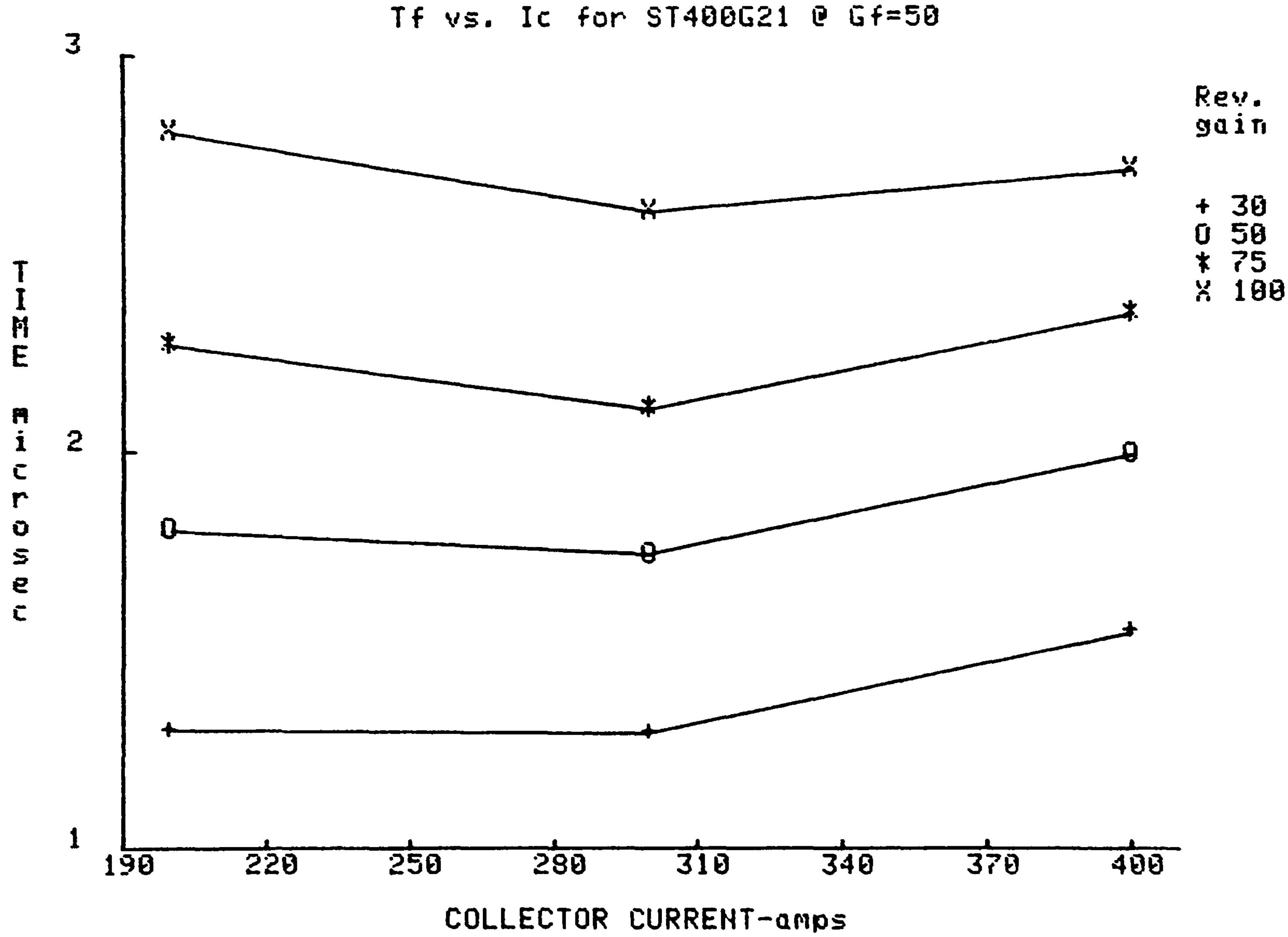
Tf vs. Ic for ST400G21 @ Gf=50
TIME microsec
3
2
1
190
220
250
280
310
340
370
400
COLLECTOR CURRENT-amps
Rev. gain
+ 30
O 50
* 75
X 100

Fig. A.11.7

Qon vs Ic for ST400G21 @ Vce=300V

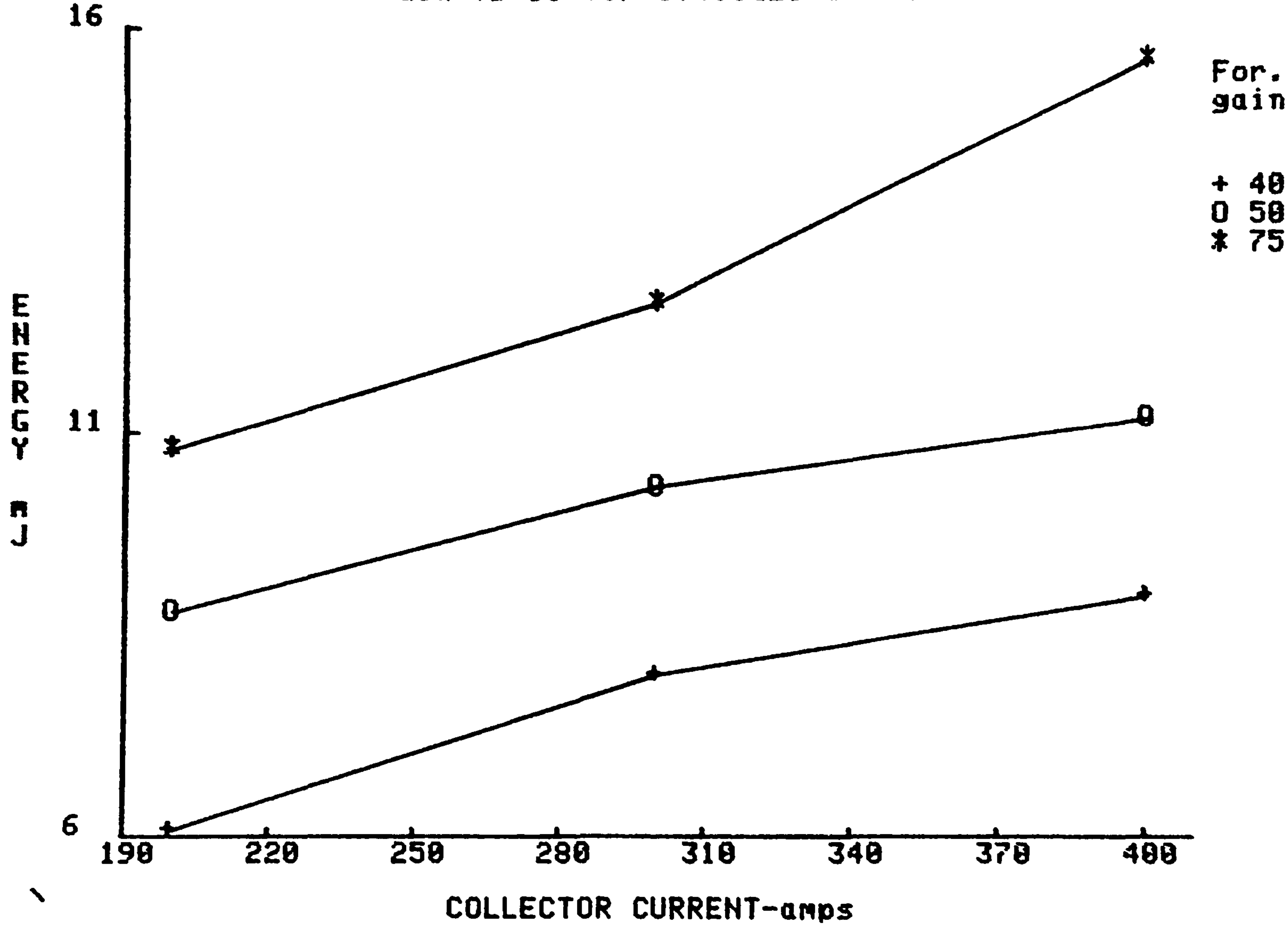

Fig. A.11.8

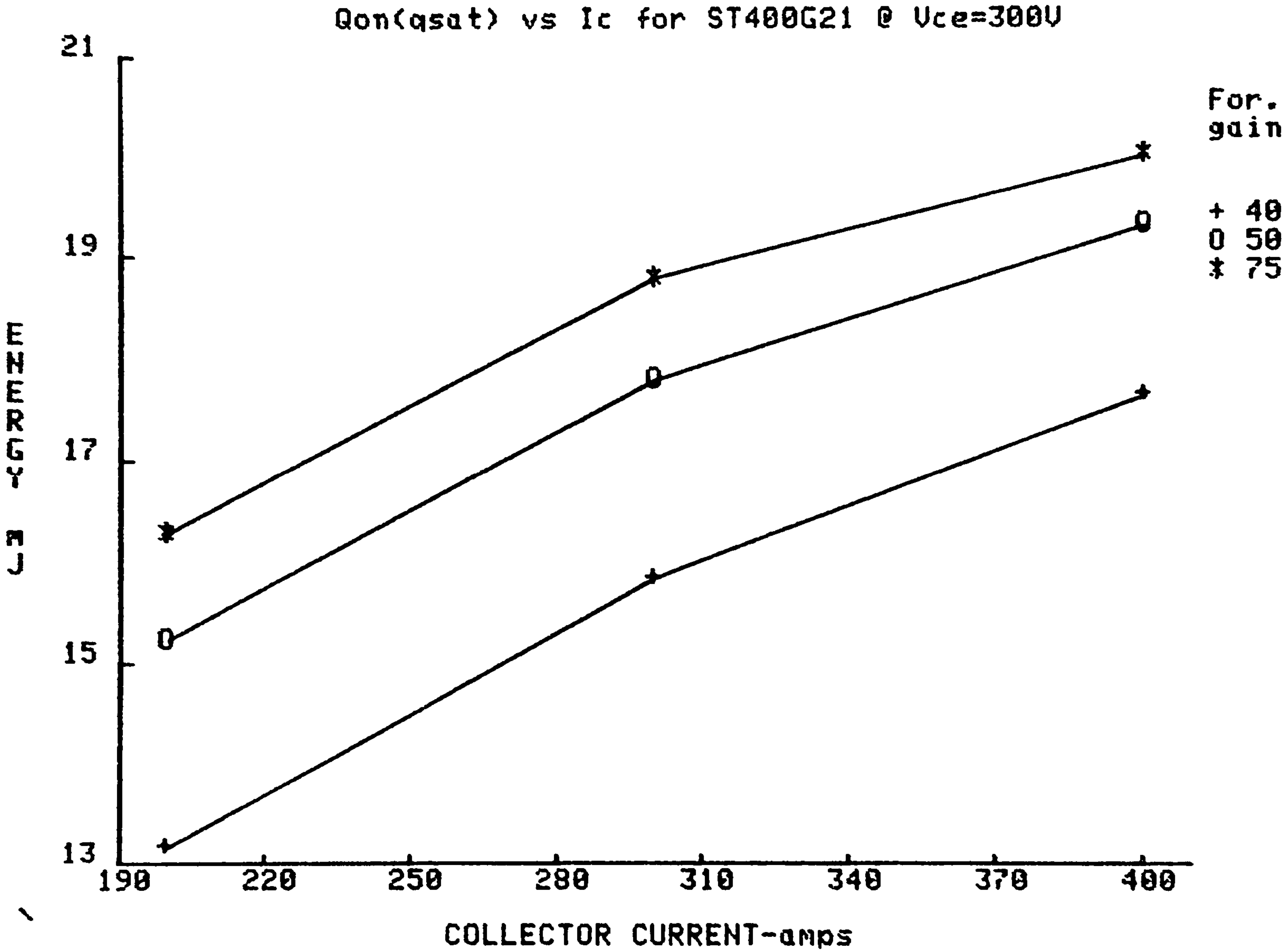
Qon(qsat) vs Ic for ST400G21 @ Vce=300V
ENERGY mJ
21
19
17
15
13
190
220
250
280
310
340
370
400
COLLECTOR CURRENT-amps
For. gain
+ 40
0 50
* 75

Fig. A.11.9

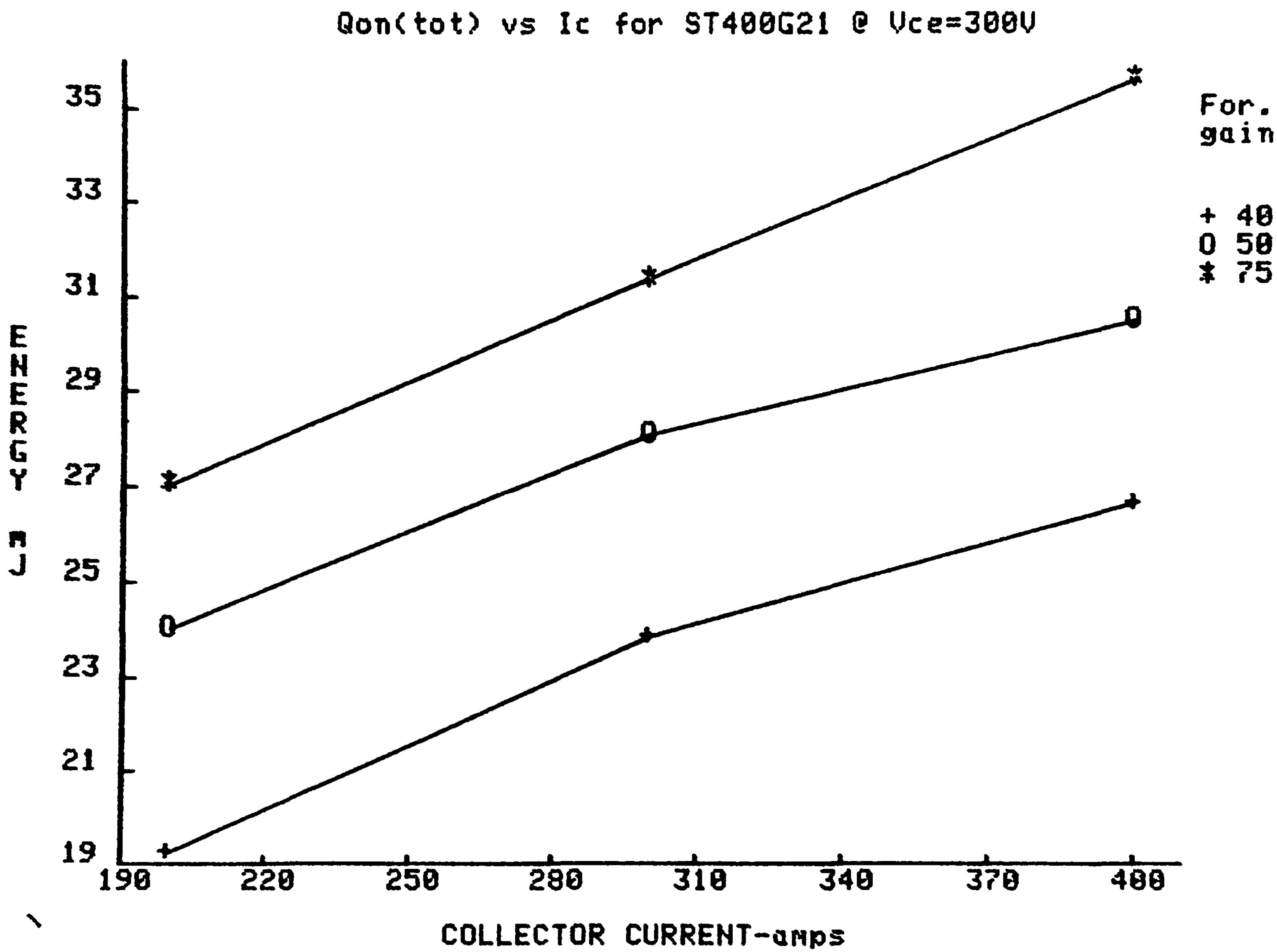
Qon(tot) vs Ic for ST400G21 @ Vce=300V
ENERGY mJ
35
33
31
29
27
25
23
21
19
190
220
250
280
310
340
370
400
COLLECTOR CURRENT-amps
For. gain
+ 40
O 50
* 75

Fig. A.21.10

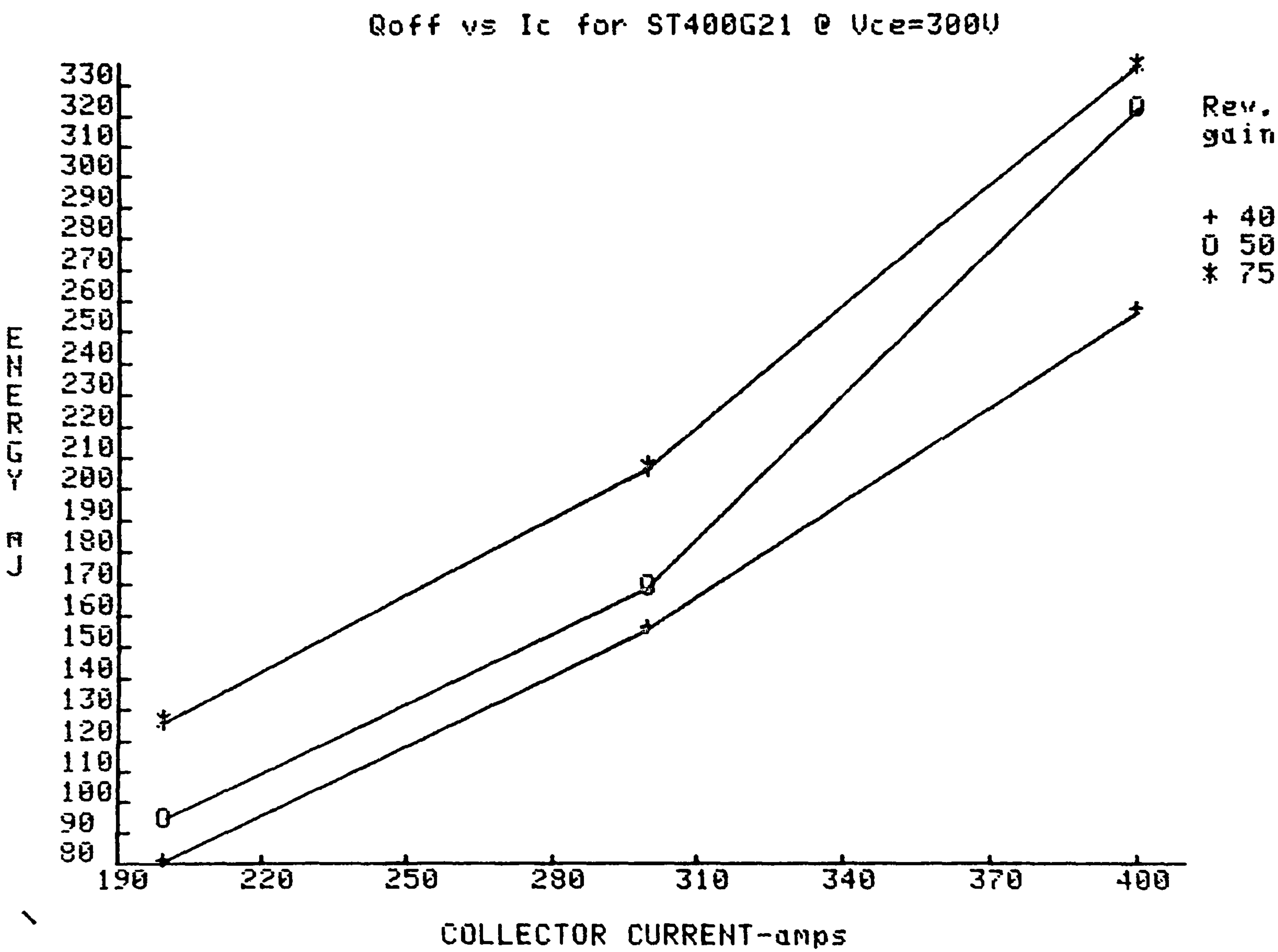

Qoff vs Ic for ST400G21 @ Vce=300V
ENERGY mJ
330
320
310
300
290
280
270
260
250
240
230
220
210
200
190
180
170
160
150
140
130
120
110
100
90
80
190
220
250
280
310
340
370
400
COLLECTOR CURRENT-amps
Rev. gain
+ 40
O 50
* 75

Fig. A.11.11

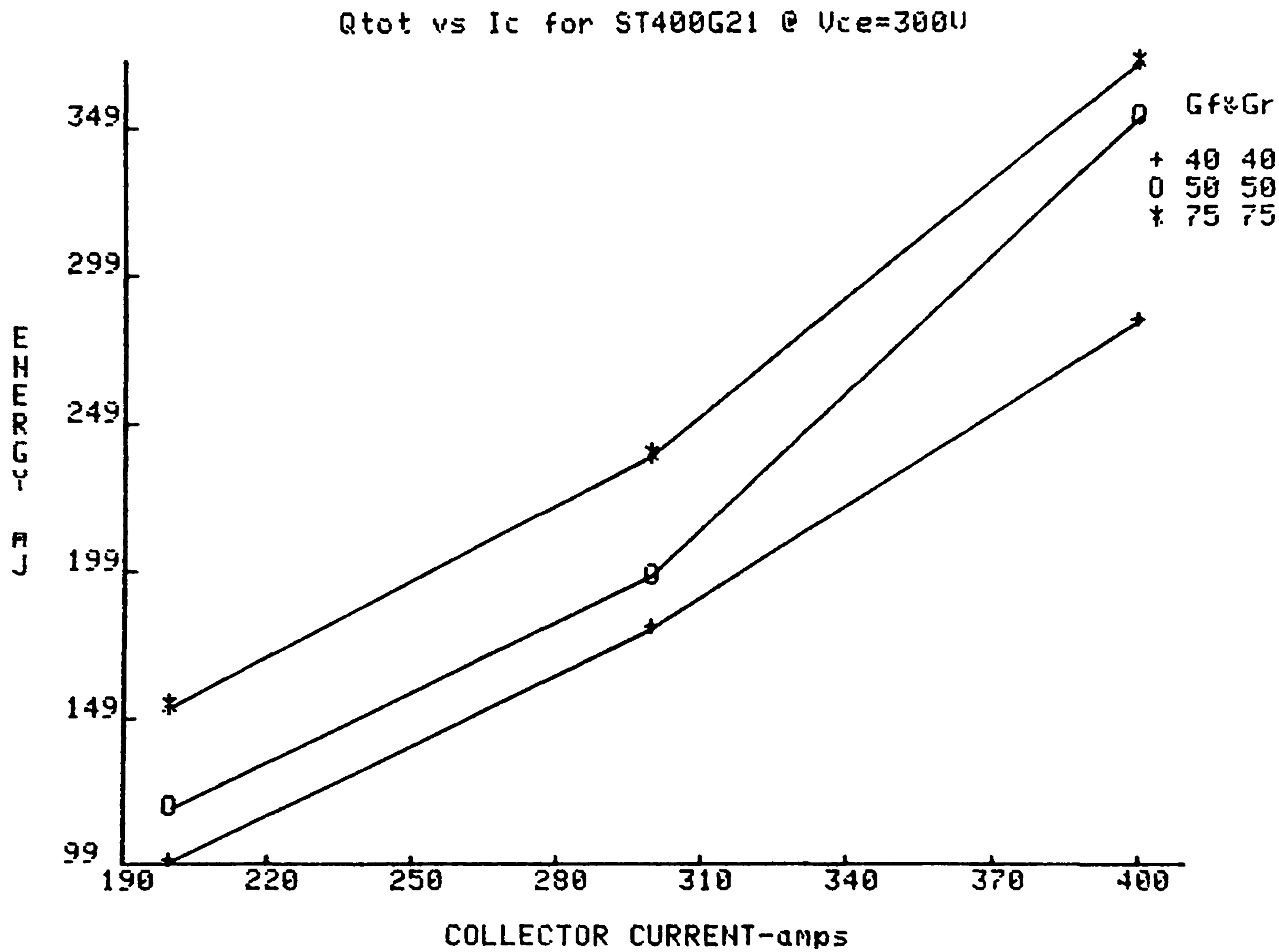
Qtot vs Ic for ST400G21 @ Vce=300V
ENERGY mJ
349
299
249
199
149
99
190
220
250
280
310
340
370
400
COLLECTOR CURRENT-amps
Gf&Gr
+ 40 40
0 50 50
* 75 75

Fig. A.11.12

Switching Loadline Characteristics: Vce vs. Ic
for Turn-on of Power Transistor with Inductive Load

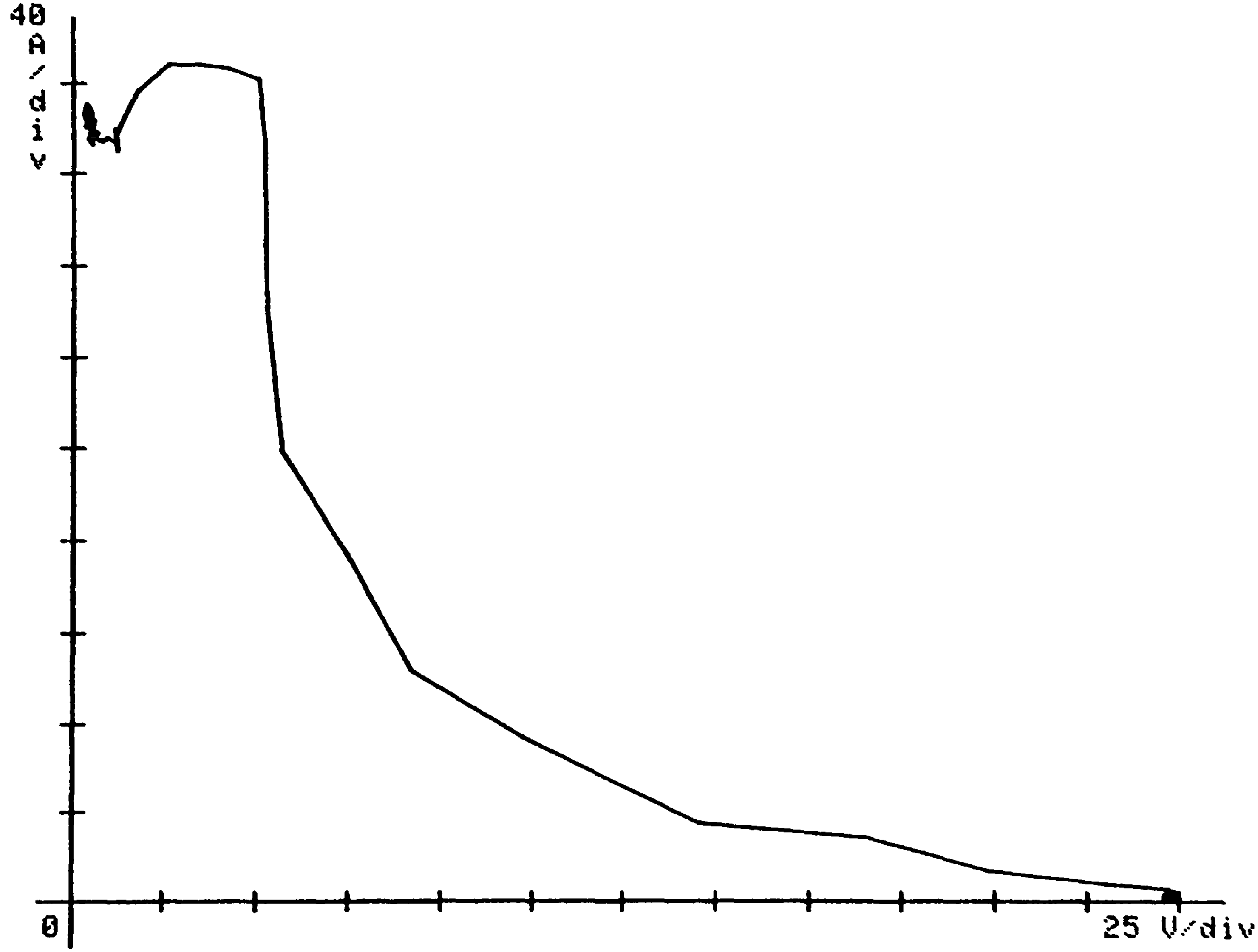

Fig. A.11.13

Switching Loadline Characteristics: Vce vs. Ic
for Turn-off of Power Trans. with Inductive Load

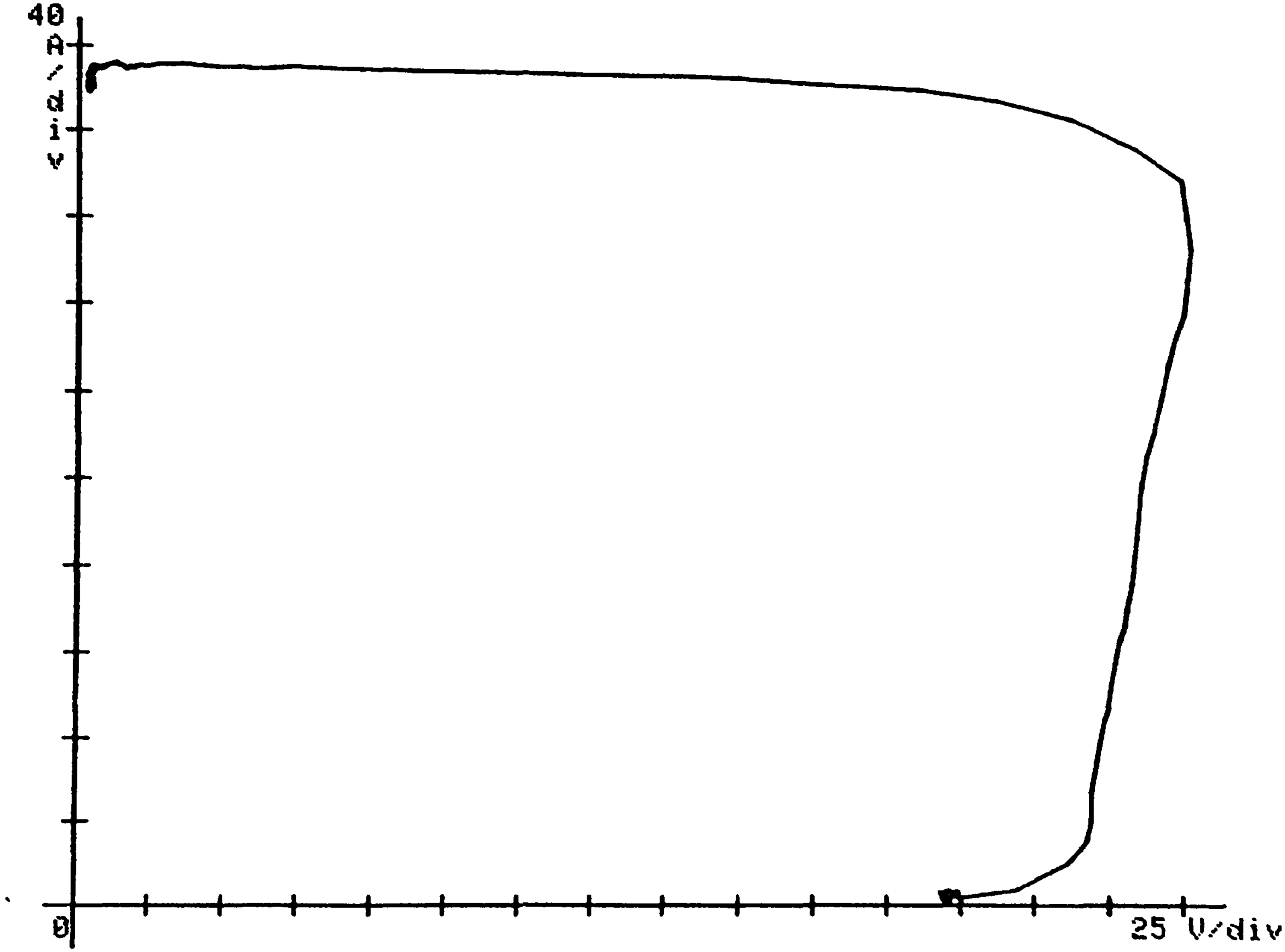

Fig.A.11.14

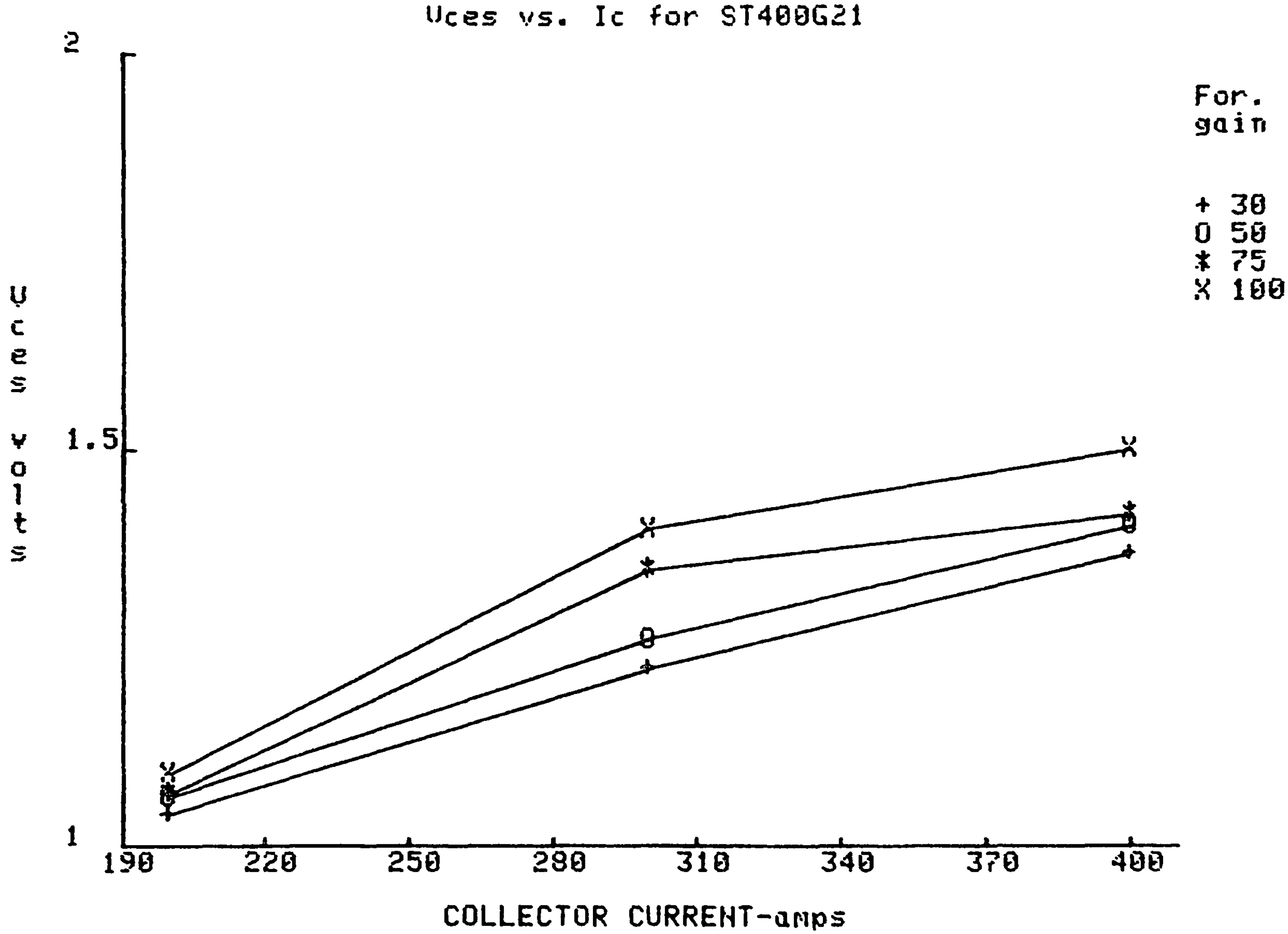

Uces vs. Ic for ST400G21
Uces volts
2
1.5
1
190
220
250
280
310
340
370
400
COLLECTOR CURRENT-amps
For. gain
+ 30
O 50
* 75
X 100

Fig. A.11.15

Hfe vs Ic for ST400G21 for Vce=3V @ Tc=35 C

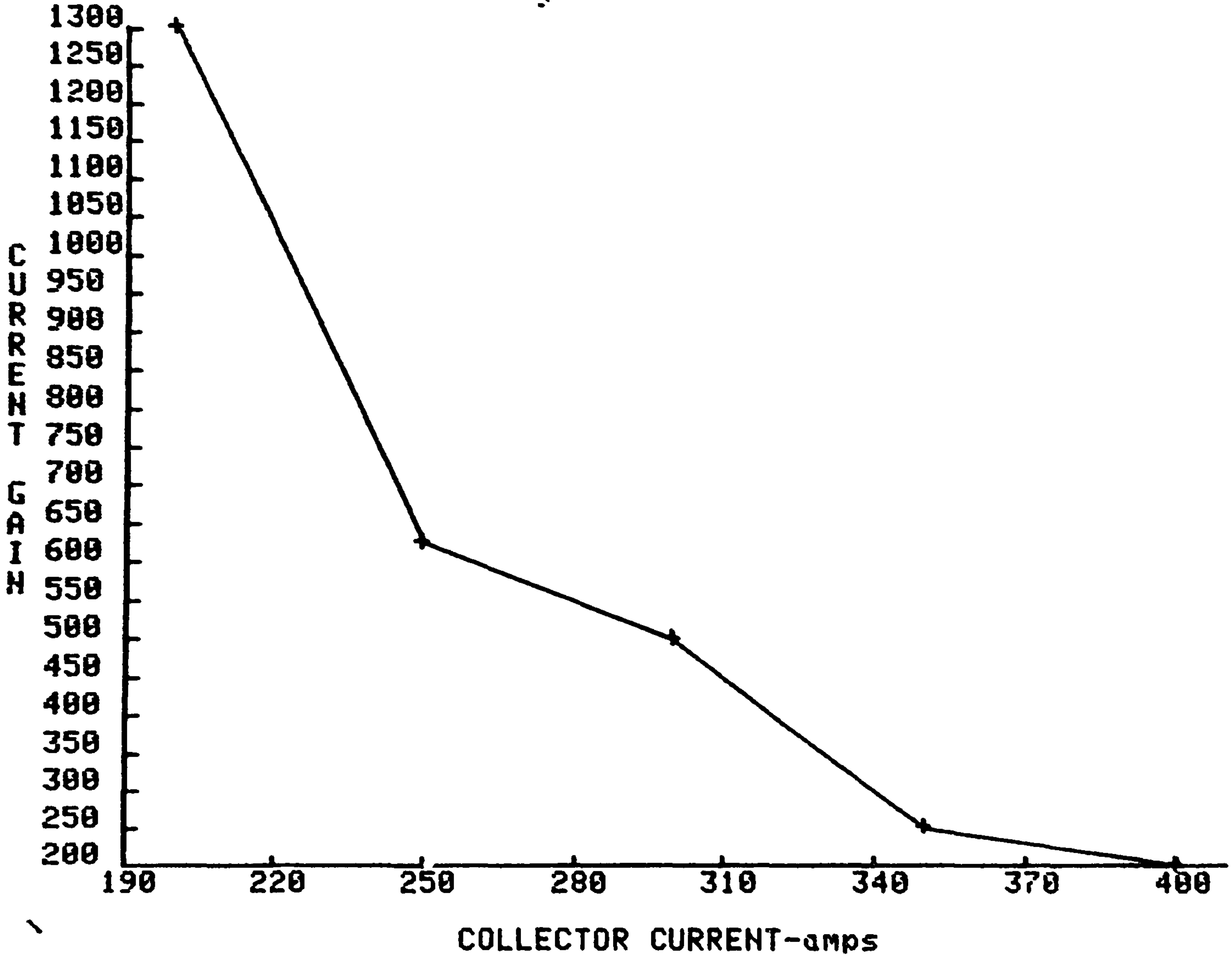

APPENDIX B

COMPARATIVE TEST DATA OF SWITCHING TIMES CHARACTERIZATION OF BIPOLAR TRANSISTORS

B.1 Comparative Data for Fuji EVM31-050 and Mitsubishi QM150DY-H

Fig. C.1.1

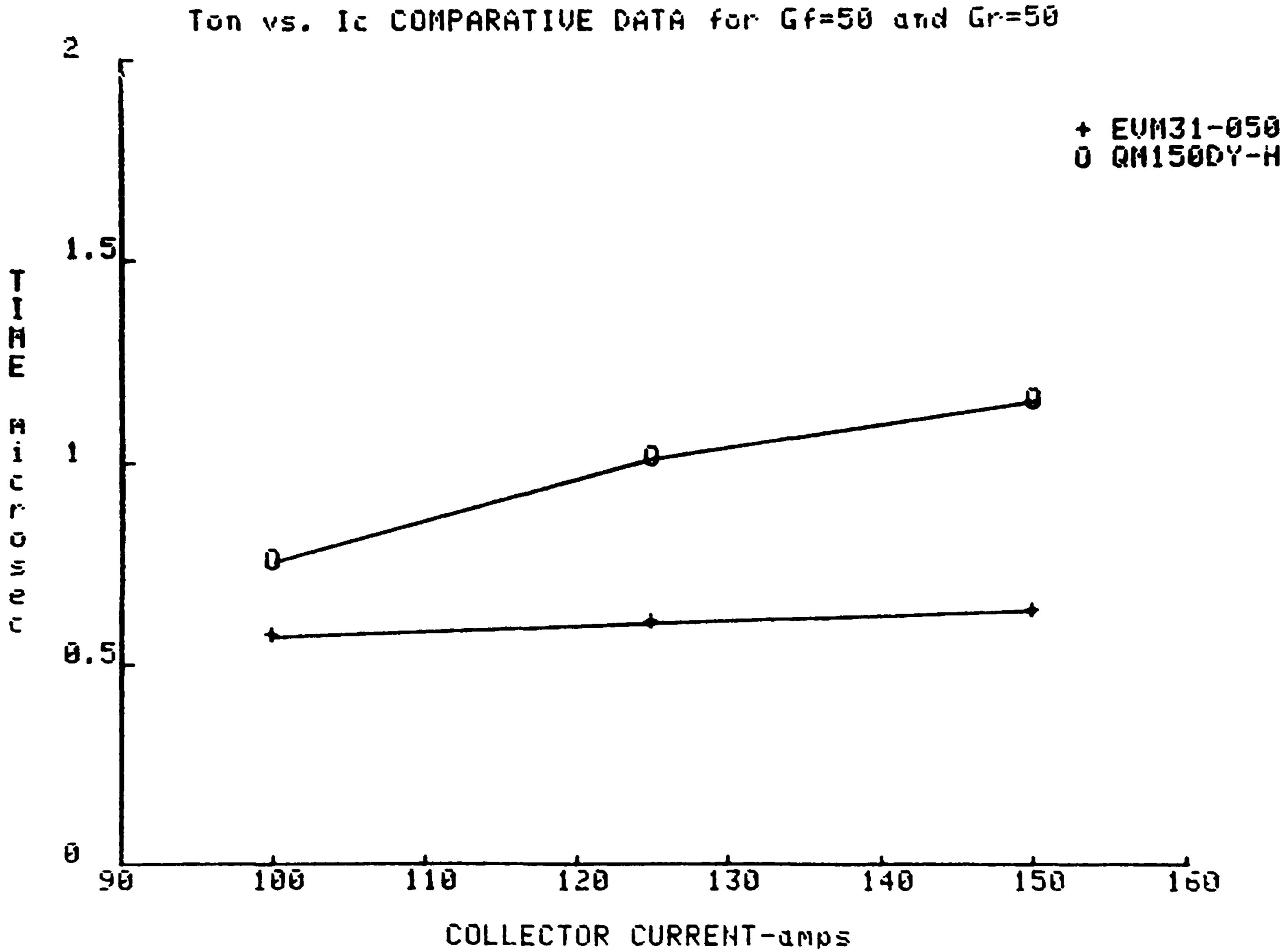

Ton vs. Ic COMPARATIVE DATA for Gf=50 and Gr=50
+ EVM31-050
0 QM150DY-H
TIME microsec
2
1.5
1
0.5
0
90
100
110
120
130
140
150
160
COLLECTOR CURRENT-amps

B.3

Fig. B.1.2

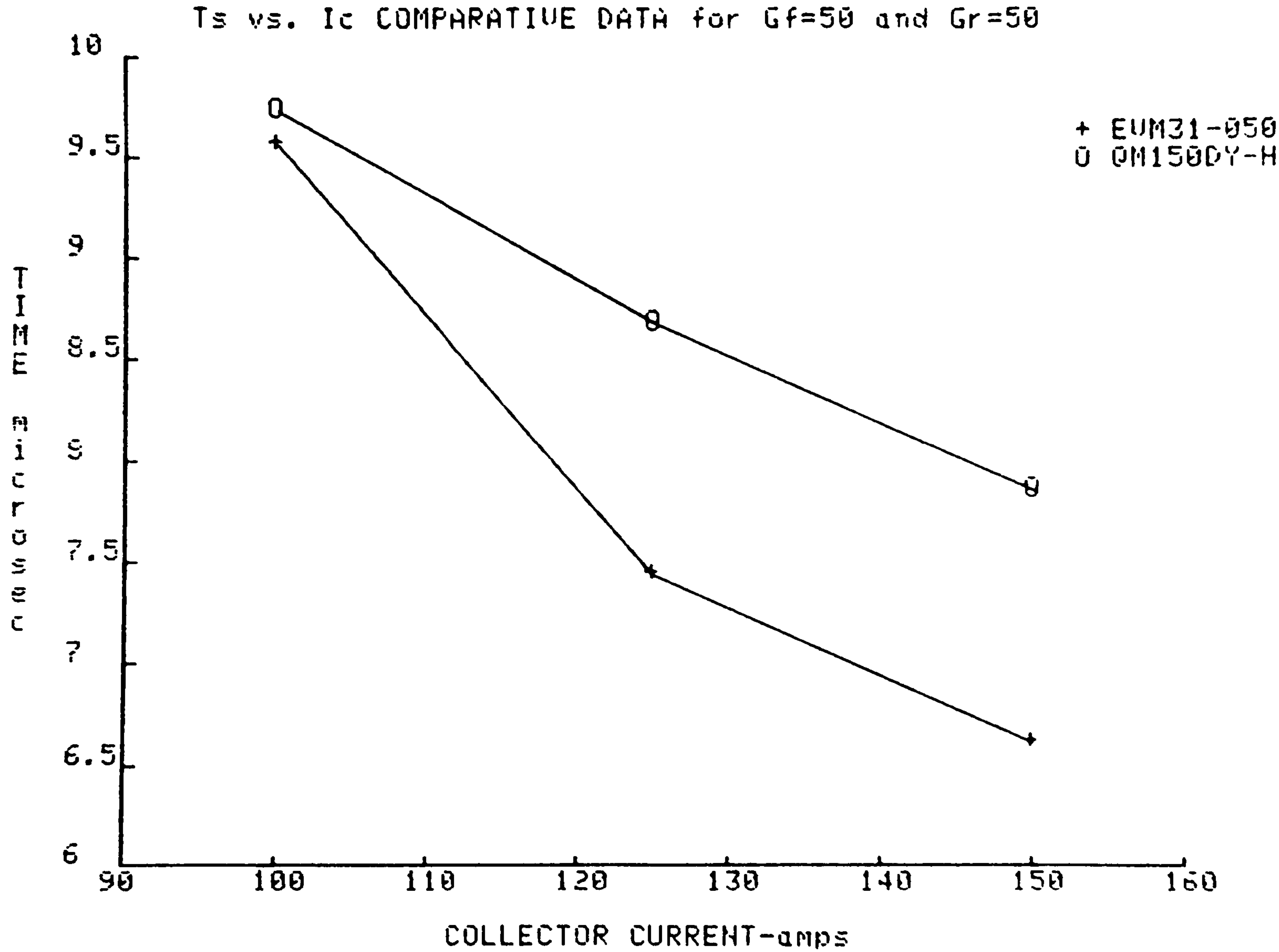
Ts vs. Ic COMPARATIVE DATA for Gf=50 and Gr=50
10
9.5
9
8.5
8
7.5
7
6.5
6
TIME microsec
90
100
110
120
130
140
150
160
COLLECTOR CURRENT-amps
+ EVM31-050
0 QM150DY-H

Fig. B.1.3

Tf vs. Ic COMPARATIVE DATA for Gr=50 and Gf=50

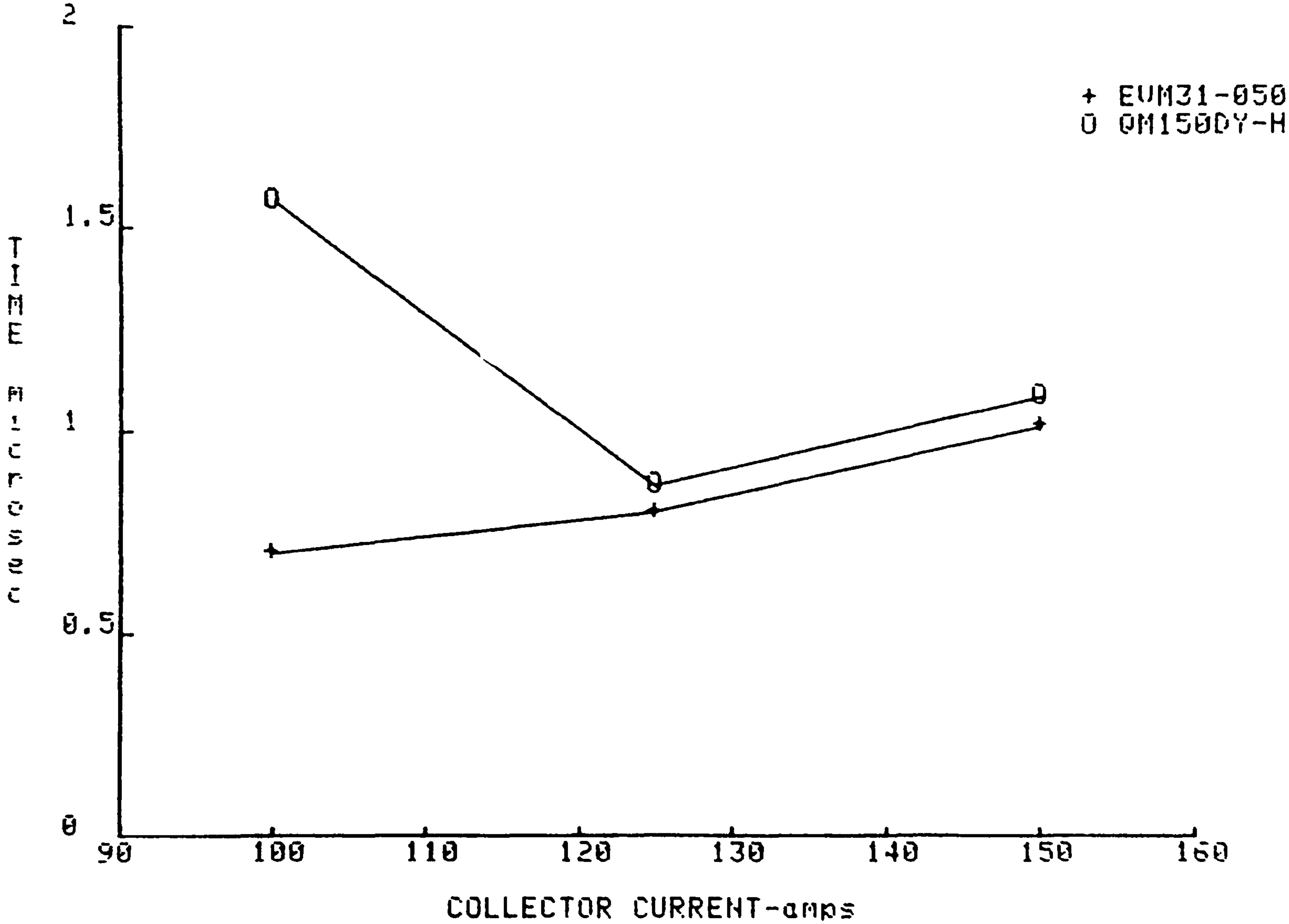

Fig. B.1.4

Qon(tot) vs Ic COMPARATIVE DATA for Vce=300V and Gf=50

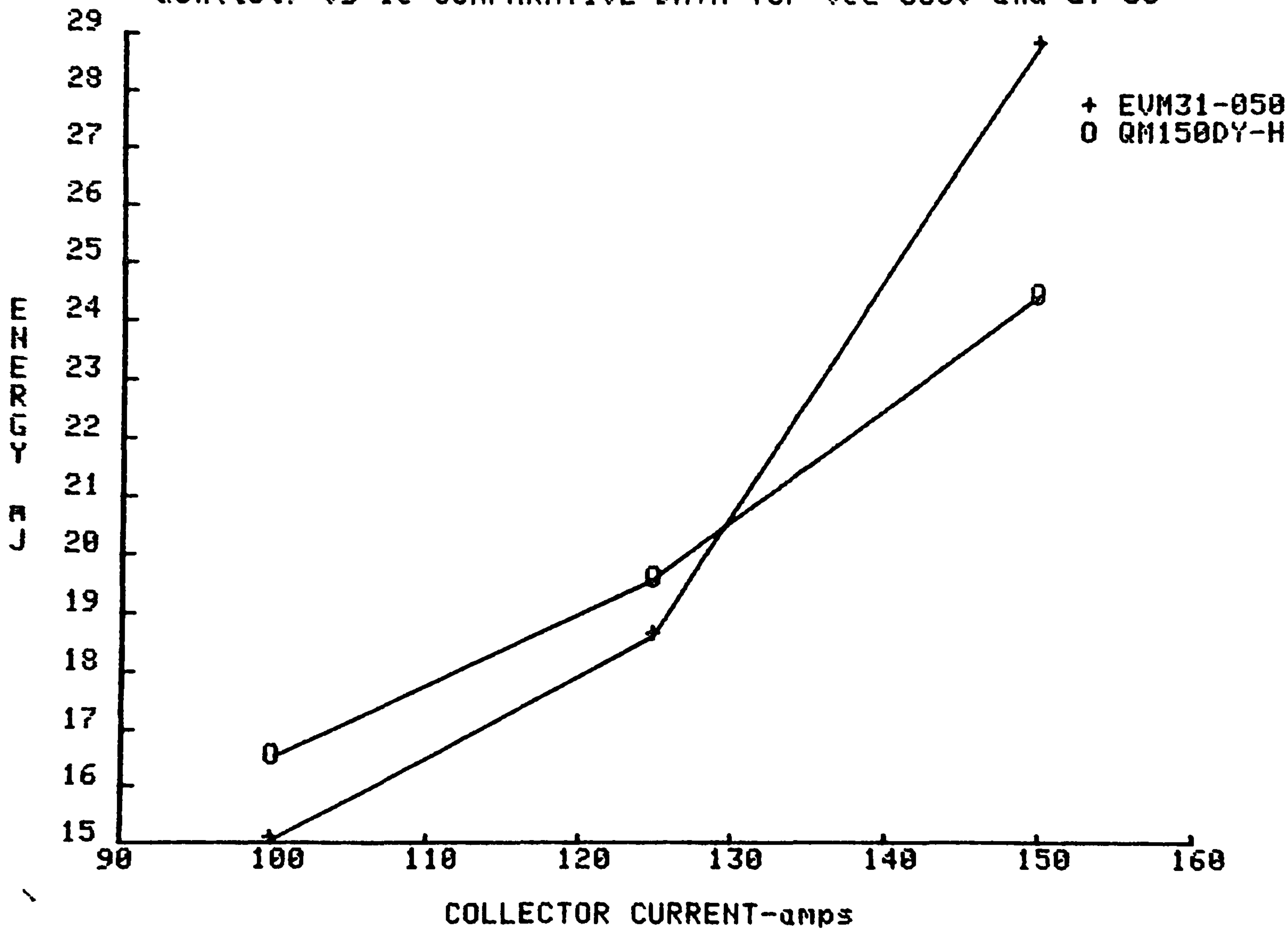

Fig. B.1.5

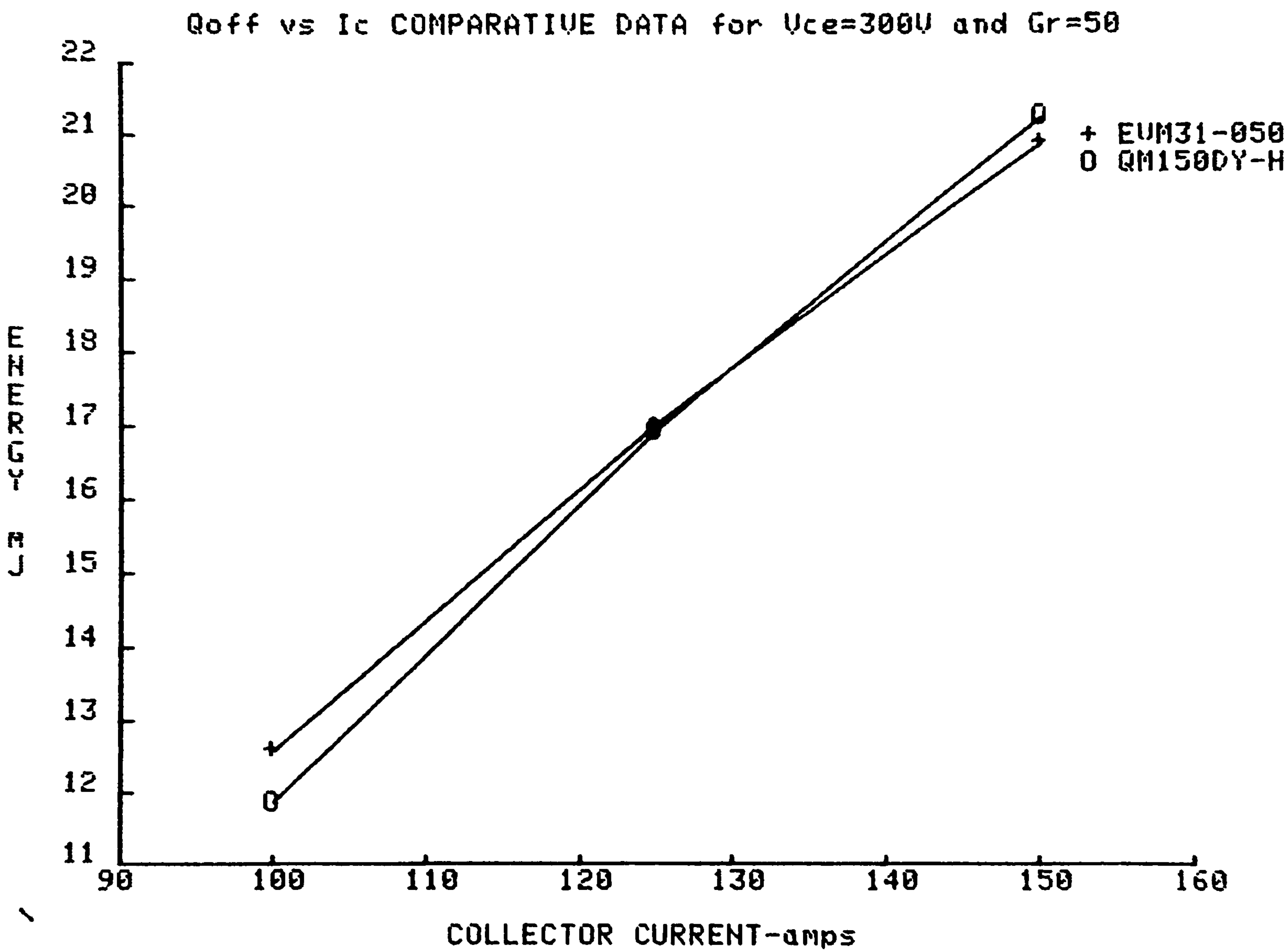

Qoff vs Ic COMPARATIVE DATA for Vce=300V and Gr=50
ENERGY mJ
22
21
20
19
18
17
16
15
14
13
12
11
90
100
110
120
130
140
150
160
COLLECTOR CURRENT-amps
+ EVM31-050
O QM150DY-H

B.7

Fig. B.1.6

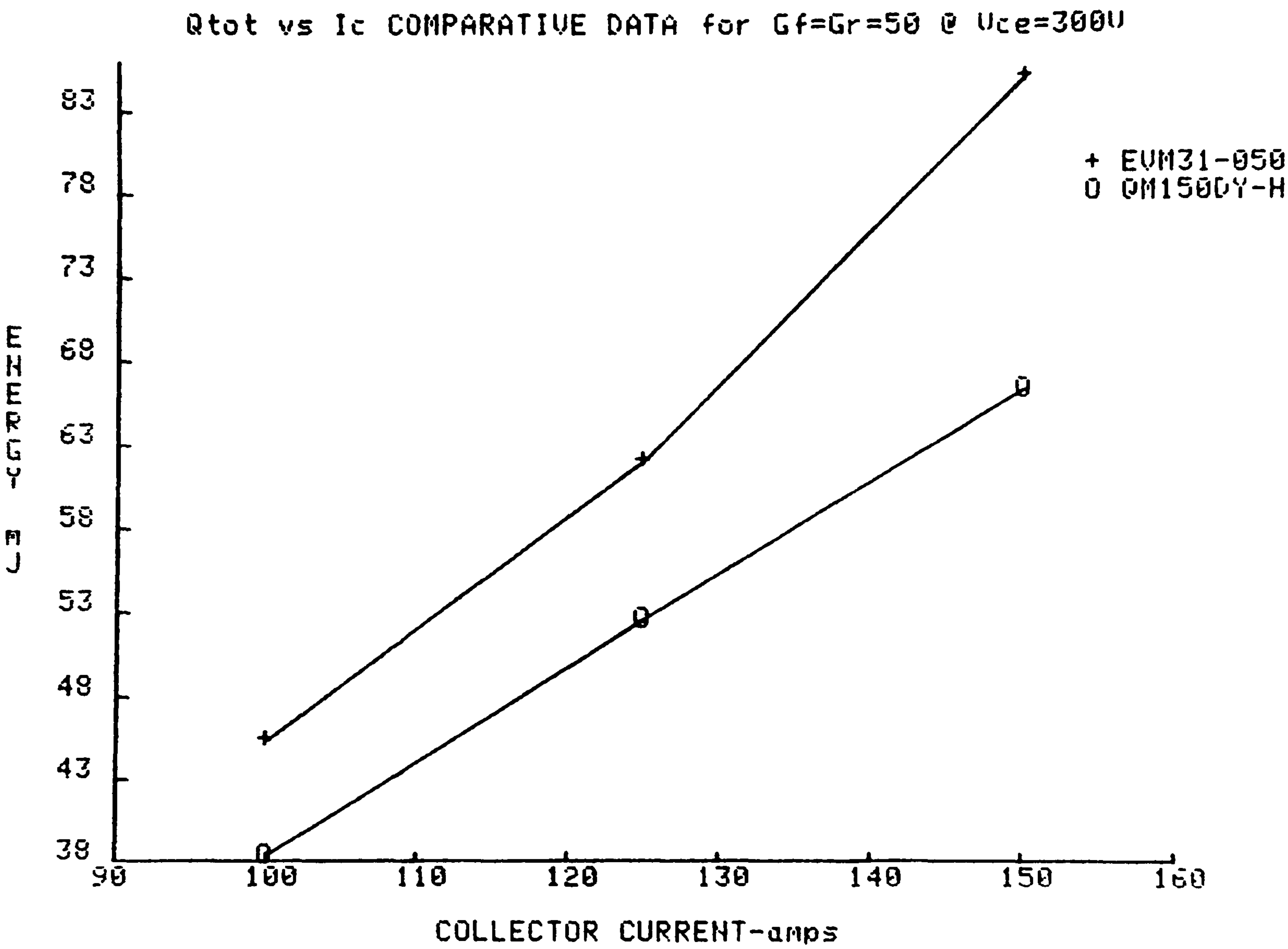
Qtot vs Ic COMPARATIVE DATA for Gf=Gr=50 @ Vce=300V
83
78
73
68
63
58
53
48
43
38
ENERGY mJ
90
100
110
120
130
140
150
160
COLLECTOR CURRENT-amps
+ EVM31-050
O QM150DY-H

Fig. B.1.7

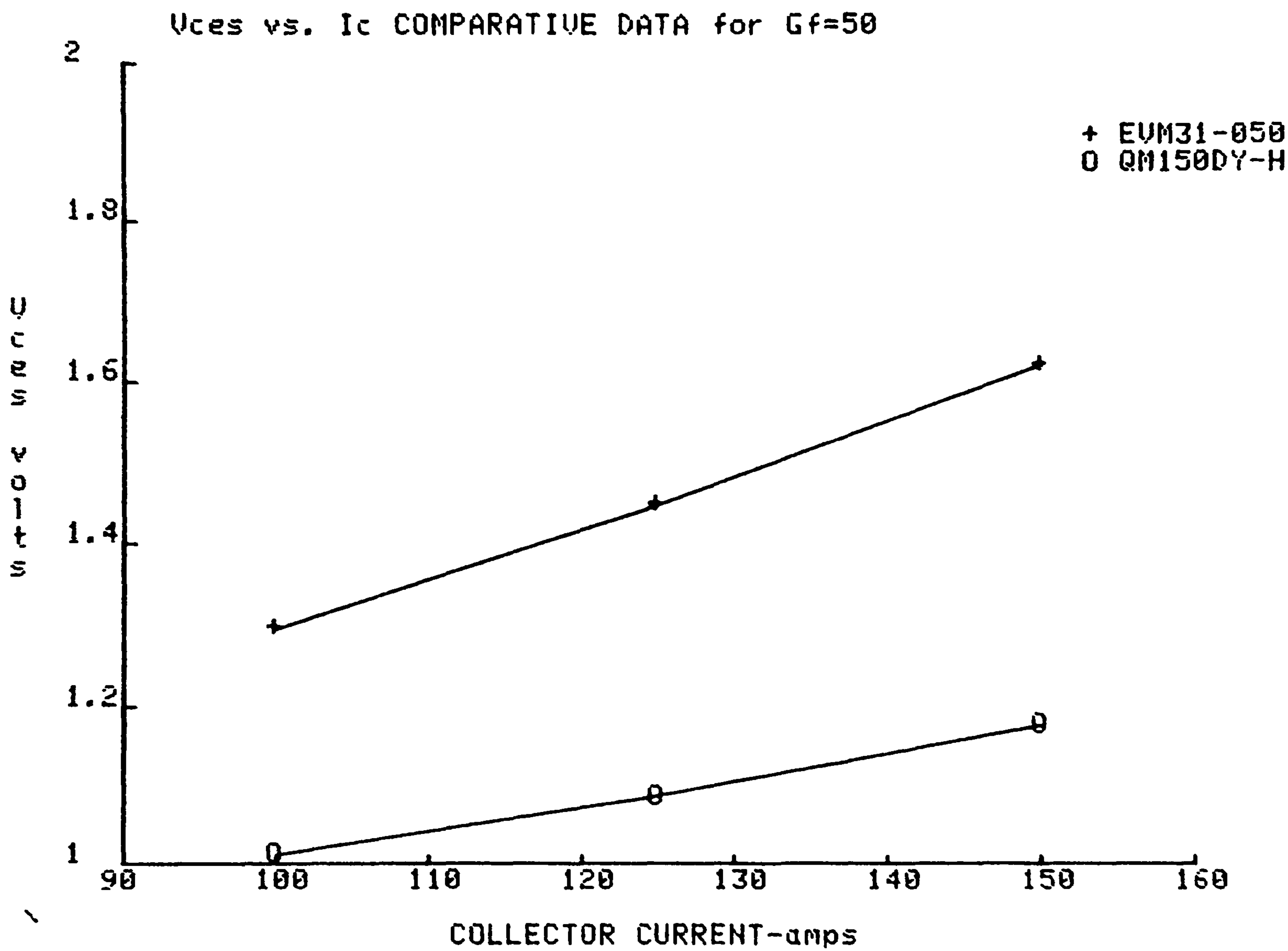
Vces vs. Ic COMPARATIVE DATA for Gf=50
2
1.8
1.6
1.4
1.2
1
90
100
110
120
130
140
150
160
Vces volts
COLLECTOR CURRENT-amps
+ EVM31-050
O QM150DY-H

Fig. B.1.8

Hfe vs Ic COMPARATIV DATA for Vce=3V @ Tc=35 C

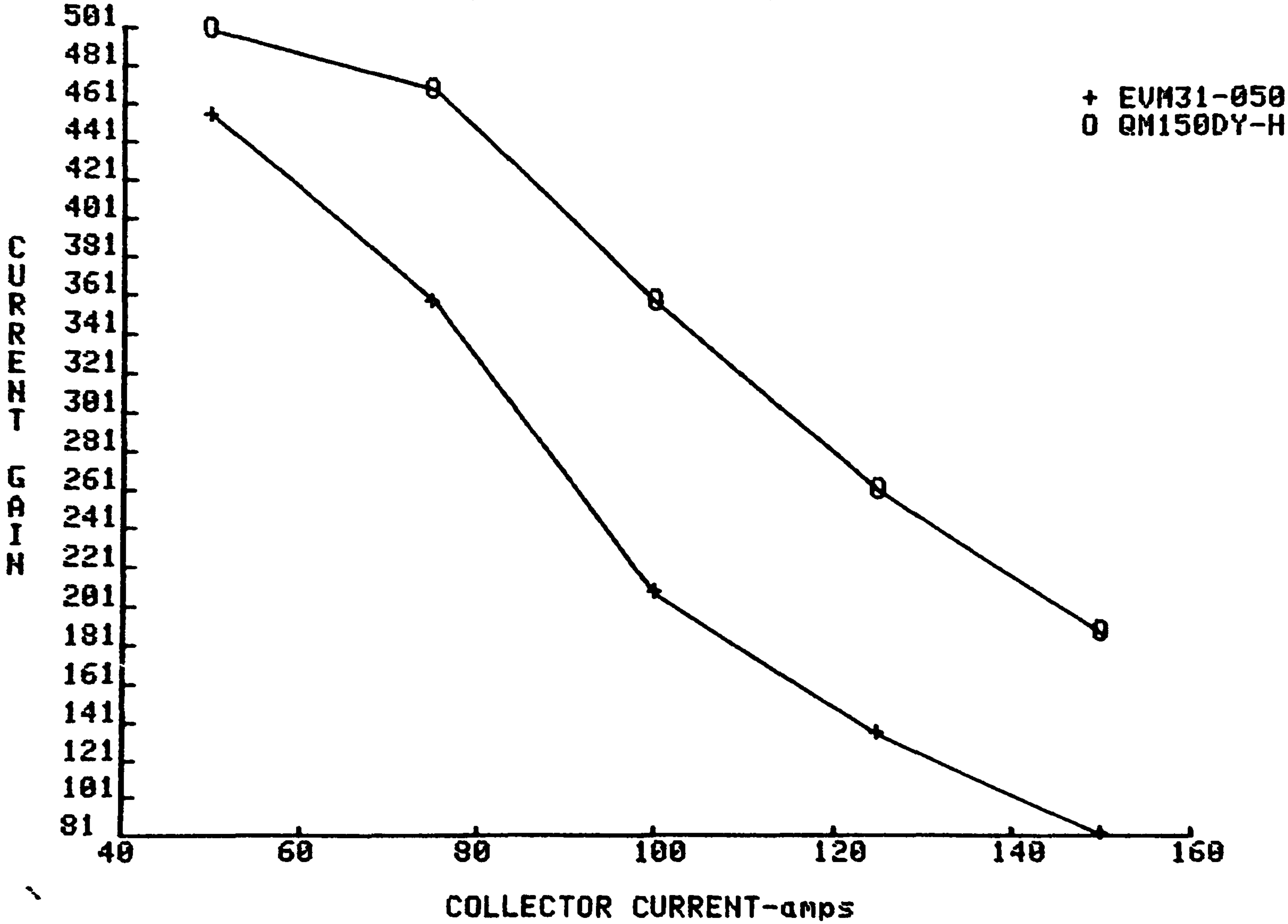

B.2 Comparative Data for Fuji ETN81-055 and Toshiba ST200M

Fig. B.2.1

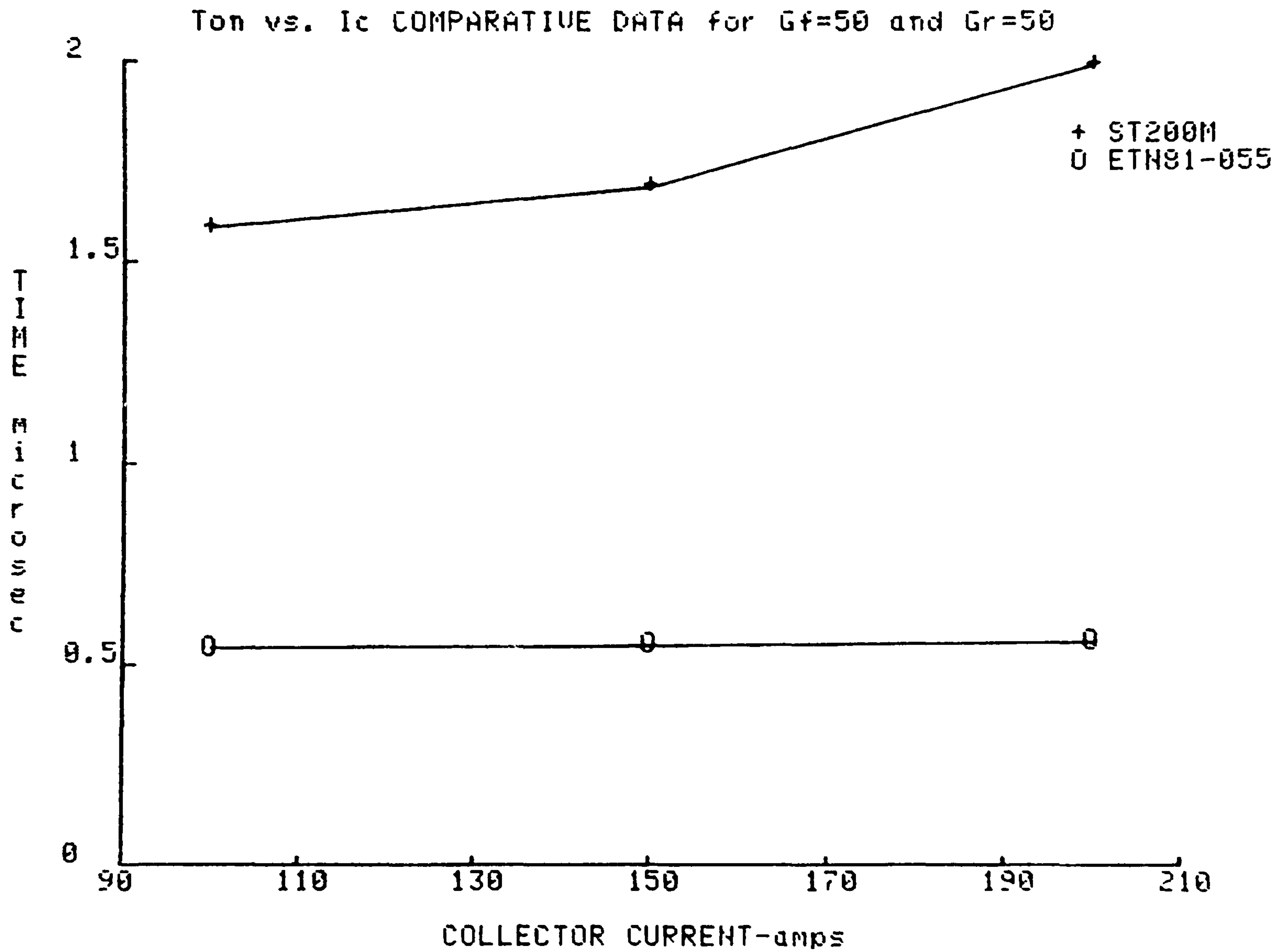
Ton vs. Ic COMPARATIVE DATA for Gf=50 and Gr=50
TIME microsec
2
1.5
1
0.5
0
90
110
130
150
170
190
210
COLLECTOR CURRENT-amps
+ ST200M
O ETN81-055

B.12

Fig. B.2.2

Ts vs. Ic COMPARATIVE DATA for Gf=50 and Gr=50

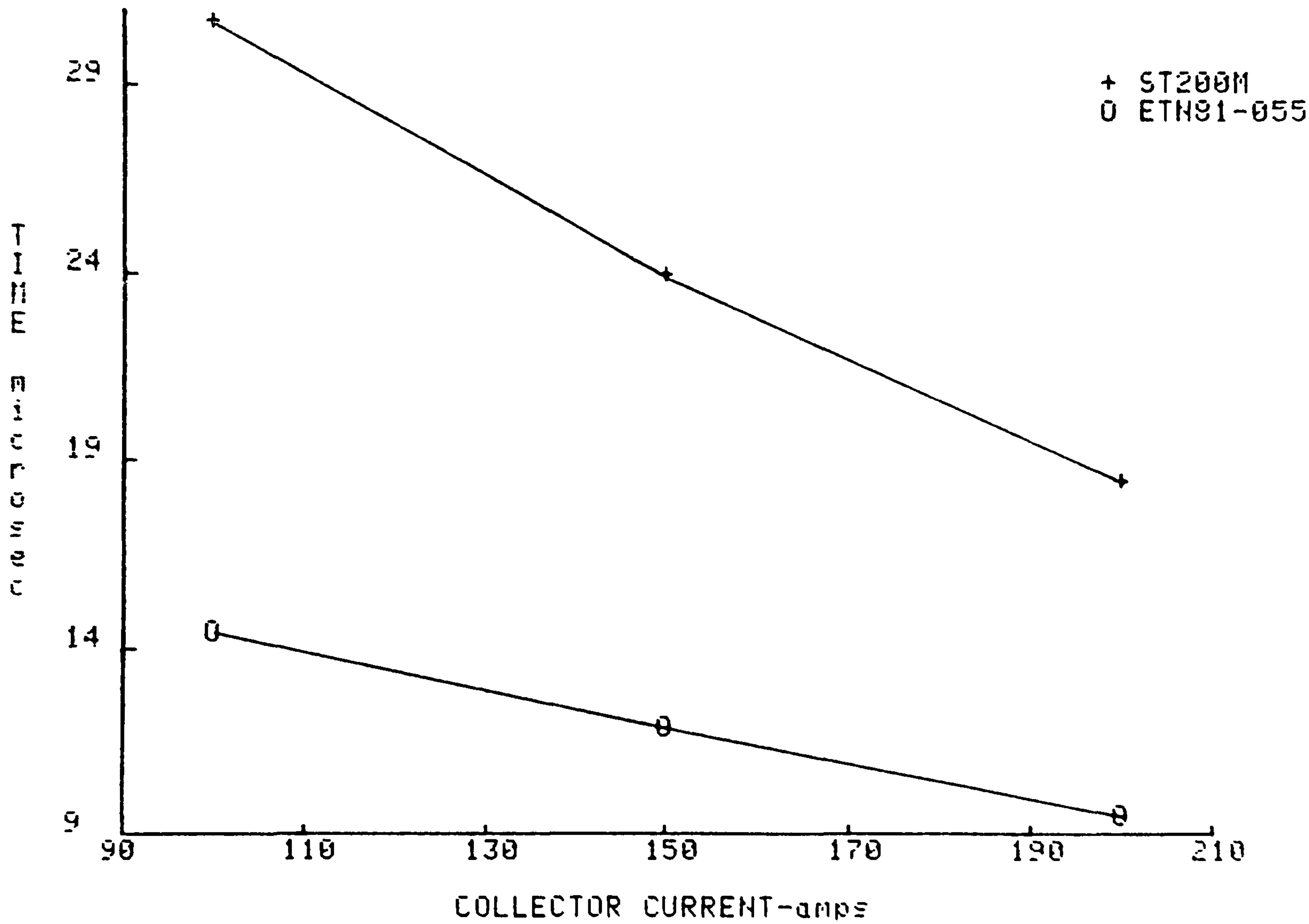

Fig. B.2.3

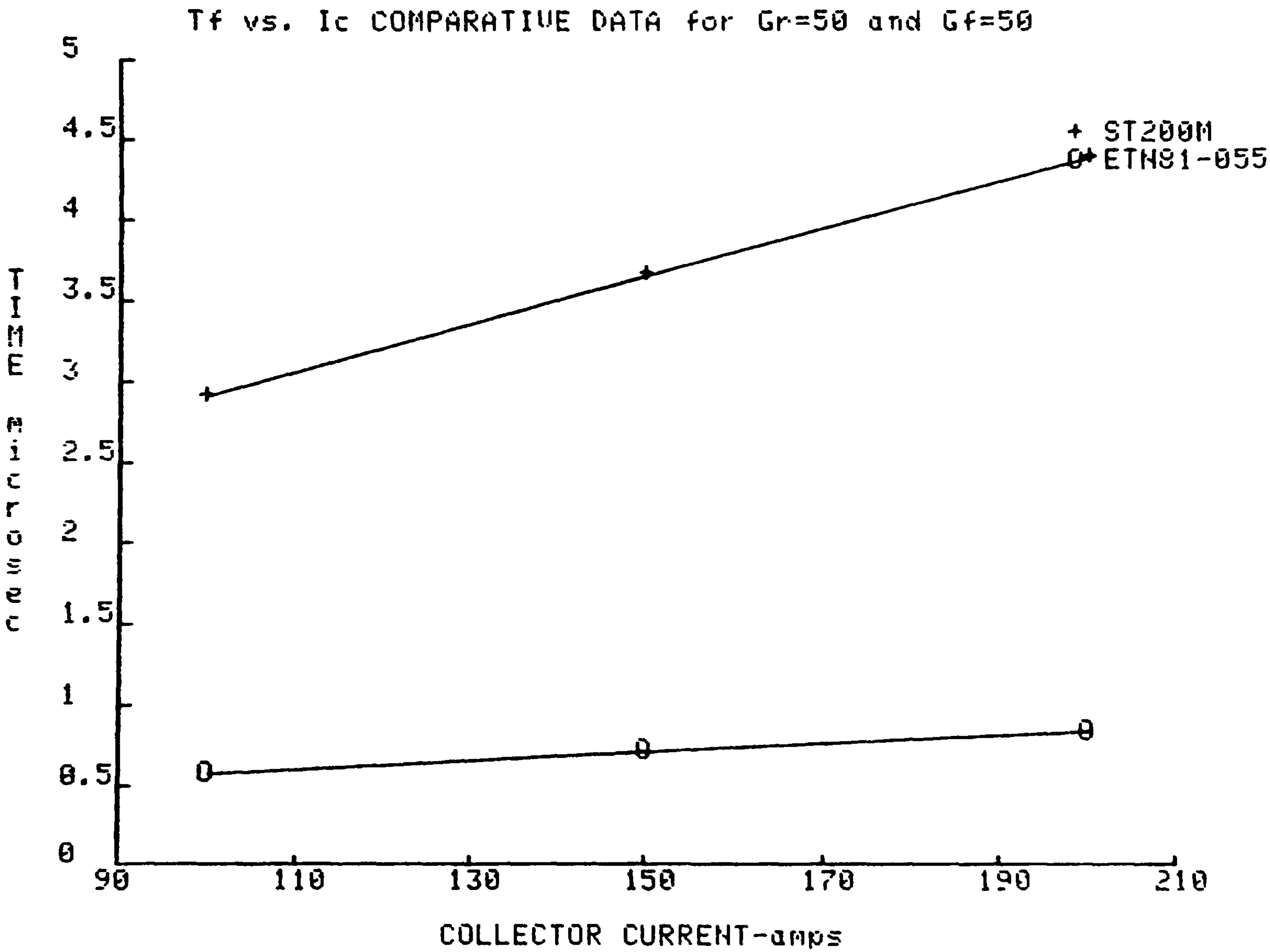

Tf vs. Ic COMPARATIVE DATA for Gr=50 and Gf=50
+ ST200M
0 ETN81-055
TIME microsec
5
4.5
4
3.5
3
2.5
2
1.5
1
0.5
0
90
110
130
150
170
190
210
COLLECTOR CURRENT-amps

Fig. B.2.4

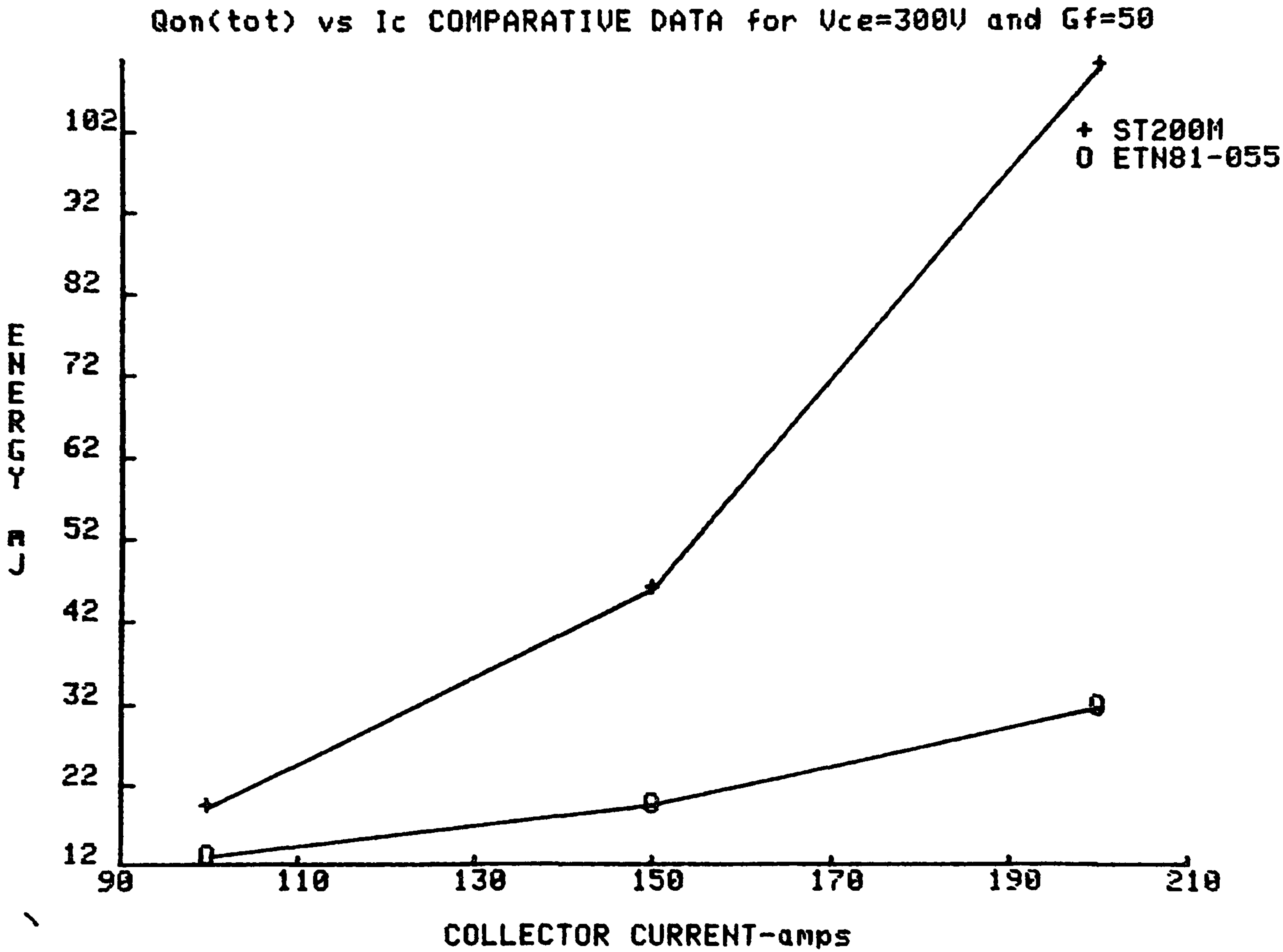
Qon(tot) vs Ic COMPARATIVE DATA for Vce=300V and Gf=50
+ ST200M
O ETN81-055
ENERGY mJ
102
92
82
72
62
52
42
32
22
12
90
110
130
150
170
190
210
COLLECTOR CURRENT-amps

Fig. B.2.5

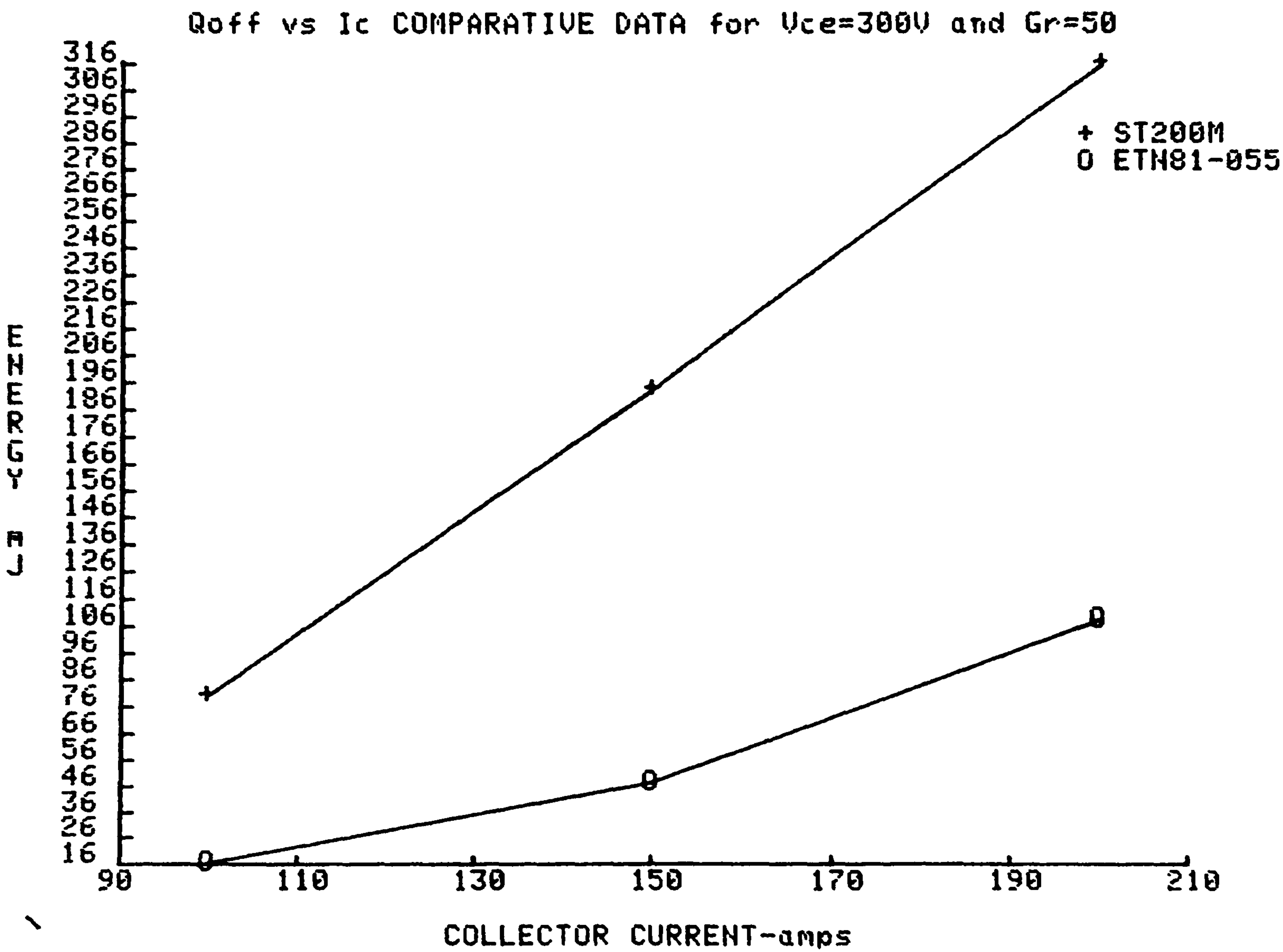
Qoff vs Ic COMPARATIVE DATA for Vce=300V and Gr=50
ENERGY mJ
316
306
296
286
276
266
256
246
236
226
216
206
196
186
176
166
156
146
136
126
116
106
96
86
76
66
56
46
36
26
16
90
110
130
150
170
190
210
COLLECTOR CURRENT-amps
+ ST200M
O ETN81-055

B.16

Fig. B.2.6

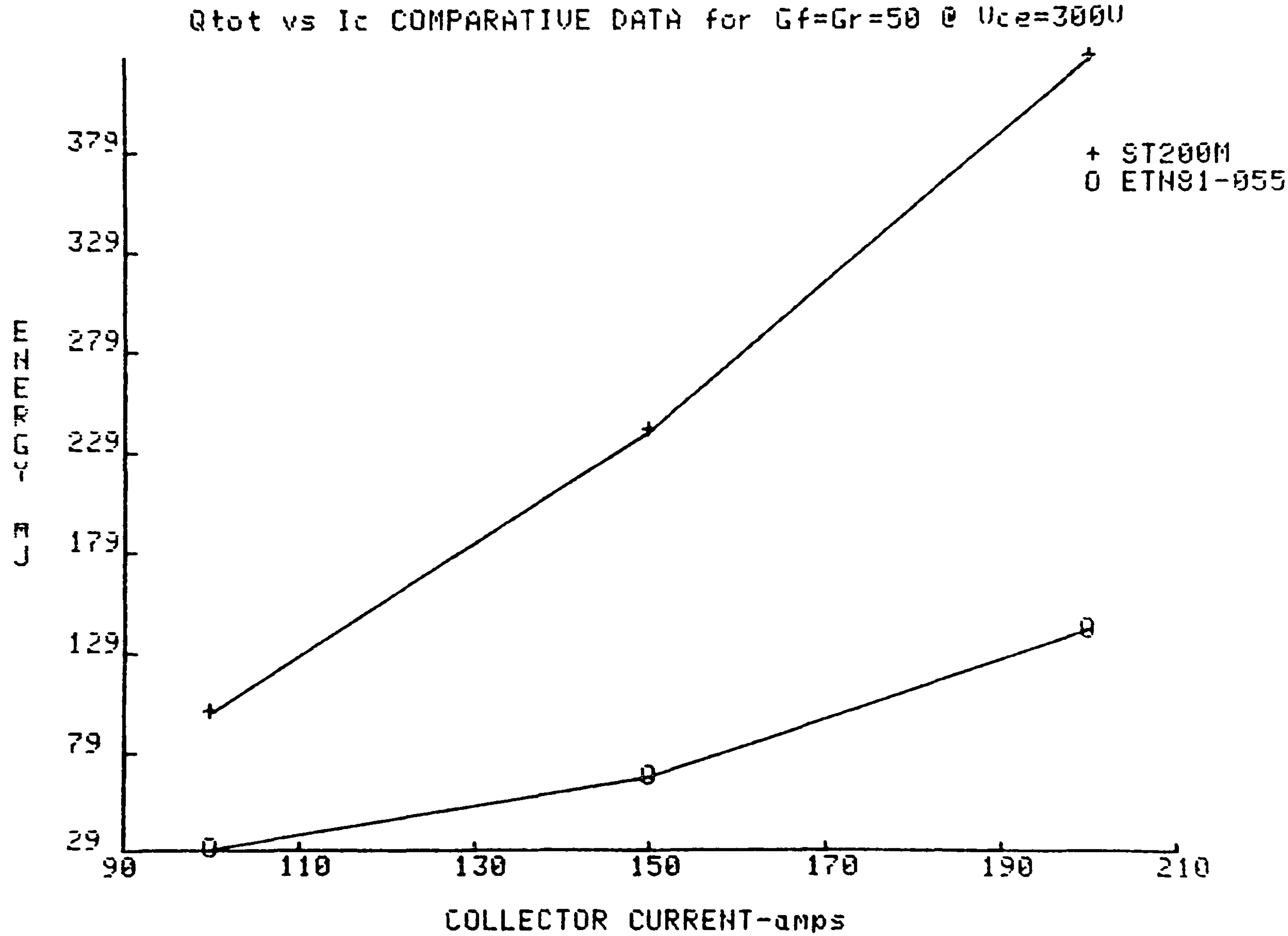
Qtot vs Ic COMPARATIVE DATA for Gf=Gr=50 @ Vce=300V
+ ST200M
0 ETN81-055
ENERGY mJ
379
329
279
229
179
129
79
29
90
110
130
150
170
190
210
COLLECTOR CURRENT-amps

Fig. B.2.7

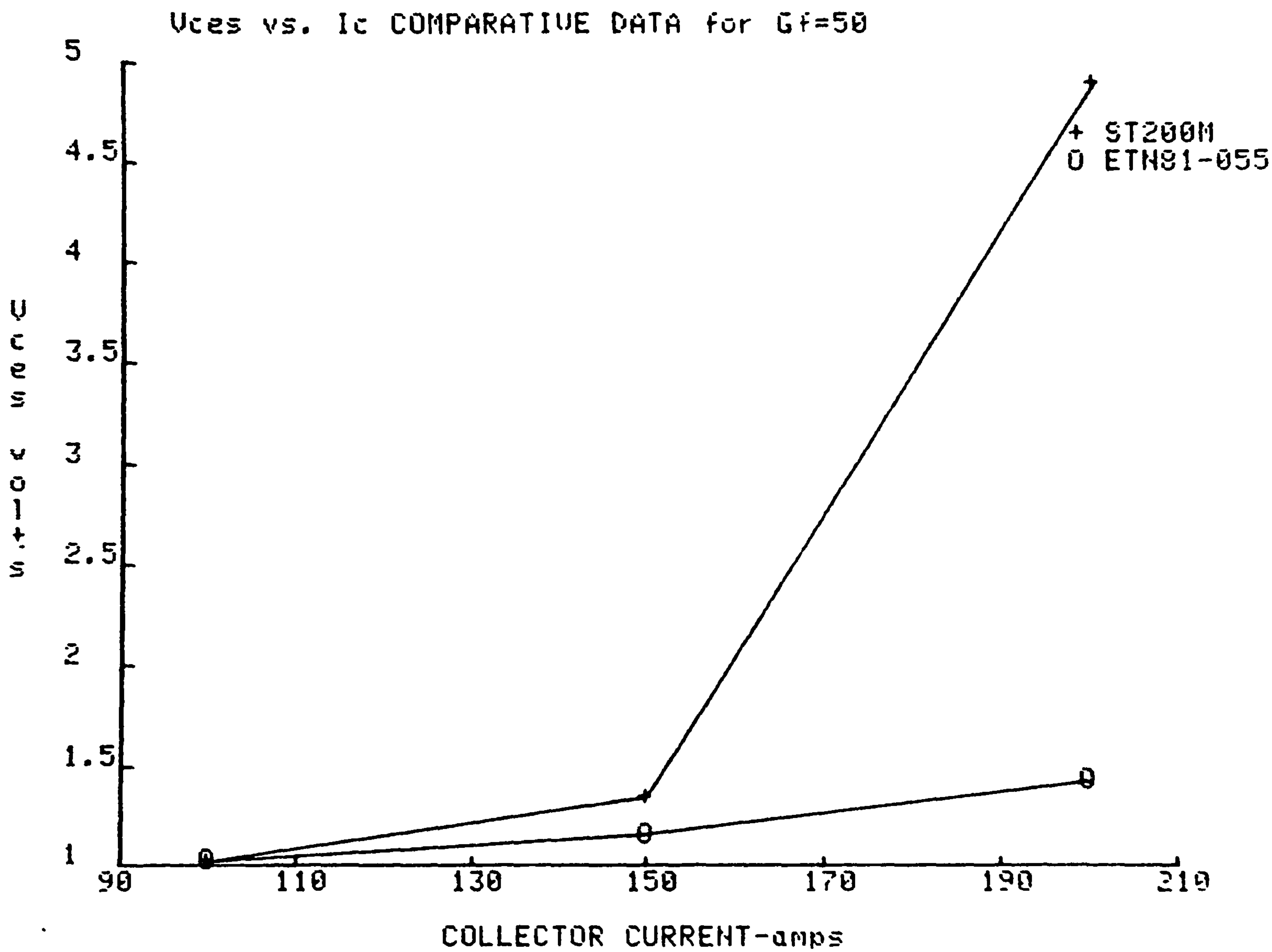
Vces vs. Ic COMPARATIVE DATA for Gf=50
5
4.5
4
3.5
3
2.5
2
1.5
1
Vces volts
90
110
130
150
170
190
210
COLLECTOR CURRENT-amps
+ ST200M
O ETN81-055

Fig. B.2.8

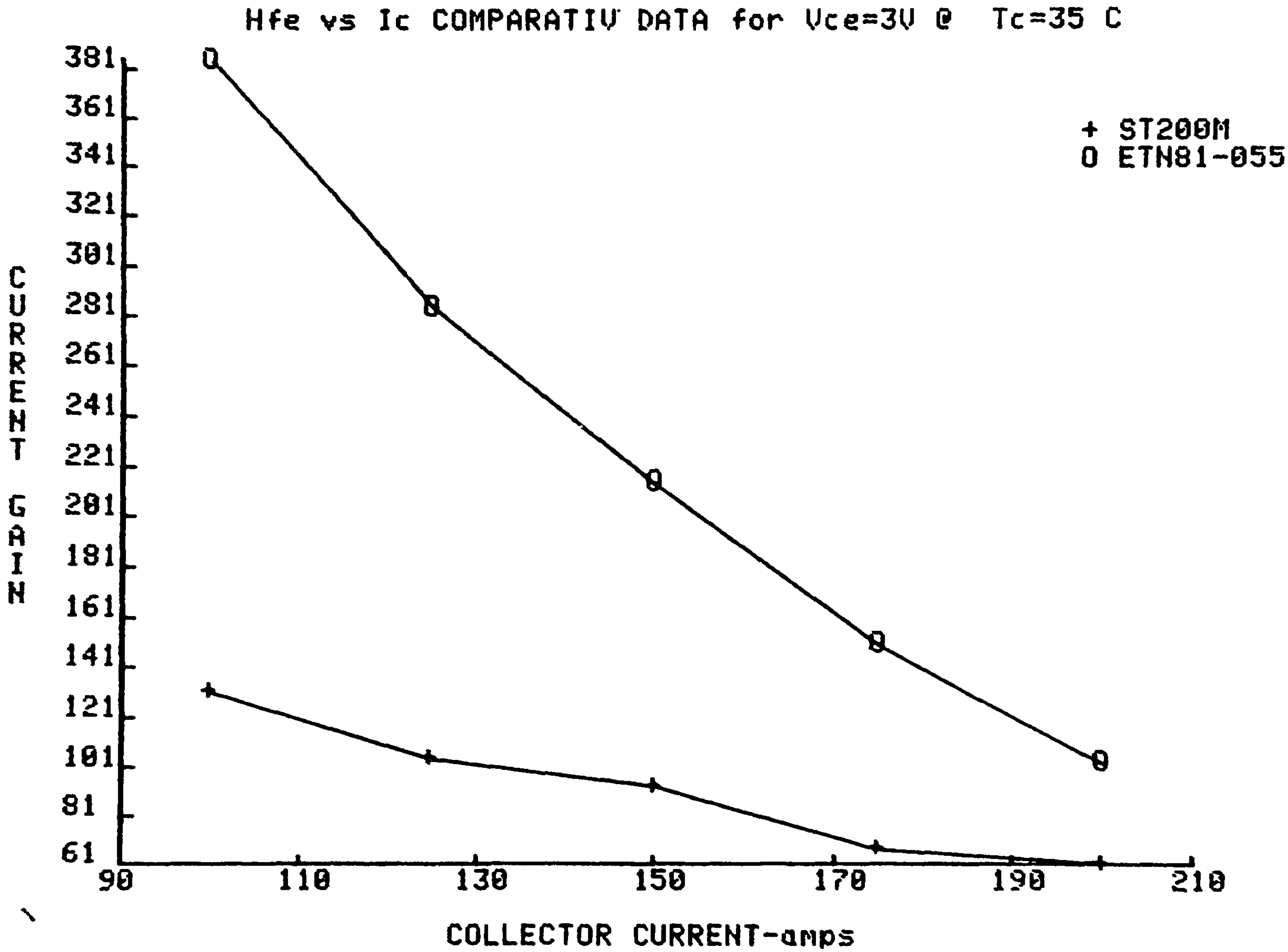
Hfe vs Ic COMPARATIV DATA for Vce=3V @ Tc=35 C
+ ST200M
O ETN81-055
CURRENT GAIN
381
361
341
321
301
281
261
241
221
201
181
161
141
121
101
81
61
90
110
130
150
170
190
210
COLLECTOR CURRENT-amps

B.3 Comparative Data for Westinghouse DA11503008, Mitsubishi QM300HA-H, Mitsubishi QM300HA-2H AND Toshiba ST300M21

Fig. B.3.1

Ton vs. Ic COMPARATIVE DATA for Gf=50 and Gr=50

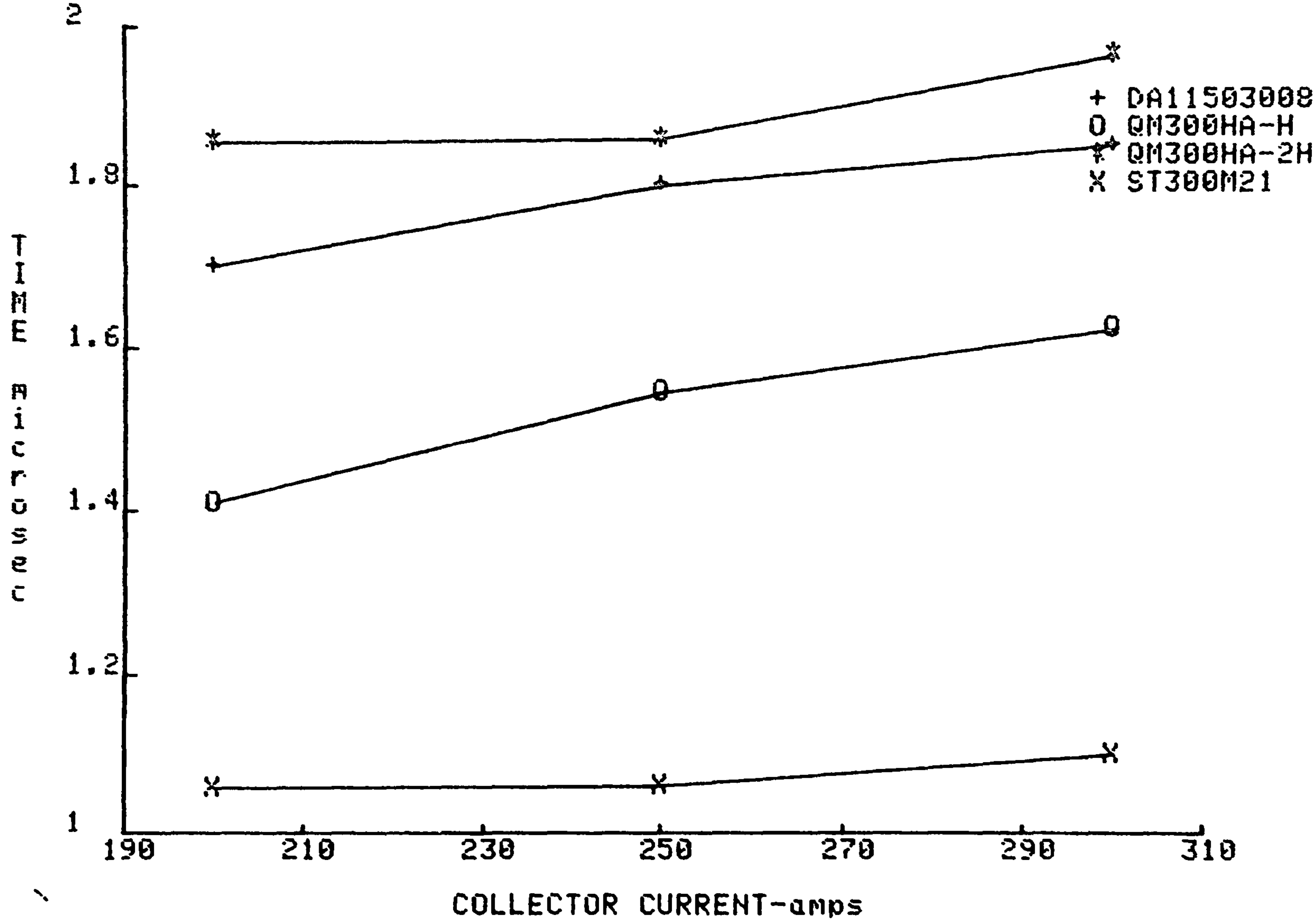

Fig. B.3.2

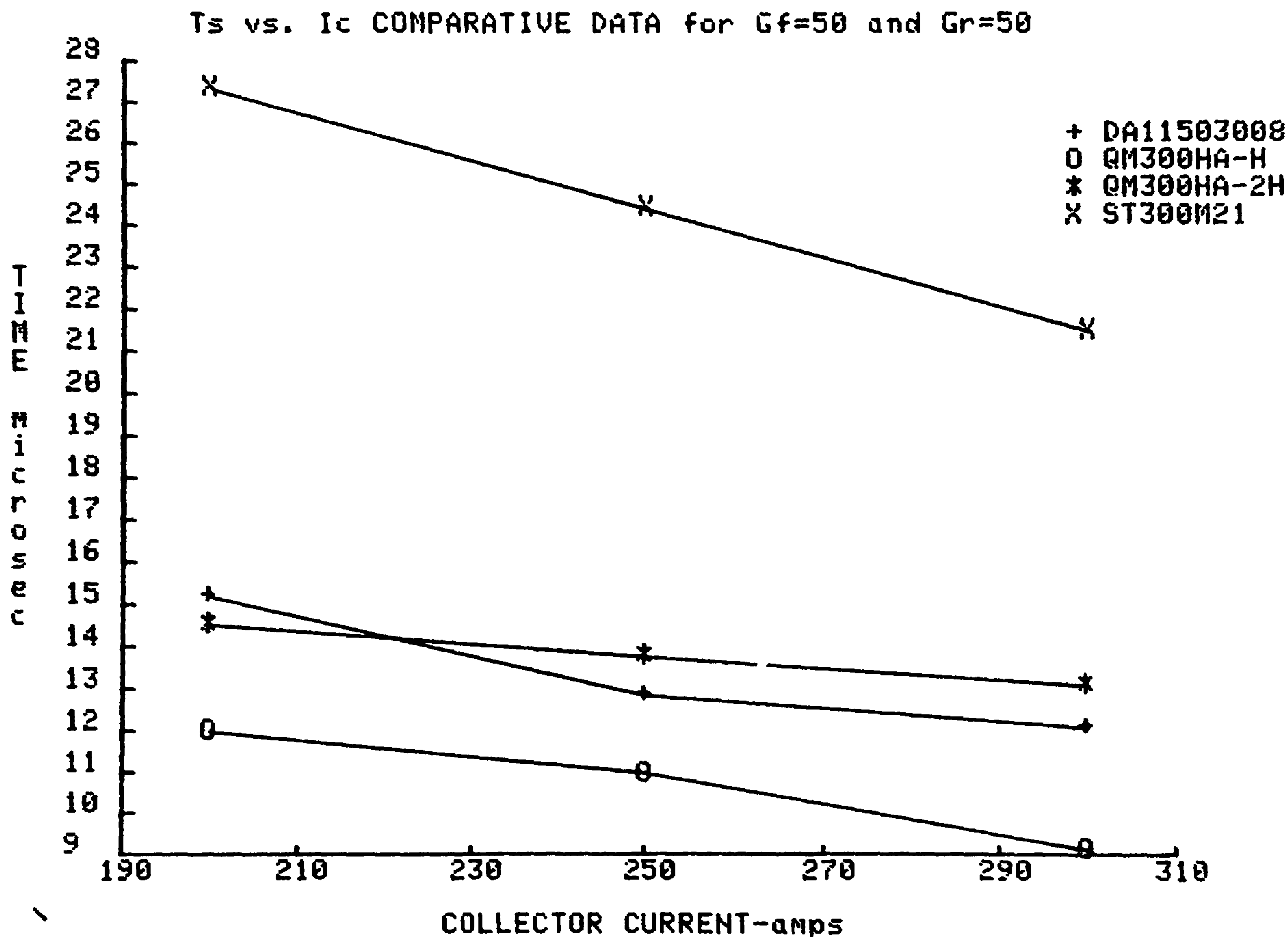
Ts vs. Ic COMPARATIVE DATA for Gf=50 and Gr=50
28
27
26
25
24
23
22
21
20
19
18
17
16
15
14
13
12
11
10
9
TIME microsec
190
210
230
250
270
290
310
COLLECTOR CURRENT-amps
+ DA11503008
O QM300HA-H
* QM300HA-2H
X ST300M21

Fig.B.3.3

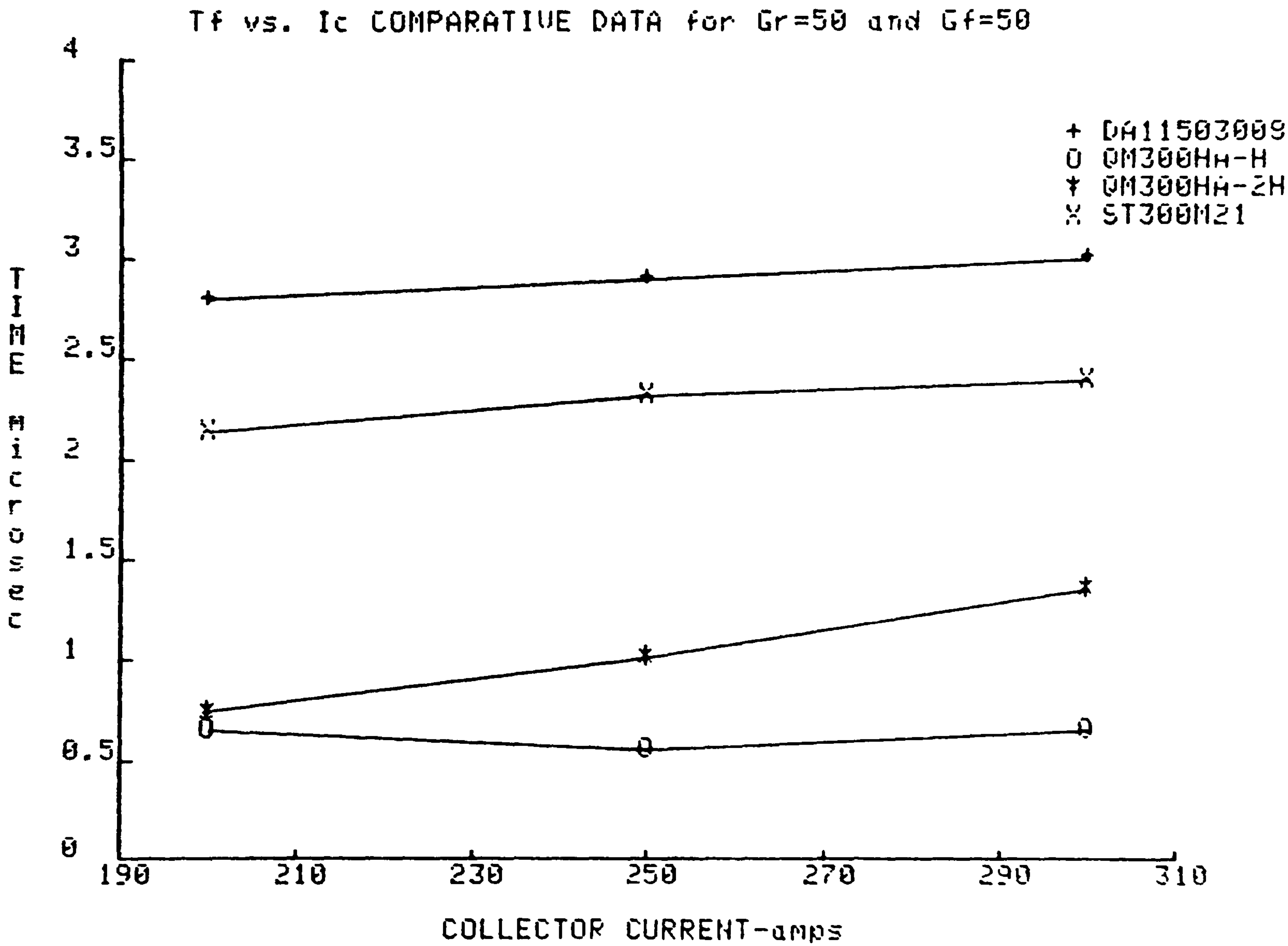
Tf vs. Ic COMPARATIVE DATA for Gr=50 and Gf=50
4
3.5
3
2.5
2
1.5
1
0.5
0
TIME microsec
+ DA11503009
O QM300HA-H
* QM300HA-2H
X ST300M21
190
210
230
250
270
290
310
COLLECTOR CURRENT-amps

Fig.B.3.4

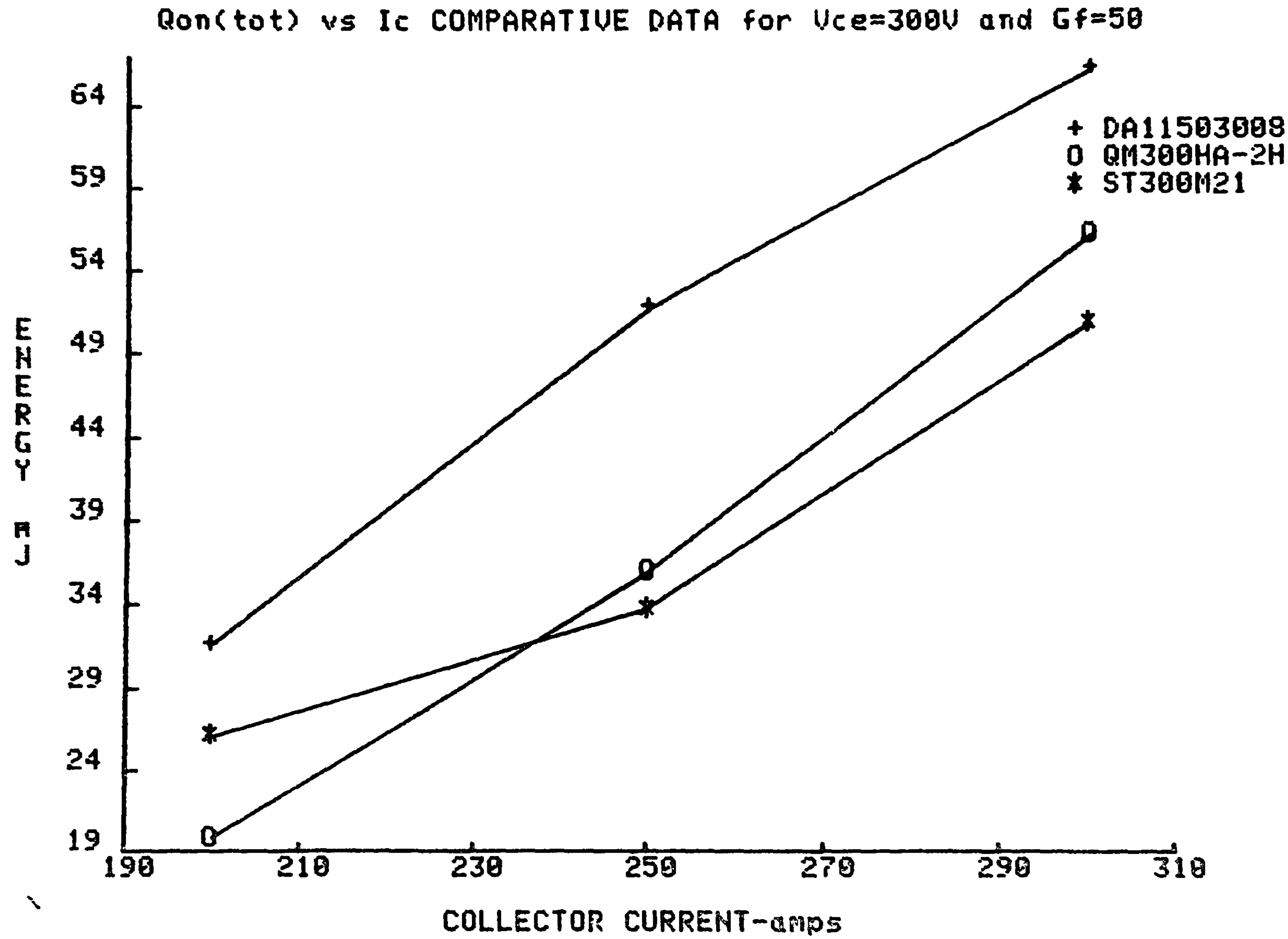
Qon(tot) vs Ic COMPARATIVE DATA for Vce=300V and Gf=50
+ DA11503008
O QM300HA-2H
* ST300M21
ENERGY mJ
64
59
54
49
44
39
34
29
24
19
190
210
230
250
270
290
310
COLLECTOR CURRENT-amps

Fig.B.3.5

Qoff vs Ic COMPARATIVE DATA for Vce=300V and Gr=50

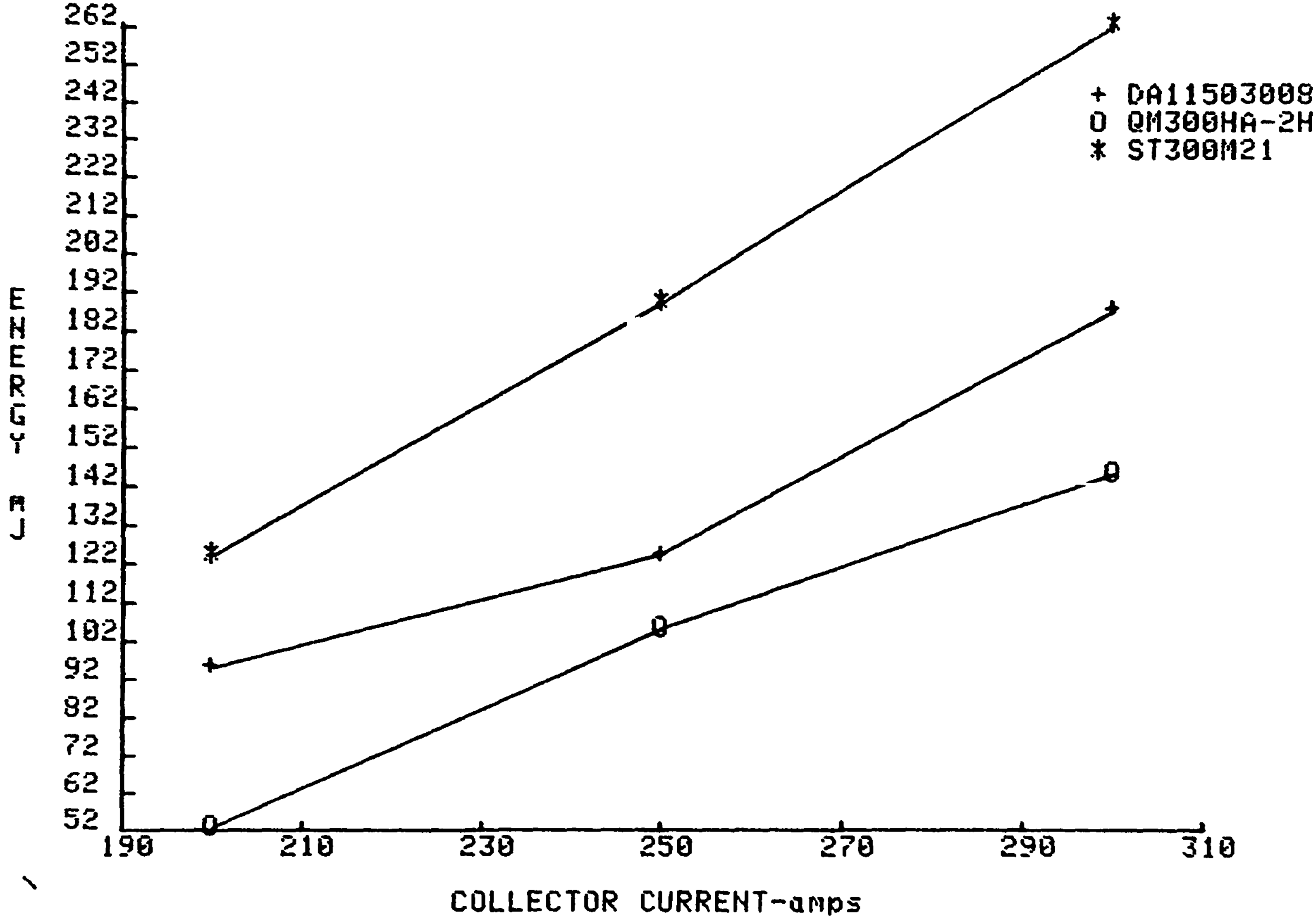

Fig. B.3.6

Qtot vs Ic COMPARATIVE DATA for Gf=Gr=50 @ Vce=300V

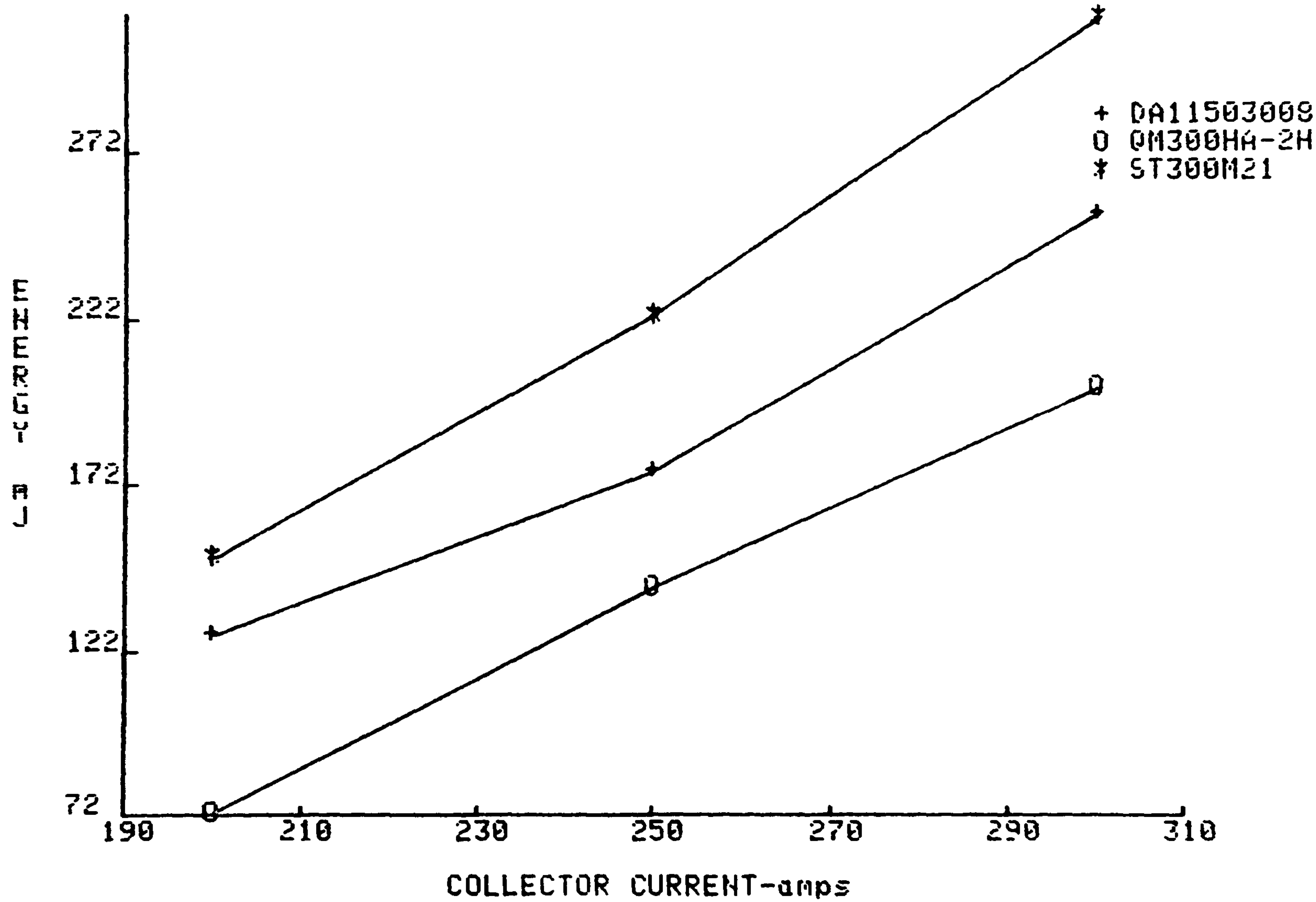

Fig. B.3.7

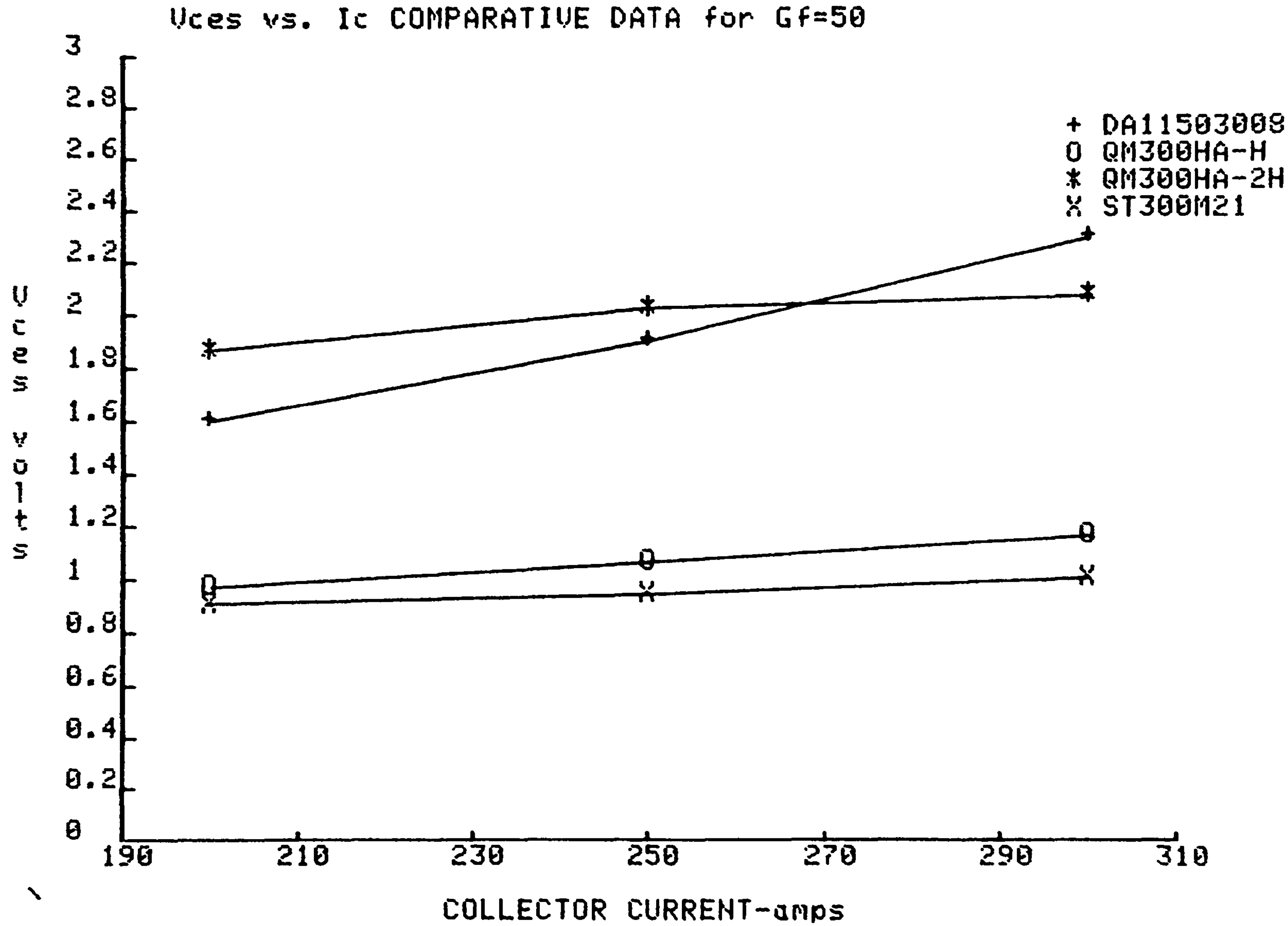
Vces vs. Ic COMPARATIVE DATA for Gf=50
V c e s volts
3
2.8
2.6
2.4
2.2
2
1.8
1.6
1.4
1.2
1
0.8
0.6
0.4
0.2
0
190
210
230
250
270
290
310
COLLECTOR CURRENT-amps
+ DA11503008
O QM300HA-H
* QM300HA-2H
X ST300M21

Fig. B.3.8

Hfe vs Ic COMPARATIVE DATA for Vce=3V @ Tc=35 C

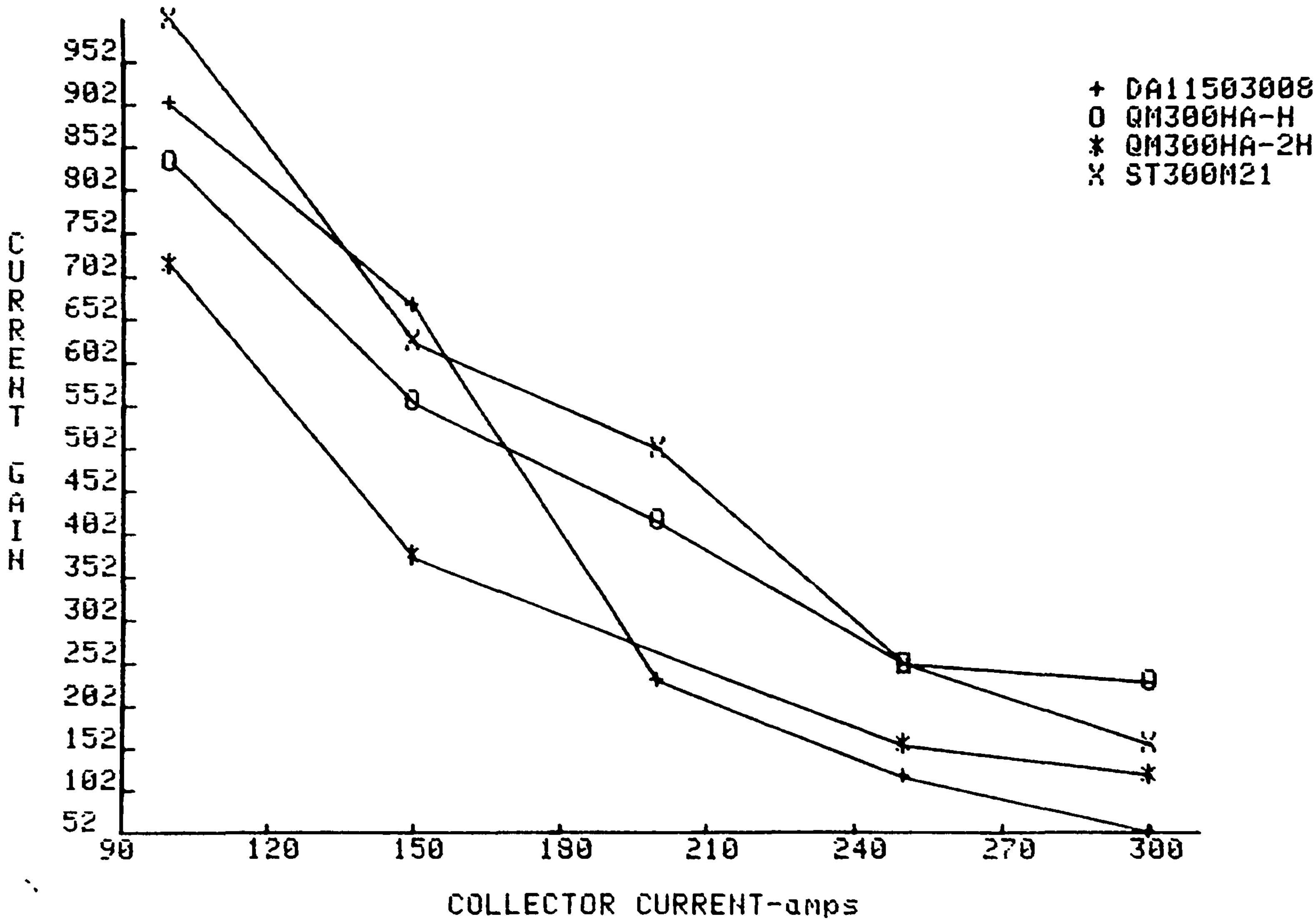

B.4 Comparative Data for Toshiba ST400G and Toshiba ST400G21

Fig. B.4.1

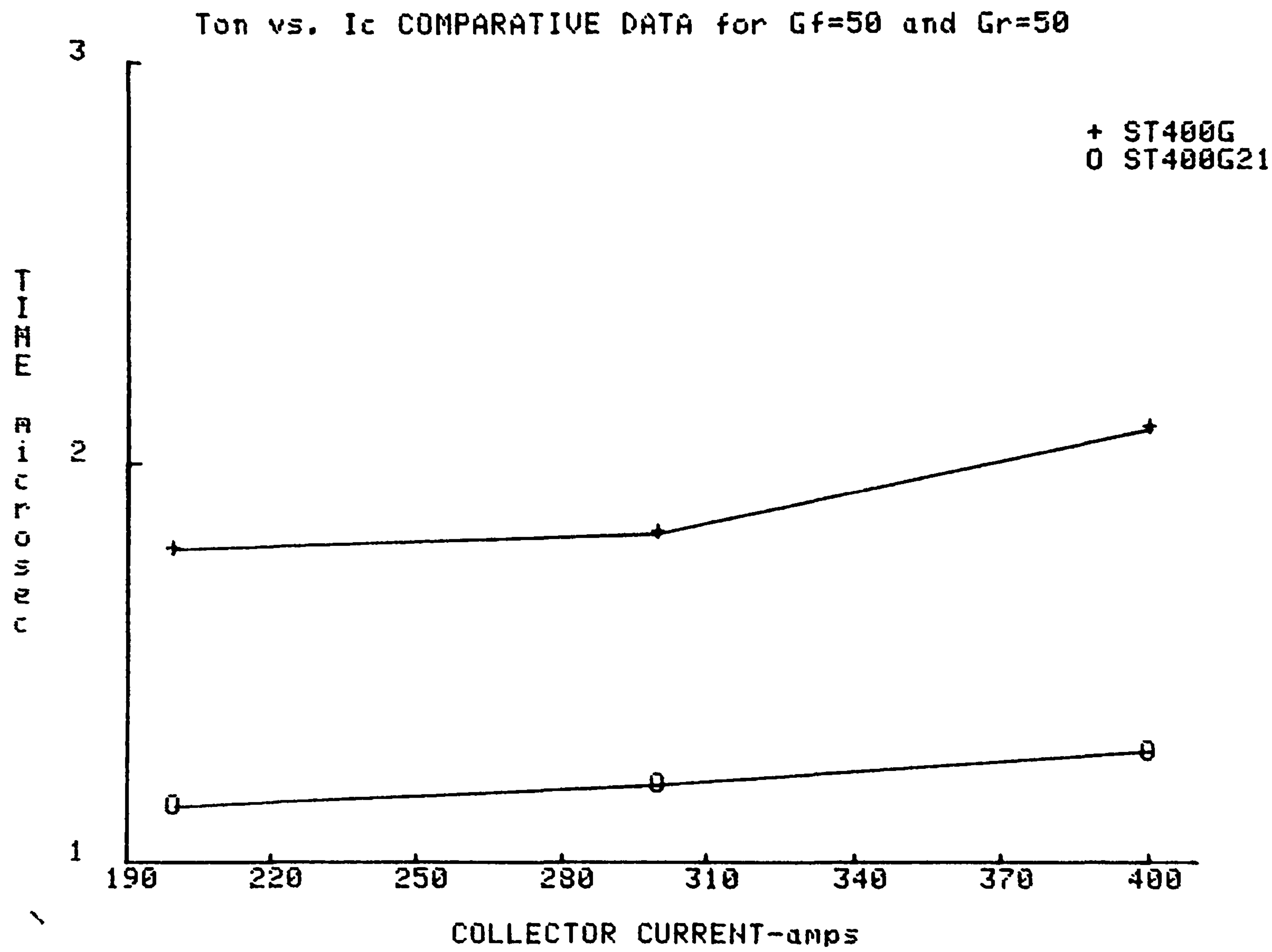

Ton vs. Ic COMPARATIVE DATA for Gf=50 and Gr=50
+ ST400G
O ST400G21
TIME microsec
3
2
1
190
220
250
280
310
340
370
400
COLLECTOR CURRENT-amps

Fig. B.4.2

Ts vs. Ic COMPARATIVE DATA for Gf=50 and Gr=50

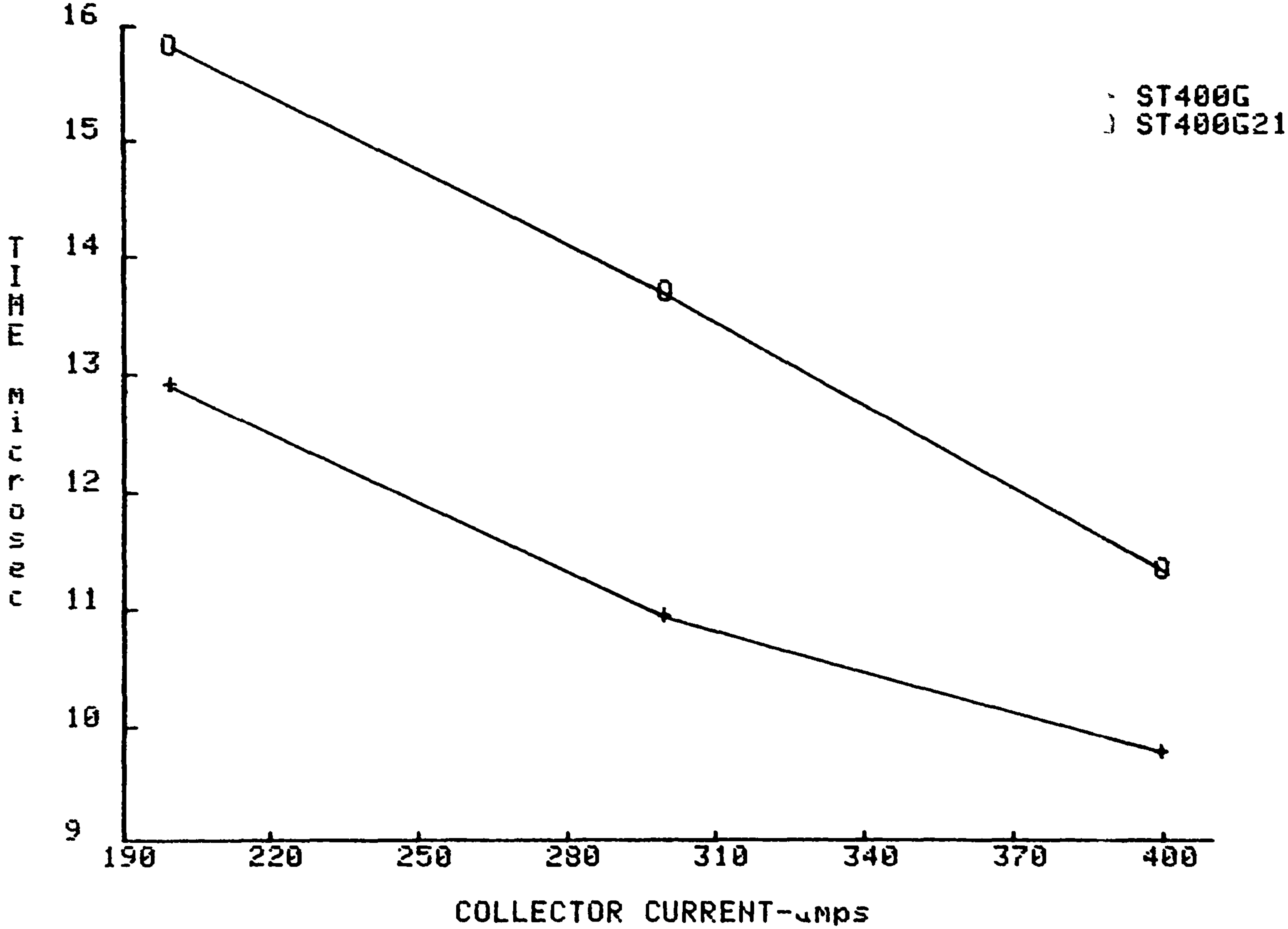

Fig. B.4.3

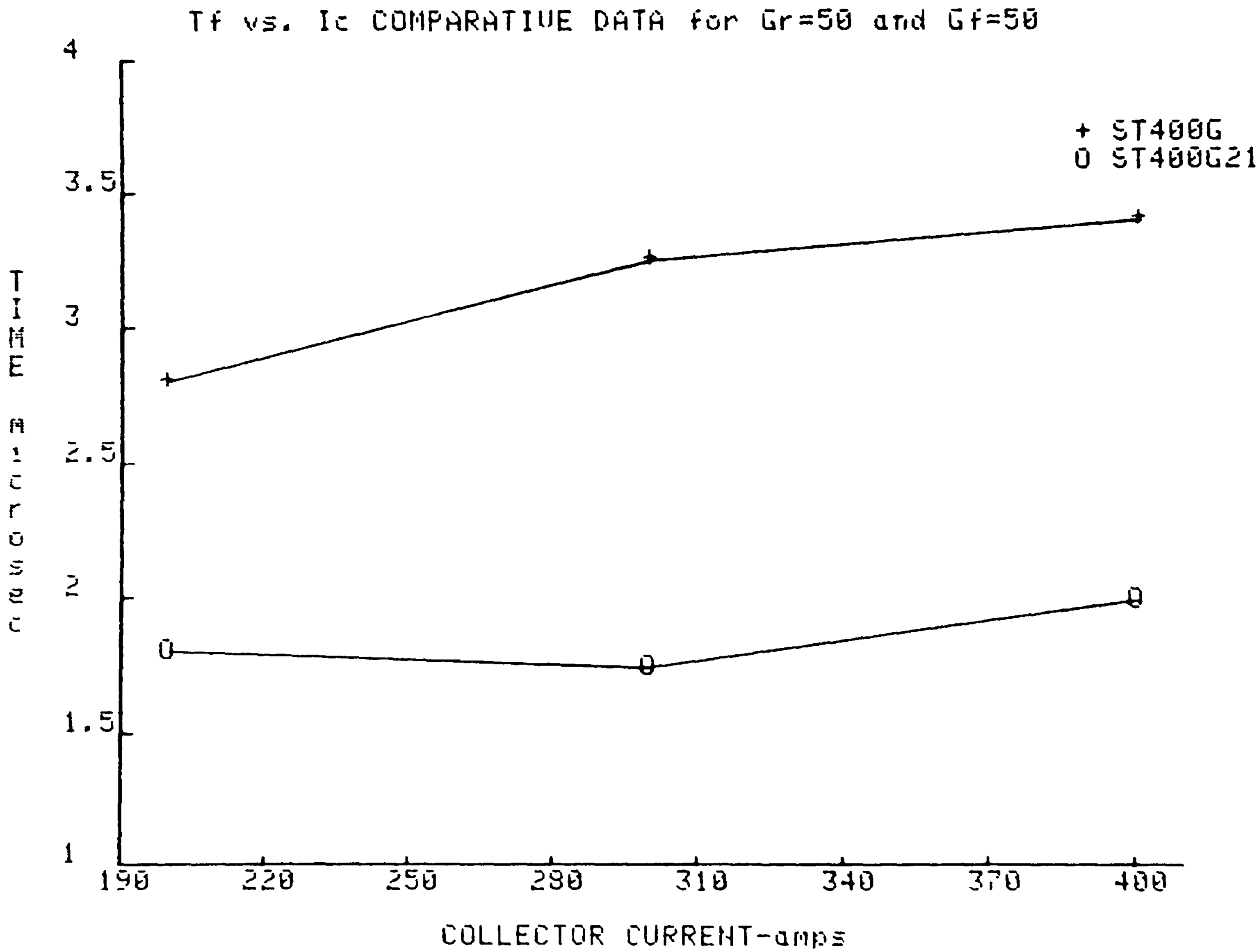

Tf vs. Ic COMPARATIVE DATA for Gr=50 and Gf=50
+ ST400G
0 ST400G21
TIME microsec
4
3.5
3
2.5
2
1.5
1
190
220
250
280
310
340
370
400
COLLECTOR CURRENT-amps

Fig. B.4.4

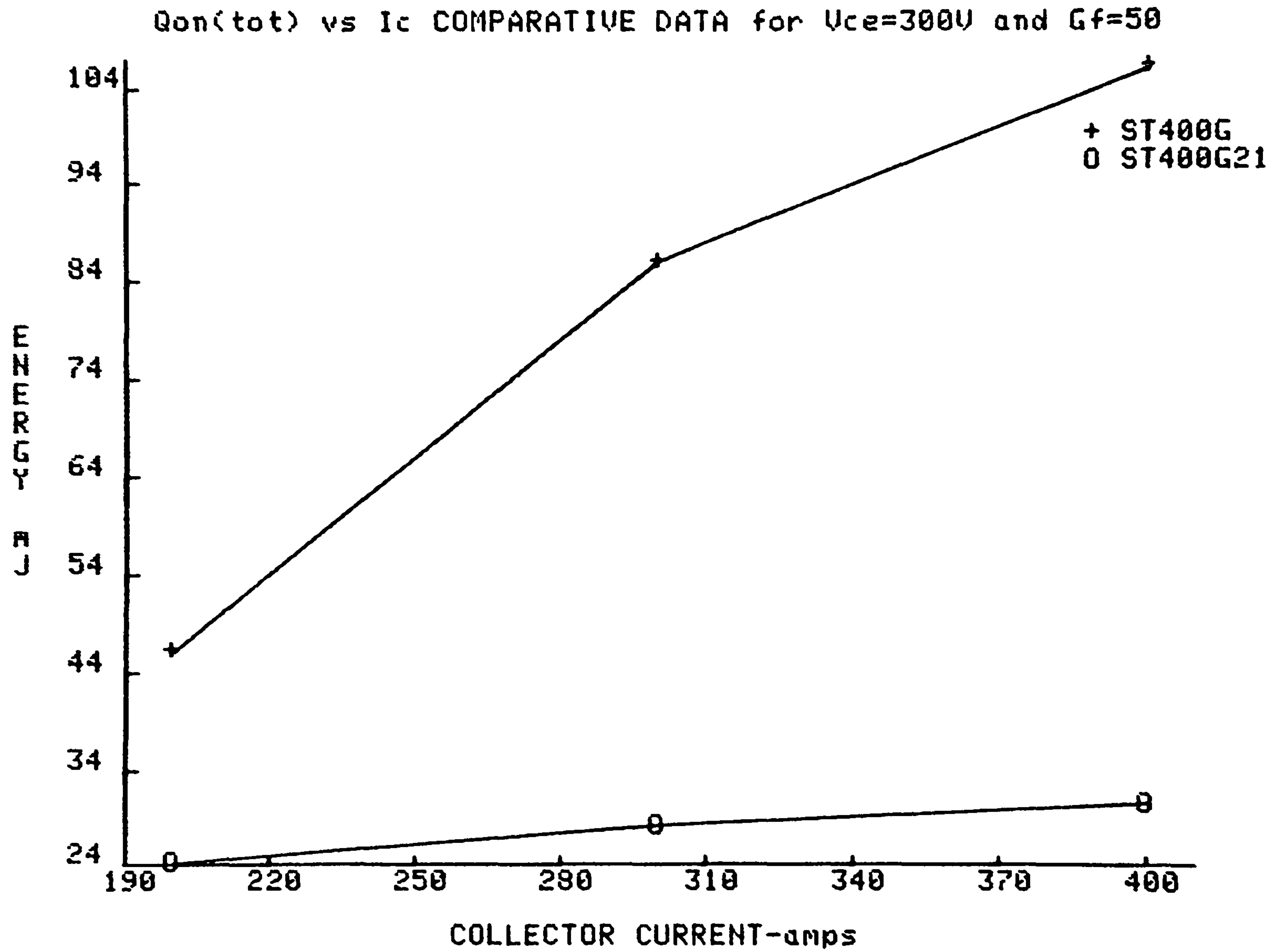
Qon(tot) vs Ic COMPARATIVE DATA for Vce=300V and Gf=50
+ ST400G
O ST400G21
ENERGY mJ
104
94
84
74
64
54
44
34
24
190
220
250
280
310
340
370
400
COLLECTOR CURRENT-amps

Fig. B.4.5

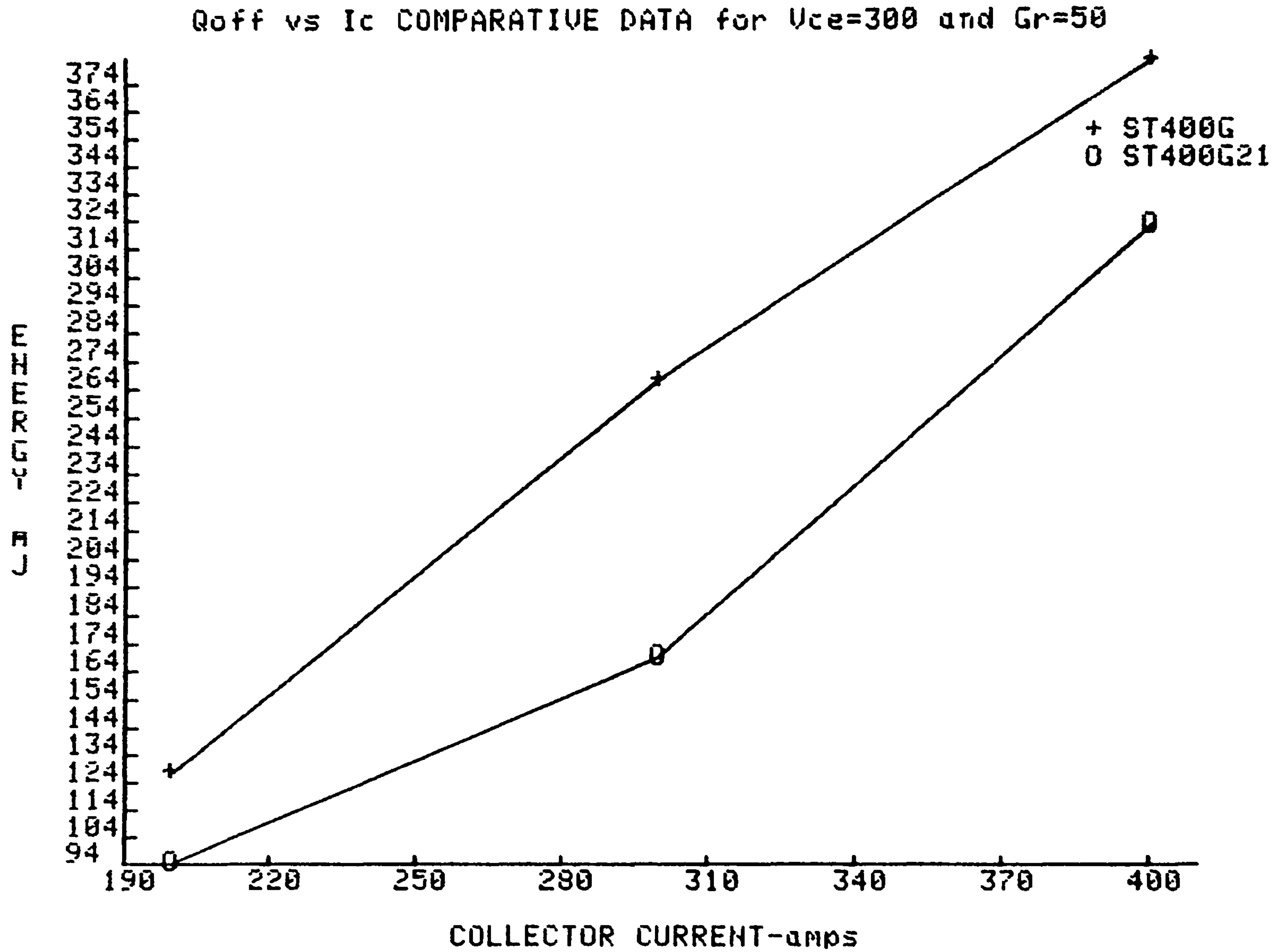

Qoff vs Ic COMPARATIVE DATA for Vce=300 and Gr=50
374
364
354
344
334
324
314
304
294
284
274
264
254
244
234
224
214
204
194
184
174
164
154
144
134
124
114
104
94
ENERGY mJ
190
220
250
280
310
340
370
400
COLLECTOR CURRENT-amps
+ ST400G
O ST400G21

Fig. P.4.6

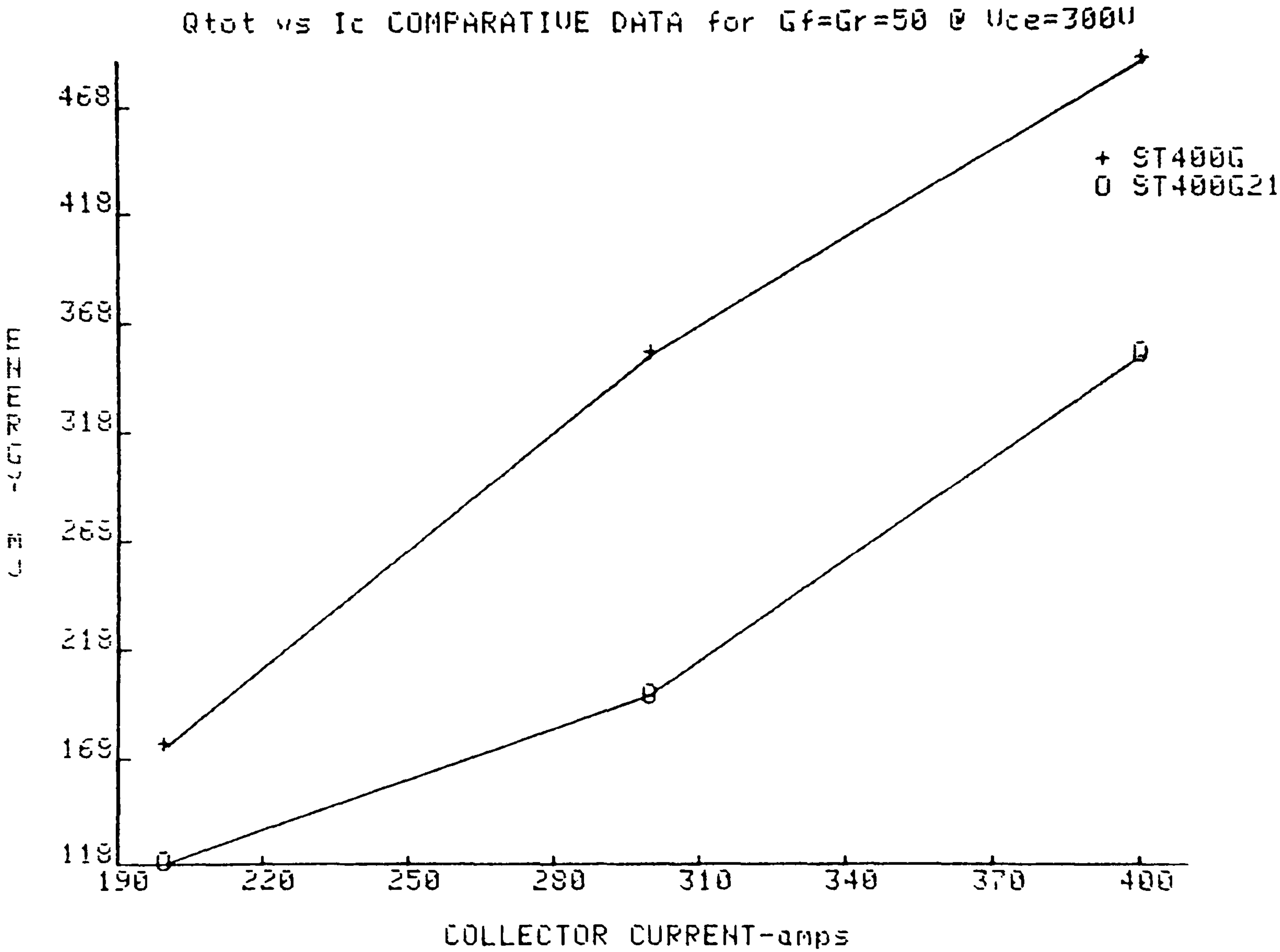

Qtot vs Ic COMPARATIVE DATA for Gf=Gr=50 @ Vce=300V
+ ST400G
O ST400G21
ENERGY- mJ
468
418
368
318
265
218
169
118
190
220
250
280
310
340
370
400
COLLECTOR CURRENT-amps

Fig. B.4.7

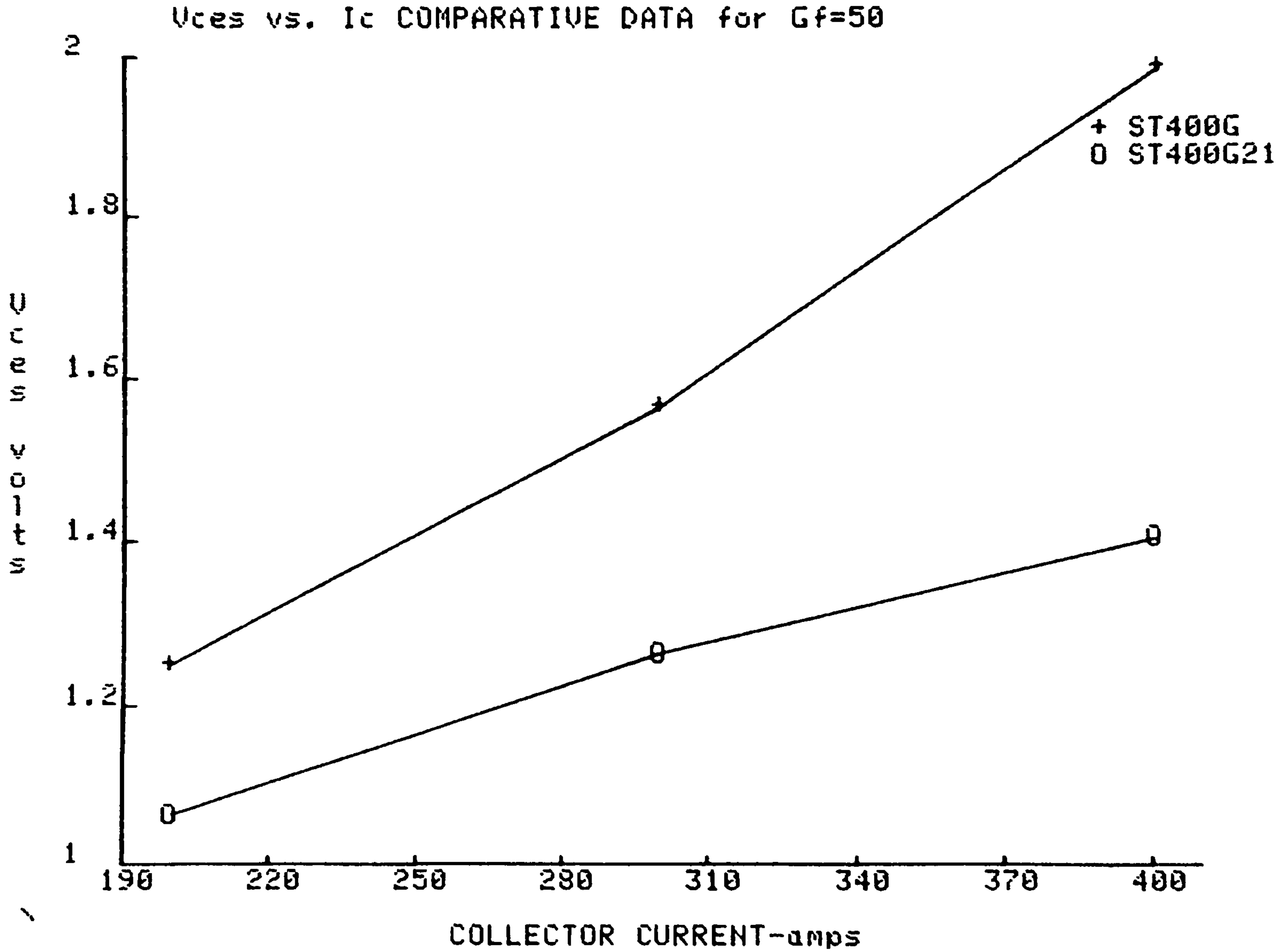

Vces vs. Ic COMPARATIVE DATA for Gf=50
+ ST400G
0 ST400G21
Vces volts
2
1.8
1.6
1.4
1.2
1
190
220
250
280
310
340
370
400
COLLECTOR CURRENT-amps

Fig. B.4.8

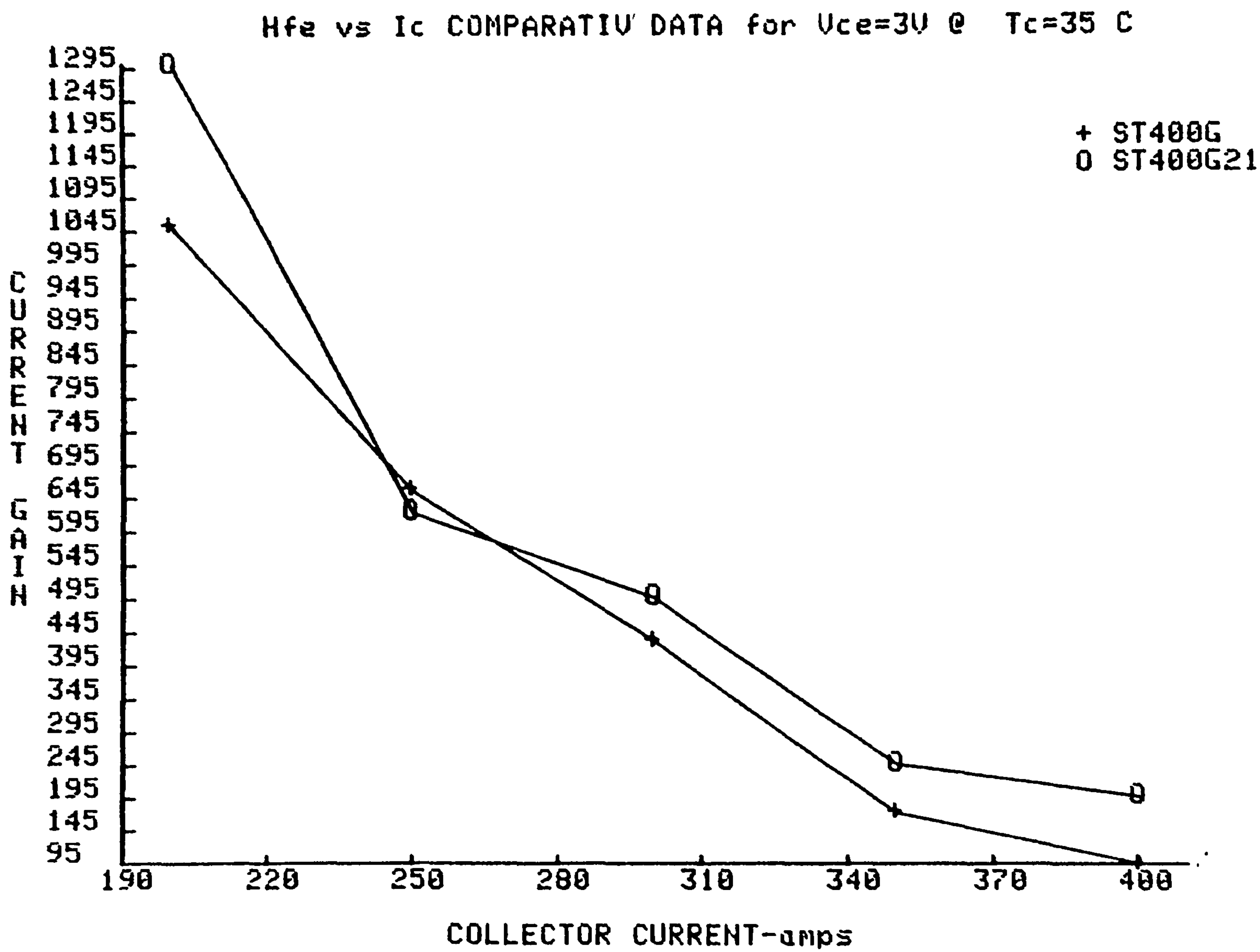

Hfe vs Ic COMPARATIV DATA for Vce=3V @ Tc=35 C
CURRENT GAIN
1295
1245
1195
1145
1095
1045
995
945
895
845
795
745
695
645
595
545
495
445
395
345
295
245
195
145
95
190
220
250
280
310
340
370
400
COLLECTOR CURRENT-amps
+ ST400G
O ST400G21

APPENDIX C

TEST DATA OF PARALLEL OPERATION OF BIPOLAR TRANSISTORS

C.1 Test Data of Parallel Operation of Fuji EVM31-050 at $T_c = 30^{o}C$

$\bar{I}_C$

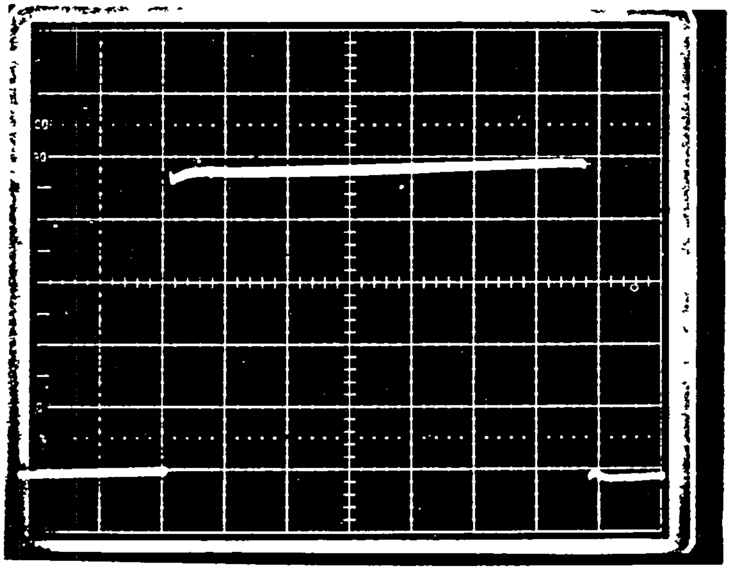

GND

Fig. C.1.1. Total collector current ($I_C = I_{C1} + I_{C2}$) of two Fuji EVM31-050 devices connected in parallel at I_C=100A
Scale: 20 μs/div; 20A/div

I_B

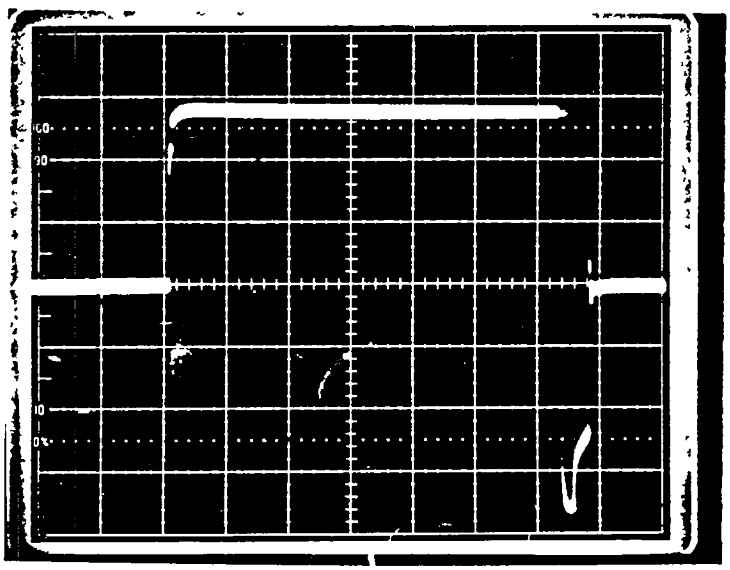

GND

Fig. C.1.2. Total base current ($I_B = I_{B1} + I_{B2}$) of two Fuji EVM31-050 devices connected in parallel at I_B=5A
Scale: 20 μs/div; 2A/div

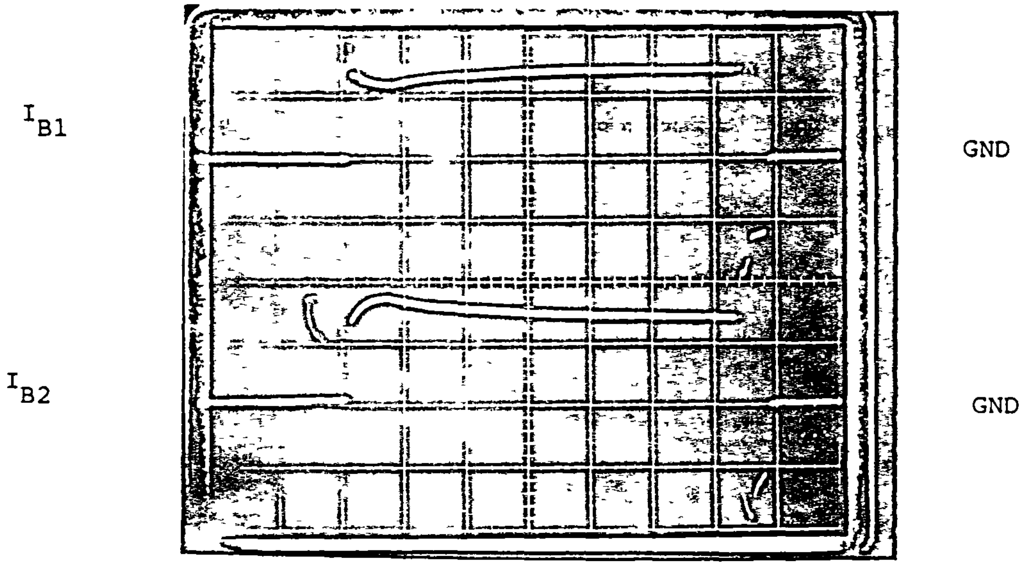

Fig. C.1.3. Individual base currents (I_{B1} and I_{B2}) of two Fuji EVM31-050 devices connected in parallel at I_c=100A; I_B=5A and T_c=30°C. Scale: 20μs/div; 2A/div.

Fig. C.1.4. Individual collector currents (I_{c1} and I_{c2}) of two Fuji EVM31-050 devices connected in parallel at I_c=100A; I_B=5A and T_c=30°C. Scale: 20μs/div, 20A/div.

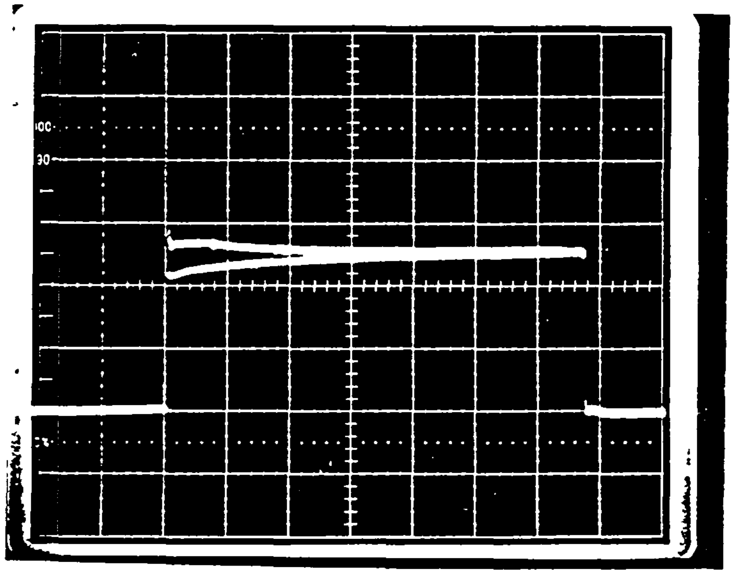

Fig. C.1.5. Individual collector currents (I_{c1} and I_{c2}) of two Fuji EVM31-050 devices connected in parallel at I_c=100A; I_B=5A and T_c=30°C. Currents are shown to overlap.
Scale: 20μs/div; 20A/div.

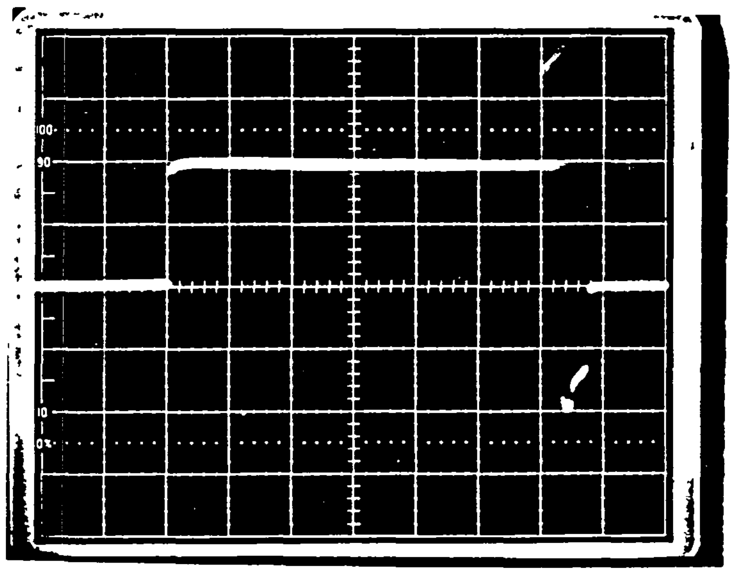

Fig. C.1.6. Total base current (I_B=I_{B1}+I_{B2}) of two Fuji EVM31-050 devices connected in parallel at I_B=10A
Scale: 20μs/div; 5A/div.

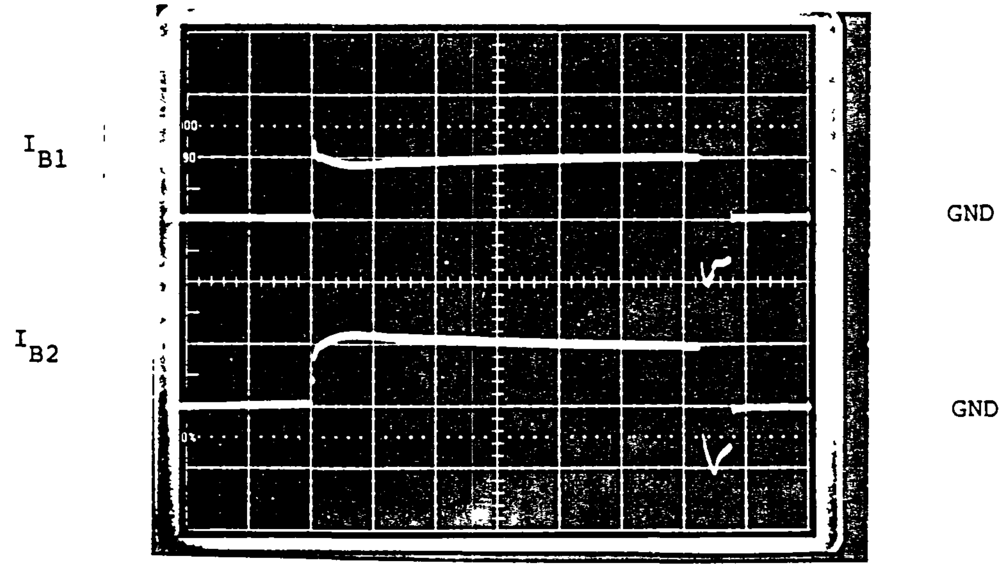

Fig. C.1.7. Individual base currents (I_{B1} and I_{B2}) of two Fuji EVM31-050 devices connected in parallel at I_C=100A; I_B=10A and T_C=30°C. Scale: 20μs/div; 5A/div.

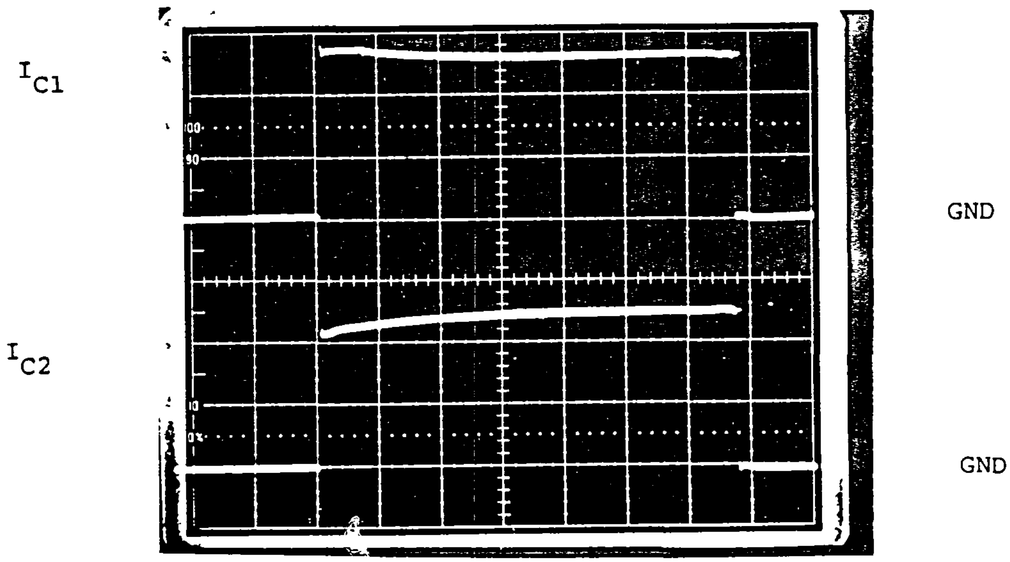

Fig. C.1.8. Individual collector currents (I_{c1} and I_{c2}) of two Fuji EVM31-050 devices connected in parallel at I_C=100A; I_B=10A and T_C=30°C. Scale: 20μs/div, 20A/div.

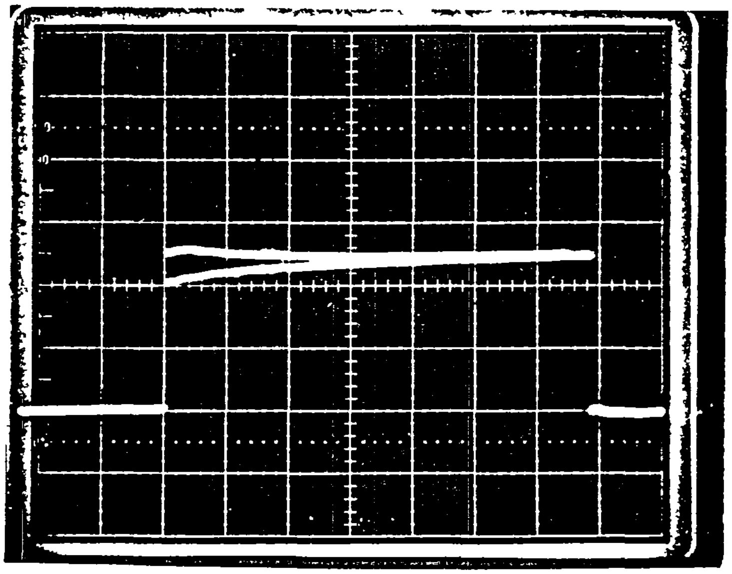

Fig. C.1. 9. Individual collector currents (I_{c1} and I_{c2}) of two Fuji EVM31-050 devices connected in parallel at I_c=100A; I_B=10A and T_c=30°C. Currents are shown to overlap.
Scale: 20μs/div; 20A/div.

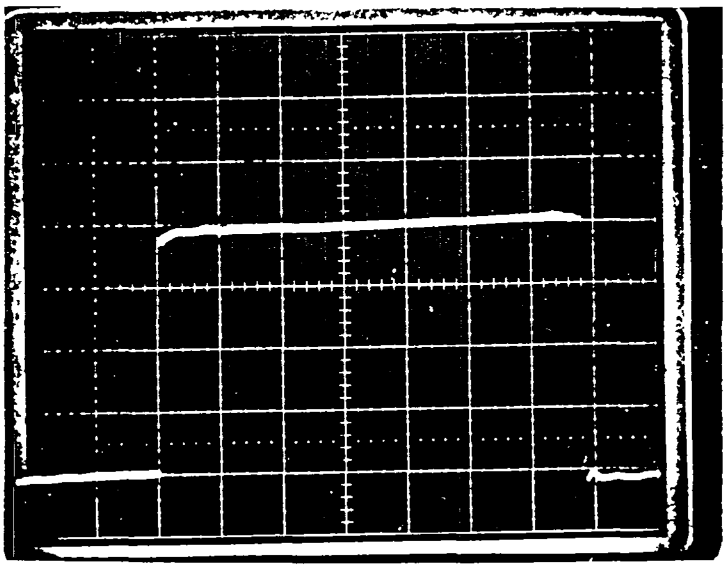

Fig. C.1.10. Total collector current ($I_C = I_{C1} + I_{C2}$) of two Fuji EVM31-050 devices connected in parallel at I_C=200A
Scale: 20 μs/div; 50A/div

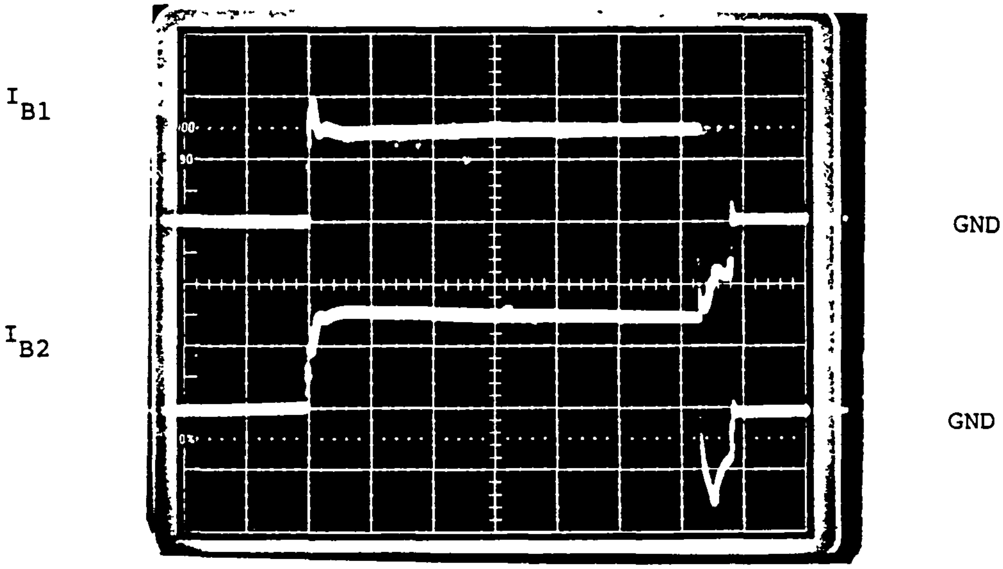

Fig. C.1.11. Individual base currents (I_{B1} and I_{B2}) of two Fuji EVM31-050 devices connected in parallel at I_C=200A; I_B=5A and T_C=30°C. Scale: 20μs/div; 5A/div.

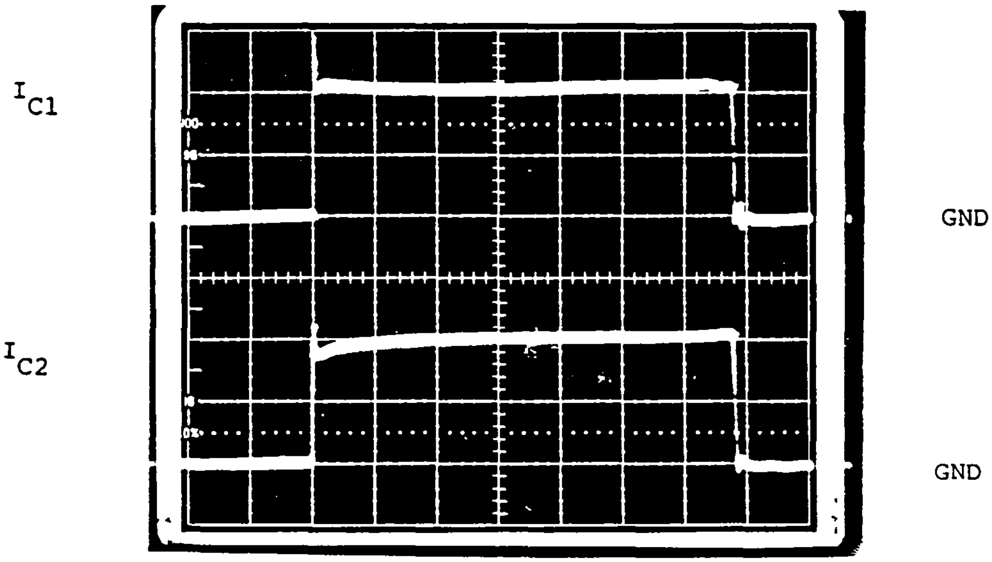

Fig. C.1.12. Individual collector currents (I_{c1} and I_{c2}) of two Fuji EVM31-050 devices connected in parallel at I_C=200A; I_B=5A and T_C=30°C. Scale: 20μs/div, 50A/div.

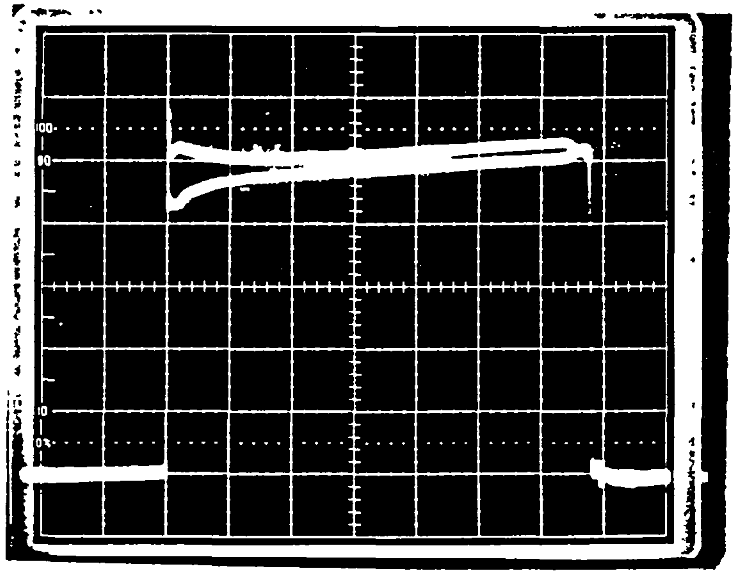

Fig. C.1.13. Individual collector currents (I_{c1} and I_{c2}) of two Fuji EVM31-050 devices connected in parallel at I_c=100A; I_B=10A and T_c=30°C. Currents are shown to overlap.
Scale: 20μs/div; 20A/div.

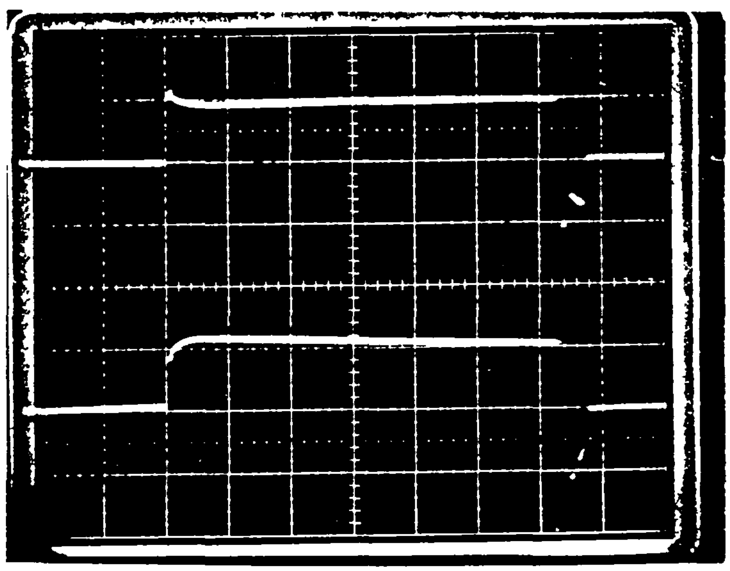

Fig. C.1.14. Individual base currents (I_{B1} and I_{B2}) of two Fuji EVM31-050 devices connected in parallel at I_c=200A; I_B=10A and T_c=30°C.
Scale: 20μs/div; 5A/div.

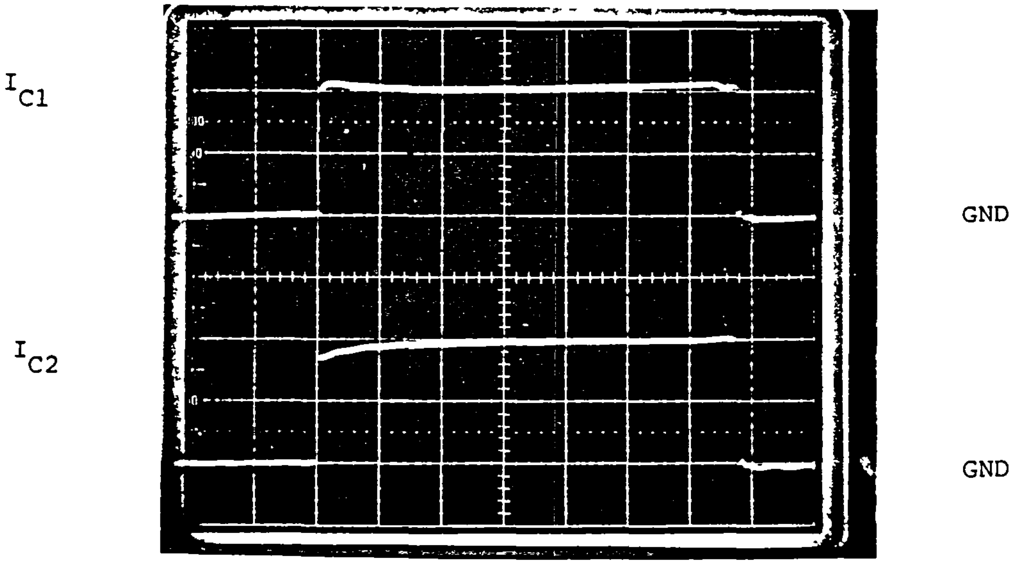

Fig. C.1.15. Individual collector currents (I_{c1} and I_{c2}) of two Fuji EVM31-050 devices connected in parallel at I_c=200A; I_B=10A and T_c=30°C. Scale: 20μs/div, 50A/div.

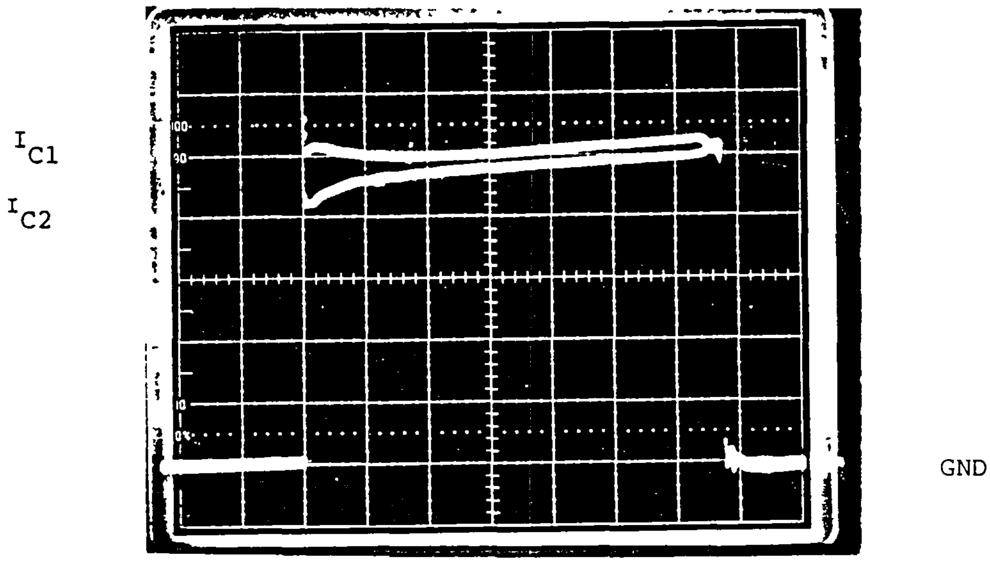

Fig. C.1.16. Individual collector currents (I_{c1} and I_{c2}) of two Fuji EVM31-050 devices connected in parallel at I_c=200A; I_B=10A and T_c=30°C. Currents are shown to overlap. Scale: 20μs/div; 50A/div.

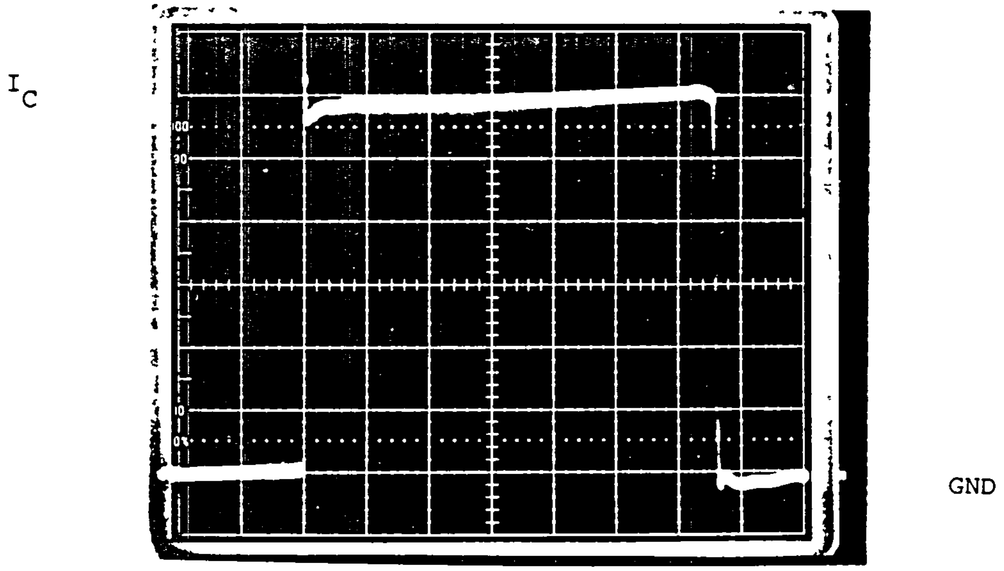

Fig. C.1.17. Total collector current ($I_C=I_{C1}+I_{C2}$) of two Fuji EVM31-050 devices connected in parallel at I_C=300A
Scale: 20 μs/div; 50A/div

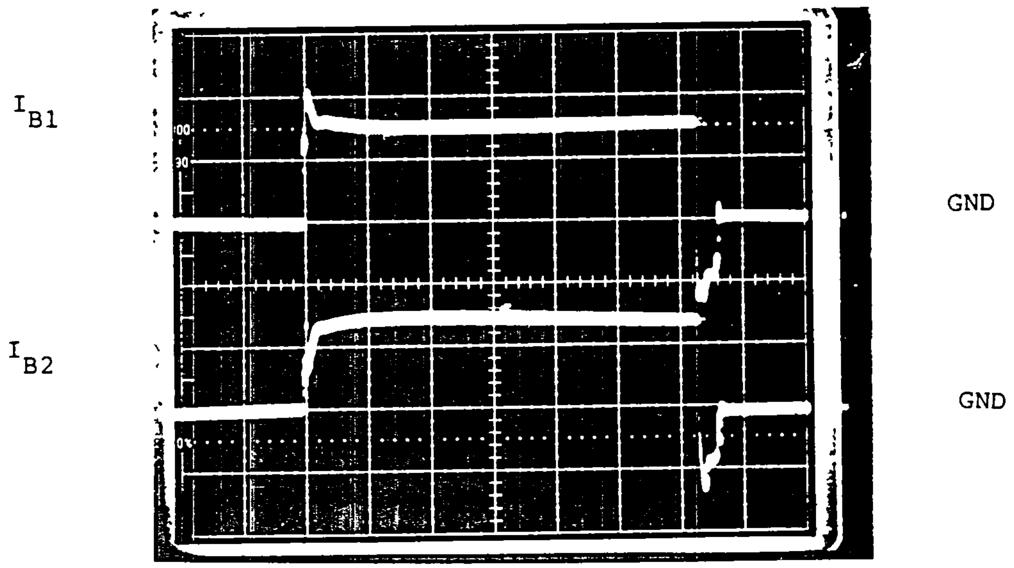

Fig. C.1.18. Individual base currents (I_{B1} and I_{B2}) of two Fuji EVM31-050 devices connected in parallel at I_c=300A; I_B=5A and T_c=30°C.
Scale: 20μs/div; 2A/div.

I_{C1}

I_{C2}

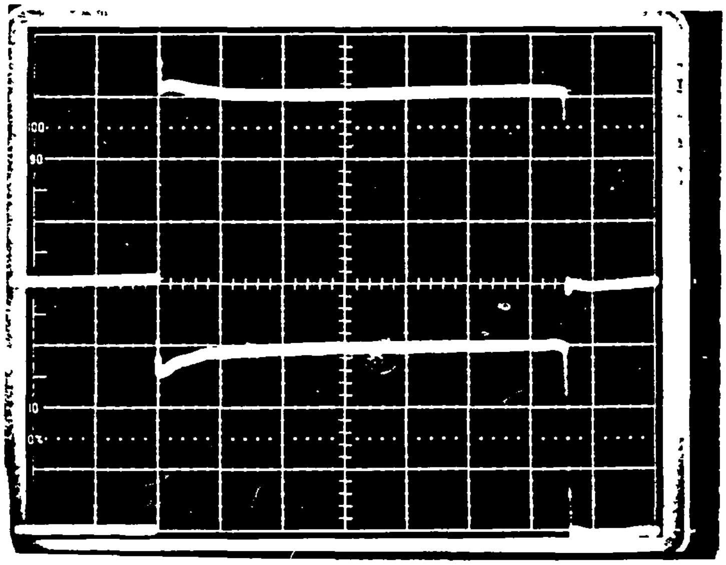

GND

GND

Fig. C.1.19. Individual collector currents (I_{c1} and I_{c2}) of two Fuji EVM31-050 devices connected in parallel at I_c=300A; I_B=5A and T_c=30°C. Scale: 20μs/div, 50A/div.

I_{C1}

I_{C2}

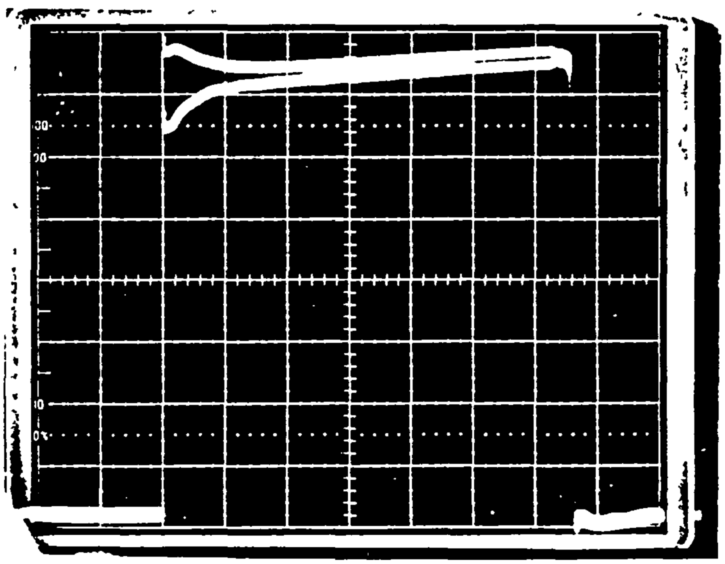

GND

Fig. C.1.20. Individual collector currents (I_{c1} and I_{c2}) of two Fuji EVM31-050 devices connected in parallel at I_c=300A; I_B=5A and T_c=30°C. Currents are shown to overlap.
Scale: 20μs/div; 50A/div.

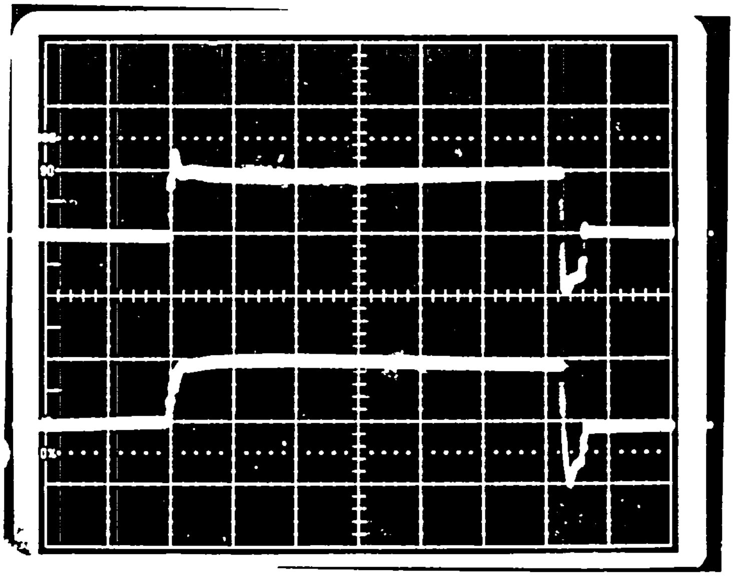

Fig. C.1.21. Individual base currents (I_{B1} and I_{B2}) of two Fuji EVM31-050 devices connected in parallel at I_c=300A; I_B=10A and T_c=30°C. Scale: 20µs/div; 2A/div.

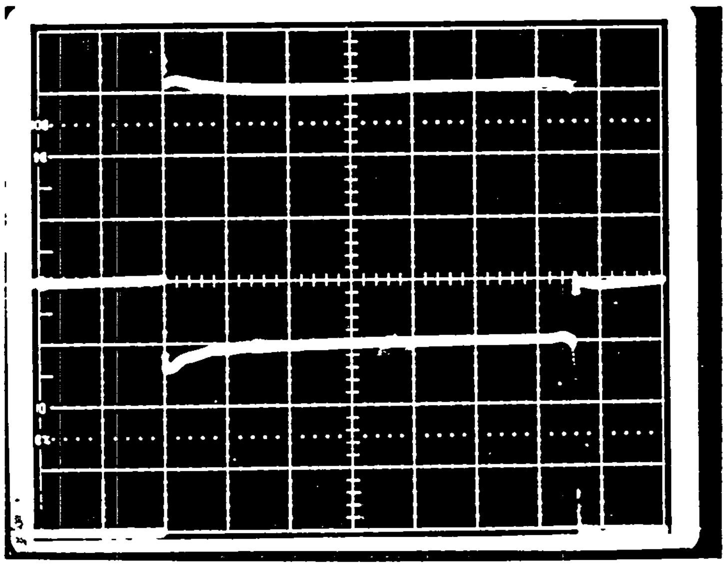

Fig. C.1.22. Individual collector currents (I_{c1} and I_{c2}) of two Fuji EVM31-050 devices connected in parallel at I_c=300A; I_B=10A and T_c=30°C. Scale: 20µs/div, 50A/div.

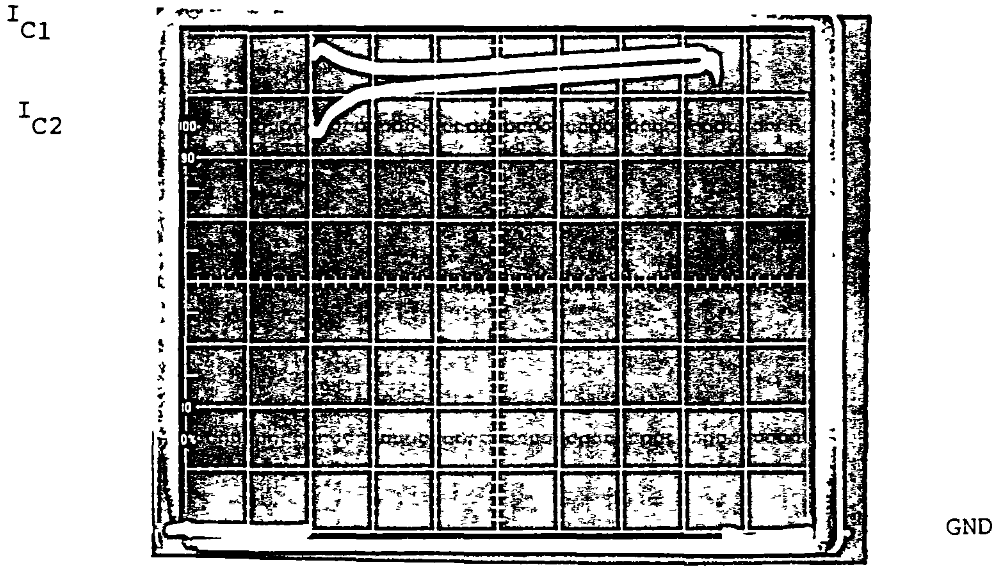

Fig. C.1.23. Individual collector currents (I_{c1} and I_{c2}) of two Fuji EVM31-050 devices connected in parallel at I_C=300A; I_B=10A and T_C=30°C. Currents are shown to overlap. Scale: 20μs/div; 50A/div.

C.2 Test Data of Parallel Operation of Fuji EVM31-050 at $T_c=100^{o}C$

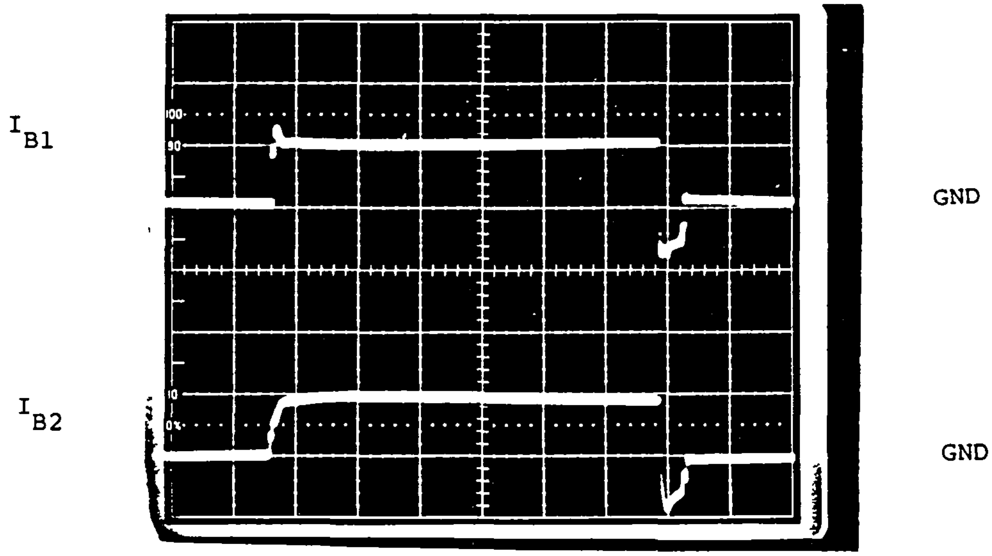

Fig. C.2.1 Individual base currents (I_{B1} and I_{B2}) of two Fuji EVM31-050 devices connected in parallel at I_C=100A; I_B=10A and T_C=100°C. Scale: 20μs/div; 5A/div.

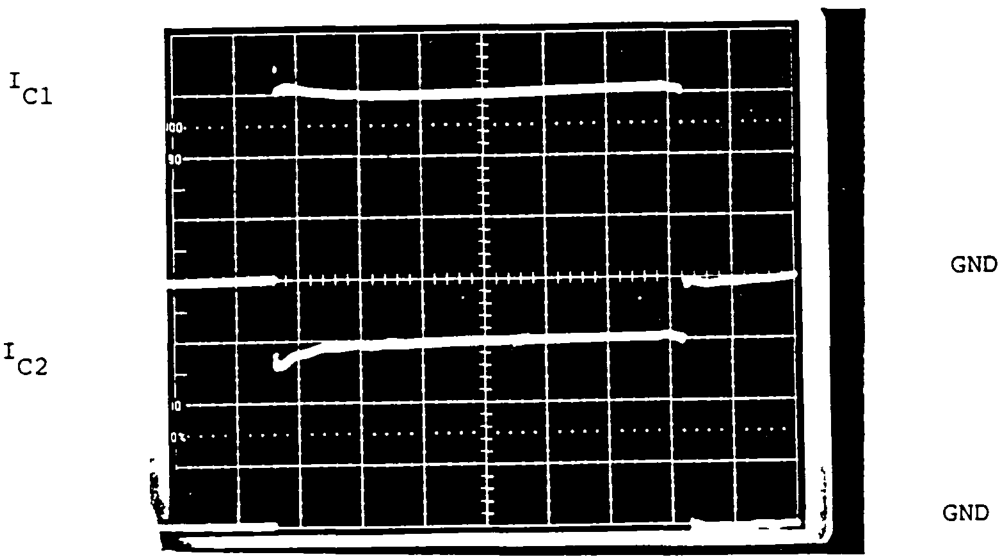

Fig. C.2.2 Individual collector currents (I_{c1} and I_{c2}) of two Fuji EVM31-050 devices connected in parallel at I_C=100A; I_B=10A and T_C=100°C. Scale: 20μs/div, 20A/div.

I_{C1}

I_{C2}

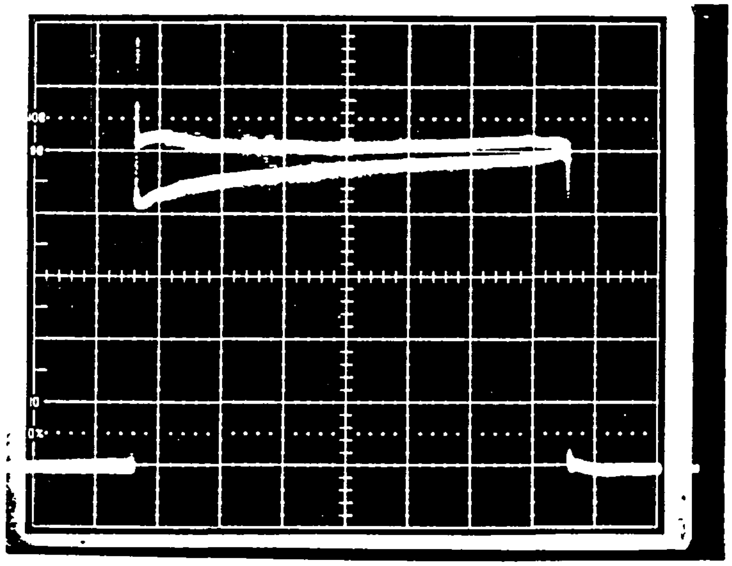

GND

Fig. C.2.3 Individual collector currents (I_{c1} and I_{c2}) of two Fuji EVM31-050 devices connected in parallel at I_c=100A; I_B=10A and T_c=100°C. Currents are shown to overlap.
Scale: 20μs/div; 20A/div.

I_{B1}

I_{B2}

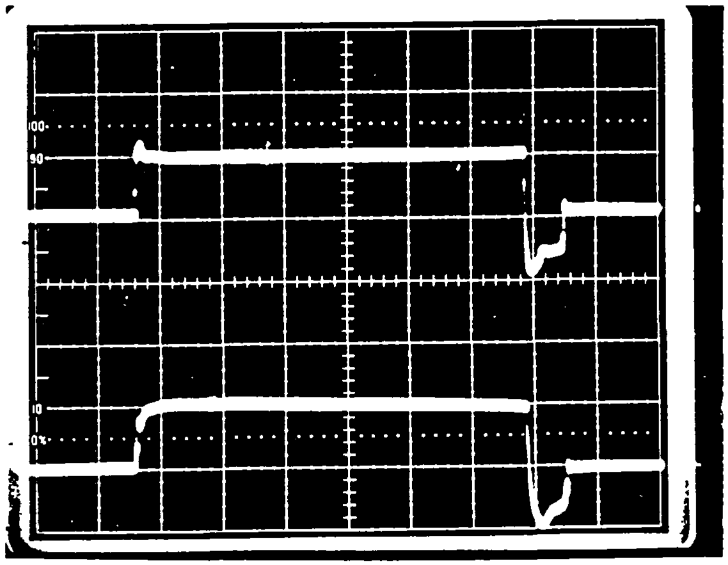

GND

GND

Fig. C.2.4 Individual base currents (I_{B1} and I_{B2}) of two Fuji EVM31-050 devices connected in parallel at I_c=200A; I_B=10A and T_c=100°C.
Scale: 20μs/div; 5A/div.

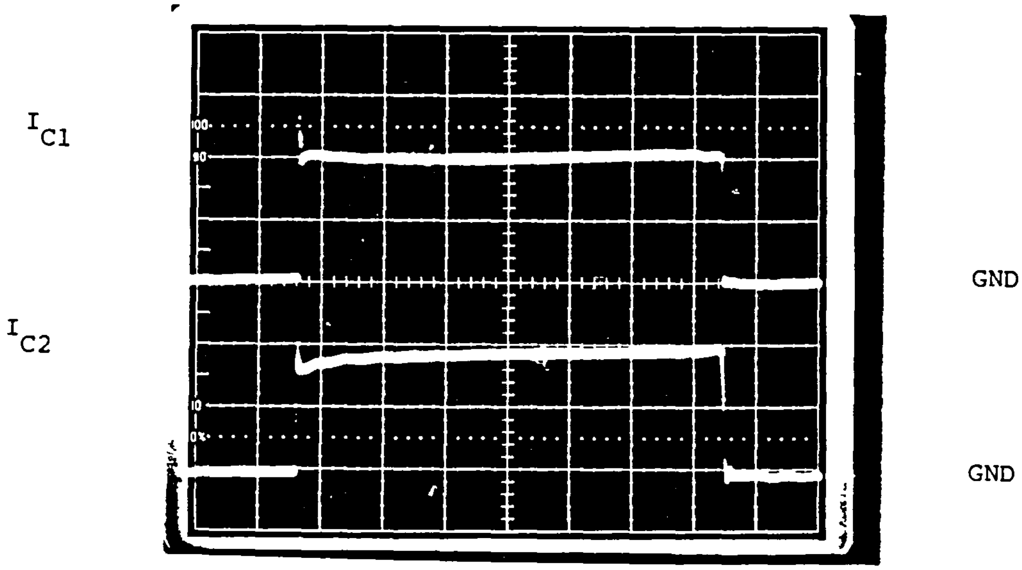

Fig. C.2.5 Individual collector currents (I_{c1} and I_{c2}) of two Fuji EVM31-050 devices connected in parallel at I_c=200A; I_B=10A and T_c=100°C. Scale: 20μs/div, 50A/div.

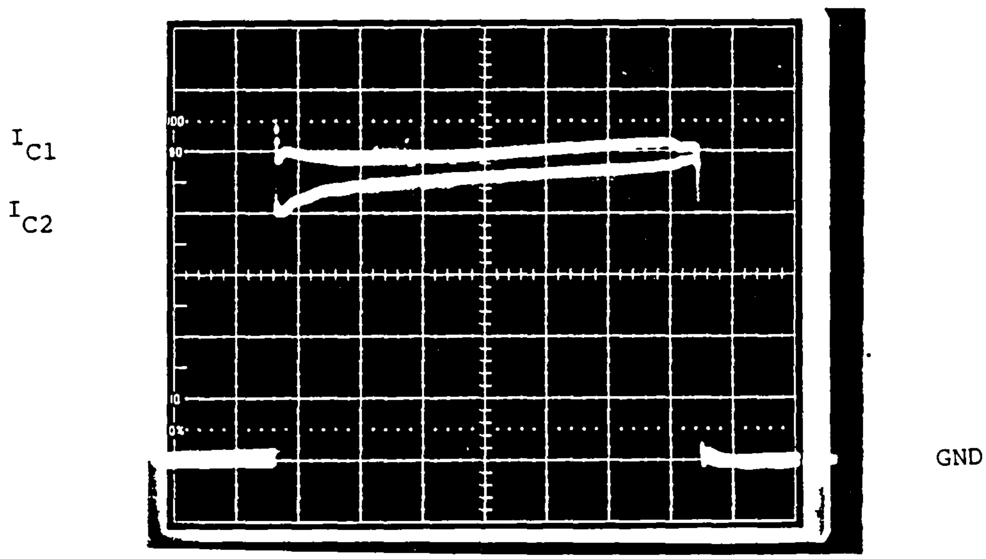

Fig. C.2.6 Individual collector currents (I_{c1} and I_{c2}) of two Fuji EVM31-050 devices connected in parallel at I_c=200A; I_B=10A and T_c=100°C. Currents are shown to overlap. Scale: 20μs/div; 50A/div.

I_{B1}

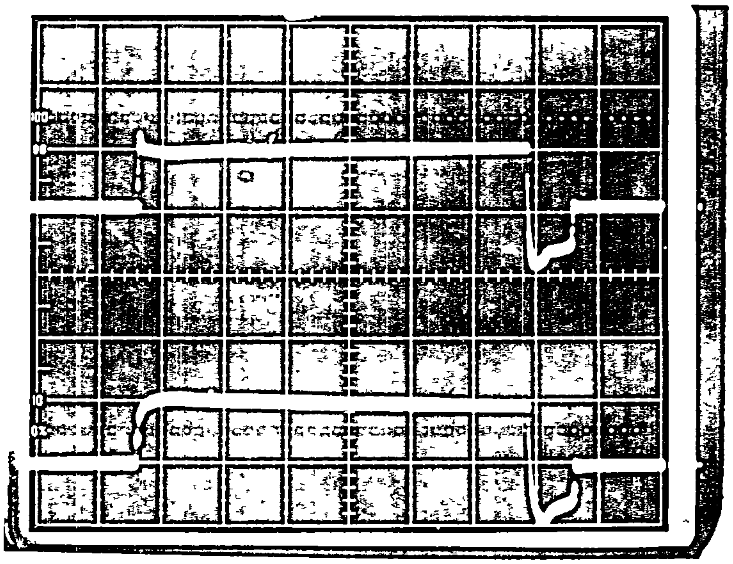

GND

I_{B2}

GND

Fig. C.2.7 Individual base currents (I_{B1} and I_{B2}) of two Fuji EVM31-050 devices connected in parallel at I_C=300A; I_B=10A and T_C=100°C. Scale: 20μs/div; 5A/div.

I_{C1}

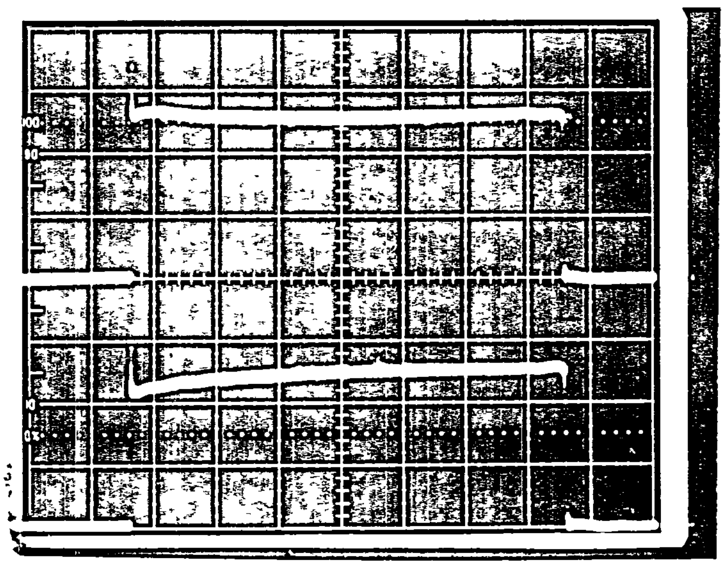

GND

I_{C2}

GND

Fig. C.2.8 Individual collector currents (I_{c1} and I_{c2}) of two Fuji EVM31-050 devices connected in parallel at I_C=300A; I_B=10A and T_C=100°C. Scale: 20μs/div, 50A/div.

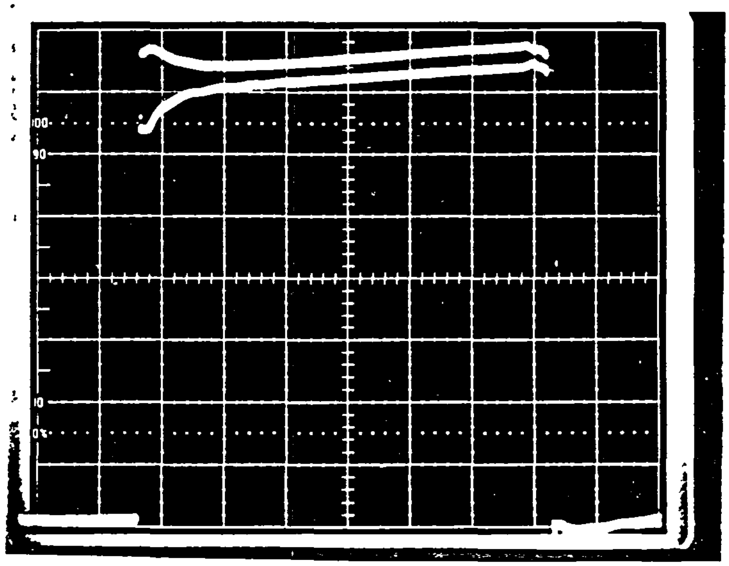

Fig. C.2.9 Individual collector currents (I_{c1} and I_{c2}) of two Fuji EVM31-050 devices connected in parallel at I_C=300A; I_B=10A and T_c=100°C. Currents are shown to overlap.
Scale: 20μs/div; 50A/div.

APPENDIX D

TEST DATA OF RBSOA CHARACTERIZATION

D.1 Test Data of RBSOA of Westinghouse KD324510

General Remark for Appendix D:

The voltage and Time Scale are Referred

to the Large Divisions of the Display

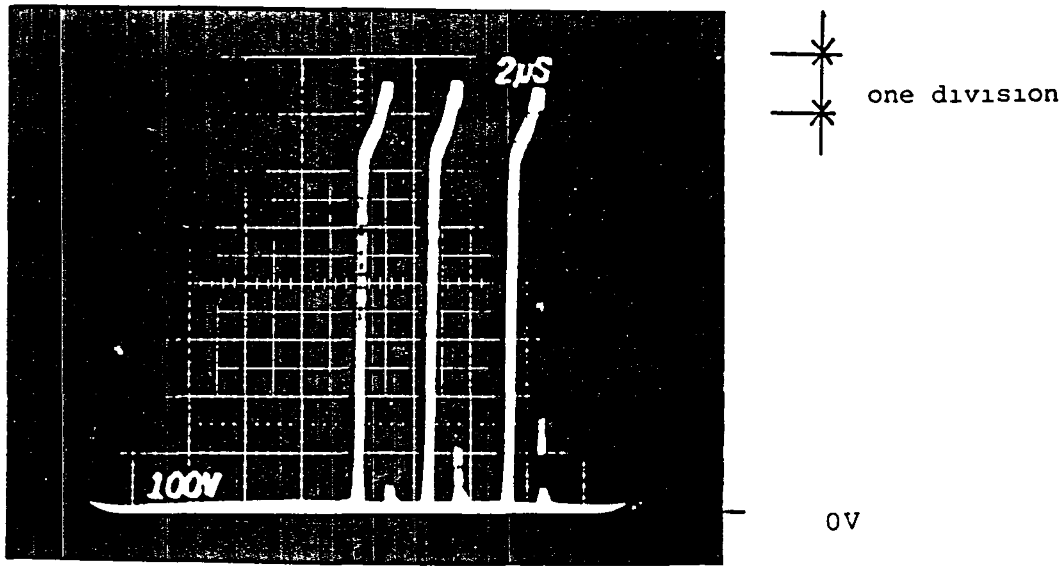

Fig. D.1.1 RBSB behavior of the Westinghouse KD324510.
Test conditions: I_c = 20A; I_{BR} = 2A;
I_{BF} = 2;4;8A.
Scale: 2 μs/div; 100V/div

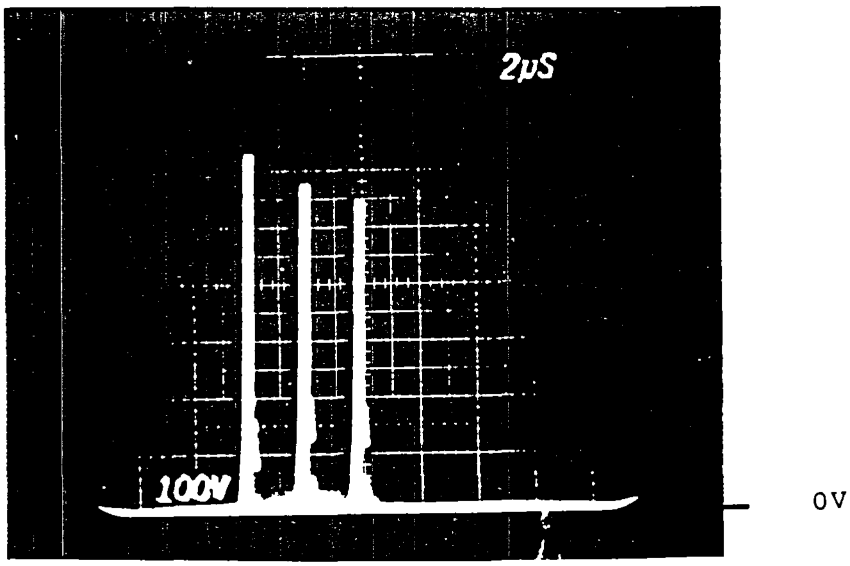

Fig. D.1.2 RBSB behavior of the Westinghouse KD324510.
Test conditions: I_c = 20A; I_{BR} = 3A;
I_{BF} = 2;4;8A.
Scale: 2 μs/div; 100V/div

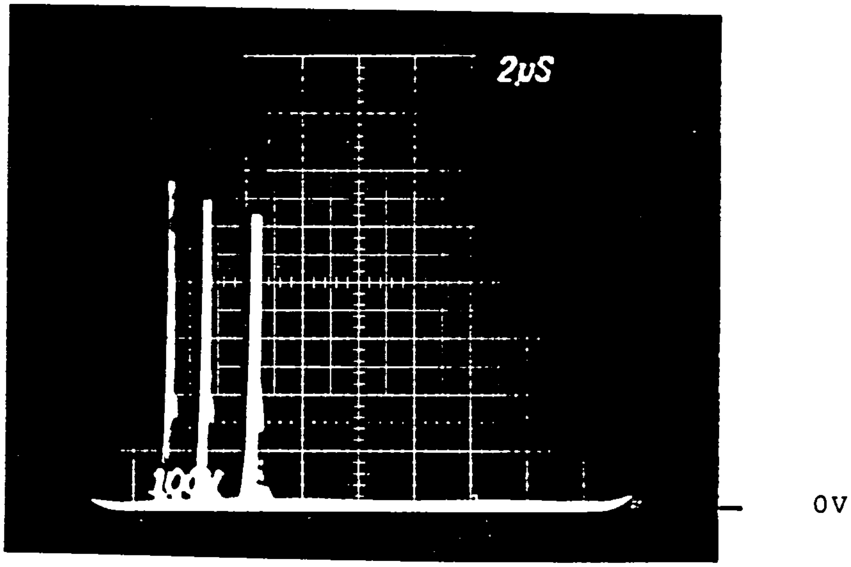

Fig. D.1.3 RBSB behavior of the Westinghous KD324510.
Test conditions: I_c = 20A; I_{BR} = 8A;
I_{BF} = 2;4;8A.
Scale: 2 µs/div; 100V/div

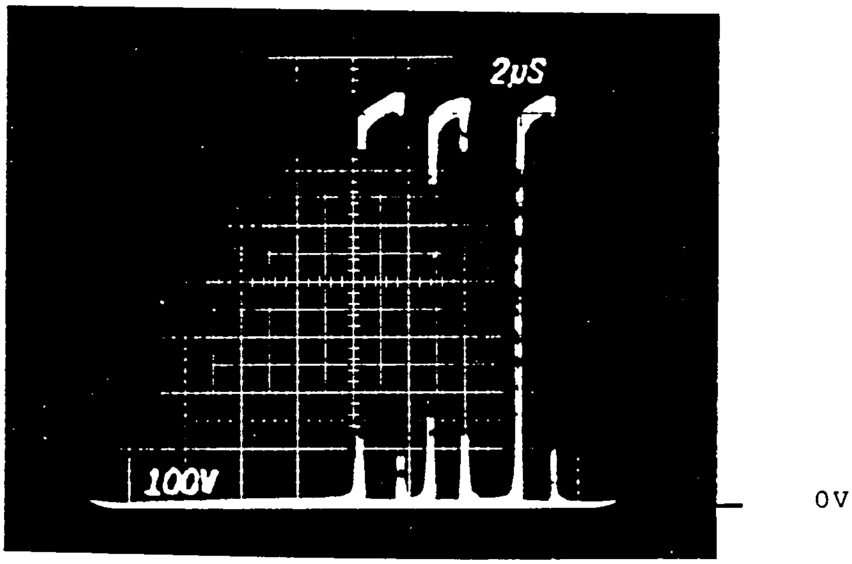

Fig. D.1.4 RBSB behavior of the Westinghouse KD324510.
Test conditions: I_c = 40A; I_{BR} = 2A;
I_{BF} = 2;4;8A.
Scale: 2 µs/div; 100V/div

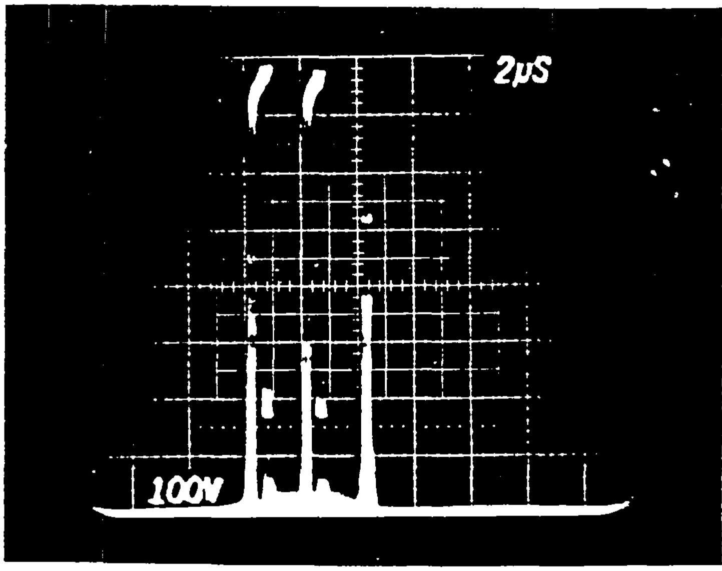

0V

Fig. D.1.5 RBSB behavior of the Westinghouse KD324510.
Test conditions: I_c = 40A; I_{BR} = 4A;
I_{BF} = 2;4;8A.
Scale: 2 μs/div; 100V/div

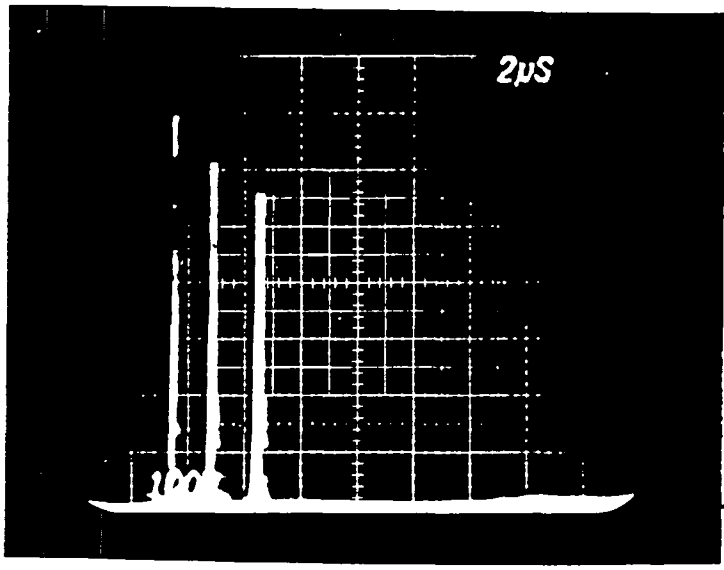

0V

Fig. D.1.6 RBSB behavior of the Westinghous KD324510.
Test conditions: I_c = 40A; I_{BR} = 8A;
I_{BF} = 2;4;8A.
Scale: 2 μs/div; 100V/div

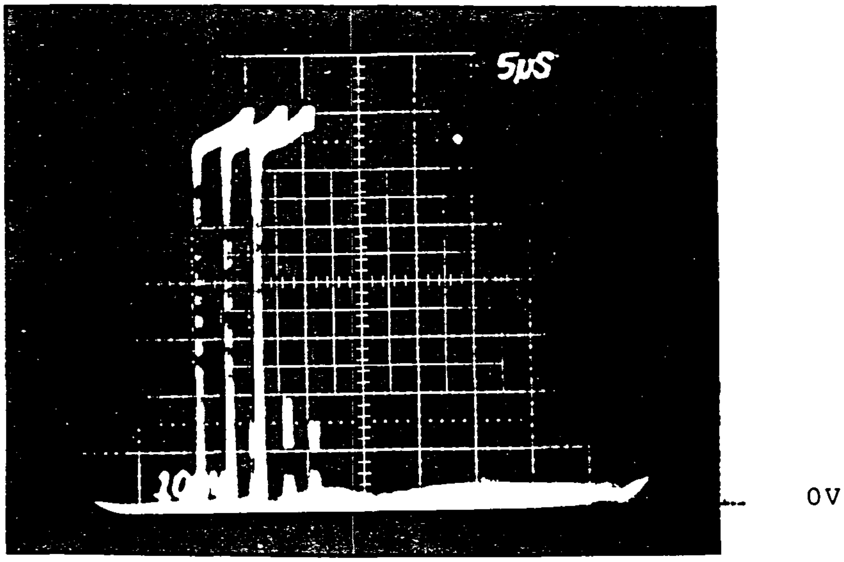

Fig. D.1.7 RBSB behavior of the Westinghouse KD324510.
Test conditions: I_c = 60A; I_{BR} = 2A;
I_{BF} = 2;4;8A.
Scale: 2 µs/div; 100V/div

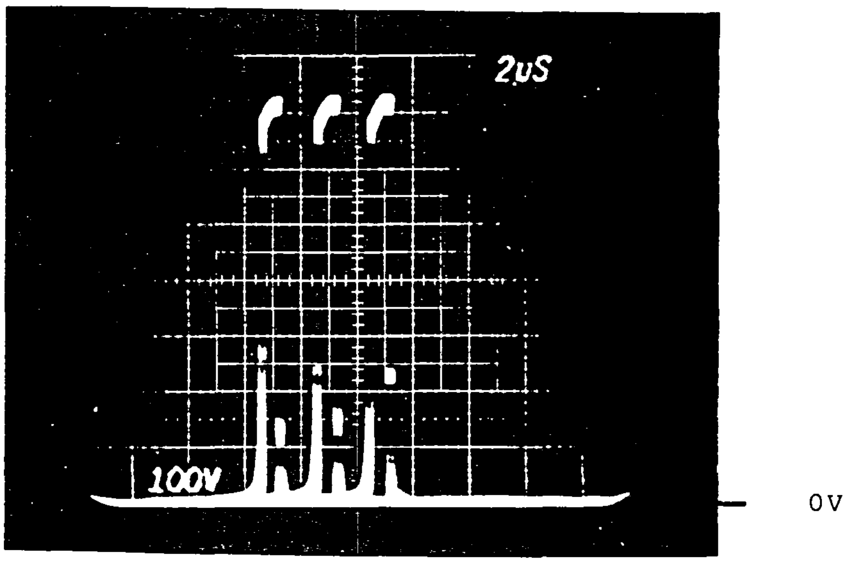

Fig. D.1.8 RBSB behavior of the Westinghouse KD324510.
Test conditions: I_c = 60A; I_{BR} = 4A;
I_{BF} = 2;4;8A.
Scale: 2 µs/div; 100V/div

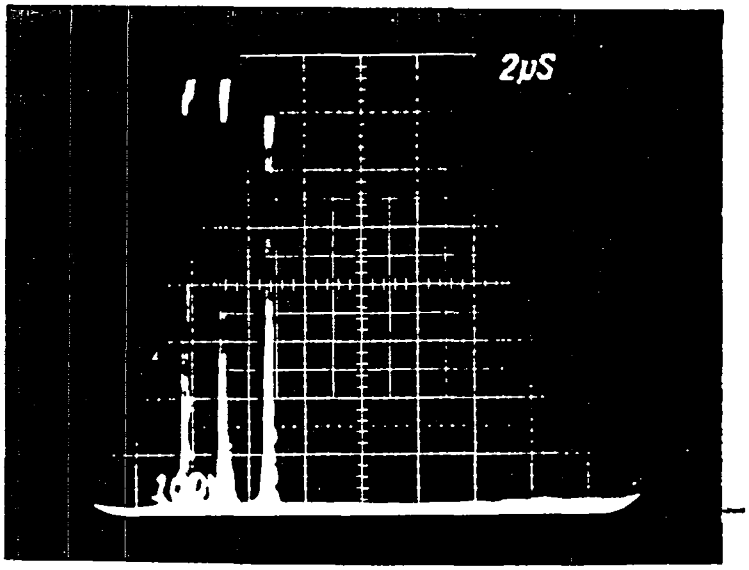

0V

Fig. D.1.9 RBSB behavior of the Westinghouse KD324510.
Test conditions: I_c = 60A; I_{BR} = 8A;
I_{BF} = 2;4;8A.
Scale: 2 μs/div; 100V/div

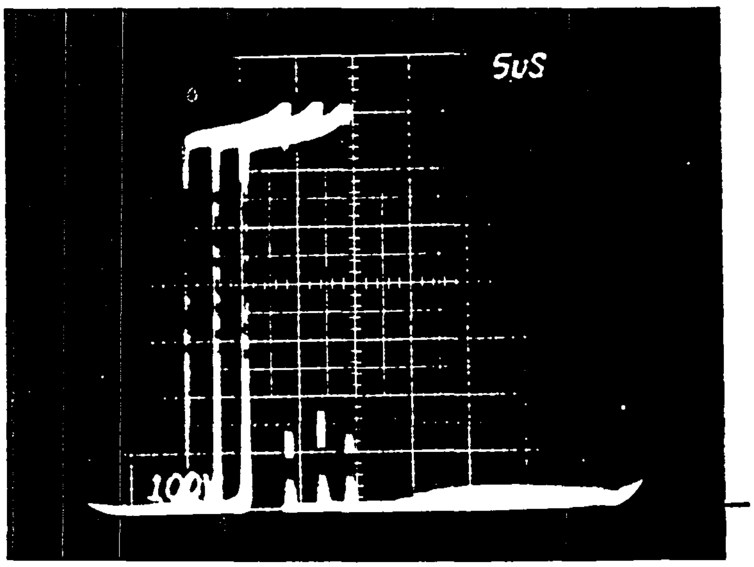

0V

Fig. D.1.10 RBSB behavior of the Westinghouse KD324510.
Test conditions: I_C = 80A; I_{BR} = 2A;
I_{BF} = 2;4;8A.
Scale: 2 μs/div; 100v/div

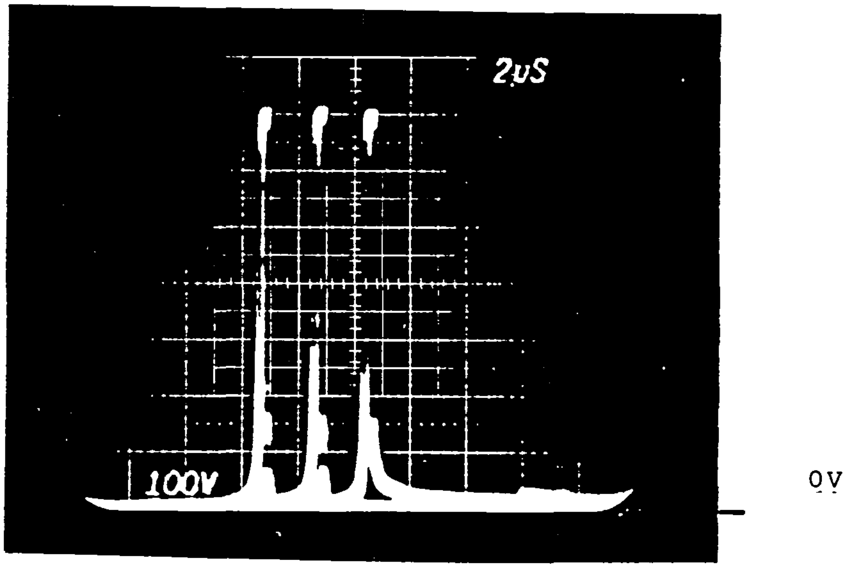

Fig. D.1.11 RBSB behavior of the Westinghouse KD324510.
Test conditions: I_c = 80A; I_{BR} = 4A;
I_{BF} = 2;4;8A.
Scale: 2 µs/div; 100V/div

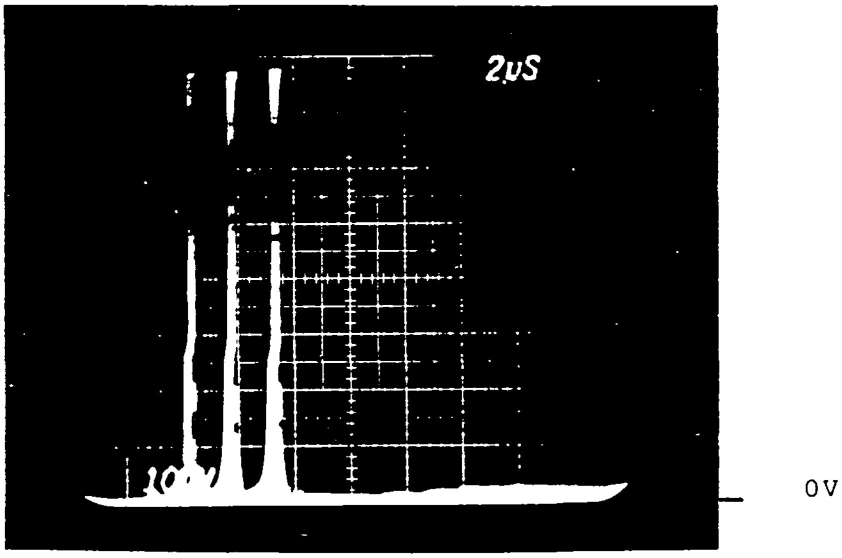

Fig. D.1.12 RBSB behavior of the Westinghouse KD324510.
Test conditions: I_c = 80A; 8_{BR} = 8A;
I_{BF} = 2;4;8A.
Scale: 2 µs/div; 100V/div

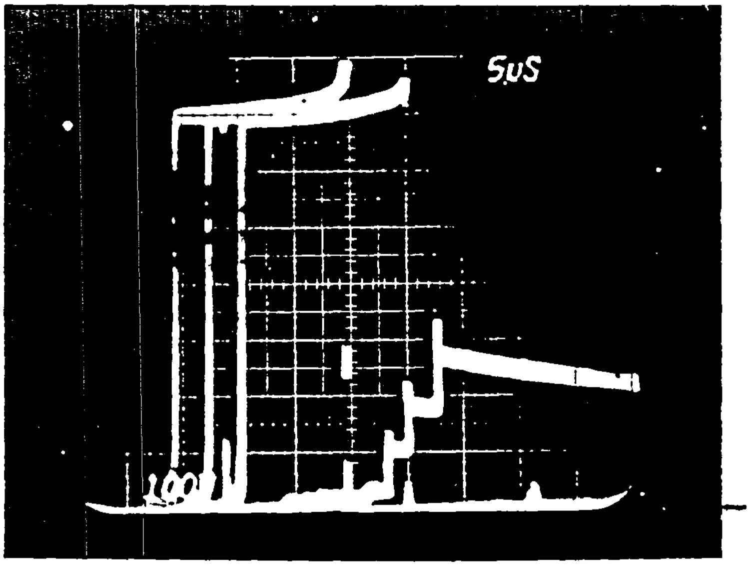

Fig. D.1.13 RBSB behavior of the Westinghouse KD324510.
Test conditions: I_c = 100A; I_{BR} = 2A;
I_{BF} = 2;4;8A.
Scale: 2 μs/div; 100V/div

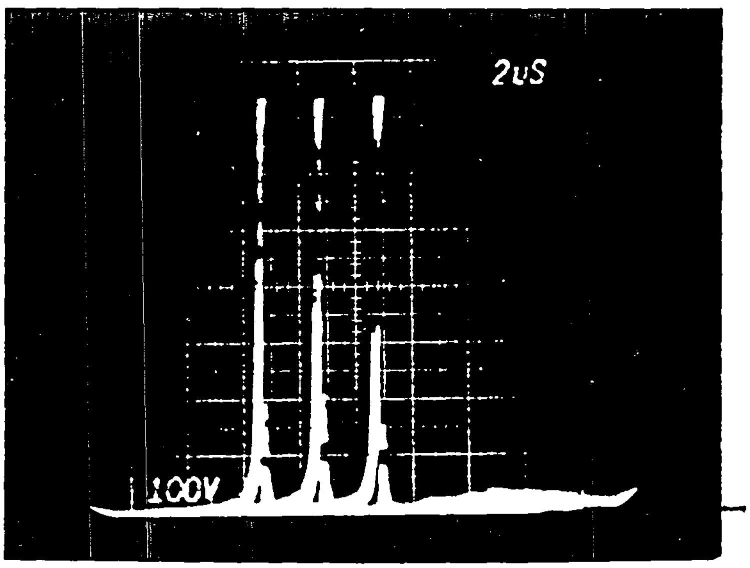

Fig. D.1.14 RBSB behavior of the Westinghouse KD324510.
Test conditions: I_c = 100A; I_{BR} = 4A;
I_{BF} = 2;4;8A.
Scale: 2 μs/div; 100V/div

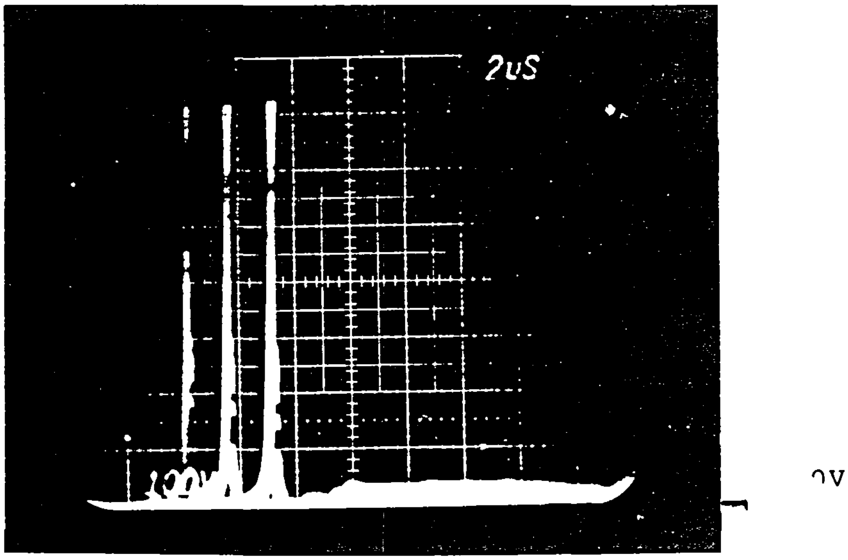

Fig. D.1.15 RBSB behavior of the Westinghouse KD324510.
Test conditions: I_c = 100A; I_{BR} = 8A;
I_{BF} = 2;4;8A.
Scale: 2 μs/div; 100V/div

D.2 Test Data of RBSOA of Westinghouse DA11503008

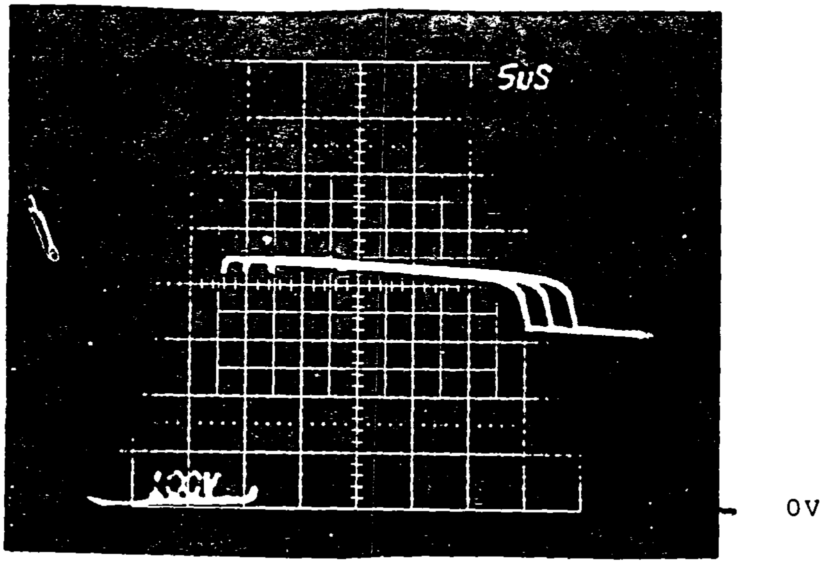

Fig. D.2.1 RBSB behavior of the Westinghouse DA 11503008. Second breakdown could not be induced using only first base drive. Test conditions: I_c = 60A; I_{BR} = 8A; I_{BF} = 2;4;8A; V_{CLAMP} = 500V
Scale: 2 μs/div; 100V/div.

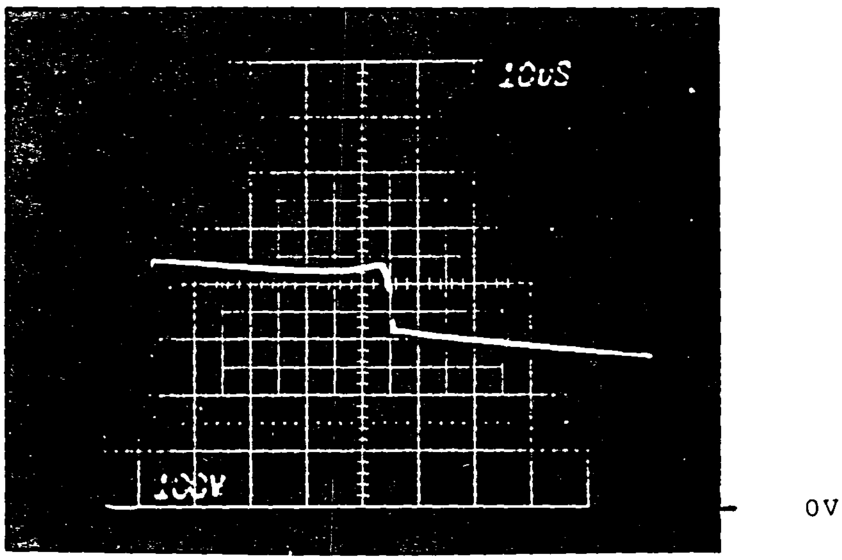

Fig. D.2.2 RBSB behavior of the Westinghouse DA 11503008. Second Breakdown could not be induced using only first base drive. Test conditions: I_c = 100A; I_{BR} = 16A; I_{BF} = 8A; V_{CLAMP} = 500V
Scale: 10 μs/div; 100V/div.

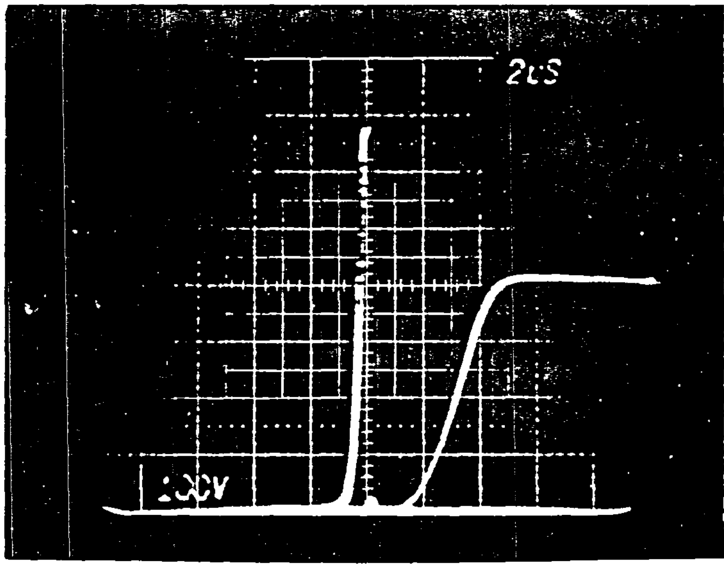

0V

Fig. D,2.3 RBSB behavior of the Westinghouse DA 11503008. The left trace corresponds to SB test with 2nd base (SB occurs) and the right corresponds to SB test without 2nd base (SB does not occur).
Test conditions: I_c = 20A; I_{BF} = 4A; I_{BR} = 4A; I_{BR2} = 4; 0A.
Scale: 2 μs/div; 100V/div.

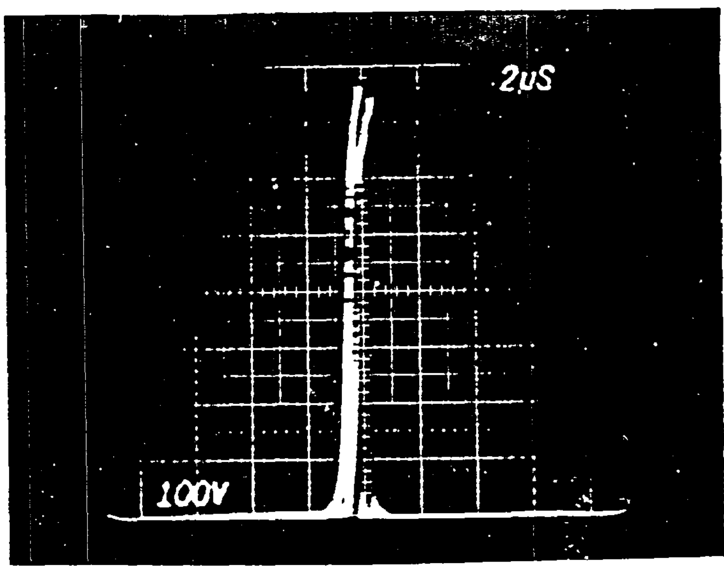

0V

Fig. D.2.4 RBSB behavior of the Westinghouse DA 99503008. The second base drive employed.
Test conditions: I_c = 40A; I_{BF} = 4A; I_{BR} = 4A; I_{BR2} = 8,4A.
Scale: 2 μs/div; 100V/div

D.3 Test Data of RBSOA of Fuji ETN81-055

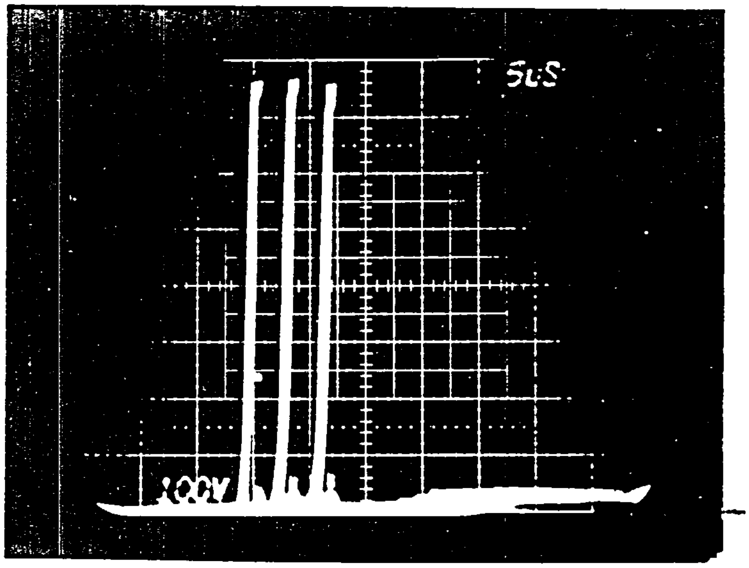

Fig. D.3.1. RBSB behavior of the Fuji ETN81-055.
Test conditions: I_C=20A; I_{BR}=2A;
I_{BF}=2,4,8A.
Scale: 5μs/div; 100 V/div.

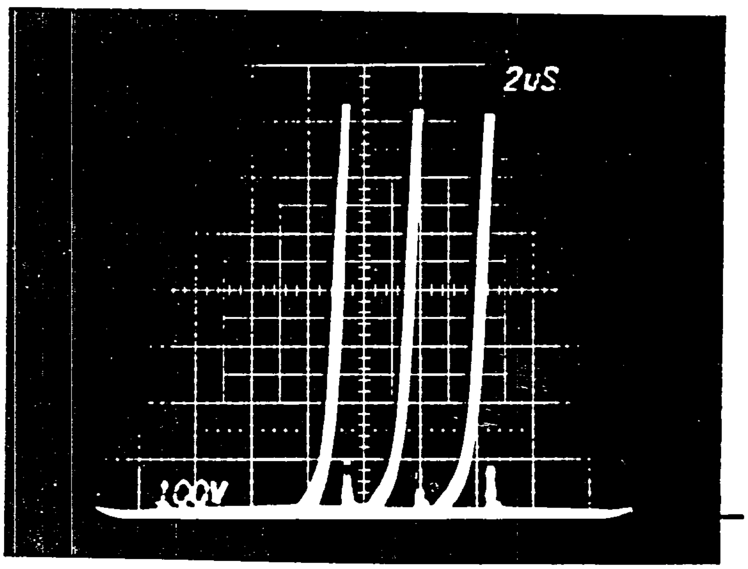

Fig. D.3.2. RBSB behavior of the Fuji ETN81-055.
Test conditions: I_C=20A; I_{BR}=4A;
I_{BF}=2,4,8A.
Scale: 2μs/div; 100 V/div.

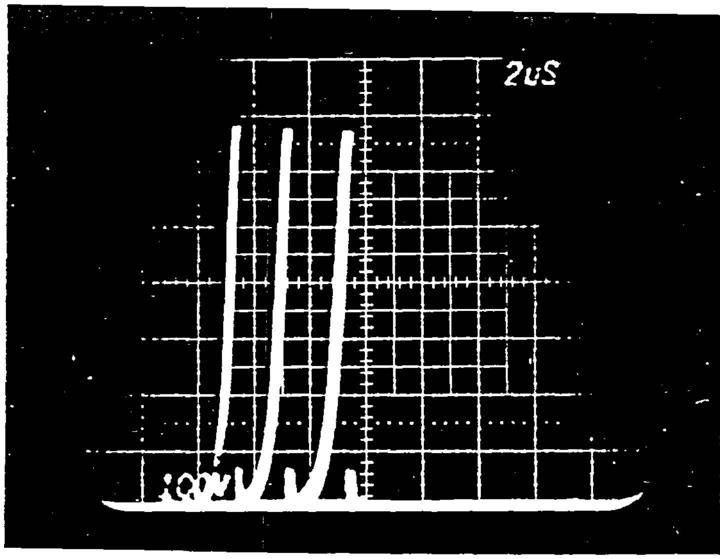

0V

Fig. D.3.3. RBSB behavior of the Fuji ETN81-055.
Test conditions: I_C=20A; I_{BR}=8A;
I_{BF}=2,4,8A.
Scale: 2μs/div; 100 V/div.

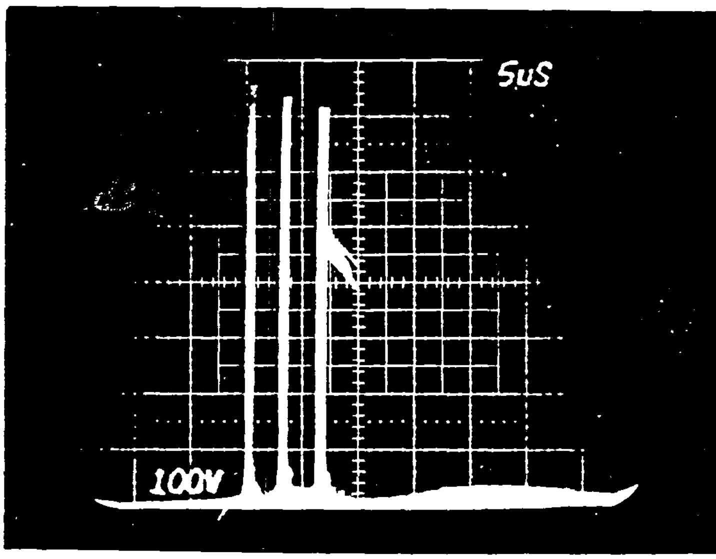

0V

Fig. D.3.4. RBSB behavior of the Fuji ETN81-055.
Test conditions: I_C=40A; I_{BR}=2A;
I_{BF}=2,4,8A.
Scale: 5μs/div; 100 V/div.

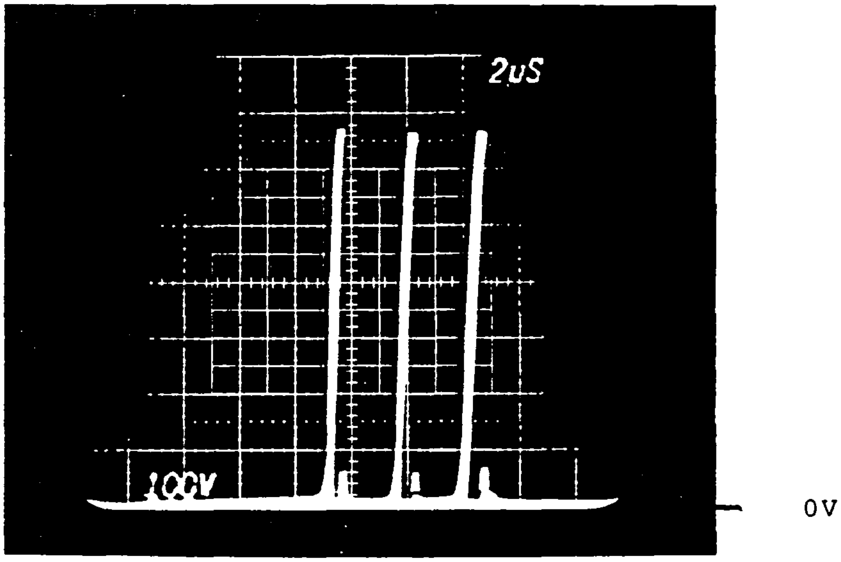

Fig. D.3.5. RBSB behavior of the Fuji ETN81-055.
Test conditions: I_c=40A; I_{BR}=4A;
I_{BF}=2,4,8A.
Scale: 2μs/div; 100 V/div.

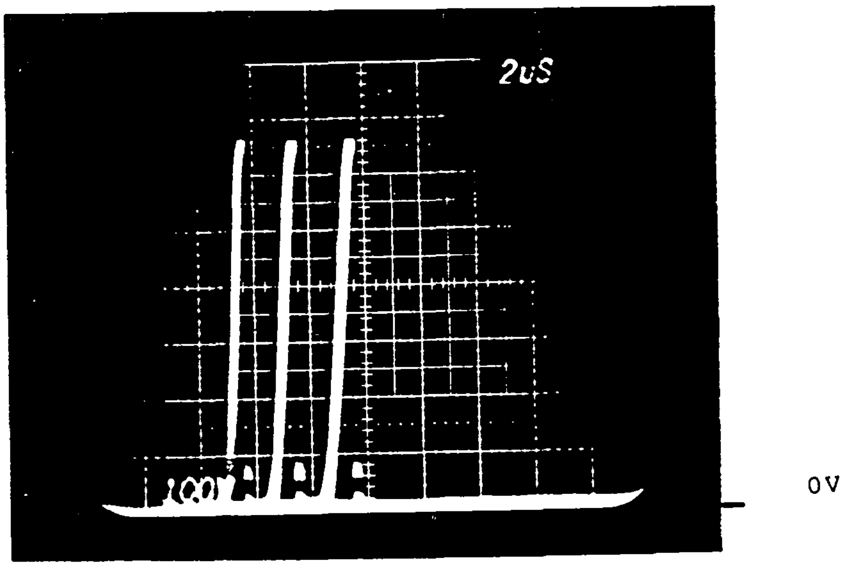

Fig. D.3.6. RBSB behavior of the Fuji ETN81-055.
Test conditions: I_c=40A; I_{BR}=8A;
I_{BF}=2,4,8A.
Scale: 2μs/div; 100 V/div.

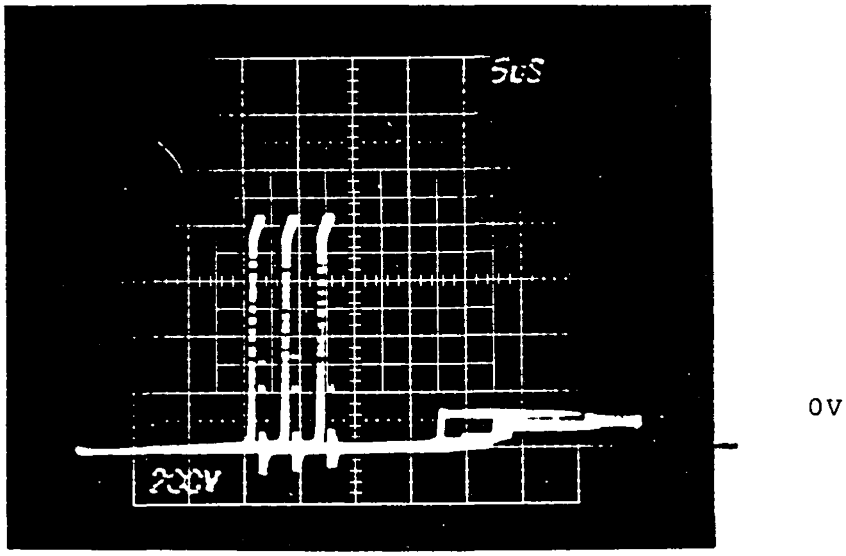

Fig. D.3.7. RBSB behavior of the Fuji ETN81-055.
Test conditions: I_c=60A; I_{BR}=2A;
I_{BF}=2,4,8A.
Scale: 5 μs/div; 100 V/div.

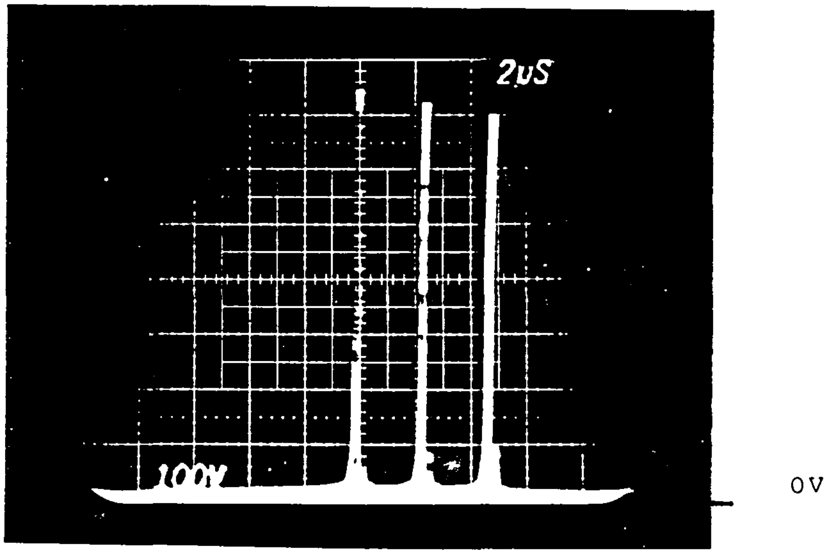

Fig. D.3.8. RBSB behavior of the Fuji ETN81-055.
Test conditions: I_c=60A; I_{BR}=4A;
I_{BF}=2,4,8A.
Scale: 2μs/div; 100 V/div.

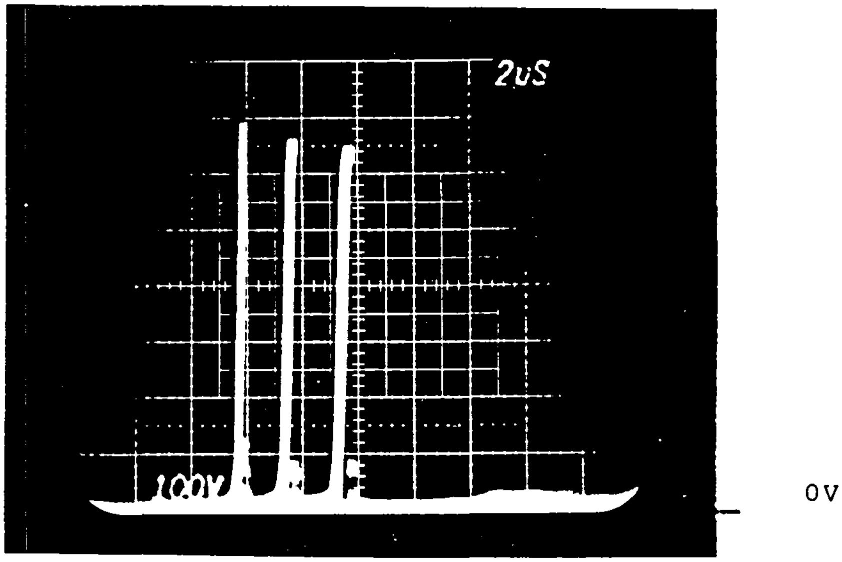

Fig. D.3.9. RBSB behavior of the Fuji ETN81-055.
Test conditions: I_C=60A; I_{BR}=8A;
I_{BF}=2,4,8A.
Scale: 2µs/div; 100 V/div.

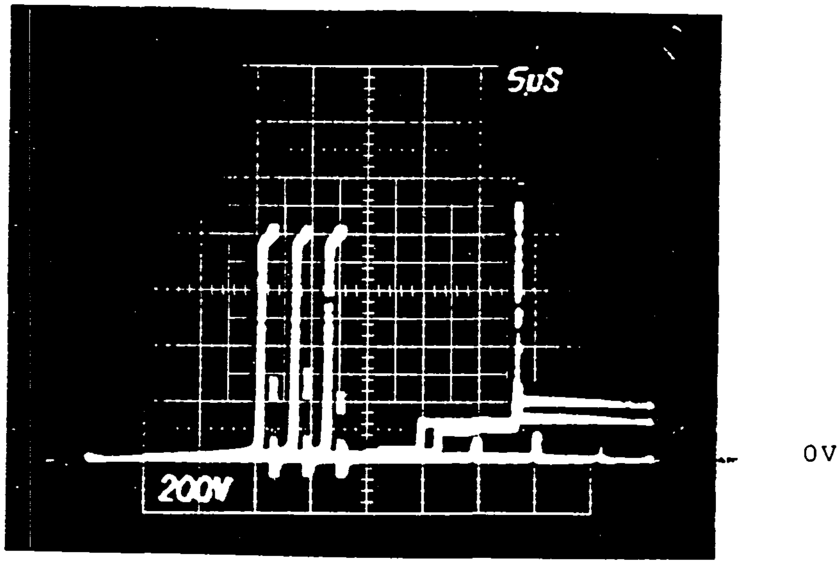

Fig. D.3.10. RBSB behavior of the Fuji ETN81-055.
Test conditions: I_C=80A; I_{BR}=2A;
I_{BF}=2,4,8A.
Scale: 5µs/div; 200 V/div.

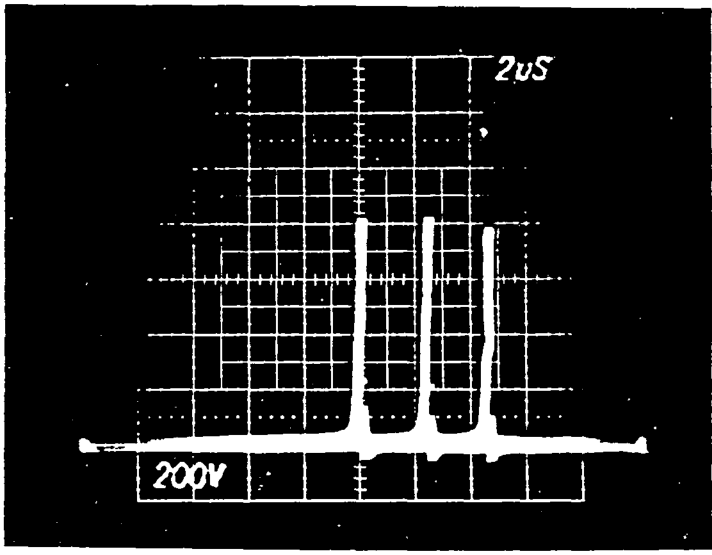

0V

Fig. D.3.11. RBSB behavior of the Fuji ETN81-055.
Test conditions: I_C=80A; I_{BR}=4A;
I_{BF}=2,4,8A.
Scale: 2μs/div; 200 V/div.

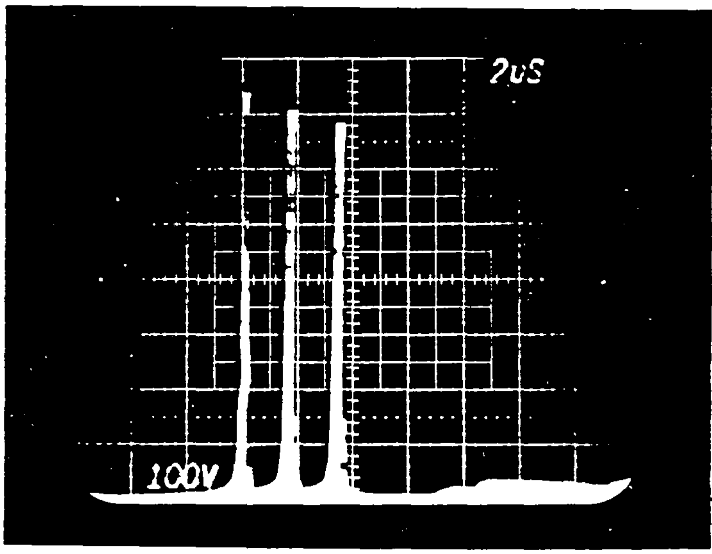

0V

Fig. D.3.12. RBSB behavior of the Fuji ETN81-055.
Test conditions: I_C=80A; I_{BR}=8A;
I_{BF}=2,4,8A.
Scale: 2μs/div; 100 V/div.

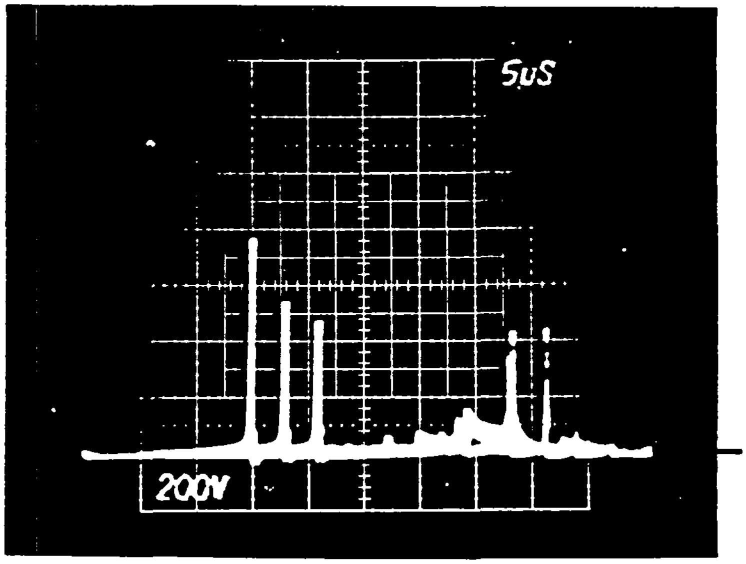

Fig. D.3.13. RBSB behavior of the Fuji ETN81-055.
Test conditions: I_C=100A; I_{BR}=2A;
I_{BF}=2,4,8A.
Scale: 5μs/div; 200 V/div.

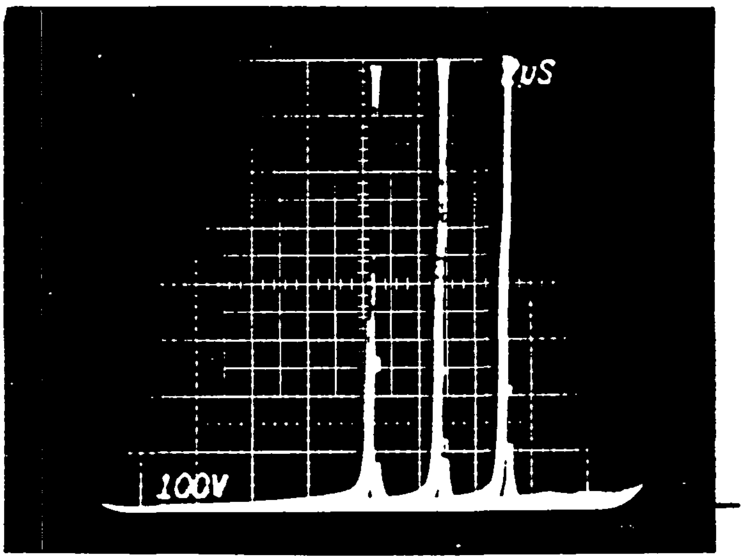

Fig. D.3.14. RBSB behavior of the Fuji ETN81-055.
Test conditions: I_C=100A; I_{BR}=4A;
I_{BF}=2,4,8A.
Scale: 2μs/div; 100 V/div.

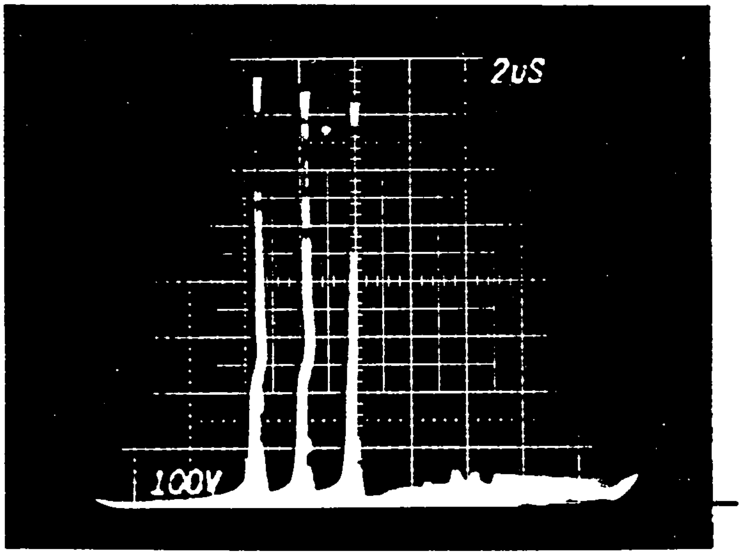

0V

Fig. D.3.15. RBSB behavior of the Fuji ETN81-055.
Test conditions: I_C=100A; I_{BR}=8A;
I_{BF}=2,4,8A.
Scale: 2μs/div; 100 V/div.

D.4 - Test Data of RBSOA of Fuji EVM31-050

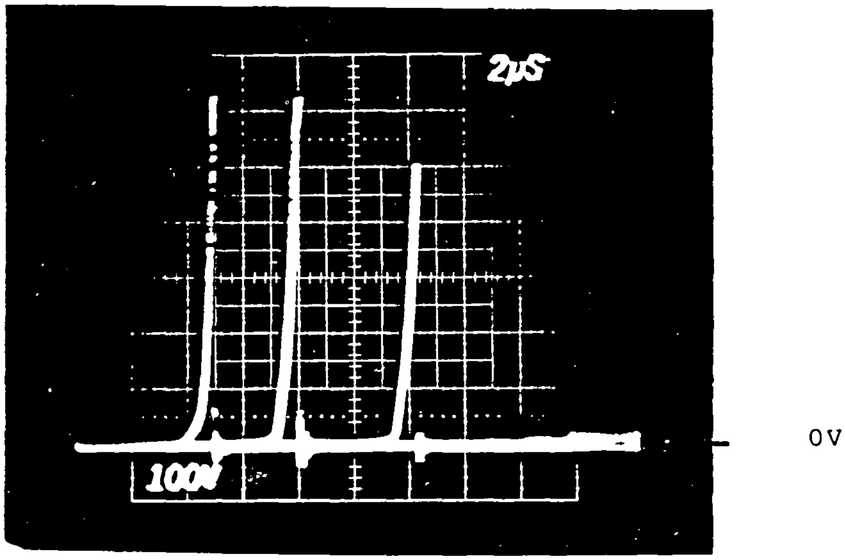

Fig. D.4.1 RBSB behavior of the Fuji EVM31-050
Test conditions: I_c = 20A; I_{BF} = 2A;
I_{BR} = 8,4,2A.
Scale: 2 μs/div; 100V/div.

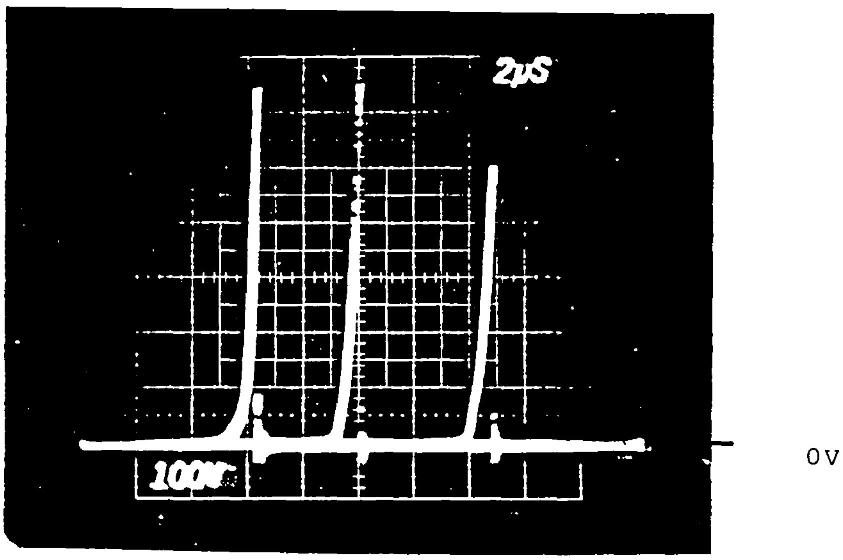

Fig. D.4.2 RBSB behavior of the Fuji EVM31-050.
Test conditions: I_c = 20A; I_{BF} = 4A;
I_{BR} = 8,4,2A.
Scale. 2 μs/div; 100V/div.

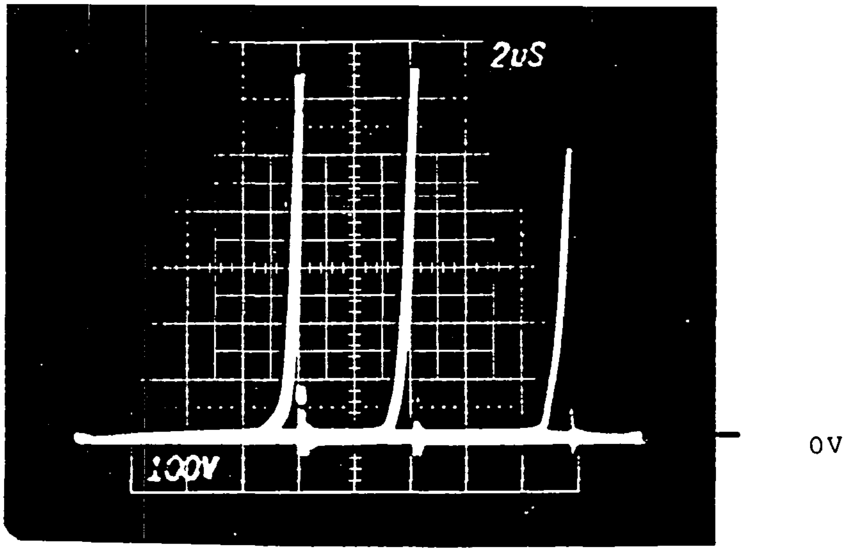

Fig. D.4.3 RBSB behavior of the Fuji EVM31-050.
Test conditions: I_c = 20A; I_{BF} = 8A;
I_{BR} = 8,4,2A.
Scale: 2 μs/div; 100V/div.

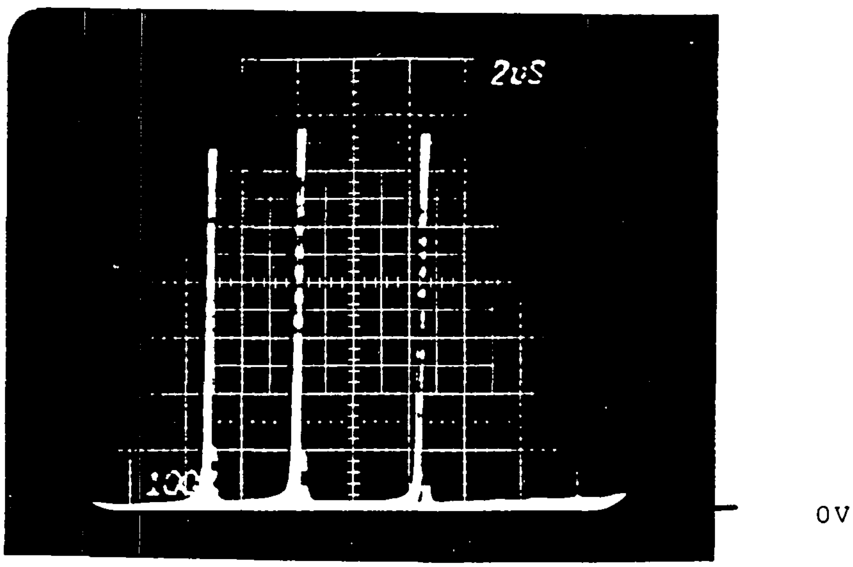

Fig. D.4.4 RBSB behavior of the Fuji EVM31-050.
Test conditions: I_c = 40A; I_{BF} = 2A;
I_{BR} = 8,4,2A.
Scale: 2 μs/div; 100v/div.

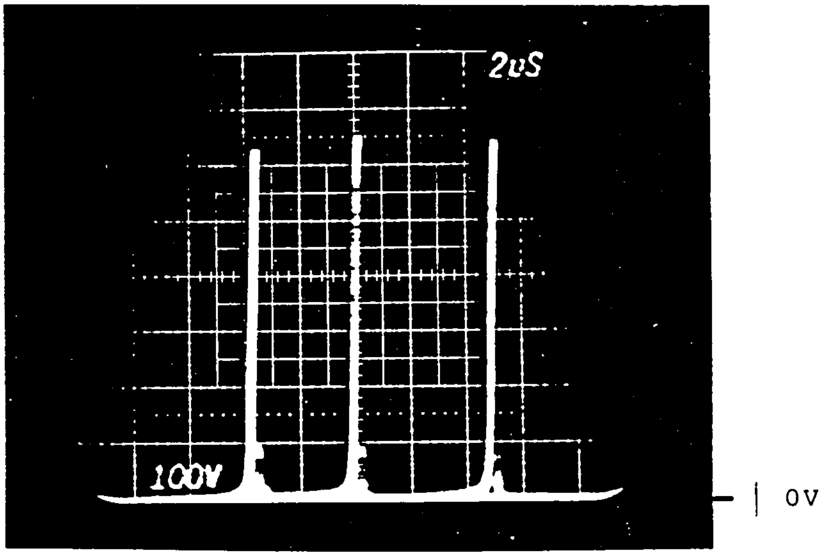

Fig. D.4.5 RBSB behavior of the Fuji EVM31-050.
Test conditions: I_c = 40A; I_{BF} = 4A;
I_{BR} = 8,4,2A.
Scale: 2 μs/div; 100V/div.

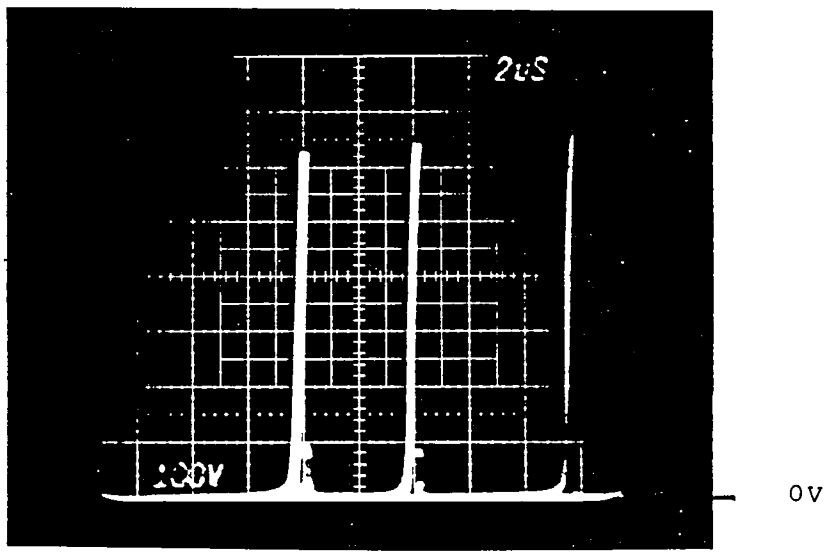

Fig. D.4.6 RBSB behavior of the Fuji EVM31-050.
Test conditions: I_c = 40A; I_{BF} = 8A;
I_{BR} = 8,4,2A.
Scale: 2 μs/div; 100V/div.

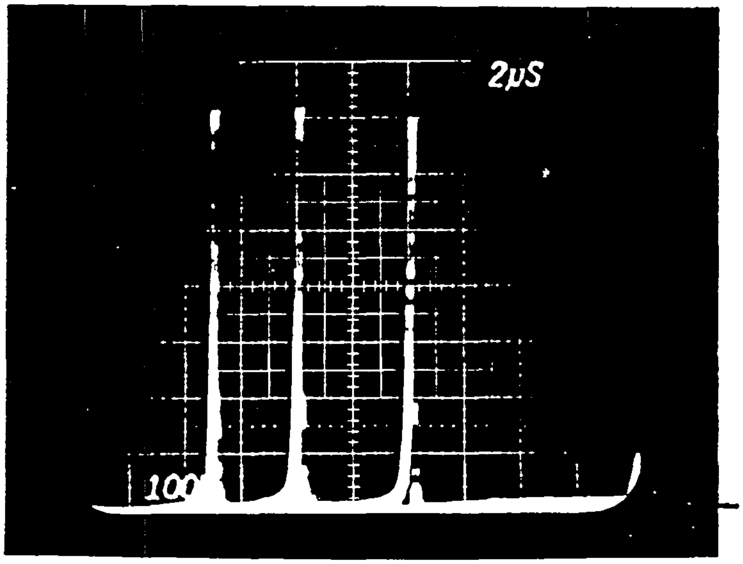

0V

Fig. D.4.7 RBSB behavior of the Fuji EVM31-050.
Test conditions: I_c = 60A; I_{BF} = 2A;
I_{BR} = 8,4,2A.
Scale: 2 µs/div; 100V/div.

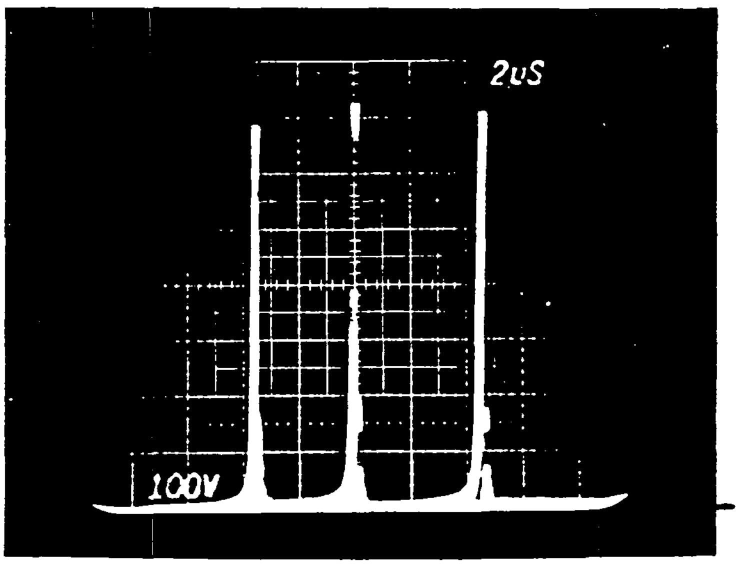

0V

Fig. D.4.8 RBSB behavior of the Fuji EVM31-050.
Test conditions: I_c = 60A; I_{BF} = 4A;
I_{BR} = 8,4,2A.
Scale: 2 µs/div; 100V/div.

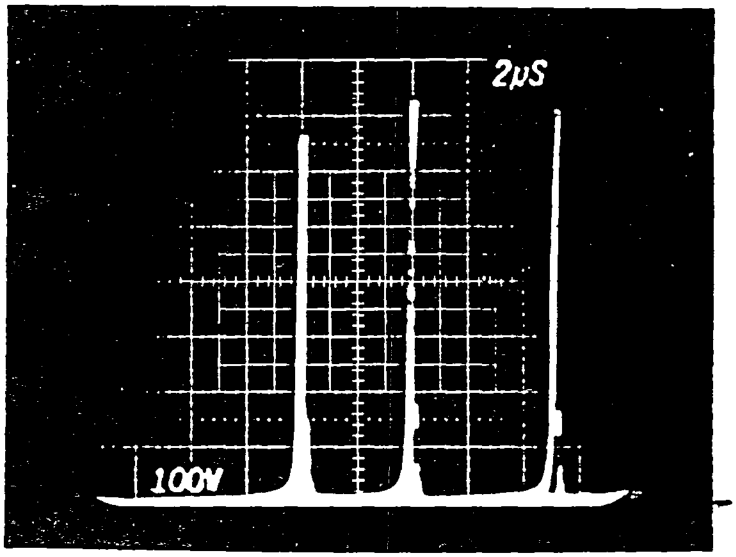

OV

Fig. D.4.9 RBSB behavior of the Fuji EVM31-050.
Test conditions: I_C = 60A; I_{BF} = 8A;
I_{BR} = 8,4,2A.
Scale: 2 μs/div; 100V/div.

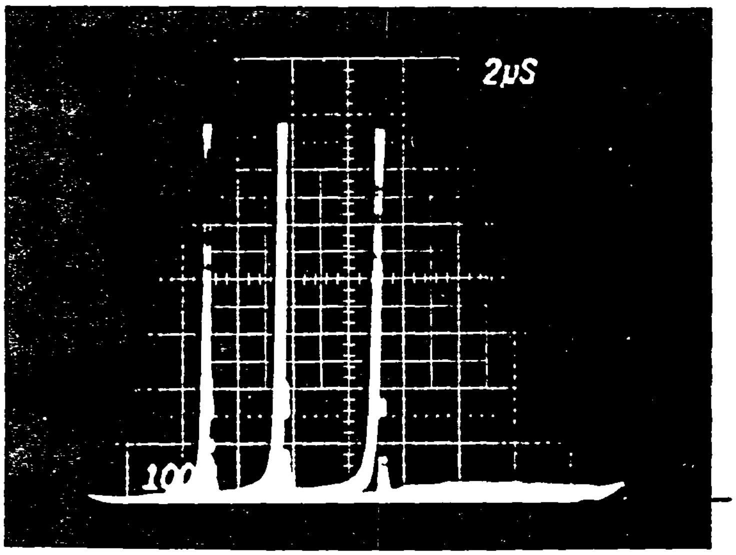

OV

Fig. D.4.10 RBSB behavior of the Fuji EVM31-050.
Test conditions: I_C = 80A; I_{BF} = 2A;
I_{BR} = 8,4,2A.
Scale: 2 μs/div; 100V/div.

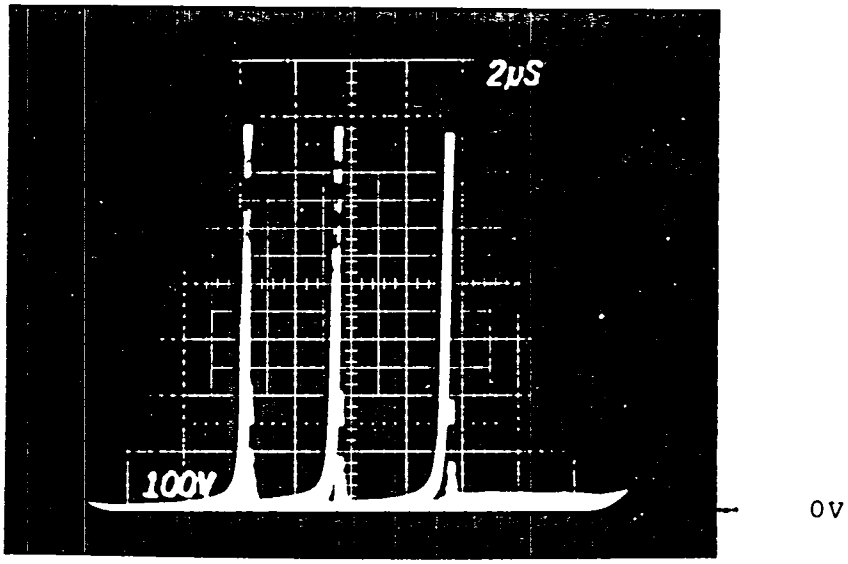

Fig. D.4.11 RBSB behavior of the Fuji EVM31-050.
Test conditions: I_c = 80A; I_{BF} = 4A;
I_{BR} = 8,4,2A.
Scale: 2 μs/div; 100v/div.

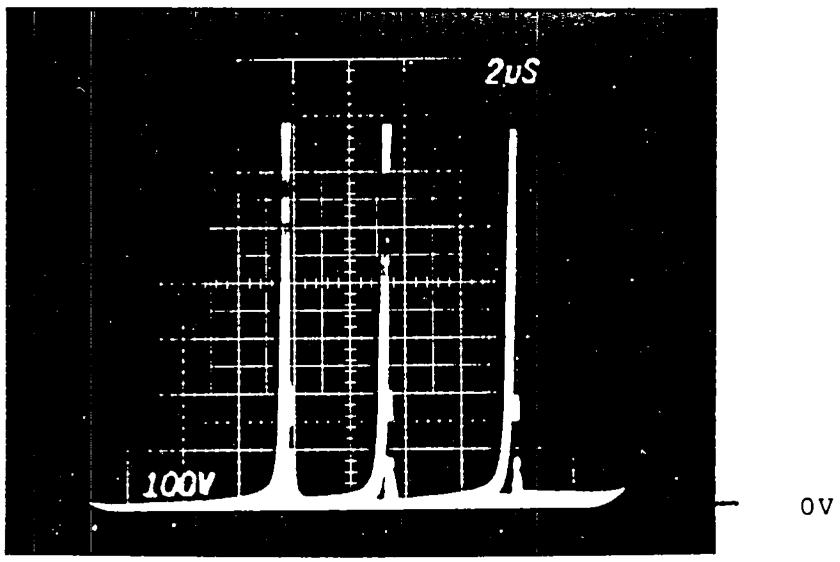

Fig. D.4.12 RBSB behavior of the Fuji EVM31-050.
Test conditions: I_c = 80A; I_{BF} = 8A;
I_{BR} = 8,4,2A.
Scale: 2 μs/div; 100V/div.

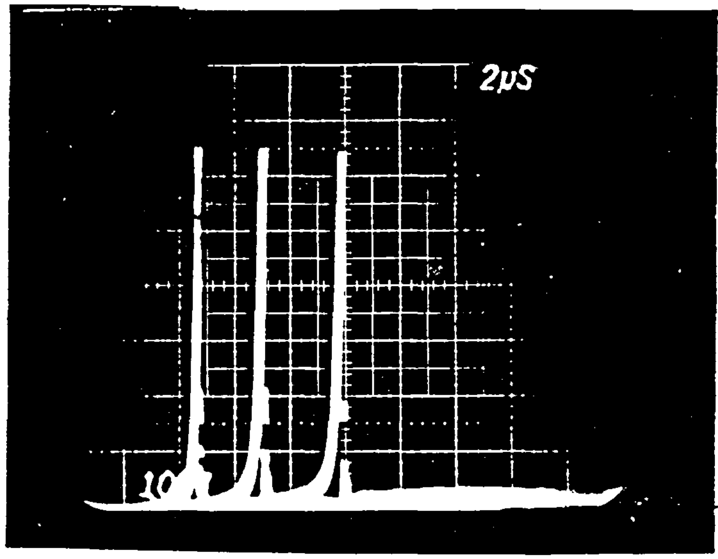

0V

Fig. D.4.13 RBSB behavior of the Fuji EVM31-050.
Test conditions: I_c = 100A; I_{BF} = 2A;
I_{BR} = 8,4,2A.
Scale: 2 µs/div; 100V/div.

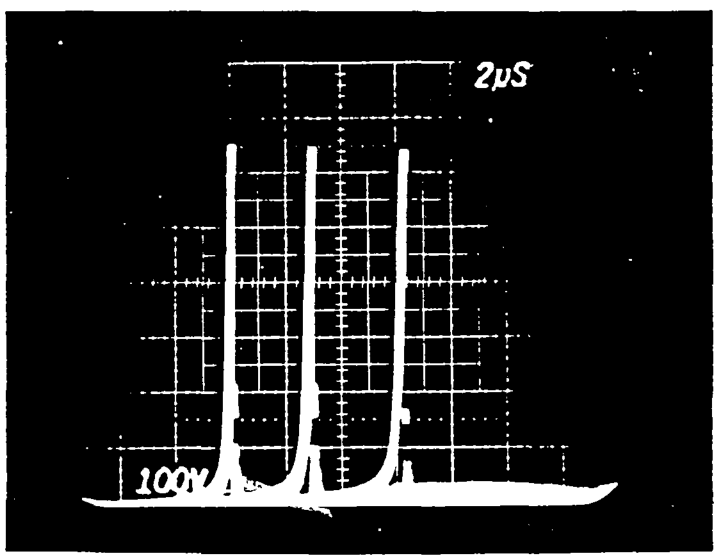

0V

Fig. D.4.14 RBSB behavior of the Fuji EVM31-050.
Test conditions: I_c = 100A; I_{BF} = 4A;
I_{BR} = 8,4,2A.
Scale: 2 µs/div; 100V/div.

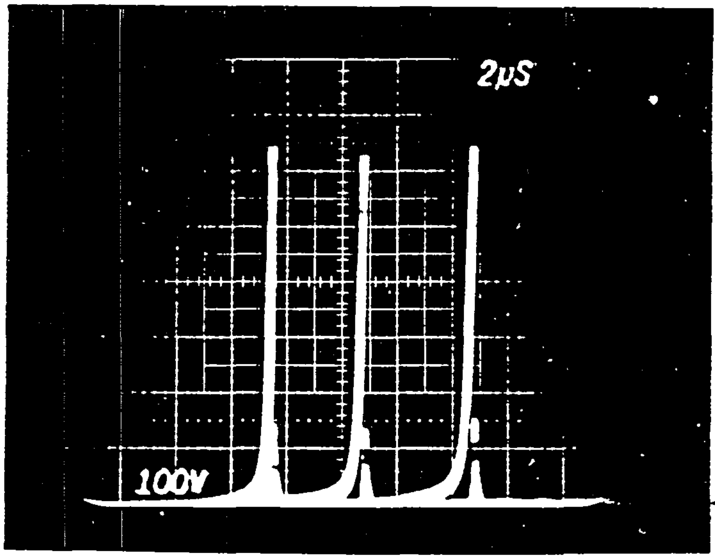

OV

Fig. D.4.15 RBSB behavior of the Fuji EVM31-050.
Test conditions: I_c = 100A; I_{BF} = 8A;
I_{BR} = 8,4,2A.
Scale: 2 μs/div; 100V/div.

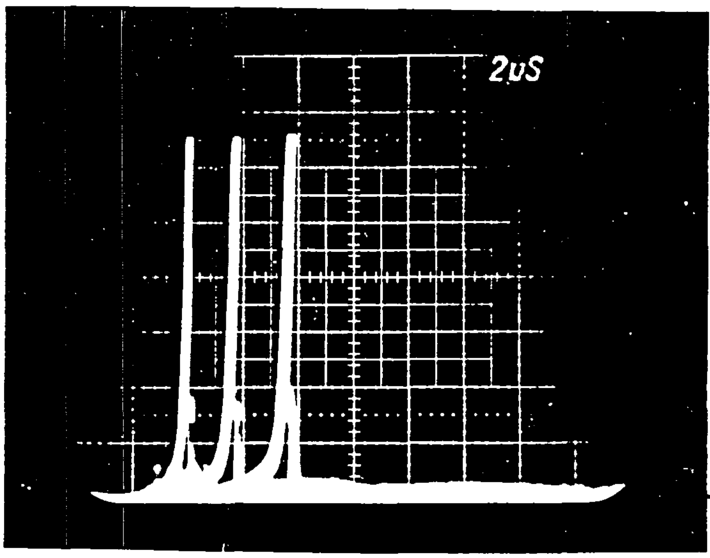

OV

Fig. D.4.16 RBSB behavior of the Fuji EVM31-050.
Test conditions: I_c = 120A; I_{BF} = 2A;
I_{BR} = 8,4,2A.
Scale: 2 μs/div; 100V/div.

D.5 Test Data of RBSOA of Mitsubishi QM150DY-H

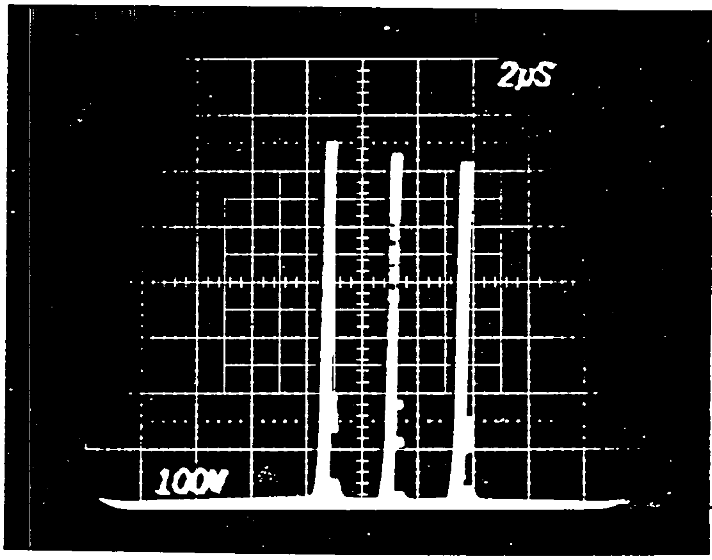

0V

Fig. D.5.1. RBSB behavior of the Mitsubishi QM150DY-H. Test conditions: I_c=20A; I_{BR}=2A; I_{BF}=2,4,8A.
Scale: 2 μs/div; 100 V/div.

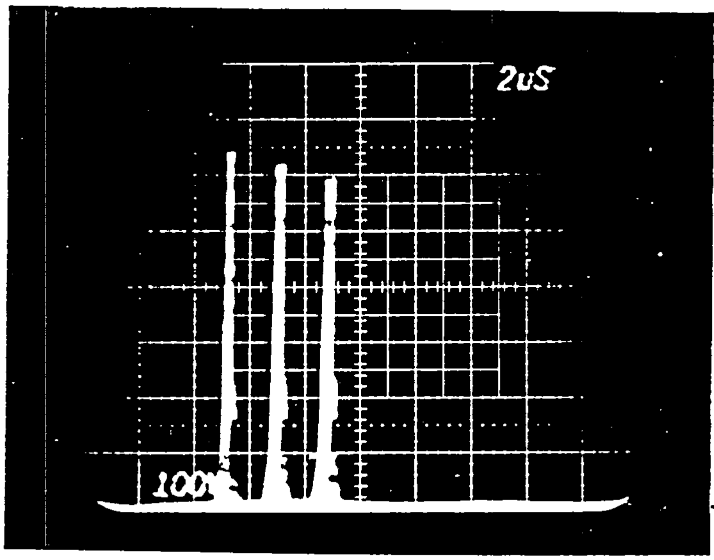

0V

Fig. D.5.2. RBSB behavior of the Mitsubishi QM150DY-H. Test conditions: I_c=20A; I_{BR}=4A; I_{BF}=2,4,8A.
Scale: 2 μs/div; 100 V/div.

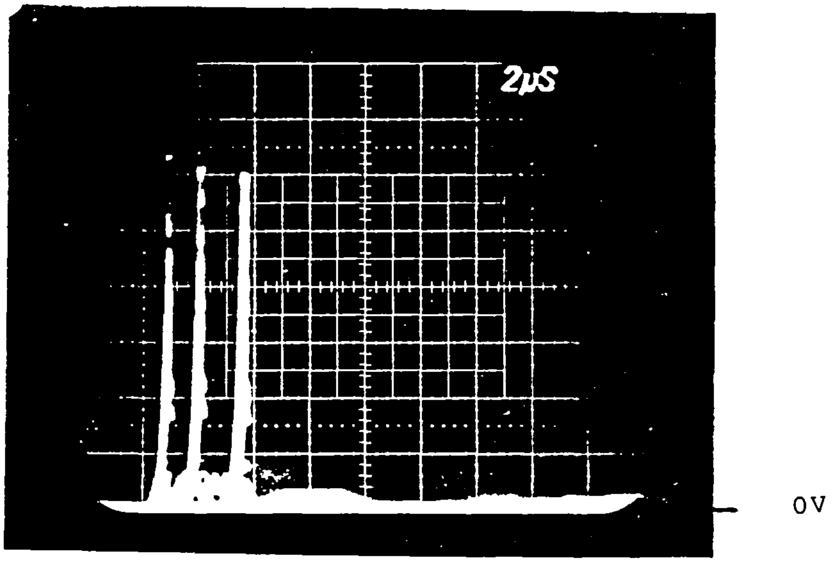

Fig. D.5.3. RBSB behavior of the Mitsubishi QM150DY-H. Test conditions: I_C=20A; I_{BR}=8A; I_{BF}=2,4,8A.
Scale: 2 μs/div; 100 V/div.

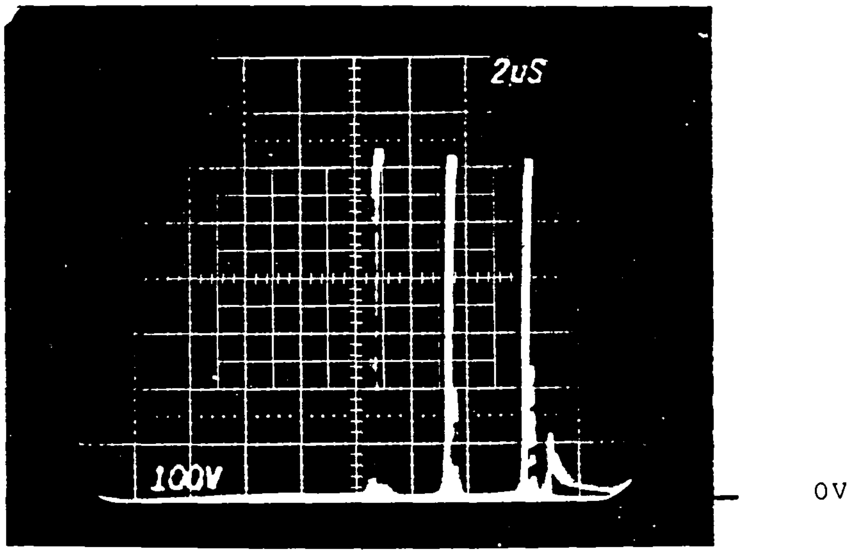

Fig. D.5.4. RBSB behavior of the Mitsubishi QM150DY-H. Test conditions: I_C=40A; I_{BR}=2A; I_{BF}=2,4,8A.
Scale: 2 μs/div; 100 V/div.

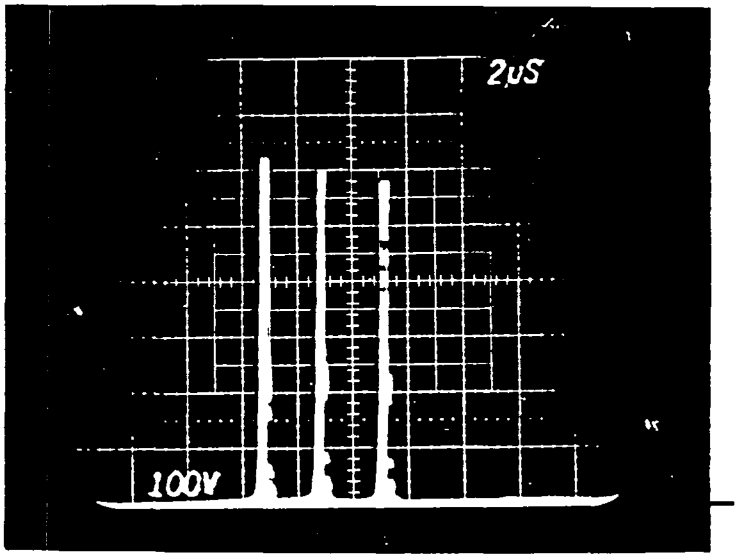

0V

Fig. D.5.5. RBSB behavior of the Mitsubishi QM150DY-H. Test conditions: I_C=40A; I_{BR}=4A; I_{BF}=2,4,8A.
Scale: 2 μs/div; 100 V/div.

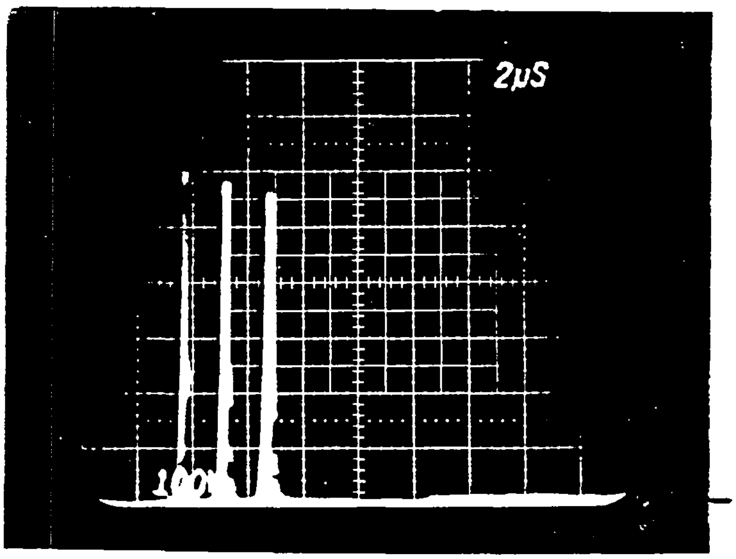

0V

Fig. D.5.6. RBSB behavior of the Mitsubishi QM150DY-H. Test conditions: I_C=40A; I_{BR}=8A; I_{BF}=2,4,8A.
Scale: 2 μs/div; 100 V/div.

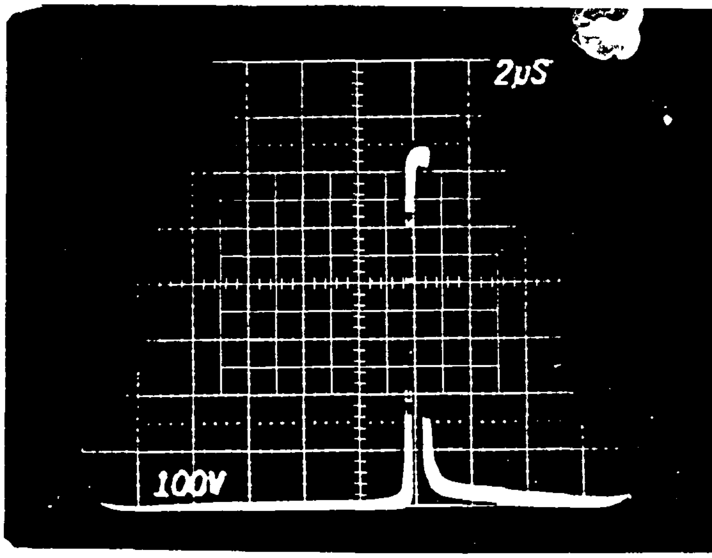

0V

Fig. D.5.7. RBSB behavior of the Mitsubishi QM150DY-H. Test conditions: I_C=60A; I_{BR}=2A; I_{BF}=2,4,8A.
Scale: 2 µs/div; 100 V/div.

D.6 Test Data of RBSDOA of Mitsubishi QM300HA-H

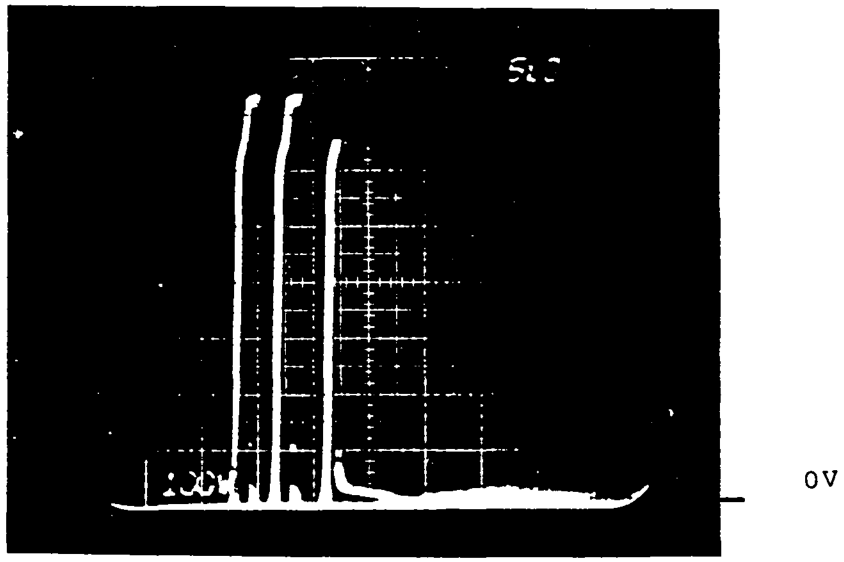

Fig. D.6.1. RBSB behavior of theMitsubishi QM300HA-H. Test conditions: I_C=20A; I_{BR}=2A; I_{BF}=2,4,8A. Scale: 5 μs/div; 100 V/div.

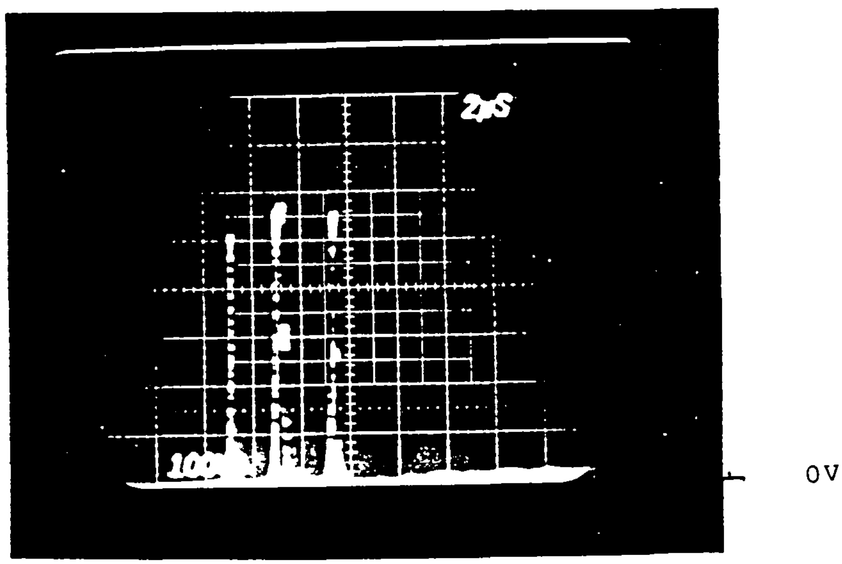

Fig. D.6.2. RBSB behavior of the Mitsubishi QM300HA-H. Test conditions: I_C=80 A; I_{BR}=5A; I_{BF}=1,2,4A. Scale: 2 μs/div; 100 V/div.

D.7 Test Data of RBSOA of Mitsubishi QM300HA-2H

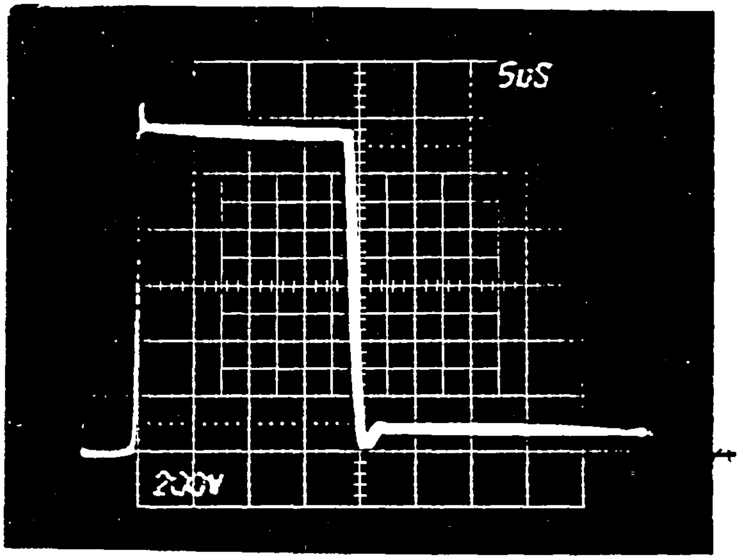

Fig. D.7.1 RBSB test for the Mitsubishi QM300HA-2H. Device did not show SB although the clamp voltage was set at the highest value as well as collector current.
Test conditions: I_c = 120A; I_{BR} = 16A; I_{BF} = 4A; V_{CCL} > 1100V
Scale: 5 μs/div; 200V/div.

D.8 Test Data of RBSOA of Toshiba ST200M

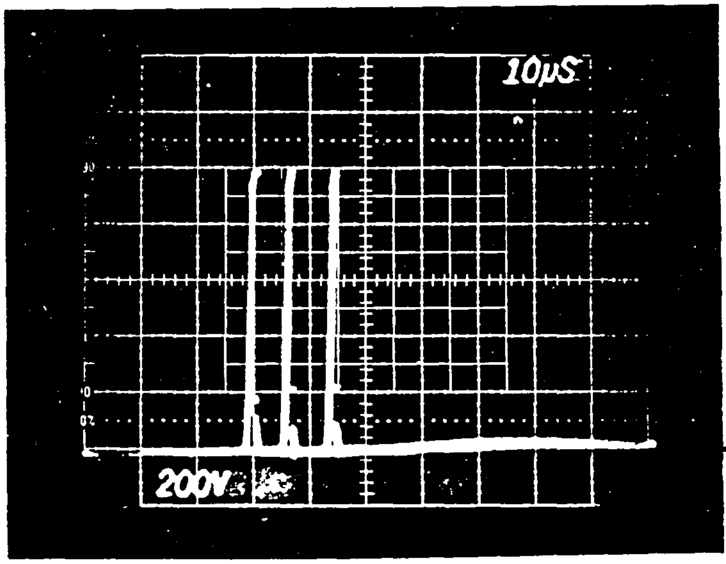

0V

Fig. D.8.1 RBSB behavior of the Toshiba ST200M.
Test conditions: I_C=20A; I_{BR}=2A; I_{BF}=2;4;8A.
Scale: 10μs/div; 200V/div.

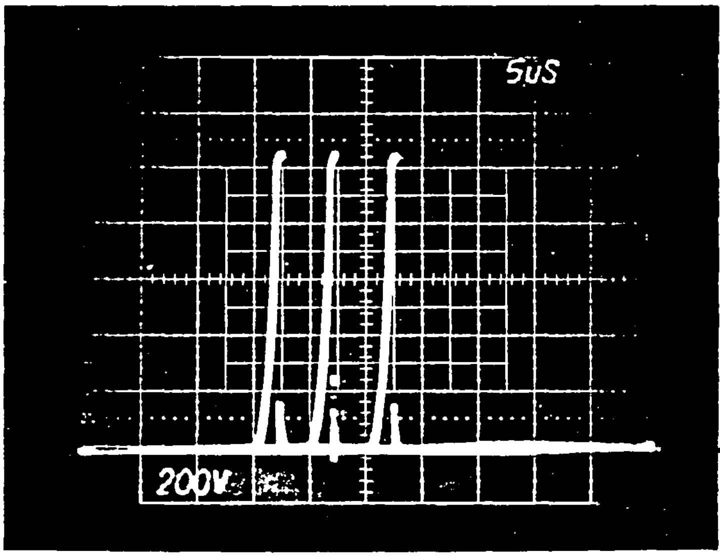

0V

Fig. D.8.2 RBSB behavior of the Toshiba ST200M.
Test conditions: I_C=20A; I_{BR}=4A; I_{BF}=2;4;8A.
Scale: 5μs/div; 200V/div

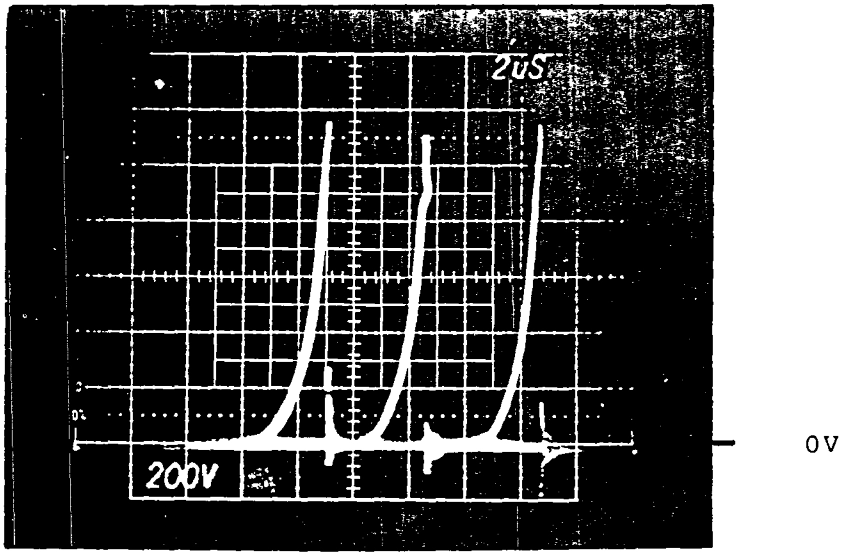

Fig. D.8.3 RBSB behavior of the Toshiba ST200M.
Test conditions: I_C=20A; I_{BR}=8A; I_{BF}=2;4;8A.
Scale: 2μs/div; 200V/div.

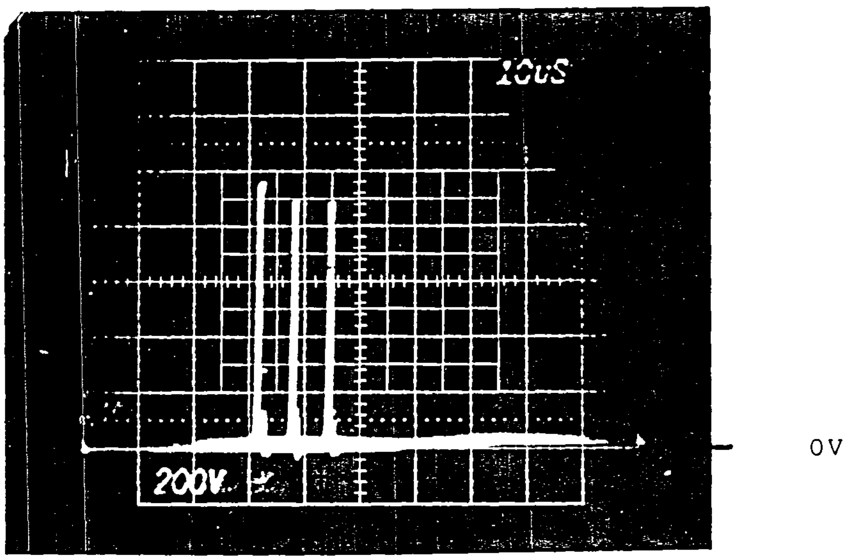

Fig. D.8.4 RBSB behavior of the Toshiba ST200M.
Test conditions: I_C=40A; I_{BR}=2A; I_{BF}=2;4;8A.
Scale: 10μs/div; 200V/div.

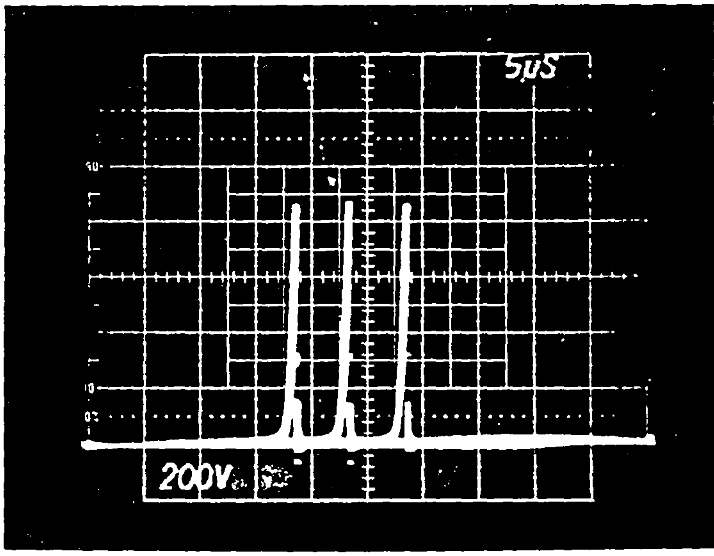

0V

Fig. D.8.5 RBSB behavior of the Toshiba ST200M.
Test conditions: I_C=40A; I_{BR}=4A; I_{BF}=2;4;8A.
Scale: 5μs/div; 200V/div.

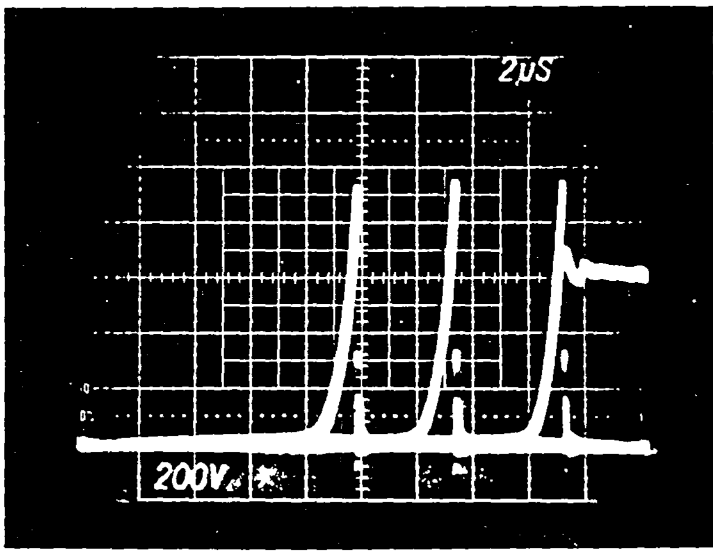

0V

Fig. D.8.6 RBSB behavior of the Toshiba ST200M.
Test conditions: I_C=40A; I_{BR}=8A; I_{BF}=2;4;8A.
Scale: 2μs/div; 200V/div.

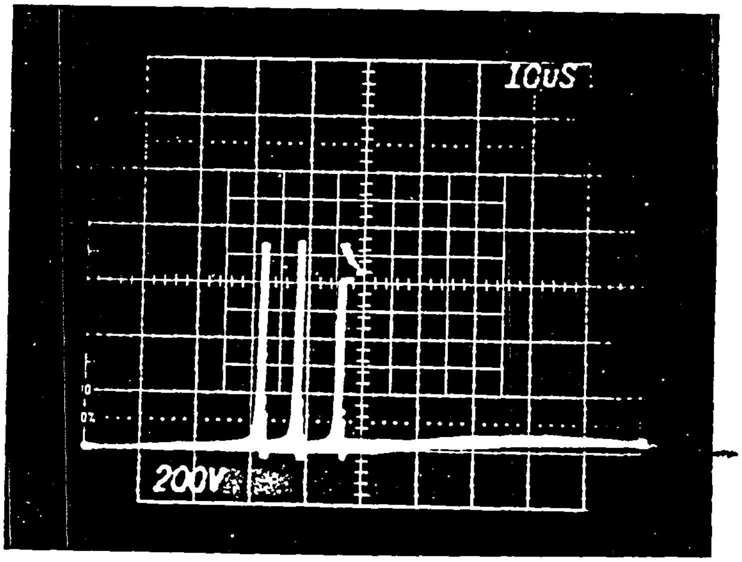

Fig. D.8.7. RBSB behavior of the Toshiba ST200M.
Test conditions. I_C=60A; I_{BR}=2A; I_{BF}=2;4;8A.
Scale: 10μs/div; 200V/div.

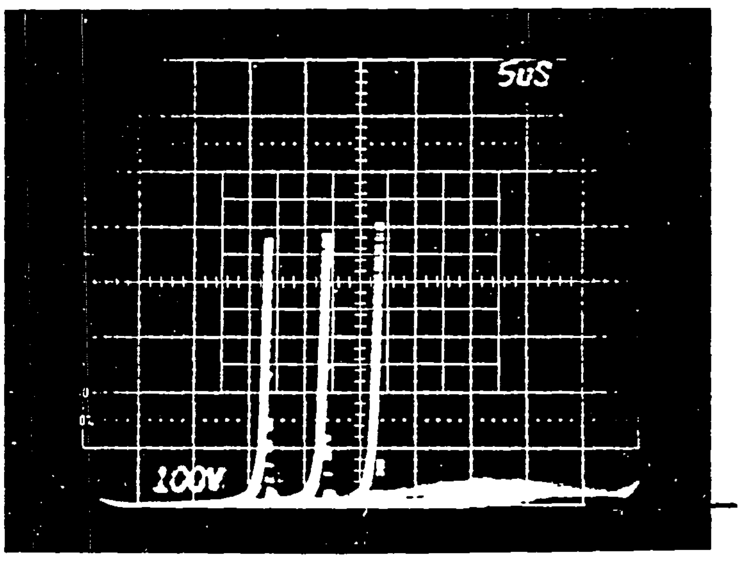

Fig. D.8.8 RBSB behavior of the Toshiba ST200M.
Test conditions: I_C=60A; I_{BR}=4A; I_{BF}=2;4;8A.
Scale: 5μs/div; 100V/div.

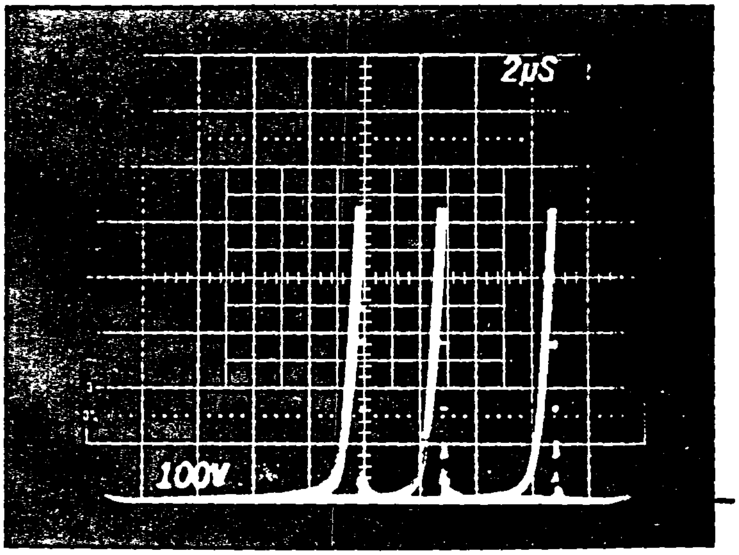

0V

Fig. D.8.9 RBSB behavior of the Toshiba ST200M.
Test conditions: $I_C=60A$; $I_{BR}=8A$; $I_{BF}=2;4;8A$.
Scale: 5μs/div; 100V/div.

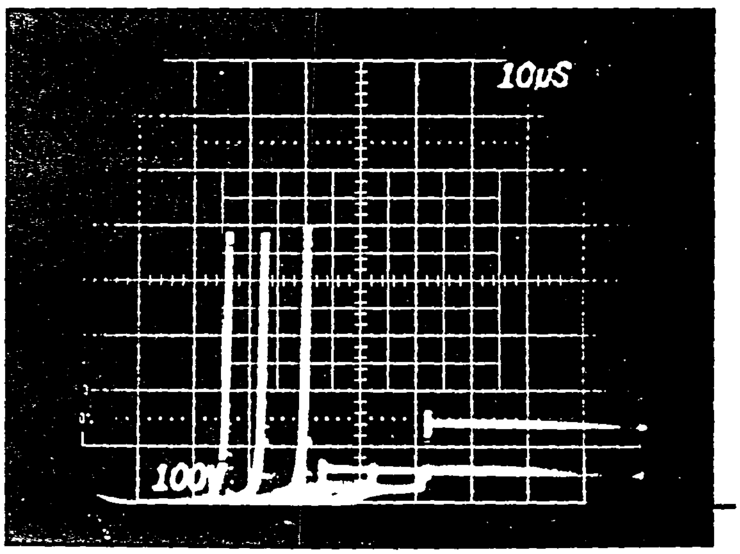

0V

Fig. D.8.10 RBSB behavior of the Toshiba ST200M.
Test conditions: $I_C=80A$; $I_{BR}=2A$; $I_{BF}=2;4;8A$.
Scale: 10μs/div; 100V/div.

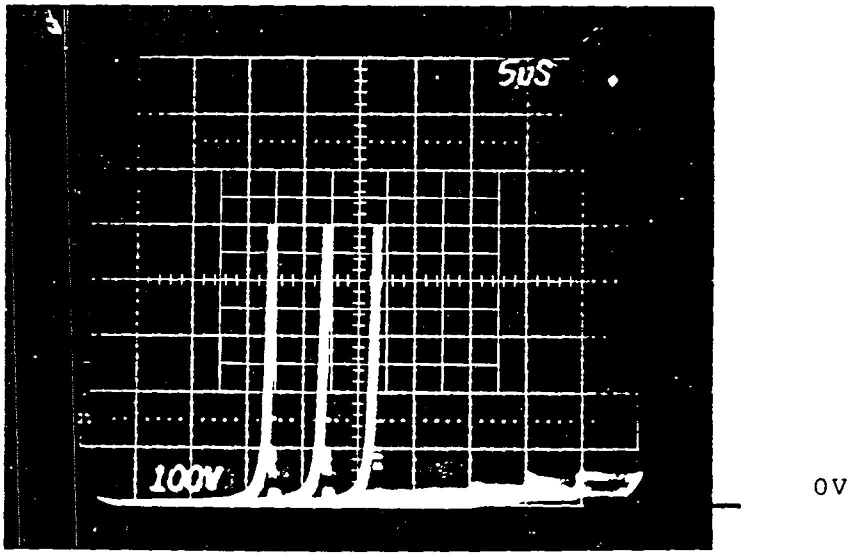

Fig. D.8.11 RBSB behavior of the Toshiba ST200M.
Test conditions: I_C=80A; I_{BR}=4A; I_{BF}=2;4;8A.
Scale: 5μs/div; 100V/div.

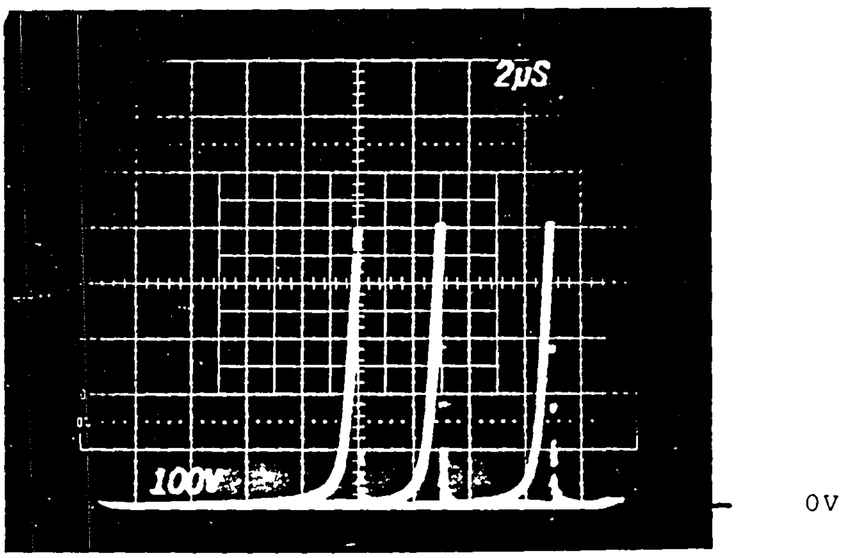

Fig. D.8.12 RBSB behavior of the Toshiba ST200M.
Test conditions: I_C=80A; I_{BR}=8A; I_{BF}=2;4;8A.
Scale: 2μs/div; 100V/div.

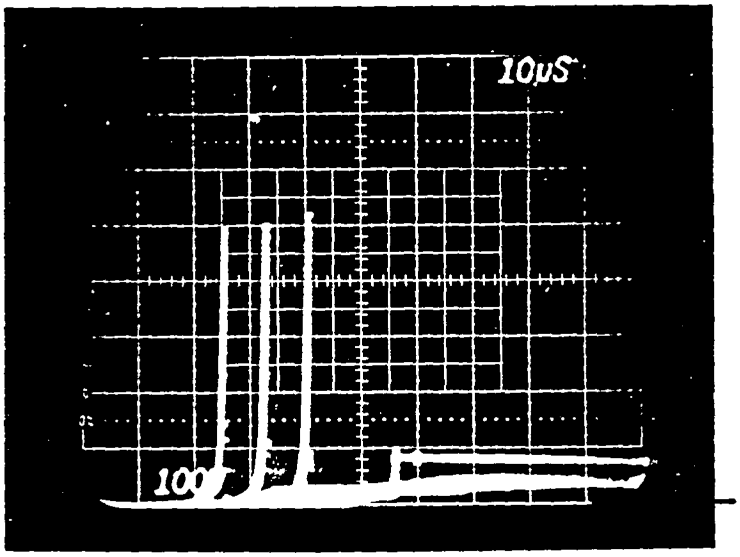

Fig. D.8.13 RBSB behavior of the Toshiba ST200M.
Test conditions: I_C=100; I_{BR}=2A; I_{BF}=2;4;8A.
Scale: 10µs/div; 100V/div.

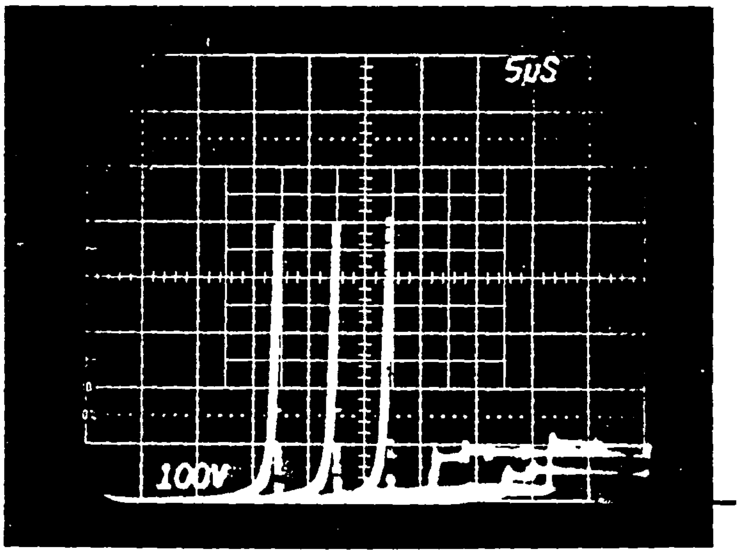

Fig. D.8.14 RBSB behavior of the Toshiba ST200M.
Test conditions: I_C=100A; I_{BR}=4A; I_{BF}=2;4;8A.
Scale: 5µs/div; 100V/div.

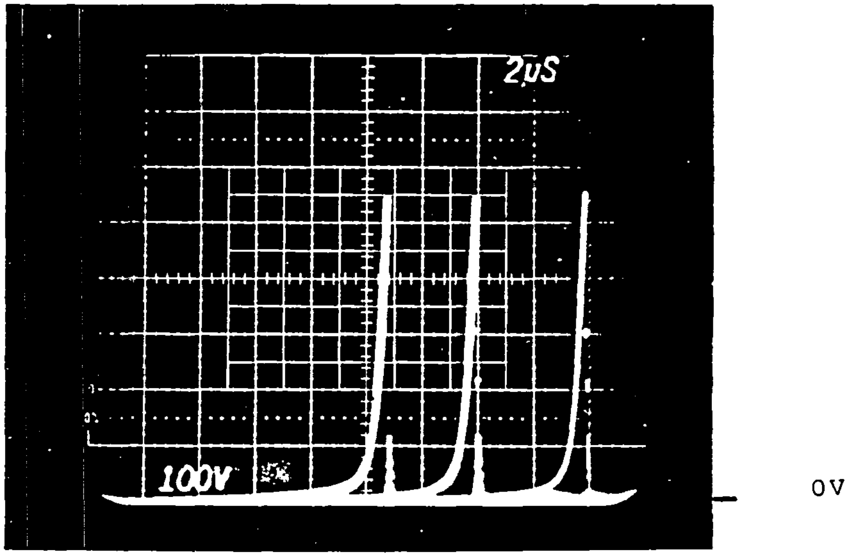

Fig. D.8.15 RBSB behavior of the Toshiba ST200M.
Test conditions: I_C=100A; I_{BR}=8A; I_{BF}=2;4;8A.
Scale: 2μs/div; 100V/div.

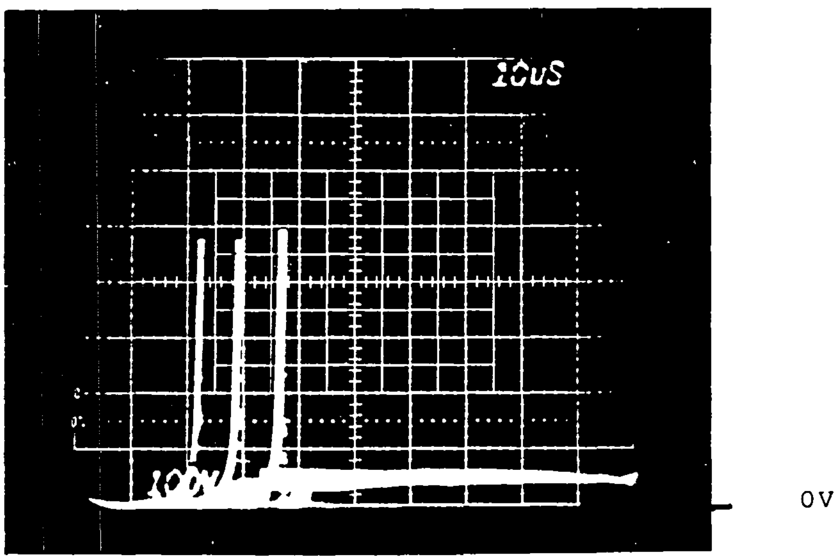

Fig. D.8.16 RBSB behavior of the Toshiba ST200M.
Test conditions: I_C=120A; I_{BR}=2A; I_{BF}=2;4;8A.
Scale: 10μs/div; 100V/div.

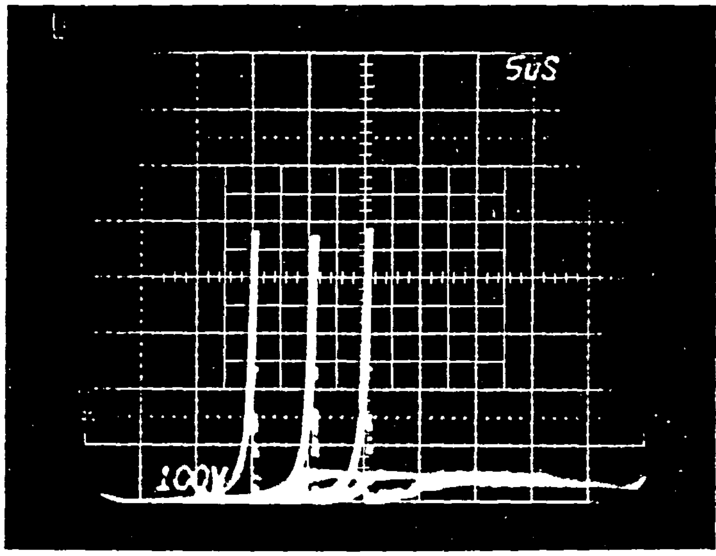

0V

Fig.D.8.17 RBSB behavior of the Toshiba ST200M.
Test conditions: I_C=120A; I_{BR}=4A; I_{BF}=2;4;8A.
Scale: 5μs/div; 100V/div.

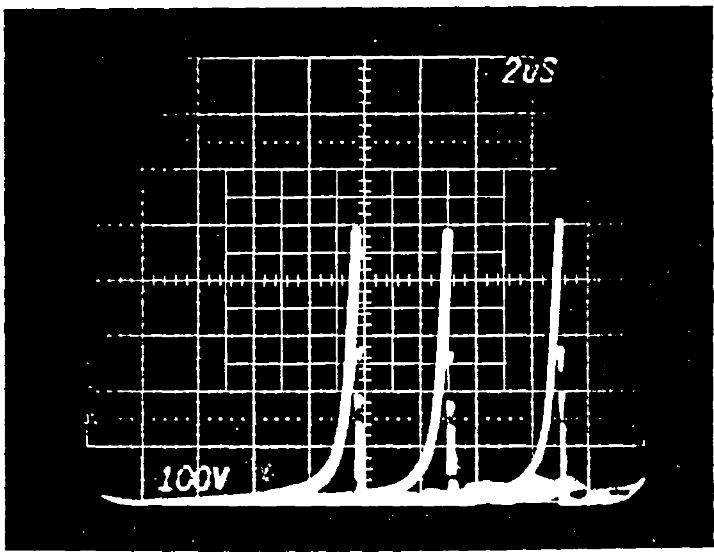

0V

Fig.D.8.18 RBSB behavior of the Toshiba ST200M.
Test conditions: I_C=120A; I_{BR}=8A; I_{BF}=2;4;8A.
Scale: 2μs/div; 100V/div.

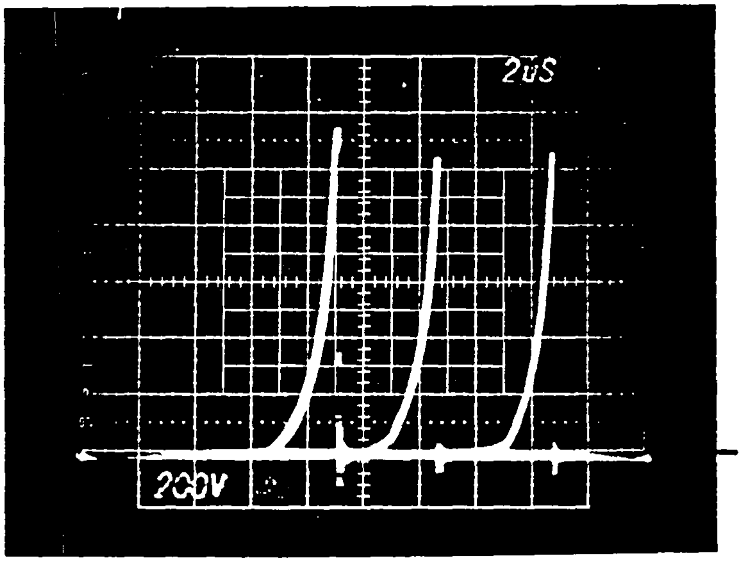

0V

Fig.D.8.19 RBSB Test of the Toshiba ST200M taken after fifty four repeatative tests (after all tests on preceding figs.) Conditions: I_C=20A; I_{BR}=8A; I_{BF}-2;4;8A.
Scale: 2µs/div; 200V/div.
(Compare this picture with that in fig.D.8.3)

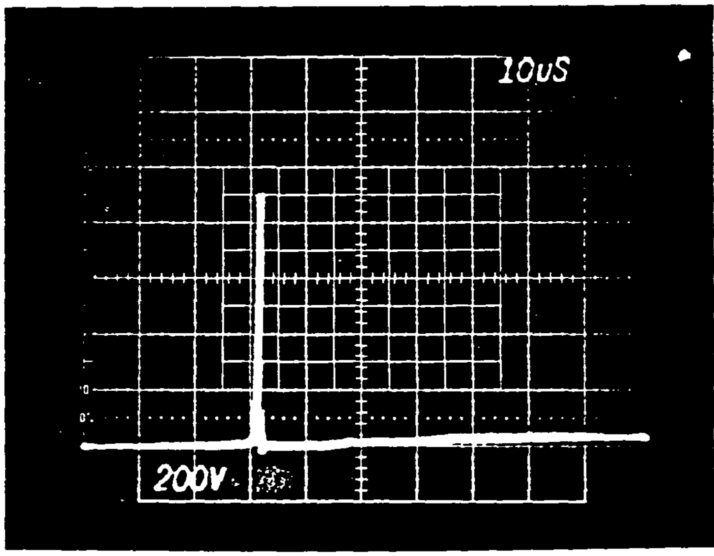

0V

Fig. D.8.20 RBSB Test of the Toshiba ST200M taken after fifty seven repeatative tests (after all tests on proceding figs.) Conditions:
I_C=40A; I_{BR}=2; I_{BF}=2A.
Scale: 10μs/div; 200V/div.
(Compare this picture with that in fig.D.8.4)

D.9 Test Data of RBSOA of Toshiba ST300M21

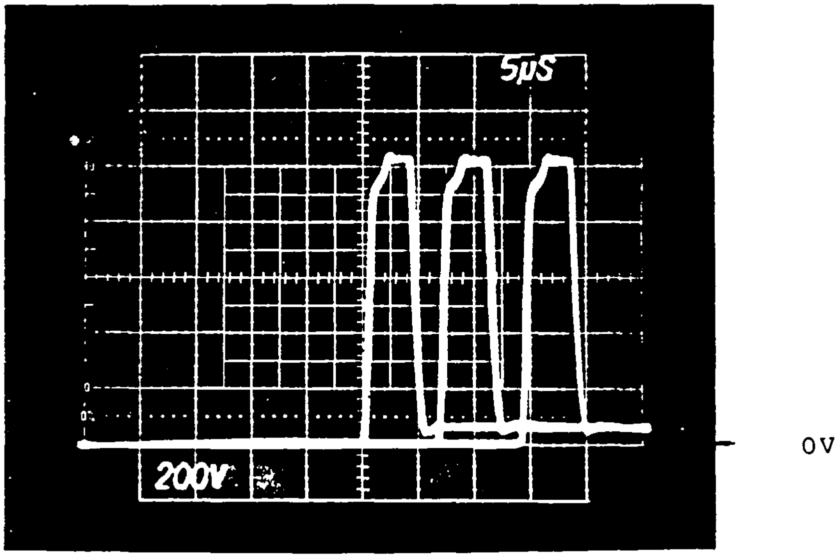

Fig. D.9.1 RBSB test for the Toshiba ST300M21
Test conditions: I_c = 20A; I_{BR} = 2A;
I_{BF} = 2,4,8A.
Scale: 5 µs/div; 200V/div.

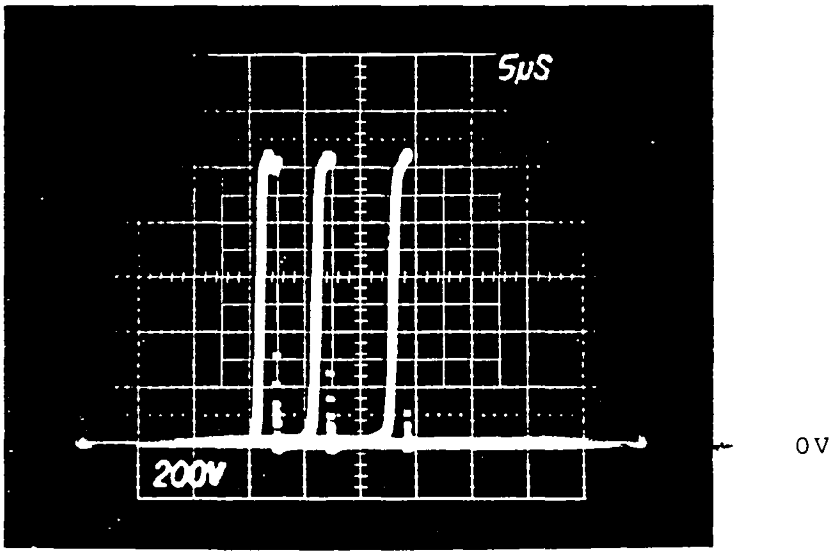

Fig. D.9.2 RBSB test for the Toshiba ST300M21
Test conditions: I_c = 20A; I_{BR} = 4A;
I_{BF} = 2,48A.
Scale: 5 µs/div; 200V/div.

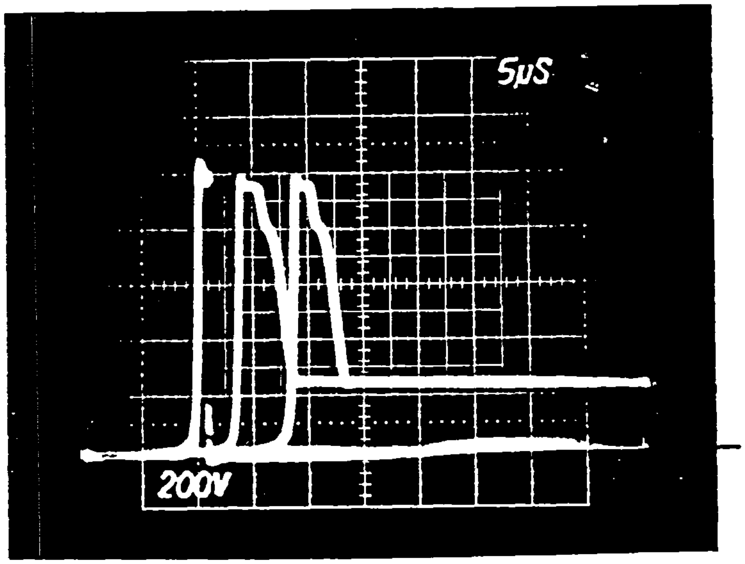

Fig. D.9.3 RBSB test for the Toshiba ST300M21
Test conditions: I_c = 20A; I_{BR} = 8A;
I_{BF} = 2,4,8A.
Scale: 5 µs/div; 200V/div.

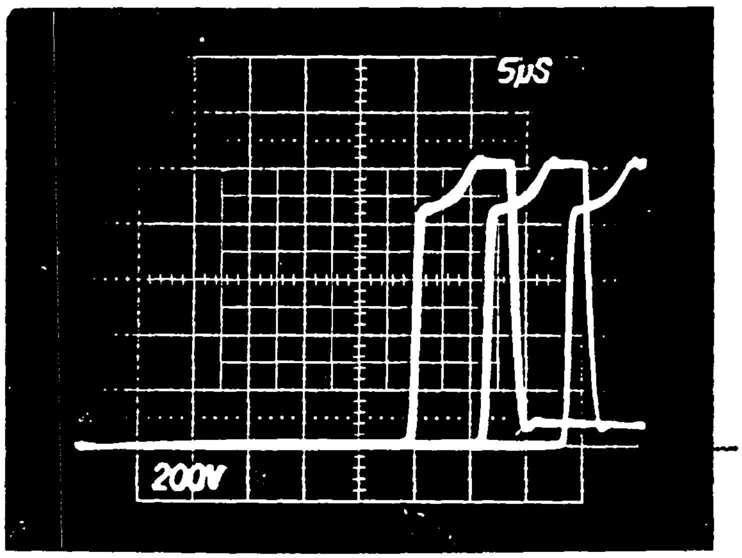

Fig. D.9.4 RBSB test for the Toshiba ST300M21
Test conditions: I_c = 40A; I_{BR} = 2A;
I_{BF} = 2,4,8A.
Scale: 5 µs/div; 200V/div.

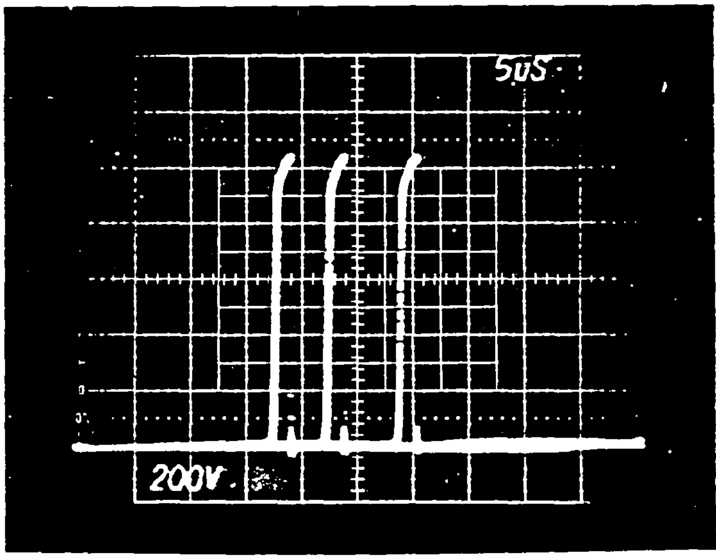

0V

Fig. D.9.5 RBSB test for the Toshiba ST300M21
Test conditions: I_c = 40A; I_{BR} = 4A;
I_{BF} = 2,4,8A.
Scale: 5 μs/div; 200V/div.

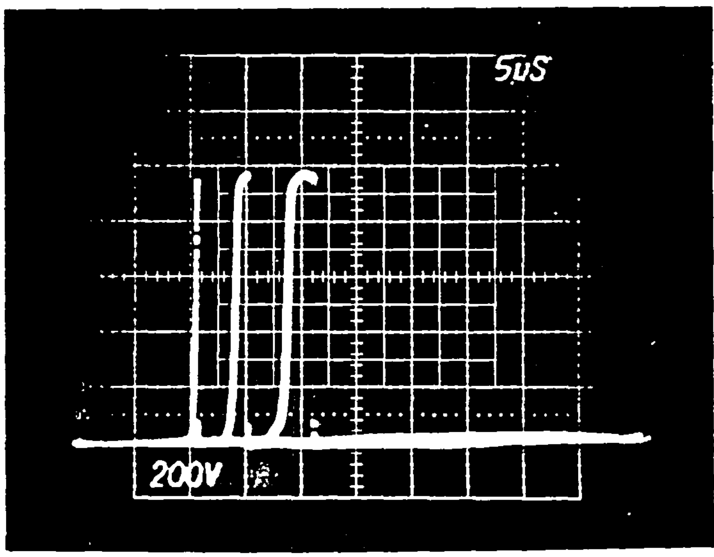

0V

Fig. D.9.6 RBSB test for the Toshiba ST300M21
Test coditions: I_c = 40A; I_{BR} = 8A;
I_{BF} = 2,4,8A.
Scale: 5 μs/div; 200V/div.

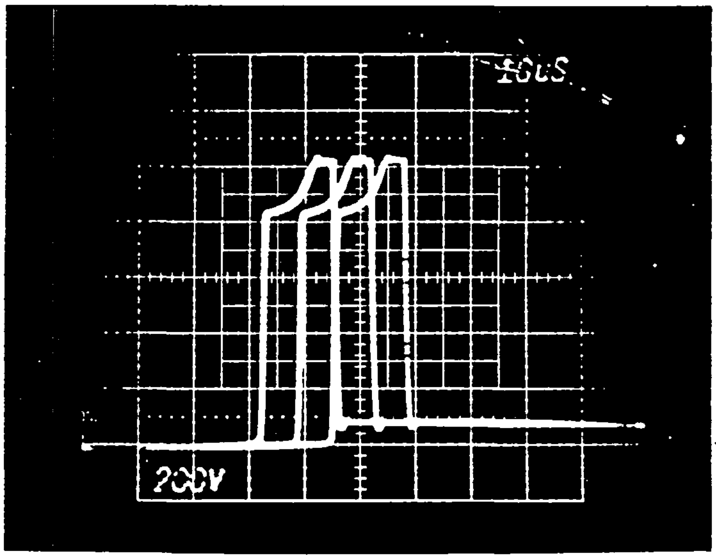

0V

Fig. D.9.7 RBSB test for the Toshiba ST300M21
Test conditions: I_c = 60A; I_{BR} = 2A;
I_{BF} = 2,4,8A.
Scale: 10 μs/div; 200V/div.

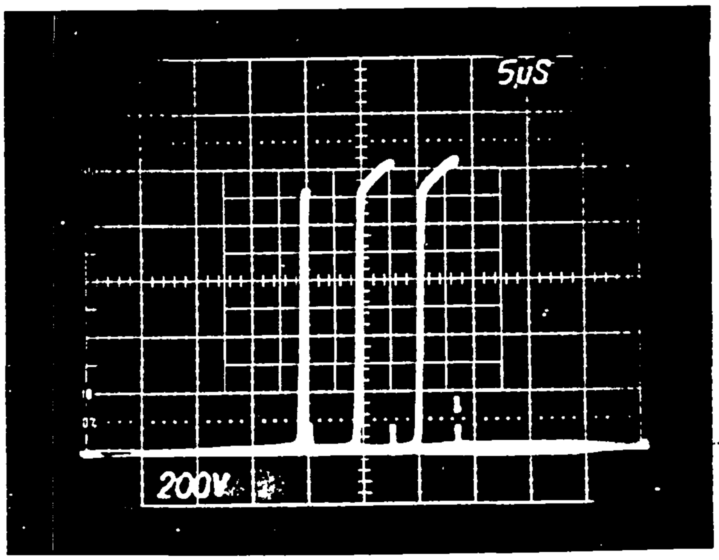

0V

Fig. D.9.8 RBSB test for the Toshiba ST300M21
Test conditions: I_c = 60A; I_{BR} = 4A;
I_{BF} = 2,4,8A.
Scale: 5 μs/div; 200V/div.

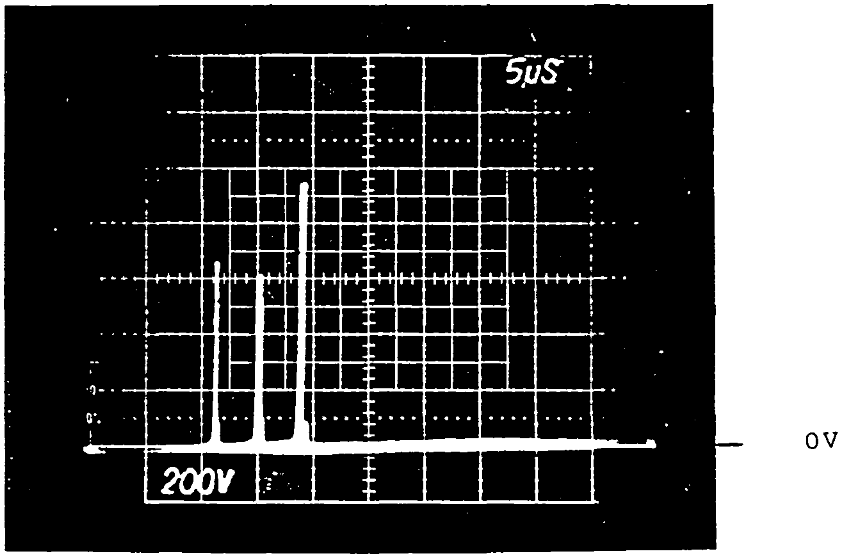

Fig. D.9.9 RBSB test for the Toshiba ST300M21
Test conditions: I_c = 60A; I_{BR} = 8A;
I_{BF} = 2,4,8A.
Scale: 5 μs/div; 200V/div.

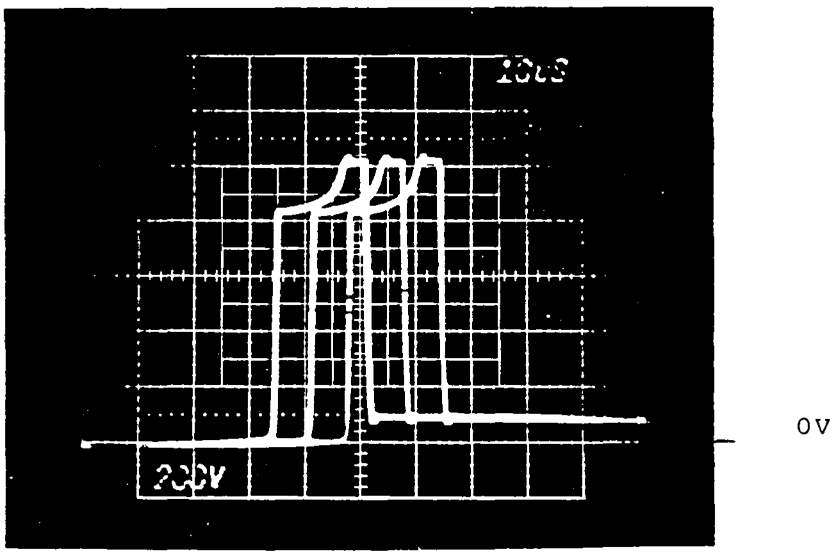

Fig. D.9.10 RBSB test for the Toshiba ST300M21
Test conditions: I_c = 80A; I_{BR} = 2A;
I_{BF} = 2,4,8A.
Scale: 10 μs/div; 200V/div.

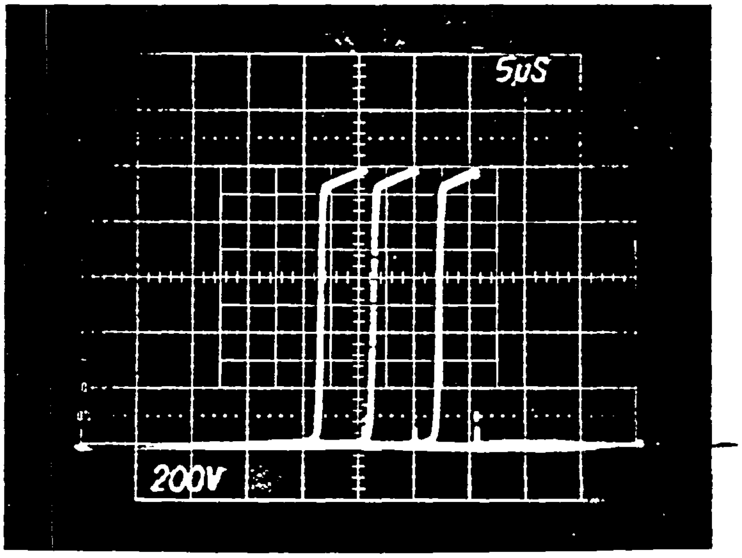

0V

Fig. D.9.11 RBSB test for the Toshiba ST300M21
Test conditions: I_c = 80A; I_{BR} = 4A;
I_{BF} = 2,4,8A.
Scale: 5 μs/div; 200V/div.

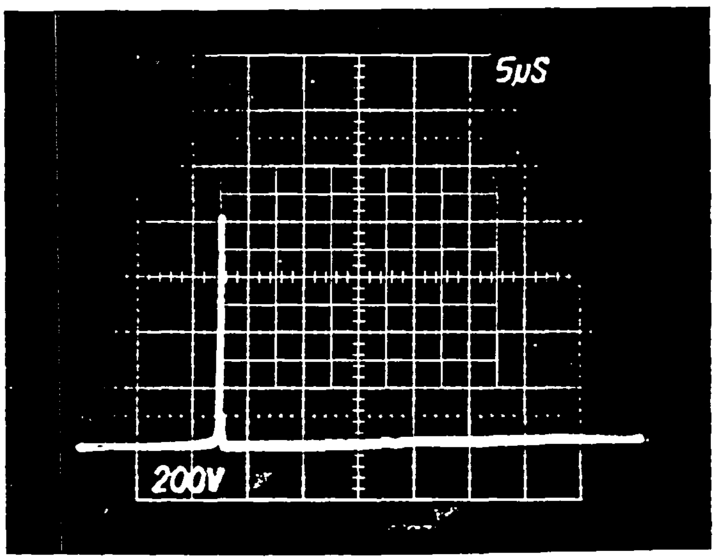

0V

Fig. D.9.12 RBSB test for the Toshiba ST300M21
Test conditions; I_c = 80A; I_{BR} = 8;
I_{BF} = 8; I_{BF} = 2.
Scale: 5 μs/div; 200V/div.

D.10 Test Data of RBSOA of Toshiba ST400G21

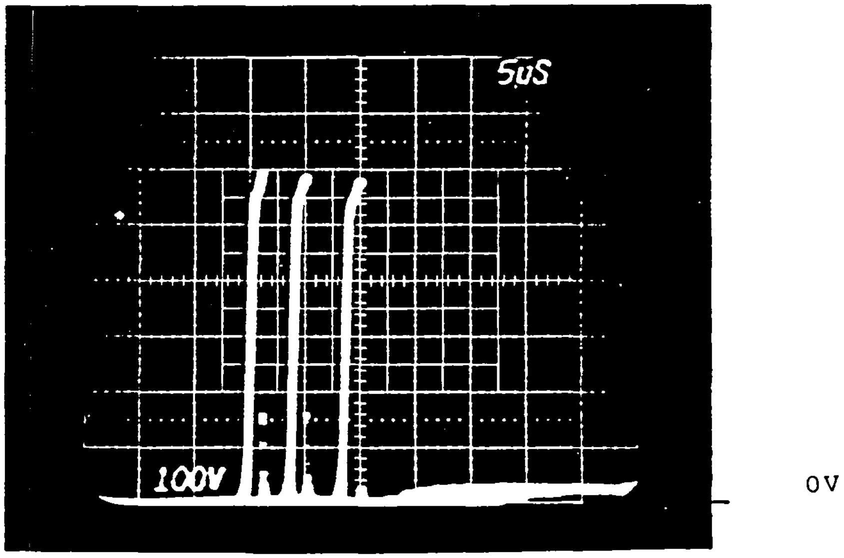

Fig. D.10.1 RBSB test for the Toshiba ST400G21
Test conditions: I_c = 20A; I_{BR} = 2A;
I_{BF} = 2,4,8A
Scale: 5 μs/div; 100V/div.

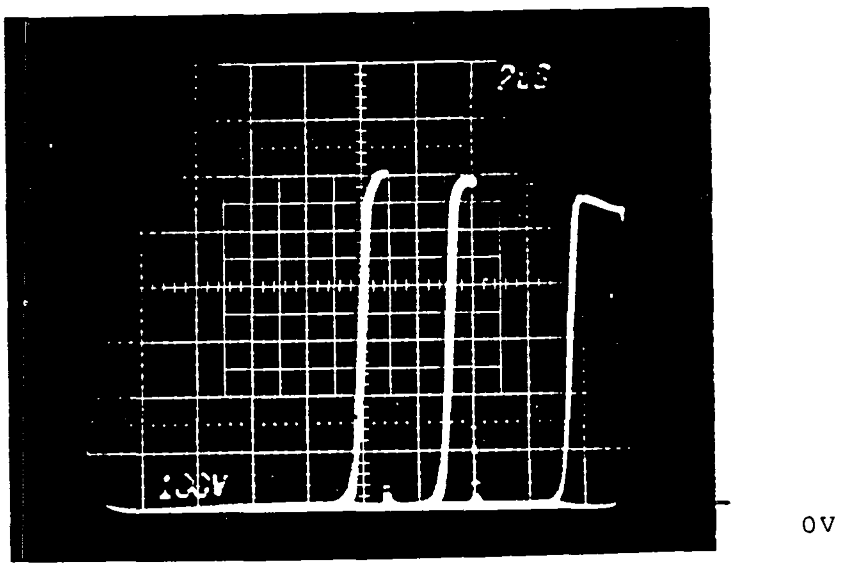

Fig. D.10.2 RBSB test for the Toshiba ST400G21
Test conditions: I_c= 20A; I_{BR} = 4A;
I_{BF} = 2,4,8A.
Scale; 2 μs/div; 100V/div.

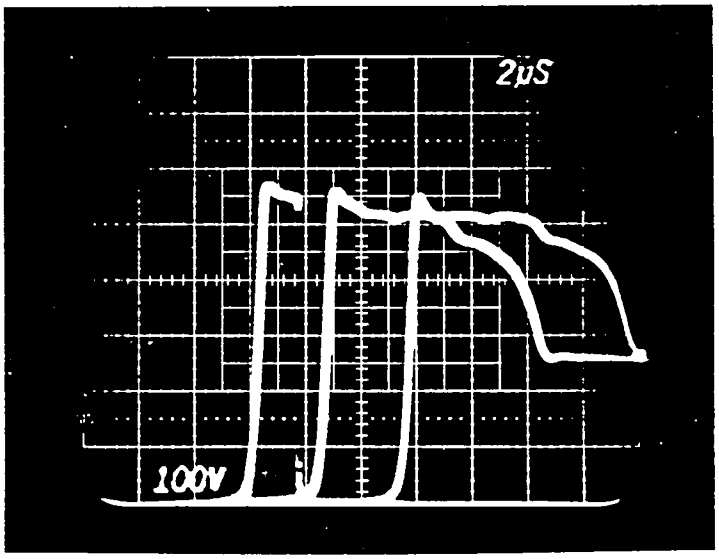

Fig. D.10.3 RBSB test for the Toshiba ST400G21
Test conditions: I_c = 20A; I_{BR} = 8A;
I_{BF} = 2,4,8A.
Scale: 2 µs/div; 100V/div.

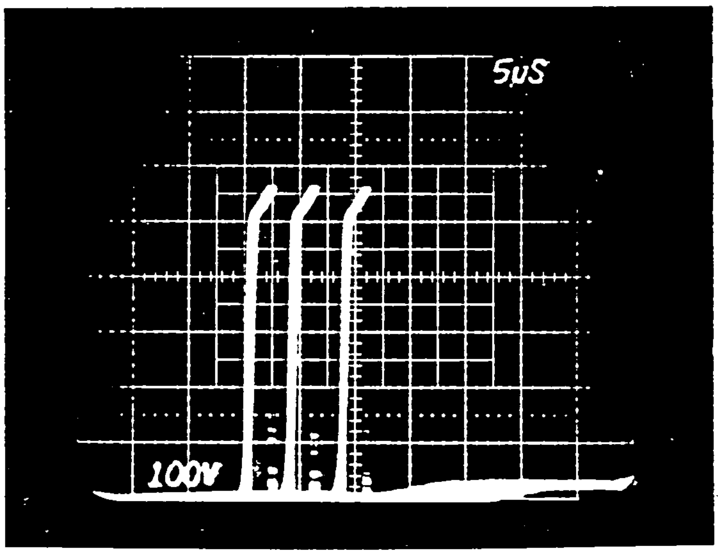

Fig. D.10.4 RBSB test for the Toshiba ST400G21
Test conditions: I_c = 40A; I_{BR} = 8A;
I_{BF} = 2,4,8A.
Scale: 5 µs/div; 100V/div.

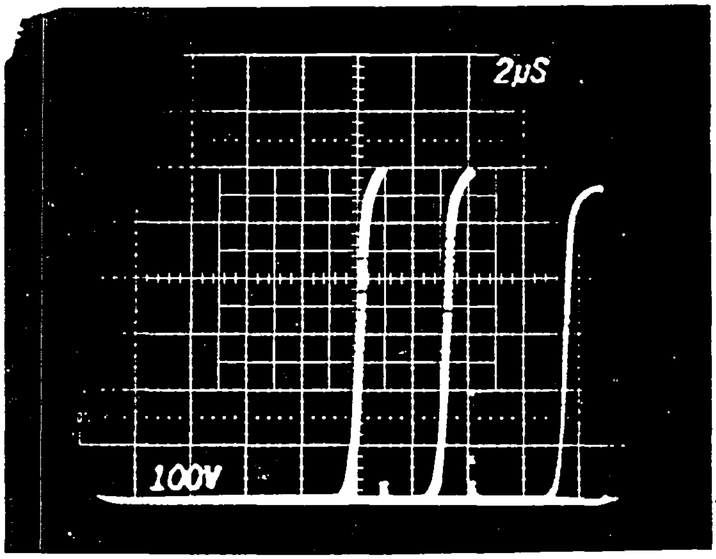

0V

Fig. D.10.5 RBSB test for the Toshiba ST400G21
Test conditions: I_c = 40A; I_{BR} = 2A;
I_{BF} = 2,4,8A.
Scale: 2 μs/div; 100V/div.

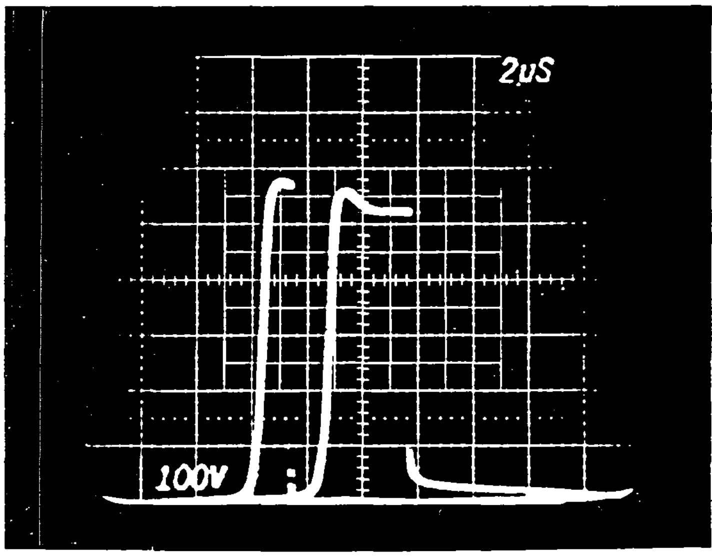

0V

Fig. D.10.6 RBSB test for the Toshiba ST400G21
Test conditions: I_c = 40A; I_{BR} = 8A;
I_{BF} = 2,4A.
Scale: 2 μs/div; 100V/div.

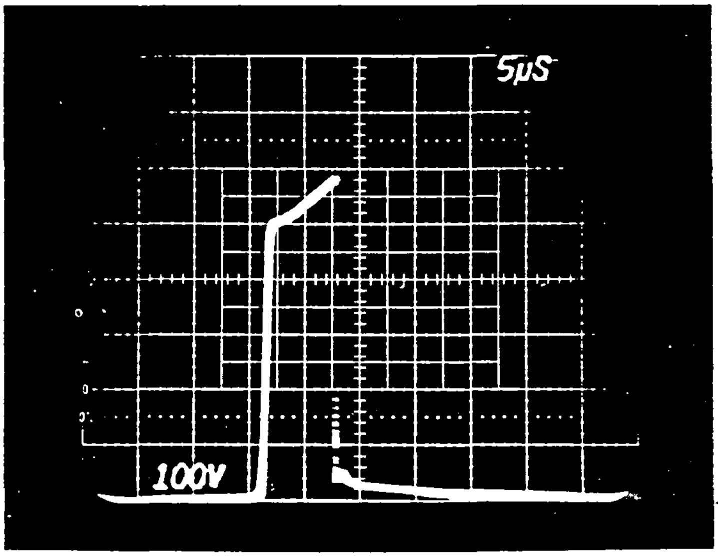

0V

Fig. D.10.7 RBSB test for the Toshiba ST400G21
Test conditions: I_c = 60A; I_{BR} = 2A;
I_{BF} = 2A.
Scale: 5 μs/div; 100V/div.

D.11 Test Data of RBSOA of Toshiba ST400G

RBSOA not characterized

D.12 Test Data of RBSOA at Elevated Temperature

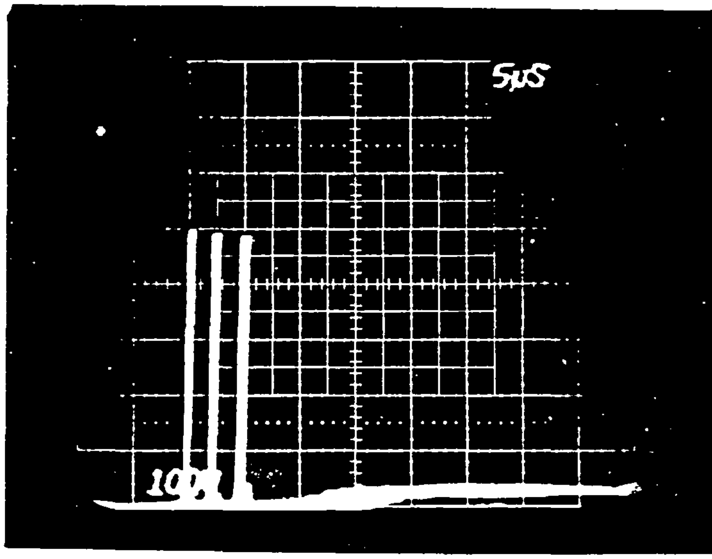

0V

Fig. D.12.1 RBSB test for the Fuji EVM31-050 at T_c=30°C. Test conditions: I_c=20A; I_{BR}=2A; I_{BF}=2,4,8A.
Scale: 5 µs/div; 100 V/div.

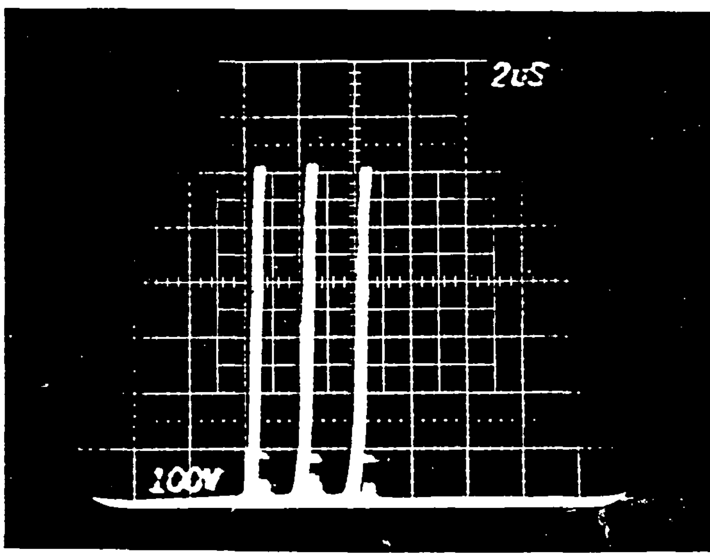

0V

Fig. D.12.2 RBSB test for the Fuji EVM31-050 at T_c=30°C. Test conditions: I_c=20A; I_{BR}=4A; I_{BF}=2,4,8A.
Scale: 2 µs/div; 100 V/div.

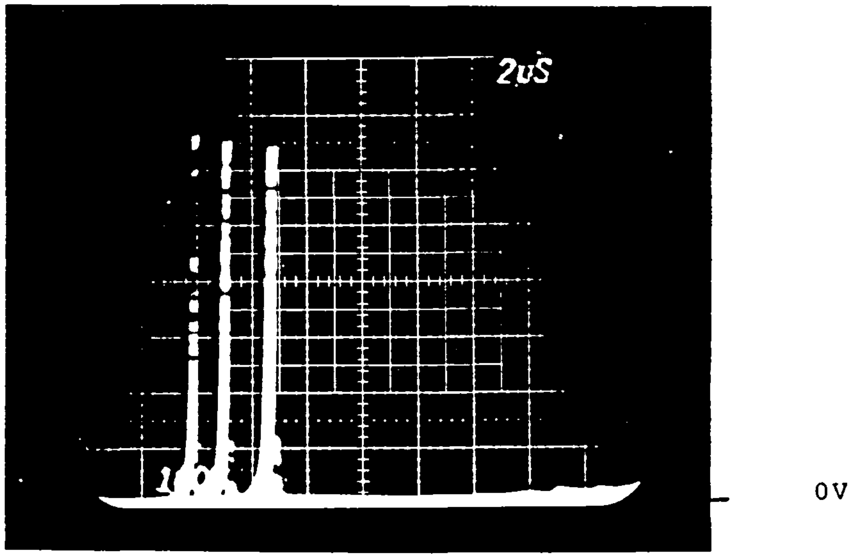

Fig. D.12.3 RBSB test for the Fuji EVM31-050 at T_c=30°C. Test conditions: I_c=20A; I_{BR}=8A; I_{BF}=2,4,8A.
Scale: 2 μs/div; 100 V/div.

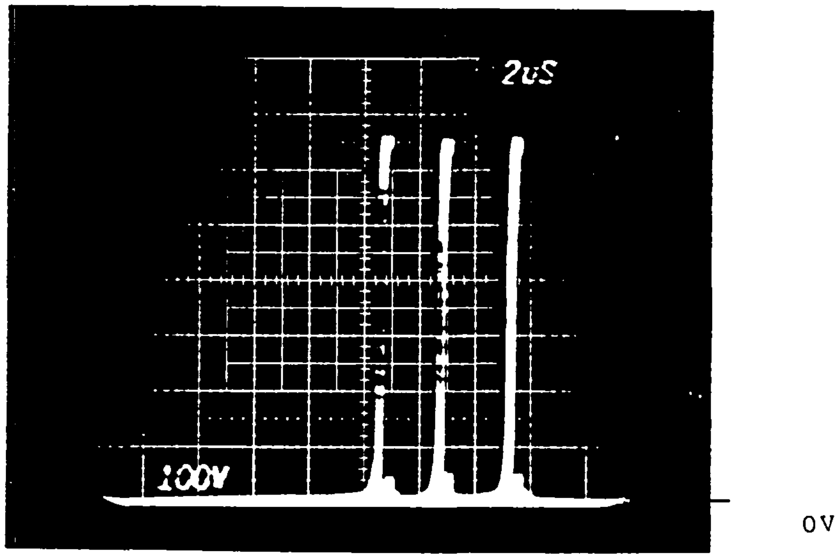

Fig. D.12.4 RBSB test for the Fuji EVM31-050 at T_c=30°C. Test conditions: I_c=40A; I_{BR}=2A; I_{BF}=2,4,8A.
Scale: 2 μs/div; 100 V/div.

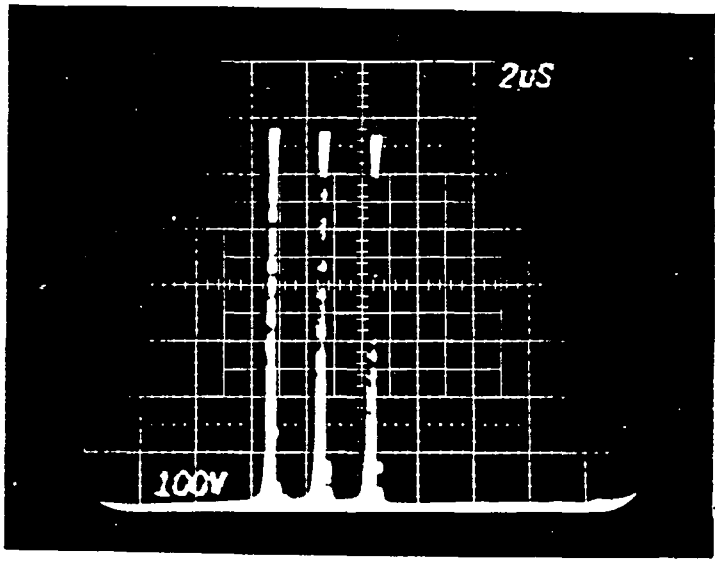

0V

Fig. D.12.5 RBSB test for the Fuji EVM31-050 at T_c=30°C. Test conditions: I_C=40A; I_{BR}=4A; I_{BF}=2,4,8A.
Scale: 2 μs/div; 100 V/div.

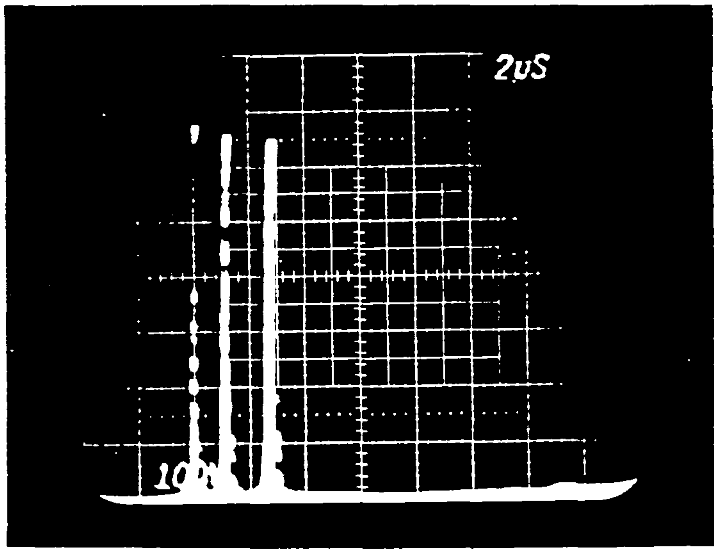

0V

Fig. D.12.6 RBSB test for the Fuji EVM31-050 at T_c=30°C. Test conditions: I_C=40A; I_{BR}=8A; I_{BF}=2,4,8A.
Scale: 2 μs/div; 100 V/div.

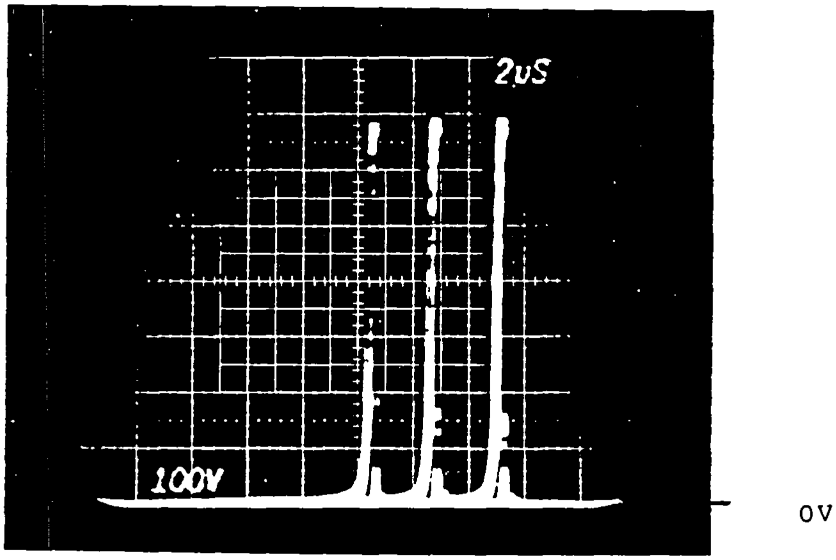

Fig. D.12.7 RBSB test for the Fuji EVM31-050 at T_c=30°C. Test conditions: I_c=60A; I_{BR}=2A; I_{BF}=2,4,8A.
Scale: 2 μs/div; 100 V/div.

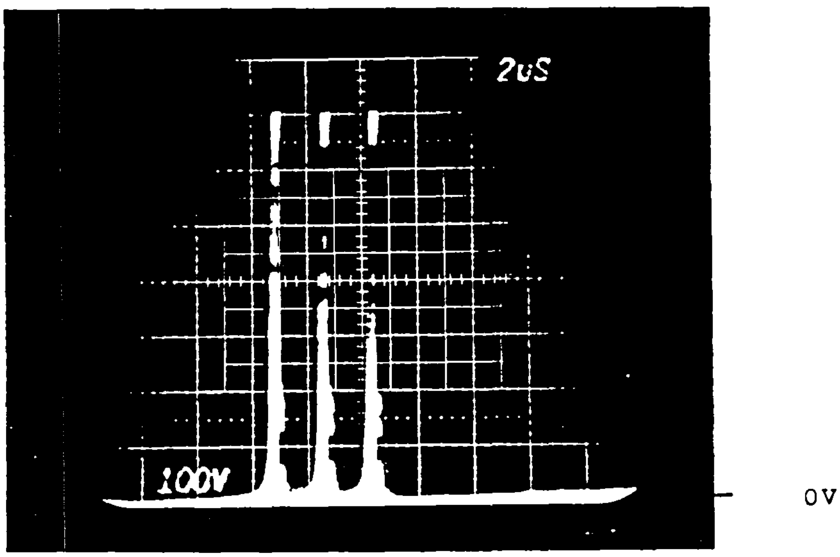

Fig. D.12 8 RBSB test for the Fuji EVM31-050 at T_c=30°C. Test conditions: I_c=60A; I_{BR}=4A; I_{BF}=2,4,8A.
Scale: 2 μs/div; 100 V/div.

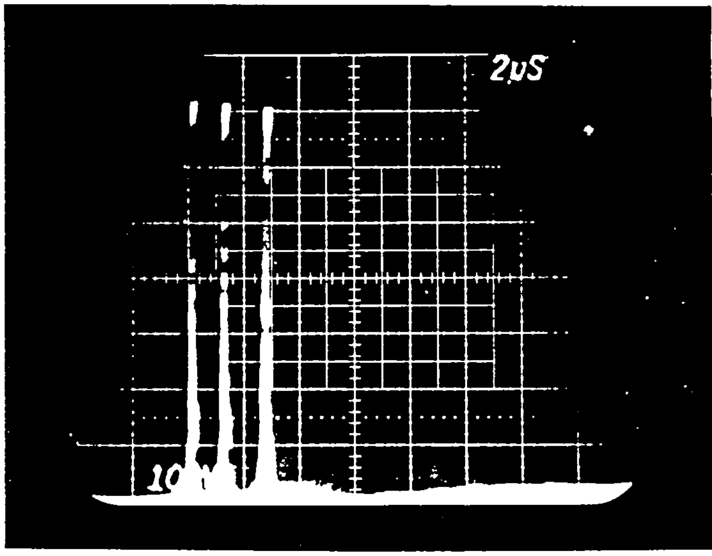

0V

Fig. D.12.9 RBSB test for the Fuji EVM31-050 at T_c=30°C. Test conditions: I_c=60A; I_{BR}=8A; I_{BF}=2,4,8A.
Scale: 2 µs/div; 100 V/div.

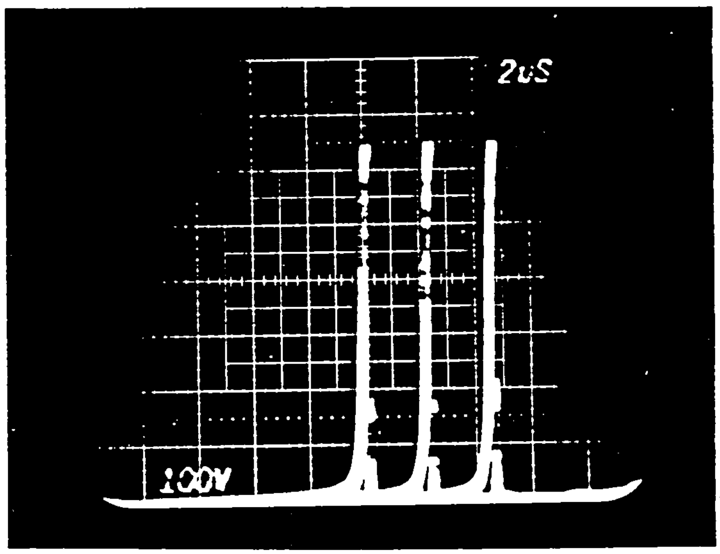

0V

Fig D.12.10 RBSB test for the Fuji EVM31-050 at T_c=30°C. Test conditions: I_c=80A; I_{BR}=2A; I_{BF}=2,4,8A.
Scale: 2 µs/div; 100 V/div.

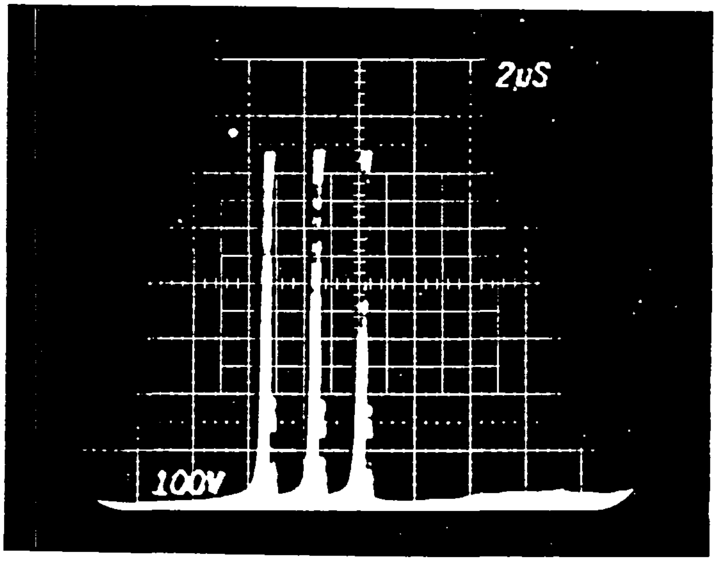

0V

Fig. D.12.11 RBSB test for the Fuji EVM31-050 at T_C=30°C. Test conditions: I_C=80A; I_{BR}=4A; I_{BF}=2,4,8A.
Scale: 2 µs/div; 100 V/div.

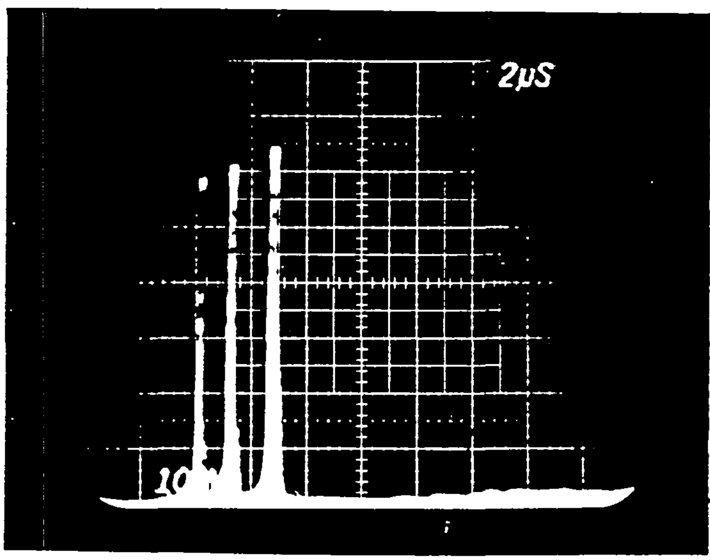

0V

Fig. D.12.12 RBSB test for the Fuji EVM31-050 at T_C=30°C. Test conditions: I_C=80A; I_{BR}=8A; I_{BF}=2,4,8A.
Scale: 2 µs/div; 100 V/div.

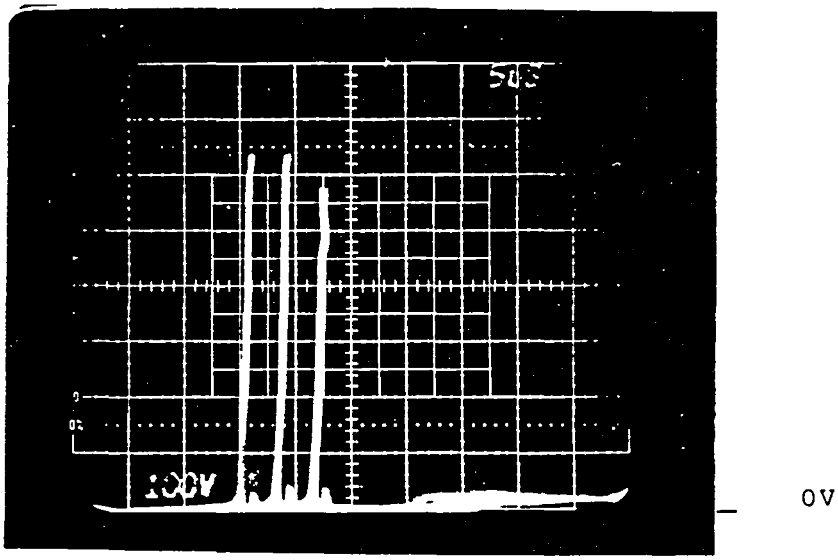

Fig. D.12.13 RBSB test for the Fuji EVM31-050 at T_c=100°C. Test conditions: I_c=20A; I_{BR}=2 A; I_{BF}=2,4,8A.
Scale: 2 μs/div; 100 V/div.

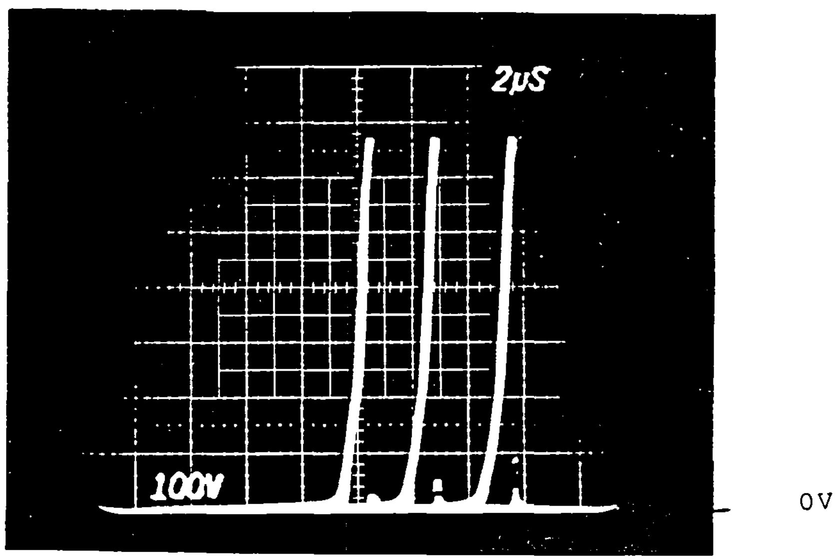

Fig. D.12.14 RBSB test for the Fuji EVM31-050 at T_c=100°C. Test conditions. I_c=20A; I_{BR}=4 A; I_{BF}=2,4,8A.
Scale: 2 μs/div, 100 V/div.

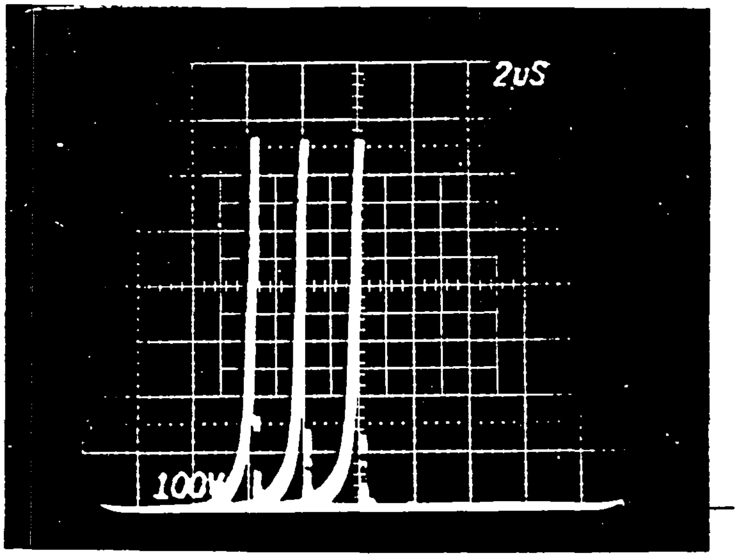

Fig. D.12.15 RBSB test for the Fuji EVM31-050 at
T_c=100°C. Test conditions: I_c=20A; I_{BR}=8A;
I_{BF}=2,4,8A.
Scale: 2 μs/div; 100 V/div.

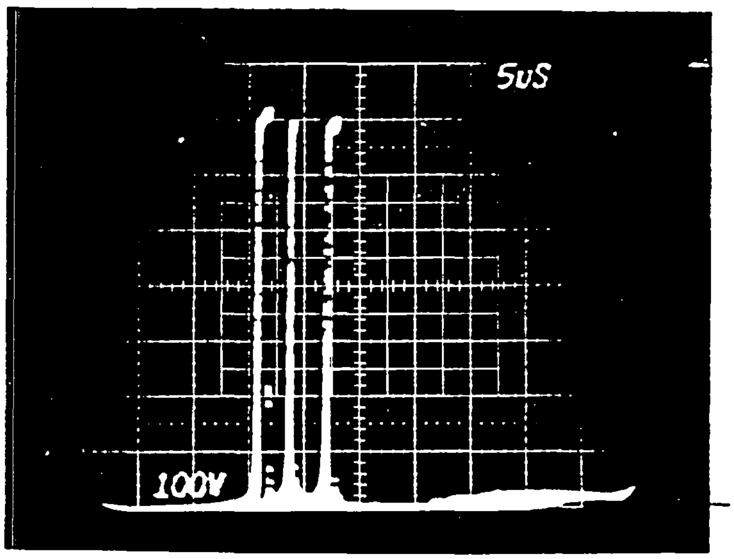

Fig. D.12.16 RBSB test for the Fuji EVM31-050 at
T_c=100°C. Test conditions: I_c=40A; I_{BR}=2A;
I_{BF}=2,4,8A.
Scale: 2 μs/div; 100 V/div.

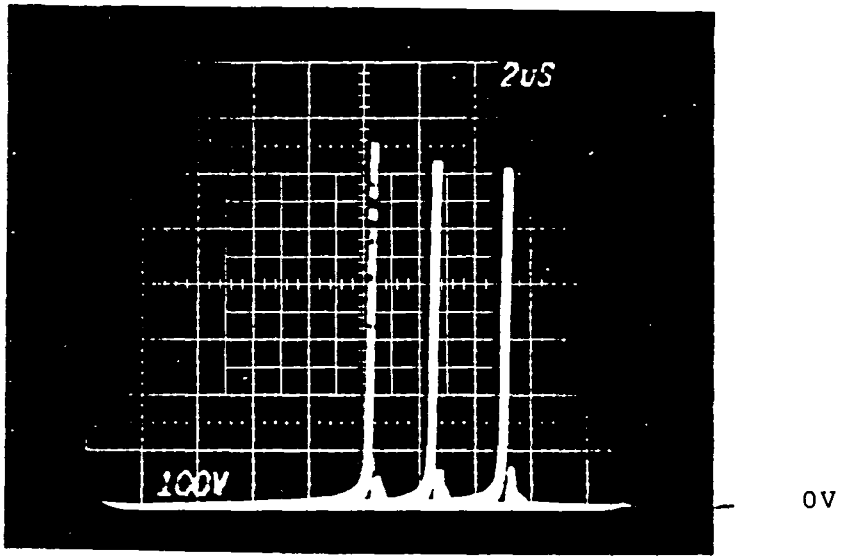

Fig. D.12.17 RBSB test for the Fuji EVM31-050 at T_C=100°C. Test conditions: I_C=40A; I_{BR}=4A; I_{BF}=2,4,8A.
Scale: 2 μs/div; 100 V/div.

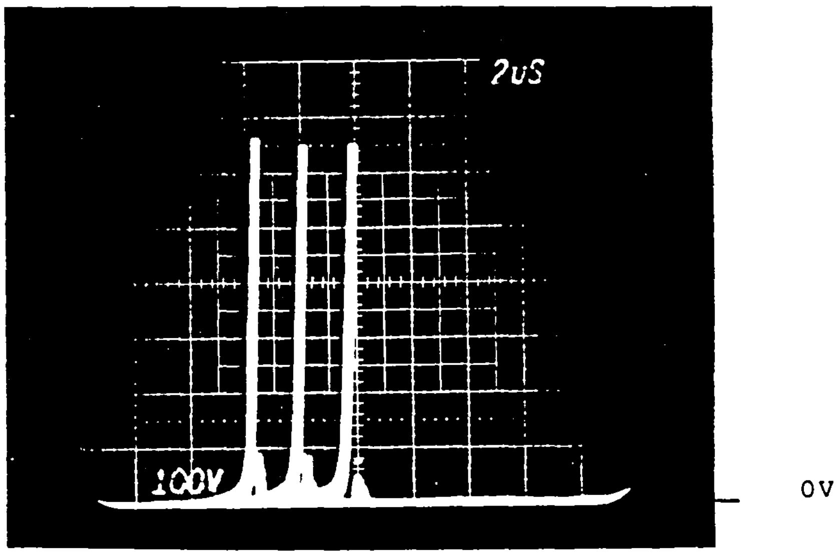

Fig. D.12.18 RBSB test for the Fuji EVM31-050 at T_C=100°C. Test conditions: I_C=40A; I_{BR}=8A; I_{BF}=2,4,8A.
Scale: 2 μs/div; 100 V/div.

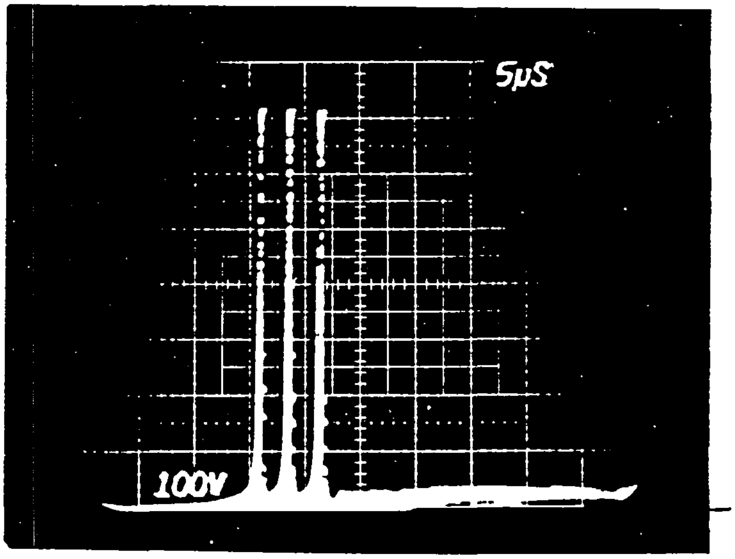

0 V

Fig. D.12.19 RBSB test for the Fuji EVM31-050 at T_c=100°C. Test conditions: I_c=60A; I_{BR}=2 A; I_{BF}=2,4,8A.
Scale: 2 μs/div; 100 V/div.

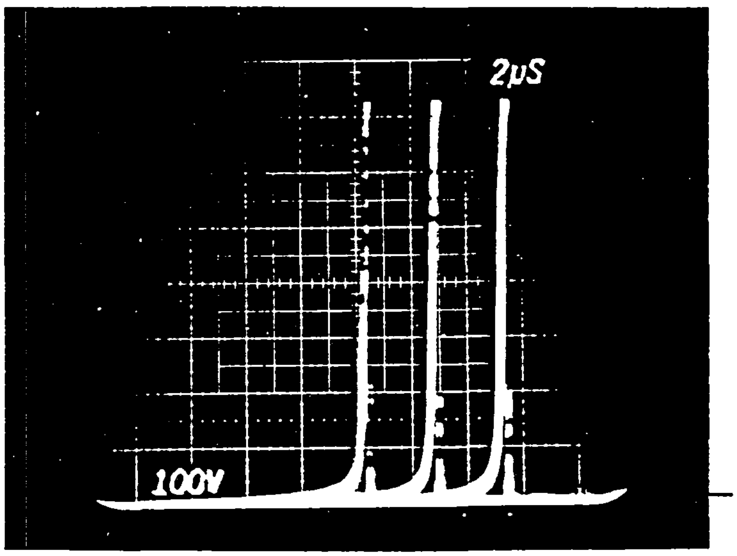

0 V

Fig. D.12.20 RBSB test for the Fuji EVM31-050 at T_c=100°C. Test conditions: I_c=60A; I_{BR}=4 A; I_{BF}=2,4,8A.
Scale: 2 μs/div; 100 V/div.

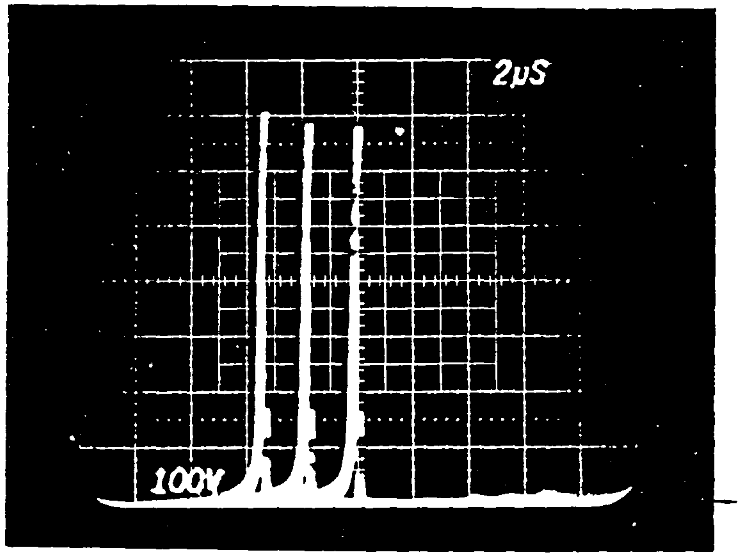

Fig. D.12.21 RBSB test for the Fuji EVM31-050 at T_C=100°C. Test conditions: I_C=60A; I_{BR}=8A; I_{BF}=2,4,8A.
Scale: 2 μs/div; 100 V/div.

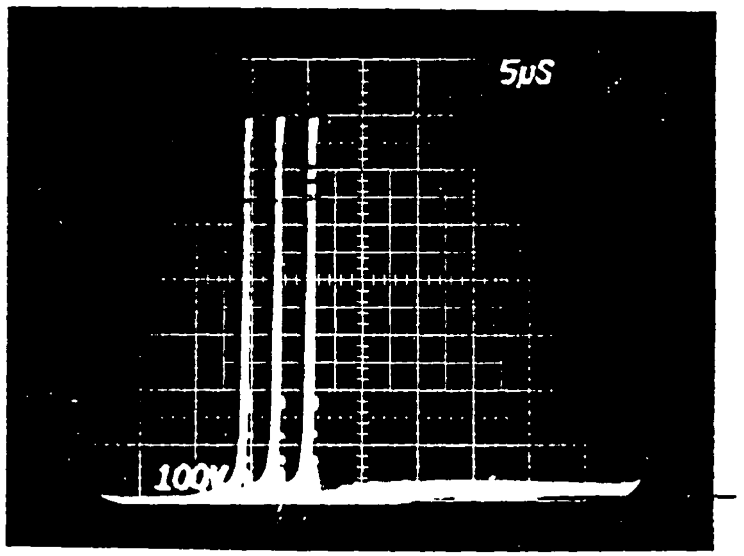

Fig. D.12.22 RBSB test for the Fuji EVM31-050 at T_C=100°C. Test conditions: I_C=80A; I_{BR}=2A; I_{BF}=2,4,8A.
Scale: 2 μs/div; 100 V/div.

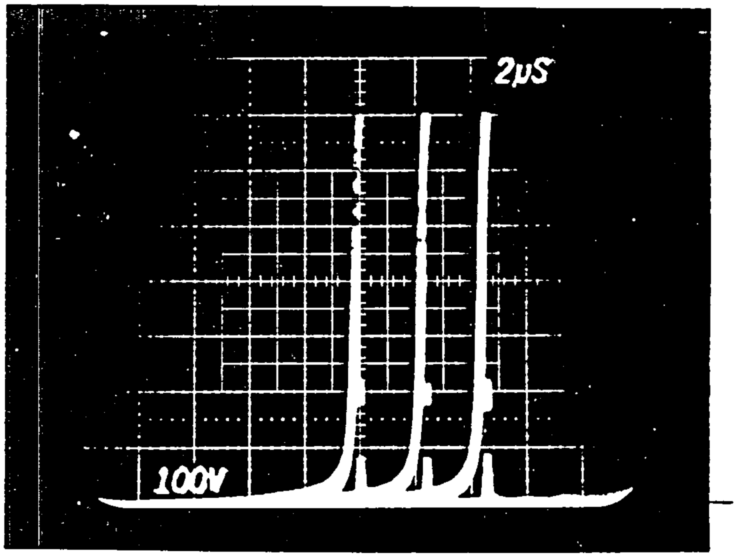

0V

Fig. D.12.23 RBSB test for the Fuji EVM31-050 at T_c=100°C. Test conditions: I_c=80A; I_{BR}=4A; I_{BF}=2,4,8A.
Scale: 2 μs/div; 100 V/div.

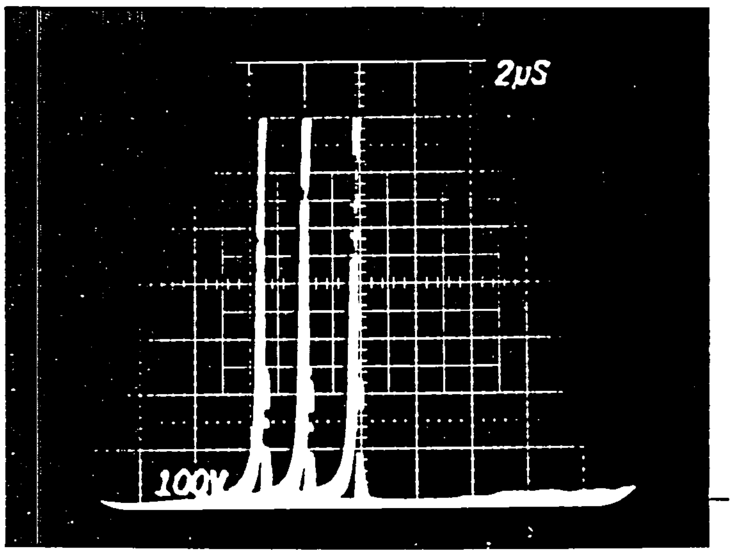

0V

Fig. D.12.24 RBSB test for the Fuji EVM31-050 at T_c=100^{o}C. Test conditions. I_c=80A; I_{BR}=8A; I_{BF}=2,4,8A.
Scale. 2μs/div; 100 V/div.

D.13 Test Data of RBSOA with Second Base Drive

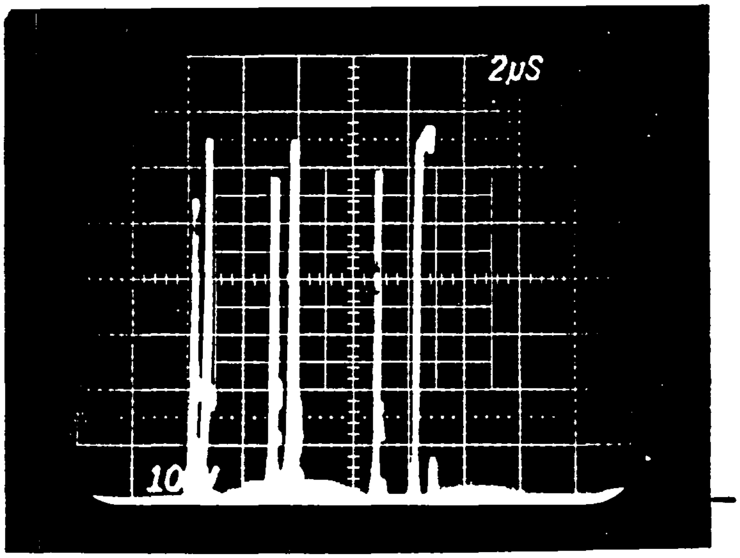

Fig. D.13.1 RBSB behavior at the Westinghouse KD324510 with the second base drive and without the second base drive being used. Test conditions: I_c = 20A; I_{BF} = 4A; I_{BR} = 8,4,2A; I_{BR2} = 8,4,4A.
Scale: 2 μs/div; ·100V/div.
(The 1st, 3rd and 5th waveterms counting from the left correspond to I_{BR} = 8,4,2A respectively while the 2nd, 4th and 6th correspond to tests with I_{BR2} = 8,4,4A, respectively).

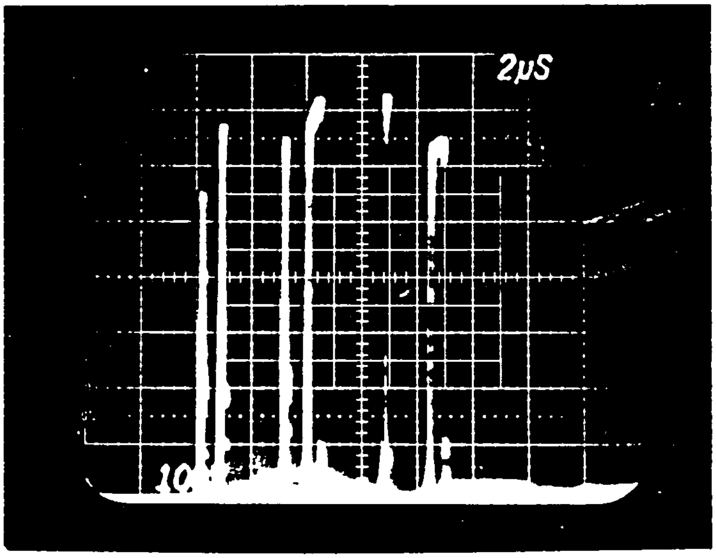

0V

Fig. D.13.2 RBSB behavior at the Westinghouse KD324510 with the second base drive and without the second base drive being used. Test condtions: I_c = 40A; I_{BF} = 4A; I_{BR} = 8,4,2A; I_{BR2} = 8,4,4A.

Scale: 2 μs/div; 100V/div.
(The 1st, 3rd and 5th waveterms counting from the left correspond to I_{BR} = 8,4,2A respectively while the 2nd, 4th and 6th correspond to tests with I_{BR2} = 8,4,4A, respectively).

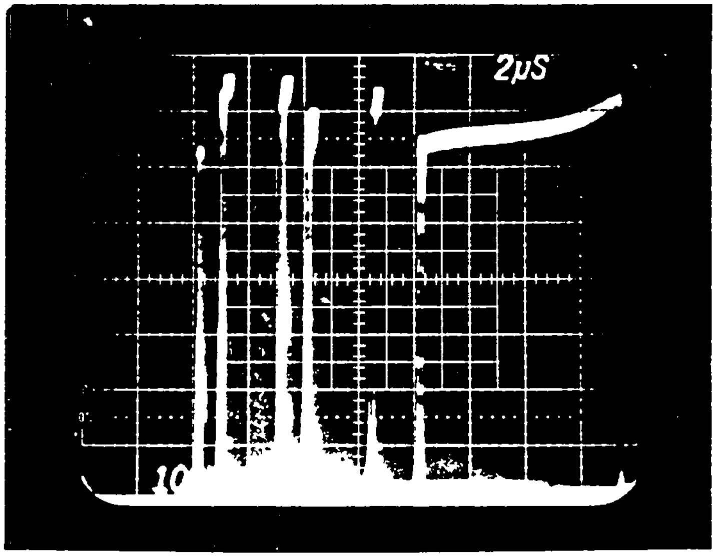

0V

Fig. D.13.3 RBSB behavior at the Westinghouse KD324510 with the second base drive and without the second base drive being used. Test conditions: I_c = 60A; I_{BF} = 4A; I_{BR} = 8,4,2A; I_{BR2} = 8,4,4A.
Scale: 2 μs/div; 100V/div.
(The 1st, 3rd and 5th waveterms counting from the left correspond to I_{BR} = 8,4,2A respectively while the 2nd, 4th and 6th correspond to tests with I_{BR2} = 8,4,4A, respectively).

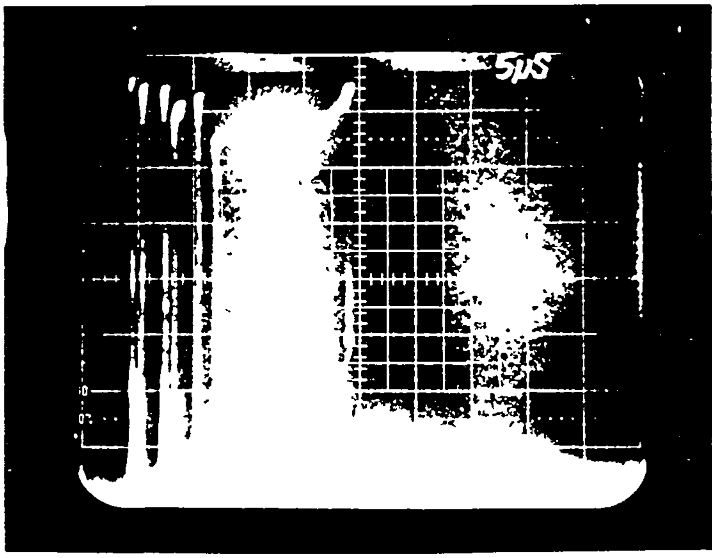

OV

Fig. D.13.4 RBSB behavior of the Westinghouse KD324510 with the second base drive and without the second base drive being used. Test conditions: I_C = 80A; I_{BF} = 4A; I_{BR} = 8,4,2A; I_{BR2} = 8,4,4A.
Scale: 2µs/div; 100V/div.
(The 1st, 3rd and 5th waveterms counting from the left correspond to I_{BR} = 8,4,2A respectively while the 2nd, 4th and 6th correspond to tests with I_{BR2} = 8,4,4A, respectively).

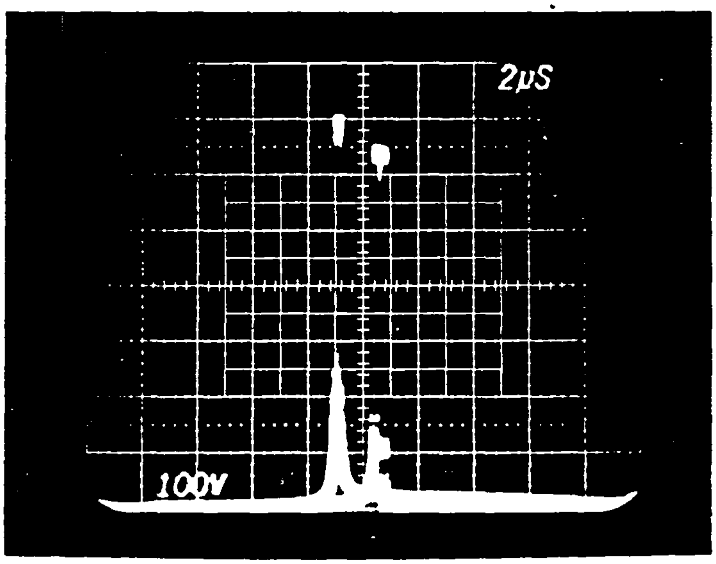

0V

Fig. D.13.5 RBSB behavior of the Westinghouse KD324510 with the second base drive being used. Test conditions: I_c = 100A; I_{BF} = 4A; I_{BR} = 2; I_{BR2} = 4A
Scale: 2 μs/div; 100V/div.
(The 1st waveterm corresponds to the second base drive test while 2nd represents test without 2nd base drive.)

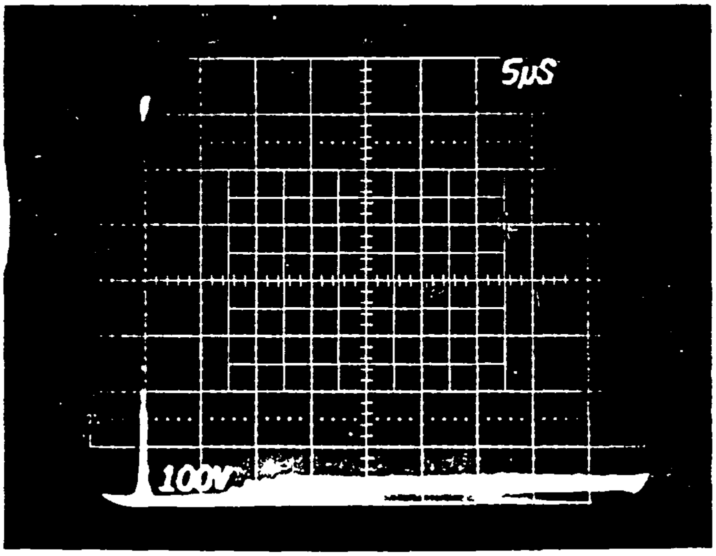

0V

Fig. D.13.6 Repeated RBSB tests for Westinghouse KD324510 as a check of the SB characteristic repeatability. Test conditions: I_c = 80A; I_{BF} = 4A; I_{BR} = 8A.
Scale: 5 μs/div; 100V/div.
(Note the same SB voltage for the same conditions in Fig. D.13.4.)

APPENDIX E

TEST DATA OF MOSFETs ON-RESISTANCE CHARACTERIZATION

E.1 Test Data of On-Resistance Characterization of the IRF441

Fig. E.1.1.

Rds(on) vs. Id for IRF 441 @ Tc=30 C

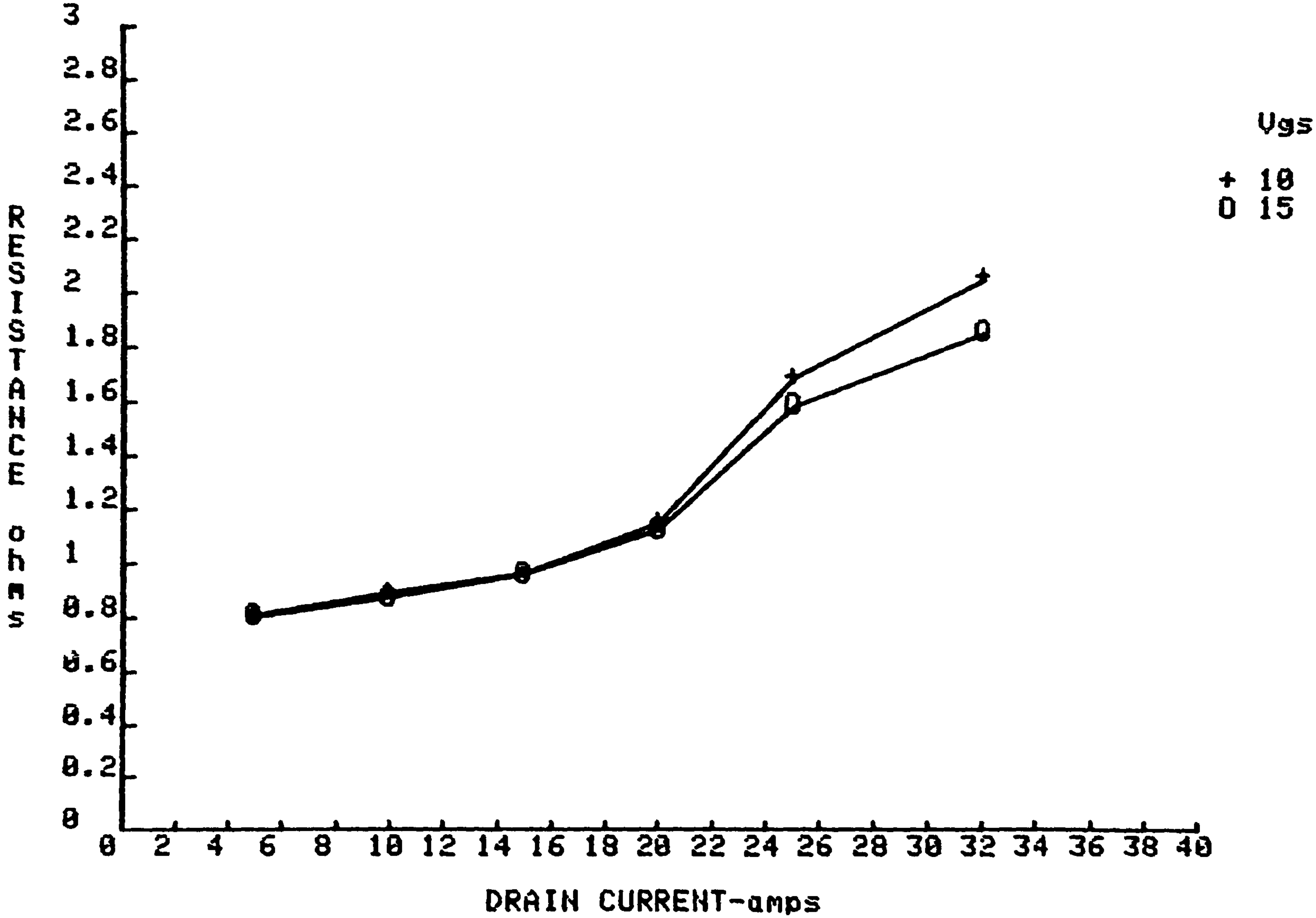

Fig. E.1.2.

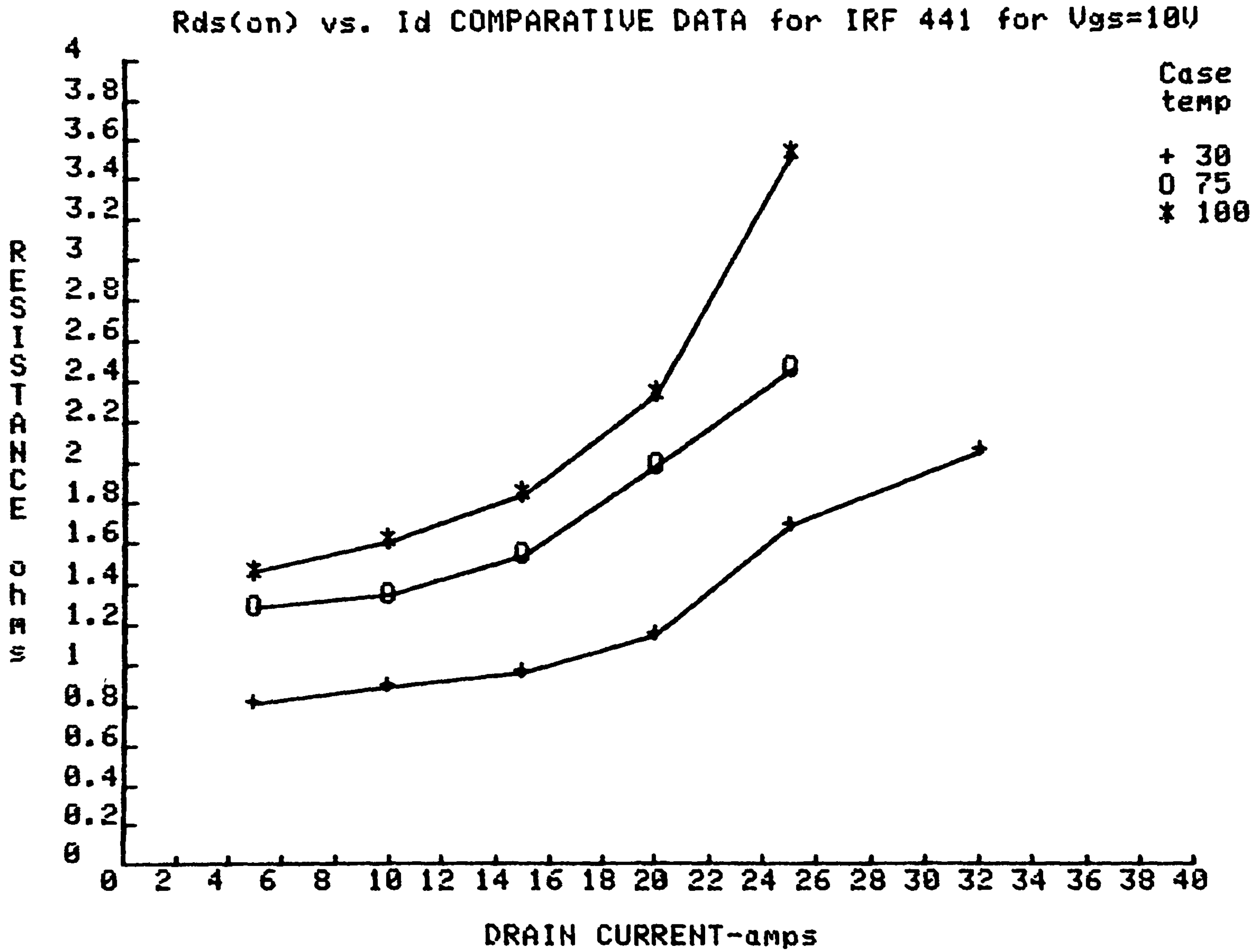
Rds(on) vs. Id COMPARATIVE DATA for IRF 441 for Vgs=10V
RESISTANCE ohms
4
3.8
3.6
3.4
3.2
3
2.8
2.6
2.4
2.2
2
1.8
1.6
1.4
1.2
1
0.8
0.6
0.4
0.2
0
0 2 4 6 8 10 12 14 16 18 20 22 24 26 28 30 32 34 36 38 40
DRAIN CURRENT-amps
Case temp
+ 30
O 75
* 100

E.2 Test Data of On-Resistance Characterization of the RCA RFK15N45

Fig. E.[illegible].1.

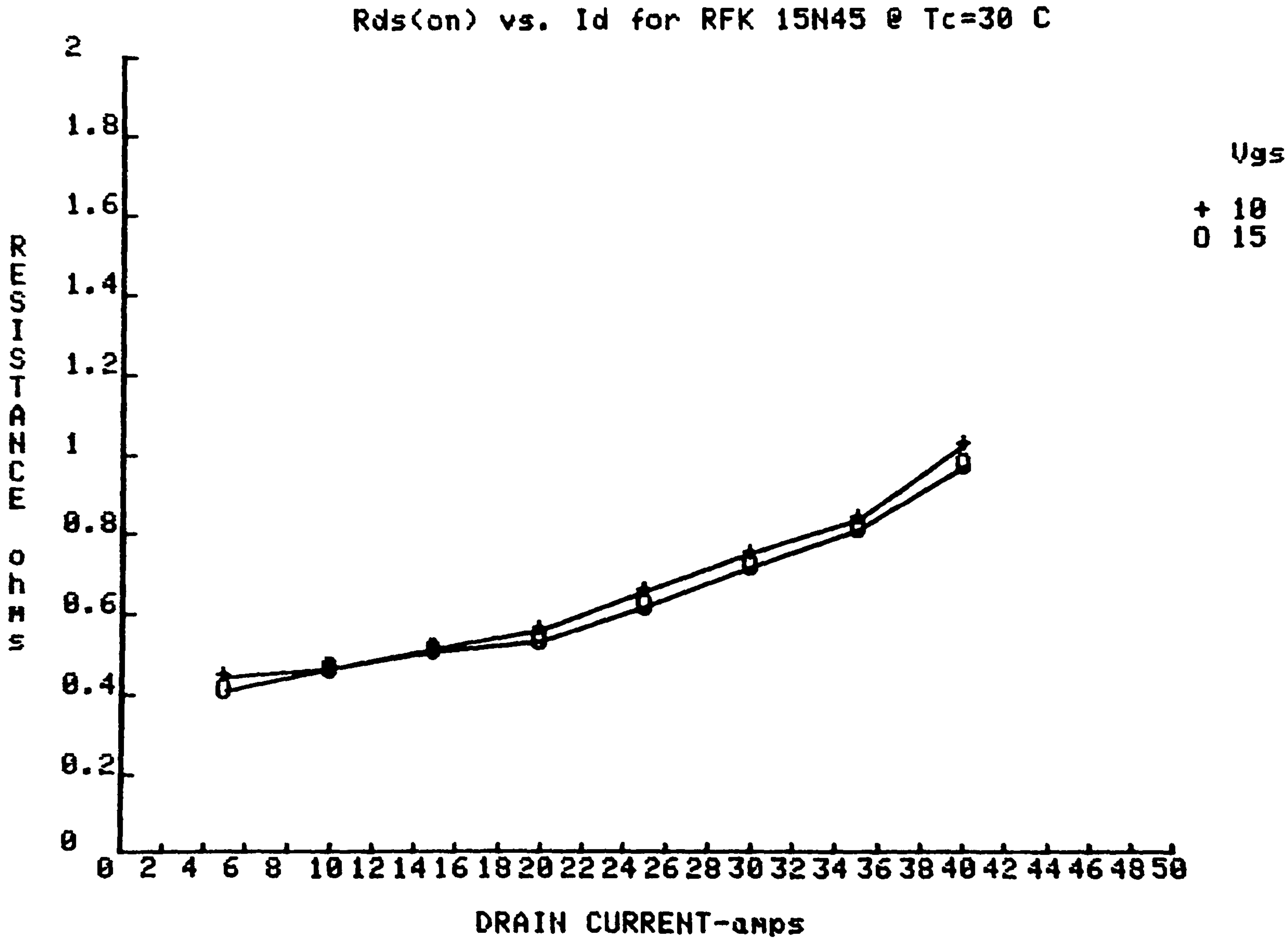
Rds(on) vs. Id for RFK 15N45 @ Tc=30 C
RESISTANCE ohms
2
1.8
1.6
1.4
1.2
1
0.8
0.6
0.4
0.2
0
0 2 4 6 8 10 12 14 16 18 20 22 24 26 28 30 32 34 36 38 40 42 44 46 48 50
DRAIN CURRENT-amps
Vgs
+ 10
O 15

Fig. E.2.2.

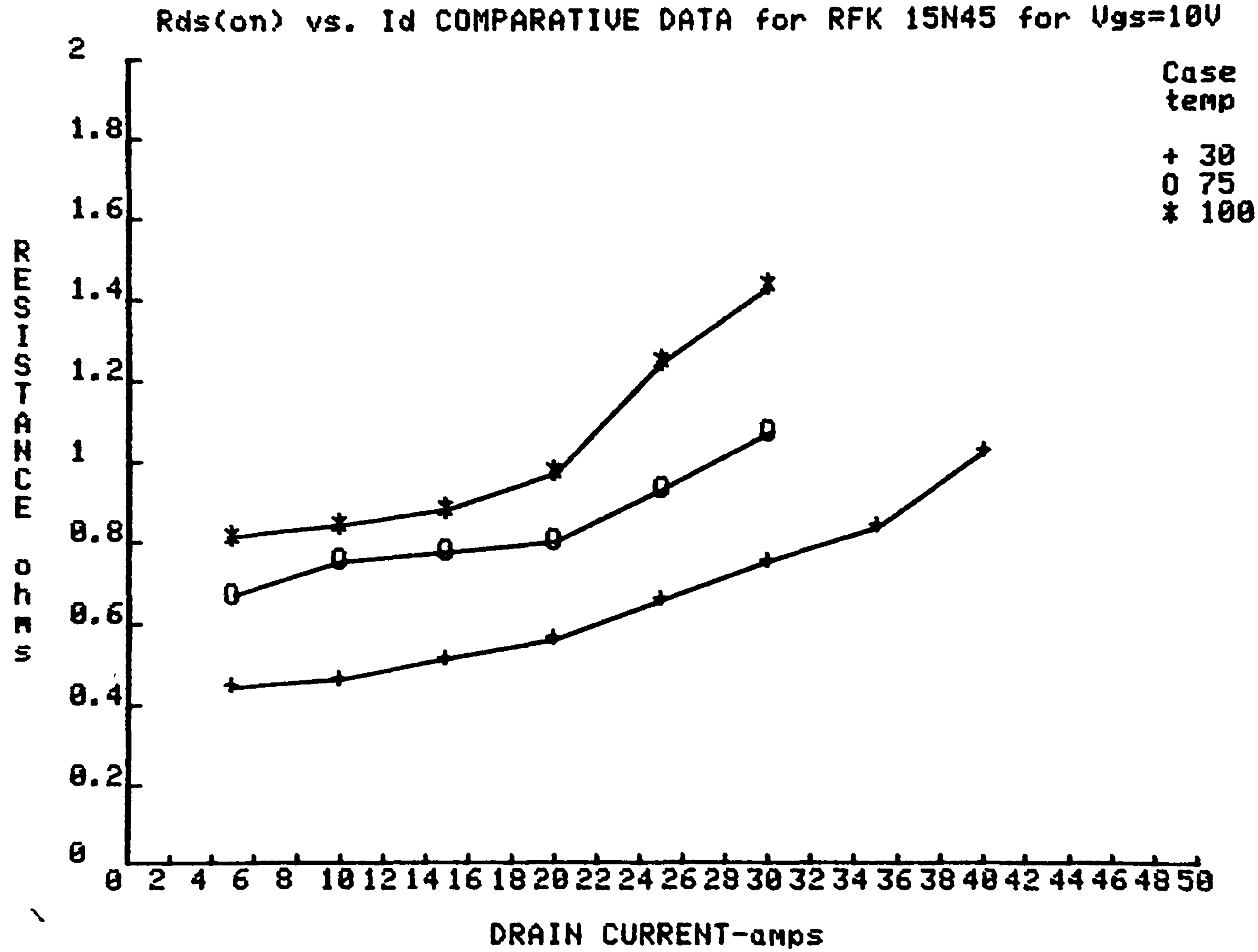
Rds(on) vs. Id COMPARATIVE DATA for RFK 15N45 for Vgs=10V
RESISTANCE ohms
2
1.8
1.6
1.4
1.2
1
0.8
0.6
0.4
0.2
0
0 2 4 6 8 10 12 14 16 18 20 22 24 26 28 30 32 34 36 38 40 42 44 46 48 50
DRAIN CURRENT-amps
Case temp
+ 30
0 75
* 100

E.7

E.3 Test Data of On-Resistance Characterization of the RCA RFK15N50

Fig. E.3.1.

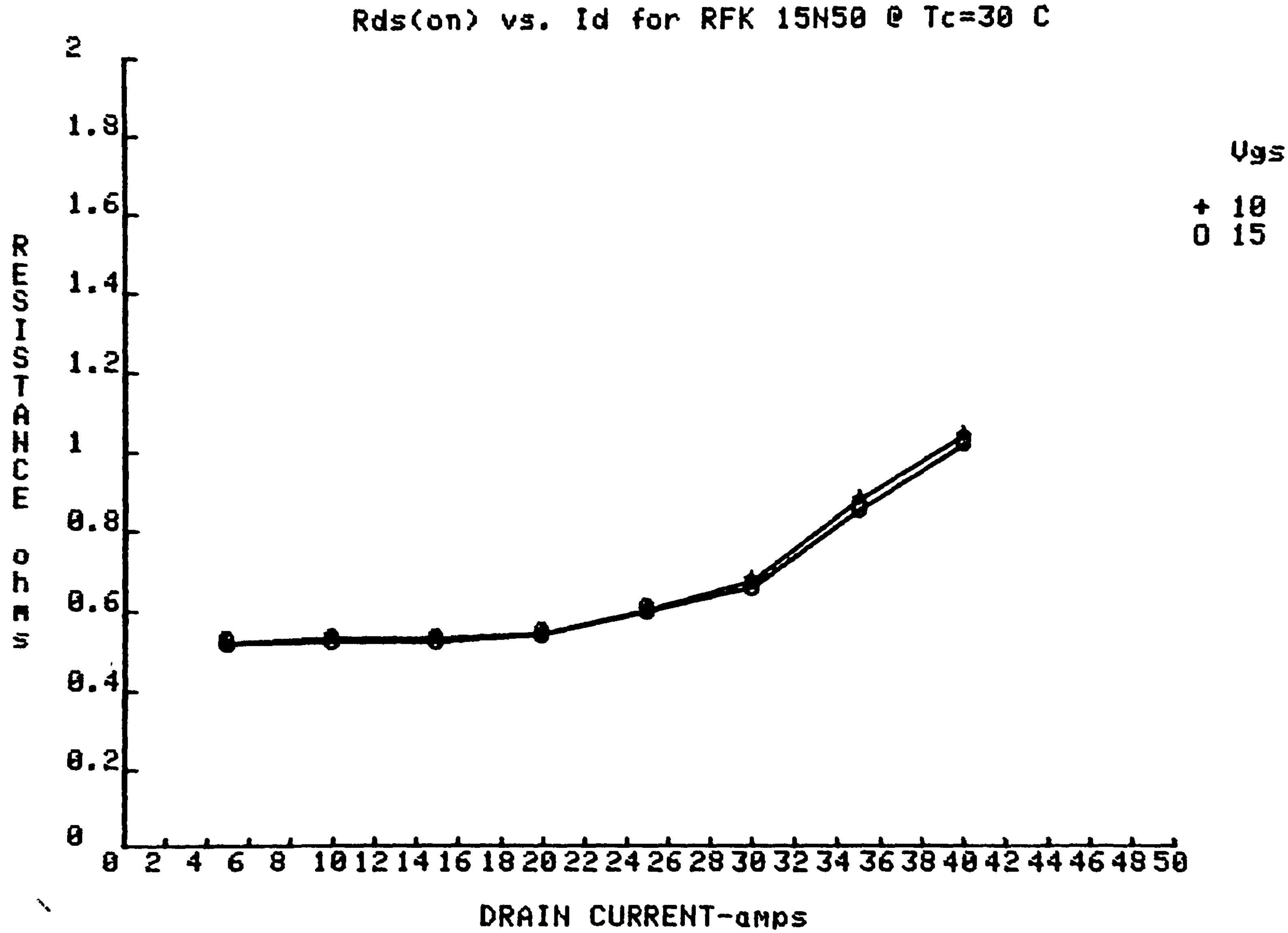
Rds(on) vs. Id for RFK 15N50 @ Tc=30 C
RESISTANCE ohms
2
1.8
1.6
1.4
1.2
1
0.8
0.6
0.4
0.2
0
0 2 4 6 8 10 12 14 16 18 20 22 24 26 28 30 32 34 36 38 40 42 44 46 48 50
DRAIN CURRENT-amps
Vgs
+ 10
O 15

E.9

Fig. E.3.2.

Rds(on) vs. Id COMPARATIVE DATA for RFK 15N50 for Vgs=10V

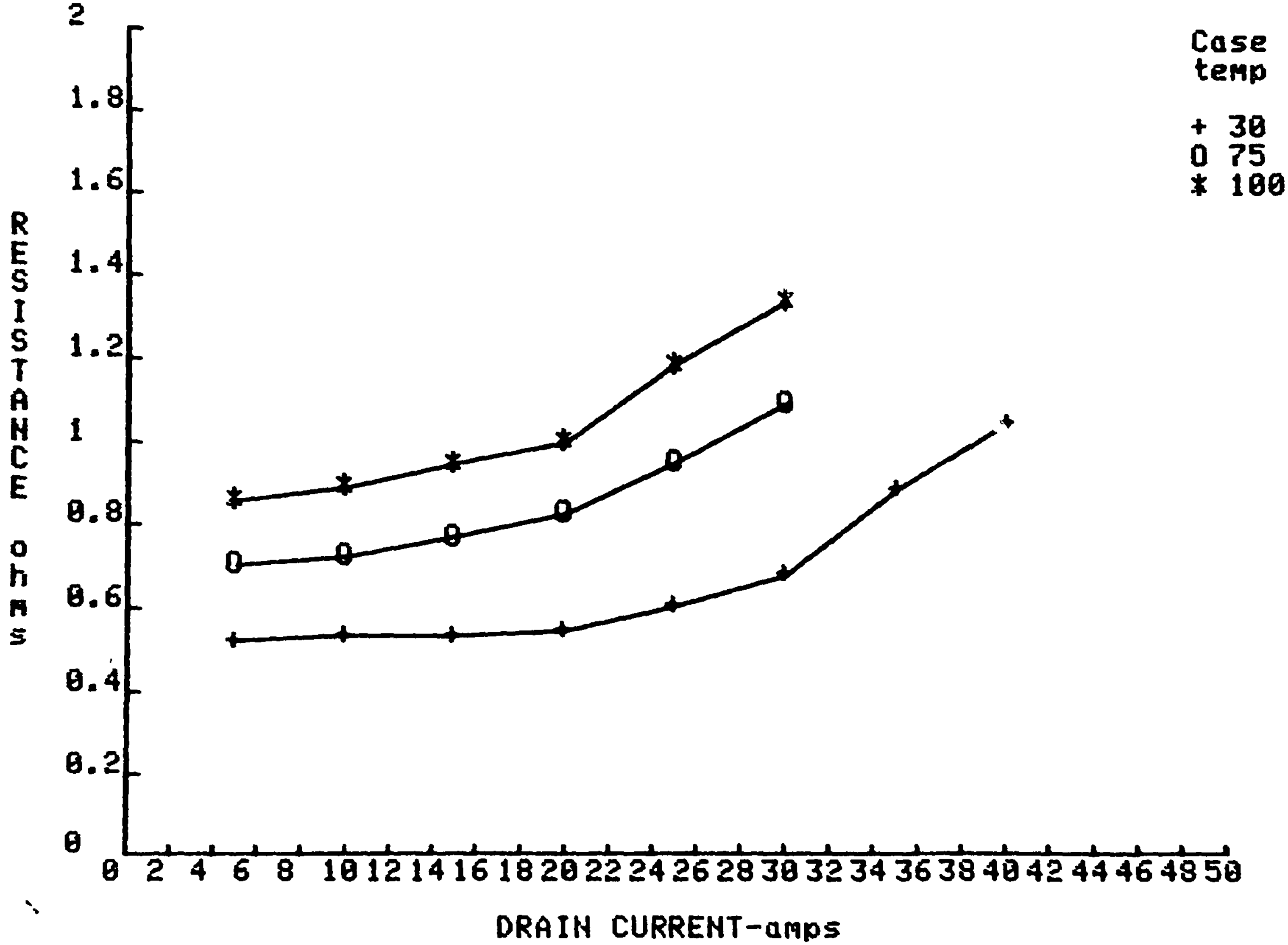

E.4 Test Data of On-Resistance Characterization of the Toshiba 2SK356

Fig. F.4.1

Rds(on) vs. Id for 2SK 356 @ Tc=30 C

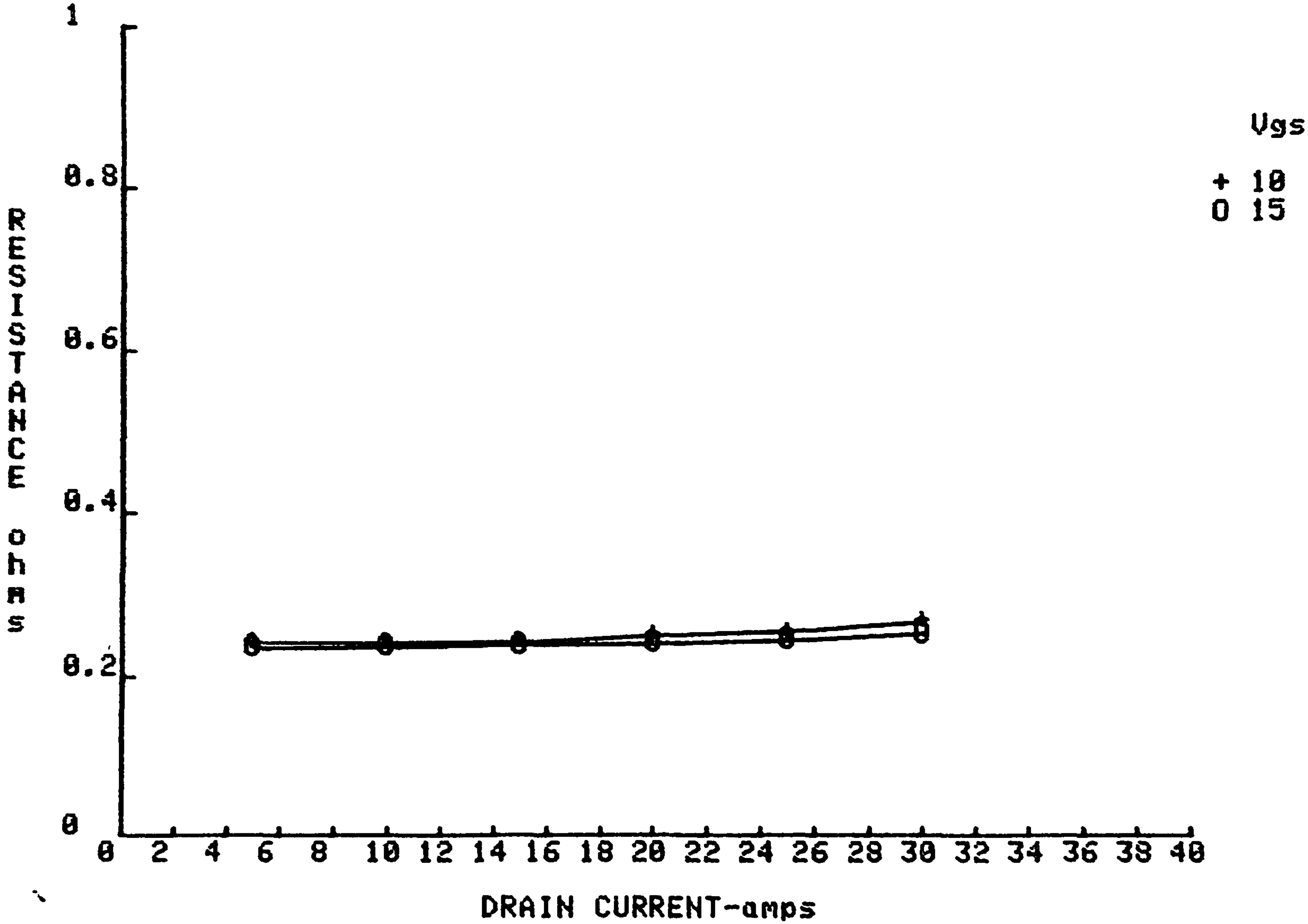

Fig. E.4.2

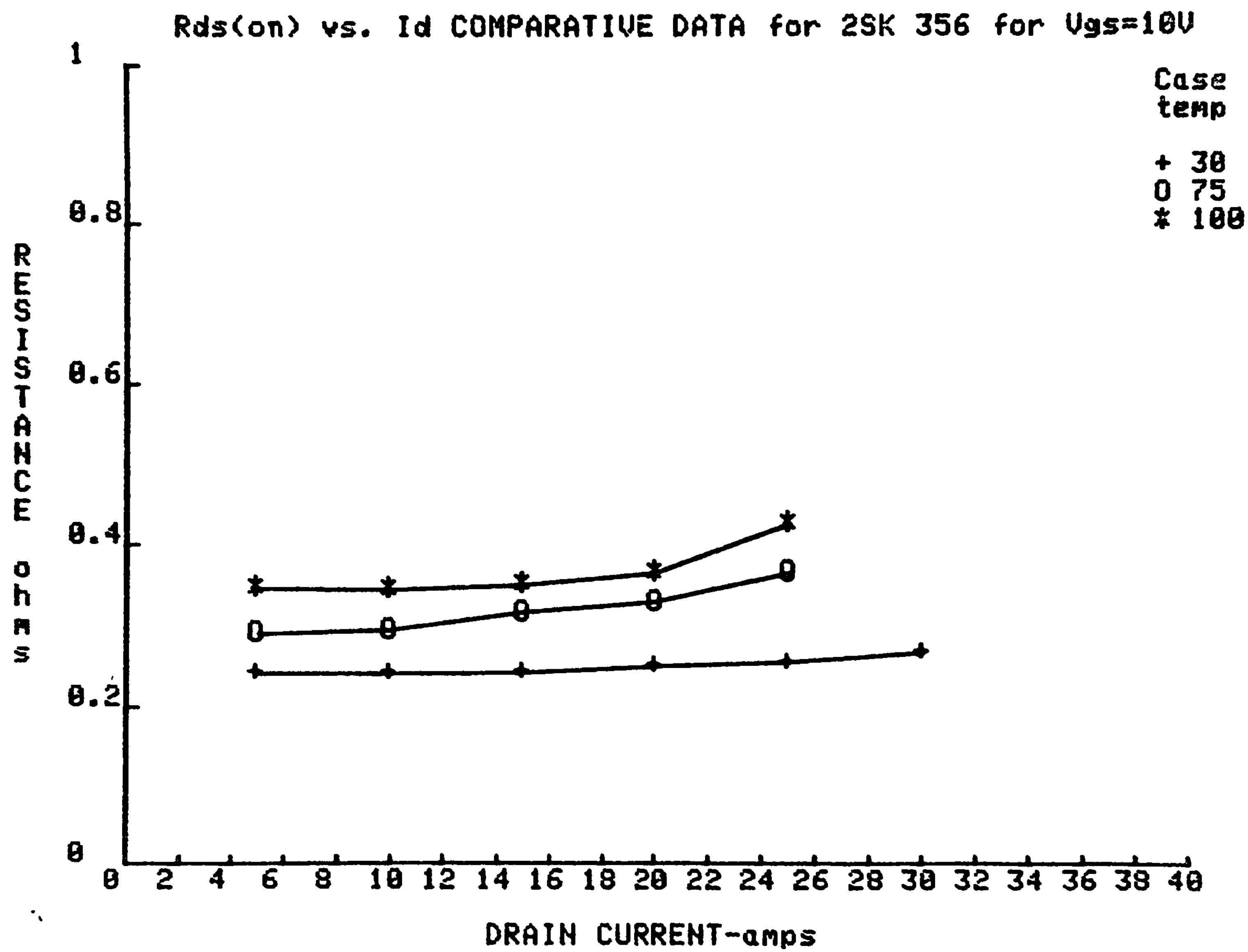
Rds(on) vs. Id COMPARATIVE DATA for 2SK 356 for Vgs=10V
Case temp
+ 30
O 75
* 100
RESISTANCE ohms
1
0.8
0.6
0.4
0.2
0
0 2 4 6 8 10 12 14 16 18 20 22 24 26 28 30 32 34 36 38 40
DRAIN CURRENT-amps

E.5 Test Data of On-Resistance Characterization of the Toshiba 2SK386

Fig. E.5.1

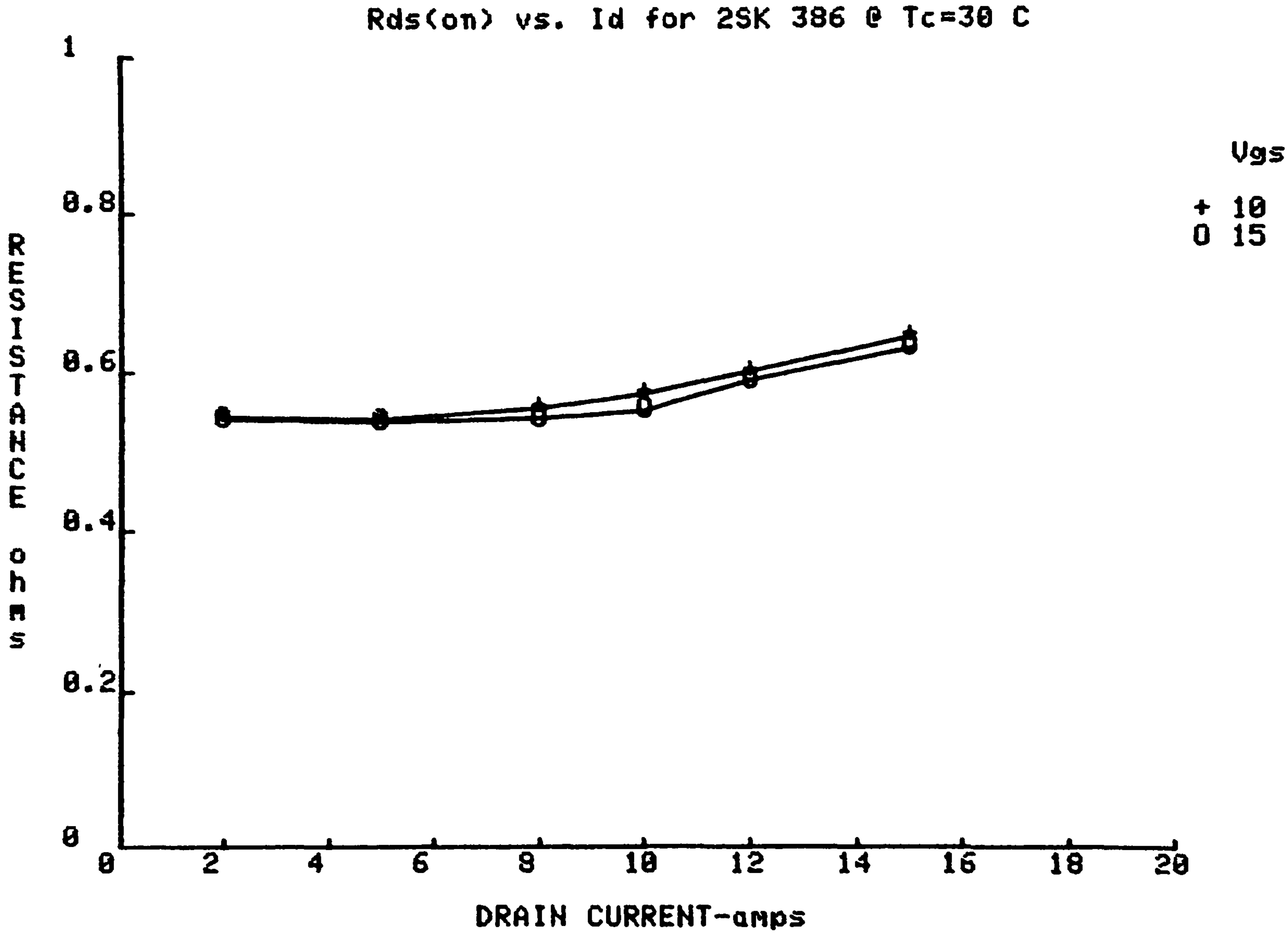
Rds(on) vs. Id for 2SK 386 @ Tc=30 C
RESISTANCE ohms
1
0.8
0.6
0.4
0.2
0
0 2 4 6 8 10 12 14 16 18 20
DRAIN CURRENT-amps
Vgs
+ 10
O 15

Fig. E.5.2

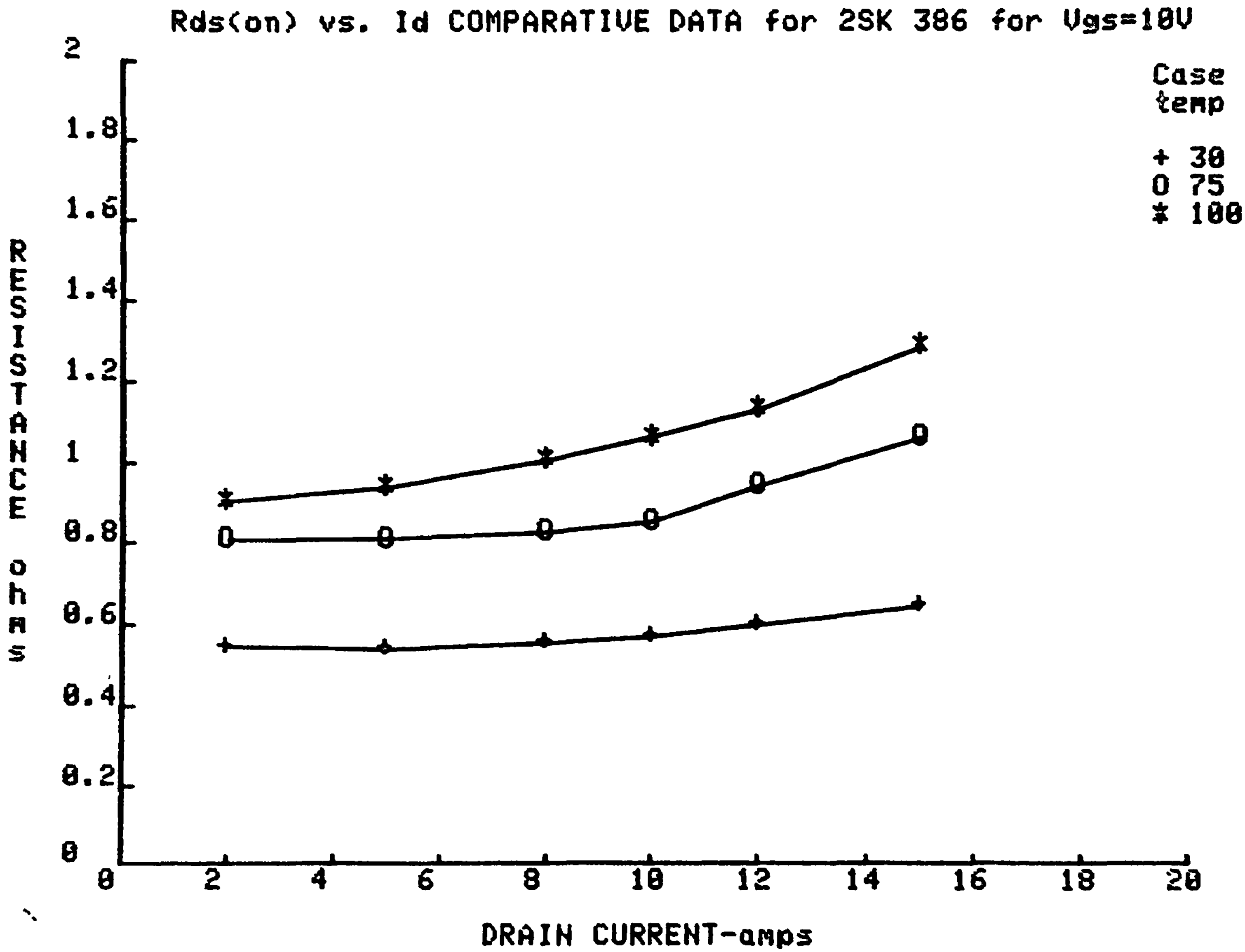

Rds(on) vs. Id COMPARATIVE DATA for 2SK 386 for Vgs=10V
RESISTANCE ohms
2
1.8
1.6
1.4
1.2
1
0.8
0.6
0.4
0.2
0
0
2
4
6
8
10
12
14
16
18
20
DRAIN CURRENT-amps
Case temp
+ 30
O 75
* 100

E.16

APPENDIX F

TEST DATA OF MOSFETs SWITCHING TIMES CHARACTERIZATION

F.1 Test Data Switching Times Characterization of the IRF 441

Fig. F.1.1.

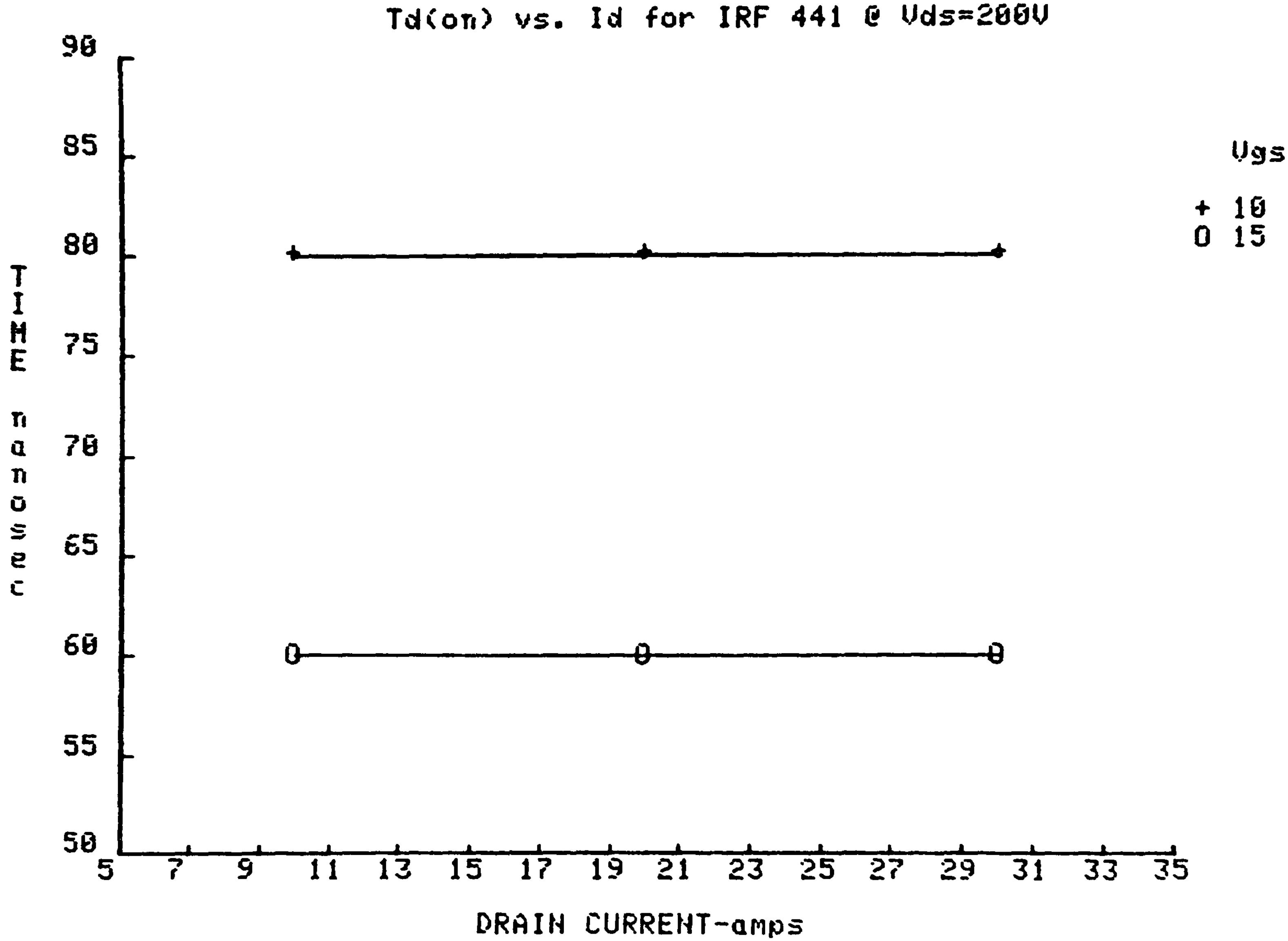
Td(on) vs. Id for IRF 441 @ Vds=200V
90
85
80
75
70
65
60
55
50
TIME nanosec
5 7 9 11 13 15 17 19 21 23 25 27 29 31 33 35
DRAIN CURRENT-amps
Vgs
+ 10
O 15

Fig. F.1.2.

Tr vs. Id for IRF 441 @ Vds=200V

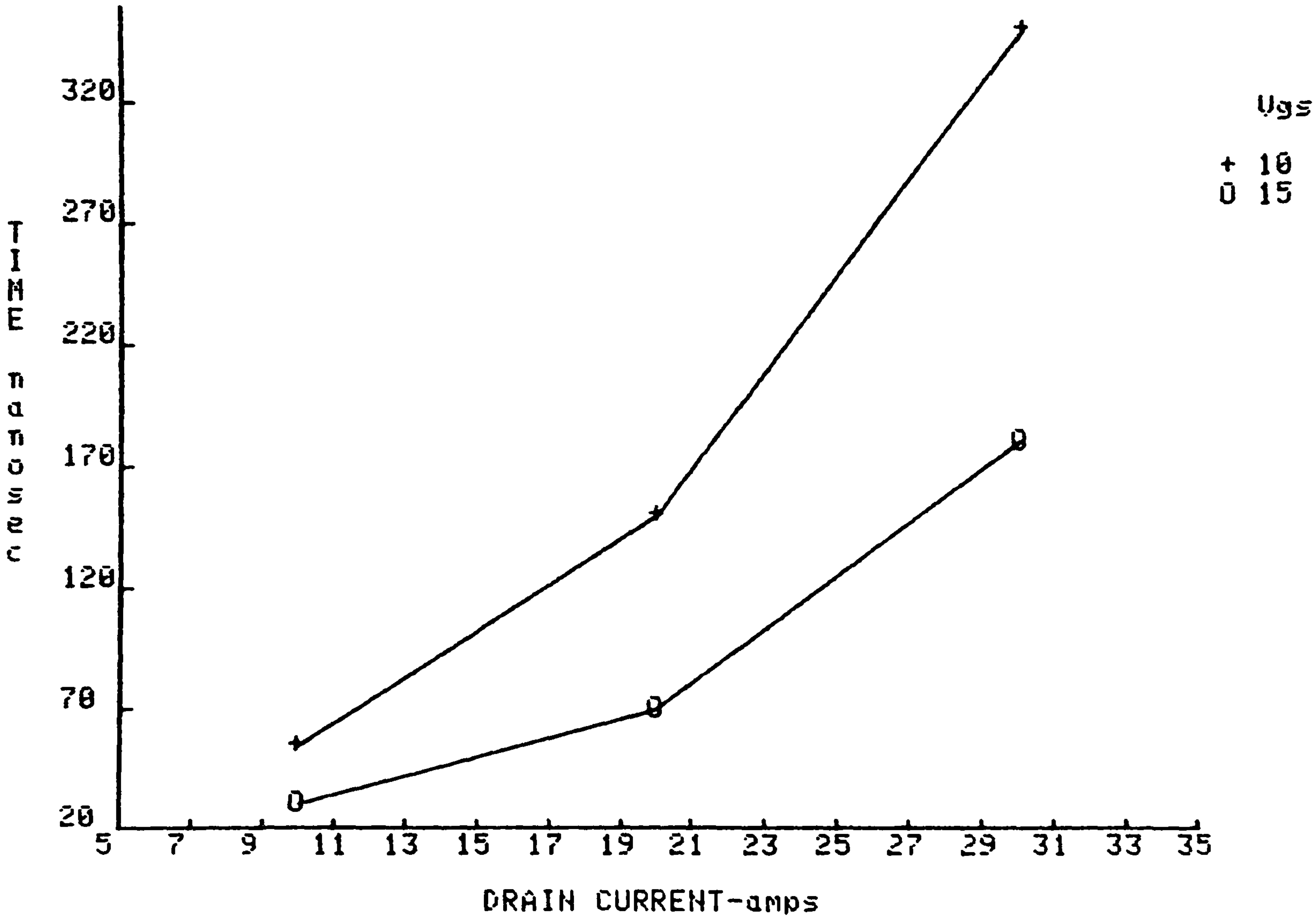

Fig. F.1.3.

Ton vs. Id for IRF 441 @ Vds=200V

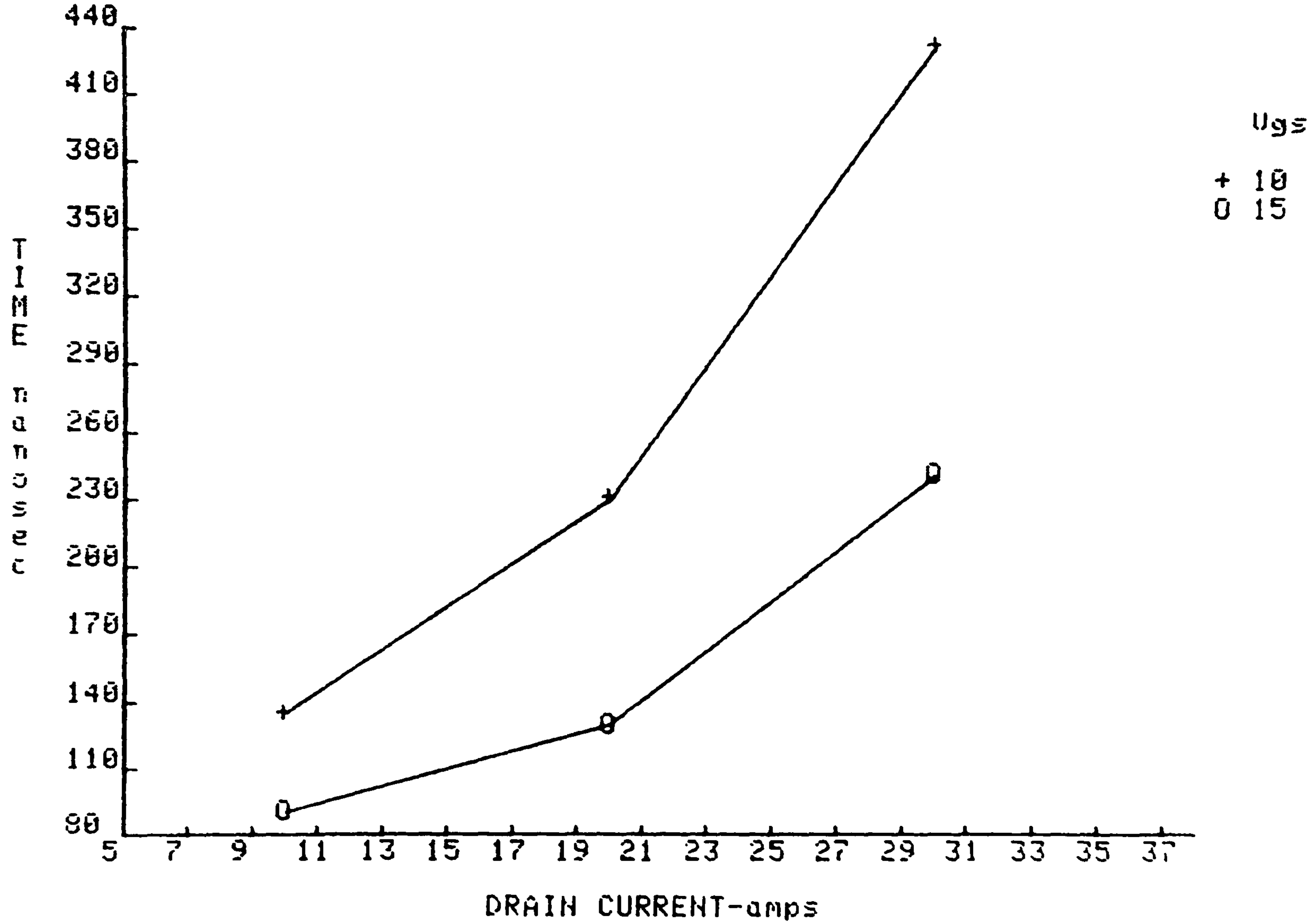

Fig. F. 1.4.

Td(off) vs. Id for IRF 441 @ Vds=200V

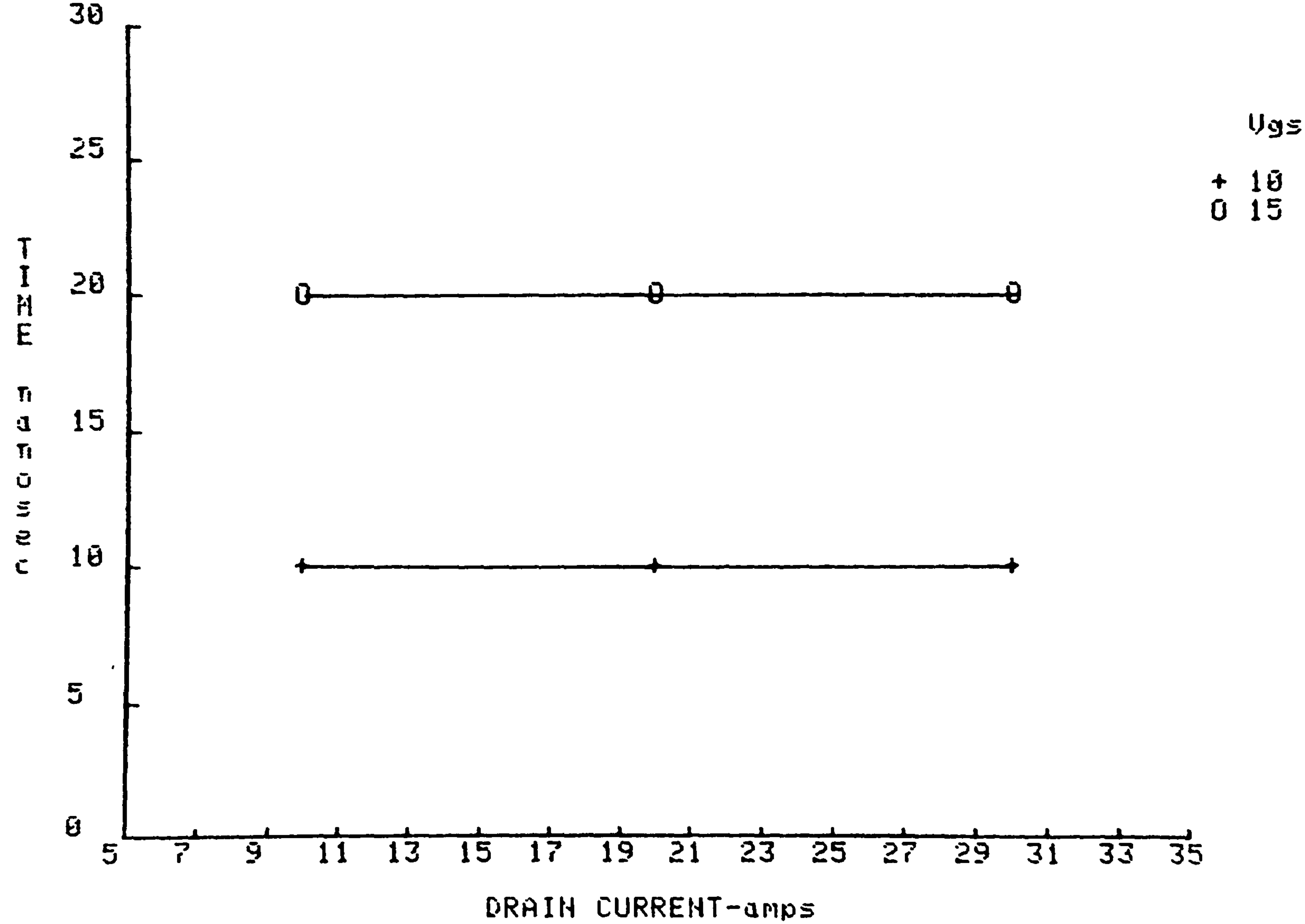

F.6

Fig. 2.1.5.

Tf vs. Id for IRF 441 @ Vds=200V

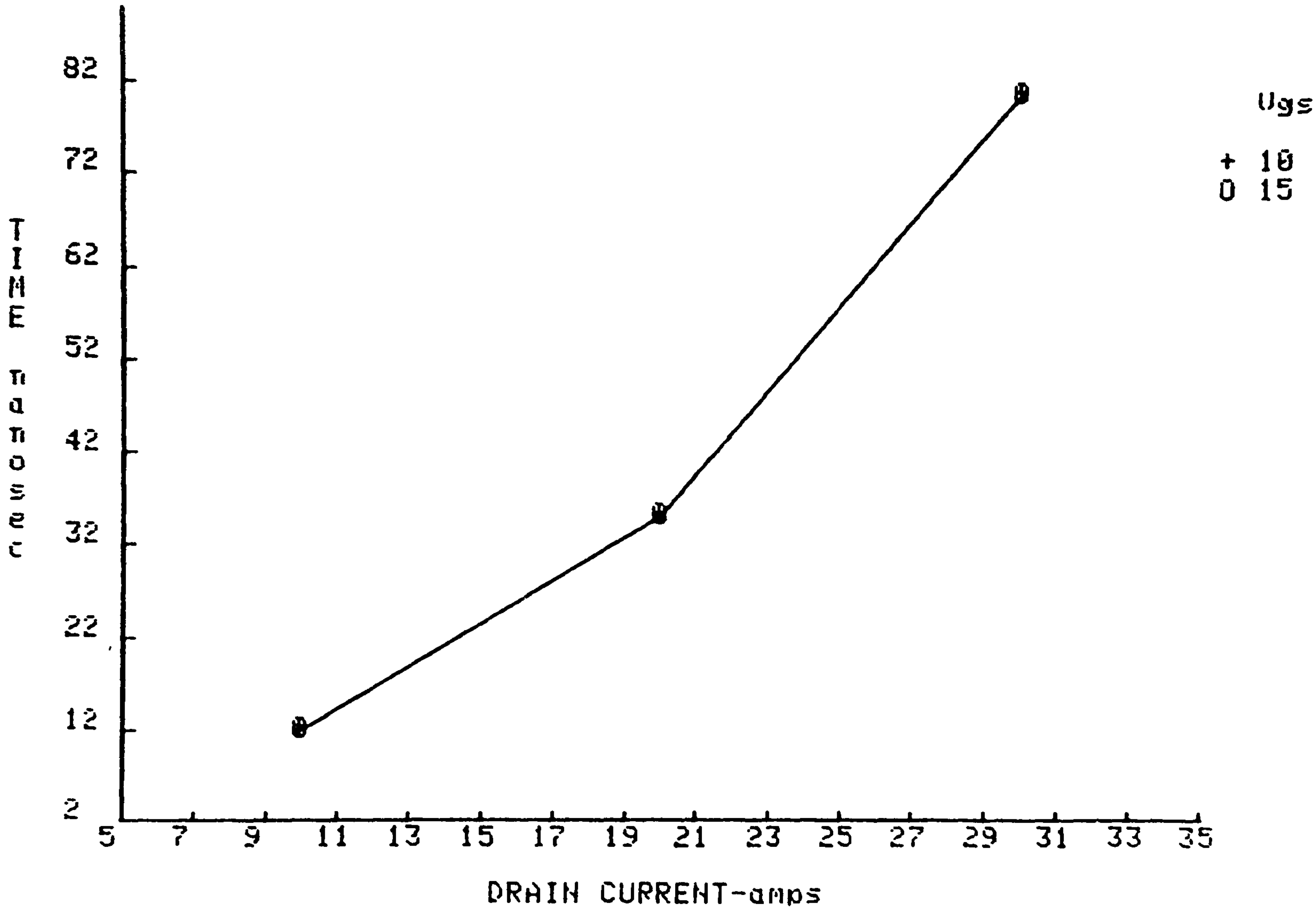

Fig. F.1.6.
Toff vs. Id for IRF 441 @ Uds=200U

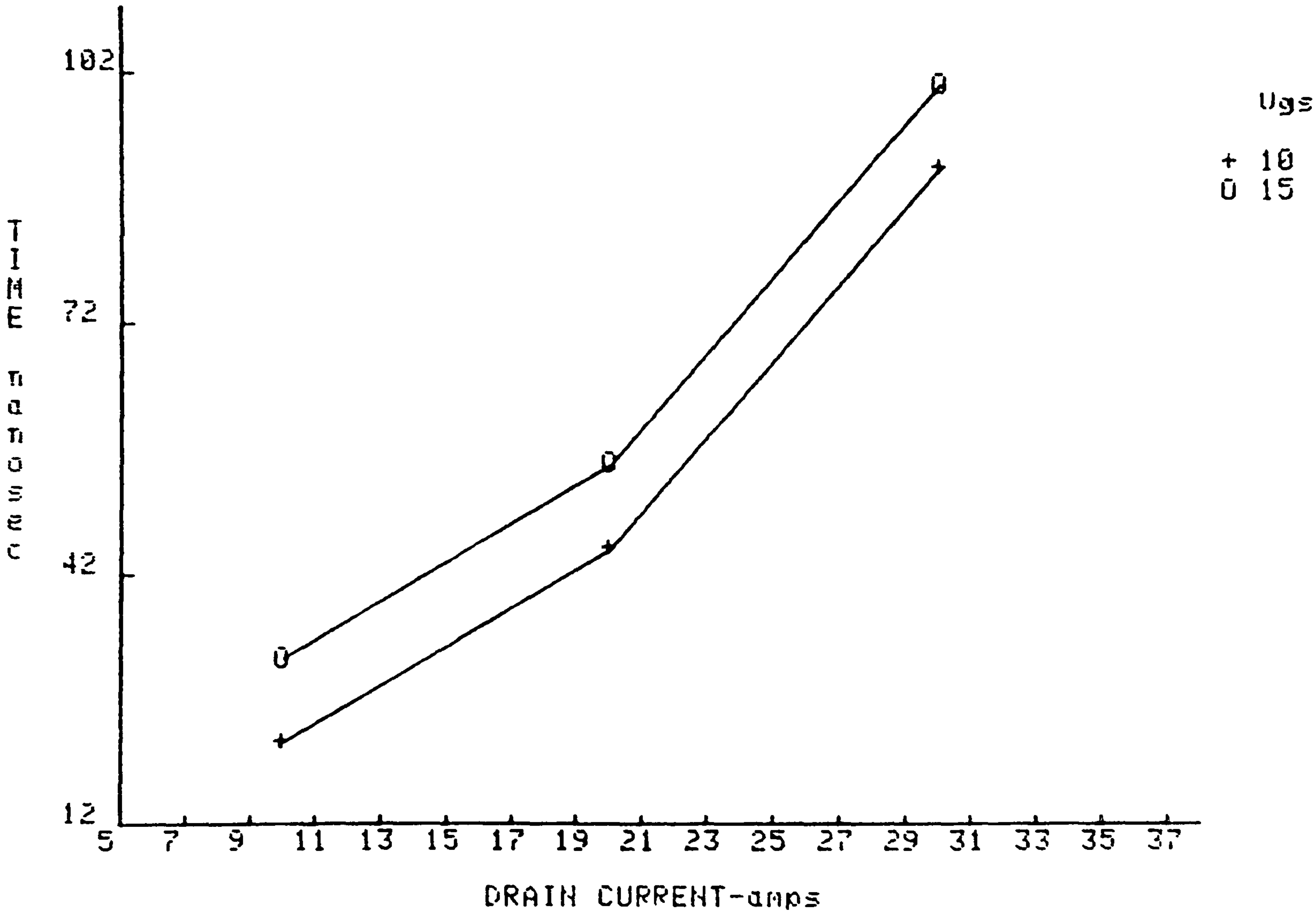

F.2 Test Data of Switching Times Characterization of the RCA RFK15N45

Fig. F.2.1

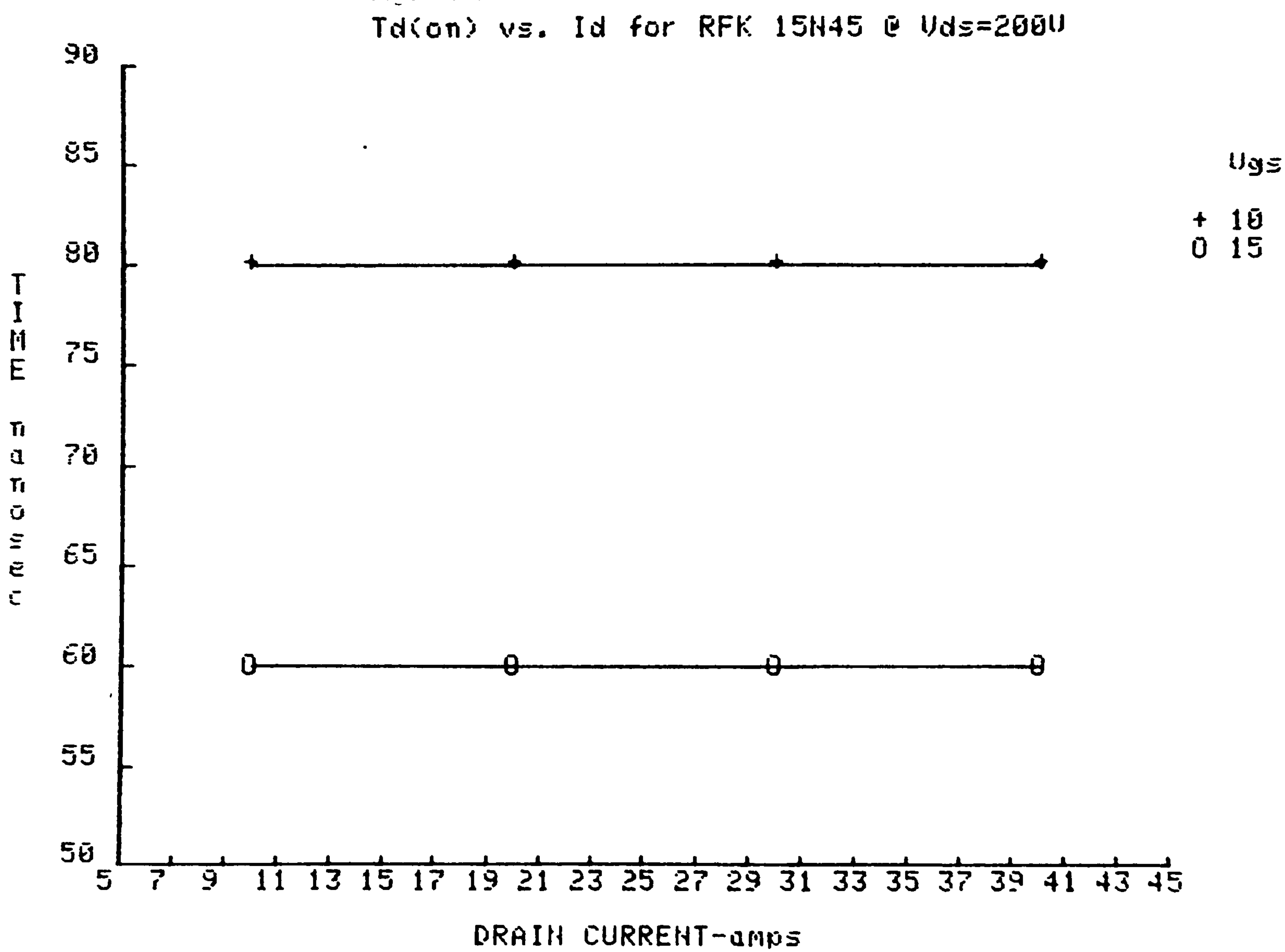
Td(on) vs. Id for RFK 15N45 @ Vds=200V
90
85
80
75
70
65
60
55
50
TIME nanosec
5 7 9 11 13 15 17 19 21 23 25 27 29 31 33 35 37 39 41 43 45
DRAIN CURRENT-amps
Vgs
+ 10
0 15

F.10

Fig. F.2.2

Tr vs. Id for RFK 15N45 @ Vds=200V

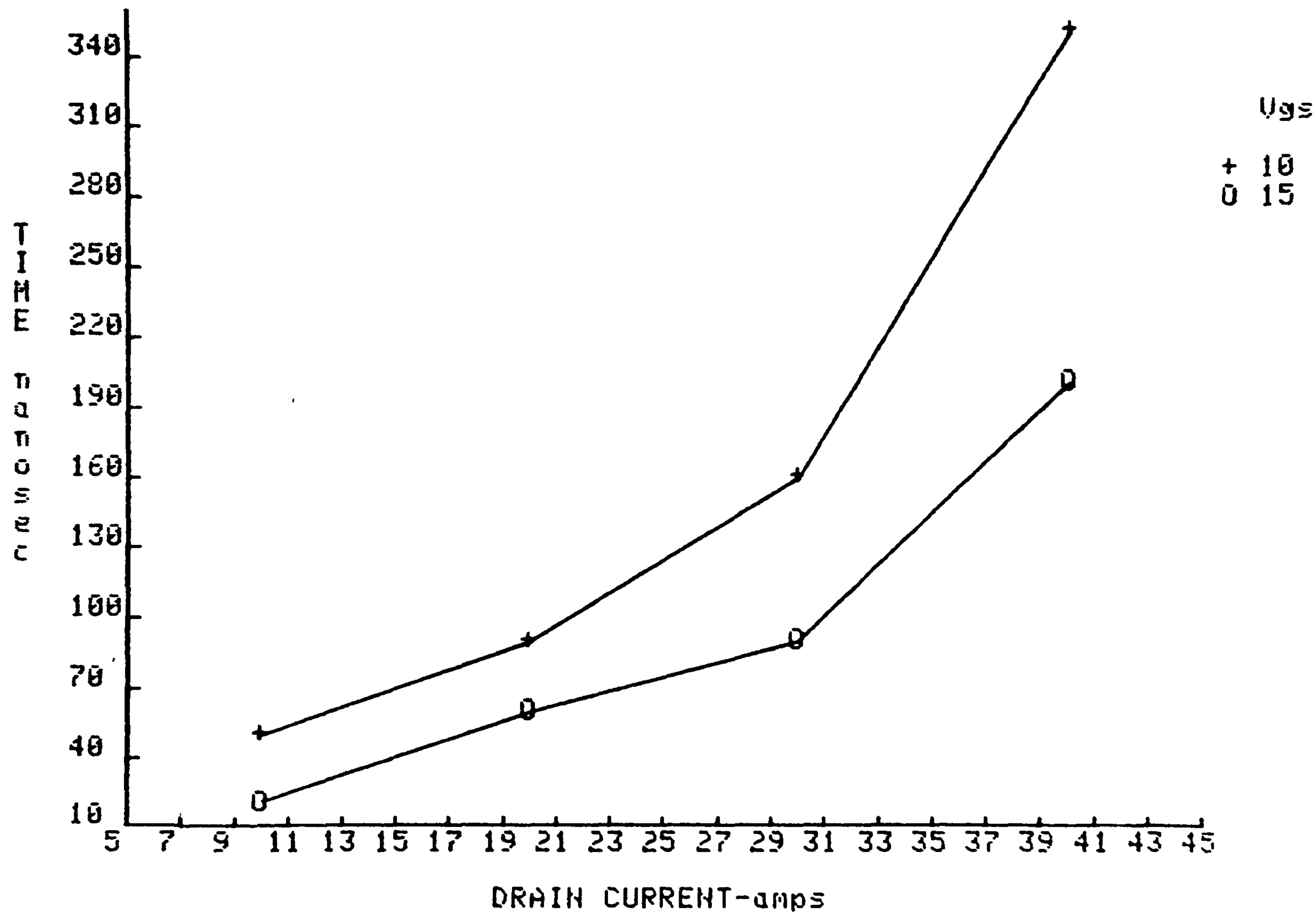

Fig. C.2.3

Ton vs. Id for RFK 15N45 @ Uds=200U

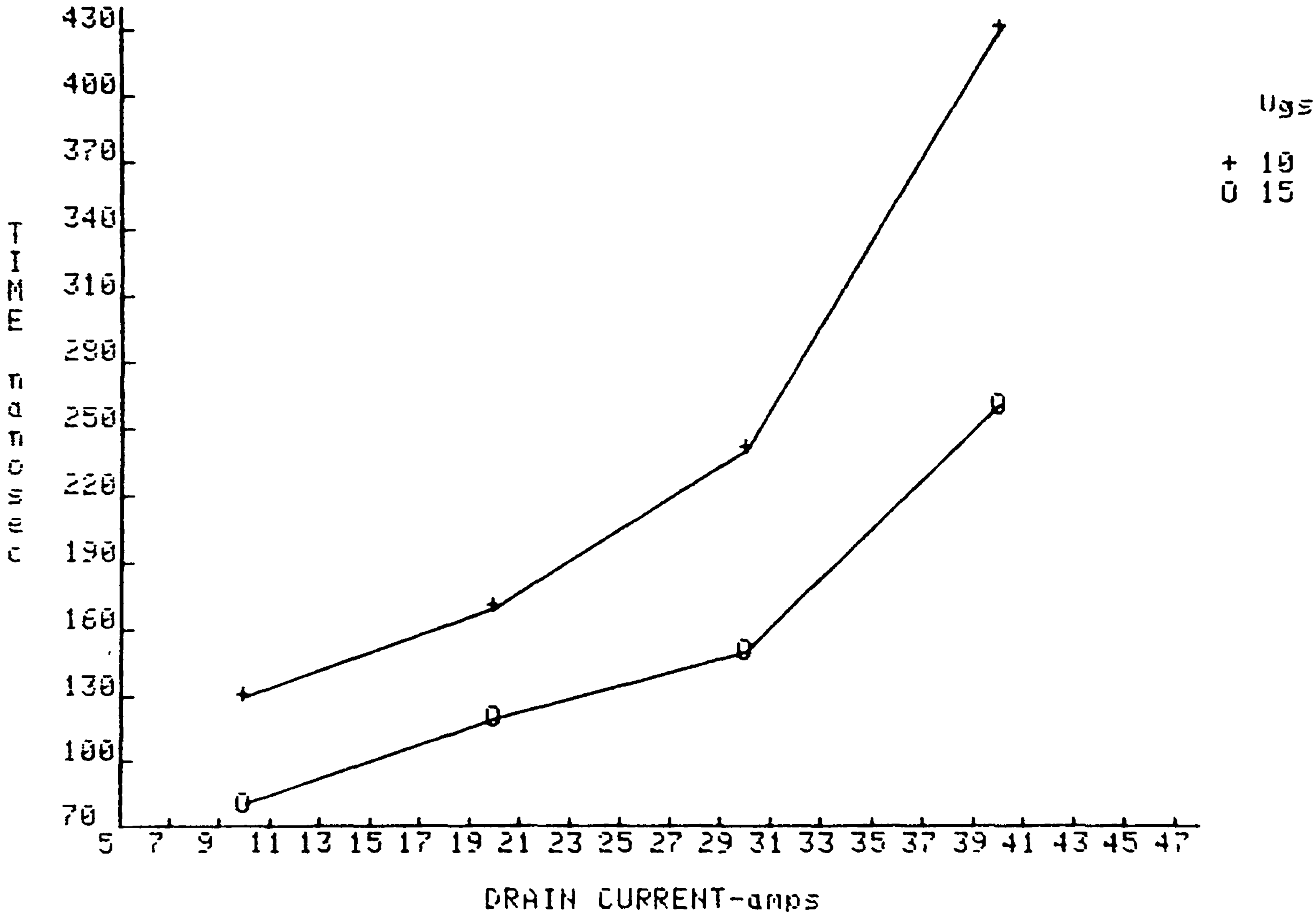

F.12

Fig. F.2.4

Td(off) vs. Id for RFK 15N45 @ Vds=200V

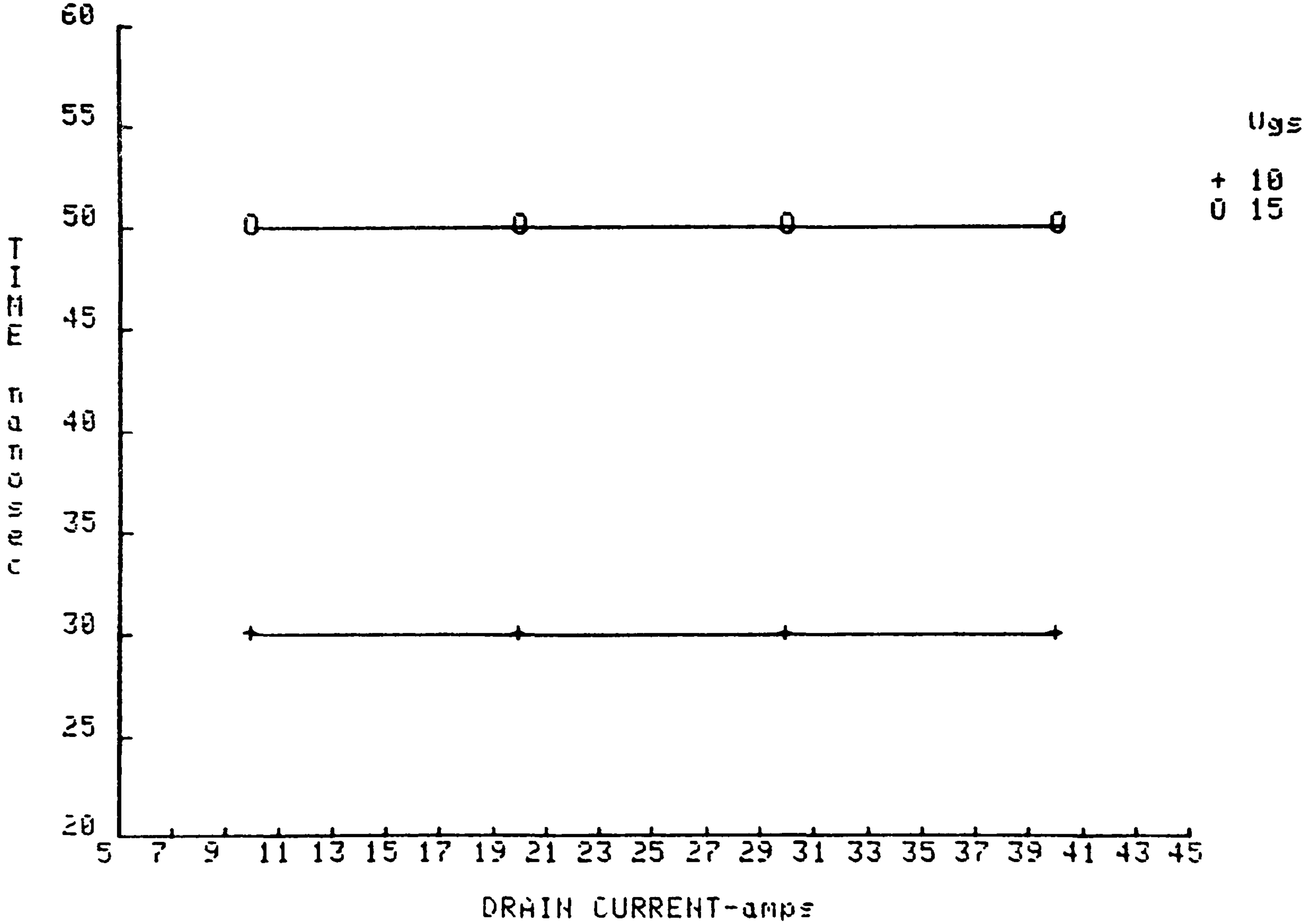

Fig. F.2.5

Tf vs. Id for RFK 15N45 @ Vds=200V

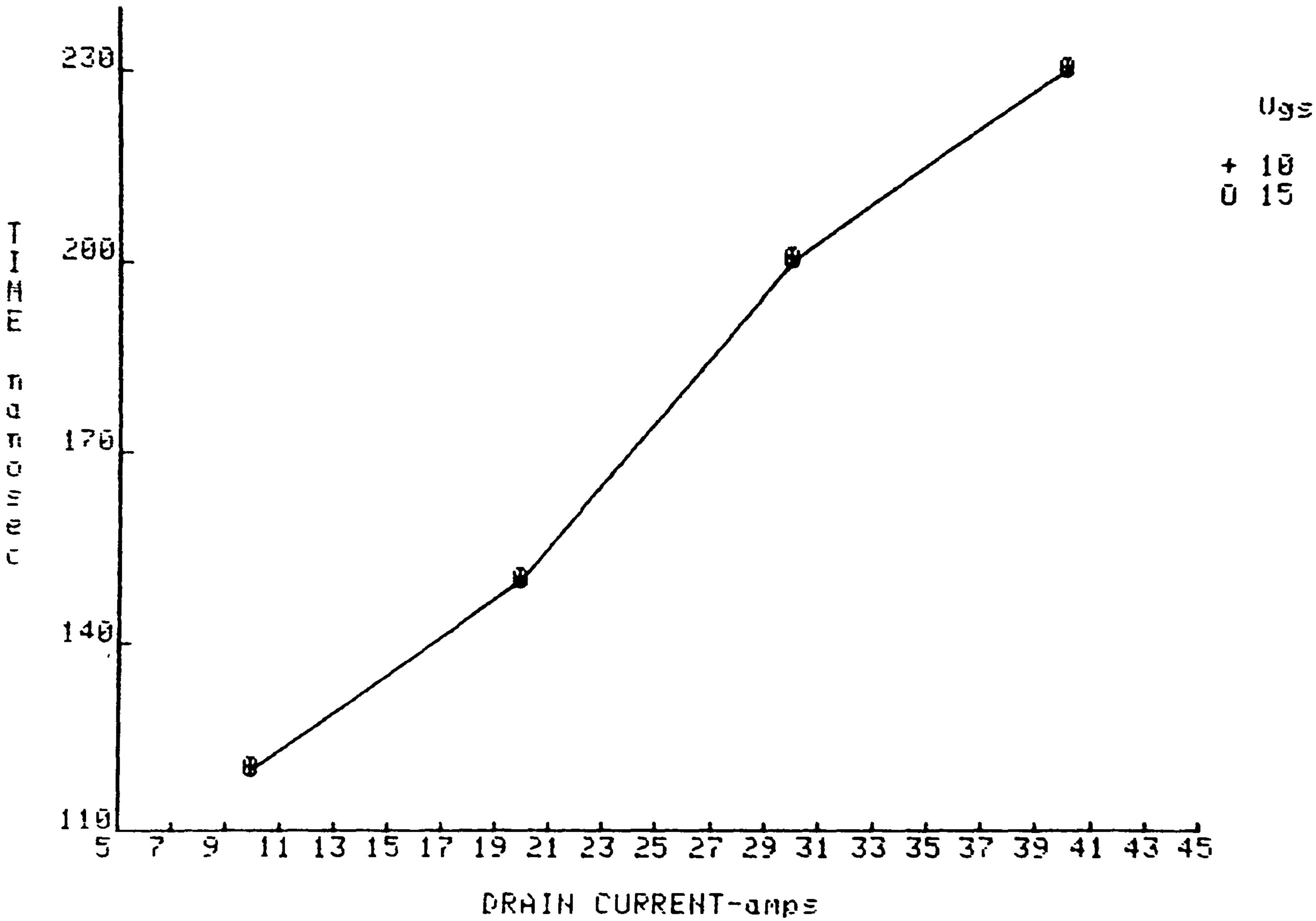

Fig. F.2.6

Toff vs. Id for RFK 15N45 @ Vds=200V

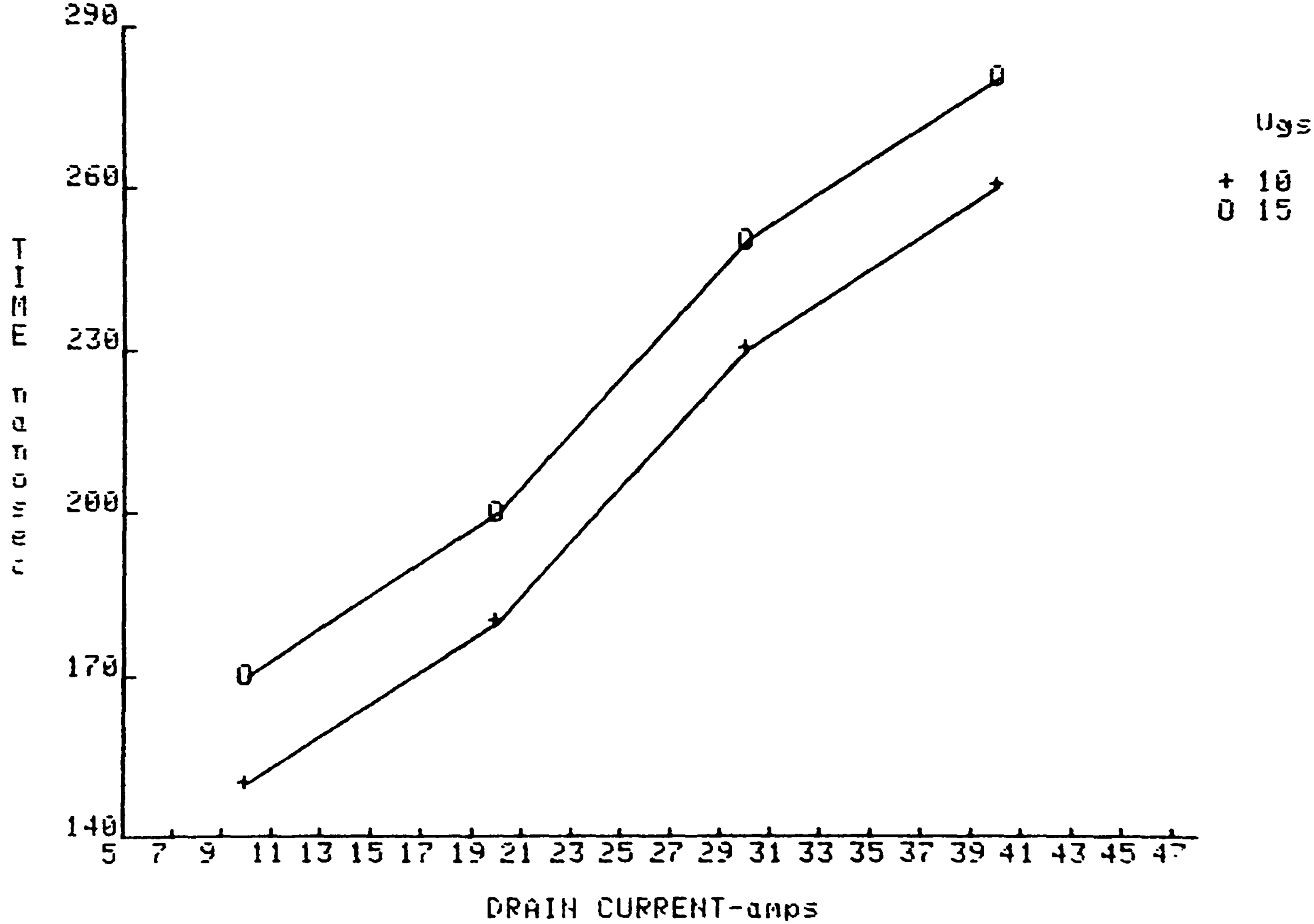

F.3 Test Data of Switching Times Characterization of the RCA RFK15N50

Fig. F.3.1.

Td(on) vs. Id for RFK 15N50 @ Vds=200V

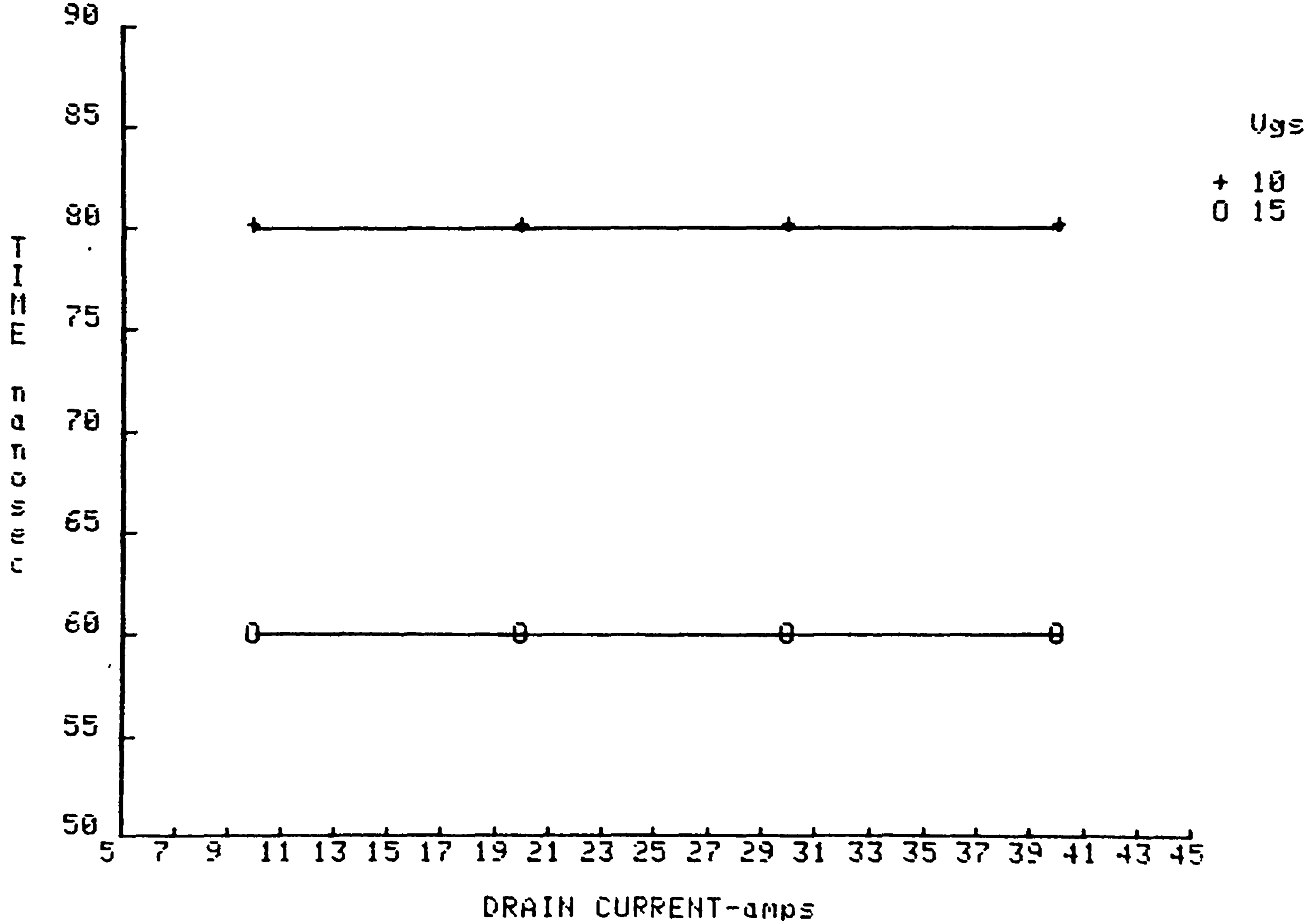

Fig. F.3.2.
Tr vs. Id for RFK 15N50 @ Vds=200V

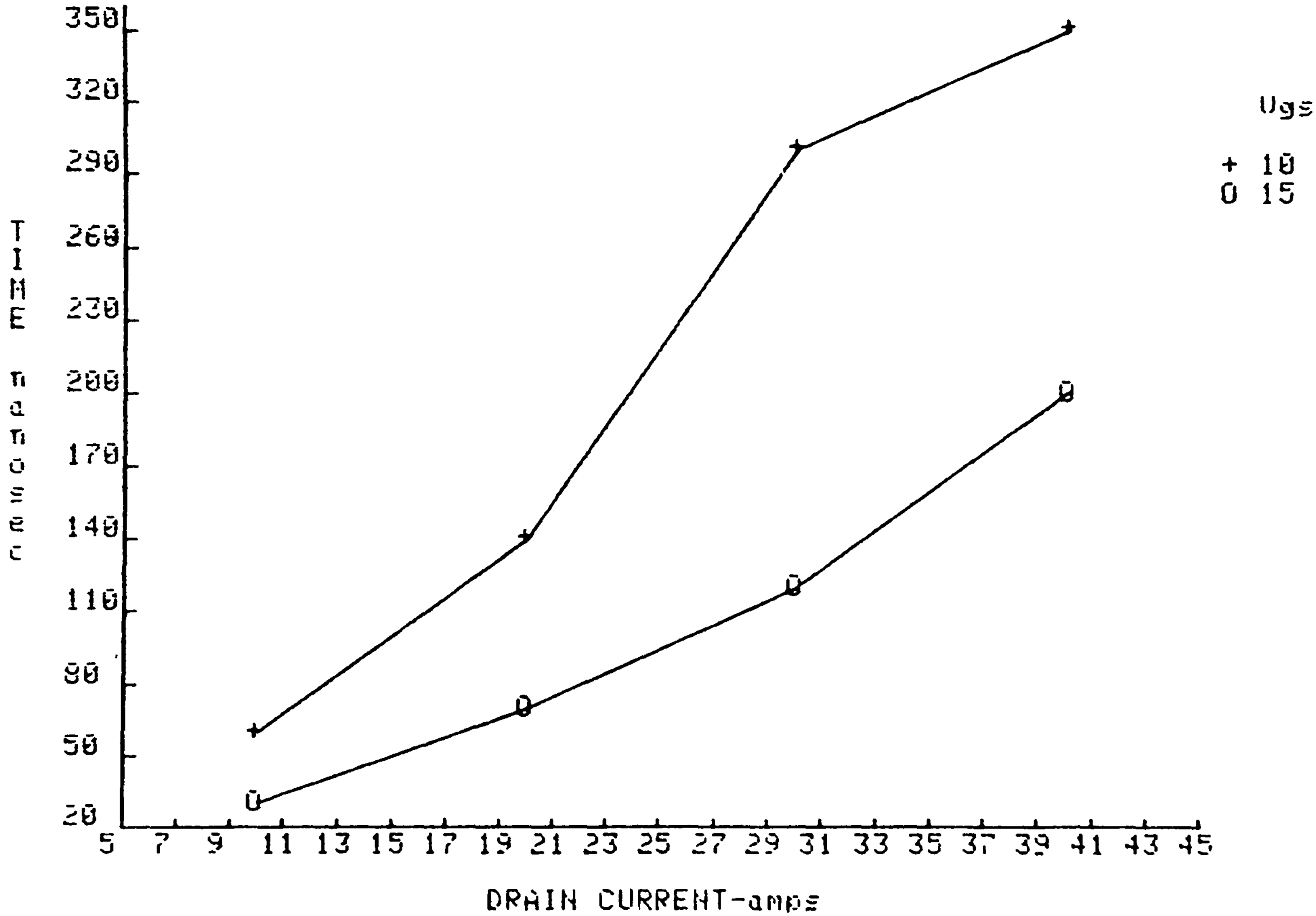

Fig. F.3.3.

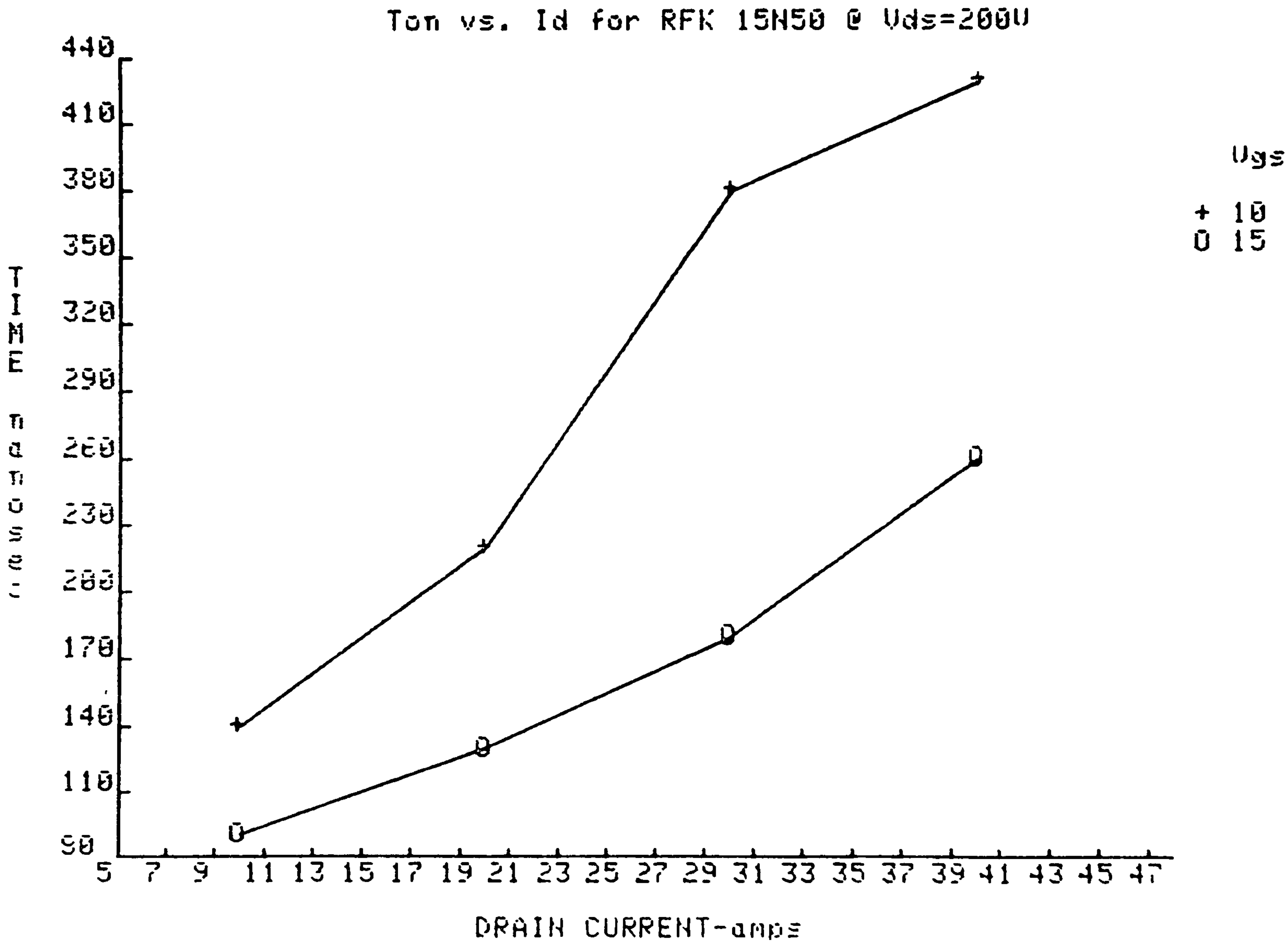
Ton vs. Id for RFK 15N50 @ Vds=200V
TIME nanosec
440
410
380
350
320
290
260
230
200
170
140
110
80
5 7 9 11 13 15 17 19 21 23 25 27 29 31 33 35 37 39 41 43 45 47
DRAIN CURRENT-amps
Vgs
+ 10
0 15

Fig. F.3.4.

Td(off) vs. Id for RFK 15N50 @ Vds=200V

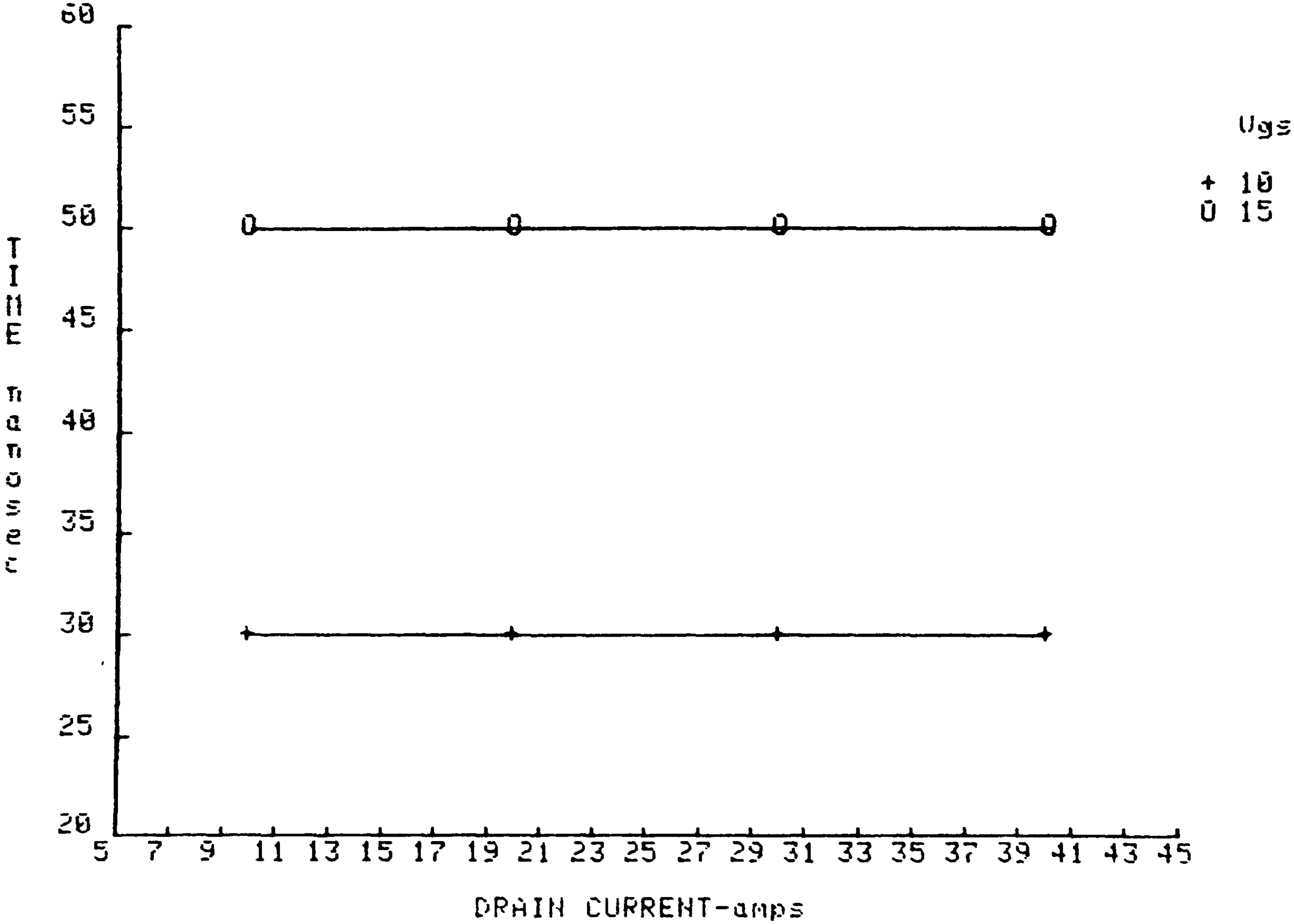

Fig. F.3.5.

Tf vs. Id for RFK 15N50 @ Vds=200V

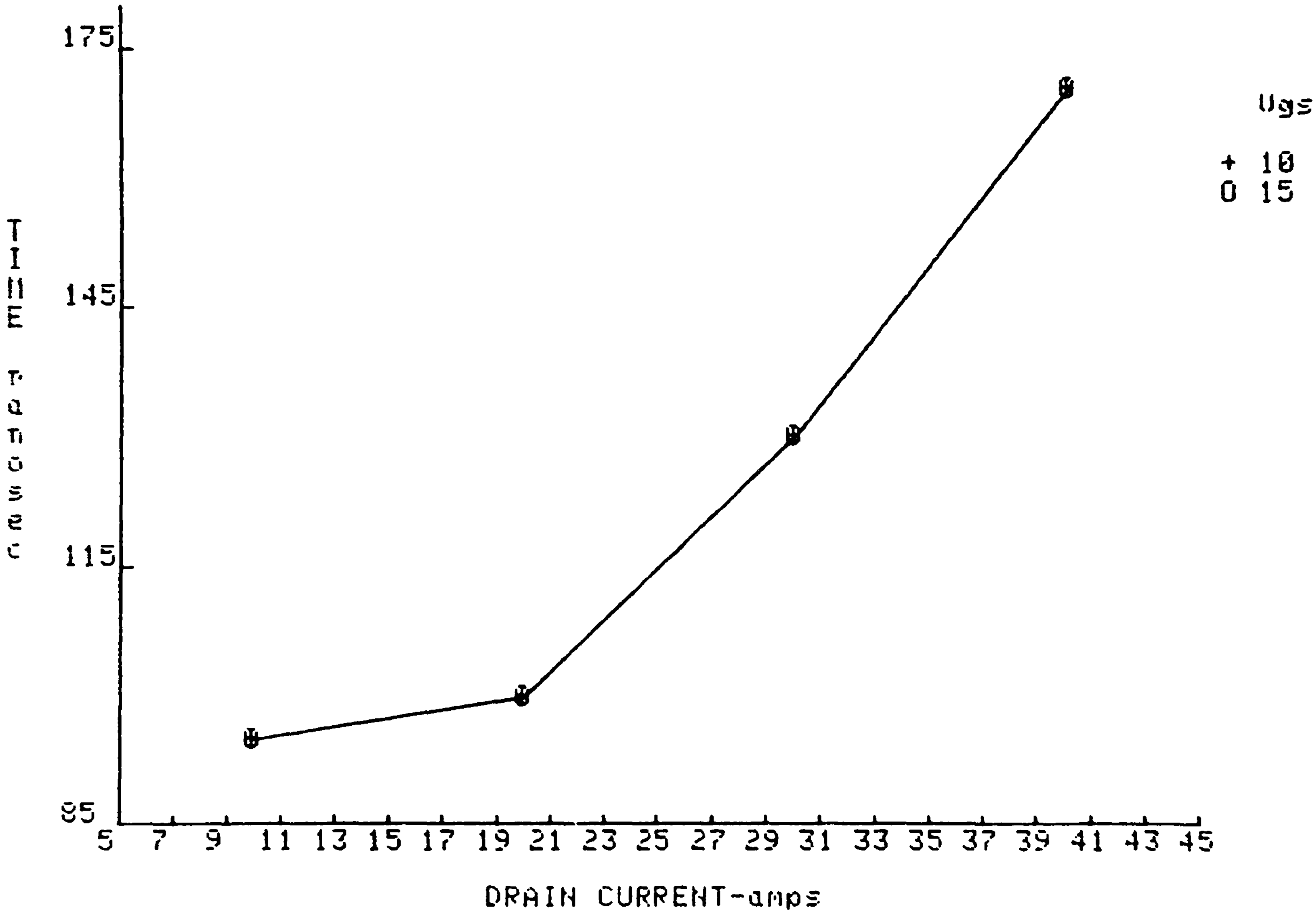

Fig. F.3.6.

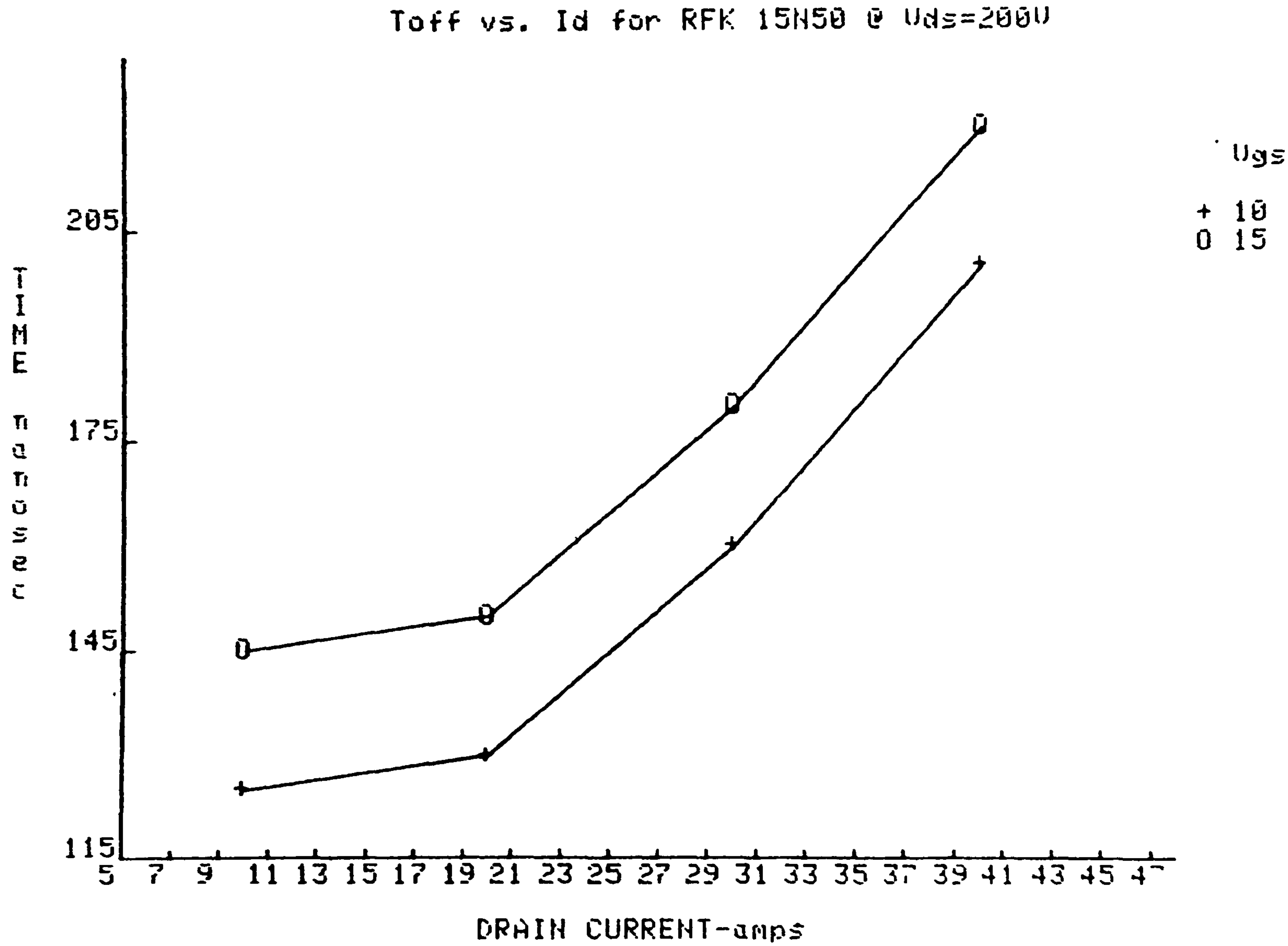
Toff vs. Id for RFK 15N50 @ Vds=200V
TIME nanosec
205
175
145
115
5 7 9 11 13 15 17 19 21 23 25 27 29 31 33 35 37 39 41 43 45 47
DRAIN CURRENT-amps
Vgs
+ 10
0 15

F.4 Test Data Switching Times Characterization of the Toshiba 2SK356

Fig. F.4.1.

Td(on) vs. Id for 2SK 356 @ Vds=200V

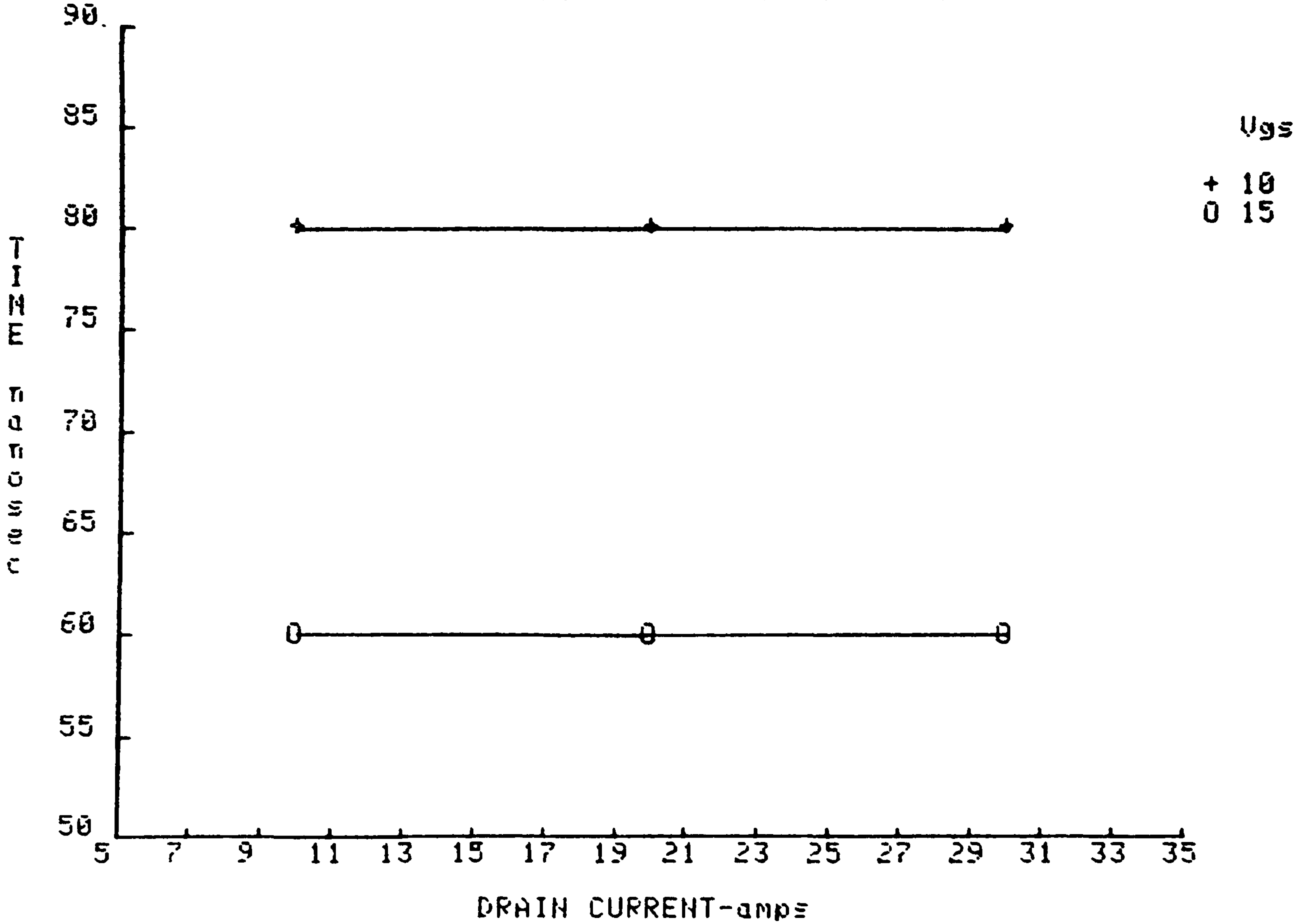

Fig. F.4.2.

Tr vs. Id for 2Sk 356 @ Vds=200V

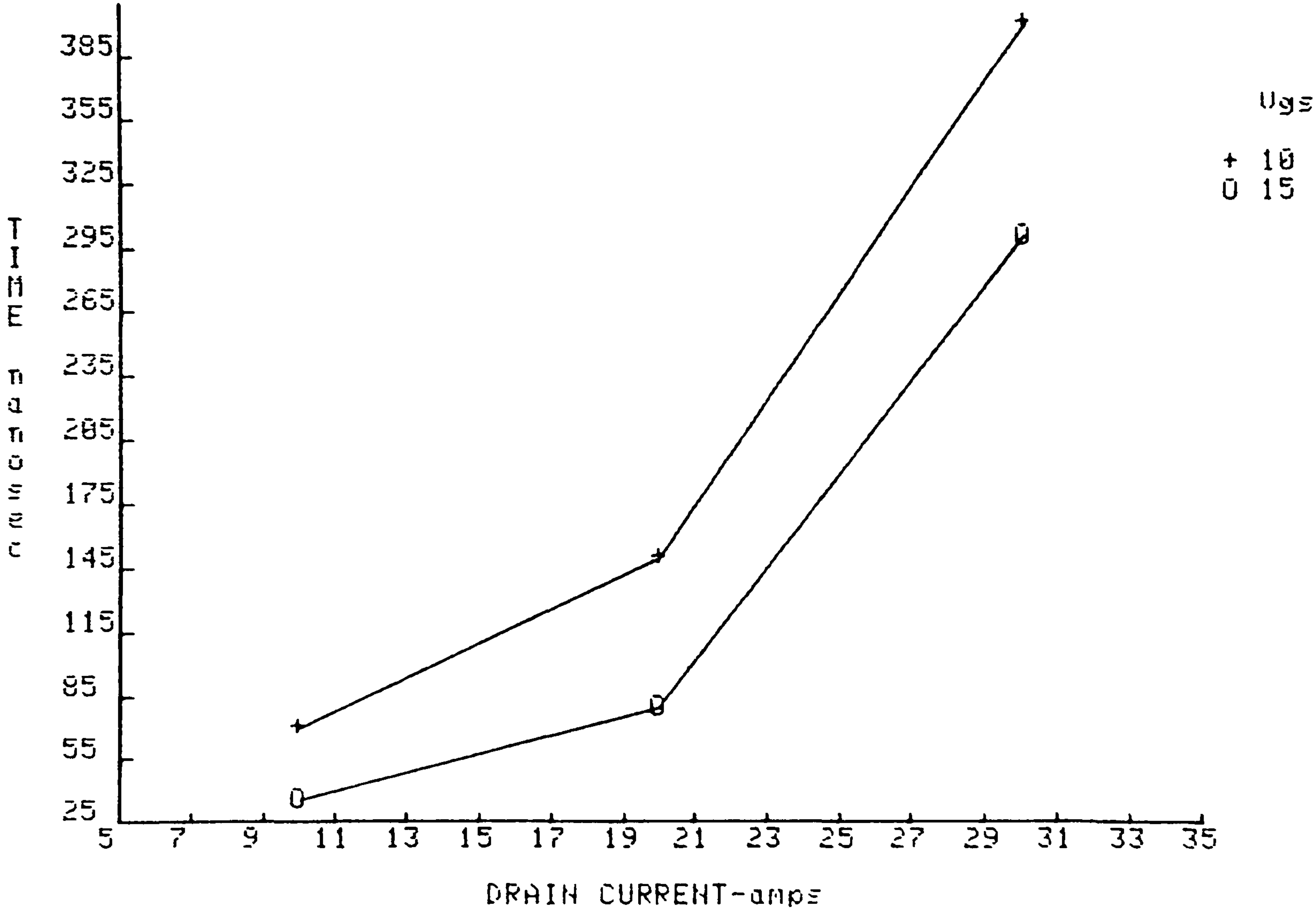

Fig. F.4.3.

Ton vs. Id for 2SK 356 @ Vds=200V

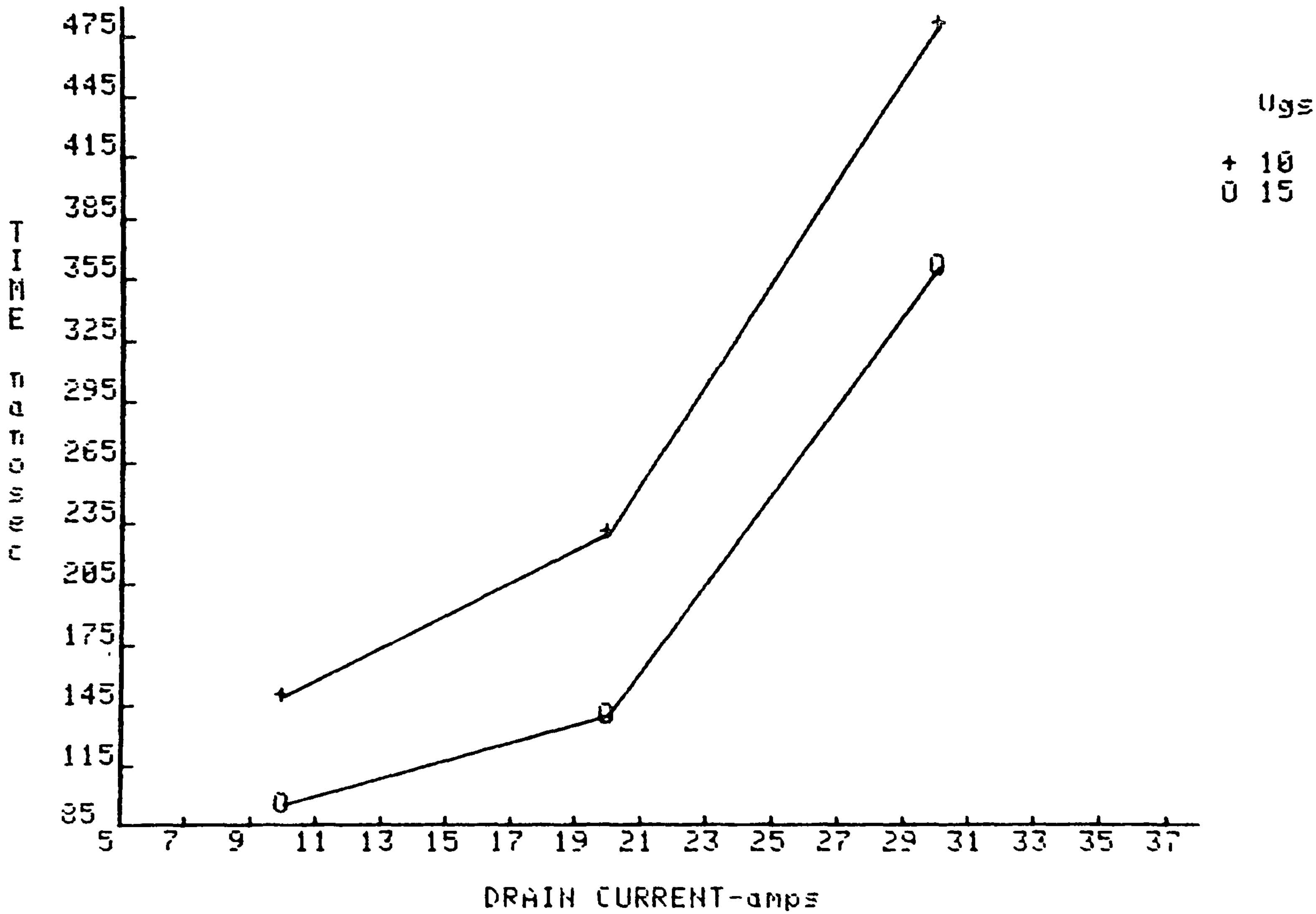

Fig. F.4.4.

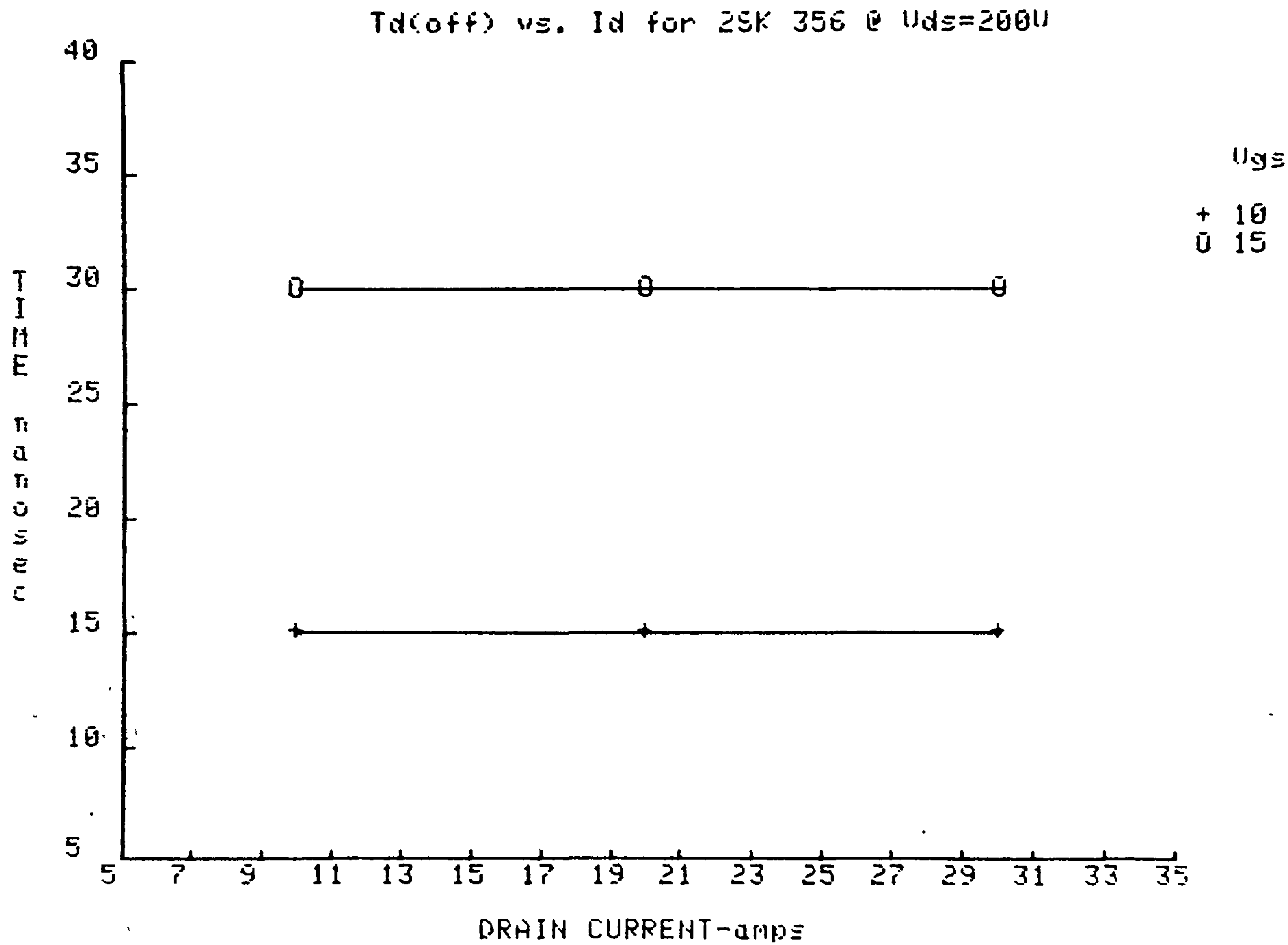
Td(off) vs. Id for 2SK 356 @ Vds=200V
40
35
30
25
20
15
10
5
TIME nanosec
5 7 9 11 13 15 17 19 21 23 25 27 29 31 33 35
DRAIN CURRENT-amps
Vgs
+ 10
0 15

Fig. F.4.5.

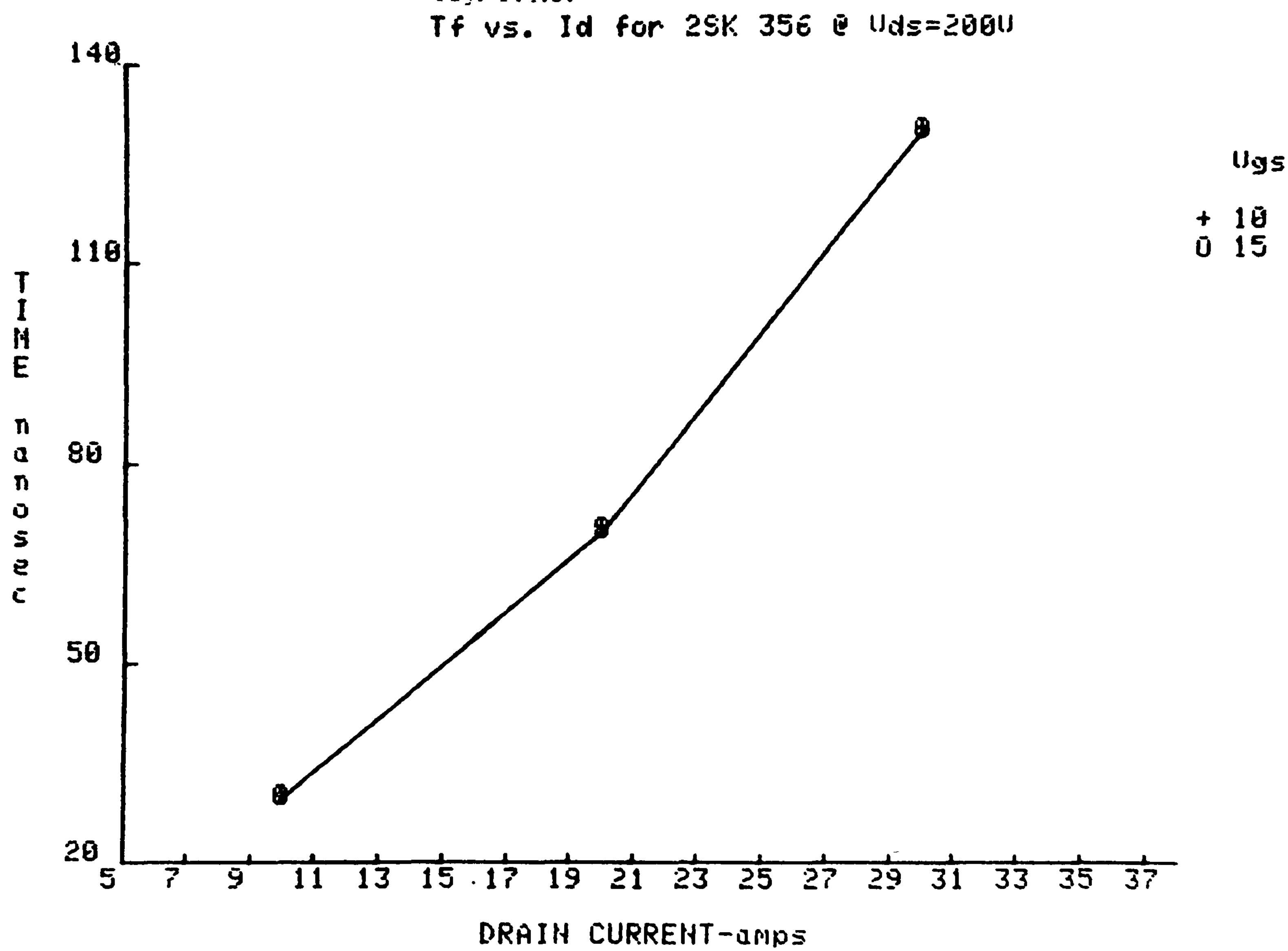
Tf vs. Id for 2SK 356 @ Vds=200V
140
110
80
50
20
TIME nanosec
5 7 9 11 13 15 17 19 21 23 25 27 29 31 33 35 37
DRAIN CURRENT-amps
Vgs
+ 10
0 15

Fig. F.4.6.

Toff vs. Id for 2SK 356 @ Vds=200V

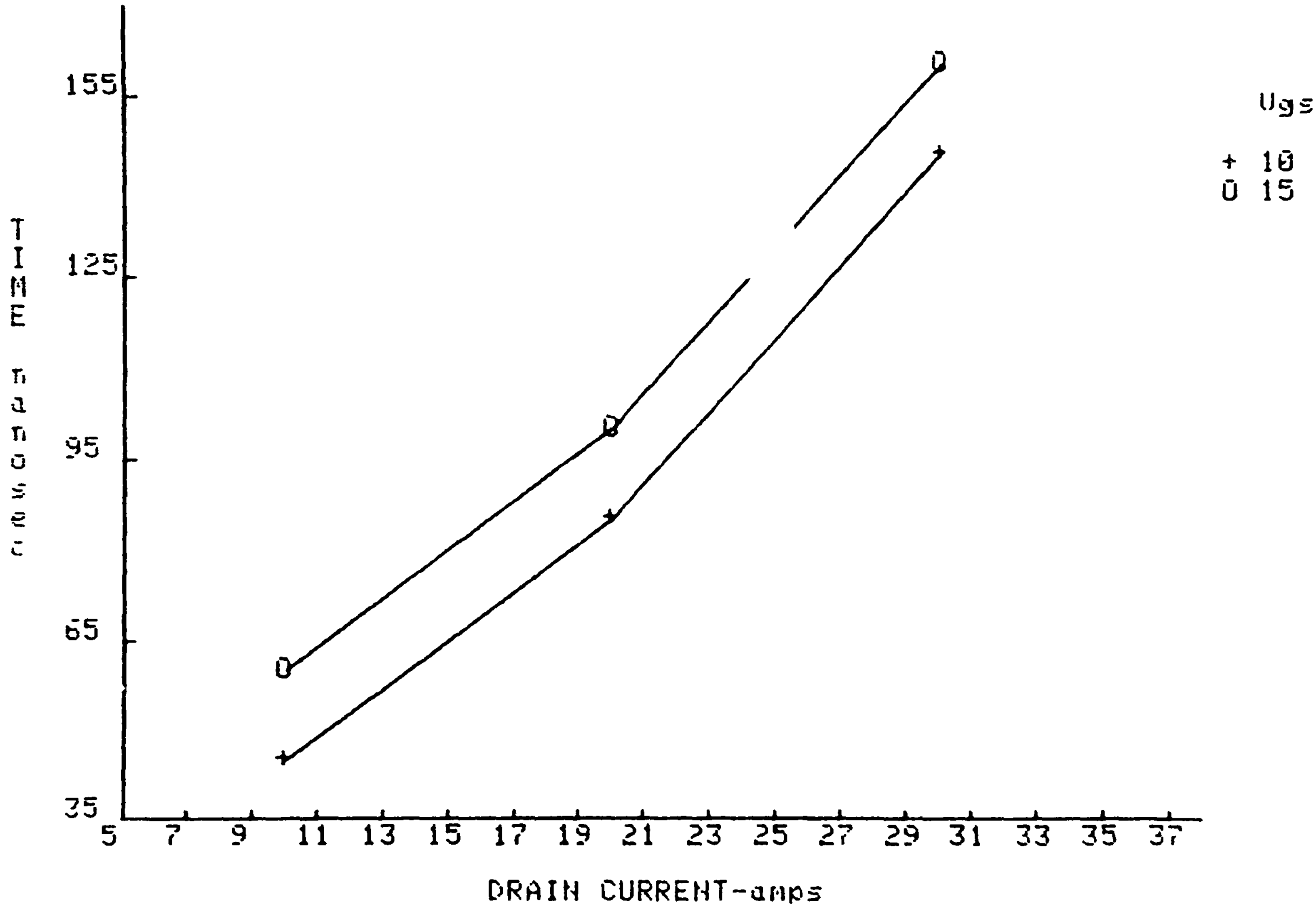

F.5 Test Data of Swıtchıng Tımes Characterıyatıon of the Toshıba

Fig. F.5.1.

Td(on) vs. Id for 2SK 386 @ Vds=200V

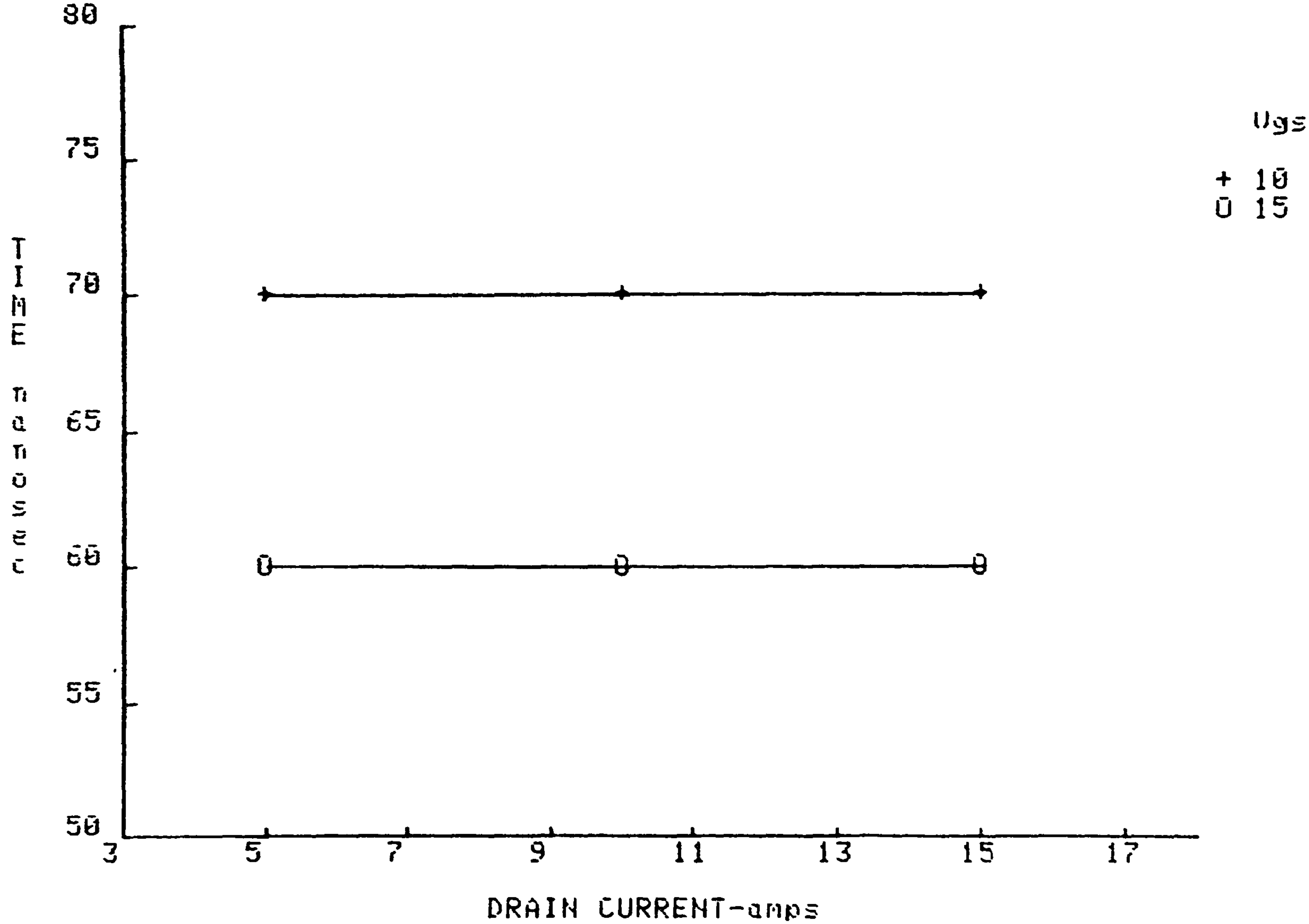

Fig. F.5.2.
Tr vs. Id for 2SK 386 @ Vds=200V

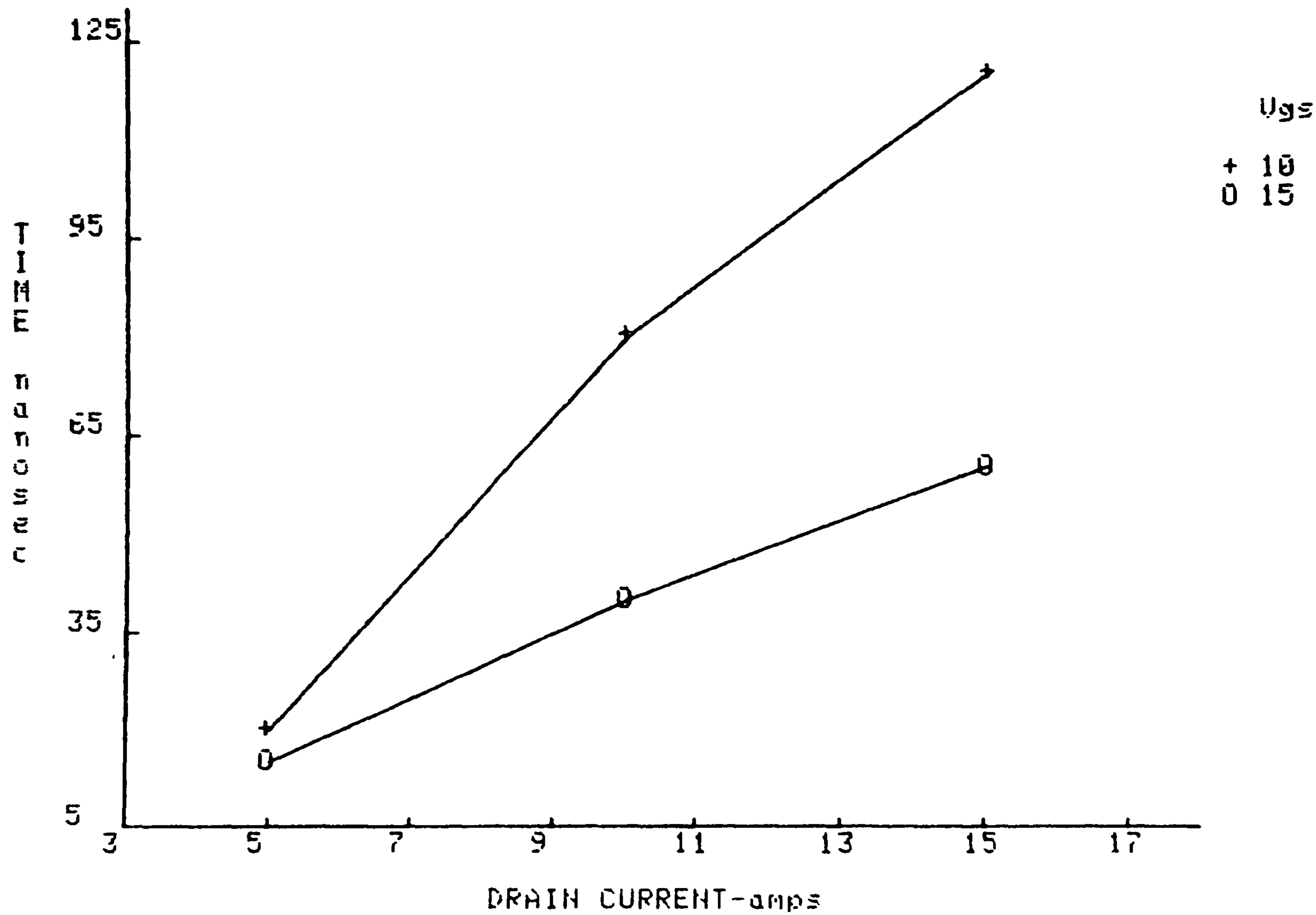

Fig. F.5.3.

Ton vs. Id for 2Sk 386 @ Vds=200V

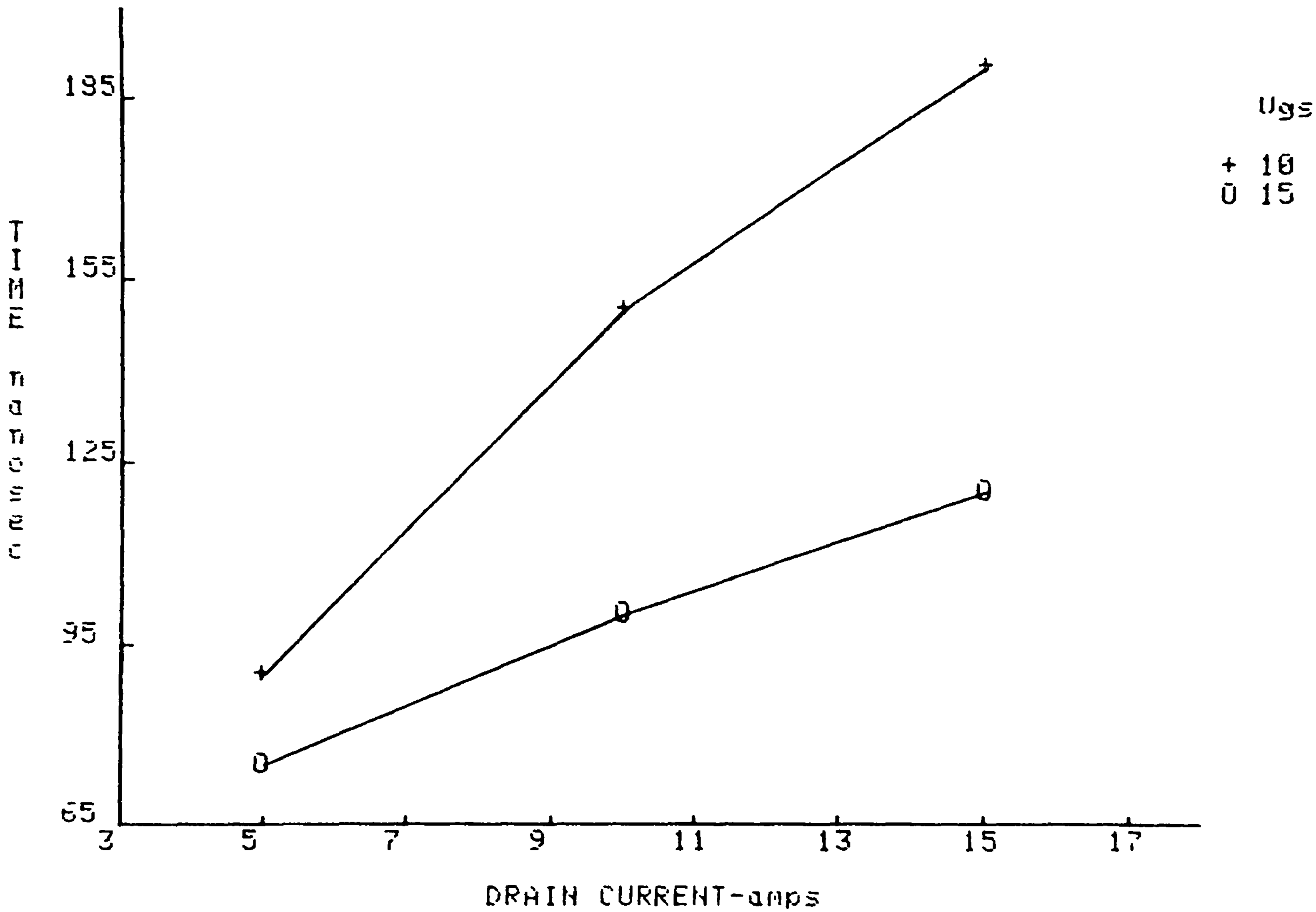

Fig. F.5.4.

Td(off) vs. Id for 2SK 386 @ Vds=200V

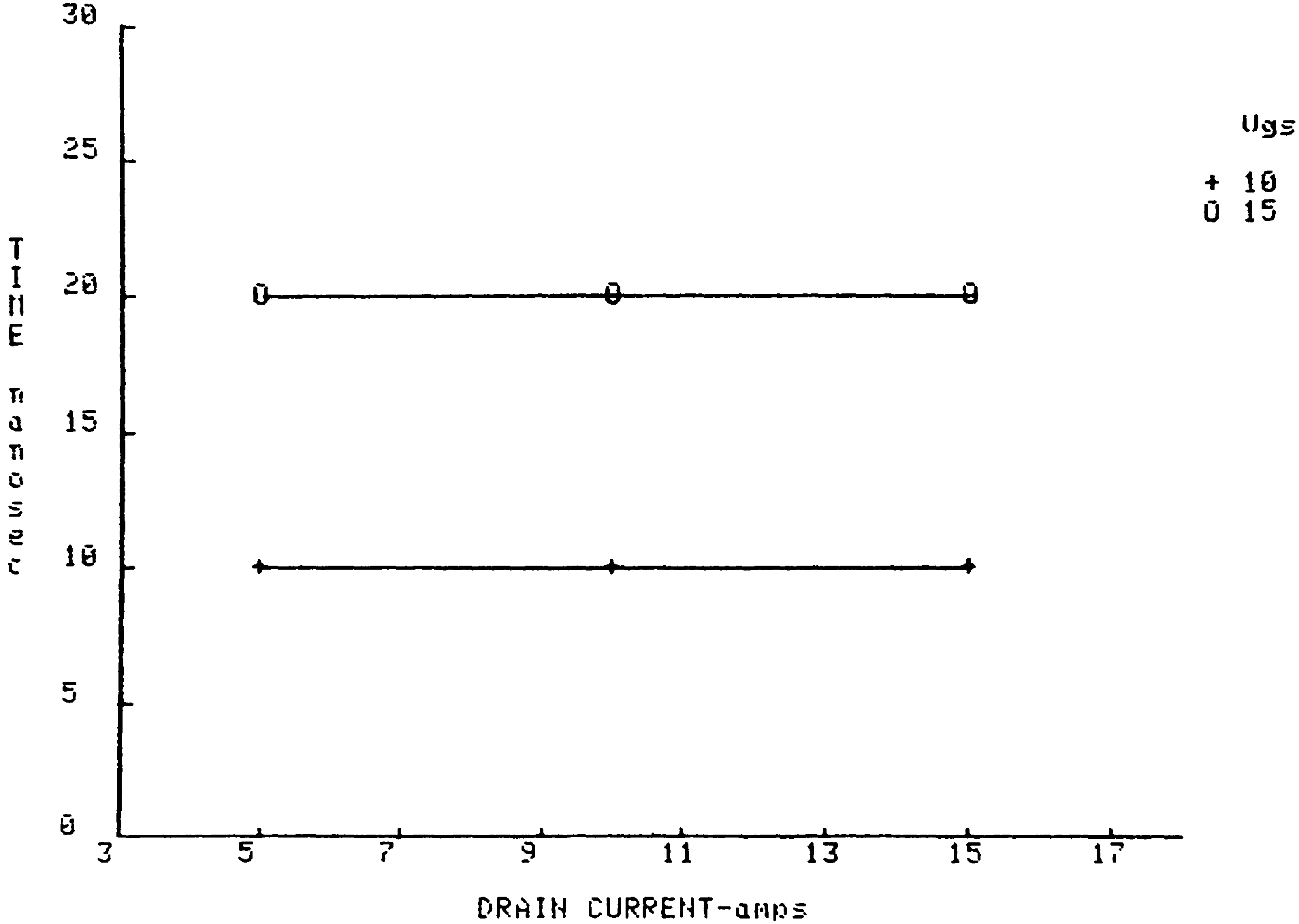

Fig. F.5.5.

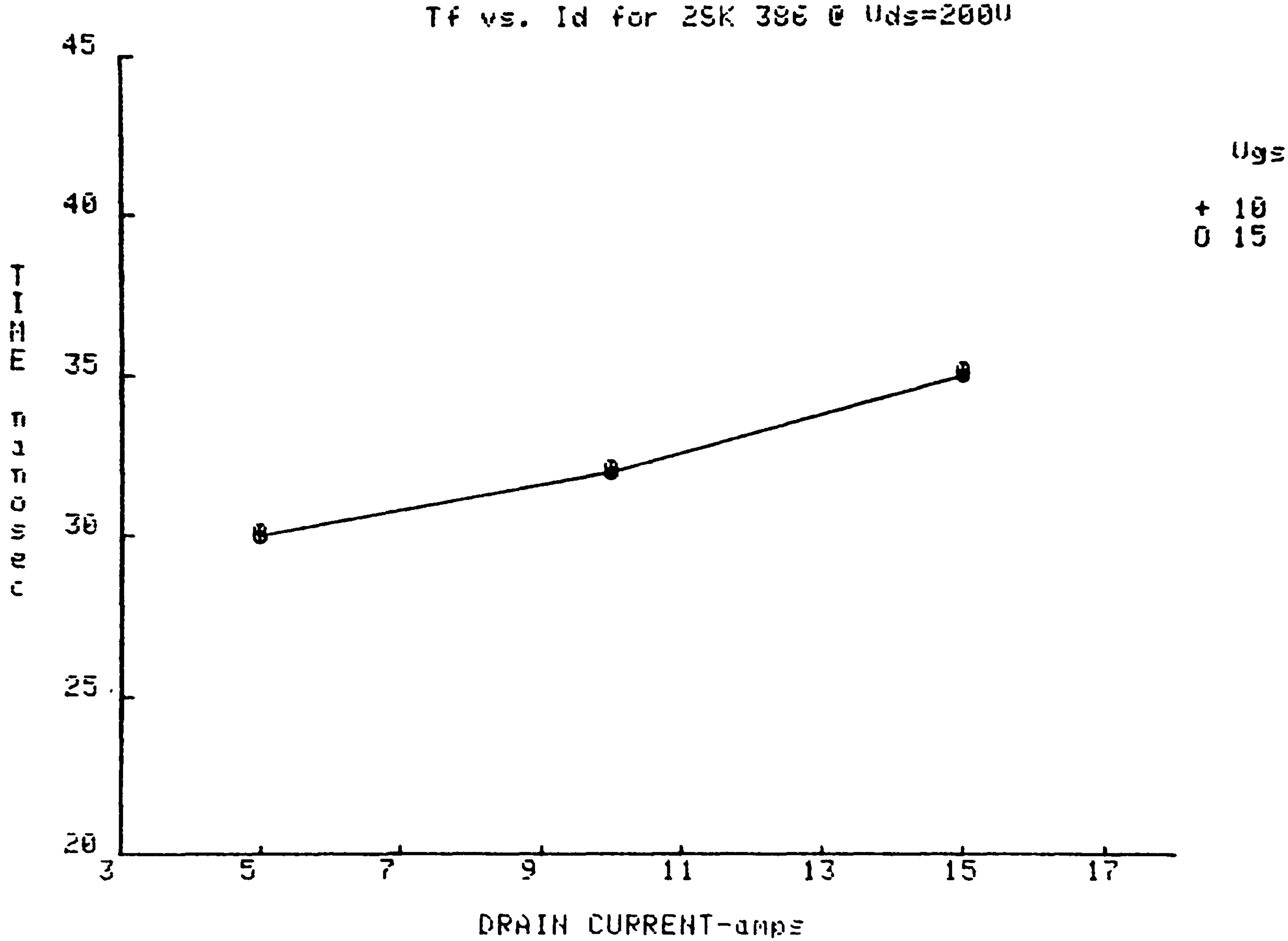

Tf vs. Id for 2SK 386 @ Vds=200V
45
40
35
30
25
20
TIME nanosec
3
5
7
9
11
13
15
17
DRAIN CURRENT-amps
Vgs
+ 10
O 15

Fig. F.5.6.

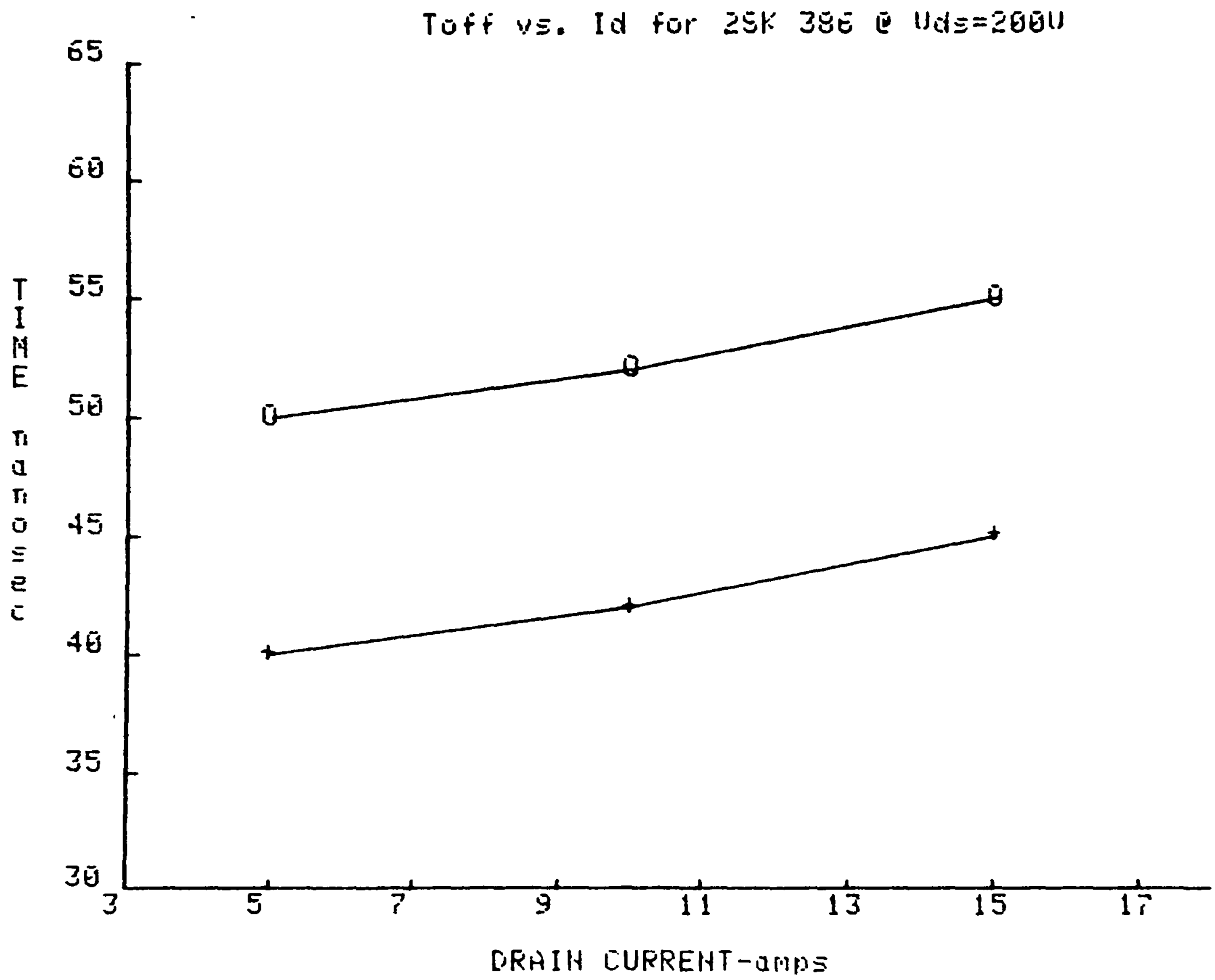

Toff vs. Id for 2SK 386 @ Vds=200V
TIME nanosec
65
60
55
50
45
40
35
30
3
5
7
9
11
13
15
17
DRAIN CURRENT-amps

APPENDIX G

COMPARATIVE TEST DATA OF MOSFETs CHARACTERIZATION

G.1 Comparative Test Data of On-Resistance at Different Case Temperatures

Fig. G.1.1

Rds(on) vs. Id COMPARATIVE DATA for Vgs=10V @ Tc=30 C

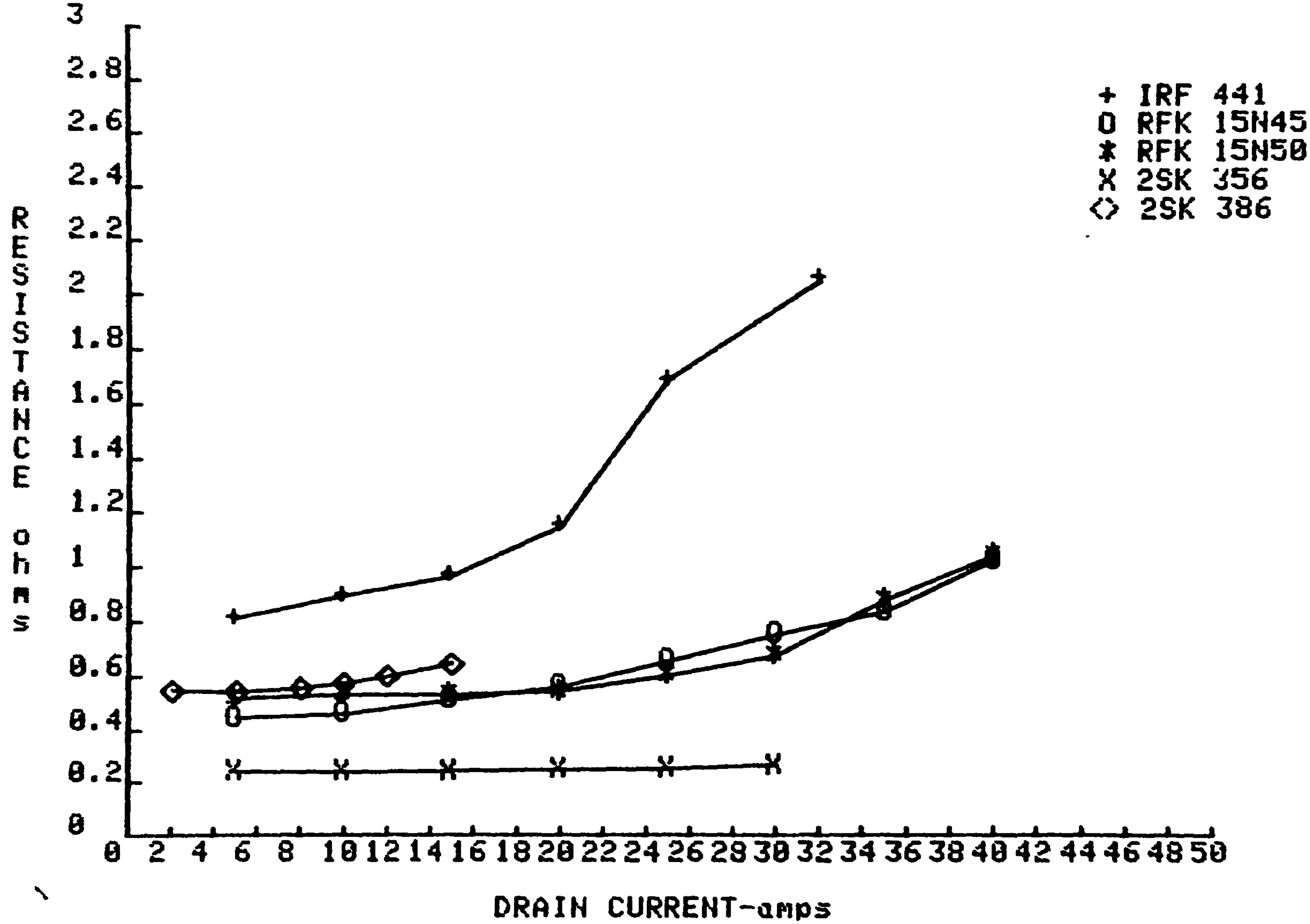

Fig. G.1.2

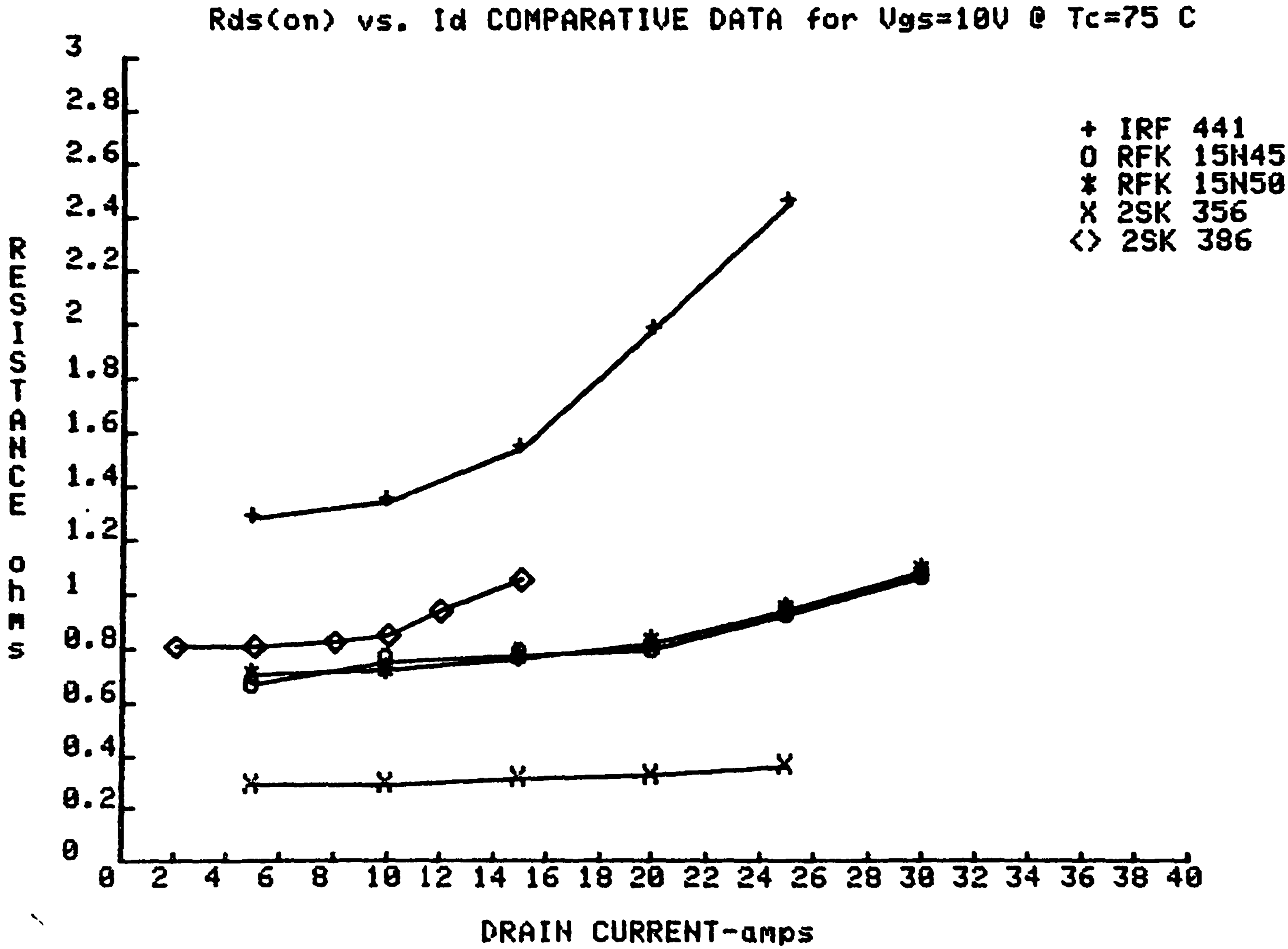
Rds(on) vs. Id COMPARATIVE DATA for Vgs=10V @ Tc=75 C
+ IRF 441
O RFK 15N45
* RFK 15N50
X 2SK 356
<> 2SK 386
RESISTANCE ohms
DRAIN CURRENT-amps
3
2.8
2.6
2.4
2.2
2
1.8
1.6
1.4
1.2
1
0.8
0.6
0.4
0.2
0
0 2 4 6 8 10 12 14 16 18 20 22 24 26 28 30 32 34 36 38 40

Fig. G.1.3

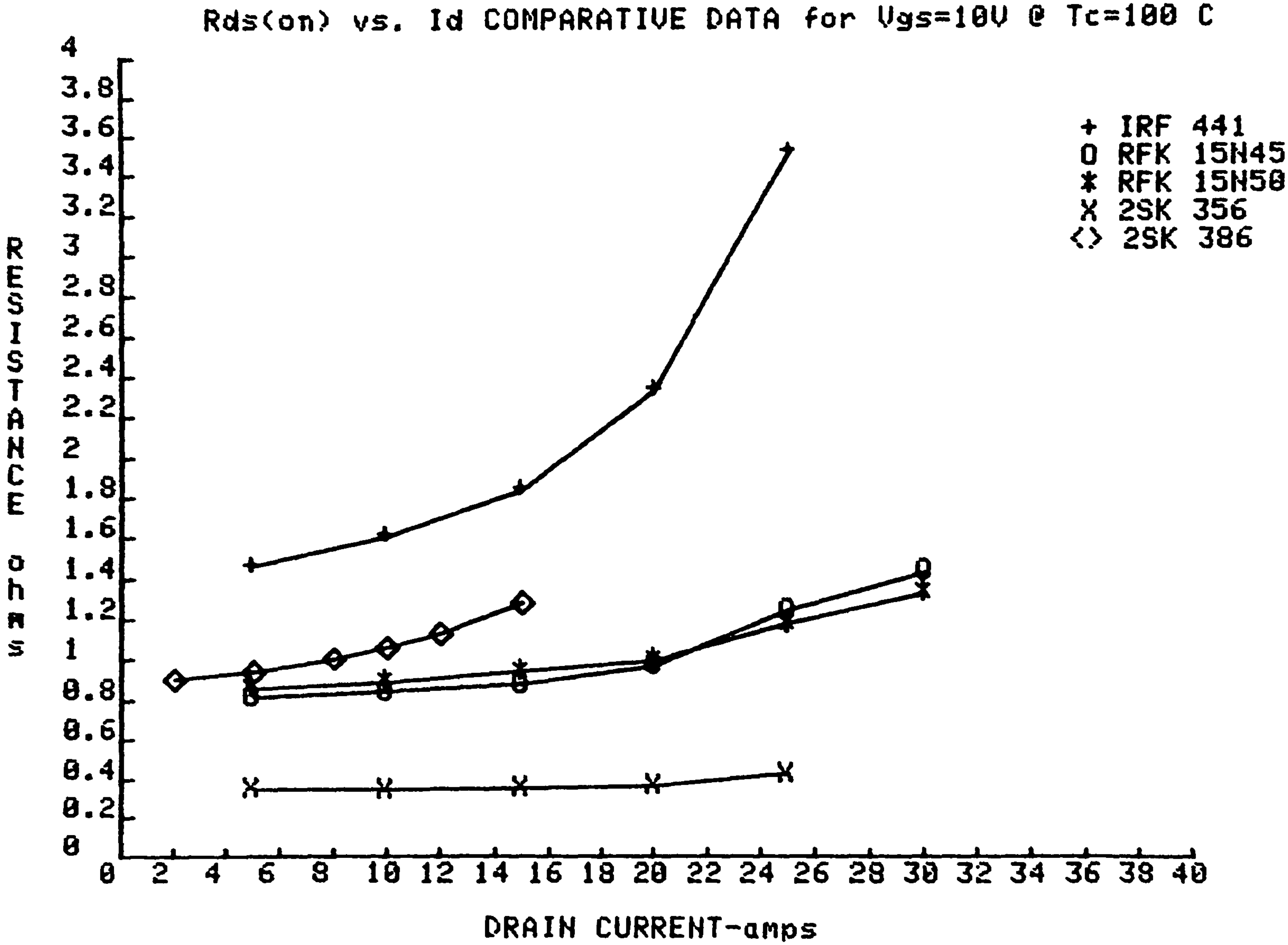

Rds(on) vs. Id COMPARATIVE DATA for Vgs=10V @ Tc=100 C
RESISTANCE ohms
DRAIN CURRENT-amps
+ IRF 441
O RFK 15N45
* RFK 15N50
X 2SK 356
<> 2SK 386
0
0.2
0.4
0.6
0.8
1
1.2
1.4
1.6
1.8
2
2.2
2.4
2.6
2.8
3
3.2
3.4
3.6
3.8
4
0 2 4 6 8 10 12 14 16 18 20 22 24 26 28 30 32 34 36 38 40

G.2 Comparative Test Data of Switching Times for V_{GS}=10V

Fig. G.2.1

Td(on) vs. Id COMPARATIVE DATA for Vgs=10V @ Vds=200V

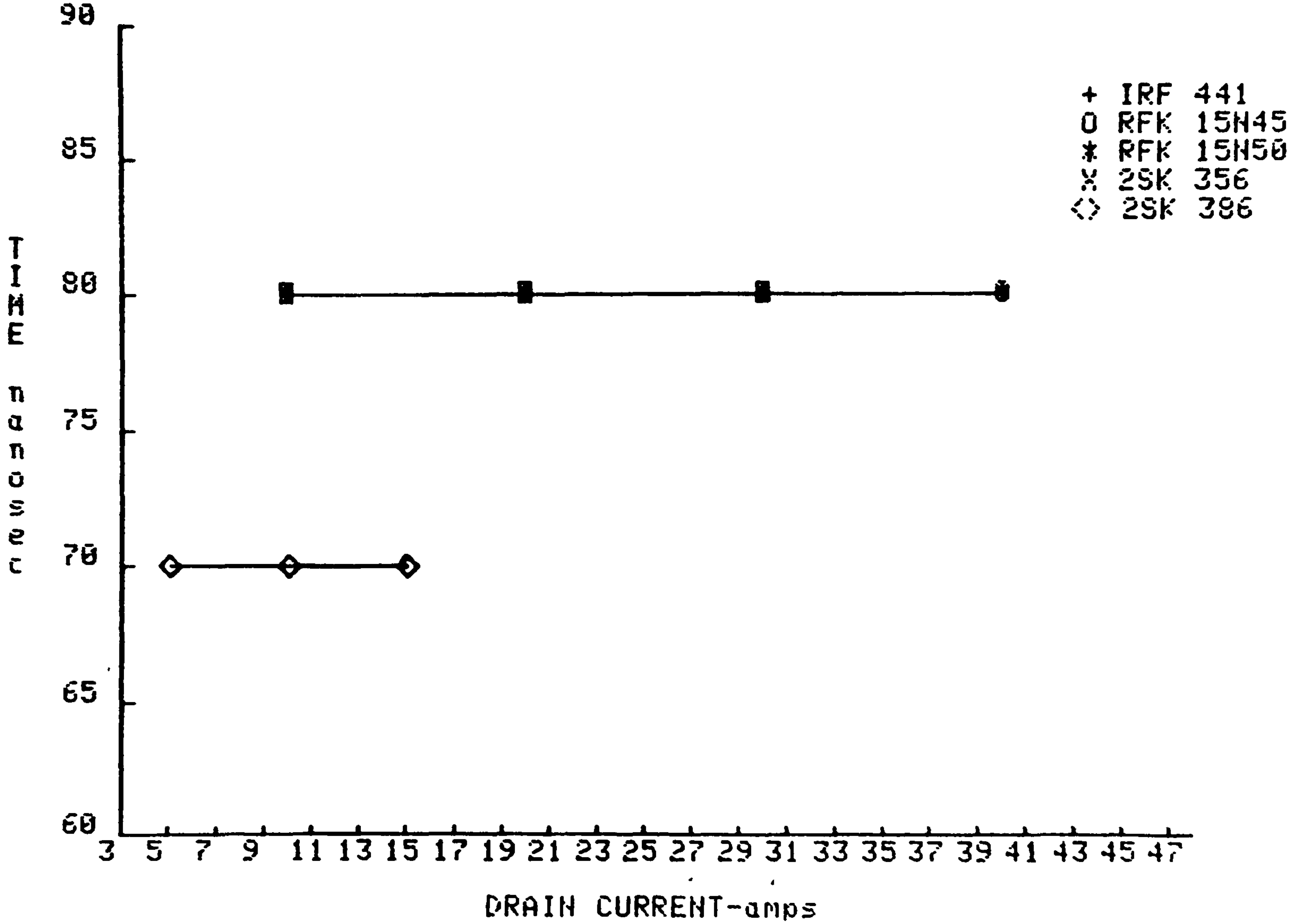

Fig. G.2.2

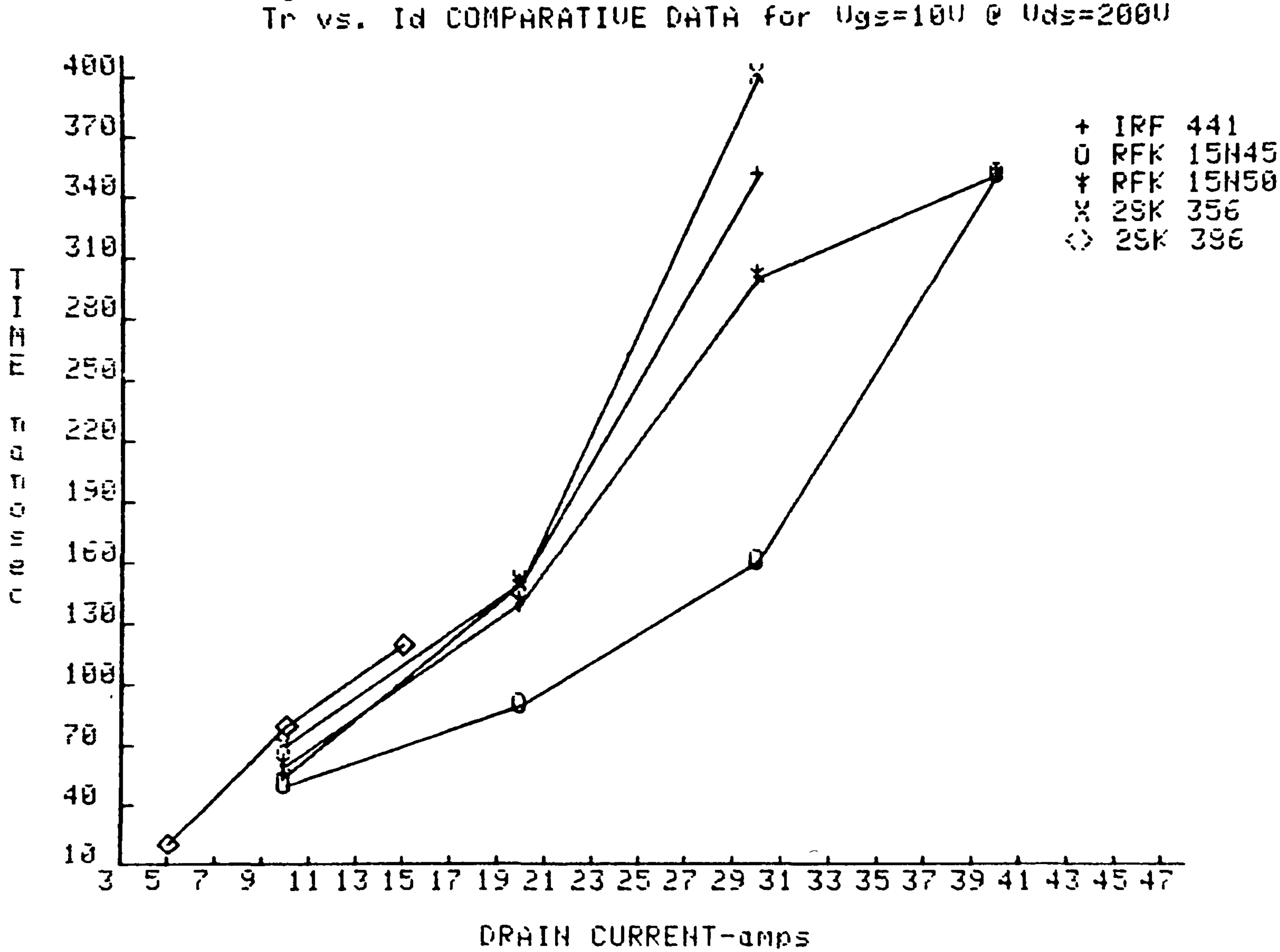
Tr vs. Id COMPARATIVE DATA for Vgs=10V @ Vds=200V
TIME nanosec
DRAIN CURRENT-amps
+ IRF 441
O RFK 15N45
RFK 15N50
X 2SK 356
◇ 2SK 396
400
370
340
310
280
250
220
190
160
130
100
70
40
10
3 5 7 9 11 13 15 17 19 21 23 25 27 29 31 33 35 37 39 41 43 45 47

Fig. G.2.3

Ton vs. Id COMPARATIVE DATA for Vgs=10V @ Vds=200V

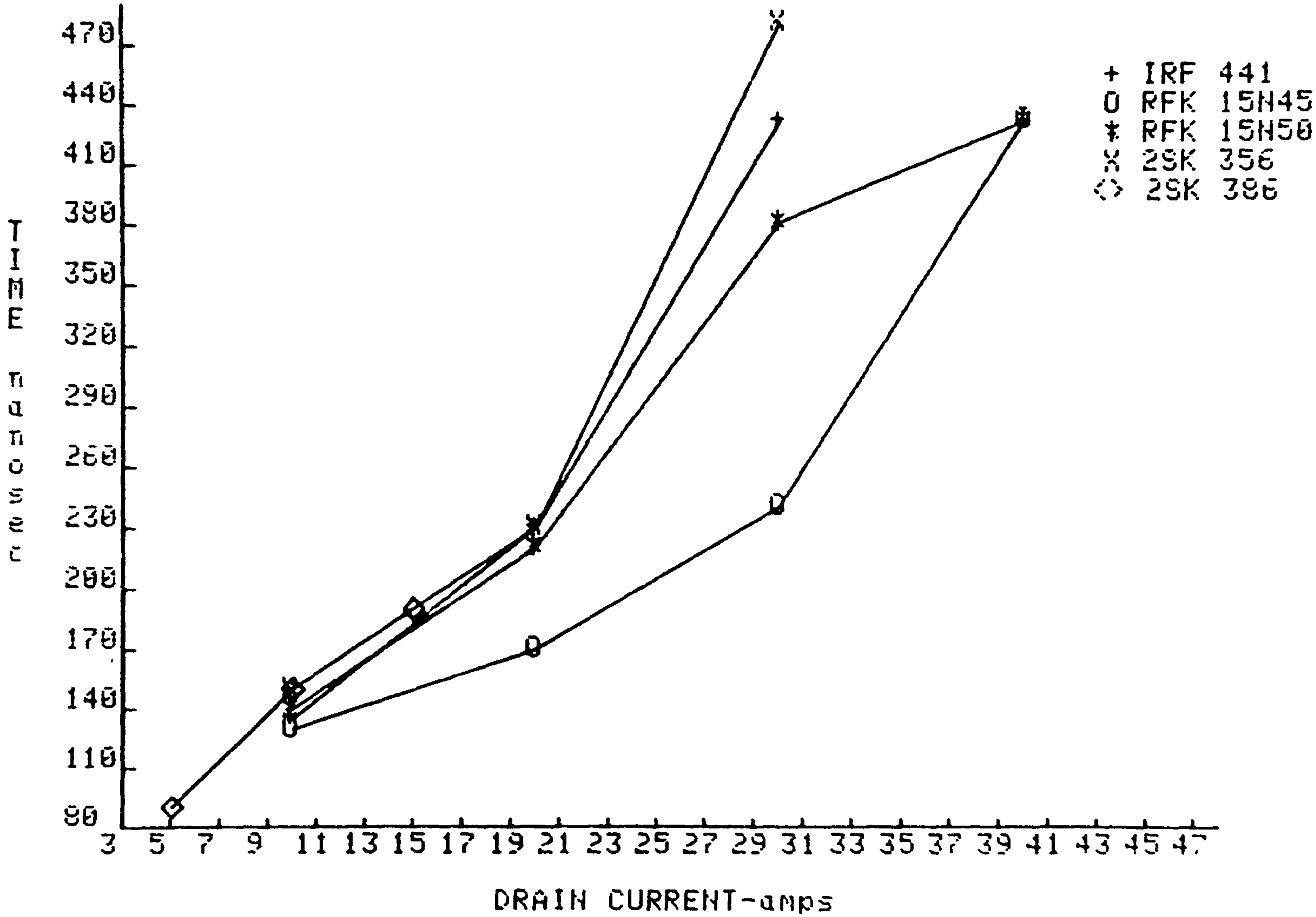

Fig. G.2.4

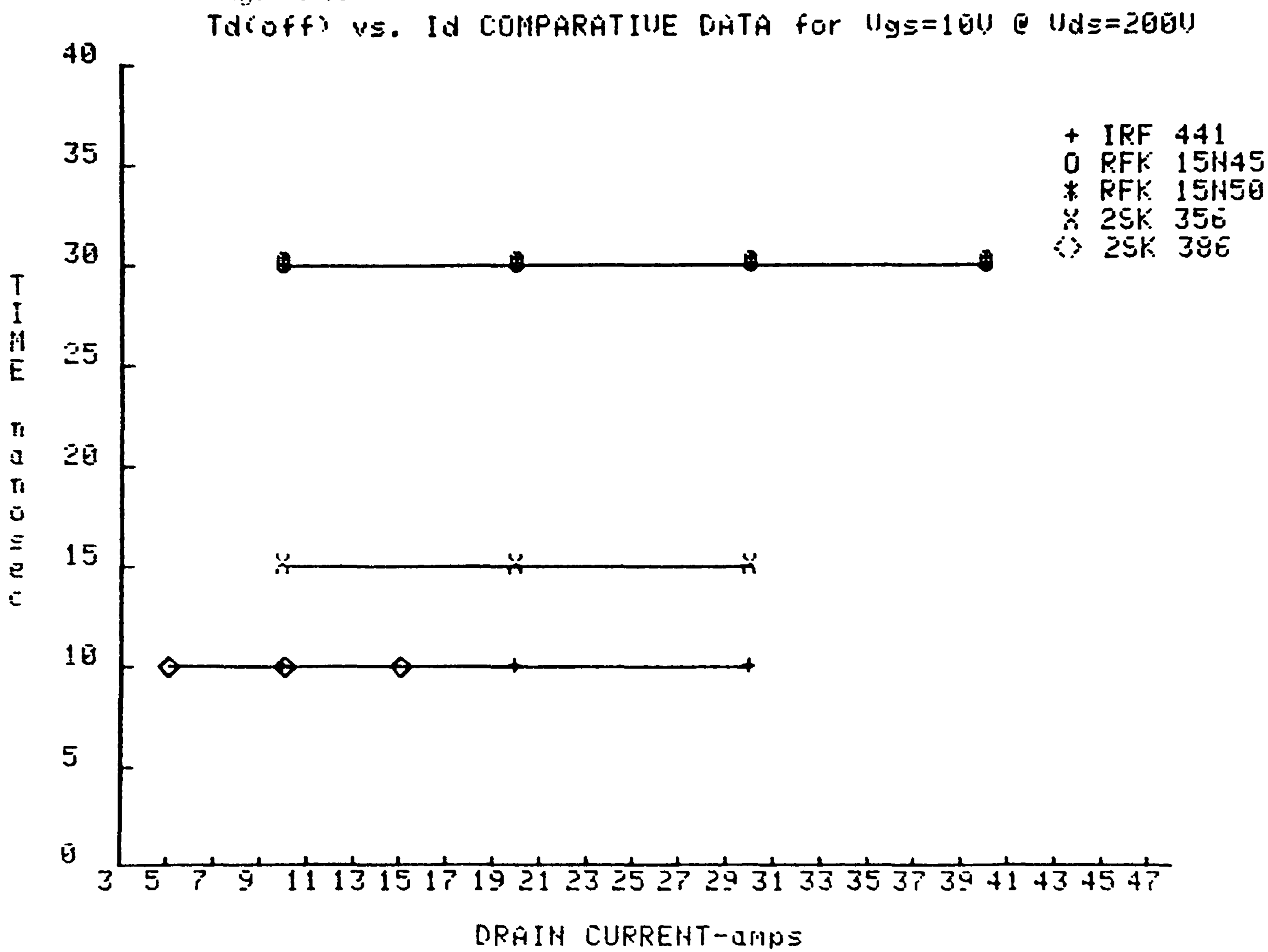

Td(off) vs. Id COMPARATIVE DATA for Vgs=10V @ Vds=200V
TIME nanosec
40
35
30
25
20
15
10
5
0
3 5 7 9 11 13 15 17 19 21 23 25 27 29 31 33 35 37 39 41 43 45 47
DRAIN CURRENT-amps
+ IRF 441
O RFK 15N45
* RFK 15N50
X 2SK 356
<> 2SK 386

Fig. G.2.5

Tf vs. Id COMPARATIVE DATA for Vgs=10V @ Vds=200V

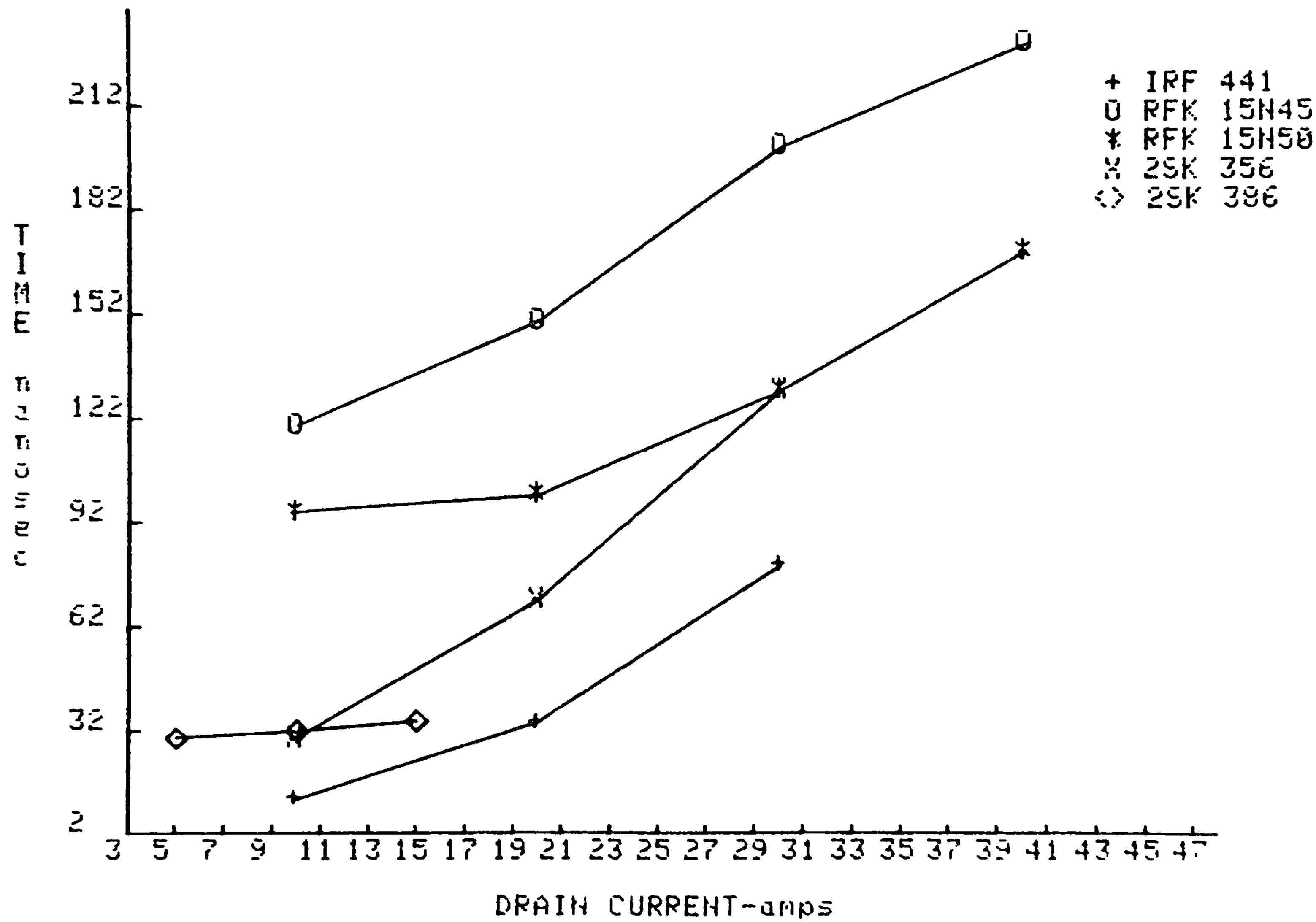

Fig. G.2.6

Toff vs. Id COMPARATIVE DATA for Vgs=10V @ Vds=200V

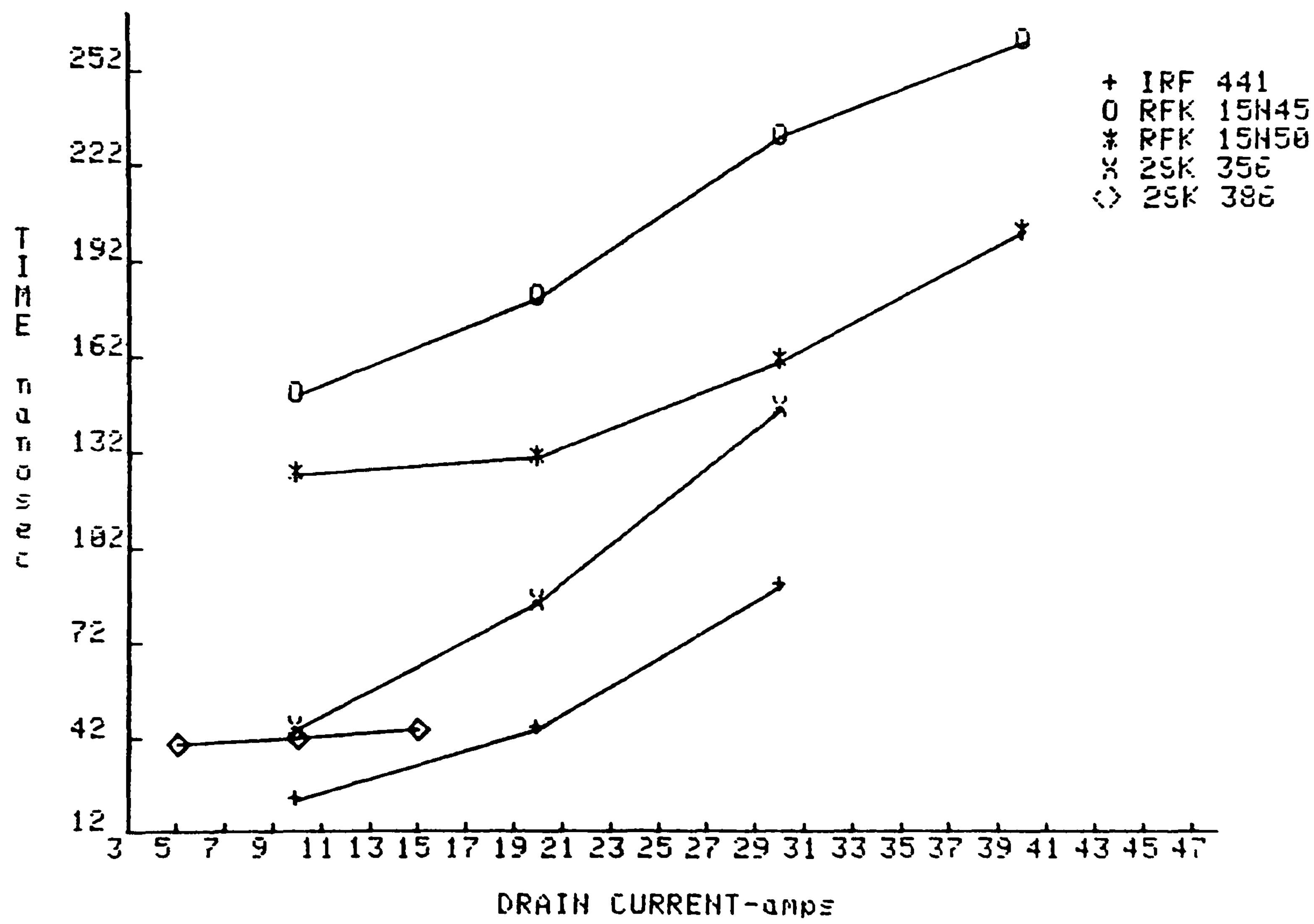

G.3 Comparative Test Data of Switching Times for V_{GS}=15V

Fig. G.3.1

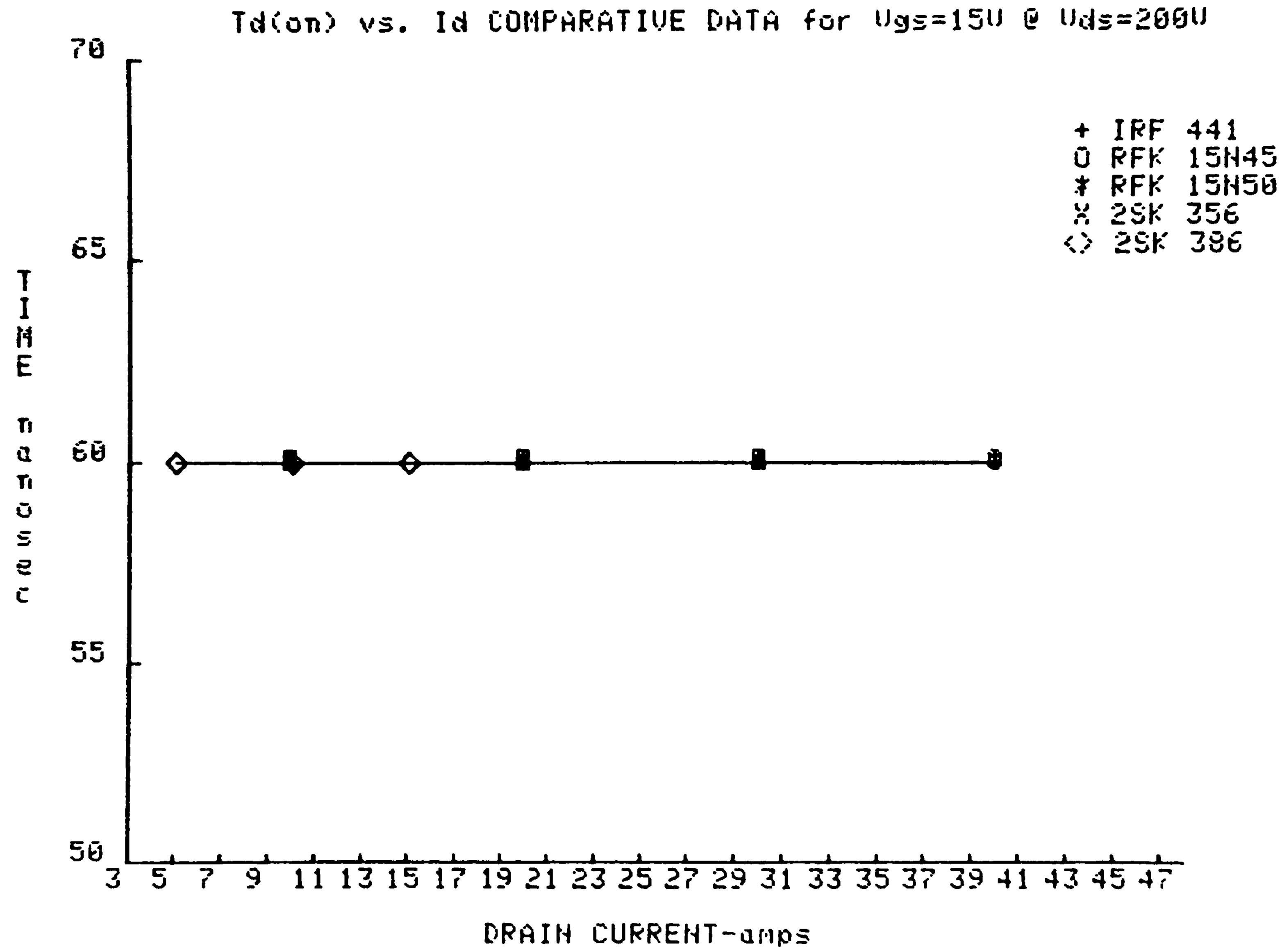

Td(on) vs. Id COMPARATIVE DATA for Vgs=15V @ Vds=200V
70
65
60
55
50
TIME nanosec
+ IRF 441
O RFK 15N45
* RFK 15N50
X 2SK 356
<> 2SK 386
3 5 7 9 11 13 15 17 19 21 23 25 27 29 31 33 35 37 39 41 43 45 47
DRAIN CURRENT-amps

Fig. G.3.2

Tr vs. Id COMPARATIVE DATA for Vgs=15V @ Vds=200V

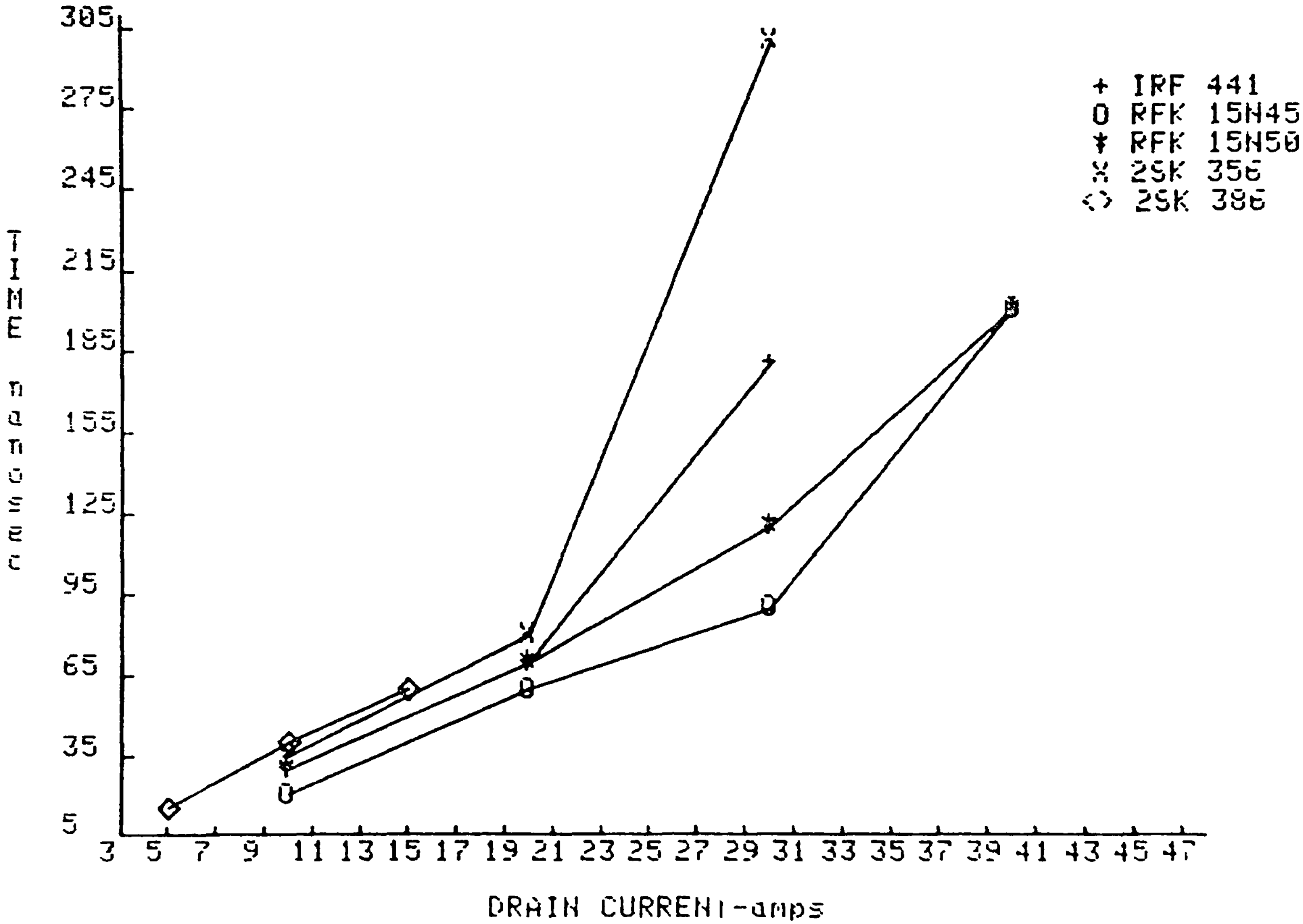

Fig. G.3.3

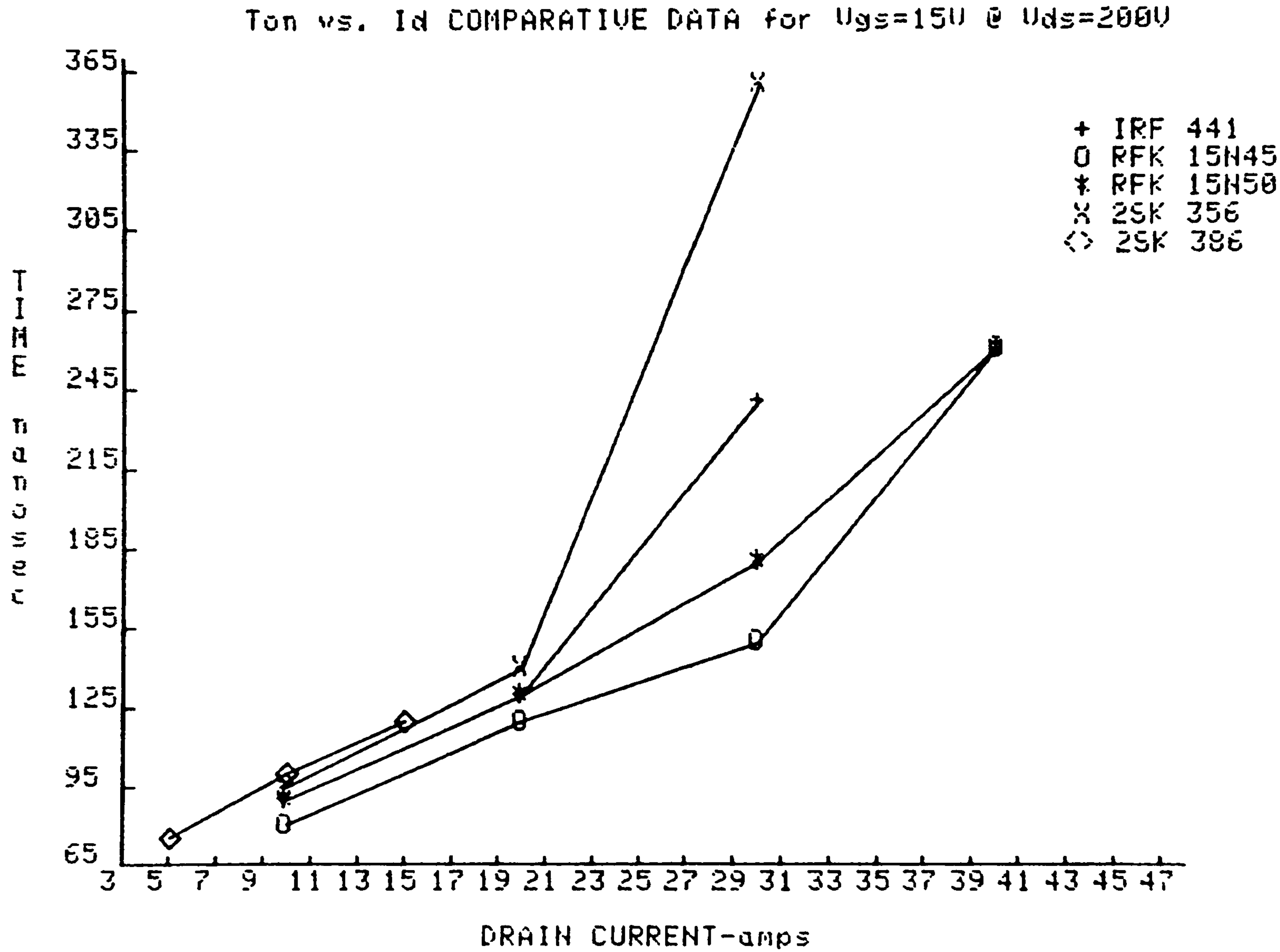
Ton vs. Id COMPARATIVE DATA for Vgs=15V @ Vds=200V
TIME nanosec
DRAIN CURRENT-amps
+ IRF 441
O RFK 15N45
* RFK 15N50
X 2SK 356
<> 2SK 386
365
335
305
275
245
215
185
155
125
95
65
3 5 7 9 11 13 15 17 19 21 23 25 27 29 31 33 35 37 39 41 43 45 47

Fig. G.3.4

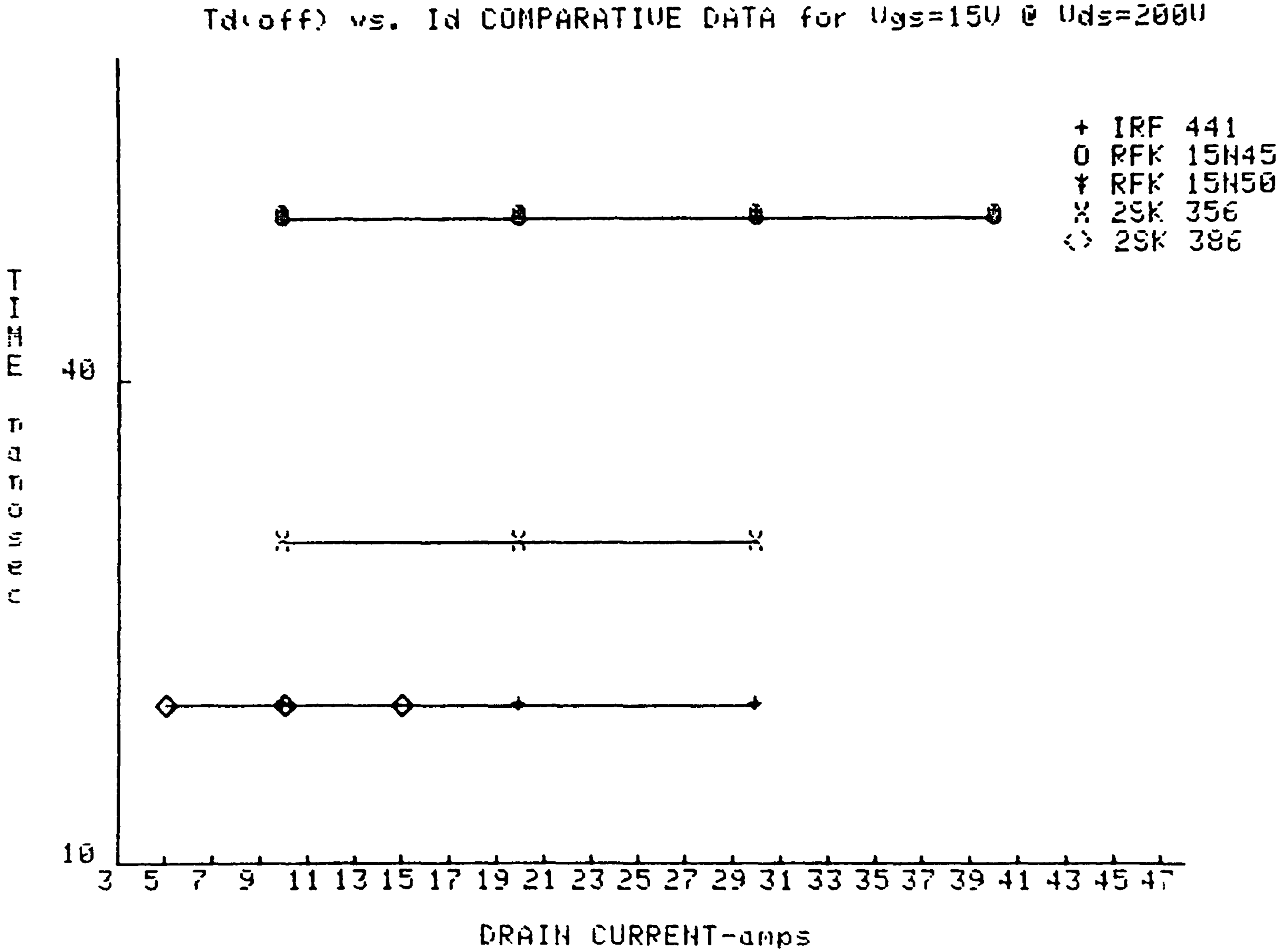
Td(off) vs. Id COMPARATIVE DATA for Vgs=15V @ Vds=200V
+ IRF 441
O RFK 15N45
† RFK 15N50
X 2SK 356
<> 2SK 386
TIME nanosec
40
10
3 5 7 9 11 13 15 17 19 21 23 25 27 29 31 33 35 37 39 41 43 45 47
DRAIN CURRENT-amps

Fig. G.3.5

Tf vs. Id COMPARATIVE DATA for Vgs=15V @ Vds=200V

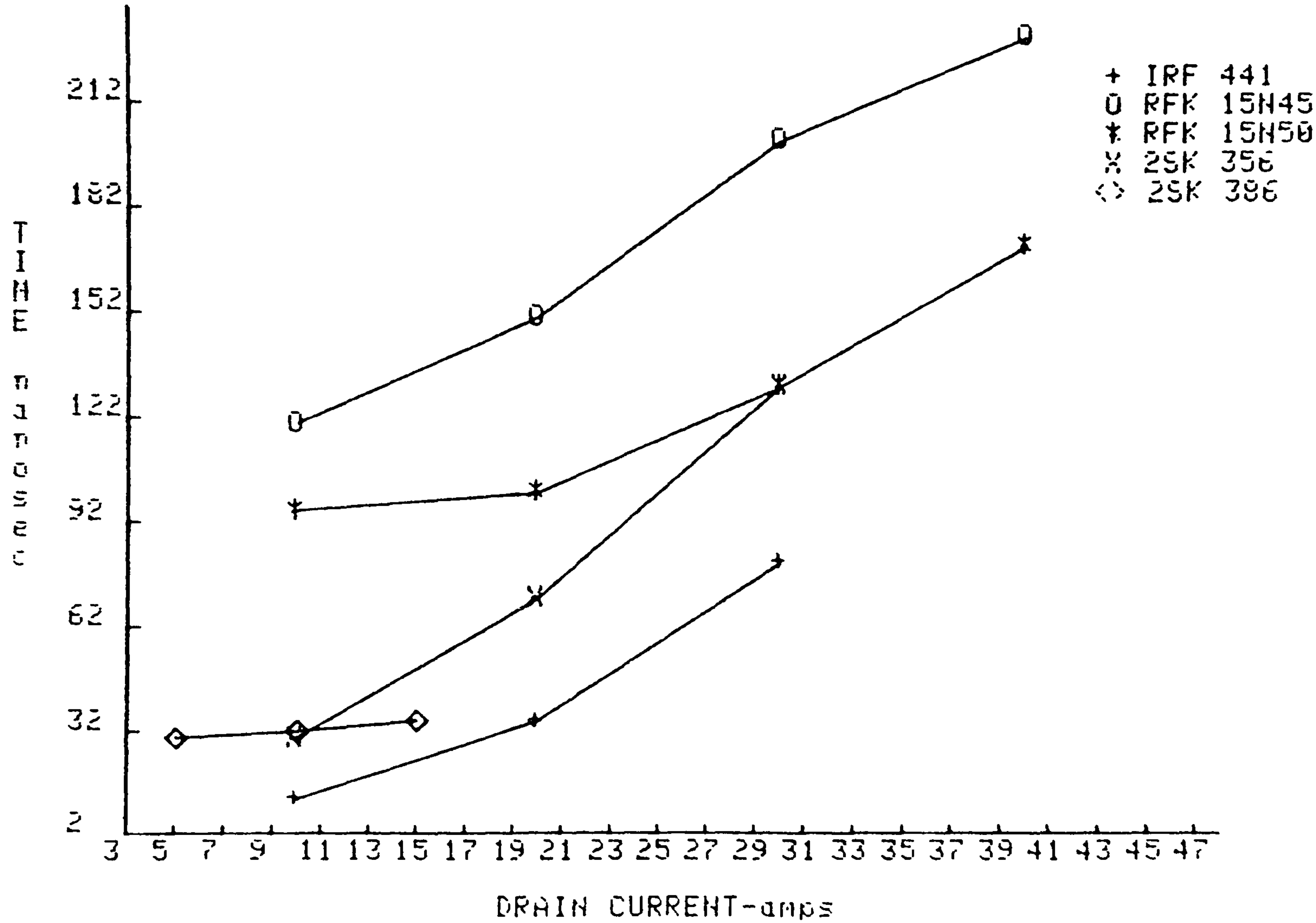

Fig. G.3.6

Toff vs. Id COMPARATIVE DATA for Vgs=15V @ Vds=200V

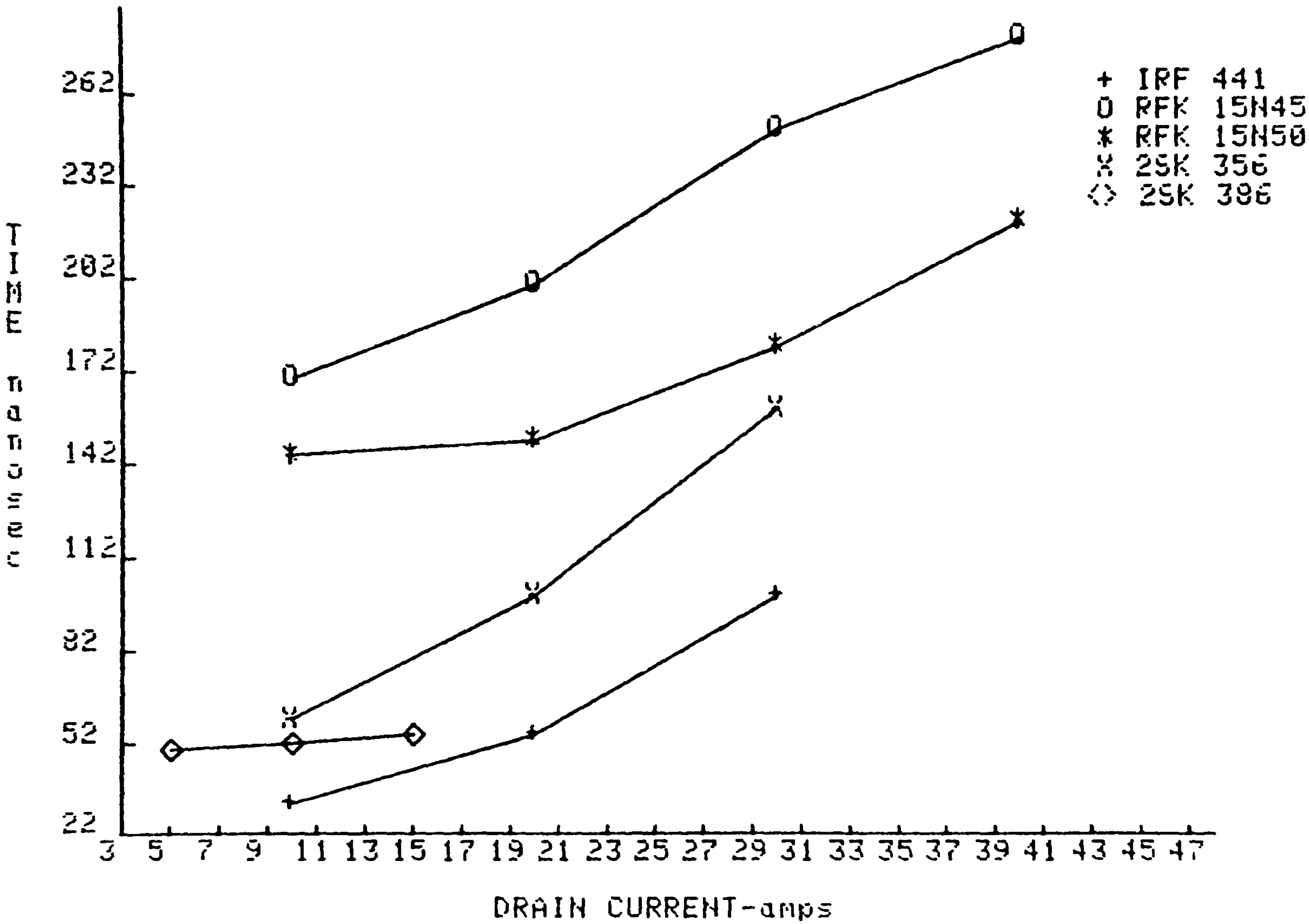

APPENDIX H

TEST DATA OF MOSFETs PARALLEL OPERATION CHARACTERIZATION

H.1 Test Data of Parallel Operation of the IRF 441

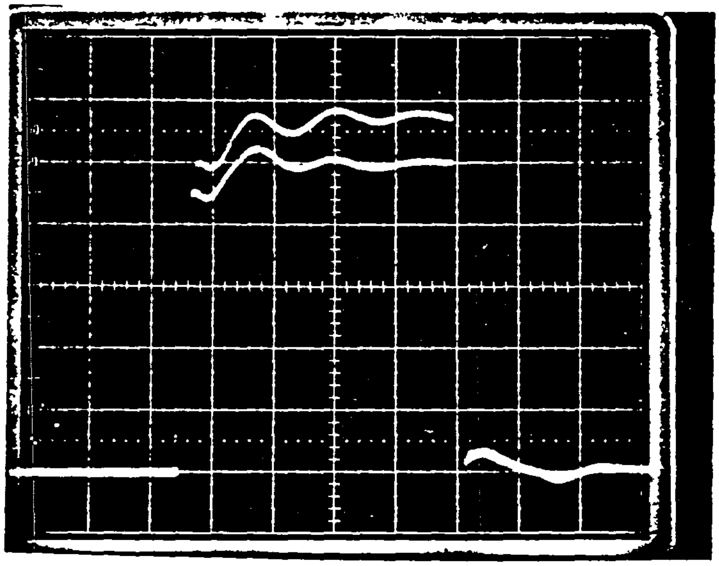

Fig. H.1.1 Drain current waveforms of two IRF 441 devices connected in parallel at 20A load current.
Scale: 500ns/div; 2A/div.

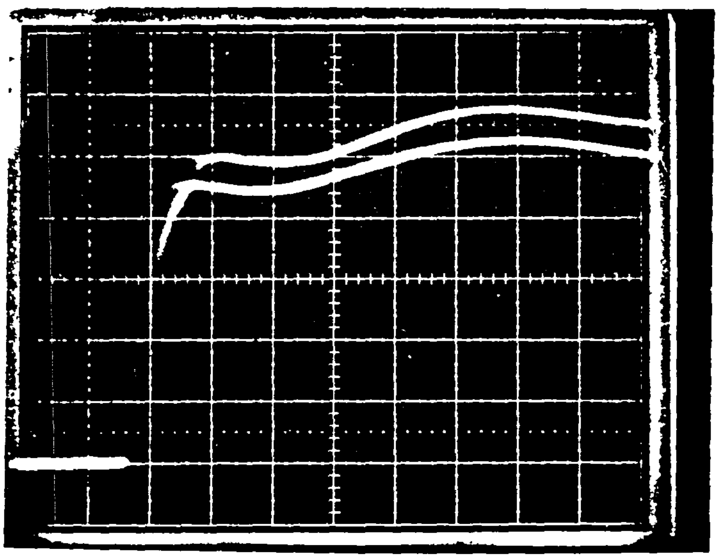

Fig. H.1.2 Drain current waveforms of two IRF 441 devices in parallel during turn-on phase at 20A load current.
Scale: 100ns/div; 2A/div.

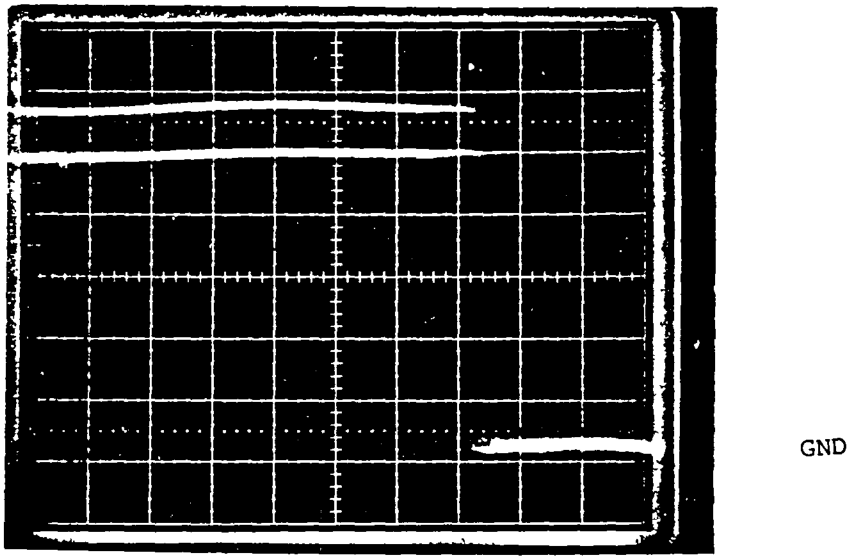

Fig. H.1.3 Drain current waveforms of two IRF 441 devices in parallel during turn-off phase at 20A load current.
Scale: 100ns/div; 2A/div.

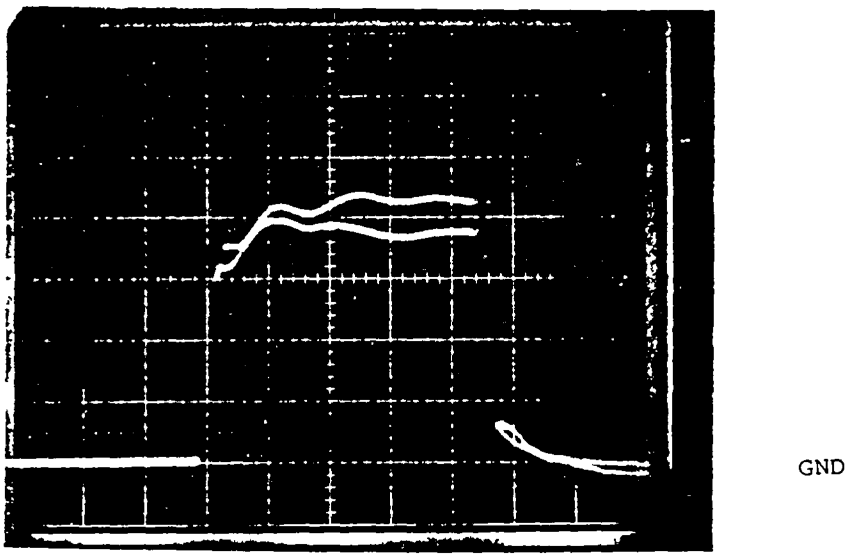

Fig. H.1.4 Drain current waveforms of two IRF 441 devices connected in parallel at 40A load current.
Scale: 500ns/div; 5A/div.

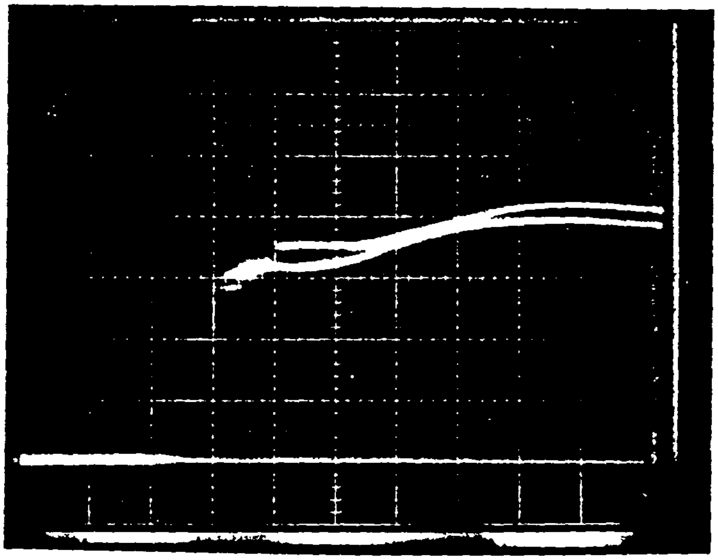

GND

Fig. H.1.5 Drain current waveforms of two IRF 441 devices in parallel during turn-on phase at 40A load current.
Scale: 100ns/div; 5A/div.

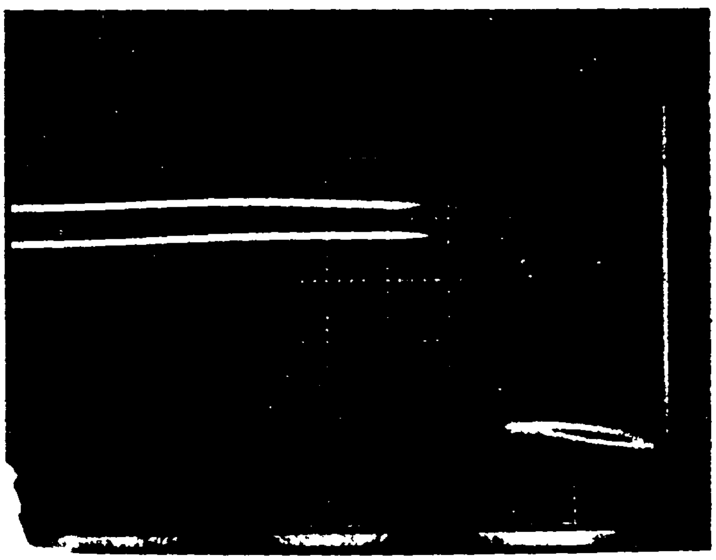

GND

Fig. H.1.6 Drain current waveforms of two IRF 441 devices in parallel during turn-off phase at 40A load current.
Scale: 100ns/div; 5A/div.

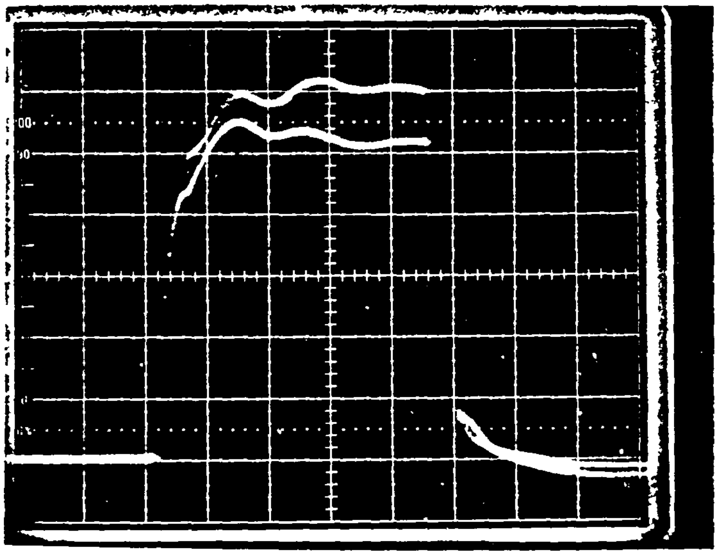

Fig. H.1.7 Drain current waveforms of two IRF 441 devices connected in parallel at 60A load current.
Scale: 500ns/div; 5A/div.

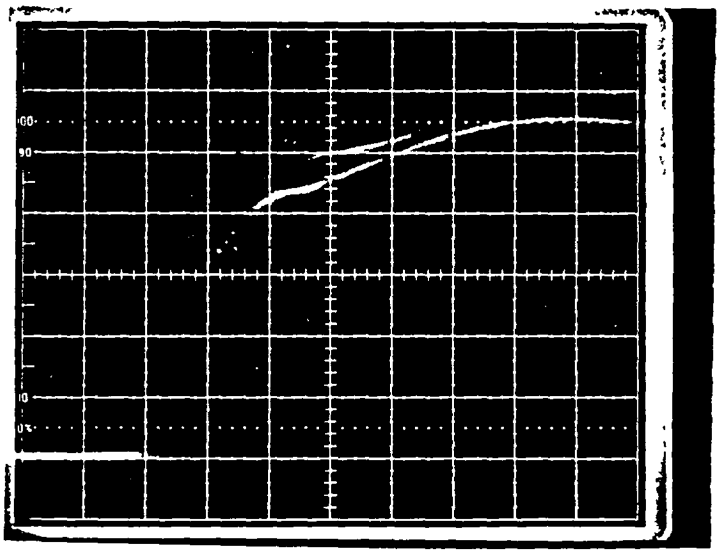

Fig. H.1.8 Drain current waveforms of two IRF 441 devices in parallel during turn-on phase at 60A load current.
Scale: 100ns/div; 5A/div.

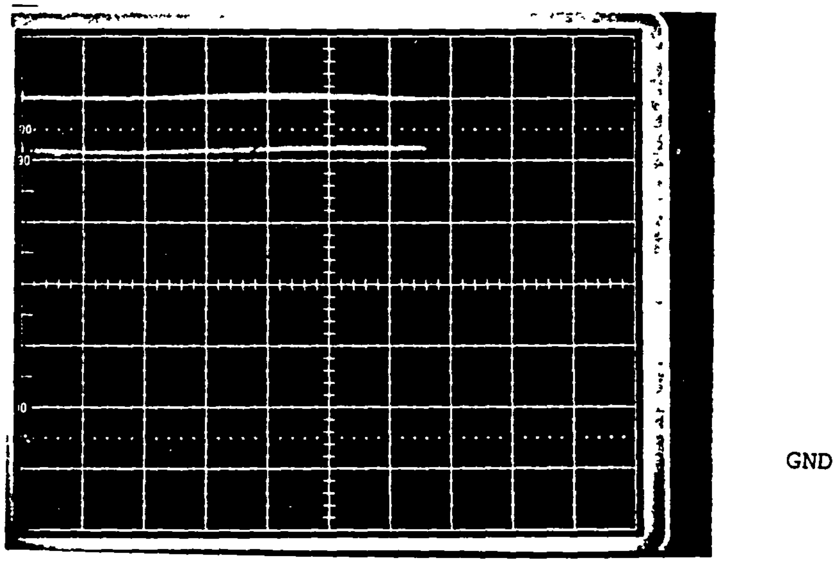

Fig. H.1.9 Drain current waveforms of two IRF 441 devices in parallel during turn-off phase at 60A load current.
Scale: 100ns/div; 5A/div.

H.2 Test Data of Parallel Operation of the RCA RFK 15N45

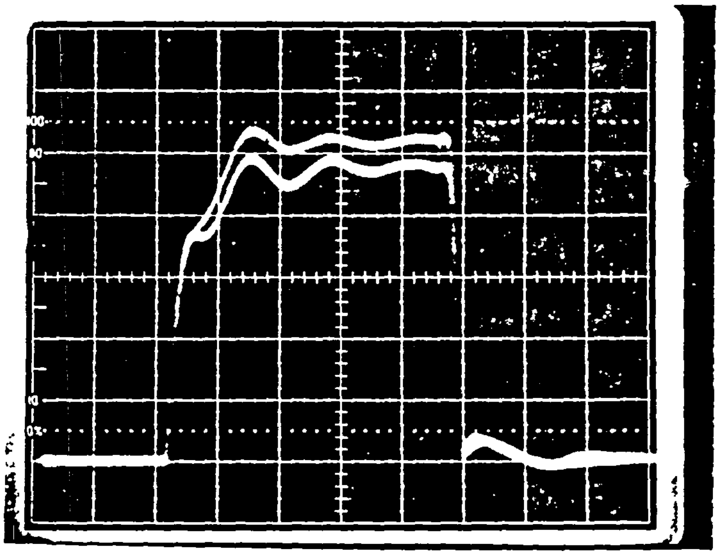

GND

Fig. H.2.1 Drain current waveforms of two RFK 15N45 devices connected in parallel at 20A load current.
Scale: 500ns/div; 2A/div.

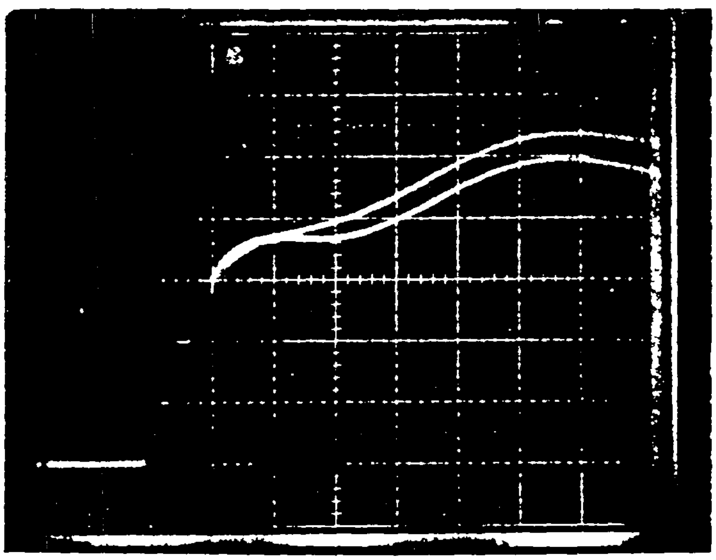

GND

Fig. H.2.2 Drain current waveforms of two RFK 15N45 devices connected in parallel during turn-on phase at 20A load current.
Scale: 100ns/div; 2A/div.

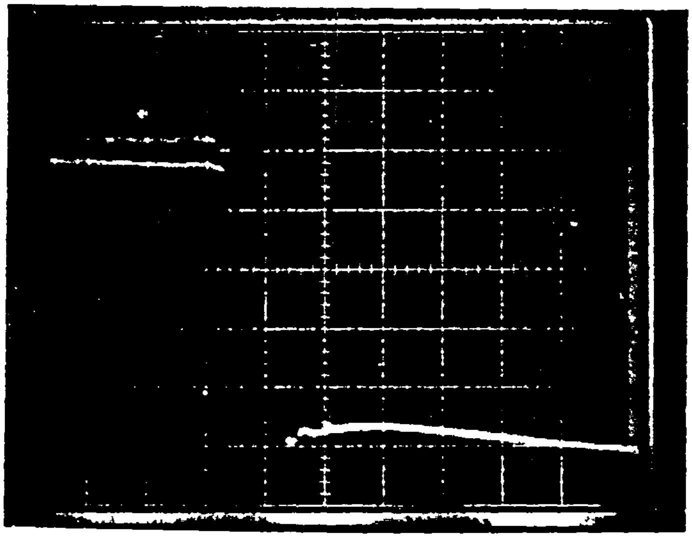

GND

Fig. H.2.3 Drain current waveforms of two RFK 15N45 devices connected in parallel during turn-off phase at 20A load current.
Scale: 100ns/div; 2A/div.

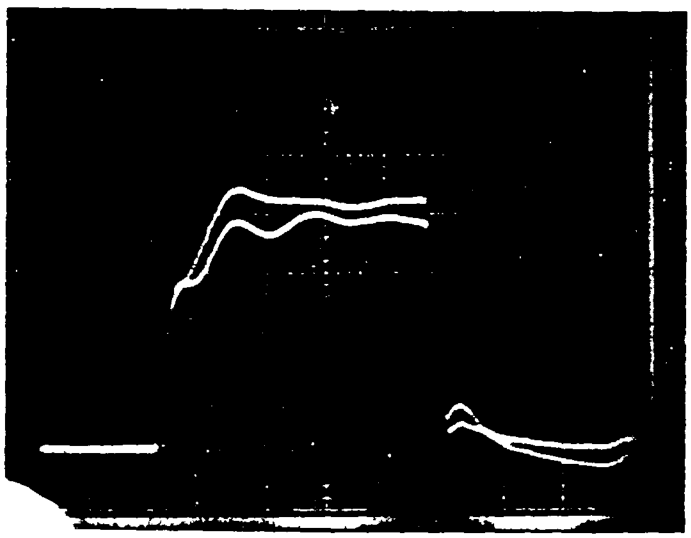

GND

Fig. H.2.4 Drain current waveforms of two RFK 15N45 devices connected in parallel at 40A load current.
Scale: 500ns/div; 5A/div.

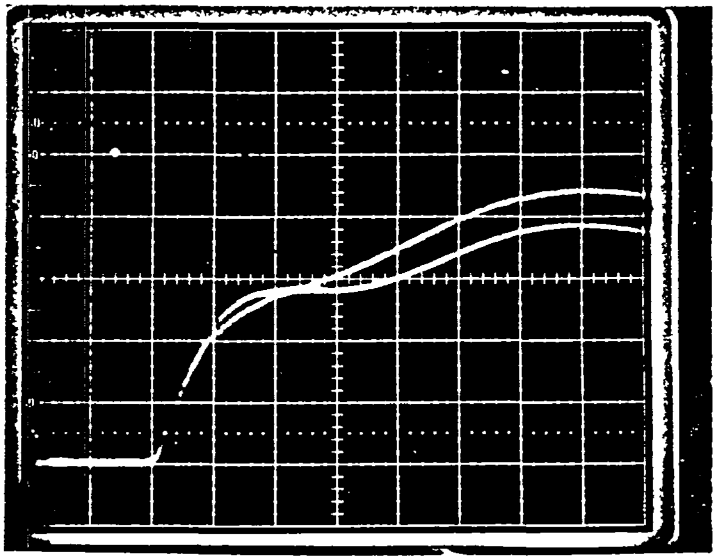

Fig. II.2.5 Drain current waveforms of two RFK 15N45 devices connected in parallel during turn-on phase at 40A load current. Scale: 100ns/div; 5A/div.

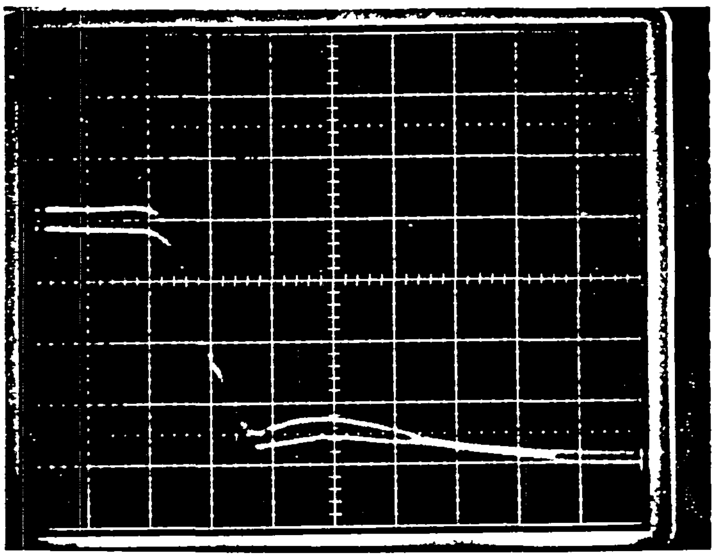

Fig. II.2.6 Drain current waveforms of two RFK 15N45 devices connected in parallel during turn-off phase at 40A load current. Scale: 100ns/div, 5A/div.

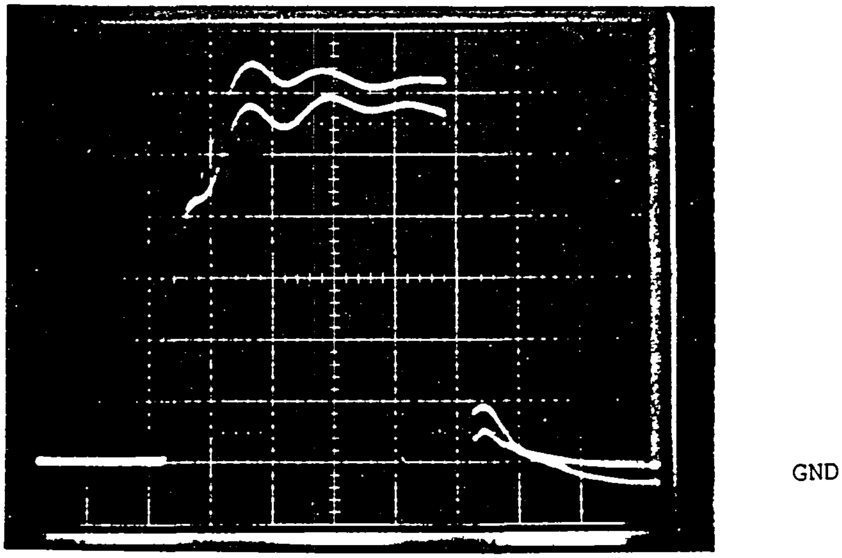

Fig. H.2.7 Drain current waveforms of two RFK 15N45 devices connected in parallel at 60A load current.
Scale: 500ns/div; 5A/div.

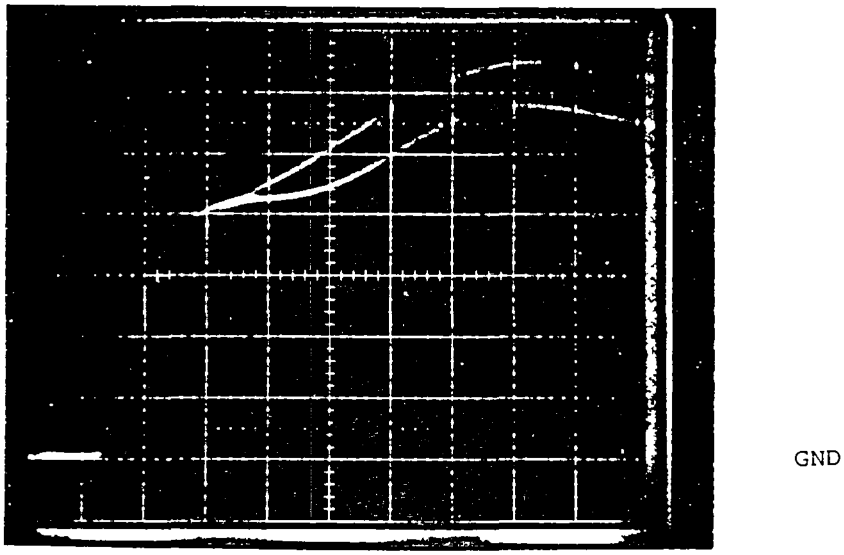

Fig. H.2.8 Drain current waveforms of two RFK 15N45 devices connected in parallel during turn-on phase at 60A load current.
Scale· 100ns/div; 5A/div.

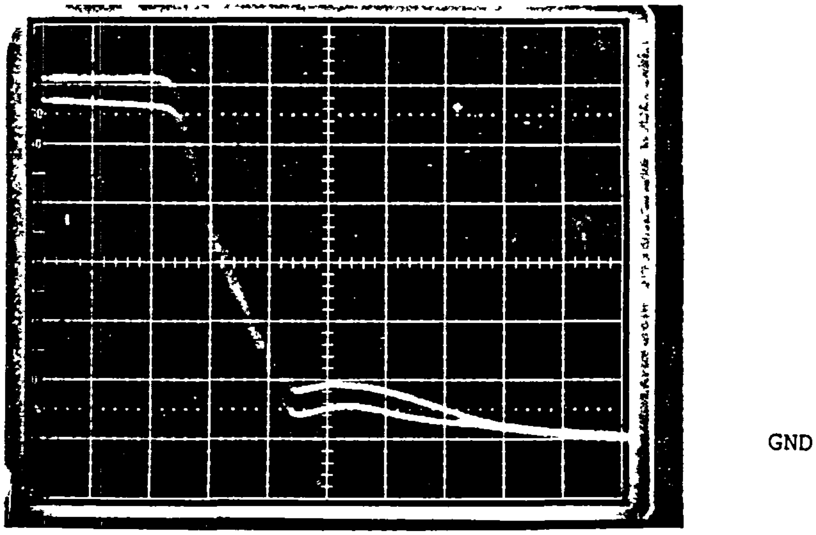

Fig. H.2.9 Drain current waveforms of two RFK 15N45 devices connected in parallel during turn-off phase at 60A load current.
Scale: 100ns/div; 5A/div.

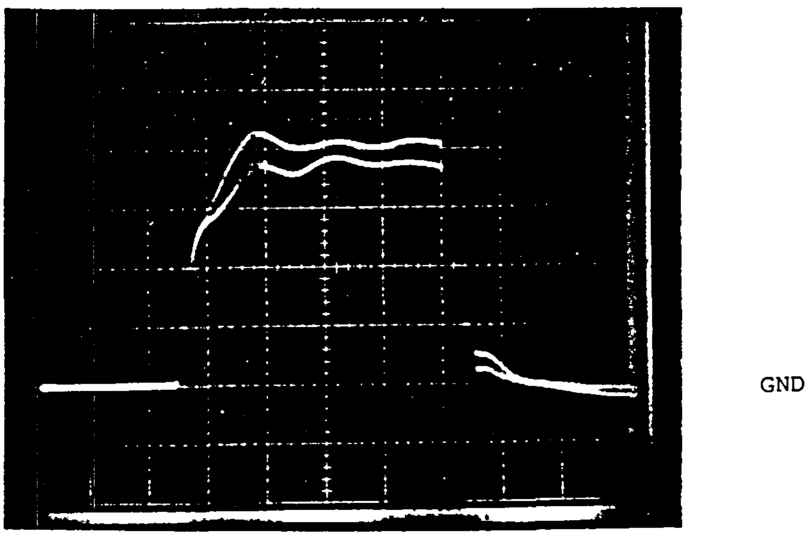

Fig. H.2.10 Drain current waveforms of two RFK 15N45 devices connected in parallel at 80A load current.
Scale: 500ns/div; 10A/div.

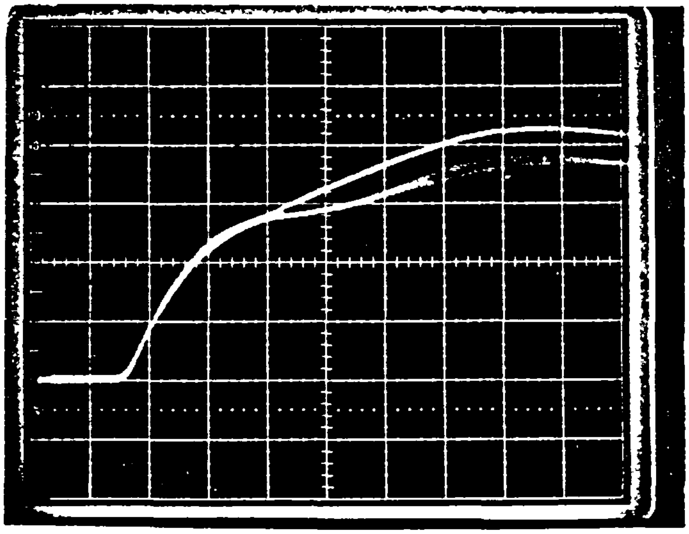

Fig. H.2.11 Drain current waveforms of two RFK 15N45 devices connected in parallel during turn-on phase at 80A load current.
Scale: 100ns/div; 10A/div.

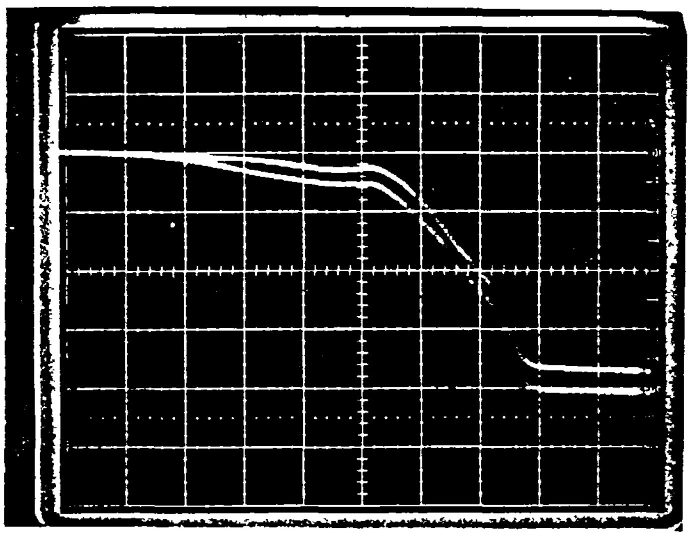

Fig. H.2.12 Drain current waveforms of two RFK 15N45 devices connected in parallel during turn-off phase at 80A load current.
Scale: 100ns/div; 10A/div.

H.3 Test Data of Parallel Operation of the RCA RFK 15N50

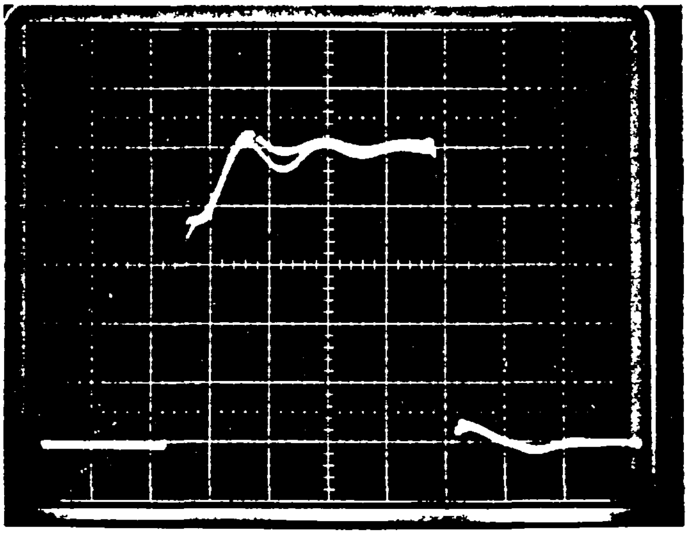

GND

Fig. H.3.1 Drain current waveforms of two RFK 15N50 devices connected in parallel at 20A load current.
Scale: 500ns/div; 2A/div.

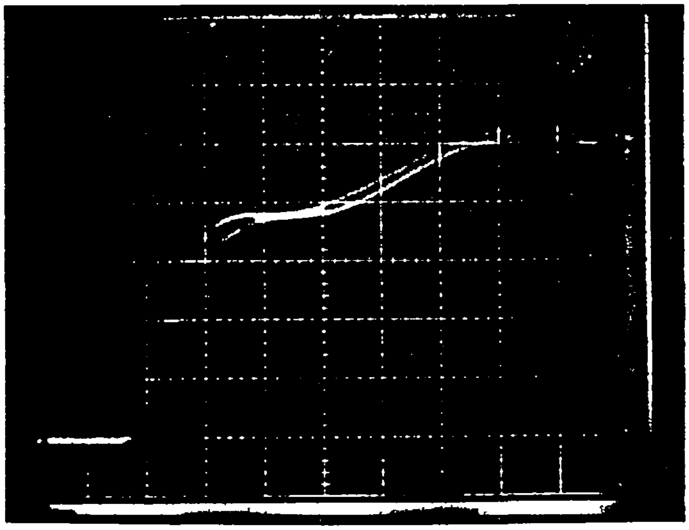

GND

Fig. H.3.2 Drain current waveforms of two RFK 15N50 devices connected in parallel during turn-on phase at 20A load current.
Scale: 100ns/div; 2A/div.

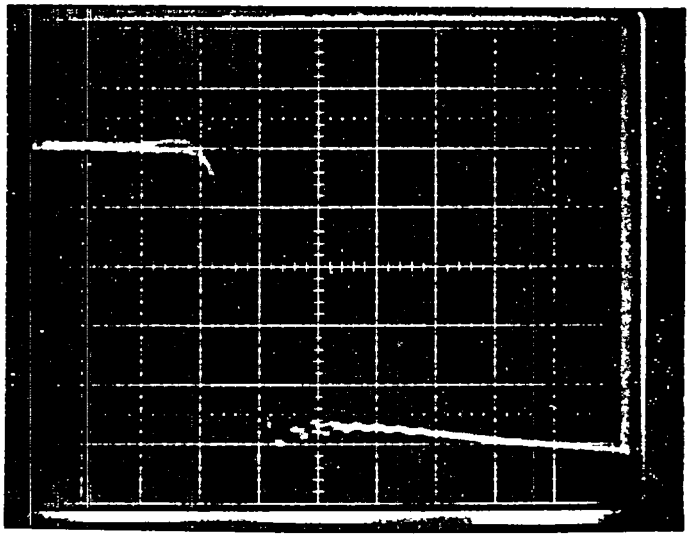

Fig. H.3.3 Drain current waveforms of two RFK 15N50 devices connected in parallel during turn-off phase at 20A load current.
Scale: 100ns/div; 2A/div.

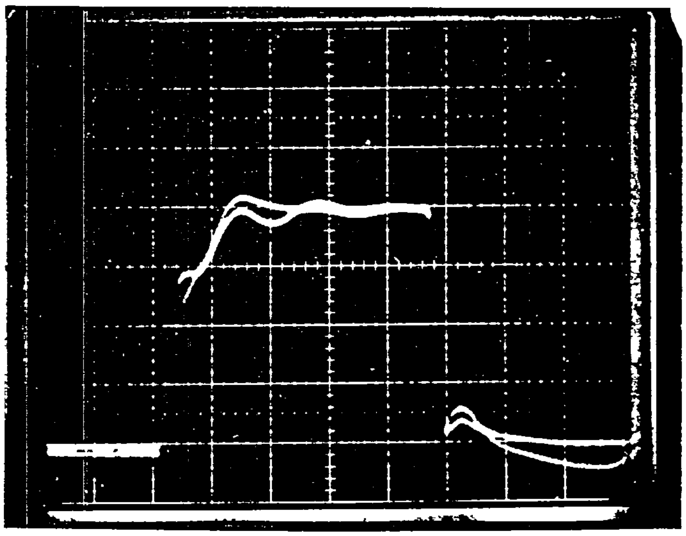

Fig. H.3.4 Drain current waveforms of two RFK 15N50 devices connected in parallel at 40A load current.
Scale: 500ns/div; 5A/div.

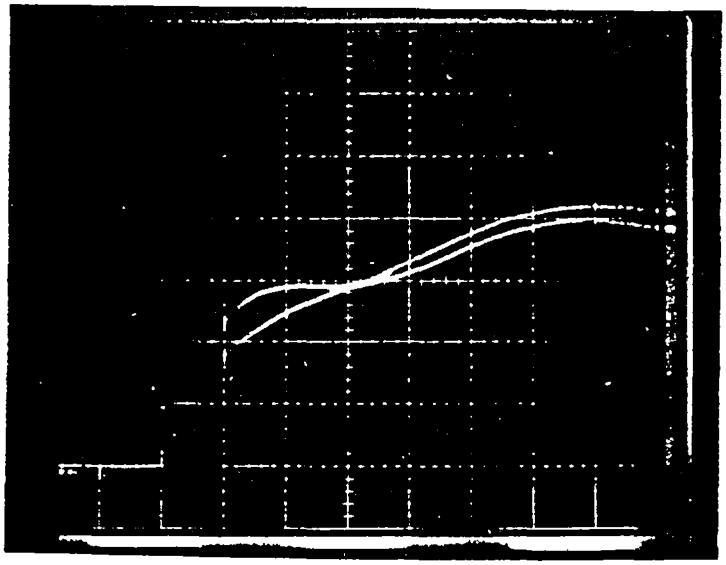

GND

Fig. H.3.5 Drain current waveforms of two RFK 15N50 devices connected in parallel during turn-on phase at 40A load current.
Scale: 100ns/div; 5A/div.

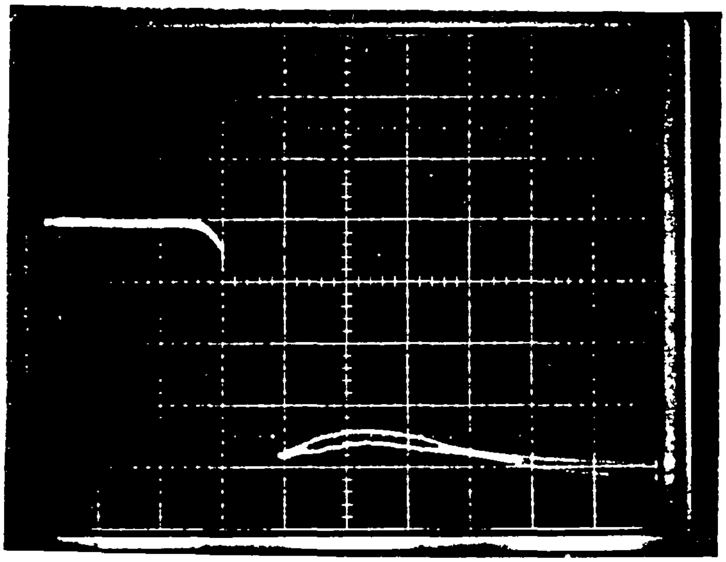

GND

Fig. H.3.6 Drain current waveforms of two RFK 15N50 devices connected in parallel during turn-off phase at 40A load current.
Scale: 100ns/div; 5A/div.

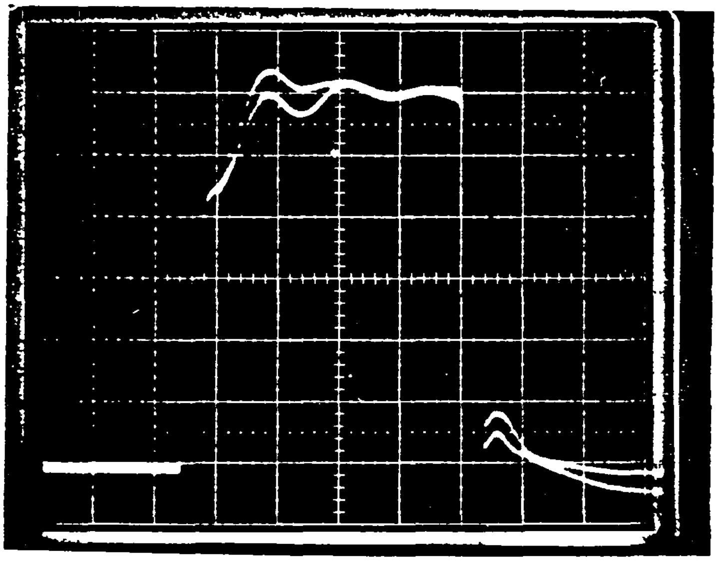

GND

Fig. H.3.7 Drain current waveforms of two RFK 15N50 devices connected in parallel at 60A load current.
Scale: 500ns/div; 5A/div.

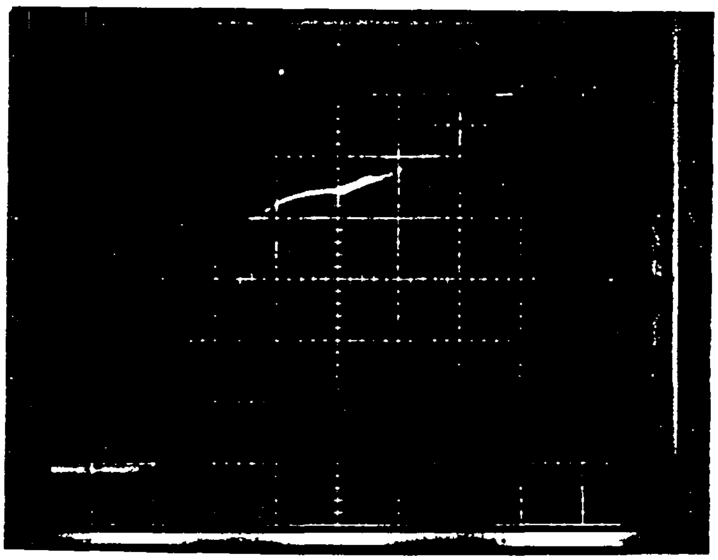

GND

Fig. H.3.8 Drain current waveforms of two RFK 15N50 devices connected in parallel during turn-on phase at 60A load current.
Scale: 100ns/div; 5A/div.

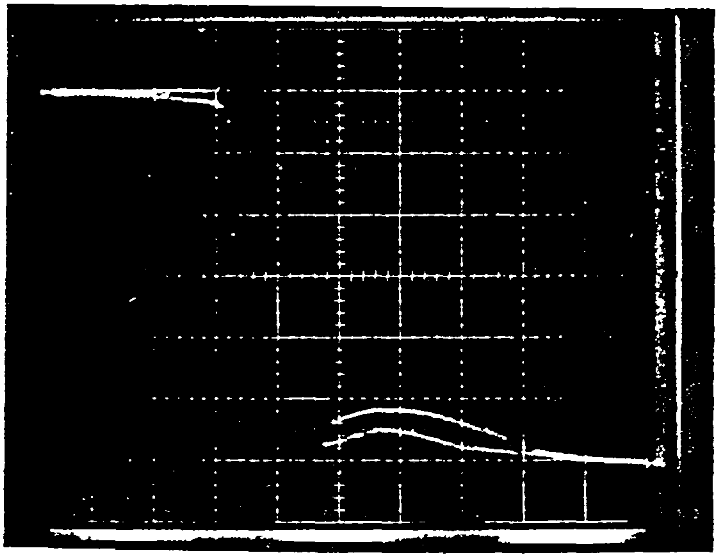

GND

Fig. H.3.9 Drain current waveforms of two RFK 15N50 devices connected in parallel during turn-off phase at 60A load current.
Scale: 100ns/div; 5A/div.

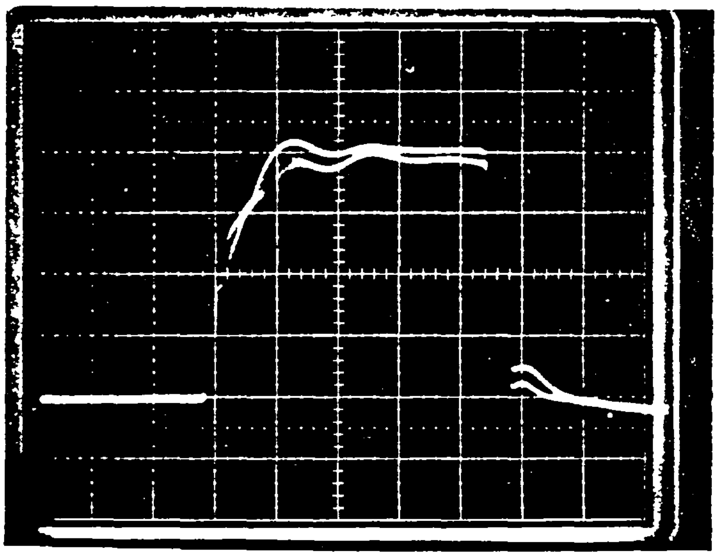

GND

Fig. H.3.10 Drain current waveforms of two RFK 15N50 devices connected in parallel at 80A load current.
Scale: 500ns/div; 10A/div.

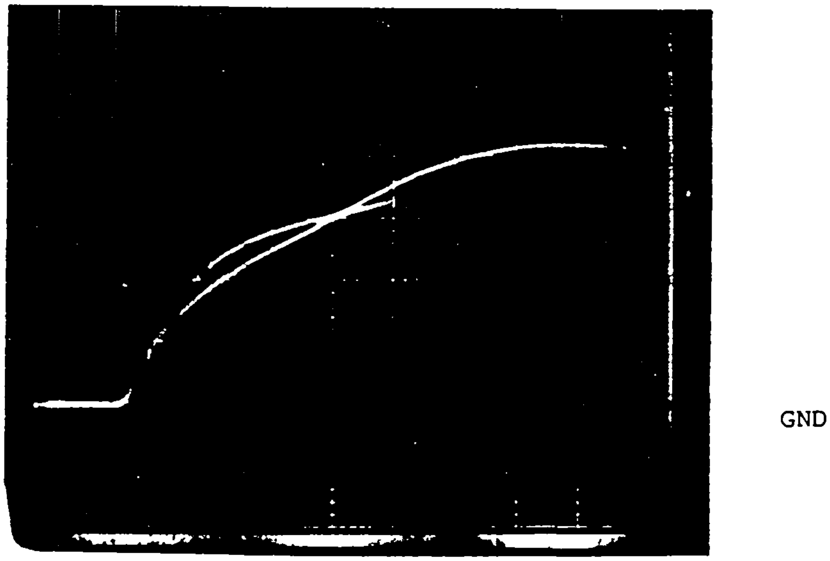

Fig. II.3.11 Drain current waveforms of two RFK 15N50 devices connected in parallel during turn-on phase at 80A load current. Scale: 100ns/div; 10A/div.

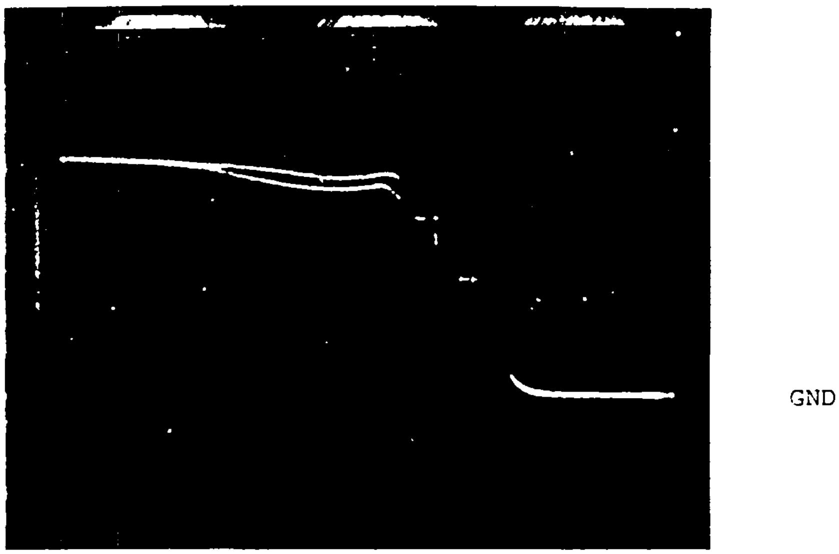

Fig. II.3.12 Drain current waveforms of two RFK 15N50 devices connected in parallel during turn-off phase at 80A load current. Scale: 100ns/div; 10A/div.

H.4 Test Data of Parallel Operation of the Toshiba 2SK356

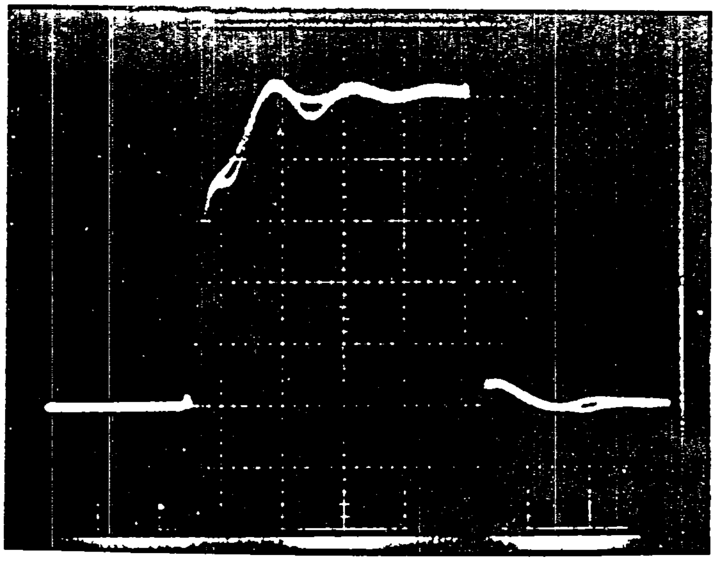

GND

Fig. H.4.1 Drain current waveforms of two 2SK356 devices connected in parallel at 20A load current.
Scale: 500ns/div; 2A/div.

GND

Fig. H.4.2 Drain current waveforms of two 2SK356 devices connected in parallel during turn-on phase at 20A load current.
Scale: 100 ns/div; 2A/div.

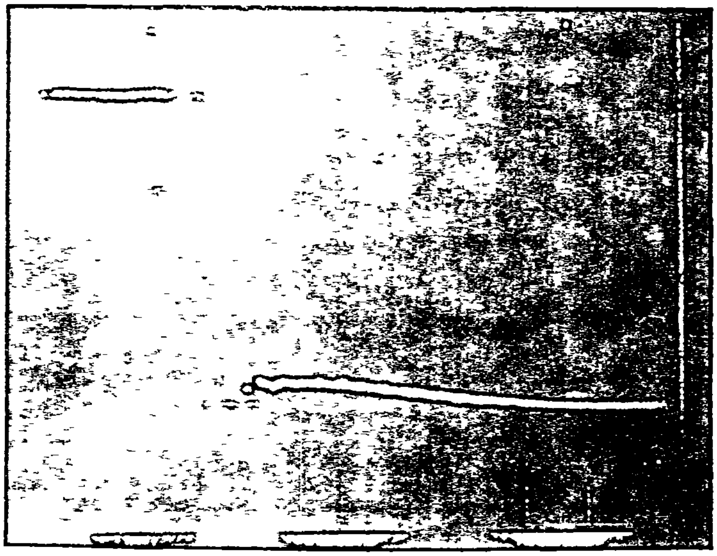

Fig. H.4.3 Drain current waveforms of two 2SK356 devices connected in parallel during turn-off phase at 20A load current.
Scale: 100 ns/div; 2A/div.

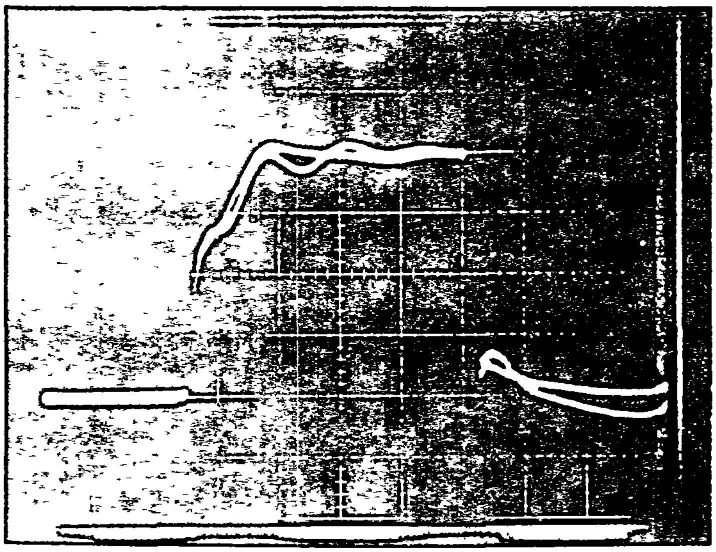

Fig. H.4.4 Drain current waveforms of two 2SK356 devices connected in parallel at 40A load current.
Scale: 500ns/div; 5A/div.

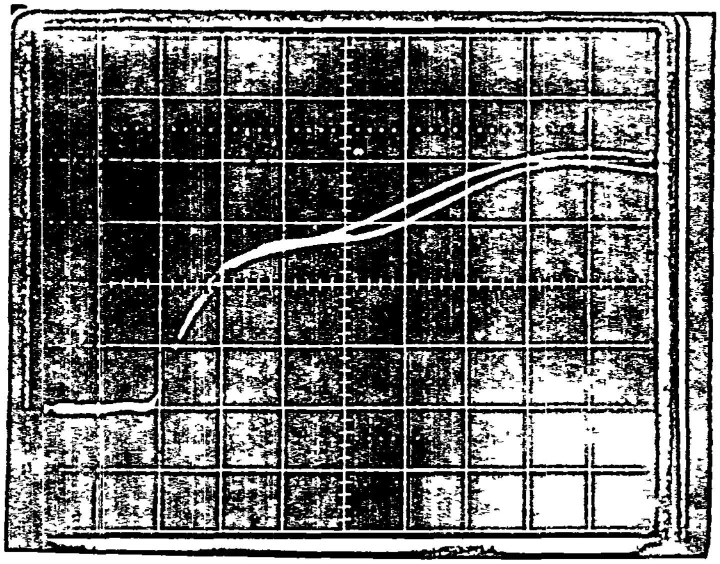

Fig. H.4.5 Drain current waveforms of two 2SK356 devices connected in parallel during turn-on phase at 40A load current. Scale: 100 ns/div; 5A/div.

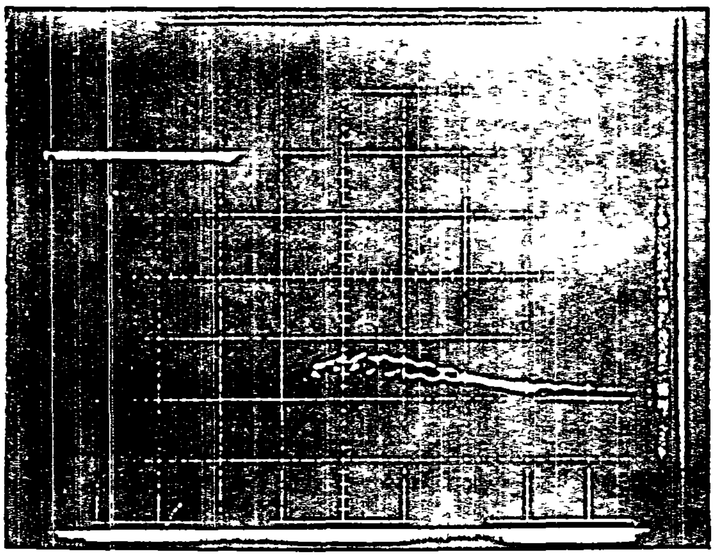

Fig. H.4.6 Drain current waveforms of two 2SK356 devices connected in parallel during turn-off phase at 40A load current. Scale: 100 ns/div; 5A/div.

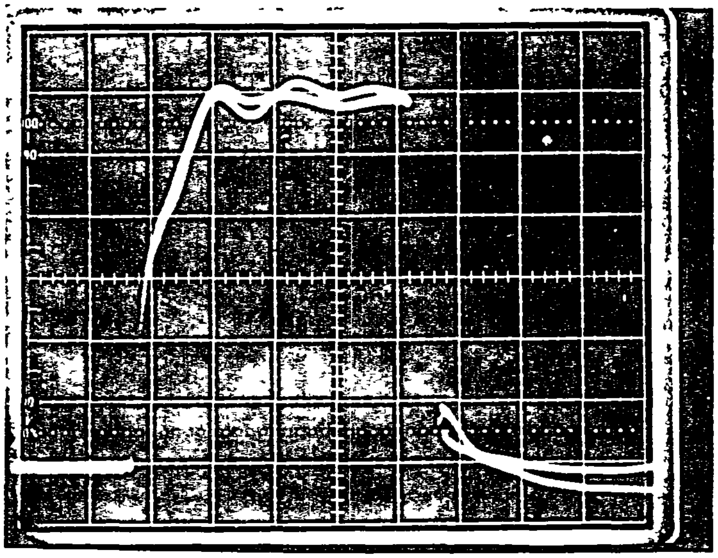

GND

Fig. H.4.7 Drain current waveforms of two 2SK356 devices connected in parallel at 60A load current.
Scale: 500 ns/div; 5A/div.

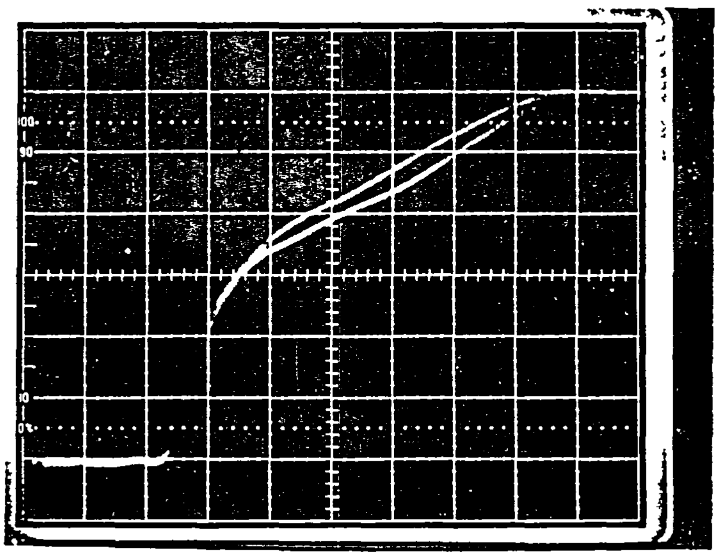

GND

Fig. H.4.8 Drain current waveforms of two 2SK356 devices connected in parallel during turn-on phase at 60A load current.
Scale: 100 ns/div; 5A/div.

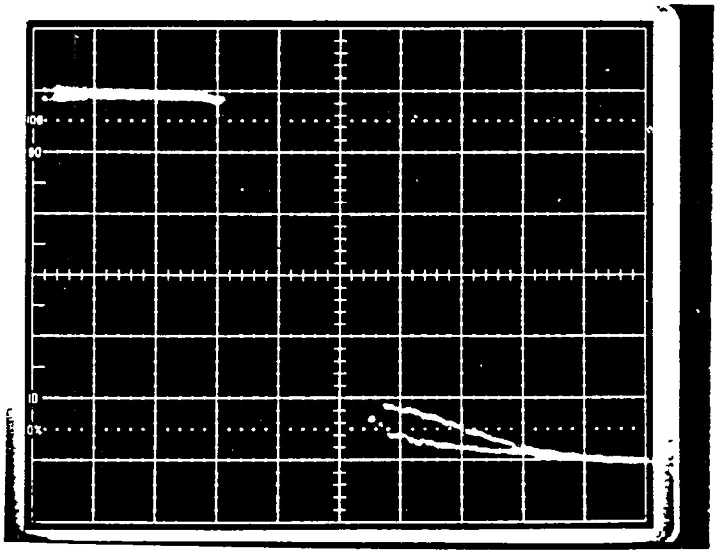

GND

Fig. II.4.9 Drain current waveforms of two 2SK356 devices connected in parallel during turn-off phase at 60A load current. Scale: 100 ns/div; 5V/div.

H.5 Test Data of Parallel Operation of the Toshiba 2SK386

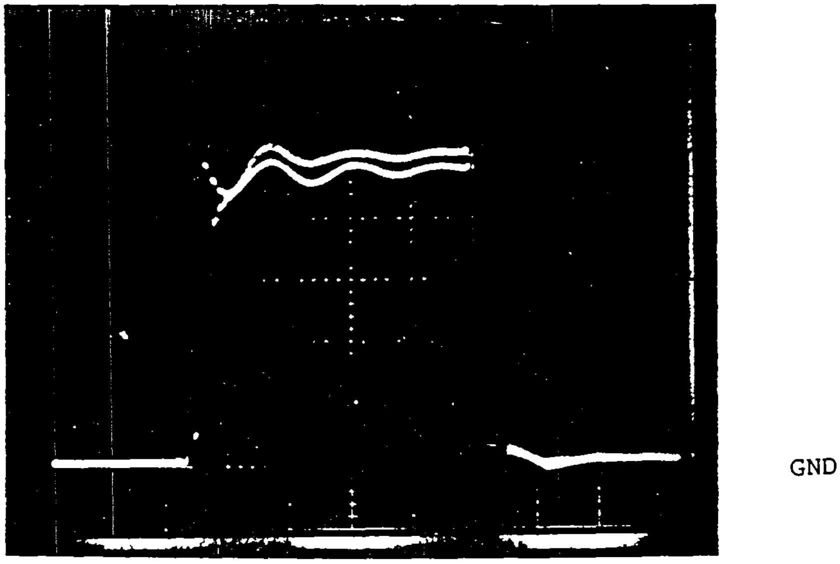

Fig. H.5.1 Drain current waveforms of two 2SK 386 devices connected in parallel at 10A load current.
Scale: 500ns/div; 1A/div.

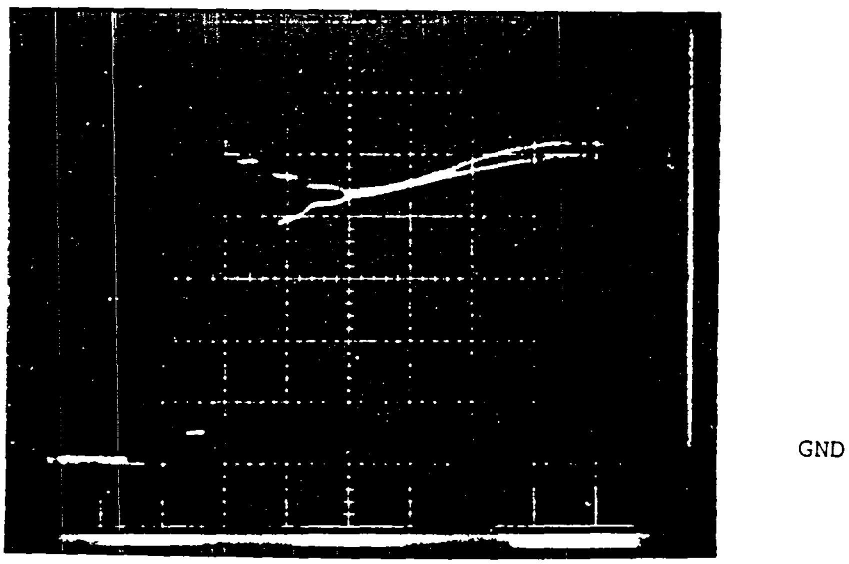

Fig. H.5.2 Drain current waveforms of two 2SK 386 devices connected in parallel during turn-on phase at 10A load current.
Scale: 100ns/div; 1A/div.

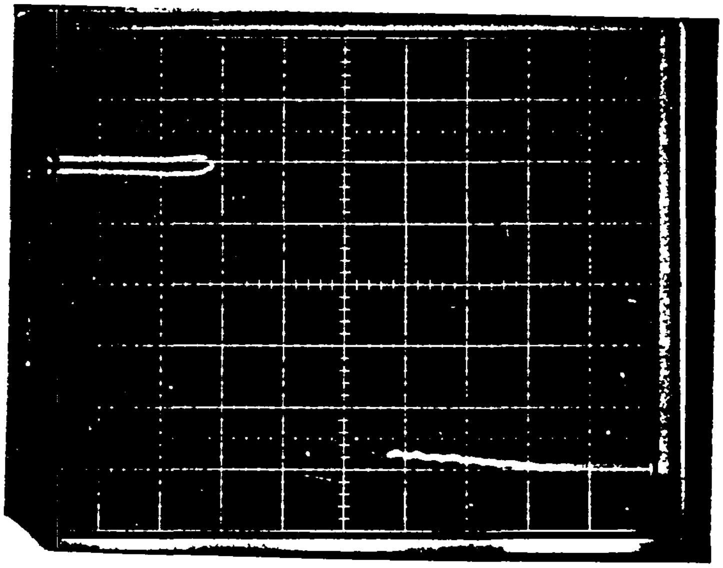

Fig. H.5.3 Drain current waveforms of two 2SK 386 devices connected in parallel during turn-on phase at 10A load current.
Scale: 100ns/div; 1A/div.

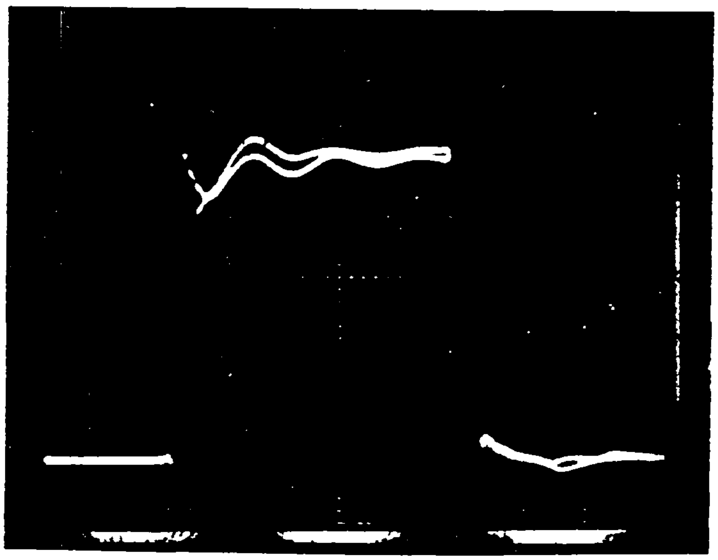

Fig. H.5.4 Drain current waveforms of two 2SK 386 devices connected in parallel at 20A load current.
Scale: 500ns/div; 2A/div.

Fig. H.5.5 Drain current waveforms of two 2SK 386 devices connected in parallel during turn-on phase at 20A load current. Scale: 100ns/div; 2A/div.

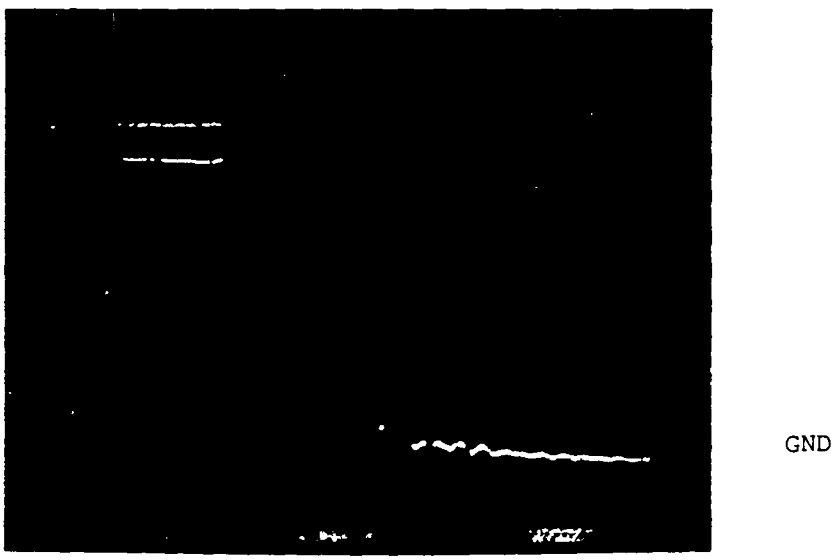

Fig. H.5.6 Drain current waveforms of two 2SK 386 devices connected in parallel during turn-off phase at 20A load current. Scale: 100ns/div; 2A/div.

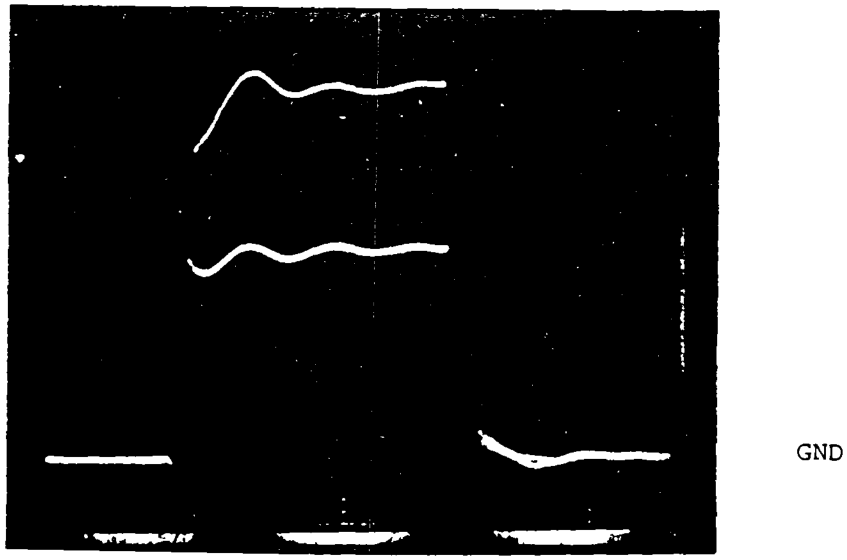

Fig. H.5.7 Drain current waveforms of two 2SK 386 devices connected in parallel at 20A load current after 3min operation. Current robbing observed.
Scale: 500ns/div: 2A/div.

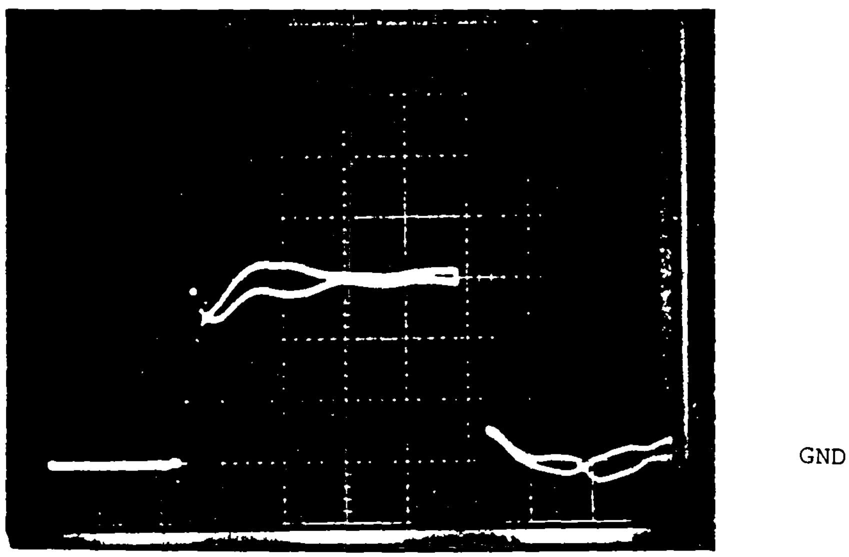

Fig. H.5.8 Drain current waveforms of two 2SK 386 devices connected in parallel at 30A load current.
Scale: 500ns/div; 5A/div.

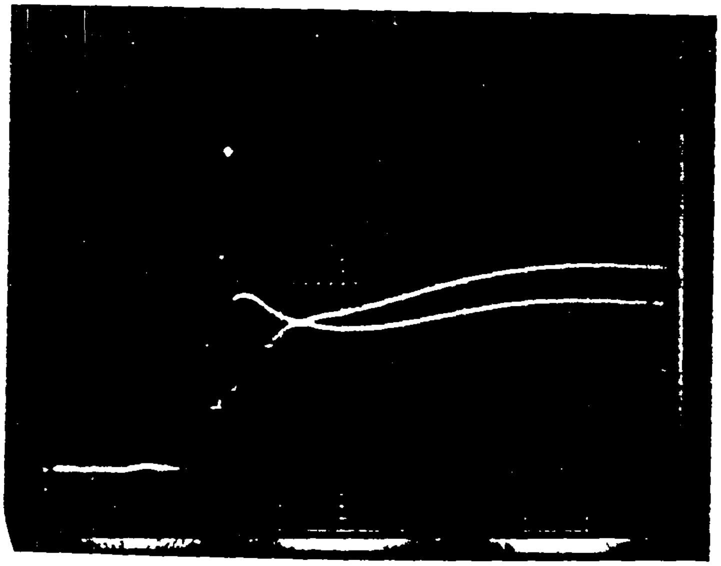

Fig. H.5.9 Drain current waveforms of two 2SK 386 devices connected in parallel during turn-on phase at 30A load current. Scale: 100ns/div; 5A/div.

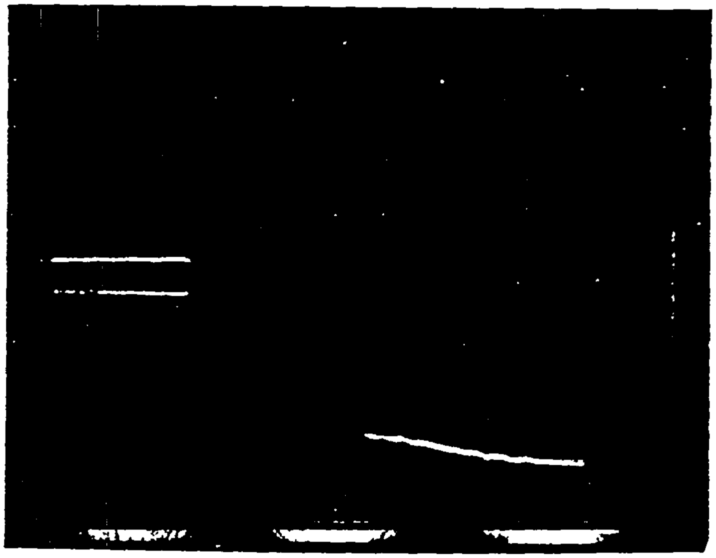

Fig. H.5.10 Drain current waveforms of two 2SK 386 devices connected in parallel during turn-off phase at 30A load current. Scale: 100ns/div, 5A/div.

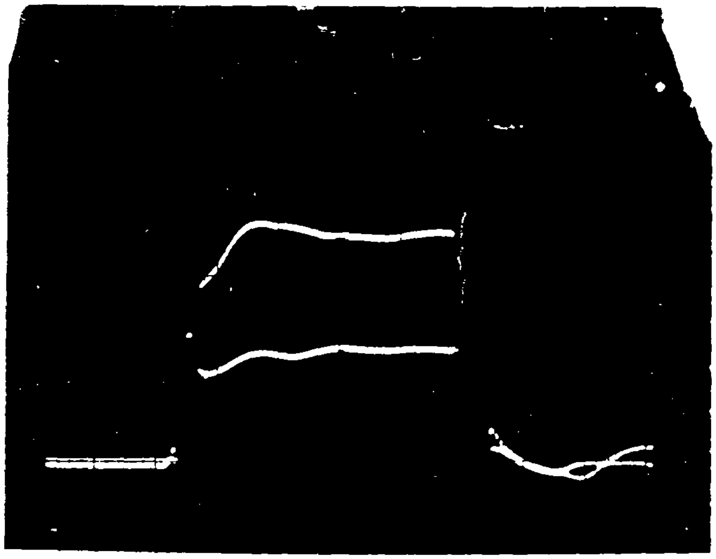

Fig. H.5.11 Drain current waveforms of two 2SK 386 devices connected in parallel at 30A load current after 3min operation. Current robbing observed.
Scale: 500ns/div: 5A/div

☆U S GOVERNMENT PRINTING OFFICE 1985-544-063/ 11050

End of Document